ISSN 1738-1142

Volume 16(1) **2018**

KOREAN RADIOACTIVE WASTE SOCIETY

2018 춘계학술논문요약집

| 일시 |

2018. 5. 30(수) ~ 6. 1(금)

| 장소 |

부산 BEXCO 컨벤션홀

Abstracts of Proceedings of the
Korean Radioactive Waste Society
SPRING 2017

사단법인 한국방사성폐기물학회
Korean Radioactive Waste Society

ISSN 1738-1142

Volume 16(1) **2018**

KOREAN RADIOACTIVE WASTE SOCIETY

2018 춘계학술논문요약집

| 일시 |

2018. 5. 30(수) ~ 6. 1(금)

| 장소 |

부산 BEXCO 컨벤션홀

Abstracts of Proceedings of the
Korean Radioactive Waste Society
SPRING 2017

사단법인 한국방사성폐기물학회
Korean Radioactive Waste Society

Contents

KOREAN
RADIOACTIVE WASTE
SOCIETY

1분과 핵주기정책 및 핵비확산 (Oral)

09:00~09:20 Survey on Standards to Harden Security of PC-Based Systems for Nuclear Facilities ····· 19
Chaechang Lee and Soomin Lim[KINAC]

09:20~09:40 Potential Utilization of Laser Flash Analysis for On-Site Measurement of UO_2 Stoichiometry ····· 21
Gyeonghun Kim, Jungsu Ahn, and Sangjoon Ahn[UNIST]

09:40~10:00 Game-Theoretic Approach for Safeguards Program of a Geological Repository for Spent Nuclear Fuels During Post-Closure Period ····· 23
Heejae Ju and Sungyeol Choi [KAIST], Il Soon Hwang[Seoul Natl. Univ.]

10:00~10:20 Accomplishment and Suggestion of ROK's NMAC for Nuclear Security ····· 25
Jae San Kim[KINAC]

11:20~11:40 Development of Safeguards Approach for the Disposal of Low and Intermediate Level Radioactive Waste Containing Uranium ····· 27
Chul Heo, Seungho Ahn, Seungmin Lee, and Junghee Son[KINAC]

11:40~12:00 Legal Policy Study on Nuclear Liability Principle of Nuclear Operator Under Korea Nuclear Liability Law ····· 29
Daesung Lee and Jaeyoung Bang[KAERI]

2분과 사용후핵연료 처분전관리 (Oral)

09:00~09:20 Evaluation of Decay Heat Distribution in the OASIS-32D Cask ····· 33
Yong IL Kim, Young Tae Han, Joon Gi Ahn, In Ho Song, and Gyu Cheon Lee[KEPCO E&C]

09:20~09:40 Stress-Based Criterion for the Creep Response of Spent Nuclear Fuel Rod ··· 35
Donghyo Lee, Seongki Lee, and Jongsung Yoo[KEPCO NF]

09:40~10:00 Validation of CFD Thermal Model for Dry Cask Simulator ····· 37
Taehyeon Kim, Yongdeog Kim, and Sunghwan Chung[KHNP-CRI]

10:00~10:20 Multi-Dimensional Modeling of Electrorefining Process of Used Nuclear Fuel With Liquid Cadmium and Rotating Cylinder Electrodes ····· 39
Dokyu Kang and Sungyeol Choi [KAIST], Jaeyeong Park[UNIST]

11:20~11:40 Development of Finite Element Model for Handling Characteristic Evaluation of Spent Nuclear Fuel ····· 41
Jaejun Lee, Hyeongkoo Kim, Seongki Lee, and Jongsung Yoo[KEPCO NF]

11:40~12:00 Method to Determine the Simplified Fuel Assembly Model for a Spent Fuel Rack Seismic Analysis From the Reactor Vessel Internal Seismic Analysis Model ····· 43
Dong-Hak Kim and Yulim Shin[KHNP-CRI]

12:00~12:20 Equivalent Drop Analysis Model of Transportation Cask Including Spent Nuclear Fuel Assembly ····· 45
Yun Young Yang, Sang Soon Cho, Woo-Seok Choi, and Ki-Seog Seo [KAERI], Daesik Yook and A Ra Go[KINS]

2분과 사용후핵연료 처분전관리 (Poster)

P0201 Determination of a Simplified Analysis Model of Spent Fuel Storage Rack for Seismic Analysis ····· 49
Yulim Shin and Dong-Hak Kim[KHNP-CRI]

P0202 Recovery of RE-less U From U/RE Ingot by Electrochemical Oxidation Process ·· 51
Si Hyung Kim, Dalsung Yoon, Junhyuk Jang, Taek-Jin Kim, Seunwoo Paek, and Sung-Jai Lee[KAERI]

P0203 U/RE Recovery Using Large-Scale LCC Electrowinning System ····· 53
Si Hyung Kim, Joon-Bo Shim, Junhyuk Jang, Sang-Woon Kwon, Young Sang Lee, Youngwoo Kwon, Gha-Young Kim, and Sung-Jai Lee[KAERI]

P0204 A Review of the Probabilistic Model for Chloride-Induced Stress Corrosion Cracking ····· 55
Hyoung Gyu Park, Sun Woo Park, and Kwang Heon Park[Kyung Hee Univ.]

P0205 Crucible Cover of Multilayer Porous Hemisphere for Cd Distillation ····· 57
S.W.Kwon, Y.S.Lee, J.H.Jung, S.H.Kim, S.J.Lee, and J.M. Hur[KAERI]

P0206 Effect of Creep Deformation on Ductility of Simulated Spent Fuel Cladding ·· 58
Jong-Dae Hong, Euijung Kim, and Dong-Hak Kook[KAERI]

P0207 Requirements for Direct Radiation From SNF Dry Storage Casks ····· 60
Sunghwan Chung, Kiyoung Kim, and Yongdeog Kim[KHNP CRI]

P0208 Criticality Safety Study for Loss of Single Fuel Rod From WH 14 Type Fuel ·· 62
Janghwan Lim, Manseok Do, Seongki Lee, and Jongsung Yoo[KEPCO NF]

P0209 Reaction of Rare Earth Elements With UCl_3 in the LiCl-KCl Salt ····· 64
Seungwoo Paek, Dal-Sung Yoon, Si Hyung Kim, Junhyuk Jang, Gha-Young Kim, and Sung-Jai Lee[KAERI]

P0210 Safety Design Criteria for Spent Nuclear Fuel Cycle Facility ····· 66
Woo Jin Jo, Seok-Jun Seo, Siwan Noh, Hyo Jik Lee, and Seung Nam Yu [KAERI]

P0211 Applicability of the ANSI/ANS-58.16 on Pyroprocessing Facilities ····· 68
Gilsung You, Seokjun Seo, Woojin Jo, Siwan Noh, Hyojik Lee, Hohee Lee, Seungnam Yu, and Jeonghoe Ku[KAERI]

P0212 Preliminary Evaluation of Process Equipment Test Mock-up for Construction of Drying System ····· 70
Byungsuk Park, Jaehoon Lim, Dongseok Ryu, Jonghui Han, and Seungnam Yu[KAERI]

P0213 Critical Effect According to Number of Spent Fuel Nuclide ····· 72
KIM Yun-sik[KONES corp.], Kim Ki-Young[KHNP]

P0214 Fuel Integrity Evaluation During the Dry Storage by FRAPCON ····· 74
Suji Yoon, Kwang heon Park, Hyung ju Yun, and Wu seung You[Kyung Hee Univ.]

P0215 Numerical Simulations of Flow Field in a Vacuum Chamber for the Drying Test Equipment of Spent Fuel ····· 76
Ju-Chan Lee, K.S. Bang, S.H. Yu, S.S. Cho, and W.S. Choi[KAERI]

P0216 Design of an Actuation Module for a Cathode Basket Lifting Mechanism ···· 78
Doyeon Kim, Dongseok Ryu, and Seungnam Yu[KAERI]

P0217 Hydrogen Content Effects on Delayed Hydride Cracking in Zircaloy-4 Cladding ·· 80
Wooyong Choi and Kwangheon Park[Kyung Hee Univ.]

P0218 Development of Forced Helium Dehydration (FHD) Test System for Spent Fuel Canister ····· 82
Kyung-Wook Shin, Gyung-Sun Chae, Byeong-Mok Park, Suk-Nam Lim, and Jae-Seok Park [SAE-AN ENGINEERING CO.]

P0219 Design of a Basket Lifting Mechanism for Pyroprocessing Automation Verifying Mockup ····· 84
Dongseok Ryu, Jongkwang Lee, and Seungnam Yoo[KAERI]

P0220 Construction of Dry Room for Pyroprocessing Automation Verification Mock-up ····· 86
Jonghui Han, Byungsuk Park, Jaehoon Lim, Dongseok Ryu, and Seungnam Yu[KAERI]

P0221 15 m Drop Analysis for Spent Nuclear Fuel Transport Cask ····· 88
JaeHoon Lim, Sang Soon Cho, Yun-young Yang, Kiseog Seo, and Woo-seok Choi[KAERI], Daesik Yook[KINS]

P0222 Radiation Shielding Evaluation for Spent Fuel Storage Pool According to Burnup ····· 90
Young-Hwan Choi and Jae-Hun Ko[KONES corp.], Ki-Young Kim[KHNP CRI]

P0223 Dynamic Optimization of the PWR SF Transportation With Constraints on Storage Capacity and SF Movement ····· 92
Hong Jang and Hyo On Nam[KAERI]

P0224 Applicaiton of Likelihood Evaluation Method for an Integrated Safety Analysis ····· 94
Seok-Jun Seo, Woojin Jo, Siwan Noh, Hongrae Jeon, Gil-Sung You, Jeong-Hoe Ku, and Seung Nam Yu [KAERI]

P0225 A Study on the Improvement of Process Operation Through Logistics Control ····· 96
Hun Suk Im, Hong Jang, and Hyo Jik Lee[KAERI]

P0226 Evaluation of Spent Fuel Damage in Actually Happenable 15 m Drop Accident Test ····· 98
Woo-seok Choi, Sangsoon Cho, Yun-young Yang, and Jae-hoon Lim[KAERI], Sanghyeok Han[Sungshin ENG], Daesik Yook[KINS]

P0227 Factors Affecting Spent Nuclear Fuel Rod Resistance Against Impact ····· 100
Sanghoon Lee[Keimyung Univ.], Belal Almomani and Dongchan Jang[KAIST]

P0228 A Simulation Study for Galvanic Reduction of Metal Chloride From LiCl-KCl Eutectic Salt ····· 102
Kwang-Rag Kim, Sung-Ki Kim, Hun-Suk Im, and Hyo-On Nam[KAERI]

P0229 Technical Review of Force-Reflecting Telemanipulator System ····· 104
Seungnam Yu, Jongkwang Lee, and Byungsuk Park[KAERI]

P0230 Electrochemical Formation of RE-Mg Alloy in LiCl-KCl-$RECl_3$ Molten Salt ·· 106
Gha-Young Kim and Sung-Jai Lee[KAERI]

3분과 고준위폐기물처분 (Oral)

09:00~09:20 Modelling of Sulphide Induced Copper Corrosion in Deep Geologocial Repository With Expected Condition ····· 111
Nakkyu Chae and Sungyeol Choi[KAIST], Heui-Joo Choi[KAERI]

09:20~09:40 Performance Evaluation of Novel Emplacement Device ····· 113
Minsoo Lee, Jong Yul Lee, and Sung-Hoon Ji[KAERI]

09:40~10:00 Preliminary Analysis on the Domestic Applicability of Deep Borehole Disposal ··· 115
Jong-Youl LEE, Min-Soo LEE, Heui-Joo CHOI, Kyung-Su KIM, and Dong-Keun CHO[KAERI]

10:00~10:20 Correlations Among Fracture Distribution, in Situ Stress States and Hydraulic Conductivity of Fractured Rock Mass ····· 117
Yeonguk Jo, Kyung-Woo Park, and Sung-Hoon Ji[KAERI]

11:20~11:40 Studies on Excavation Damage by Blasting in Underground Research Laboratories ····· 119
Seung-Hoon Park and Sangki Kwon[Inha Univ.]

11:40~12:00 Groundwater Flow Modeling Based on the Site Descriptive Model Around KURT ····· 121
Kyung-Woo PARK, Su-Lim Jung, and Sung-Hoon Ji[KAERI]

12:00~12:20 Application of Complementary Indicators for the Performance Assessment of Disposal Facility in Korea ····· 123
Yongheum Jo, Sol-Chan Han, and Jong-Il Yun[KAIST]

12:20~12:40 Numerical Analysis of Upward Movement of Dummy Canister at Engineered Barrier Emplacement Experiment ····· 125
Changsoo Lee, Jaewon Lee, and Geon Young Kim[KAERI]

3분과 고준위폐기물처분 (Poster)

P0301 Shearing Analysis of Disassembly Machine in HeadEnd ····· 129
Younghwan Kim, Yungzon Cho, and Youngsoon Lee[KAERI]

P0302 Thermal Conductivity Investigation of Korean Bentonite Buffer Materials ····· 131
Seok Yoon, Wanhyoung Cho, Changsoo Lee, and Geonyoung Kim[KAERI]

P0303 Nuclide Transport Behavior in the Fracture Around a Conceptual German HLW Repository ····· 133
Youn-Myoung Lee[KAERI], Thorsten Schaefer[KIT]

P0304 Numerical Evaluation for In-Situ Tests Investigating a Local Hydraulic Property on a Borehole ····· 135
Nak-Youl Ko and Sung-Hoon Ji[KAERI]

P0305 Development of Modeling Interface for a Process-Based Total System Performance Assessment of a Geological Disposal System ····· 137
Jung-Woo Kim, Jaewon Lee, and Dong-Keun Cho[KAERI]

P0306 Statistical Approach of the Geochemical Mobility of Geogenic Uranium in Groundwater of KURT ····· 139
Jihye Jeong, Jang-Soon Kwon, Yong-Kwon Koh, and Jae-Kwang Lee[KAERI]

P0307 Characteristics of KyungJu-II Bentonite Heated With Different Potassium Concentrations ····· 141
Wan Hyoung Cho, Ji-Hun Ryu, and Jae Kwang Lee[KAERI]

P0308 Preliminary Evaluation of Rare Earth Effect on Burnup Limit in TRU Fuel ·· 143
Byoung Oon Lee, Chan Bock Lee, June Hyung Kim, Jin Sik Cheon, Jeong Yong Park, and Sung Ho Kim[KAERI]

P0309 Effects of Microbial Activity on the Biochemical Alteration of KJ-II Bentonite Under Alkaline-Reducing Conditions ····· 145
Hyo-Jin Seo, Seung Yeop Lee, Jae-Kwang Lee, and Wan Hyoung Cho[KAERI]

P0310 Introduction of the IAEA URF Network and Role of the KAERI ····· 147
Geon Young Kim, Kyungsu Kim, Min-Hoon Baik, and Young-Chul Choi[KAERI]

P0311 Modelling Transport of Radionuclides Observed in In-Situ Tracer Tests Based on Microstructure Characterization ····· 149
Dong Kyu Park and Sung-Hoon Ji[KAERI]

P0312 The State-of-the Art of the Geological Evolution Research to Verify the Long-Term Safety of Disposal Site ····· 151
Soolim Jung and Sung-Hoon Ji[KAERI]

P0313 Numerical Modelling of Gas Injection Experiment Using Damage Model ····· 153
Jaewon Lee, Changsoo Lee, and Geon Young Kim[KAERI]

P0314 Recent Suction and Temperature-Controlled Tests for Measuring the Mechanical Properties of Unsaturated Bentonite Buffer ····· 155
Jaw Owan Lee and Geon Young Kim[KAERI]

P0315 Application of Mazars Damage Model to KURT Rock Under Thermo-Hydro-Mechanical Coupled Conditions ····· 157
Jin-Seop Kim, Young-Chul Choi, Seok Yoon, and Geon-Young Kim[KAERI]

4분과 중저준위폐기물관리 (Oral)

09:00~09:20 Newly Developed Technology Introduction: Radioactive Spent Resin Treatment System Using Combined Dewatering Hopper ····· 161
JongSeo Choi, Sung-Hyun Heo, Yun Jae Lee, and Gi-Ho Park[DAEWOO E&C]

09:20~09:40 Development of the PHWR Spent Resin Treatment Technology to Secure Disposal Safety ····· 163
Kyu-Tae Park, Jung-Min Yoo, Hyeon-Oh Park, and Young-Ku Choi[Sunkwang T&S Co.,Ltd]

09:40~10:00 Consequence Analysis on the Transportation Accident of Spent Resin Waste From a Heavy Water-Cooled Reactor to the Gyeongju Disposal Facility ···· 165
Ki Joon Kang, UkJae Lee, Jaeseong Min, and Hee Reyoung Kim[UNIST]

10:00~10:20 Radiological Safety Analysis in Transportation for Radioactive Wastes Disposal ··· 167
Woo Nyun Choi and Hee Reyoung Kim[UNIST]

11:20~11:40 Potential Management Options of Radioactive Large Metallic Components From NPPs in Operation and Decommissioning ····· 169
Jin-ho Park, Jae hak Cheong, and Joo-ho Hwang[KyungHee Univ.]

11:40~12:00 Probabilistic Safety Assessment for LILW Silo Repository in Earthquake Scenario Using Domestic Earthquake List ····· 171
Sol-Chan Han and Jong-Il Yun[KAIST]

12:00~12:20 Solidification of HyBRID Waste Using Geopolymer Waste Form ····· 173
Jinmo Ahn, Won-Seok Kim, Seongye Kwon, and Wooyong Um[POSTECH],
Seonbyeong Kim and Wangkyu Choi[KAERI]

12:20~12:40 A Study on the Proper Amount of $Ba(OH)_2$ for Wastewater Treatment From the SP-HyBRID Decontamination Process ····· 175
J.Y. Jung, H.C. Eun, S.Y. Park, H.J. Won, J.S. Park, S.B. Kim, and B.K. Seo[KAERI],
S.J. Park[Chungnam Natl. Univ.]

4분과 중저준위폐기물관리 (Poster)

P0401 Radiation Shielding Evaluation for IP-2 Transport Container Including Activated Cutting Waste of KORI Unit 1 RV/RVI ····· 179
Jae-Hun Ko, Duk-Woon Jung, and Dong-Kyu Lee[KONES corp.],
Young-Hwan Hwang[KHNP CRI]

P0402 Radionuclide Inventory of Past Radioactive Waste in NPPs ····· 181
HeeJin Ahn[KHNP CRI], HongJoo Ahn[KAERI]

P0403 5-bromo-Ph4-BTPhen Ligand for Selective Removal of Strontium and Cobalt From Water ····· 183
Jiseon Jang and Dae Sung Lee[Kyungpook Natl. Univ.], Laurence M. Harwood, Joe Cowell, and Ashfaq Afsar[Univ. of Reading]

P0404 Treatment of Radwastes From Medical Radioisotope Production ····· 184
Seung-Kon Lee, Suseung Lee, Myunggoo Kang, Kyungsoek Woo, and Junsig Lee[KAERI]

P0405 Study on Predictive Models for Leaching Behavior of Waste Glasses Based on Machine Learning Algorithms ····· 186
Jae Hwan Yang[KAERI]

P0406 A Comparative Study on Domestic and Overseas WTS for Implementation of the Integrated Radioactive Waste Tracking System ····· 188
Sun Il Kim, Hak Yun Lee, Ki Tae Yang, and Jong Soon Song[Chosun Univ.]

P0407 An Experimental Study on the Pelletization of Powdered Radioactive Waste Using the Roll Compaction System ····· 190
Jongsoon Song, Minyoung Jung, and Sanghyun Lim[Chosun Univ.]

P0408 Implementation of Waste Tracking System (WTS) for Solidification Process and Management ····· 192
Sungjong Kim, Changhwan Cho, Jawon Jeng , and Wooseok Heo[MIRAEEN Co. Ltd]

P0409 Characteristics Testing of Solidified Radioactive Waste From Nuclear Fuel Manufacturing ····· 194
Sungjong Kim and Changhwan Cho[MIRAEEN Co. Ltd], Seunghoon Han, Youngjong Ju, Hyunkyu Kang, and Jungwoo Lee[KEPCO NF]

P0410 Leaching Test of Lime Precipitate Radioactive Waste Containing Uranium ·· 196
Changhwan Cho and Sungjong Kim[MIRAEEN Co. Ltd], Seunghoon Han, Youngjong Ju, Jungwoo Lee, and Jeongmyeong Kim[KEPCO NF]

P0411 Evaluation of Structural Stability for Cement Waste Form of Lime Waste ···· 198
Jong Sik Shon, Gi Yong Kim, Ki-baek Shin, Junhyuck Im, and Dae Seok Hong[KAERI]

P0412 The Applicability of Core Sampling to Treatment of ITER Type B Radwaste ···· 200
Sunggeun Kim, Myungchul Park, Wanho Oh, and Sangbok Ahn[KAERI]

P0413 The Homogeneity Test and Analysis For Solidified Specimen of Low and Intermediate Level of Radioactive Wastes ····· 202
Jawon Jeng and Sungjong Kim[MIRAEEN Co., Ltd.],
Seunghoon Han, Youngjong Ju, Jungwoo Lee, and Jeongmyeon Kim[KEPCO NF]

P0414 Solidification of Spent Resin for Safe Storage ····· 204
Won-Seok Kim, Jaehyuk Kang, Taeho Jung, and Wooyong Um[POSTECH],
Mi-suk Jang and Jong-seon Jeon[Nuclear Engineering Service & Solution Corp.]

P0415 A Study on Characteristic for Manufacturing Immobilization of Green Body for Moist Particulate and Sludge-Type Radioactive Waste ····· 206
Yongho Hong, Minsu Kim, Heekyung Kim, Hyoungmin Park, Dongchul Kim, and Taekyu Lee [ACT Co., Ltd.], Byunggu Lee, Seonghun Yoon, and Jeongsu Kim[TAEKWANG Co., Ltd.]

P0416 Mixing Treatment of Radioactive Wastes and Structural Stability Evaluation of Solid Waste Form From the FMPP ····· 208
Jong Sik Shon, Junhyuck Im, Gi Yong Kim, Dong-Ju Lee, and Dae-Seok Hong[KAERI]

P0417 Collection of Samples for Periodically Validating the Scale Factor ····· 210
Bong-Ki Ko, Kyung-Ho Kim, Myoung-Ju Yoo, and Young-Ku Choi[Sunkwang T&S Co.,Ltd.]

P0418 Developing the Process of Collecting Samples of the Waste Filter for NPP Waste ····· 212
Kyung-Ho Kim, Bong-Ki Ko, Dong-Je Lee, and Young-Ku Choi[Sunkwang T&S Co.,Ltd.]

P0419 Evaluation on Glass Mold Integrity of Cold Crucible Induction Melter for Discharging Glass Melt ····· 214
Sunghoon Hong, Seok-Ju Hwang, and Cheon-Woo Kim[KHNP CRI],
Toshiro Oniki[IHI Yokohama Engineering Center]

P0420 Cost-Benefit Analysis for Regulatory Clearance of VLLW Metal Radwastes at KAERI ····· 216
Ki-baek Shin, Dae-seok Hong, Il-sik Kang, and Gi Yong Kim[KAERI],
In Ho Kim[Chungnam Natl. Univ.]

P0421 Safety Analysis of Radwastes Storage Buildings in KAERI : Earthquake Case ··· 218
Jongjin Kim, Hong Rae Jeon, Dong Ju Lee, Jeong-guk Kim, and Dae-Seok Hong[KAERI]

P0422 Waste Characteristics Evaluating Strategy of KRR1&2 Reclassified Wastes by Applying the IAEA TECDOC 1537 ····· 220
JeongWook Moon, GuenHo Kim, JeongGuk Kim, JongJin Kim, JongWon Choi, and DaeSeok Hong[KAERI]

P0423 A Study on the Application of the Reactor Power Cutback System to WH1000 Type NPP ····· 222
Beyongho Yi and Jongsoon Song[Chosun Univ.]

5분과 제염해체 (Oral)

09:00~09:20 Performance Evaluation of Decontamination Foam According to the Characteristics of Surface Contamination ····· 227
Wangkyu Choi, Seungeun Kim, Chonghun Jung, Seonbyeong Kim, and Bumkyoung Seo[KAERI]

09:20~09:40 Study of Chemical Separation Methods for the Treatment of a Uranium Containing Process Effluent ····· 229
Maeng-Kyo Oh and Chang-Ha Lee[Yonsei Univ.], Keun-Young Lee, Richard I. Foster, and Kwang-Wook Kim[KAERI]

09:40~10:00 Dismantling Scenario of Reactor Vessel (RV) in KORI 1 ····· 231
Kwang-Soo Park, Hae-Woong Kim, Gyu-Ho Jang, Hee-Dong Sohn, and Jin-Woo Choi[Doosan HI&C]

10:00~10:20 Characteristics of and Implications From Radioactive Discharge Data Before and After Post-Shutdown of Nuclear Power Plants in United States ····· 233
Na Yoon Choi and Jae Hak Cheong[Kyung Hee Univ.]

11:20~11:40 Establishment of DF (Decontamination Factor) Target for Kori-1 Full System Chemical Decontamination ····· 235
Dooho Lee[KHNP CRI]

11:40~12:00 Formation of Meta-Anokelite for the Decontamination of Uranium Bearing Effluents: From Laboratory to Pilot Plant ····· 237
Richard I. Foster, Kwang-Wook Kim, Maeng-Kyo Oh, Min-Jeong Kim, and Keun-Young Lee[KAERI]

12:00~12:20 Development of Testbed for Advanced Remote Dismantling System ····· 239
Dongjun Hyun, Ikjune Kim, Sungmoon Joo, Jonghwan Lee, and Shin Young Kang[KAERI]

12:20~12:40 Preliminary Evaluation for the Nuclide Inventory of the RCP Suction Leg for Decommissioning of Kori Unit 1 ····· 241
Jonghoa Kim, Homin Jeon, Yongsik Kim, Jaejoon Song, Kyeongho Han, and Jangsoo Seo[Sae-An Engineering Co., Ltd]

5분과 제염해체 (Poster)

P0501 The Main Issues of Large Components From Decommissioning to Storage and Disposal of a Nuclear Facility ····· 245
KwanSeong Jeong, SeungKook Park, and BumKyung Seo[KAERI]

P0502 A Study on the Effect of Internal Exposure of Worker due to Radioactive Aerosols Generated During NPP Dismantling Process ····· 247
Sun Il Kim, Hak Yun Lee, and Jong Soon Song[Chosun Univ.]

P0503 Review of the Practical Cost Estimations for Decommissioning of Nuclear Facilities ····· 249
KwanSeong Jeong, SeungKook Park, DaeSeo Koo, InHye Hahm, JaeHyun Ha, SangBum Hong, and BumKyoung Seo[KAERI]

P0504 Review of Operating Conditons for Full System Decontamination Operation Procedure Development of Kori-1 Nuclear Power Plant ····· 251
Hak-Soo Kim and Cho-Rong Kim[KHNP CRI]

P0505 Underwater Laser Cutting Experiment of Stainless Steel Plate Using Supersonic Conical Nozzle for Nuclear Decommissioning ····· 253
Seong Y. Oh, Jae Sung Shin, Sangwoo Seon, Taek Soo Kim, Hyunmin Park, Lim Lee, Chin-Man Chung, and Jonghwan Lee[KAERI]

P0506 Canceled
Review of Management for Problematic Waste During Kori Unit 1 Decommissioning
Ji Young Song, Jin Ho Park, Hyun Woo Kim, Gang Woo Ryu, and Kwang Pyo Kim[Kyung Hee Univ.]

P0507 Risk Informed Economic Assessment for the Decommissioning Project ····· 257
Younggook Kim, Taesik Yun, and Hyunmin Kim[KHNP CRI]

P0508 Suggestion of Safeguards Regulatory Framework for Decommissioning ····· 259
Junghee Son, Seungmin Lee, and Chul Heo[KINAC]

P0509 Remote Sample Taking Techniques From a Large Metallic Radwaste ····· 261
Kwonpyo Hong, Sanghee Jung, Myungchul Park, Sunggeun Kim, and Wanho Oh[KAERI]

P0510 Cutting Process Update Method to Simulate the Nuclear Facility Decommission ·· 263
Ikjune Kim, Dongjun Hyun, Jonghwan Lee, Shinyoung Kang, and Sungmoon Joo[KAERI]

P0511 Electrolytic Reduction of Palladium in DBSO/Ionic Liquid System ····· 265
Iksoo Kim, Dongyong Chung, and Keunyoung Lee[KAERI]

P0512 Comparison of Radiolytic Decomposition of Oxidation Decontamination Solutions ·· 267
N.O. Chang, H.J. Won, S.Y. Park, and S.B. Kim [KAERI], Y.S. Kim[Hanyang Univ.]

P0513 Effective Cross Section Estimation of ^{36}Cl and ^{41}Ca in Concrete of Kori Unit 1 ····· 269
Mee Jang, Hyunchul Kim, Chang Jong Kim, and Jong Myoung Lim[KAERI]

P0514 The Applicability of pH Measurement as an Indicator for Estimation of Oxalic Acid Concentration ····· 271
Jin-Hee Kim, Hyun-kyu Lee, Won-Zin Oh, and Sang-June Choi[Kyungpook Natl. Univ.]

P0515 Trend and Current State of Decommissioning Waste Quantity and Cost in Korea ····· 273
Jae Yong Oh and Taesik Yun[KHNP CRI]

P0516 Kori-1 Decommissioning Project Expense Evaluation ····· 275
Jae Yong Oh, Jihwan Yu, Younggook Kim, Gilim Kim, Hyejin Jung, and Wook Sohn [KHNP CRI]

P0517 Risk Assessment Method for the Decommissioning Activities by Using Risk Matrix ····· 277
Hyung-Woo Seo, Kwang-Ho Jo, and Kun-Man Kwon[KHNP CRI]

P0518 Design of the Advance Remote Dismantling System Framework ····· 279
Jonghwan Lee, Sungmoon Joo, Dongjun Hyun, and Ikjune Kim[KAERI]

P0519 Establishment of Technology Requirements for Environmental Information Feedback to Dismantle Core Facilities of Nuclear Power Plants ····· 281
Jonghwan Lee, Ikjune Kim, Sungmoon Joo, Dongjun Hyun, and Shin Young Kang[KAERI]

P0520 Strategy of the Kori-1 Final Decommissioning Plan Base on IAEA Safety Assessment Methodology ····· 283
Kwang-Ho Jo, Hyung-Woo Seo, and Kun-Man Kwon[KHNP CRI]

P0521 Measurement of Minimum Detectable Activity for Clearance Level ····· 285
Min-Seung Ko, Jae-Yong Lee, Kyung-Min Kim, and Yong-Soo Kim[Hanyang Univ.]

P0522 Comparison Study of MARSSIM and EURSSEM Methodology for Final Status Survey ·· 287
Inhye Hahm, Sang Bum Hong, and Bum-Kyoung Seo[KAERI]

P0523 A Study on the Conceptual Design of Package for the RV/RVI Cutting Wastes During Decommissioning of Kori Unit-1 NPP ····· 289
Duk-Woon Jung, Hyosub Kim, Dong-gyu Lee, and Kyu-Sub Choi[KONES corp.], Young-Hwan Hwang[KHNP CRI]

P0524 Spontaneous Reductive Decomposition Behavior of Permanganic Acid Depending on Initial Concentration and Reaction Temperature for the Chemical Decontamination of NPP ····· 291
Hyun-Kyu Lee, June-Hyun Kim, Jin-Hee Kim, Wonzin Oh, and Sang-June Choi [Kyungpook Natl. Univ.]

P0525 Scenarios of Effective Treatment Process of Decommissioned Radioactive Metal Waste ····· 293
Daeseo Koo, Seung-Kook Park, Kwan Seong Jeong, Jea Hyun Ha, In Hye Hahm, Sang Bum Hong, Bum Kyoung Seo, and Kook-Nam Park[KAERI]

P0526 A Fundamental Study for Development of Radioactive Waste Content and Solidifying During the Dissolution of Concrete in Decommissioning Nuclear Power Plant ····· 295
Youngbum Mun, Hyunkook Choi, Jaeyoung Kim, and Donghee An[Sungshin Cement Co., LTD]

P0527 Preliminary Study on Virtual Waste Package Concept Associated With Consolidated Configuration Management for Decommissioning of Nuclear Power Plant ····· 297
Jae Min Lee, Na Yoon Choi, Ji Woo Lee, Jae Hak Cheong, and Joo Ho Whang[Kyung Hee Univ.]

P0528 Performance Shaping Factors for the Human Reliability in Decommissioning Activities ····· 299
Byung-Sik Lee and Hyun-Jae Yoo[Dankook Univ.]

P0529 Evaluation of Oxide Removal Rate by Oxidation/Reduction Continuous Process Based on Permanganic acid-Oxalic acid ····· 301
Chorong Kim and Hak-Soo Kim[KHNP CRI]

P0530 The Cost Estimation for Decommissioning of a Nuclear Fuel Cycle Facility Using CERREX Based on ISDC Structure ····· 303
JaeHyun Ha, KwanSeong Jeong, SeungKook Park, DaeSeo Koo, InHye Hahm, SangBum Hong, and BumKyoung Seo[KAERI]

P0531 A Study on the Development of Interview Procedure for HSA at Kori Unit 1 ··· 305
Donghee Lee, Wook Sohn, Sukbon Yoon, and Suhee Lee[KHNP CRI]

P0532 Study on the Common Ion Effect on Cs^+ Extraction by Using Ionic Liquid ··· 307
Hayeon Ryu, Seungyeon Cho, Jungweon Choi, Wonzin Oh, and Sang-june Choi [Kyungpook Natl. Univ.]

P0533 Change of Adsorption/Desorption of Cesium on Illite Depending on the Ionic Strength of Ion Exchange Electrolyte ····· 309
Sung Man Kim, Chan Woo Park, Il-Gook Kim, Kune-Woo Lee, and In-ho Yoon[KAERI], So-Jin Park[Chungnam Natl. Univ.]

P0534 Suggestion of Kori-1 NPP Decommissioning Target Facilities ····· 311
Hyunmin Kim, Hyejin Jung, and Wook Sohn [KHNP CRI]

P0535 Study on Installation of Plasma Melter Refractory ····· 313
Seokju Hwang, Hyun-jae Cho, and Cheon-Woo Kim[KHNP CRI]

P0536 Development of RV Decommissioning Mockup ····· 315
Seokju Hwang, Young Hwan Hwang, and Cheon-Woo Kim[KHNP CRI]

P0537 Study on Segmentation Plan for Kori Unit 1 Reactor Vessel Internal ····· 317
Young Hwan Hwang, Seok-Ju Hwang, Ju-Young Yoon, and Cheon-Woo Kim[KHNP CRI]

P0538 Process Development for Kori Unit 1 Reactor Vessel Segmentation ····· 319
Young Hwan Hwang, Seok-Ju Hwang, Ju-Young Yoon, and Cheon-Woo Kim[KHNP CRI]

P0539 Review of Decommissioning Radioactive Waste Management and Treatment Technology for Waste Type ····· 321
Mi-Hyun Lee and Cheon-Woo Kim [KHNP CRI]

P0540 Discussion on Bioshield Dismantling Process of Kori Unit 1 ····· 323
Ju-Young Yoon and Cheon-Woo Kim[KHNP CRI]

P0541 Study on the Characteristics of Electro-Decontamination by Pilot Scale Equipment ····· 325
Ki-Chul Kim, Dong-Yeon Kim, and Jung-hyun Lee[KEPCO KPS]

P0542 A Study of Traceability Change Management Based on Decommissioning Information for a Nuclear Facility ····· 327
Yunjeong Hong, Heeseoung Park, Jongjin Kim, and Jeong-guk Kim[KAERI]

P0543 3D Scanner Calibration Methodology for Advanced Remote Dismantling System ·· 329
Sang Min Lee [Korea Univ. of Tech. and Edu.], Jonghwan Lee, Dongjun Hyun, Ikjune Kim, and Shin Young Kang[KAERI]

P0544 Development of Decommissioning Project Management System Platform ···· 331
Kook-Nam Park, In-Hye Hahm, Dae-Seo Koo, and Sang-Bum Hong[KAERI],
Jung-Sup Oh and Moon-Joo Gil[ETRI]

P0545 Generation Characterization of Metal Wastes During the Decommissioning of PWR NPPs ····· 333
Ji-Hoon Lee and Kang-Ok Cho[KHNP CRI]

P0546 An Equilibrium Calculation on Removal of Sulfate and Metal Ions in a Wastewater Generated From the SP-HyBRID Decontamination Process ····· 335
H.C. Eun, J.Y. Jung, S.Y. Park, J.S. Park, H.J. Won, S.B. Kim, and B.K. Seo[KAERI]

P0547 Development of Decommissioning Waste Information Tracking System for the Life-Cycle of Decommissioning Nuclear Facilities ····· 337
Sang Bum Hong, In Hye Hahm, Jae Hyun Ha, Kwan Seong Jeong, Seung Kook Park, Dae Seo Koo, Kook Nam Park, and Bum Kyoung Seo[KAERI]

P0548 Review for Remediation Technology of Radiocesium-Contaminated Soil ····· 339
In-Ho Yoon, Ilgook Kim, Chan-Woo Park, Hee-Man Yang, Sung-Man Kim,
and Kune-Woo Lee[KAERI]

P0549 Ferrous Oxalate Precipitation Behavior Depending on Ferrous Concentration and Temperature for Reductive Chemical Decontamination of Nuclear Power Plant ····· 341
Sae-Binna Lee, Hyun-Kyu Lee, June-Hyun Kim, Jin-Hee Kim, Yoon-Ji Park, Won-Zin Oh, and Sang-June Choi[Kyungpook Natl. Univ]

P0550 Flow-Through Electrochemical Membrane System for the Selective Removal of Cobalt Ions ····· 343
Joosung Park, Youngkun Chung, and Seoktae Kang[KAIST], Keun-Young Lee[KAERI]

P0551 Evaluation of Material Integrity by AP-OX Oxidation-Reduction Process Environments ····· 345
Kyunghee Lee, Hyukchul Kwon, and Dooho Lee[KHNP CRI]

P0552 Review on North Korea's Critical Nuclear Facilities Decommissioning From the Planning Point of View ····· 347
Yong-soo Kim[Hanyang Univ.]

6분과 방사선환경 및 안전 (Oral)

초청발표

09:00~09:30 Fukushima Mapping Project After the Fukushima Dai-ichi Nuclear Power Station Accident ····· 351
Satoshi Mikami[JAEA]

09:30~09:50 Review on the Optimized Public Protective Action on NPP Having 30 km UPZ Risk Based on the New Protective Action Guidance ····· 353
Goanyup Lee, Bongseok Kim, Hyunki Kim, Haecho Lee, Jongsoo Kim, Kanghyeon Lee, and Seungyeon Baek[KAERI]

09:50~10:10 Radiological Risk Assessment of ^{232}Th and ^{238}U in Water Leach Purification (WLP) Residue Using Modified SPLP Method ····· 355
Nur Shahidah Abdul Rashid and Wooyong Um[POSTECH],
Zetty Izzaty Saleh, Nurul Syiffa Mahzan, Khoo Kok Siong, and Syazwani Mohd Fadzil[UKM]

초청발표

11:20~11:40 Experience of Airborne Radiation Monitoring After the Fukushima Dai-ichi Nuclear Station Accident ····· 357
Yukihisa Sanada[JAEA]

11:40~12:00 Large-Area Compton Camera for Three-Dimensional Imaging of Radioactive Contamination in Concrete ····· 359
Young-su Kim, Jae Hyeon Kim, Junyoung Lee, and Chan Hyeong Kim[Hanyang Univ.]

12:00~12:20 Experimental Setup for Accuracy Analysis of Multi-Detector Boron Meter ·· 361
Si Hyeong Sung, Jin Bok Cho, and Hee Reyoung Kim[UNIST]

12:20~12:40 Proposed Regulatory Standards for the Industrial NORM Waste Management ·· 363
Yeoungsuk Go, Eun Lee, Jaeman Kim, and Suk K. Sim[Environment & Energy Technology, Inc.]

6분과 방사선환경 및 안전 (Poster)

P0601 Domestic Data on the Radionuclide Transfer From Soils to Rice Plants ····· 367
Yong-Ho Choi, Kwang-Muk Lim, In Jun, Dong-Kwon Keum, and Hyo-Joon Jeong[KAERI]

P0602 Establishment of Alarm Management System for Radiation Emergency Response ····· 369
Hae Cho Lee, G.Y. Lee, J.S. Kim, H.K. kim, B.S. Kim, J.S. Kim, G.H. Lee, and S.Y. Baek[KAERI]
W.S. Heo and K.Y. Sohn[MIRAEEN Co., LTD]

P0603 Development of Air Suction Control System for Continuous Air Contamination Monitor ····· 371
Jongsoo Kim, Sung-Ho Lee, O-Young Kwon, and Hae-Cho Lee[KAERI]

P0604 Evaluation of Trapping Characteristics for Volatile Kr/Xe Off-Gas ····· 373
Seok-Min Hong, Jae Hwan Yang, and Yung-Zun Cho[KAERI]

P0605 Analysis of the Natural Radionuclides Concentrations of Atmospheric PM_{10} Aerosols of Jeju Gosan Site in 2015 ····· 375
Chung-Hun Han, Duk-Woo Kim, Hang-ku Lee, and Jae-Woo Park[Jeju Natl. Univ.]

P0606 A Preliminary Study for Residual Radioactivity Assessment After Neutron Irradiation of Silicon Carbide ····· 377
Ki-Man Lee, Byung-Gun Park, and Gwang-Min Sun[KAERI]

P0607 Analysis of Minimum Detectable Activity for Noble Gas Monitor Using System Modeling ····· 379
Sung-Ho Lee, Jong-Soo Kim, and Tae-Woo Go[KAERI]

P0608 Canceled
Safety Evaluation of a NORM Site Restoration in Korea
Zu-Hee Woo, Yong-Jae Kim, Byung-Uck Chang, and Jae-Ho Jang[KINS], Ki-Beom Son[Kyunghee Univ.]

P0609 Review of Decommisssioning Risks ····· 383
Gi-Lim Kim, Taesik Yun, and Jihwan Yu[KHNP-CRI]

P0610 A Case Study on the Effect of Filter Micron Rating Change of Filtration System in Lancing Process ····· 385
Kyung-Wook Shin, Yun-Sang Jung, Sam-Hyun Kim, Yong-Seok Choi, Byeong-Mok Park, Gyung-Sun Chae, and Hee-Kon Jang[SAE-AN ENGINEERING CO.]

P0611 Analysis of Exposure Dose by RESRAD Sensitivity Analysis ····· 387
Sang June Park, Ji Hyang Byon, and Seokyoung-Ahn [Pusan Natl. Univ.], Suhee Lee[KHNP-CRI]

P0612 Radiological Effect of Aerosols From Decommissioning and Decontamination ··· 389
Min-Ho Lee, Nakkue Chae, and Sungyeol Choi[KAIST]

P0613 Effectiveness Verification of the Representative Sampling Location Scale Down to Reflect the Latest Standards ····· 391
Ju-Young Yoon and Dong-guk Lee[KHNP-CRI]

P0614 Impact of Operating Nuclear Power Plants to Decommissioning Workers ··· 393
EunHee Lee and ChangLak Kim[KINGS]

P0615 Tritium Release Under Unlikely and Extremely Unlikely Loading Condition of the HCCR TBS at PD-1 Phase ····· 395
Hyung Gon Jin, Dong Won Lee, Jae Sung Yoon, Suk Kwon Kim, Eo Hwak Lee, Seong Dae Park, and Chang Wook Shin[KAERI], Seungyon Cho[NFRI]

P0616 Vacuum Suction Force Analysis of Concrete Wall Climbing Device for Dry Cask Storage System ····· 397
Kyoung Won Yoon, Jin Yoo, Misuk Jang, and Seoung Rae Kim
[Nuclear Engineering Service & Solution Co., Ltd]

P0617 Estimated Activity of CPP Wastewater and Radioactivity of Evaporative Concentrates ····· 399
Ki Bang Sung[KHNP-CRI]

P0618 The Determination of Depth Distributions of Radioactive Cesium in the Ground Using In Situ Gamma-Ray Spectrometry ····· 401
Young-Yong Ji, Kun Ho Chung, Mun Ja Kang, and Wanno Lee [KAERI], Taehyung Lim [SI Detection Co. Ltd.]

7분과 방사화학 (Oral)

초청발표

09:00~09:30 What are Required for Ensuring the Safe Disposal of Radioactive Wastes? ·· 405
Sol-Chan Han, Yongheum Jo, and Jong-Il Yun [KAIST]

09:30~10:00 DFT Study on the U(IV)-PNPP Complex in Water ····· 407
Keunhong Jeong [KMA], Wansik Cha [KAERI] , Kyungwon Kwak [IBS]

10:00~10:20 First Principles Computational Studies of Spontaneous Reduction Reaction of Eu(III) in Eutectic LiCl-KCl Molten Salt ····· 409
Choah Kwon, Seung Hyo Noh, Hoje Chun, and Byungchan Han[Yonsei Univ.], Il Soon Hwang[Seoul Natl. Univ.]

11:20~11:40 On-Line Monitoring of Metal Ions in LiCl-KCl Melt ····· 411
Sang-Eun Bae, Suhee Choi, Tae-Hong Park, Jong-Yun Kim, and Ji-Hye Kim[KAERI]

11:40~12:00 The Effect of Target Material and the Neutron Spectrum on Nuclear Transmutation of ^{99}Tc and ^{129}I in Nuclear Reactors ····· 413
Seung Gu Kang and Hyun Chul Lee[Pusan Natl. Univ.]

12:00~12:20 Rotating Disk Electrode Measurements of the Electrochemical Reduction Reaction of Sm^{3+} and Eu^{3+} in LiCl-KCl Melt ····· 415
Suhee Choi, Sang-Eun Bae, and Tae-Hong Park[KAERI]

12:20~12:40 Luminescence Studies of U(VI)-Laponite System in Aqueous Phase ····· 417
Wansik Cha, Hee-Kyung Kim, Sue Young Hong, and Euo Chang Jung[KAERI]

7분과 방사화학 (Poster)

P0701 Electrochemical Behavior of Er Ion and Bi Ion in LiCl-KCl Molten Salt ····· 421
Beom Kyu Kim, Hwa Jeong Han, Ji Hye Park, Won Ki Kim, and Byung Gi Park [Soonchunhyang Univ.]

P0702 Preliminary Test of ^{55}Fe and ^{63}Ni Analysis Method in Concrete Sample ····· 423
Kahee Jeong, Jong-Ki Choi, and Kyu-Min Song [KHNP CRI], Jong-Myoung Lim[KAERI]

P0703 Determination of Cerium Isotopes and Total Burnup in Irradiated Pellet Based on Isotope Dilution Mass Spectrometric Measurement ····· 425
Jung Suk Kim, Yang-Soon Park, Byungman Kang, Kyungwon Suh, Kwang Soon Choi, and Yeong Keong Ha[KAERI]

1분과

핵주기정책 및 핵비확산 (Oral)

Survey on Standards to Harden Security of PC-Based Systems for Nuclear Facilities

Chaechang Lee* and Soomin Lim

Korea Institute of Nuclear Nonproliferation and Control, 1534 Yuseong-daero, Yuseong-gu, Daejeon, Republic of Korea

*chiching@kinac.re.kr, s2min@kinac.re.kr

1. Introduction

As cyber attack technique evolves, various devices and software are developed to prevent the attack. However, no matter how advanced the security technology is, it is difficult to introduce and utilize it in systems that operate nuclear power plant. Before introducing security equipment into existing systems, design changes are needed and the impact on the operation of the plant, such as an increase of latency and response time, should be considered. Compatibility with the security software should also be considered.

In this paper, we will discuss the standards for enhancing security by using security configurations of existing operating systems of PC-based nuclear facilities, which are difficult to install security software and deploy security equipment.

2. Standards on Security Configurations

2.1 FDCC

The Federal Desktop Core Configuration (FDCC) is a list of security settings recommended by the National Institute of Standards and Technology for general-purpose microcomputers that are connected directly to the network of a United States government agency [1]. From March 2007, the US Air Force had applied the FDCC, which is the predecessor of the United States Government Configuration Baseline (USGCB), to Windows XP version. Currently, the USGCB has been replaced with Windows 7 to maintain the organization security configurations.

2.2 USGCB

USGCB is intended to provide federal agencies with guidance on best practices for configuring information protection [2]. It aims to enhance system security by reducing costs and increasing efficiency through standardization of IT systems to address security threats that have yet to be discovered. In other words, it recommends the secure security settings of all PCs used by federal agencies to protect hosts within federal agencies from various cyber threats. Security settings, such as access privilege restrictions, can be used to reduce the risk of operating system vulnerabilities by applying the standard that are stricter than the default security configurations of the supplied PC.

The USGCB, which adds Windows Vista, Windows 7 and RHEL 5 setup to FDCC, has been patched more than 39 times and also provides security configurations for Internet Explorer 7 and 8 versions.

2.3 CCE

The Common Configuration Enumeration (CCE) is intended to provide a unique identifier for security-related system configuration by quickly and accurately associating configuration data from

various information sources and tools [3]. While the USGCB is a set of security enhancement items for specific operating systems, the CCE defines security enhancement items from servers to applications such as Apache and Internet Information Services (IIS). The project was started at MITRE and is now managed by NIST.

2.4 NIST 800-53

The NIST Special Publication 800-53 standard provides a list of security controls for the US federal information system [4]. It addresses the steps in the risk management framework dealing with security control choices for federal information systems in accordance with the security requirements of the Federal Information Processing Standard (FIPS). The fifth revised version, Security and Privacy Controls for Information Systems and Organizations, is now available as a draft on August, 2017.

The US Nuclear Regulatory Commission (NRC) regulates nuclear licensees with Regulatory Guide (RG) 5.71, Cyber Security Programs for Nuclear Facilities, which is including all controls designated as the “High” baseline within the third revised NIST 800-53.

3. Conclusion

In this paper, we discussed standards to harden security of PC-based systems by using its own security configurations. Since digital computer and communications systems and networks in nuclear facilities have restrictions to install security software and to deploy security equipment, nuclear licensees should utilize their own security configurations.

In the next study, we will try to verify the effectiveness of the security configuration enhancement presented above by attempting cyber attacks using known vulnerabilities to the hosts to which the security configuration enhancement items are applied and to the hosts that are not applied.

REFERENCES

[1] Wikipedia, “Federal Desktop Core Configuration”, https://en.wikipedia.org (accessed April 9, 2018).

[2] NIST, “United States Government Configuration Baseline, https://csrc.nist.gov (accessed April 9, 2018).

[3] CCE, “Common Configuration Enumeration (CCE)”, https://cce.mitre.org (accessed April 9, 2018).

[4] NIST, “Security and Privacy Controls for Information Systems and Organizations”, SP 800-53 (2017).

Potential Utilization of Laser Flash Analysis for On-Site Measurement of UO_2 Stoichiometry

Gyeonghun Kim, Jungsu Ahn, and Sangjoon Ahn*
Department of Nuclear Engineering, Ulsan National Institute of Science and Technology, Ulju, Ulsan, Republic of Korea
* sjahn99@unist.ac.kr

1. Introduction

Oxide fuel stoichiometry often comes at a great importance during IAEA and SSAC inspection for nuclear material accountancy. By and large, thermogravimetric analysis (TGA) has been used for that matter ever since its first introduction about 60 years ago [1]. One shortcoming of the TGA method is the lack of decent hand-carry device for on-site inspection due to the nature of the methodology. To address this issue, we suggest the utilization of thermal conductivity profile up to lower temperatures (~ 300 °C) and measured the thermal conductivity of stoichiometry-specific CeO_{2-x} pellets, as a surrogate material for non-stoichiometric UO_2, using laser flash analyzer (LFA) to demonstrate the feasibility of the method.

2. Experimental Methodology

2.1 Sample preparation

As-received CeO_2 powder (99.9%, 1-μm, Avention) was pressed into green pellets (9.8 mmD × 2 mmL) under 250 MPa using hydraulic press (KSHM-010P, Kumsung). The green pellets were then heated at 5 °C/min rate up to 1500 °C and held for 1 h ~ 20 h under low oxygen partial pressure (~0.01 %) argon gas atmosphere. Oxygen partial pressure (p_{O_2}) in argon gas was monitored using oxygen sensor (C-100, Nano-ionics Korea) throughout the sintering process.

Various hypo-stoichiometric CeO_{2-x} pellets ($0 < x < 0.05$) were fabricated referring to the constitutional Ce-O phase diagram [2] with equilibrium oxygen partial pressure at 1500 °C. The non-stoichiometric equilibrium reached over 10 h sintering time.

The sample density was measured at room temperature using the Archimedes method.

2.2 Thermogravimetric analysis (TGA)

The stoichiometry of sintered pellets were reaffirmed using TGA (STA 449 F5, NETZSCH).

2.3 Laser flash analysis (LFA)

The thermal diffusivity of stoichiometry-specific CeO_{2-x} pellets were measured from 25 °C to 300 °C using LFA (LFA 467 HT, NETZSCH).

3. Results & Discussion

3.1. Density

The measured density of sintered CeO_2 were ranging from 96.3 to 97.6 %TD, which are well matched with density of fresh UO_2 fuel for LWR (95 % ~ 97 %TD).

Table 1. Measured density of sintered non-stoichiometric CeO_2 pellets

Sintering time	Measured density (g/cm^3)	% TD
1 h	6.98	96.68
5 h	6.96	96.39
10 h	7.02	97.18
20 h	7.04	97.56

3.2. Stoichiometry

Fig. 1 shows a TGA mass gain of non-stoichiometric CeO_2 sample sintered 20 h. Subtle mass drop through the second isothermal step was regarded as balance drift error. Measured mass changes were calibrated by adding average mass drop.

Mass gain from oxidation of non-stoichiometric CeO_2 to stoichiometric CeO_2 is converted into O/Ce ratio as follows:

$$\mathrm{O/Ce} = \frac{(1 - w_{Ce}) / A_O}{w_{Ce} / A_{Ce}} \quad (1)$$

$$w_{Ce} = \left(\frac{A_{Ce}}{A_{Ce} + 2A_O} \right) \left(\frac{m_2}{m_1} \right) \quad (2)$$

where m_1 and m_2 are mass of non-stoichiometric and

stoichiometric CeO_2 respectively, A_{Ce} is atomic mass of cerium, A_O is atomic mass of oxygen, and W_{Ce} is mass fraction of cerium in CeO_2.

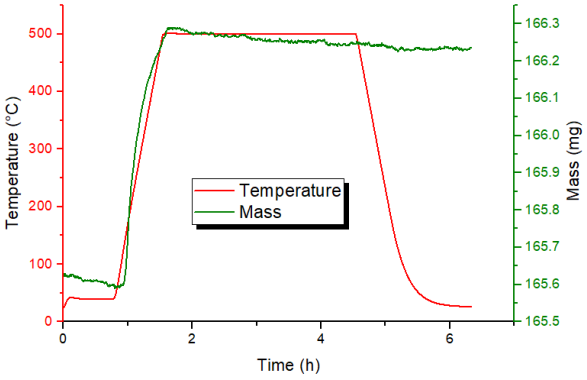

Fig. 1. TGA curve of non-stoichiometric CeO_2.

Calculated from measured mass gains of the heating curve up to 500 °C showed agreement with intended stoichiometry within ± 0.005.

3.3. Thermal conductivity

Using measured density and diffusivity data of in this study and heat capacity data of Nelson et al.[3], thermal conductivity of sample was calculated as follows:

$$k = \alpha \cdot \rho \cdot C_p \tag{3}$$

where α is thermal diffusivity, ρ is density, and C_p is heat capacity.

Thermal conductivity of samples with different density was adjusted to independently evaluate the stoichiometry effect on thermal conductivity using the following equation:

$$k_2 = k_1 \frac{\rho_2}{\rho_1} \tag{4}$$

where k_1 and ρ_1 are the thermal conductivity and measured density, and k_2 and ρ_2 are the same variables for the density of interest (96 % TD).

Fig. 2 shows measured thermal conductivity of non-stoichiometric CeO_2, which drastically lowered with small stoichiometry deviation at low temperature. Hence, a portable LFA device can be designed by adopting reduced size furnace and insulator for low temperature operation only.

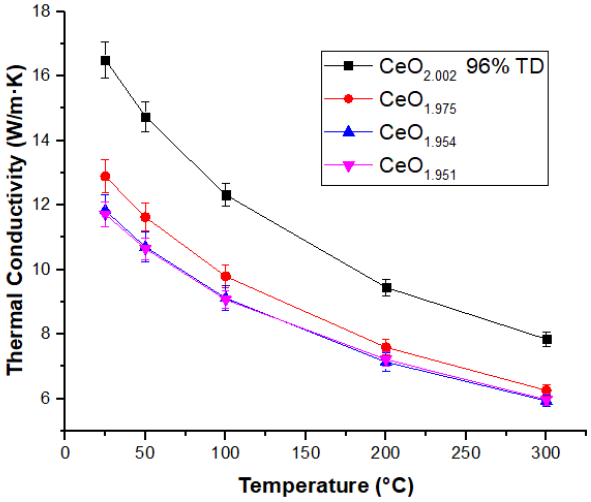

Fig. 2. Thermal conductivity of non-stoichiometric CeO_2.

4. Conclusions

Various stoichiometric specific CeO_{2-x} pellets were fabricated as the surrogate of non-stoichiometric UO_2 pellets. Collected thermal conductivity profiles indicate clear potential of LFA method to be used for on-site measurement of UO_2 fuel stoichiometry.

ACKNOWLEDGEMENT

This work was supported by the Korea Institute of Nuclear Nonproliferation and Control (Management and Evaluation of Environmental Sampling, GP2009-0015).

REFERENCES

[1] L. G. Stonhill, “The Determination of Atomic Ratios In The Uranium-Oxygen System by A Thermogravimetric Method,” Can. J. Chem., vol. 37, no. 2, pp. 454–459 (1959).

[2] T. B. Lindemer, O. R. National, and O. Ridge, “chemical thermodynamic representation of very nonstoichiometric phases CeO_{2-x},” vol. 10, no. 2, pp. 129–136 (1986).

[3] A. T. Nelson, D. R. Rittman, J. T. White, J. T. Dunwoody, M. Kato, and K. J. McClellan, “An Evaluation of the Thermophysical Properties of Stoichiometric CeO2 in Comparison to UO2 and PuO2,” J. Am. Ceram. Soc., vol. 97, no. 11, pp. 3652–3659 (2014).

Game-Theoretic Approach for Safeguards Program of a Geological Repository for Spent Nuclear Fuels During Post-Closure Period

Heejae Ju [1], Il Soon Hwang [2], and Sungyeol Choi [1,*]

[1]Korea Advanced Institute of Science and Technology, 291 Daehak-ro, Yuseong-gu, Daejeon, Republic of Korea

[2]Seoul National University, 1 Gwanak-ro, Gwanak-gu, Seoul, Republic of Korea

*sungyeolchoi@kaist.ac.kr

1. Introduction

The traditional safeguards approach to conventional nuclear facilities has been challenged by a deep geological repository (DGR) for spent nuclear fuels (SNF). One of the key questions on the safeguards of a DGR is that when the safeguards can be terminated. Since significant amount of plutonium will remain over 10,000 years in one disposal canister, long-term safeguards on DGR should be required to prevent an unauthorized access unless rigid physical protection by a repository itself is provided. Recently, this issue led to international consensus that long-term safeguards of a repository is unavoidable. In this case, continuous safeguards cost can be imposed. Considering that the principle objective of a DGR is the minimization of burden to future generation, a possibility of long-term economic cost by safeguards program of DGR should be discussed in decision making process for SNF management policy. This paper suggests a game-theoretic approach for an assessment of economic cost by safeguards on a DGR during post-closure period.

2. Literature review

Plutonium in SNF is classified as Reactor-Grade plutonium (RG-Pu) with an isotopic composition of fissile plutonium isotopes (mainly Pu239) around 60 ~ 80 wt%. The use of RG-Pu is an attractive option for nuclear diversion because this material is expected to be directly used as explosive [1]. Therefore, plutonium in SNF will be weapon-usable over 10,000 years of cooling time [2].

Under the safeguards agreements between the IAEA and the states, safeguards shall terminate provided that the State and the Agency agree that the nuclear material is ‘practicably irrecoverable’ [3]. Unfortunately, a clear definition of the term ‘practicably irrecoverable’ is absent yet [4]. Nevertheless, the IAEA states that a recovery of nuclear material subject to safeguards from a DGR during post-closure period is feasible by clandestine human intrusion [1]. Accordingly, to terminate safeguards on a DGR, the state needs to prove that a clandestine human intrusion is not desirable without clear guideline for this issue. This may lead discord between the international agency and the state. In practice, STUK, the radiation and nuclear safety authority in Finland, pointed out the concern for non-termination of safeguards on the DGR in Finland [5].

3. Methodology

The game theory is useful method to improve understanding the situation of strategic decision making. This study has applied the game theory for quantitative analysis on the relationship between the desirability (motivation) of clandestine intruder and the efforts of safeguards subject. A game theoretic approach to safeguards problems is reasonable because the both players in the game would be rational: they should be intelligent enough to carry out their strategies which need advanced knowledge on nuclear engineering. However, such consideration for safeguards system of a decommissioned DGR has not been made. Therefore, this thesis tries to suggest a game theoretic model to find optimized safeguards option for safeguards agents for a decommissioned DGR.

4. Pu Mine Game Model

A problem of clandestine human intrusion can be though as plutonium mine game. The players participating in plutonium mine game represent two groups including the group of malicious actors who try to procure plutonium and safeguards agent who tries to defend a DGR from malicious actor group. For convenience, the group of malicious actors is designated by intruder. Fig. 1 illustrates simple

strategic form of plutonium mine game. Each player has two strategies. Safeguards agent chooses one of two strategies, either safeguards or no safeguards: and simultaneously intruder chooses one of strategies described in columns, intrude or not intrude. Accordingly, four strategy combinations exist. Each strategy combination defines a pair of payoff for each player. For example, the strategy combination of (safeguards, intrude) results in payoff a1 for safeguards agent and payoff a2 for intruder.

The preference of decision of each player is determined by the decision of another player. The intruder has incentive to intrude a DGR owing to significant value of plutonium. The safeguards agent would like to assure so that intrusion attempt does not exist but doing so requires cost for safeguards system. If intruder does not try to intrude, the safeguards agent would prefer no safeguards strategy. Such preferences of each player are marked with red arrows in. The circular arrow structure in Fig. 1 shows that there is no strategy combination satisfying both players. Rational players would try to maximize their payoff. Therefore, the players will mix their strategy with a certain probability to lead an equilibrium of the game.

Consider that intruder chooses to intrude a DGR with the probability of p. Then the payoff to the safeguards agent with safeguards strategy is expressed as follows:

$$\text{Payoff} = a_1 \cdot p + c_1 \cdot (1-p) \quad (1)$$

Likewise, the payoff to safeguards agent with no safeguards strategy is expressed as follows:

$$\text{Payoff} = b_1 \cdot p + d_1 \cdot (1-p) \quad (2)$$

The safeguards agent is indifferent on his decision when the values of (1 and (2 are same. Thus, the equilibrium probability of intrude strategy, p^*, is defined as follows:

$$p^* = (d_1 - c_1)/(a_1 + d_1 - b_1 - c_1) \quad (3)$$

Similarly, the equilibrium probability of safeguards strategy, q^*, is defined as follows:

$$q^* = (d_2 - b_2)/(a_2 + d_2 - b_2 - c_2) \quad (4)$$

The equilibrium probability of each player is the criteria for decision making. Intruder would intrude if the frequency of safeguards actions is lower that the equilibrium probability of safeguards strategy, q^*. Safeguards agent would not safeguard if the frequency of intrusion is lower than the equilibrium probability of intrude strategy, p^*. Accordingly, minimum safeguards cost required to defense clandestine intrusion can be estimated.

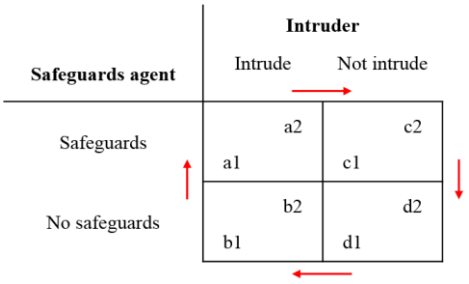

Fig. 1. Strategic form of plutonium mine game with the preference of each player (arrow).

5. Conclusion

The game theory model, named plutonium mine game model, is suggested based on the assumption that the decision of malicious actors would be determined by cost benefit of their strategies. Considering that such approach has used to be applied not only to conventional nuclear facilities but also other conflict situation, the suggested approach would be appropriate for decision making on safeguards program during post-closure period. It would be expected that the suggested model helps society to build consensus on long-term safeguards problem on a DGR which has not been accomplished.

REFERENCES

[1] IAEA, “Technological Implications of International Safeguards for Geological Disposal of Spent Fuel and Radioactive Waste”, IAEA (2010).

[2] H. Ju, “Risk Assessment of Future Human Intrusions into Deep Geological Repositories for Radioactive Wastes”, SNU (2018).

[3] IAEA, “The Structure and Contents of Agreements Between the Agency and States Required in Connection with Treaty on the Non-Proliferation of Nuclear Weapon (INFCIRC/153)”, IAEA (1972).

[4] IAEA, “Issues in radioactive waste disposal (IAEA-TECDOC-909), IAEA (1996).

[5] O. Okko, et. al., “Developing Safeguards for Final Disposal of Spent Nuclear Fuel in Finland”, Symposium on International Safeguards, IAEA (2014).

Accomplishment and Suggestion of ROK's Nuclear Material Accountancy and Control (NMAC) for Nuclear Security

Jae San Kim*

Korea Institute of Nuclear Nonproliferation and Control, 1534 Yuseong-daero, Yuseong-gu, Daejeon, Republic of Korea

*jaesan@kinac.re.kr

1. Introduction

Nuclear material accountancy and control (NMAC) is not only an obligation under IAEA Safeguards, but also it is one of the important measures to national nuclear security regulation.

The importance of NMAC to nuclear security has been emphasized by international organization like IAEA, GICNT and nuclear security summit. The various guidance from IAEA INFCIRC/225/Rev5, etc. recognized that strengthening the NMAC system is indispensable for nuclear security aspects like access control to nuclear material, detection/deterrence of theft or unauthorized removal, insider intrusion, etc. This paper describes background, features, and institutionalization of ROK's NMAC system. Also, it includes the explanation of ROK's NMAC regulation activities, introduce new type of NMAC inspection system that can help the nuclear security. And finally, it will suggest the consideration for more strengthening the NMAC for nuclear security regulation.

2. NMAC regulation activities in ROK

By the end of 2017, a total of 43 material balance areas (MBAs) were subjected to IAEA-led and national inspections. As the ROK's NAMC regulation activities, KINAC performed 10 regular inspections on licensees' accountancy management of certain nuclear materials. In addition to the regular inspections, one pre-check was performed prior to specific nuclear materials' first entry into the facility, and six inspections on a rolling basis to check whether licensees were following the accountancy provisions at all times. Now, NMAC regulation has been able to assure that facilities' NMAC system not only has a substantial quality but also functions systematically since January 2015. Changed NMAC regulation has differences rather than the previous things. The fundamental NMAC regulation objective has been to assure the compliance of requirements and implementation of NMAC legal obligations. And the NMAC inspection system was restructured for strengthening the national NMAC regulation.

Fig. 1. Structure of the accounting and control system of nuclear material.

3. Consideration for strengthening the NMAC in nuclear security regulation

Through the NMAC system, the nuclear materials in facilities were controlled through maintaining accurate bookkeeping and balance of the inventory of

material etc. And it can help to detect and deter the unauthorized removal of nuclear material that are interested in nuclear security. There are common points between NMAC and nuclear security inspection. Accounting information used by both sides is the same. Both inspections are focused to provide assurance that all nuclear material is accounted for, to provide a timely detection of material loss or diversion, to determine amount and location of any missing material and to deter and detect unauthorized removal of nuclear material. Well controlled facilities' NMAC system is possible to maintain and report accurate, timely, complete, and reliable information on the locations, quantities, and characteristics of nuclear material in the facility's possession. And it can ensure continuity of knowledge to enhance the ability to deter and detect unauthorized removal.

For example, checking the management of nuclear material is one element in physical protection inspection in ROK. In this check point, we have inspected the suitability of facilities' NMAC management, tracking of their locations, movements and changes of nuclear materials, security measures of storage area, and recovery procedures of stolen materials, etc. Those activities can also cover in national NMAC inspections procedures.

Presently, national NMAC and physical protection inspection are being divided and performed independently in ROK. And additionally, facility operators who are charging with NMAC are closely related with the nuclear safeguards activities and NMAC implementation but they are usually not engaged in the physical protection parts. In order to make up this activity, if the both inspections will be performed at the same time ideally, it can lead to more synergy of NMAC for nuclear security. And when the NMAC inspection was performed in nuclear facilities, the information of NMAC should be delivered to the physical protection parts.

4. Conclusion

NMAC and physical protection are complementary systems to deter and detect unauthorized removal of nuclear material that is concerned in nuclear security. Well controlled NMAC system should be able to detect unauthorized removal of nuclear material. So the facility operators should additionally consider the NMAC activities as one of the protective layers. Also, the national NMAC regulation have strengthened for assuring the substantial quality and systematical function in nuclear security.

REFERENCES

[1] K. H. Kim, M. S. Kim, S. H. Ahn, A New Regulation Policy for Accounting and Control of Nuclear Material, KINAC (2016).

[2] Importance of MC&A to Nuclear Security, Center for International and Security Studies at Maryland, February 2014.

Development of Safeguards Approach for the Disposal of Low and Intermediate Level Radioactive Waste Containing Uranium

Chul Heo*, Seungho Ahn, Seungmin Lee, and Junghee Son
Korea institute of Nuclear Nonproliferation and Control, 1534, Yuseong-daero, Yuseong-gu, Daejeon, KOREA
*hc0228@kinac.re.kr

1. Introduction

KNF has established a waste transport plan that includes uranium in 2017 in accordance with the plan to dispose of low and intermediate level radioactive waste agreed with Daejeon city. However, due to the absence of the IAEA safeguards standards for the waste, the transportation was difficult. The ROK and the IAEA have established safeguards approach to uranium waste and disposal facility to transfer the wastes generated from the nuclear fuel processing facility to the low and intermediate level radioactive waste storage facility.

In this paper, we describe the development process of the safeguards approach for the disposal of low and intermediate level radioactive waste containing uranium

2. Process of Establishing Safeguards Approach

2.1 Termination of Safeguards for Waste

The ROK and the IAEA discussed the safeguards approach to uranium waste through minutes and official letter exchange through the 18th, 19th Safeguards Implementation Working Group Meeting. The following three points were derived.[1]

- Identification of regulatory requirements for uranium waste through an analysis of the ROK-IAEA comprehensive safeguards agreement and additional protocol obligations
- In order to transfer the uranium waste to the low and intermediate level radioactive waste storage facility, consult with the IAEA department in advance to obtain a positive answer.
- In case the uranium waste is transported to the low and intermediate level radioactive waste storage facility and stored in the underground storage room, the inspectors cannot access it. Therefore, the ROK consults with the IAEA in establishing procedures that do not require further verification.

2.2 Follow-up action

The IAEA carried out inspection for enrichment measurement of uranium waste to be transported solidified in cement in KNF (2017.5.26. 2017.8.1~17.). The KINAC provided technical support for inspection of uranium waste.

Through the ongoing consultation with the IAEA, the ROK reviewed and approved the regulation on the management of special nuclear material for the low and intermediate level radioactive waste storage facility.

Based on the results of the IAEA consultation, the ROK has consulted with KORAD to minimize the burden on the IAEA inspection and to incorporate the facility into a safeguards facility.

2.3 Preliminary assessment

The IAEA, by measuring the enrichment of cement solidified uranium waste, confirmed the consistency with the previously reported values and concluded that the IAEA internal standards are met based on the quantitative measurement results. This completes the IAEA preliminary assessment of the adequacy of the uranium sequestration method in waste.

- In the case of uranium waste, when the deviation between the inspection result and existing declared concentration is less than 15%, it is satisfied with IAEA standard

3. Safeguards Approach

The ROK has agreed with the IAEA to designate a low and intermediate level radioactive waste storage facility as a facility to be safeguarded and to exclude uranium waste in the facility from being subject to IAEA inspection.[2]

Table 1. Standard Application

Nuclear material waste	Uranium waste (Retained waste)
Periodic IAEA inspection of nuclear material waste Report every change in inventory Report results after annual inventory taking	No Periodic IAEA inspection (implement DIV, CA) Report only on receipt of nuclear material waste No annual inventory taking

4. Conclusion

The ROK actively and proactively established safeguards approach to the disposal of nuclear material waste in consultation with the operators and the IAEA. This will ensure that IAEA safeguards are implemented in accordance with safeguards agreement, while minimizing the burden of reporting IAEA inspection and quantitative controls on disposal facility.

The establishment of such safeguards approach will be useful in establishing safeguards approach to the disposal of low and intermediate level radioactive waste storage facility of nuclear material waste generated in other nuclear facilities, not nuclear fuel processing facility. It can also be used to develop safeguards approach to future nuclear facilities related to nuclear material waste such as permanent disposal facilities.

REFERENCES

[1] 18th, 19th IMWG Meeting Minutes, 2017.

[2] Comprehensive Safeguards Agreement(1975) & Additional Protocol(2004), ROK-IAEA.

Legal Policy Study on Nuclear Liability Principle of Nuclear Operator Under Korea Nuclear Liability Law

Daesung Lee and Jaeyoung Bang
Korea Atomic Energy Research Institute, Daedeok-daero989ben-gil 111,Yuseong-gu, Daejeon, Republic of Korea
dslee@kaeri.re.kr

1. Introduction

Since the Fukushima nuclear power plant accident in Japan 2011 and the Kyungjoo earthquake in Korea 2016, Korea government has insisted on diminishing of nuclear energy dependency and strengthened the safety regulation of nuclear power plants. In the aftermath of the above transition of the current administration, new amendment of the Korea nuclear liability law is proposed to congress, which deletes current maximum liability limit of nuclear facility operator (300 million SDR[1] ; about ₩ 500 billion Won) per nuclear accident. This means that, in the event of any nuclear accident, the responsibility of the nuclear power plant operator will be unlimited without cause. In this study, we analyze the international trend of nuclear liability system and explain what to consider before changing nuclear operators′ liability from limited liability to infinite liability system.

2. Trends of Nuclear Damage Liability System

2.1 International trends

According to the OECD NEA data(Table1), Japan, Russian Federation, and Germany among the 10 largest nuclear power plants countries (based on total electric power of nuclear plants) are obliged to bear unlimited liability to nuclear operators in case of nuclear accident. Remaining 70% of big nuclear power generation countries (United States, France, China, etc.) maintain a limited liability regime.

[1] International Monetary Fund's special drawing rights

Table 1. Nuclear Operator′s Total Liability Limit

Unlimited	Japan, Russian Federation, Germany
Limited	United States, France, China, Korea, Canada, Ukraine, United Kingdom

The table shows that 70% of major nuclear energy country still keeps a limited liability regime as a main stream.

2.2 Domestic trend

Korea increased its nuclear liability limit up to 300 million SDR(about ₩500 billion Won) as the current one by revising the Nuclear Damage Compensation Act in 2001. The amount is same as with most of international nuclear liability convention such as the Vienna Convention or the Paris Convention. Newly proposed amendment regarding nuclear liability will change from limited liability concept to charging unlimited liability to nuclear operators in nuclear accident.

3. Analysis of the Proposed Amendment of Nuclear Liability Law

The amendment of nuclear liability law, proposed by Park Jung, congress member, is intended to remove maximum liability limit.

3.1 Benefits of unlimited liability

Unlimited liability will strengthen the responsibilities of the nuclear power plant operator, and in the event of a nuclear accident, all damage will be borne by the nuclear power plant operator without any restriction, thereby providing complete

damage relief and forcing safer facility management.

3.2 Concerns of the change: Infinite liability

3.2.1 Korea Hydro & Nuclear Power Co., Ltd. monopolizes the operation of all nuclear power plants in Korea. Under the situation of this single nuclear power plant operator, there is a substantial public interest to maintain corporate integrity and constancy from lawsuits such as foreclosure or injunction arising out of minor nuclear accident for stable supply of electric power to the public. In fact, fuel contractors and subcontractors may stop supply of fuel or services if the legal integrity of the nuclear power plant is unstable or dangerous such as bankruptcy or default situation under the unlimited liability regime. Thus, Issue of keeping integrity of nuclear operator under nuclear accident shall be treated well before changing the liability law.

3.2.2 In the event of damage to neighboring countries due to nuclear accidents, if KHNP, single monopolized nuclear power plant operators, directly pays all damages to neighboring countries without any limitation, there may be a diplomatic crisis with neighboring country because the countries will seek a perfect compensation of their countries victim without any consideration of KHNP′s business soundness. Additionally, China is a country of nuclear limited liability regime, so Korea victim caused by China nuclear accident shall not be compensated perfectly under the China law. It will be unfair treatment to the Korea.

3.2.3 Korea has chosen a "strict liability" concept in nuclear liability in which nuclear operators bear all responsibility for irrespective of the reason for the accident when a nuclear accident occurs. This is possible because a predictable burden is set that the maximum limit is finite. However, if nuclear operator′s liability becomes infinite there may be unfair balance between strict liability and the infinite burden to nuclear operators.

4. Policy Harmonization

Considering practical needs of raising a total liability amount in nuclear damages and compensation, we can compromise the needs and maintaining current limited liability system. That is to say, raising a maximum limit of nuclear operator up to double or further may be the answer for the balance. Though nuclear liability is put to nuclear operators unlimited the operators is only able to assume the liability up to its asset limit, not more than that as a corporate body.

5. Conclusion

We have looked at international trends in nuclear energy liability limits. It is necessary to comprehend the legislative intention of the countries which still maintain the limited liability system in order to balance between keeping a sound nuclear industry for sustainable energy supply and protection of the victims from nuclear accident. Before changing a nuclear liability regime by new amendment of nuclear liability law, the more detailed and harmonized consideration and debate would be required.

REFERENCES

[1] OECD NEA, Article ″Nuclear Operator′s Third Party Liability Amounts and Financial SecurityLimits″http://www.oecdnea.org/law/table-liability-coverage-limits.pdf (April 2018).

2분과

사용후핵연료 처분전관리 (Oral)

Evaluation of Decay Heat Distribution in the OASIS-32D Cask

Yong IL Kim, Young Tae Han, Joon Gi Ahn, In Ho Song, and Gyu Cheon Lee
KEPCO Engineering & Construction Company, 989-111, Daedeokdaero, Yuseong-gu, Daejeon, Republic of Korea
yongil@kepco-enc.com

1. Introduction

The decay heat distribution from spent nuclear fuels in the OASIS-32D cask has been evaluated. The OASIS-32D is a dual purpose cask for spent fuel transport and storage under developing by KEPCO E&C. It is designed to store 32 PWR spent fuel assemblies (FA) that have been cooled for 10 years. The decay energy from spent fuels is used as a heat source for the thermal analysis of the cask design. In thermal analysis, it is generally assumed that all the decay heat is released from the spent fuel. However, in reality, gamma rays emitted from the spent fuel react with adjacent substances, and some of the decay heat is generated in the surrounding structure. For the evaluation of the spatial distribution of decay heat from spent fuel in the cask, the gamma energy depositions in each structure of the cask were obtained by carrying out gamma ray transport calculation.

2. Methods and Results

2.1 Source term calculation

The spent fuels for the decay heat distribution calculation in the OASIS-32D are PLUS7 with an initial enrichment of 3.0 wt%. The PLUS7 fuels are assumed to be burned for three cycles at a power level of 40 MWt/MTU in the reactor core and have an average discharge burnup of 45 GWD/MTU. The amounts of decay energy from each particle (α, β, and γ) and decay gamma spectrum from spent nuclear fuels are calculated by ORIGEN-ARP module in the SCALE 6.1 code [1].

2.2 Gamma transport calculation

The alpha and beta particles have very short ranges so it can be considered to deposit all of their energies into the fuel pellet. The neutron and gamma rays emitted from spent fuel pellets react with surrounding materials and distribute their energies in the fuel regions and in the structure materials of the cask. The deposition energy of neutrons is negligible compared to that of other particles (α, β, or γ), so gamma transport calculation has been performed by MCNP5 code [5] to obtain the decay heat distribution in the components of OASIS-32D cask. The ratio of gamma decay energy to total decay energy (30.9%), derived from ORIGEN-ARP depletion calculation results, is used in conjunction with the total gamma deposition energy to evaluate the decay heat confined in the fuel region.

In the MCNP modeling, the PLUS7 fuel assemblies are homogenized as the materials of UO_2 fuels and Zircaloy clads. And all the cask components such as basket, neutron absorber, reinforcement structure, canister, cask shell, and external neutron shields are modeled as their actual shapes as shown in Fig. 1.

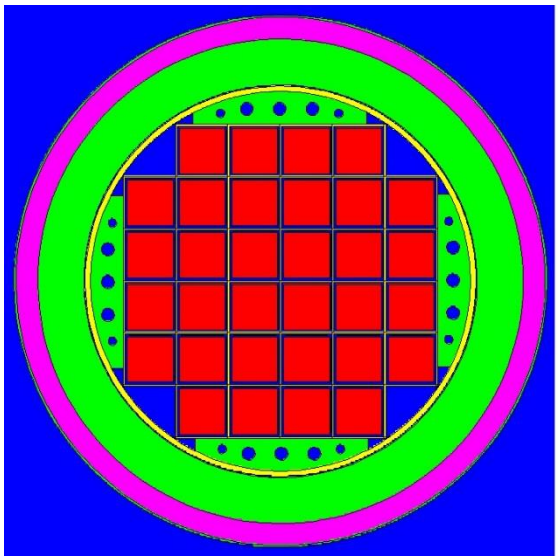

Fig. 1. MCNP model for transport calculation.

The cross-section data used in the MCNP5 gamma transport calculation is continuous cross-section data based on the ENDF/B-VI nuclear data library. The source energy distribution is based on the gamma spectra from spent fuel with a cooling time of 10 years and the axial burnup profile is reflected in the spatial distribution of the source.

Table 1 shows the deposition fractions of gamma energy to each material region and the deposition fractions of total decay energy generated from spent fuel assemblies as a result of gamma-ray transport calculation.

Table 1. Energy deposition ratio at each component

Component	Gamma Energy	Total Decay Energy
FA	93.22%	97.88%
Neutron Absorber	0.24%	0.07%
Basket	4.90%	1.51%
Reinforcement Structure	0.49%	0.15%
Canister	0.84%	0.26%
Cask Shell	0.31%	0.10%
Neutron Shield	0.00%	0.00%

3. Conclusions

The decay heat deposited in the spent fuel assemblies was evaluated to be 98% of the total decay heat. When realistic heat source distribution is required for the OASIS-32D thermal analysis, it is possible to apply the decay heat distribution results in this paper. However, the analysis result that the 98% heat source is distributed within the fuel assemblies suggests that the current thermal analysis assumption that all the heat sources are present in spent fuel is appropriate and guarantees some safety margin of the cask thermal analysis.

REFERENCES

[1] “SCALE: A Comprehensive Modeling and Simulation Suite for Nuclear Safety Analysis and Design,” ORNL/TM-2005/39, Version 6.1, Oak Ridge National Laboratory, June 2011.

[2] “MCNP-A General Monte Carlo N-Particle Transport Code, Version 5-1.51,” Los Alamos National Laboratory, LA-UR-09-00384, January 2009.

Stress-Based Criterion for the Creep Response of Spent Nuclear Fuel Rod

Donghyo Lee*, Seongki Lee, and Jongsung Yoo
KEPCO NF, 242, Daedeok-daero 989beon-gil, Yuseong-gu, Daejeon, Republic of Korea
*donghyo@knfc.co.kr

1. Introduction

Among potential damage mechanisms postulated for spent fuel in dry storage, creep has been identified as the most likely mechanism [1]. In this report, we reviewed and analyzed the evaluating process of creep by stress-based criterion.

2. Creep Criteria

2.1 Strain-Based Criterion

1% creep strain criterion was extended from fuel design practice as a conservative limit, however test and simulation results, Fig. 1 and 2 showed that tertiary creep which could propagate to creep rupture did not occur, although creep strain exceeded 1%.

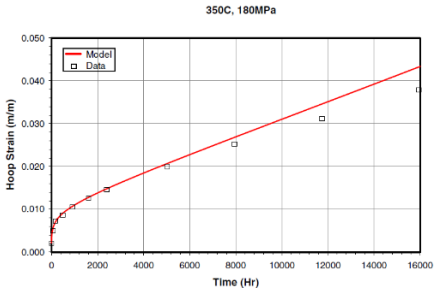

Fig. 1. FALCON analysis and test results.

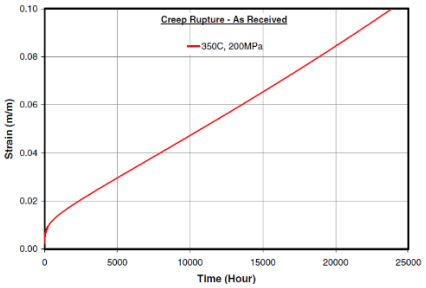

Fig. 2. FALCON analysis result.

2.2 Stress-Based Criterion

Strain alone is not an adequate measure for judging cladding integrity. Stress-based criterion is founded on the concept that, in order to creep failure to break out, the cladding effective stress must rise above the yield strength. The criterion consists of two basic elements: a stress and a Minor rule.

Relative damage in the cladding due to creep is defined by Minor rule,

$$D = \sum \Delta D_i = \sum \Delta t_i / t_{yi} \quad (1)$$

where D is the damage index, Δt_i is the i^{th} time step size, and t_{yi} is the experimentally determined time to yield at the conditions prevailing at time t_i.

Under constant pressure creep tests, stress is continuously changing with time,

$$\sigma_{\theta\theta} = \sigma_{\theta 0} / e^{-2\dot{\varepsilon}_{si} t_i} \quad (2)$$

Eq. (2) can be rewritten as follows,

$$\sigma_y = \sigma_i / e^{-2\dot{\varepsilon}_{si} t_{yi}} \quad (3)$$

where, $\dot{\varepsilon}_{si}$ is the steady-state creep rate. Solving for t_{yi} from Eq. (3) yields,

$$t_{yi} = -\ln\left(\frac{\sigma_i}{\sigma_{yi}}\right) / 2\dot{\varepsilon}_{si} \quad (4)$$

and the damage index becomes,

$$D = \sum \Delta t_i / \{-\ln(\sigma_i / \sigma_{yi}) / 2\dot{\varepsilon}_{si}\} \quad (5)$$

Eq. (5) has been implemented in FALCON, as shown in Fig. 3.

A damage index value of unity implies 50% probability of yield.

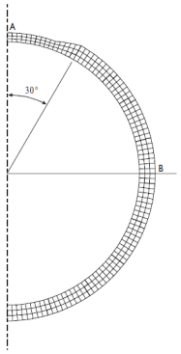

Fig. **3**. FALCON R-θ grid for local effects creep analysis.

3. Results and Discussion

The fuel rod analysis case is given in Table 1. It assumes severer condition than dry storage condition. Three response parameters are calculated by R- θ analysis: stress, strain, and damage index. These are plotted in Fig. 4 and 5, and Table 2 shows a summary of the results. In Fig. 4 the peak strain exceeds 1%, however the damage index is less than 1 in Fig. 5. Therefore, cladding remains in elastic regime.

Table 1. Fuel rod analysis case

Peak Temp.(℃)		Pressure(MPa)
Initial Storage	During Drying	Initial Storage
400	440	19.1

Table 2. Summary of fuel rod analysis results

Stress Change (%)	Peak Strain (%)	Damage Index (%)
-16	9	43

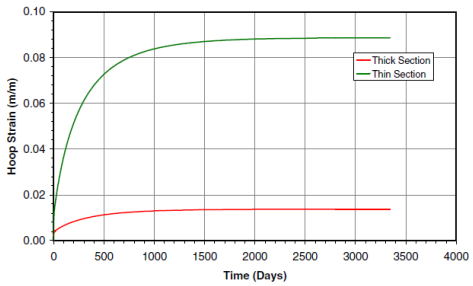

Fig. 4. FALCON analysis results – (a) Strain history.

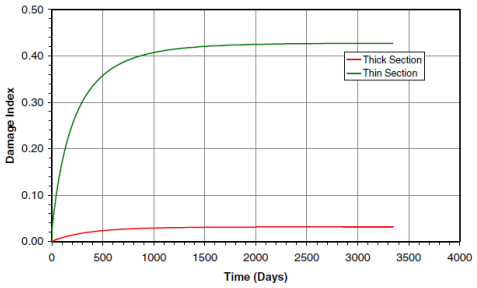

Fig. 5. FALCON analysis results – (b) Damage index history.

4. Conclusion

It is demonstrated that occurrence of creep rupture during dry storage is a remote possibility by FALCON analysis. Also, creep rupture of cladding should be evaluated by not only strain and but also stress.

5. Acknowledgement

This work was supported by the Korea Institute of Energy Technology Evaluation and Planning(KETEP) and the Ministry of Trade, Industry & Energy(MOTIE) of the Republic of Korea (No. 2014171020166C).

6. References

[1] Y. Rashid, R. Dunham, “Creep Modeling and Analysis Methodology for Spent Fuel in Dry Storage”, EPRI, Palo Alto, CA, (2001) 1003135.

Validation of CFD Thermal Model for Dry Cask Simulator

Taehyeon Kim*, Yongdeog Kim, and Sunghwan Chung

KHNP-CRI, 70, 1312beon-gil, Yuseong-daero Yuseong-gu, Daejeon, Republic of Korea

*taehyeon.kim@khnp.co.kr

1. Introduction

The Electric Power Research Institute(EPRI) of USA is coordinating the Extended Storage Collaborating Program(ESCP) to evaluate aging effects for extended storage of spent nuclear fuel(SNF). ESCP consideration engages in functions important to safety that storage facilities must maintain including thermal performance. Recently, a storage cask demands for higher heat loads and high-burnup fuel become the norm, possible margins are decreased to the point that expected peak cladding temperatures(PCT) are very close to the permissible limits. Several type of casks showed almost no-margin in PCT without verification and validation(V&V) and uncertainty quantification. The computational fluid dynamics(CFD) code was continually used in thermal hydraulic analyses of casks to reduce analytical uncertainty[1]. Therefore, V&V must be performed to assess accuracy and reliability in CFD. In this research, CFD calculations are carried out to validate for CFD models and approximations with experimental results of the EPRI dry cask simulator(DCS).

2. Validation of Thermal Model

2.1 Test Apparatus

The DCS system designed to produce temperature data sets under well-controlled boundary-conditions with a various heat loads, internal gas pressure and surrounding situations[2]. Fig. 1 shows the general design overview. The DCS system has two ducting shells that were used to emulate conditions for vertical dry storage systems with canister. Canister pressure vessel are located in inner shell that includes basket structure and Incoloy-clad test 9x9 fuel assembly of prototypic boiled water reactor. Axial and radial temperature profiles are measured for a various range of heat loads and helium pressure in pressure vessel. Ambient air is drawn into inlet ducts at lower side of the DCS, flows upward along the heated outer wall of the pressure vessel and discharged outlet openings arear in the outer shell at the upper side of the DCS. Inlet velocity is measured by hot wire anemometer to calculate mass flow rate of air.

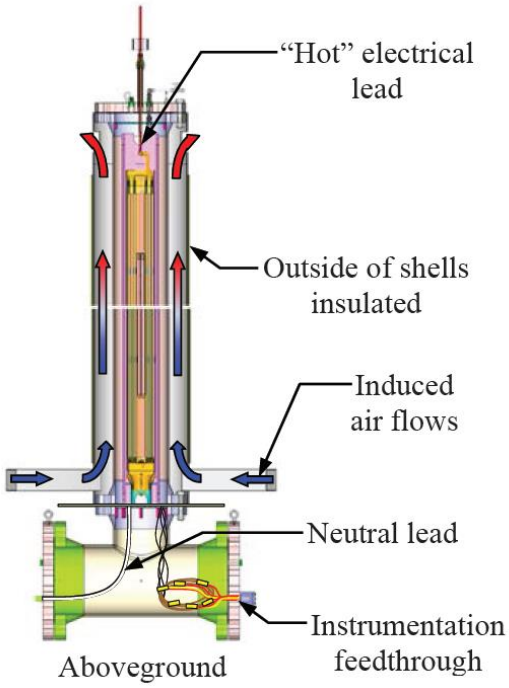

Fig. 1. The plan view of dry cask simulator.

2.2 CFD thermal analysis model

The CFD thermal model focus on the calculation for fuel cladding, inner helium gas, and air cooling temperatures. A 3D analytical geometry using a $1/8^{th}$ symmetry, as shown in Fig. 2 was used to evaluate temperatures. Boundary conditions were used to simulate experimental conditions for the DCS. The laminar model was used in the inner helium gas flow, and realizable k-epsilon model was used in the external air flow with full buoyancy effects. The surface to surface model with view factor was used for radiation heat transfer. The second order upwind scheme was used for momentum, turbulence, energy and radiation heat transfer. The velocity-pressure coupling method is SIMPLE.

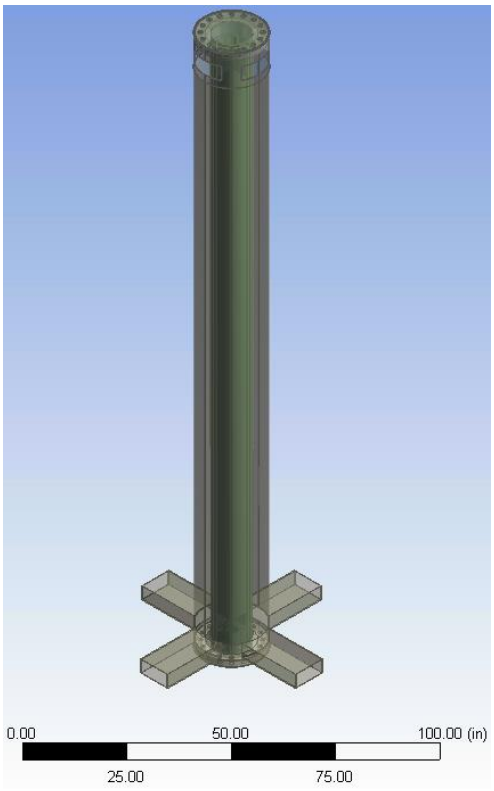

Fig. 2. The CFD analysis geometry of dry cask simulator.

Thermal Property of fluids and solids materials are presented in the DSC handbook[2] and material inventory of CFD code[3]. Ideal gas conditions are used helium and air densities.

3. Results and Discussion

Fig. 3 show temperature contour at middle plane that located in the height of 3.023 m. Fuels temperature higher than basket and helium region except near fuel region. Fig. 4 shows the steady state transverse temperature profile at middle plane. This figure shows the location and value of the temperature for each region of the test apparatus and CFD results. Maximum temperature different is 5.8K at the vessel structure and minimum is 0.5K at the basket structure. The results show good agreement between the experimental results and the CFD calculations for the DCS.

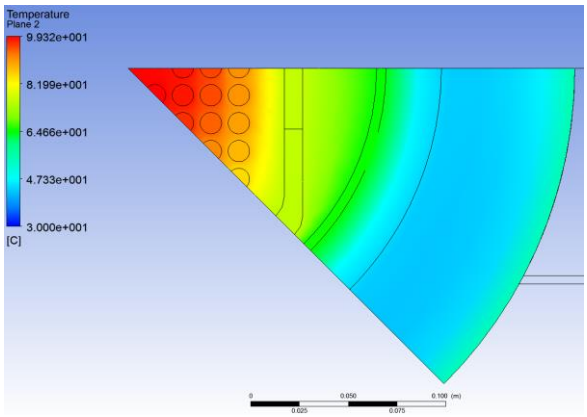

Fig. 3. The temperature contour of measured location (z=3.023).

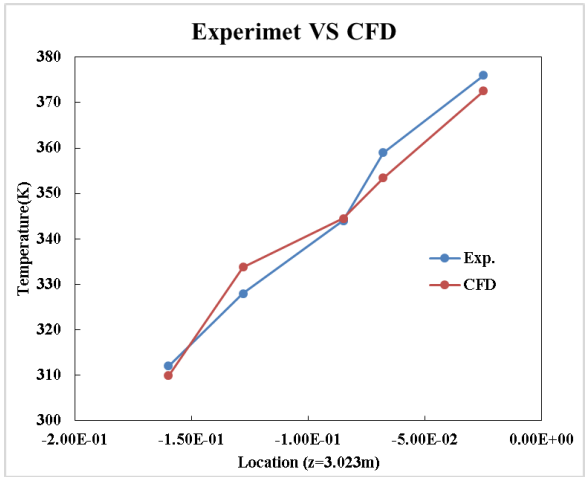

Fig. 4. Steady state temperature as a function of location.

REFERENCES

[1] A. ZIGH and J. SOLIS, “Computations Fluid Dynamics Best Practice Guidelines for Dry Cask Application,” Nuclear Regulatory Commission, NUREG-2152, (2013).

[2] E.R. Lindgren and S.G. Durbin, “Materials and dimensional reference handbook of the boiling water reactor dry cask simulator”, Sandia National Laboratories (2017).

[3] Fluent 17.2. ANSYS Fluent Theory Guide 17.0, ANSYS Inc, USA (2016).

Multi-Dimensional Modeling of Electrorefining Process of Used Nuclear Fuel With Liquid Cadmium and Rotating Cylinder Electrodes

Dokyu Kang [a], Jaeyeong Park [b], and Sungyeol Choi [a,*]
[a] Department of Nuclear and Quantum Engineering, Korea Advanced Institute of Science and Technology, Yuseong-gu, Daejeon 34141, Korea
[b] School of Mechanical, Aerospace and Nuclear Engineering, Ulsan National Institute of Science and Technology, 50 UNIST-gil, Ulju-gun, Ulsan, 44919, Korea
sungyeolchoi@kaist.ac.kr

1. Introduction

Electrorefining process is the actual process separating the recyclable U species from the products of electroreduction process [1]. Thus the separation efficiency of electrorefining process determines the efficiency of the whole pyroprocessing.

This study aimed to construct computational electrorefining model. Electrorefining process accompanies electrochemical reaction and mass transport. To reflect these multi-physics in the electrorefining reaction and optimize the computational load, the 3D hydrodynamic model and 2D multi-species model were developed.

The results were validated by the experimental data of lab-scale electrorefining process conducted by Argonne National Laboratory (ANL) at 1992 [2].

2. Method

2.1 Cell configuration

This model brought initial conditions and geometry from the lab-scale ANL experiment. The configuration of electrorefining cell is shown in Fig. 1.

The molten salt region in contact with the cathode and anode, where the region highlighted by the red line in the Fig. 1, was only considered in this model to focus on the reactions over the surface of the electrodes.

2.2 Numerical approach

In this paper, 3D and 2D computational electrorefining models were developed with a CFD software COMSOL 5.1.

The 3D model only considered U single species and calculated velocity distribution and the thickness of diffusion dominant region caused by the rotating cylinder cathode.

The calculated thickness was applied to the 2D model which ignores fluid dynamics and assumes well mixed state of bulk region and only consider mass transport of diffusion in the diffusion dominant region. 2D model involved three species U, Pu, and Nd and focused on the competitive reactions of them.

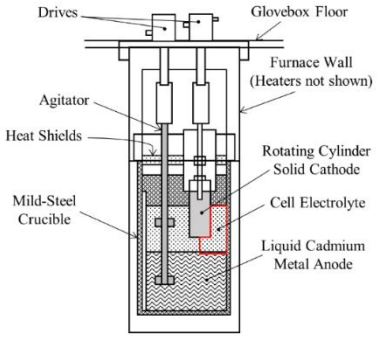

Fig. 1. ANL lab-scale electro-refining cell [2].

2.3 Mathematical equations

The Nernst-Planck equation was calculated to reflect mass transport caused by the convection and diffusion. The electromigration was neglected because of the sufficient supporting electrolyte.

$$N_i = -D_i \nabla C_i + C_i v - \frac{n_i F}{RT} D_i C_i \nabla \phi \quad (1)$$

The Navier-Stokes equation was applied to the 3D hydrodynamic model to reflect the convection effect of rotating cylinder cathode.

$$\rho\left(\frac{\delta v}{\delta t} + v \cdot \nabla v\right) = -\nabla p + \nabla \cdot \mu(\nabla v + (\nabla v)^T) + f \quad (2)$$

The modified Butler-Volmer equation was applied to the 2D multi-species model to calculate the competitive reactions of reactants.

$$i_{loc,i} = i_{ex,i} \frac{exp\left(\frac{\pm\alpha_i n_i F \eta_i}{RT}\right)}{1+\frac{i_{ex,i}}{i_{L,i}} exp\left(\frac{\pm\alpha_i n_i F \eta_i}{RT}\right)} \quad (3)$$

The limiting current was defined as follow:

$$i_{L,i} = \frac{n_i F D_i C_{bulk,i}}{\delta} \quad (4)$$

3. Results and Discussions

3.1 3D hydrodynamic model

The velocity distribution of U in the molten salt was investigated with the 3D model (Fig. 2). The highest velocity was formed in the vicinity of the rotating cathode. On the other hand, the lowest velocity was formed right below the cathode bottom and the region far from the cathode. Because of the active mass transport by the convection, very thin diffusion dominant layer was formed near the cathode.

The calculated thickness of the diffusion dominant layer was 0.0045 cm and it was applied to the 2D model. However, we expect the actual thickness should be thinner because we only consider the convection effect of the cathode.

3.2 2D multi-species model

The amount of metal deposition on the cathode was investigated with 2D multi-species model (Fig. 3). The early deposition reaction was dominated by the U. However, the time after 50 hours, the Pu started to participate in the reduction reaction and the reduction rate of U started to decrease. Although the Nd also exist in the molten salt, Nd was not involved in the metal deposition on the cathode until the end of the process. It is because Nd is chemically very stable in chloride form [3].

4. Conclusion

In this paper, the hydrodynamic effect of the rotating cylinder electrode was investigated with 3D model and the calculated thickness of diffusion dominant region was applied to the 2D multi-species model. The simulated result of metal deposition on the cathode was well matched to the reference experimental data of ANL.

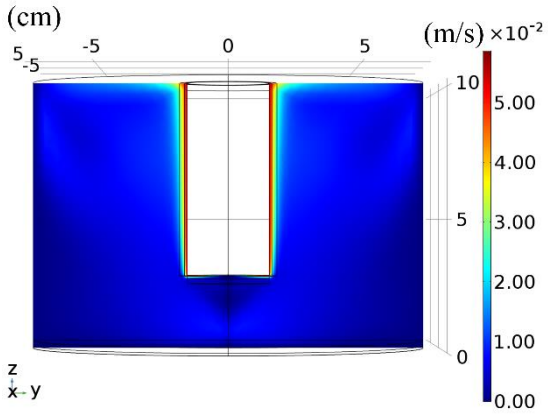

Fig. 2. Velocity (m/s) of U in molten salt at the *yz*-cross section of 3D hydrodynamic model analyzing a rotating cylinder solid electrode.

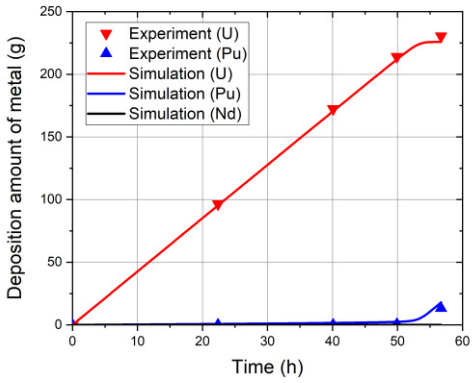

Fig. 3. Amount of metal deposition on the cathode.

ACKNOWLEDGEMENTS

This work was supported by the National Research Foundation of Korea (NRF) funded by the Ministry of Science and ICT (The grant number: NRF-2016M2B2B1945249).

REFERENCES

[1] H.-S. Lee, G.-I. Park, K.-H. Kang, J.-M. Hur, J.-G. Kim, D.-H. Ahn, Y.-Z. Cho, E.-H. Kim, Pyroprocessing technology development at KAERI, Nuclear Engineering and Technology, 43 (2011) 317-328.

[2] Z. Tomczuk, J.P. Ackerman, R.D. Wolson, W.E. Miller, Uranium Transport to Solid Electrodes in Pyrochemical Reprocessing of Nuclear Fuel, Journal of The Electrochemical Society, 139 (1992) 3523-3528.

[3] J. Zhang, Electrochemistry of actinides and fission products in molten salts—Data review, Journal of Nuclear Materials, 447 (2014) 271-284.

Development of Finite Element Model for Handling Characteristic Evaluation of Spent Nuclear Fuel

Jaejun Lee*, Hyeongkoo Kim, Seongki Lee, and Jongsung Yoo

KEPCO NF, 242, Daedeok-daero 989beon-gil, Yuseong-gu, Daejeon, Republic of Korea

*jaejunlee@knfc.co.kr

1. Introduction

Spent Nuclear Fuels (SNFs) have been stored in spent fuel pools of the each pressurized water reactor nuclear power plant since the plants started commercial operation. The estimations for quantities of the SNFs are around 13,000 tons [1]. The top nozzles of some SNFs were separated during handling due to the Inter-Granular Stress Corrosion Cracking (IGSCC) [2].

To evaluate the handling characteristics of the SNF, a Finite Element (FE) model was developed considering the top region in the fuel, and the analyses were performed using the developed model in this study. The model is generated based on the Westinghouse (WH) 17×17 type fuel assembly (FA) because the FA is the heaviest among the FAs with the IGSCC concern.

2. Finite Element Model for the Guide Tube to Top Nozzle Joint

2.1 Single Guide Tube to Top Nozzle Joint

The analyses and tests were carried out using the single guide tube to top nozzle joint. The analysis model and test specimen are illustrated in Fig. 1 and 2. The boundary and loading conditions were that the end of guide tube was fixed and the top nozzle plate was moved.

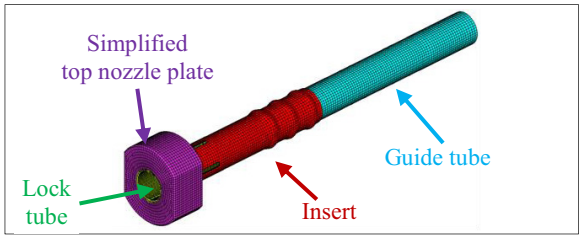

Fig. 1. FE model for single guide tube to top nozzle joint.

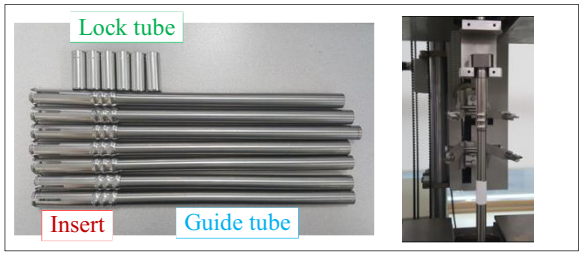

Fig. 2. Test specimen and equipment for single guide tube to top nozzle joint.

2.2 Full FE Model for Guide Tube to Top Nozzle Joint

The full FE model was generated for the top region of WH 17 type FA. The model consists of a top nozzle, 24 inserts, 24 guide tubes and 24 lock tubes. Fig. 3 shows the full FE model and the loading/boundary conditions.

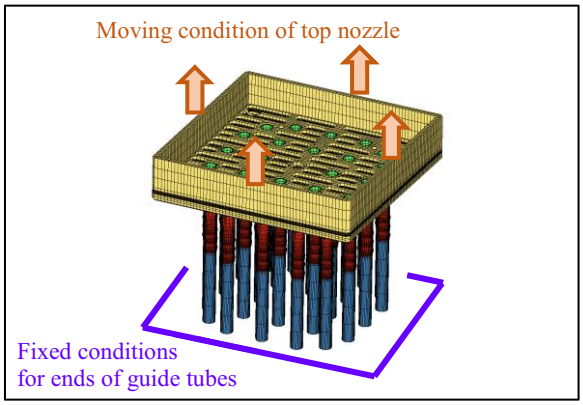

Fig. 3. Full FE model for single guide tube to top nozzle joint.

3. Results of Analysis and Test

The analyses and tests were performed until the separation between the insert and the top nozzle. Fig. 4, 5 and 6 are the non-dimensional load-displacement curves from each analysis and test. The each non-dimensional value is calculated based on the average values of maximum reaction forces and displacements from the tests.

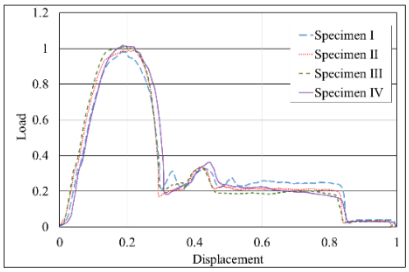

Fig. 4. Load-displacement curve for single test model.

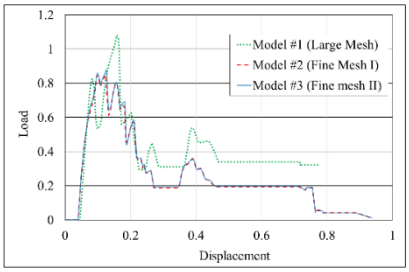

Fig. 5. Load-displacement curve for single FE model.

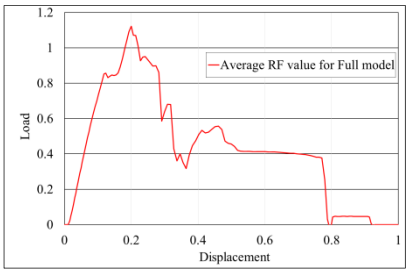

Fig. 6. Load-displacement curve for full FE model.

Fig. 4 and 5 is the test and analysis results for the single model and Fig. 6 is the analysis results for full FE model. In Fig. 6, each load for displacement is average value for 24 guide tubes. The reason for using the average value is to evaluate the suitability of the full FE model from comparisons between the full model and the single model results.

From these comparisons, it can be known that the trends are similar although the non-dimensional loads are a little different. However, the maximum load of Model #1 (large mesh) in the single FE model and that of full FE model are very similar. If the fine meshes are used in the full FE model, the load values may be approached to the test values for the single model.

4. Conclusion

The full FE model is developed to evaluate the handling characteristics of the SNF. The suitability of the developed FE model is verified from the comparisons among analysis/test results. In the future, the test will be performed using the same full specimen as the full FE model.

ACKNOWLEDGMENTS

This work was supported by the Korea Institute of Energy Technology Evaluation and Planning(KETEP) and the Ministry of Trade, Industry & Energy(MOTIE) of the Republic of Korea (No. 2014171020166C).

REFERENCES

[1] O. C. KWON, S. Y. KIM, Y. I. YOO, N. G. PARK, S. K. LEE and J. S. YOO, “R&D Activities of Spent Nuclear Fuel Integrity Evaluation during Handling and Trans-portation for Long-term Storage,” PATRAM 2016, Sep. 18-23, 2016, Kobe, Japan.

[2] IAEA, Spent Fuel Performance Assessment and Research, IAEA-TECDOC-1343, IAEA, Vienna, Austria (2003).

Method to Determine the Simplified Fuel Assembly Model for a Spent Fuel Rack Seismic Analysis From the Reactor Vessel Internal Seismic Analysis Model

Dong-Hak Kim* and Yulim Shin

Korea Hydro & Nuclear Power Co., Ltd. Central Research Institute, 70, Yuseong-daero 1312beon-gil, Yuseong-gu, Daejeon, Republic of Korea

Donghak.kim@khnp.co.kr

1. Introduction

The evaluation of the fuel assembly stored in spent fuel storage rack under a seismic condition is required by U.S. Nuclear Regulatory Commission (U.S. NRC) Standard Review Plan (SRP) 3.8.4 App. D Rev.4[1]. The effect of the end-of-life(EOL) condition on the evaluation of the fuel assembly(FA) stored in spent fuel storage rack should be also considered. To consider the evaluation of the fuel assembly for the spent fuel rack seismic analysis, the method to determine the simplified fuel assembly model should be studied.

The model of the reactor vessel internals plus core are used to evaluate the response of the fuel assemblies at the core to seismic excitation. The analysis model of fuel assembly is determined from the series of tests under the boundary condition to simulate the core support and fuel alignment plates. In this paper, the method to determine the analysis model of fuel assembly for the spent fuel rack seismic analysis from that for the models of the reactor vessel internals plus core is studied. At first, the effect of boundary condition is evaluated. The other effects are discussed on the method to determine the analysis model of fuel assembly.

2. Simplified model of fuel assembly

Fig. 1 shows the simplified beam model of FA for reactor vessel internals[2] and the simplified beam model of fuel rack including rack and FA[3]. The beam model of FA for reactor vessel internals is determined from a series of tests under the boundary condition to simulate the core support and fuel alignment plates. Especially, the flexural rigidity of beam model is determined by simulating the test results using the beam model of FA.

The spent fuel storage rack model has the beam model for FA and rack, respectively. The beam model for FA should be determined to properly evaluate the integrity of FA and exactly simulate a motion of FA and an impact between FA and rack.

3. Effect of boundary condition

The tilt test of FA was conducted by fixing the core support and loading on the top of FA. The tilt test results are compared with the analysis results using the beam model of FA which simulates the boundary condition of tilt test. The natural frequency of an analysis model is lower than that of test results.

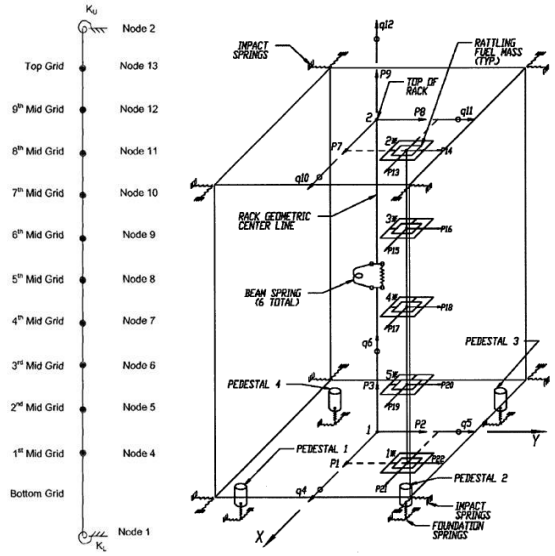

(a) Reactor vessel internals (b) spent fuel storage rack

Fig. 1. The simplified model of FA.

The boundary condition of tests to determine the beam model was determined to simulate the core support and fuel alignment plates. FA is compressed by fuel alignment plates. The flexural rigidity of model is determined by lowering the error of displacement between test and analysis. The displacement of center of FA is the largest value because of the fixed condition at the end of FA. The flexural rigidity of model for reactor vessel internals is determined to simulate the displacement of FA center exactly so using the beam model for reactor vessel internals to simulate FA for spent fuel storage rack should be justified.

4. Discussion

The natural frequency is the most important factor for the flexural rigidity of model. The natural frequency of FA is various with the amplitude of the vibration test. The natural frequency of FA for APR1400 reactor vessel internal is determined at the large amplitude. The natural frequency of FA for the WEC NPP such as Kori#2 was determined at the zero-amplitude. The natural frequency of FA is different between the methodologies of reactor vessel internal seismic analysis.

Also, a natural frequency of FA under end-of-life conditions is lower than that under beginning-of-life conditions. So, the effect of the FA natural frequency should be considered.

5. Conclusion

The justification for the use of a FA model for reactor vessel internal seismic analysis should be evaluated by the sensitivity analysis for the effect on the flexural rigidity of FA model. The range of the flexural rigidity should be determined by considering the effect of the boundary condition, the amplitude and EOL condition

REFERENCES

[1] U.S. Nuclear Regulatory Commission, Standard Review Plane, Section 3.8.4, Rev.4, September 2013.

[2] Combustion Engineering Report, “Structural Analysis of Fuel Assemblies for Seismic and Loss of Coolant Accident Lading,” CENPD-178-P, Rev.1-P (1981).

[3] Holtec Report, “Licensing report for South Texas Project units 3&4 ABWR spent fuel racks,” HI-2135462, Rev.2 (2014).

Equivalent Drop Analysis Model of Transportation Cask Including Spent Nuclear Fuel Assembly

Yun Young Yang [a], Sang Soon Cho [a*], Woo-Seok Choi [a], Ki-Seog Seo [a], Daesik Yook [b], and A Ra Go [b]

[a]Radwaste Transportation and Storage Technology Team, Korea Atomic Energy Research Institute, 111, Daedeok-daero 989 beon-gil, Yuseong-gu, Daejeon, Republic of Korea

[b]Dept. of Radiation Safety Research, Korea Institute of Nuclear Safety, 62 Gwahak-no, Yuseong-gu, Daejeon, Republic of Korea

*sscho96@kaeri.re.kr

1. Introduction

The purpose of this study is to develop an equivalent analysis model for evaluating the integrity of a spent fuel cladding tube from drop impacts under normal transport conditions and accident conditions of a transportation cask. This study proposes the equivalent drop analysis FE model of the transportation cask including the spent nuclear fuel assembly under normal transport and accident conditions, and a verification test was performed for showing the reliability of the equivalent analysis model.

2. Equivalent Drop Analysis FE Model

2.1 Spent Nuclear Fuel Assembly FE Model

The fuel assembly consists of a 16x16 fuel cladding, a bottom nozzle, a top nozzle, an intermediate support grid, an upper support grid, a bottom support grid, an outer guide tube, and a center guide tube. The fuel claddings, grids and guide tubes are modeled using beam elements, and the bottom nozzle is modeled as solid elements. The springs and dimples in grids are modeled using the spring connectors. Fig. 1 is a finite element model of spent nuclear fuel assembly developed in previous study[1, 2].

2.2 Equivalent Drop Analysis FE Model

Fig. 2 shows the bottom vertical impact analysis model in which the basket and the impact limiter are connected to the finite element model of spent fuel assembly in section 2.1. As shown in Fig. 2, the basket is modeled on the outside of the nuclear fuel assembly, and the horizontal displacement of the nuclear fuel assembly are restricted by adding contact conditions between the cladding and the basket, the support grid and the basket. The impact limiter is modeled as the beam element with a circular cross section, and whose diameter and height are used with the actual dimension of the impact limiter. The impact energy can be absorbed by applying the elasto-plastic properties of the impact limiter into the beam element. The element between the fuel assembly and the impact limiter is connected by a spring element to model the stiffness between the bottom nozzle-canister-cask. The magnitude of the stiffness between these components was determined by comparing with the drop analysis results using the detailed FE model[1].

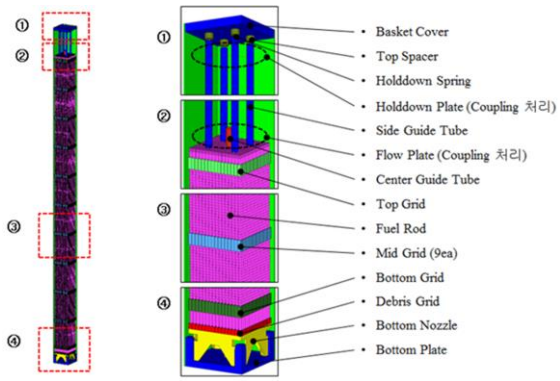

Fig. 1. Detailed FE Model of Spent Nuclear Fuel Assembly.

3. Analysis Results

Fig. 3(a) shows the deformed shape and the stress distribution of the detailed transportation cask FE model containing the spent fuel assembly model in case of 9 m vertical drop analysis. Permanent deformation occurred in the impact limiter at the bottom of the cask and large plastic strain occurred in the cladding of the fuel assemblies in the canister. Fig. 3(b) shows the result of the vertical drop analysis of the 9 m height using the equivalent drop analysis model including the spent fuel assembly. The analysis showed very similar results to those of the detailed FE model.

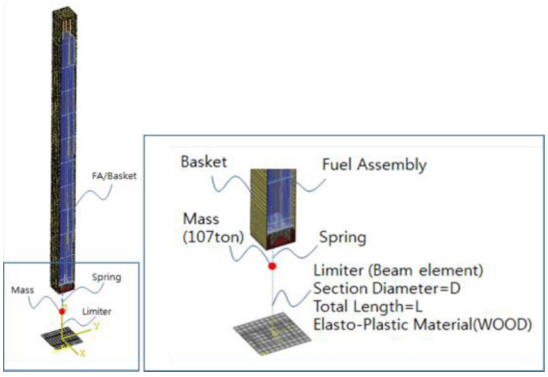

Fig. 2. Equivalent Drop Analysis FE Model of Transportation Cask including Detailed Spent Nuclear Fuel FE Model.

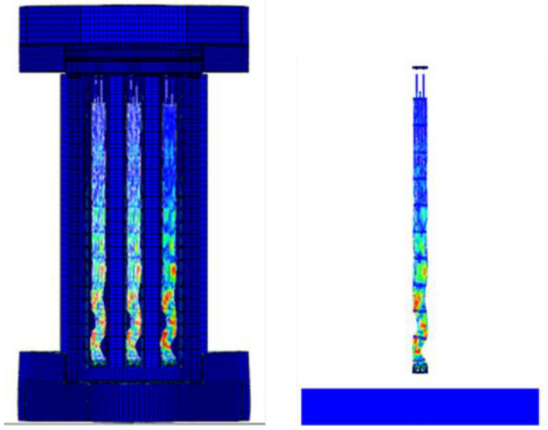

(a) Detailed FE model (b) Equivalent FE model

Fig. 3. Comparisons of deformed shape and stress distribution between Detailed FE model and Equivalent FE model in case of 9m Vertical Drop.

4. Conclusions

This study presents the equivalent finite element model for the vertical drop analysis of the transportation cask including the spent nuclear fuel assembly under normal transport and accident conditions. The analysis results showed that the present equivalent FE model had the reliability by comparing with the drop analysis results using the detailed FE model.

REFERENCES

[1] D. T. Tang, J. Guttmann, B. J. Koeppel and H. E. Adkins, “High Burn-up Spent Nuclear Fuel Structural Response when subjected to a Hypothetical Impact Accident”, Proc. of ASME/JSME Pressure Vessels and Piping Division Conference, July 25-27, 2004, USA.

[2] S.S. Cho, W.S. Choi, K.S. Seo and Y.Y. Yang, “Drop Analysis of Spent Nuclear Fuel including Cladding”, Proc. of the KRS 2016 Fall Conference, 14(2), Oct. 12-14, 2016, Jeju.

2분과

사용후핵연료 처분전관리 (Poster)

Determination of a Simplified Analysis Model of Spent Fuel Storage Rack for Seismic Analysis

Yulim Shin* and Dong-Hak Kim

Korea Hydro & Nuclear Power Co., Ltd. Central Research Institute, 70, Yuseong-daero 1312beon-gil, Yuseong-gu, Daejeon, Republic of Korea

Yulim.shin@khnp.co.kr

1. Introduction

A whole-pool-multi-racks (WPMR) model which simulates whole racks stored in the spent fuel pool to consider the impacts between racks and rack-to-pool is used for a seismic analysis of a stent fuel storage rack[1]. A simplified model of a stent fuel storage rack is determined to simulate a movement of racks and an impact between racks or rack-to-pool. In this paper, the method to determine a simplified model of a spent fuel storage rack for seismic analysis is studied. A simplified model is determined to simulate the dynamic behavior of a spent fuel storage rack. To determine a simplified model of a spent fuel storage rack, the detailed finite element analysis is conducted.

2. Detailed model of rack

The 9 X 10 spent fuel storage rack is modeled as shown in Fig. 1. The welding between cells is considered. To consider a dynamic behavior, the modal analysis is conducted. Fig. 2 shows an x-direction and a y-direction displacement of a detailed model at the first and third modes, respectively. The first and third modes show the bending mode of rack. Deformations of the other modes show the distortion mode as shown in Fig. 3.

Fig. 1. Detailed model of rack.

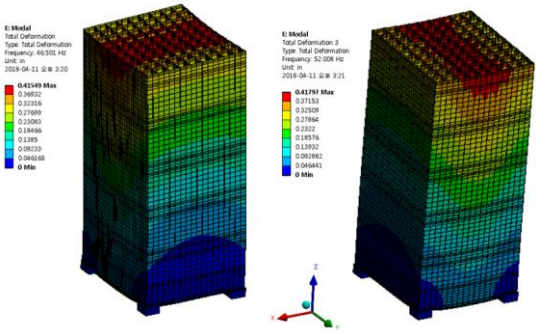

Fig. 2. The 1st and 3rd mode shape of a detailed model.

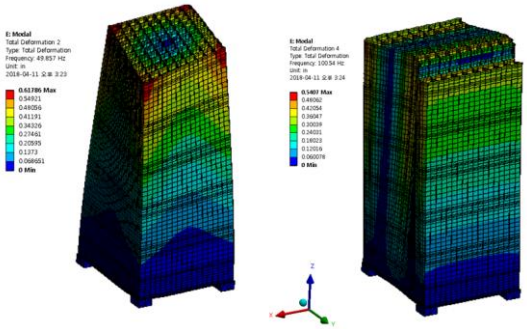

Fig. 3. The 2nd and 4th mode shape of detailed model.

3. Simplified model of rack

Fig. 4 shows the schematic model of a simplified rack model. Fig. 4(a) shows the sample of a seismic

rack model[2]. The simplified model as shown in Fig. 4(b) is simulated for a seismic rack model. A rack is simulated by a mass-beam model as parts of a cell, bottom plate and reg. The bottom plate is modeled as a rigid body by using a large flexural rigidity because all bottom plate is welded with a cell. A flexural rigidity of rack leg can be determined as a geometric shape. A flexural rigidity of rack cell which considers the welding effect needs to be determined.

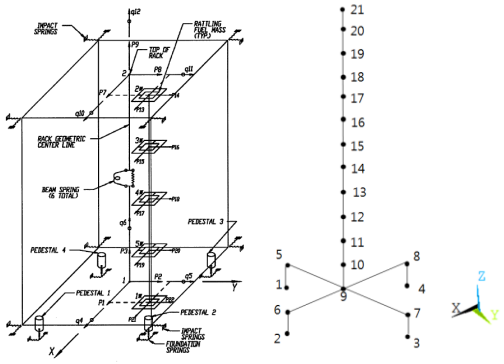

(a) Seismic rack model[2] (b) simplified model

Fig. 4. Simplified model of a rack.

A simplified model can simulate the directional behavior of a spent fuel storage rack as shown in Fig. 2 so a flexural rigidity of rack cell is determined which has the same natural frequency as that of detailed model. The first and third modes are the major mode to simulate the impact between racks and rack-to-pool.

A flexural rigidity of a rack cell has a directional value. The ratio of a flexural rigidity in an x-direction to that in a y-direction is determined by a theoretical ratio considering geometry. Table 1 shows the natural frequencies of a simplified and a detailed model. The first and the second natural frequencies of a simplified model are similar with the first and the third natural frequencies of a detailed model.

Table 1. Natural frequency of rack

	1st	2nd	3rd	4th
Detailed model	46.501	49.857	52.008	100.54
Simplified model	46.603	50.443	216.55	239.64

4. Conclusion

The method to determine a simplified model of rack for a seismic analysis of a spent fuel storage rack is studied. A rack is simulated by a mass-beam model as parts of a cell, bottom plate and reg. A flexural rigidity of rack cell is determined which has the same natural frequency as that of detailed model. The major modes to simulate the impact between racks and rack-to-pool are only considered. The ratio of a flexural rigidity in an x-direction to that in a y-direction is determined by a theoretical ratio considering geometry.

REFERENCES

[1] G. DeGrassi, “Review of the Technical Basis and Verification of Current Analysis Methods Used to Predict Seismic Response of Spent Fuel Storage Racks”, NUREG/CR-5912(BNL-NUREG-52335) (1992).

[2] Holtec Report, “Licensing report for South Texas Project units 3&4 ABWR spent fuel racks,” HI-2135462, Rev.2 (2014).

Recovery of RE-less U From U/RE Ingot by Electrochemical Oxidation Process

Si Hyung Kim*, Dalsung Yoon, Junhyuk Jang, Taek-Jin Kim, Seunwoo Paek, and Sung-Jai Lee

Korea Atomic Energy Research Institute, Daedeok-daero989ben-gil 111,Yuseong-gu, Daejeon, Republic of Korea

*exodus@kaeri.re.kr

1. Introduction

SFR fuel is majorly composed of U and Pu, where the amount of impurities such as RE (rare earth) needs to be controlled as low as possible, for example, below 1% of the fuel composition. But, it is very difficult to recover U/Pu material having so low RE amount from LCC electrowinning process [1, 2]. In order to decrease RE amount in the U/Pu/RE mixture obtained from LCC electrowinning, some treatments should be done. In this study, selective oxidation behavior of RE components in U/RE ingot was studied using an electrochemical process.

2. Experimental

Fig. 1 shows the experimental configuration for the electrochemical oxidation process, where LiCl-KCl-3.6wt% $LaCl_3$ was contained in an alumina crucible. U/Ce/Nd anode ingot having a weight of about 3.8 g was contained in an alumina crucible and zinc cathode buttons having a weight of about 35g in another alumina crucible as shown in Fig. 1. For the measurement of the potentials of the electrodes, Ag/AgCl electrode was used as a reference. The melting point of zinc is about 420℃ and so the zinc buttons are melted at the reaction temperature of 500℃.

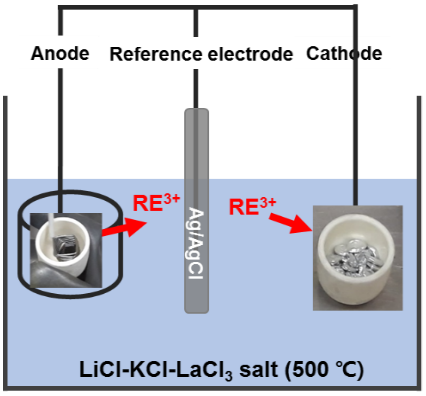

Fig. 1. Experimental configuration for electrochemical oxidation process.

Fig. 2(a) shows the U/Ce/Nd ingot, where upper and lower parts of the ingot show the different colors. This is owing to the density difference of the U/Ce/Nd. The densities of the U and RE (Ce/Nd) was about 19 g/cm^3 and 7 g/cm^3, respectively. According to the EPMA analysis, some RE particles was seen in U matrix and some U particles in RE matrix. Fig. 2(b) shows the CV result of the LiCl-KCl-$LaCl_3$ salt at 500℃. Any other components was not detected except La in the salt.

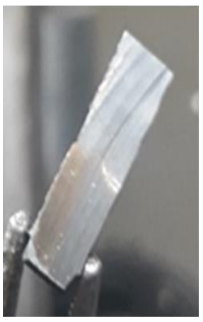

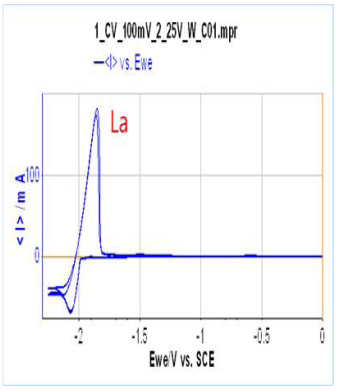

(a) U/Ce/Nd ingot (b) CV in LiCl-KCl-$LaCl_3$ salt

Fig. 2. The anode ingot and CV result of the LiCl-KCl-$LaCl_3$ salt.

3. Results and Discussion

3.1 Oxidation of the anode

After the anode and the cathode was connected to a potentiostat equipment, -1.7V was applied to the anode as a working electrode. Fig. 3(a) shows the variation of the zinc cathode potential and the current, respectively. About 250 mA was applied at the initial time and nearly 0.2 mA after 5 hours. Current value of 0 mA means no reaction between the electrodes. So, the oxidation experiment was terminated around 6 hours. Fig. 3(b) shows the CV result of the final salt to check the existence of U in the salt. U peak was not seen. During the oxidation process, it is expected that most of the Ce/Nd components was oxidized to the chloride forms and some La/Ce/Nd components was deposited to the liquid zinc cathode.

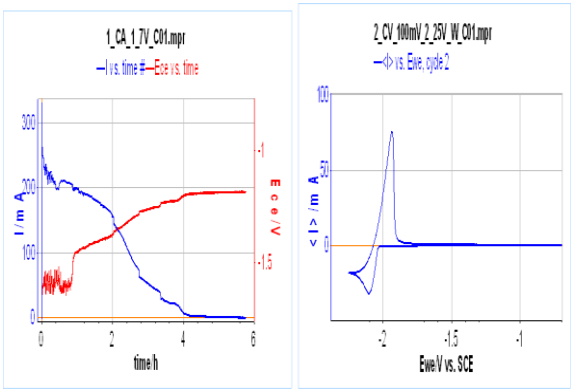

(a) current change (b) CV result of final salt

Fig. 3. Change of current value during the oxidation process and CV result of the final salt.

3.2 SEM/EPMA analysis

Fig. 4 shows the SEM/EPMA photographs of the anode ingot after the oxidation reaction. Only U part was remained and RE matrix part was all oxidized into the salt. But, RE particles still existed in the U matrix part even after the oxidation. It is predicted from this result that most of the RE particles distributed in the U matrix would not be oxidized because RE particles would be predominantly distributed in the inner part rather than the surface part of U matrix.

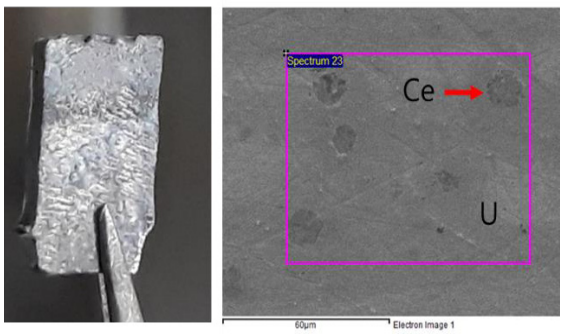

Fig. 4. SEM/EPMA analysis results of anode ingot after the oxidation reaction.

3.3 Distillation of the zinc cathode

While the anode was oxidized into the salt, metal ions of the salt would be deposited into the zinc cathode. After the oxidation was terminated, zinc cathode product was distilled in the alumina crucible around 850℃ at 1 torr to recover the deposited metal components. Fig. 5(a) shows the variation of the temperature and the weight during the distillation. Weight difference of about 35g occurred and it corresponds to the weight of the zinc cathode material. Fig. 5(b) shows the metal product remained in the alumina crucible after the distillation. The metal is being chemically analyzed to identify its composition.

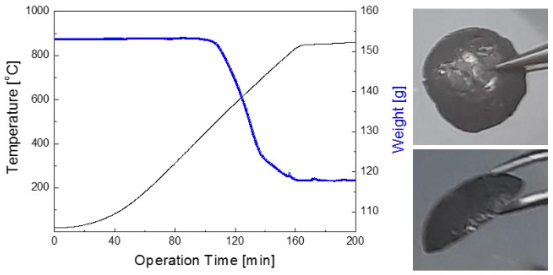

(a) weight change (b) recovered metal

Fig. 5. Weight loss and the recovered metal after the distillation of the zinc cathode product.

4. Summary

Selective oxidation of RE elements from the U/RE metal ingot was studied in this paper using electrochemical process. Constant potential of -1.7V was applied between anode and cathode, where the potential value corresponds to standard potentials between actinide and rare earth materials. When the current values approached to nearly 0 mA, the reaction was finished. It is confirmed from the EPMA analysis that only U part of the U/RE ingot was remained. The metal recovered to the zinc cathode was obtained through the distillation process and it is being chemically analyzed in the KAERI analytical laboratory.

ACKNOWLEDGEMENT

This work was supported by a National Research Foundation of Korea (NRF) grant funded by the Korean Government (MSIP) (No. 2017M2A8A5015079)

REFERENCES

[1] Li, S.X.; Herrmann, S.D.; Goff, K.M.; Simpson, M.F.; Benedict, R.W. (2009) Actinide recovery experiments with bench-scale liquid cadmium cathode in real fission product-laden molten salt. Nucl. Mater. 165:190-199.

[2] Uozumi, K.; Iizuka, M.; Kato, T.; Inoue, T.; Shirai. O.; Iwai, T.; Arai, Y. (2004) Electrochemical behaviors of uranium and plutonium at simultaneous recoveries into liquid cadmium cathode. J. Nucl. Mater.325:34-43.

U/RE Recovery Using Large-Scale LCC Electrowinning System

Si Hyung Kim*, Joon-Bo Shim, Junhyuk Jang, Sang-Woon Kwon, Young Sang Lee, Youngwoo Kwon, Gha-Young Kim, and Sung-Jai Lee

Korea Atomic Energy Research Institute, Daedeok-daero989ben-gil 111,Yuseong-gu, Daejeon, Republic of Korea

*exodus@kaeri.re.kr

1. Introduction

The electrowinning system of KAERI is composed of three processes : (i) LCC (liquid cadmium cathode) electrowinning process for group recovery of actinides [1, 2], (ii) RAR (residual actinides recovery) process to collect most of residual actinides in a molten salt after the LCC electrowinning process, and (iii) Cd (Cadmium) distillation process of LCC deposits obtained from LCC electrowinning and RAR processes. The recovered U/TRUs are transferred to an ingot casting furnace to produce a metal fuel ingot. In this experiment, thermogravimetry (TG) was used to make a metal ingot. In this study, large-scale electrowinning system has been tested to obtain U/RE ingot using a LiCl-KCl eutectic salt containing U and rare earth elements (REs) such as Nd, Ce, and La.

2. Experimental

For the experiments of LCC process, several electrodes such as a graphite anode, a Cd cathode, a reference electrode (Ag/1mol%AgCl) and a monitoring electrode (glassy carbon anode + tungsten cathode) were used as shown in Fig. 1. The configuration of graphite anode is shown as Fig. 1(a). Namely, a graphite rod is serially surrounded by dense Al_2O_3 tube and porous SiC tube. Because electrolyte salt can be migrated and diffused to the surface of the graphite through the pores of the SiC tube, the electrode reaction can be properly happened. Cl_2 gas created on the surface of the graphite during the electrode reaction will be moved toward the Cl_2 vent line. In this stage, the dense Al_2O_3 tube plays a role of preventing Cl_2 gas from diffusing out of the anode housing. About 7.3 kg of Cd was contained in a new BeO crucible manufactured by MATERION Corporation in the USA. A potentiostat with the maximum current of 20 A (Bio Logic Company) was used for this study.

Thermogravimetry (TG) shown in Fig. 2 was used for the consolidation process of the product recovered from the Cd distiller. TG is composed of the 2-zone furnace and glove box. Operating temperature can be increased to 1200℃ below 0.1 torr.

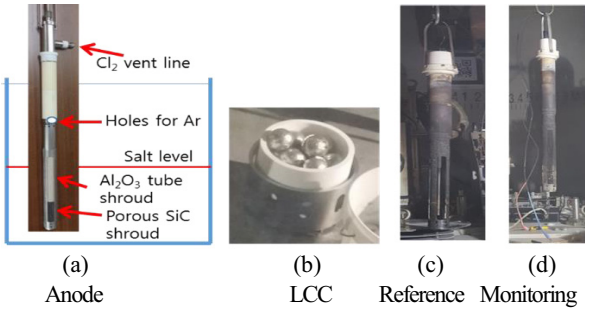

Fig. 1. Electrodes used for LCC process.

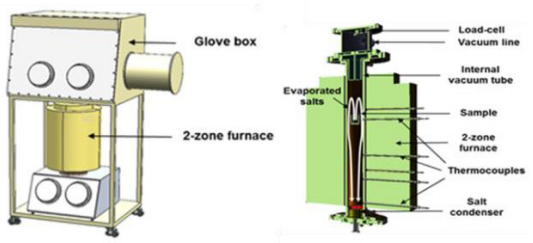

Fig. 2. Thermogravimetry equipment.

3. Results and Discussion

Fig. 3(a) shows the variation of the anode and cathode potential at the current density of 50 mA/cm^2 for 18 hours around 500℃, where liquid Cd was used as a cathode. Cathode potential gradually moved to the positive direction as the time increases to 16 hours. Beyond that time, the cathode potential went abruptly upward. So, the deposition was terminated on that time.

Fig. 3(b) shows the comparison of the CVs before and after the deposition. Before the deposition, peak height of U was higher than that of RE, showing the concentration of U is larger than that of RE. By the way, the peak height of U is lower than that of RE in the salt after the deposition, indicating much more U ions rather than RE ions were deposited on the liquid Cd. Oxidation peaks between -0.4 and -0.6V disappeared and thereby multiple peaks were not also seen.

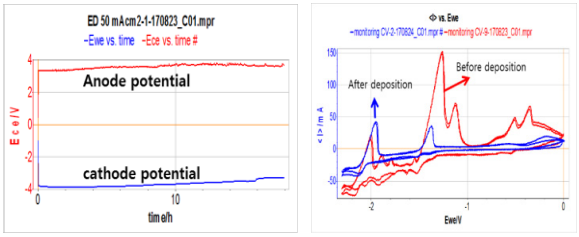

(a) Potential (b) CV result

Fig. 3. Potential change during the deposition and comparison of CVs before and after deposition.

After the electrodeposition, LCC assembly was raised above the salt to see deposits and the status of the BeO crucible. Some deposits were observed to be attached along the outer surface of the crucible as shown in Fig. 4(a). Fig. 4(b) is the BeO crucible separated from the LCC assembly. It is observed that some deposits were attached along the inner surface of the crucible. It is predicted from Fig. 3 and Fig. 4 that some deposits began to grow out of the crucible from beyond the 16 hours deposition and so U amount recovered in Cd might be decreased compared to the theoretical U amount.

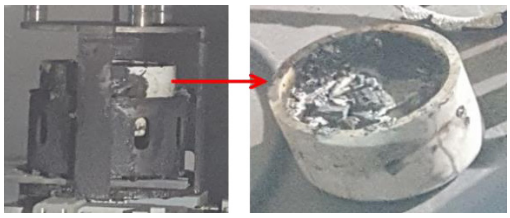

(a) LCC assembly (b) BeO crucible containing Cd

Fig. 4. BeO crucible containing Cd deposits.

Cd ingot containing U and RE elements obtained through LCC process was transferred to Cd distiller to remove Cd. The Cd in the LCC deposit was distilled very slowly at low temperature (600℃) to avoid a Cd splatter. And then, the distillation experiment was performed at 900 °C for the evaporation of the covered salt. U/RE product of about 107g was recovered from Cd distiller. For the consolidation process, U/RE product was contained into the Al_2O_3 crucible having a diameter of 5cm and the Al_2O_3 crucible was installed into the sample position of TG as shown in Fig. 2. After the consolidation process at 1200℃ around 0.1 torr, the weight loss of the sample was about 6g as shown in Fig. 5(a). The volume of the product in Al_2O_3 crucible decreased after the consolidation process. But, the product of Fig. 5(b) was not metal ingot and relatively easily broken to pieces by some shock. It was considered that most of the U/RE product had been considerably oxidized during the Cd distillation.

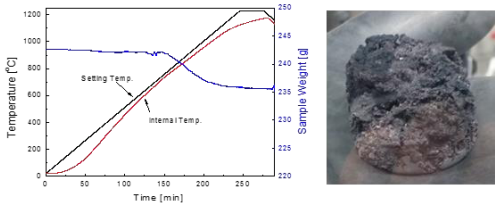

(a) Weight change (b) U/RE product

Fig. 5. Weight change and U/RE product after consolidation.

4. Summary

U/RE was electrochemically recovered to LCC at 50 mA/cm^2 from LiCl-KCl salt containing 0.5wt%UCl_3, 0.22wt%$NdCl_3$, 0.15wt%$CeCl_3$ and 0.07wt%$LaCl_3$. The Cd in the LCC deposit was removed during the distillation using Cd distiller. U/RE product of 107g obtained from the distiller was installed to TG and then heated to 1200℃ to be consolidated. Dense U/RE metal ingot was not acquired through the consolidation process because U/RE product had been partially already oxidized during the distillation process.

ACKNOWLEDGEMENT

This work was supported by a National Research Foundation of Korea (NRF) grant funded by the Korean Government (MSIP) (No. 2017M2A8A5015079)

REFERENCES

[1] Vaden, D.; Li, S.X.; Westphal, B.R.; Davies, K.B. (2008) Engineering-scale liquid cadmium cathode experiments. Nucl. Tech. 162:124-128.

[2] Kato, T.; Inoue, T.; Iwai, T.; Arai, Y. (2006) Separation behaviors of actinides from rare-earths in molten salt electrorefining using saturated liquid cadmium cathode. J. Nucl. Mater.357:105-114.

A Review of the Probabilistic Model for Chloride-Induced Stress Corrosion Cracking

Hyoung Gyu Park, Sun Woo Park, and Kwang Heon Park*
Department of Nuclear Engineering, Kyung Hee University, 1732 Deokyoung-daero, Giheung-gu, Yong-in, Gyeonggi-do, Republic of Korea
*kpark@khu.ac.kr

1. Introduction

It is important to study how to manage spent nuclear fuel (SNF) dry cask storage in S. Korea, because the dry cask has been chosen as the interim storage instead of the wet pool. One type of degradation is Chloride-Induced Stress Corrosion Cracking (CISCC), leading to release the radioisotope from the canister.

The Electric Power Research Institute (EPRI) and the U.S. NRC have undertaken research on the CISCC mechanism [1]. In addition, Sandia National Laboratories (SNL) has extensively researched the effect of CISCC on the management of dry storage canisters, suggesting a probabilistic model for CISCC [2].

The aim of this study is to review probabilistic CISCC model and to analyze the model more specifically.

2. Probabilistic CISCC Model

SNL suggests the probabilistic model to predict the potential impact, including timing and location, of stress corrosion cracking (SCC). The model consists with three periods; incubation before pit initiation, pit growth, and crack growth.

2.1 Incubation before pit initiation

The canister surface temperature and realistic environmental conditions are important factors in the incubation period. The canister surface temperature can vary with the decay heat of the spent fuel and the location and environment of the storage sites. Due to the canister surface temperature, the relative humidity (RH) could vary, and it affects to the deliquescence of the brine on the canister (Fig.1).

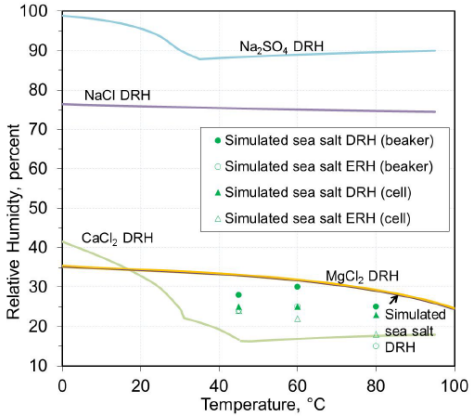

Fig. 1. Summary of Simulated Sea Salt Deliquescence [1].

To analyze the environmental conditions, dusts were collected from the dry storage canisters at Hope Creek and Diablo Canyon in the US. It was identified that the dusts at Hope Creek were composed of Fe, Si, Ca, K, and S, because Hope Creek is located near the territory and river. On the contrary, Diablo Canyon is located near the Pacific Ocean. Therefore, Cl was additionally observed at that site. SEM/EDS, XRF, ICP-OES, and IC were used for the analysis of the dusts at the SNL [2].

2.2 Pit growth

The maximum pit size model and pit-to-crack transition model were introduced to describe the pit and crack. Z.Y. Chen et al. [3] proposed an analytic expression to calculate the bounding conditions of pitting under atmospheric conditions. The expression could predict the maximum pit size based on the maximum cathode current. The expression can be written as:

$$\ln I_{c,max} = \frac{4\pi k W_L \Delta E_{max}}{I_{c,max}} + \ln\left[\frac{\pi e r_a^2 \int_{E_{corr}}^{E_{rp}} (i_c - i_p)\, dE}{\Delta E_{max}}\right] \quad (1)$$

Where $I_{c,max}$ is the maximum cathodic current, k is the conductivity of the electrolyte, W_L is the

electrolyte layer thickness, ΔE_{max} is the difference between E_{rp} and E_{corr}, r_a is the radius of the pit, E_{rp} is the potential to the pit, E_{corr} is the potential from the cathode edge, and i_c and i_p are the cathodic and passive current density, respectively.

Y. Kondo [4] suggested the corrosion pit growth rate to predict the pit-to-crack transition using the concept of the stress intensity factor range (ΔK). The proposed expression can be written as:

$$\frac{dc}{dN} = \left(\frac{1}{3}\right) C_p{}^3 f^{-1} \alpha^2 \pi^2 Q^{-2} (2.24\sigma_a)^4 \Delta K^{-4} \quad (2)$$

Where c is the radius of the crack, C_p is the coefficient, f is the frequencies, α is the aspect ratio (= a/c), Q is the shape factor, and σ_a is the stress amplitude.

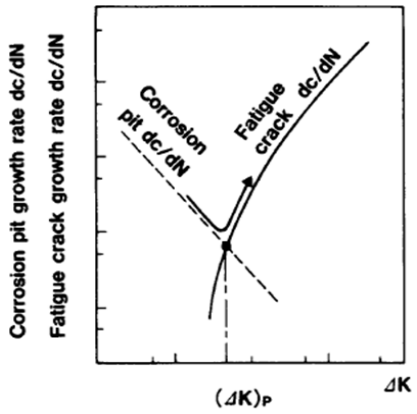

Fig. 2. Effect of the stress amplitude on the critical pit condition [4].

2.3 Crack growth

Mock-up canister tests have been studied to measure the effect of the weld residual stress (WRS) [5]. The residual stress at the heat-affected zone (HAZ) is an important factor for SCC. A variety of methods is available to measure residual stress.

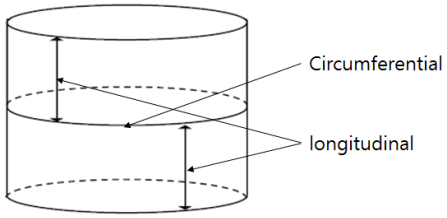

Fig. 3. The location of the welds on the mock-up canister.

According to the welded regions in Fig.3, the residual hoop and axial stress were measured. Because the residual stress causes the rate of cracking to quicken, the values of residual stress must be known.

3. Conclusion

The probabilistic CISCC model proposed by SNL was analyzed more detailed in this review paper. CISCC is one of the issues in the degradation of the dry storage. CISCC has been widely studied by the EPRI, U.S. NRC, and SNL.

The government of S. Korea decided to use the dry cask as an interim storage method instead of the wet pool. However, there is not enough information about the degradation of the dry storage in S. Korea. This review paper would be useful for the management of the dry storage.

REFERENCES

[1] X. He, T.S. Mintz, R. Pabalan, L. Miller, and G. Oberson, “Assessment of Stress Corrosion Cracking Susceptibility for Austenitic Stainless Steels Exposed to Atmospheric Chloride and Non-Chloride Salts”, Report No. NUREG/CR-7170, 2014, Washington, DC.

[2] C.R. Bryan, and D.G. Enos, “Analysis of Dust Samples Collected from Spent Nuclear Fuel Interim Storage Containers at Hope Creek, Delaware, and Diablo Canyon, California”, SAND2014-16383, Sandia National Laboratories, 2014.

[3] Z.Y. Chen, and R.G. Kelly, “Computational Modeling of Bounding Conditions for Pit Size on Stainless Steel in Atmospheric Environments”, Journal of the Electrochemical Society, 157(2), C69-C78 (2010).

[4] Y. Kondo, “Prediction of Fatigue Crack Initiation Life Based on Pit Growth”, Corrosion, 45(1), 7-11 (1989).

[5] D.G. Enos, and C.R. Bryan, “Characterization of Canister Mockup Weld Residual Stresses”, SAND2016-12375R, Sandia National Laboratories, 2016.

Crucible Cover of Multilayer Porous Hemisphere for Cd Distillation

S.W.Kwon*, Y.S.Lee, J.H.Jung, S.H.Kim, S.J.Lee, and J.M. Hur
Korea Atomic Energy Research Institute, 989-111 Daedukdaero, Yuseong, Daejeon, 34057, Korea
*swkwon@kaeri.re.kr

Abstract

The electrorefining process is generally composed of two recovery steps in pyroprocessing – the deposit of uranium onto a solid cathode and the recovery of the remaining uranium and TRU elements simultaneously by a liquid cadmium cathode. The liquid cathode processing is necessary to separate cadmium from the actinide elements since the actinide deposits are dissolved or precipitated in a liquid cathode. Distillation process was employed for the cathode processing. It is very important to avoid a splattering of cadmium during evaporation due to the high vapor pressure. In this study, a multi-layer porous round cover was proposed and examined to develop a splatter shield for the Cd distillation crucible. Cadmium vapor can be released through the holes of the shield, whereas liquid drops can be collected in the multiple hemisphere. The collected drops flow on the round surface of the cover and flow down into the crucible. The crucible cover was fabricated and tested in the Cd distiller. The cover was made with three stainless steel round plates with a diameter of 33.50 mm. The distance between the hemispheres and the diameter of the holes are 10 and 1 mm, respectively. About 40 grams of Cd and about 4 grams of Bi was distilled at a reduced pressure for two hours at 470℃. After the Cd distillation experiment, cadmium was not detected and more than 90 % of Bi remained in the ICP-OES analysis. Therefore the crucible cover can be a candidate for the splatter shield of the Cd distillation crucible. Further development of the crucible cover is necessary for the decision of the optimum cover geometry and the operating conditions of the Cd distiller.

ACKNOWLEDGEMENT

This work was supported by a National Research Foundation of Korea (NRF) grant funded by the Korean Government (MSIP) (No. **2017M2A8A5015079**)

Effect of Creep Deformation on Ductility of Simulated Spent Fuel Cladding

*Jong-Dae Hong, Euijung Kim, and Dong-Hak Kook
Nuclear Fuel Safety Research Division, Korea Atomic Energy Research Institute,
989-111 Daedeok-daero, Yuseong-gu, Daejeon, Republic of Korea
* jongd@kaeri.re.kr

1. Introduction

At present, the only licensed method for storing domestic commercial PWR spent fuel is wet storage (or pool storage). But the saturation of pool is imminent, and dry storage process is essential before disposal. Dry storage is considered as well-developed technology for spent fuel management with no critical problems. Meanwhile, one of potential degradation mechanism for spent fuel cladding during dry storage is creep, although it does not degrade the cladding integrity.

Creep will deform the cladding, but the effect of creep deformation on ductility has yet to be reported. In this regards, cladding ductility before and after creep deformation were evaluated by ring compression test (RCT). In addition, hydride distribution was observed by optical microscope to confirm the changes of microstructure.

2. Experimental

2.1 Test material

The test material used in this study was unirradiated CWSR Zircaloy-4 cladding, which has been widely used in PWR fuel cladding. The initial cladding thickness (t) and outer diameter (OD) are 0.57 mm and 9.5 mm (Westinghouse 17X17 type). To simulate the behavior of spent fuel cladding, hydrogen is charged using the Sievert method under mixed argon/hydrogen condition at 400°C.

2.2 Test condition [1]

Creep tests were performed in a muffle furnace by internally pressurization method using 150mm long specimens, because that method is only available to apply stress uniformly without stress concentration at specific points. Assembled specimens constantly pressurized by argon gas to achieve the target hoop stresses. Temperature was continuously monitored and maintained with an accuracy of ± 4°C. The creep strain was calculated from average outer diameter measurement which was performed 10 times (axially 5 points and circumferentially 2 points per specimen). The schematic illustration of the sample and fixtures for the creep test are shown in Fig. 1.

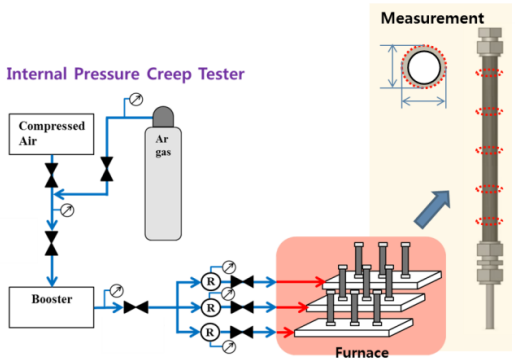

Fig. 1. Creep test method [1].

RCT at RT, 100°C, and 300°C was performed to compare the ductility before and after creep test. Also, microstructural analysis was performed to confirm hydride distribution.

3. Results and Discussion

3.1 Creep deformation

Creep strain as a function of time at 400°C, 120 MPa with various hydrogen contained specimens are shown in Fig. 2. After short primary creep, secondary creep behaviors were maintained during test time. Fresh (As-received) and 100 ppm H specimen shows 1% strain in 120 hours, and creep strain decreases as hydrogen content in specimen increases. 600 ppm H specimen reaches to 1% strain about 1500 hours. Because hydrogen leads to a significant creep strengthening and precipitated hydrides act as obstacles to dislocation glide [2,3].

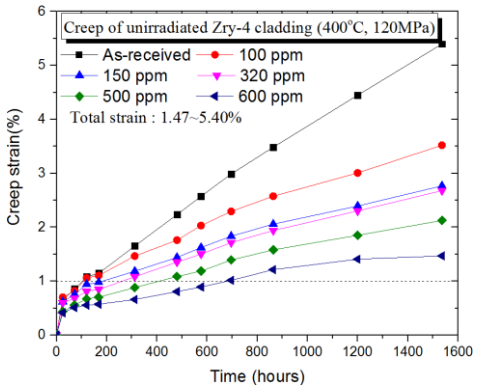

Fig. 2. Creep strain of unirradiated Zircaloy-4 cladding at 400°C, 120MPa.

3.2 Effect of creep deformation on ductility

Fig. 3 shows the measured offset strain by RCT at RT, 100°C, and 300°C. Regardless of creep deformation the ductility decreases as temperature decrease (Fig. 4). The offset strain decreases for specimens having high hydrogen content over 500 ppm, but the offset strain even at RT is enough to maintain ductile property within the all tested ranges of hydrogen contents. The trends of offset strain after creep deformation is identical with that no deformation condition. It implies that creep deformation does not have a significant effect on the ductility.

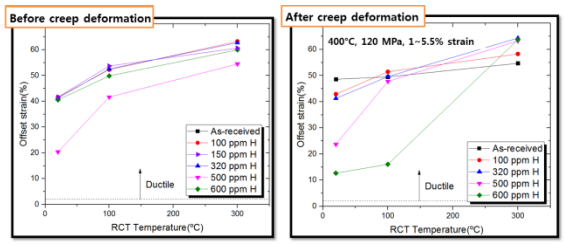

(a) (b)

Fig. 3. Results of ring compression test (a) before creep deformation (b) after creep deformation.

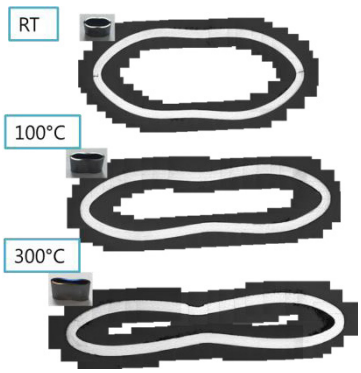

Fig. 4. Microstructure of Zircaloy-4 after creep deformation and RCT (400°C, 120MPa, 320ppm).

Meanwhile, as shown in Fig. 5, microstructure after creep deformation is same as that before deformation. Circumferential hydrides distribute uniformly and its amounts increases as charged hydrogen contents.

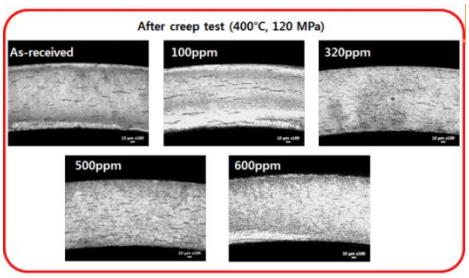

Fig. 5. Microstructure of Zircaloy-4 after creep deformation.

4. Conclusion

To clarify the effect of creep deformation on ductility, creep tests of unirradiated Zircaloy-4 cladding were performed below practical dry storage condition. To compare ductility before and after creep deformation, RCT at various temperatures were performed. That result implies that creep deformation does not have a significant effect on the ductility.

ACKNOWLEGMENTS

This work was supported by the Radioactive Waste Management Technology Program of the Korea Institute of Energy Technology Evaluation and Planning (KETEP), granted financial resource from the Ministry of Trade, Industry & Energy, Republic of Korea. (No. 2014171020166A)

REFERENCES

[1] J.D. Hong, E. Kim, Y.S. Yang, D.H. Kook, “Mechanical property degradation of unirradiated Zircaloy-4 cladding after creep deformation”, Nuclear Technology, *In Press*.

[2] A. Sarkar et al, “Creep Behavior of Hydrogenated Zirconium Alloys”, J. Mater. Eng. Perform. 23(10), 3649-3656 (2014).

[3] P. Bouffioux and N. Rupa, “Impact of Hydrogen on Plasticity and Creep of Unirradiated Zircaloy-4 Cladding Tubes”, ASTM STP 1354, 399-422 (2000).

Requirements for Direct Radiation From SNF Dry Storage Casks

Sunghwan Chung*, Kiyoung Kim, and Yongdeog Kim
Central Research Institute, Korea Hydro & Nuclear Power Co., Ltd.,
70, Yuseong-daero 1312beon-gil, Yuseong-gu, Daejeon, Republic of Korea
*sunghchung@khnp.co.kr

1. Introduction

Dry storage casks for spent nuclear fuel(SNF) must be designed to meet the regulatory requirements in Korea Nuclear Safety Act[1] and US 10CFR72[2]. Shielding features for SNF dry storage casks must restrict direct radiation dose so that total dose due to radiation from the casks is within the regulatory limits. And dose rates for dry storage casks must be consistent with ALARA principles, which are incorporated into storage cask design to the extent practical. But dose rate limits for protection against direct radiation from SNF dry storage casks are not explicitly specified in any domestic and foreign regulation. Radiation dose rate limits for SNF dry storage cask based on US and Korea regulatory requirements were examined.

2. Regulatory requirements

Regulations in US 10CFR72 require that SNF dry storage casks are designed to provide sufficient radiation protection during normal operations, off-normal conditions, accidents and natural phenomenon events, all of which are referred as design-basis conditions, and that shielding design descriptions of storage casks to be in compliance with regulatory limits. Radiation limits rely on a variety of factors of cask array geometry of storage facilities, working time in storage facilities such as monitoring or remote operations, proximity to work areas or public access areas and other limitations for cask operations.

US 10CFR72 establishes radiation dose limits for SNF dry storage facilities(Fig.1) including dry storage buildings(Fig.2) : annual normal operations dose limit is 0.25mSv (10CFR72. 104(a)) and accident exposure limit 50mSv(10CFR72. 106(b)), for individual on or beyond controlled area boundary of storage facilities.

But specific dose rate limits on individual dry storage casks is not imposed. In SRP of USNRC NUREG-1536[3], NRC has accepted surface dose rates on SNF dry storage casks from 0.2 to 4mSv/h in shielding assessment of canister-based storage cask designs(Fig.3). Radiation dose rate limits of transport casks under normal conditions of transportation in accordance with IAEA SSR-6[4] and US 10CFR71[5] is 2mSv/h on cask surfaces and 0.1mSv/h at 1m distance from casks for non-exclusive use or 10mSv/h on cask surfaces for exclusive use. These radiations dose rate limits are the same as those of Korea's regulatory requirements. Transportable dry storage casks(Fig.4) must be designed to meet these radiation dose rate limits for transport casks.

SNF dry storage facilities will be designated as a radiation control area. Radiation dose rate limits for the radiation control area shall be applied to the design of dry storage facilities in accordance with Korea's relevant regulations such as regulations on technical standards for radiation safety control[6]. In Article 3 of Regulation on technical standards, radiation dose rate limit outside the radiation control area is limited to 0.4mSv per week, which is based on annual worker exposure dose limit of 20mSv. And in Article 5 of regulation on technical standards, external radiation dose rate limits to maintain shielding capacity of maximum nuclear fuel materials storable at storage facilities is 1mSv per week, which is based on annual exposure dose limit of 50mSv. These limits are the same as design criteria on shielding structure of Korea NSSC notice for radiation protection[7].

Fig. 1. SNF dry storage facility.

Fig. 2. SNF dry storage building.

Fig. 3. Canister-based dry storage casks.

Fig. 4. Transportable dry storage casks.

3. Conclusion

Radiation shielding features of SNF dry storage casks must be sufficient for the design to fulfill the radiation dose requirements in the related regulations. US 10CFR72 establishes radiation limits of annual doses for normal operations and total dose from accidents, which are applied for individuals on or beyond controlled area boundary of SNF dry storage facilities. The regulations don't specify radiation limits for dry storage cask surfaces nor at distance from cask surfaces, unlike transport casks. Radiation dose rates on dry storage cask surfaces to comply with the radiation requirements of 10CFR72 depends on radiation dose limits of storage facilities including cask arrangement. Since SNF dry storage facilities including storage buildings will be designated as a radiation control area, the storage facilities shall be designed to meet radiation dose limits for the radiation control area in accordance with Korea regulations on technical standards for radiation safety control. Radiation dose rate limits outside SNF dry storage facilities shall not exceed 0.4mSv/week.

Radiation dose rate limits on dry storage cask surfaces are not specified in any domestic or foreign regulation. Although it is possible to refer to US regulatory guidance, it may be desirable to apply radiation dose limits for shielding structure design requirements of domestic regulations. Radiation dose rate limits for SNF dry storage casks shall not exceed 1mSv/week in accordance with Korea regulations on technical standards for radiation safety control. And transportable dry storage casks must be designed to meet radiation dose rate limits for transport casks in accordance with the related regulations.

However, radiation dose rate limits of the canister-based dry storage casks and the transportable dry storage casks differ from each other. Radiation dose rate limits of dry storage casks shall be set so that radiation dose rate limits of storage facilities are within radiation limits of the radiation control area, regardless of which storage casks are stored.

REFERENCES

[1] Korea Act No.14839, Nuclear Safety Act

[2] US 10 CFR Part 72, Licensing Requirements for the Independent Storage of Spent Nuclear Fuel

[3] USNRC NUREG-1536, Standard Review Plan for Spent Fuel Dry Storage Systems at a General License Facility

[4] IAEA Safety Standards Series No.SSR-6(2012 Edition), Regulations for the Safe Transport of Radioactive Material

[5] US 10 CFR Part 71, Packaging and Transportation of Radioactive Material

[6] Korea NSSC Regulation No.19, Regulations on Technical standards for Radiation Safety Control

[7] Korea NSSC Notice 2014-34, Radiation Protection

Criticality Safety Study for Loss of Single Fuel Rod From WH 14 Type Fuel

Janghwan Lim*, Manseok Do, Seongki Lee, and Jongsung Yoo
KEPCO NF, 242, Daedeok-daero 989beon-gil, Yuseong-gu, Daejeon, Republic of Korea
*jhlim@knfc.co.kr

1. Introduction

As of the end of June 2017, 17,574 assemblies of PWR type Spent Nuclear Fuel (SNF) and 430,576 bundles of PHWR type SNF are temporarily stored in the Spent Fuel Pool (SFP). It is expected that the storage capacity of the SFP in the Nuclear Power Plant (NPP) will be saturated in 2024, starting from Kori NPP. Thus it is necessary to transport SNF from NPP site to intermediate storage facilities. The objective of this study, the effect of single failed fuel rod is to confirm on the criticality safety whether is significant.

2. Background and Scope of Work

2.1 NUREG/CR-6835 [1]

The objective of this report is to investigate the consequences of potential fuel failure on criticality safety and external dose rates for SNF storage and transport casks, with emphasis on high-burnup SNF. Analyses were performed to assess the impact of several damaged/failed fuel scenarios on the effective neutron multiplication factor (k_{eff}) and external dose rates.

2.2 Failure Scenarios

For the criticality safety analyses, five different fuel failure scenarios that would impact criticality safety were defined and studied in [1]. Only scenario #1 (Individual fuel rod collapse resulting in rods being absent from the assembly lattice) is studied and will later the other scenarios

3. Analysis Results

3.1 KN-12 Transport Cask Basket Model

Using KENO-VI, a Monte Carlo transport simulation code included in the SCALE computer code system [2], basket-cell model was developed to perform criticality safety calculations for scenario #1. For conservative analysis, the basket was loaded with fresh PWR assemblies enriched to 5 wt% ^{235}U. The fuel assembly types are WH 14×14 fuel assemblies (STD, OFA).

3.2 Assumptions and Analysis results

Full water flooding was assumed, including water in the gap between the fuel pellets and cladding. All of the top and bottom end fittings, grid spacers, and other hardware were removed. The basket-cell models are reflected to form an infinite array (all direction) of fuel baskets conservatively.

Fuel failure scenario #1 was evaluated by comparing the calculated values of k_{eff} with multiplication factors from baseline basket-cell models with intact (undamaged) fuel assemblies. The baseline k_{eff} values are given in Table 1.

Table 1. Baseline calculated k_{eff} values with intact (undamaged) fuel

Fuel Type	Basket-cell model k_{eff}
14OFA	1.00208
14STD	0.99249

This scenario involves fuel failure which an individual fuel rod collapses, resulting in the removal of that rod from the assembly lattice. To conduct the analysis, each single rod in a basket-cell model was removed at a time to quantify its effect on k_{eff}. Fig.1 through 2 show the change in k_{eff} for removal of each single fuel rod in the 14×14 assembly lattice.

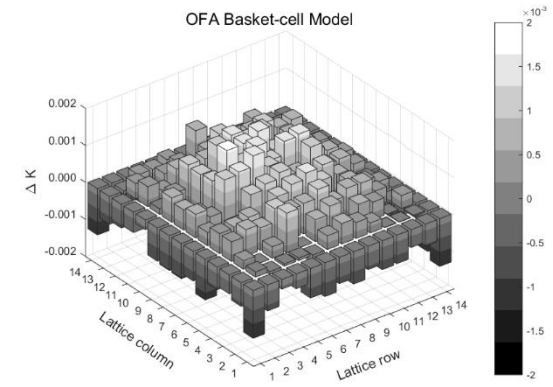

Fig. 1. Change in k_{eff} for single rod removal in the KN-12 basket cell for the 14×14 OFA fuel assembly.

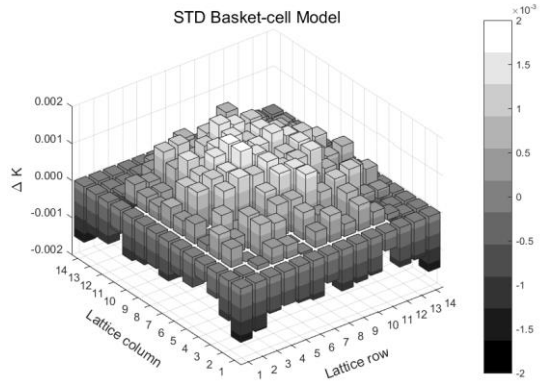

Fig. 2. Change in k_{eff} for single rod removal in the KN-12 basket cell for the 14×14 STD fuel assembly.

4. Conclusion

As a result, the Δk values(baseline – fuel rod loss position) of 14OFA was largest. The Δk values resulting from single rod removal in the basket-cell model range from -0.00129 for rods near the edge of the lattice to +0.00170 for rods near the center. Thus, it is confirmed that the study for the consequences of potential fuel failure is significant because fuel assemblies are designed to be undermoderated, and the loss of a fuel pin from the lattice causes a local area of higher moderation, which can increase k_{eff}.

ACKNOWLEDGEMENT

This work was supported by the Korea Institute of Energy Technology Evaluation and Planning (KETEP) and the Ministry of Trade, Industry & Energy (MOTIE) of the Republic of Korea (No.2014171020166C).

REFERENCES

[1] K.R. Elam, J.C. Wagner, and C.V. Parks, “Effects of Fuel Failure on Criticality Safety and Radiation Dose for Spent Fuel Casks”, NUREG/CR-6835, ORNL/TM-2002/255.

[2] B.T. Rearden, M.A. Jessee, “SCALE Code System”, ORNL/TM-2005/39 Version 6.2.1.

Reaction of Rare Earth Elements With UCl_3 in the LiCl-KCl Salt

Seungwoo Paek*, Dal-Sung Yoon, Si Hyung Kim, Junhyuk Jang, Gha-Young Kim, and Sung-Jai Lee
Korea Atomic Energy Research Institute, 111, Daedeok-daero 989beon-gil, Yuseong-gu, Daejeon, Republic of Korea
swpaek@kaeri.re.kr

1. Introduction

The pyroprocessing technology has been developed for the treatment of light-water reactor spent fuel, to recycle that fuel into sodium-cooled fast reactor in Korea Atomic Energy Research Institute [1]. TRU products supplied to SFR through pyroprocessing treatment may affect the combustion of nuclear fuel and the integrity of the fuel claddings if the rare earth content is high [2]. Accordingly, it is necessary to keep the rare earth content of TRU product as low as possible for SFR fuel to be used. In this study, we attempted to test the removal of rare earth elements from metal alloy of uranium, cerium, and neodymium using uranium tri-chloride as an oxidant.

2. Experimental

The metal alloy containing U, Nd, and Ce, was prepared by melting of metals in an induction melting furnace. The ratio of U/RE in the alloy was about 2.5 and the ratio of Ce/Nd was about 3. A STS crucible and mesh basket were used as reactor vessel and metal alloy holder, respectively.

All experiments were conducted in a glove box with purified argon and the concentration of oxygen and water were maintained to be below 5 ppm. The concentrations of each element in the salt were measured by ICP-OES. The surface of metal ingot was investigated by XRD and SEM-EDS. red, and in Times New Roman 13-point, boldface type. Capitalize the first letter of nouns, pronouns, verbs, adjectives, and adverbs. Leave one blank line after the title.

3. Results and Discussion

3.1 Reaction of RE metals with UCl_3

The RE elements in the U alloy can be removed by the reaction with UCl_3 according to the following equation.

$$RE(Nd/Ce) + UCl_3 = RE(Nd/Ce)Cl_3 + U \quad (1)$$

This reaction is based on the difference in Gibbs free energy of chloride formation, and the order of magnitude is Ce>Nd>U. Metals of Nd and Ce are then oxidized to $NdCl_3$ and $CeCl_3$ and UCl_3 is reduced to U metal. It is therefore possible to remove RE metals (Nd/Ce) from U alloy.

3.2 RE removal reaction

Fig. 1 shows the CV (Cyclic Voltammetry) curves before and after the reaction was terminated within one hour. In response to the reaction with the RE metals of U/RE ingot, UCl_3 peak was disappeared and RE chlorides peak was created.

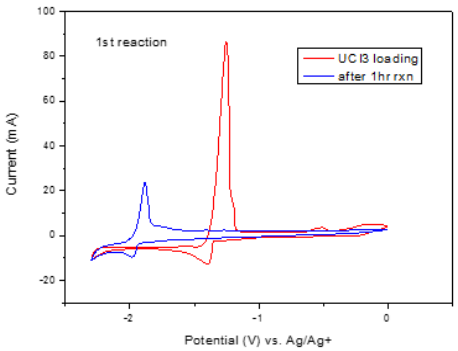

Fig. 1. CV curves of the reaction.

The changes in concentration of U, Nd, and Ce in the salt over the reaction time are shown in Table 1. Only UCl_3 existed in the salt before the reaction (S0), but after one hour (S1), UCl_3 was completely consumed and RE elements (Nd/Ce) were created. The concentration measured two hours after the reaction (S2) showed a concentration similar to that of S1 sample, indicating that the reaction was terminated within one hour. The concentration ratio of Ce/Nd in the salt after the reaction was approximately 3, which was equivalent to the ratio used in the preparation of the U/RE ingot. In order to review the mass balance of the experimental results, a comparison of the amount of UCl_3 used for the reaction with $RECl_3$ produced resulted in UCl_3 consumption was approximately 85 % of the $RECl_3$. This is considered to be reasonable value considering the experimental and analysis errors.

Table 1. Concentration of U, Nd, Ce in the salt by ICP analysis

(ppm)	U	Nd	Ce
S0	4956	ND	ND
S1	ND	746	2099
S2	ND	739	2013

4. Conclusions

In this study, as part of the study to remove the RE elements from the TRU product, which is a product of pyroprocessing, it was shown that experiment using UCl_3 as an oxidant allowed the RE elements to be effectively eliminated from an (U/RE) alloy.

ACKNOWLEDGEMENT

This work was supported by a National Research Foundation (NRF) grant funded by the Korean government (MSIP) (No.2017M2A8A5015079).

REFERENCES

[1] K. C. Song, et al., “Status of Pyroprocessing Development in Korea”, Nuclear Engineering and Technology, 42, 131-144 (2010).

[2] Y. I. Kim et al, “SFR Development Strategy for the Re-use of Spent Fuel in Korea”, Nuclear Engineering and Technology, 40(6), 517-526 (2008).

Safety Design Criteria for Spent Nuclear Fuel Cycle Facility

Woo Jin Jo*, Seok-Jun Seo, Siwan Noh, Hyo Jik Lee, and Seung Nam Yu

Korea Atomic Energy Research Institute, 111 Daedeok-daero, 989beon-gil, Daejeon, Republic of Korea

*wjjo@kaeri.re.kr

1. Introduction

As part of its international efforts to promote the recycling of Spent Nuclear Fuel for use of sustainable nuclear energy, the development and demonstration of Sodium-cooled Fast Reactor, and the increase of non-proliferation, KAERI conducted the preliminary concept design of the Korea Advanced Pyroprocessing Facility (KAPF) based on the design requirements and criteria.

As mentioned in the preliminary plan ('14), KAERI carried out a preliminary feasibility study on pyroprocessing that can review safety and safeguards to help license for large-scale pilot plants. However, the regulations and regulation guides that can be referenced in Korea are mostly applicable only to nuclear power plants among nuclear facilities, which is difficult to apply directly to KAPF. Therefore, KAERI are studying Integrated Safety Analysis (ISA) for nuclear fuel cycle facility using US-NRC regulation guidance and SECY reports. An ISA identifies potential accident sequences in the facility's operations and designates items relied on for safety (IROFS) to either prevent such accidents or mitigate their consequences to an acceptable level.

In this paper, the safety classification of nuclear power plants is analyzed and the applicability of Codes&Standards for the safety design of nuclear fuel cycle facilities such as KAPF is evaluated based on the analysis study as mentioned above in order to compensate the gap of domestic regulations and regulation guides

2. Safety Classification

2.1 Status of Safety Classification for Nuclear Power Plants

In Korea, the safety classification of the nuclear facilities, including the nuclear fuel cycle facilities and nuclear power plants, are established based on the Announcements of Nuclear Safety and Security Commission and KEPIC Standards. Because the background of such a safety classification eventually begins with safety analysis of the nuclear power plants, the requirements and technical standards applicable to only nuclear power plants are proposed. In particular, the Codes&Standards referred to in ANSI/ANS-51.1 say that the design of a nuclear power plants requires the integration of a number of interdisciplinary considerations to ensure that nuclear safety criteria are adequately identified and implemented.

2.2 Status of Safety Classicization for Nuclear Fuel Cycle Facilities

Domestic regulations on the nuclear fuel cycle facilities provide legal requirements such as permission, inspection, decommission and declaration in the Nuclear Safety Act Chapter 4 (Nuclear Fuel Cycle Business and Use, Etc. of Nuclear Materials). In addition, it refers to common regulatory oversight, supplementary provisions, and penalties as the nuclear facilities as well as the nuclear power plants.

More details on the nuclear fuel cycle facilities are mentioned in the enforcement rule of Nuclear Safety and Security Commission (Regulations on Technical Standards for Nuclear Reactor Facilities, Etc.). Chapter 3 of this enforcement rule provides comprehensive technical standards such as location, Structure, Installations, Performance, Operation, Quality Assurance, and Disassembly of the nuclear fuel cycle facilities. However, compared with the contents of Chapter 2 of this enforcement rule that provides for the nuclear reactors, so only Article 93 say that the material and structure of the vessels, pipes, pumps and valves that are utilized at the nuclear fuel cycle facilities and major supporting structures thereof shall meet the technical standards by the safety classes and standards. Even in Article

93, there is no guidance on detailed classification criteria or applicable items.

2.3 Limitation of safety classification of the nuclear fuel cycle facilities

As mentioned previously, relatively many discussions and developments in the nuclear power plants have resulted in a consistent framework, but very poor conditions at the nuclear fuel cycle facilities. The notice referred to in Article 93 of the Enforcement Rule of the Nuclear Safety and Security Commission, the only guidance for safety classification of the nuclear fuel cycle facilities, is based on ANSI/ANS-51.1-1983. This Codes&Stadnards only apply to the nuclear power plants. Nevertheless, Article 98 of the Enforcement Rule of the Nuclear Safety and Security Commission states that certain standards may not apply in those cased where it is acknowledged by the Nuclear Safety and Security Commission that such standards are not directly applicable to the nuclear fuel cycle facilities as the purpose of the facilities is for research/experiment or due to the facility and technical characteristics thereof, or that safety is not affected even if such standards are not applied. Therefore, for KAPF and other research facilities, there is a possibility to apply regulations that are similar to general industrial facilities.

3. Safety Design Criteria for KAPF

In this paper, safety classification was conducted by Integrated Safety Analysis (ISA). An ISA identifies potential accident sequences in the facility's operations and designates IROFS to either prevent such accidents or mitigate their consequences to an acceptable level.

3.1 Consequence categorization

Based on the KAPF preliminary feasibility study for facility safety results and ANSI/ANS-58.16-2014, a consequence classification was proposed as below:

KAPF ISA	ANSI/ANS-58.16-2014 safety categories
Very High Consequence	Hazard SC-3
High Consequence	Hazard SC-2
Intermediate Consequence	Hazard SC-1
Low Consequence	

3.2 Safety Design Criteria for KAPF

In this paper, Codes&Standards for SSC applicable to design basis accidents corresponding to SC-2, SC-3 are summarized as follows, referring to ANSI/ANS ANSI/ANS-58.16-2014 and DOE O 420.1C. However, if there is a separate Codes&Standards for the nuclear fuel cycle facilities, such as the nuclear power plants (ANSI/ANS-58.14), it should be prioritized.

Design Criteria	Classification	Standard number	Title
General Design Criteria	Single-failure criterion	IEEE STD 379 -2014	IEEE Standard for Application of the Single-Failure Criterion to Nuclear Power Generating Station Safety Systems
		ANSI/ANS-58.9 -2002 (R2015)	Single Failure Criteria for Light Water Reactor Safety-Related Fluid Systems
			. . .
	Quality Assurance	10 CFR Part 830, Subpart A	Quality Assurance Requirements
		DOE O 414.1D	Quality Assurance

4. Conclusion

In this paper, safety design criteria were established for deigning large-scale spent fuel processing facilities such as KAPF, and design, manufacture, construction, maintenance, and quality control of safety-critical structures, systems and components derived from ISA.

As already mentioned above, a consistent Codes&Standards or design was possible to apply for nuclear power plants since most structures are similar to those of the existing and new ones. However, there are no consistent regulations, guidelines, or Codes&Standards for the nuclear fuel cycle facilities, including large-scale spent fuel processing facilities with similar histories. It is true that the common regulatory or guidelines cannot be applied compared to the nuclear power plants because the nuclear fuel cycle facility is variable depending on the purpose and situation of them.

This paper attempts to establish a framework of Codes&Standards applicable to the spent nuclear processing facilities such as KAPF based on the results of preliminary safety analysis with KAPF preliminary concept design. Therefore, in order to design and construct such nuclear fuel cycle facilities at this time, use all of the Codes&Standards and guidelines that may be referenced by the licensee (designer, developer) prepare the licensing steps.

Applicability of the ANSI/ANS-58.16 on Pyroprocessing Facilities

Gilsung You*, Seokjun Seo, Woojin Jo, Siwan Noh, Hyojik Lee, Hohee Lee, Seungnam Yu, and Jeonghoe Ku
Korea Atomic Energy Research Institute, Daedeok-daero989ben-gil 111,Yuseong-gu, Daejeon, Republic of Korea
*yougil@kaeri.re.kr

1. Introduction

KAERI is being developed pyroprocessing technology for spent fuel recycling. For this it is necessary to develop a facility with hot cells, which can handle the processes safely [1]. In this paper the ANSI/ANS-58.16-2014 for nonreactor nuclear facilities, included fuel cycle facilities, was introduced and also studied for its applicability on pyroprocessing facilities developing in KAERI.

2. ANSI/ANS-58.16-2014 [2]

2.1 Scope and Purposes

The American National Standard Institute (ANSI)/American Nuclear Society (ANS) American National Standard ANSI/ANS-58.16-2014 provides criteria for the categorization of structures, systems, and components (SSCs) and specific administrative controls (SACs) as hazard controls, for nonreactor nuclear facilities. Standards for the design of hazard controls are identified based on a safety category (SC).

The safety categorization criteria specified in the standard will

(1) establish an objective and technically based rationale for the determination of safety categorization;

(2) ensure that all hazard controls required by the safety design basis are appropriately categorized;

(3) establish a basis for consistency (i.e., minimize categorization differences among similar items in a facility).

The purpose of the standard is the following:

(1) Specify criteria for categorization of safety SSCs;

(2) Select industry codes and standards for reliable design, construction, and operations commensurate with the safety categorization.

2.2 General safety criteria for safety categorization of controls

Safety Category	Unmitigated Consequences		
	Facility Worker	Collocated Worker	Public
SC-1 (Low Consequence)	Radiological/toxicological exposures to workers less than that in SC-2, but above regulatory limits for normal operations (i.e., defense-in-depth).	Radiological/toxicological exposures to workers less than that in SC-2, but above regulatory limits for normal operations (i.e., defense-in-depth).	Radiological/toxicological exposures to an individual of the public less than that in SC-2, but above regulatory limits for normal operations (i.e., defense-in-depth).
SC-2 (Intermediate Consequence)	Significant radiological/ toxicological exposures and potentially serious effects (may place workers' long-term health in question).	Significant radiological/ toxicological exposures and potentially serious effects (may place collocated workers' health in question).	Radiological/toxicological exposures to an individual of the public would not be expected to cause health consequences, but may require emergency response actions.
SC-3 (High Consequence)	Radiological/toxicological exposures that potentially endanger life if not limited.	Radiological/toxicological exposures that potentially endanger life if not limited.	Radiological/toxicological exposures that may cause long-lasting health effects to an individual of the public.

2.3 Design Criteria

Once the safety functions and SCs needed for protection of the public, collocated workers, and facility workers are identified, this information shall be translated into selected hazard controls (SSCs and/or SACs) and design requirements for SC-2 and SC-3 hazard controls as discussed below categories.

- General Design Criteria
- Civil-structural
- Mechanical

• process system; ventilation system; handling equipment; fire safety equipment; explosion safety equipment
- Electrical, instrumentation, and controls
- Quality assurance
- Specific administrative controls

3. Applicability of the ANSI/ANS-58.16 on Pyroprocessing Facilities

In Korea SF recycling facilities are regulated as one of fuel cycle facilities under the Korean nuclear safety law [3]. The law describes the safety requirements for the license and operation of fuel cycle facilities. Although the safety requirements for fuel cycle facilities are a little different compared with those of nuclear power plants, but a large parts of the requirements use the same technical criteria with nuclear power plants. The Korean nuclear safety law for fuel cycle facilities does not require some different safety classifications and industrial standard codes, which are different from those of nuclear power plants.

The United States also did not have a standard safety classification and the adaptable industrial standard codes for fuel cycle facilities. US NRC and DOE regulate fuel cycle facilities to use some safety classification and analysis methods different with nuclear reactors. In 2014 the ANSI/ANS published the standard, ANSI/ANS-58.16-2014, for the nonreactor nuclear facilities. As introduced in the section 2, the ANSI/ANS-58.16-2014 requires the safety classification and adaptable industrial codes of the nonreactor nuclear facilities different from those of the nuclear reactor facilities. In the future US NRC and DOE will be expected to change the regulation methods and criteria following to the ANSI/ANS-58.16-2014.

Korea has the same regulation structures with US NRC for the most parts of nuclear power plants, and the regulations of the fuel cycle facilities are the same with nuclear power plants. The Korean safety classification and adaptable industrial standard codes for fuel cycle facilities, therefore, are nearly the same with those of US NRC for nuclear power plants.

If Korean nuclear safety law for fuel cycle facilities will be changed to refer or to follow the ANSI/ANS-58.16-2014, the regulatory bodies can check and test by using more specific safety criteria for fuel cycle facilities. This will be able to increase a total and some detail safeties of fuel cycle facilities including pyroprocessing facilities.

4. Conclusions

Korea has nearly the same nuclear regulation structures with those of the US NRC adaptable for nuclear power plants. The Korean regulations for fuel cycle facilities are also the same with nuclear power plants. The Korean safety classification and adaptable industrial standard codes for fuel cycle facilities, therefore, are nearly the same with those of the US NRC for nuclear power plants.

In 2014 the ANSI/ANS published the standard, ANSI/ANS-58.16-2014, for the nonreactor nuclear facilities as introduced in the Section 2.

If Korean nuclear safety law for fuel cycle facilities will be changed to refer or to follow the ANSI/ANS-58.16-2014, it is expected that the safety of pyroprocessing facilities also will be increased.

REFERENCES

[1] Gil-Sung You, et al., “Concept and safety studies of an integrated pyroprocess facility, Nuclear Engineering Design,” No. 241, pp. 415～424 (2011)
[2] ANSI/ANS, “Safety categorization and design criteria for nonreactor nuclear facilities,” ANSI/ANS 58.16-2014 (2014)
[3] Korean Nuclear Safety Law

Preliminary Evaluation of Process Equipment Test Mock-up for Construction of Drying System

Byungsuk Park*, Jaehoon Lim, Dongseok Ryu, Jonghui Han, and Seungnam Yu

Korea Atomic Energy Research Institute, Daedeok-daero989ben-gil 111,Yuseong-gu, Daejeon, Republic of Korea

*nbspark@kaeri.re.kr

1. Introduction

Pyro-process researches are performed in a salt environment. Because salt causes corrosion, moisture in air must be removed. At the development stage, however, workers and test equipment must be able to access frerly. Thus, as a part of the construction of the drying room, the room of the panel structure except the drying system was constructed first. In this study, we introduce the basic test results for the constructed room.

2. Mock-up for Process Equipment Test

The mock-up for process equipment test consists of an auxiliary room and a process room. The auxiliary room ($8m^3$) serves as an access passage for workers or process equipment between the outside of the mock-up and the process room. The door sizes of the rooms are 1.3m (W) x 1.9m (H), respectively. The door of the auxiliary room is a rotation type with airtight and the door of the process room is a slide type. The process room ($104m^3$) has two tempered glass windows on the front and right side and a double ceiling structure. Below the first ceiling, a gantry crane with a capacity of 0.5 ton was installed, and a gantry handling system was installed under the crane. The 25A pipe was extended to the inside of the process room to supply the compressed dry air provided by the KAERI.

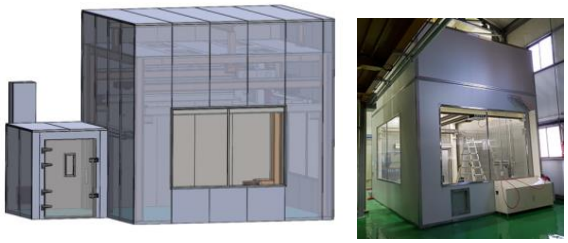

Fig.1. Mock-up for Process Equipment Test.

3. Preliminary Evaluation

3.1 Purging with Dry Air

As shown in Fig. 2, the compressed dry air is supplied into the process room through a floating area flowmeter (model GA-101, air 1~10 CMH) installed in the compressed air pipe (25A). The supply flow rate is set by reading the scale by adjusting the manual valve attached to the front of the flow meter with tick mark. The dew point of dry air supplied by the KAERI is below -40 °C. The dew point inside the room is measured with a dewpoint transmitter (VAISALA, Model DMT143, -80 to 20 ℃ Td).

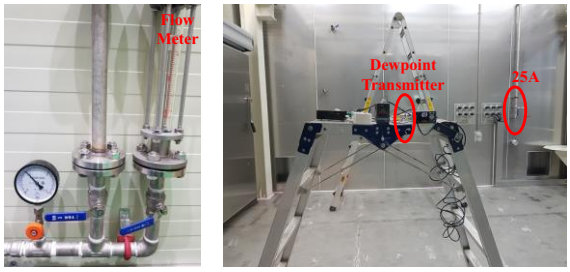

Fig.2. Flow Meter and Dewpoint Transmitter.

3.2 Leak Test of Mock-up

To calculate the leak rate of the mock-up, a test was performed to purge the dry air. When a constant flow is continuously supplied to the mock-up, the pressure remains constant after a certain period of time.

This is the leakage rate at that pressure. Table 1 shows the pressure information obtained while changing the purge flow rate.

As the pressure increases, it is shown that leakage rate increases.

Table 1. Pressure according to Purge Flow Rate

Flow Rate (CMH)	Pressure (mmAq)
1	1.2
2	1.4
3	1.8
4	2.3
5	2.8
6	3.5
7	4.3
8	4.8
9	5.5
10	6.4

3.3 Dew Point Test with Constant Purge Flow

It was purged at a flow rate of 10CMH inside the process room of the mock-up. The initial dew point of the process room was 3.6 ℃ (about 8,000 ppm), and after 10 days, the dew point was -40 ℃ (about 127 ppm). Fig. 3 shows the results.

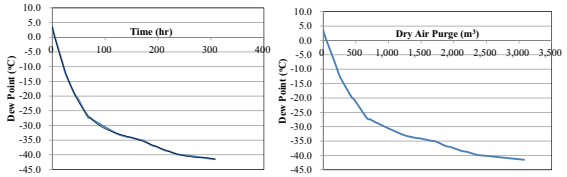

Fig. 3. Dry Air Purge with 10 CMH.

3.4 Dew Point Test with Variable Purge Flow

The dew point was measured while changing the purge flow rate to observe the dew point change. As shown in Table 2, when the purge flow rate is decreased from 10 CMH to 1CMH, the dew point is increased. The dew point is increased even if the flow rate is increased up from 1 CMH to 4 CMH. When the flow rate exceeds 5 CMH, the dew point is not increased but decreased.

Table 2. Dew Point according to Purge Flow Rate

Flow Rate (CMH)	Purge Time (hr)	Dew Point (°C)	Δ•∇	Pressure (mmAq)
10	-	-44.7	-	6.4
1	14	-41.2	Δ	1.2
2	5.5	-40.3	Δ	1.4
3	3.5	-40.1	Δ	1.8
4	44	-39.3	Δ	2.3
5	19	-40.2	∇	2.8
6	8	-40.9	∇	3.5

4. Conclusion

From the test results, it was confirmed that dry air should be purged above 5 CMH to maintain the dew point below -40℃. We plan to utilize the results to build a hybrid drying system in the future.

REFERENCES

[1] Byungsuk Park, et al., “A Consideration on the Dehumidification Methods for Designing the Dry Room”, Proc. of the KRS 2017 Autumn Conference, 15(2), 109-110.

Critical Effect According to Number of Spent Fuel Nuclide

KIM Yun-sik[a*] and Kim Ki-Young[b]

[a] Korea Nuclear Engineering & Service corp. 341-4 Jangdae-dong, Yueong-Gu, Daejeon, Republic of Korea

[b] Korea Hydro & Nuclear Power Co., Ltd. 1312, Yueong-daero, Yueong-Gu, Daejeon, Republic of Korea

[*] yunsik@kones21.com

1. Introduction

Spent fuel nuclides are important variables on the effect of burnup credit in criticality analysis of spent fuel pool and transportation / storage cask.

This paper shows that criticality reactivity changes according to the number of spent fuel nuclides applied to the analysis in the same wet spent fuel pool system.

2. Modeling Approach and Assumptions

2.1 Spent Fuel

The spent fuel data applied to the analysis are as follows.

- Design : 17x17 WH V5H
- Enrichment : 4.5wt%
- Burnup : 45,000MWd/MTU
- Cooling : 5 year

2.2 Spent fuel pool

The spent fuel pool is modeled as an infinite array of 2x2 model as shown in Figure 1 below. To model the isotopic content of fuel assembly in three dimensions, the axial burnup profiles from NUREG/CR-6801 are used. [1]

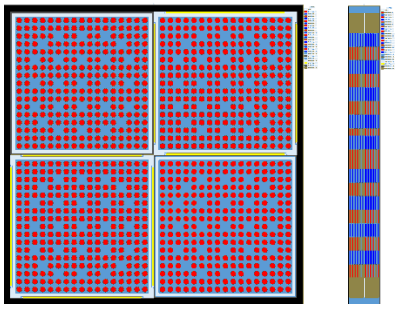

Fig. 1. Analysis model.

2.3 Computer Codes, Cross Section Library

For this analysis, SCALE 6.1 and the 238-group ENDF/B-VII cross section library was used. SCALE 6.1 is the most recent release of the SCALE code system which has been heavily used throughout the world for criticality analysis. The SCALE code system is a series of modules run by sequence drivers. For this work, TRITON sequence was used for depletion and CSAS5 sequence was used for calculation of k_{eff}. [2]

2.4 nuclides used in the analysis

The nuclides used in the analysis were sorted in ascending order of the number density of the nuclides, and the number was increased by 20 each.

First, we selected 28 nuclides from NUREG-6665. In the second, 22 nuclides were added to the above nuclides to select 50 nuclides. From the third, up to 310 nuclides were selected by adding 20 nuclides. [3]

3. Analysis Result

The criticality calculations were performed for 15 cases. As a result of calculation, the reactivity decreased as the number of nuclides increased as shown in Table 1 and Fig. 2. When 28 nuclides of NUREG-6665 were applied, the reactivity was 0.91544, and when 310 nuclides were applied, it was 0.89279. The reactivity difference between the maximum case and the minimum case was 0.02295.

Table 1. Result of criticality calculations for each case

Number of nuclides	$k_{-eff} \pm \sigma$
28	0.91544 ±0.00020
50	0.91366 ±0.00020
70	0.90583 ±0.00019
90	0.90066 ±0.00018
110	0.89795 ±0.00020
130	0.89554 ±0.00019
150	0.89385 ±0.00020
170	0.89401 ±0.00019
190	0.89279 ±0.00019
210	0.89250 ±0.00018
230	0.89271 ±0.00019
250	0.89252 ±0.00018
270	0.89299 ±0.00022
290	0.89249 ±0.00020
310	0.89279 ±0.00019

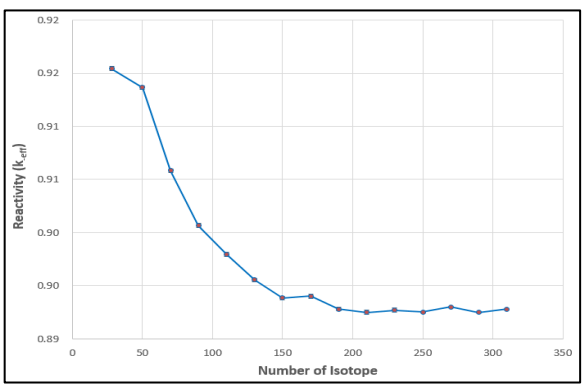

Fig. 2. Trend of reactivity change for each case.

4. Conclusions

This paper shows that criticality reactivity changes according to the number of spent fuel nuclides applied to the analysis. 15 cases from 28 to 310 depending on the number of spent nuclear fuel nuclides were calculated. As a result of calculation, the reactivity decreased as the number of nuclides increased. And reactivity converged after 150 nuclides. Therefore, it is considered that the number of nuclides to be applied in the critical analysis is selected to be approximately 150 based on the number density of radionuclides. The results of this study are expected to be used as basic data for the selection of the critical analysis applied nuclides based on burnup credit.

REFERENCES

[1] J.C. Wagner, M. D. DeHart, and, C. V. Parks, Recommendations for Addressing Axial Burnup in PWR Burnup Credit Analyses, US NRC, NUREG/CR-6801, Oak Ridge National Laboratory, 2003.

[2] Scale. A Comprehensive Modeling and Simulation Suite for Nuclear Safety Analysis and Design, Version 6.1, 2011.

[3] C. V. Parks, M. D. DeHart, and J.C. Wagner, Review and Prioritizationo f Technical Issues Related to Burnup Credit for LWR Fuel, US NRC, NUREG/CR-6665, Oak Ridge National Laboratory, 2000.

Fuel Integrity Evaluation During the Dry Storage by FRAPCON

Suji Yoon[a], Kwang heon Park[a*], Hyung ju Yun, and Wu seung You

[a]Department of Nuclear Engineering, Kyung Hee University, 1732 Deokyoungdaero, Giheung-gu, 17104, Yongin-Si, Republic of Korea

[*] kpark@khu.ac.kr

1. Introduction

Currently, it is needed to store spent nuclear fuels in dry condition(dry storage). During the dry storage, spent fuels have to meet regulatory requirement. Regulatory commission limits the cladding temperature to 400℃ for fuel with a burnup greater than 45 GWD/MTU. The 400℃ is set to prevent damage of the fuel rod cladding and the dry storage cask components related to high temperature. Also, it is important to analyze the hoop stress and determine if it remains below the 90 MPa for hydride reorientation in high-burnup fuel.

Recently, David j. Richmond[3] shows that the hoop stress may be related to the axial cladding temperature and oxidation profiles of the rods as well as the rod internal pressure at the end of life and in storage[3].

The aim of this paper is to predict spent fuel integrity evaluation such as the axial cladding temperature and the hoop stress in the dry storage.

2. Methods and Results

2.1 Analysis methods

FRAPCON-4.0 and COBRA-SFS were used. FRAPCON-4.0 is the fuel performance code in reactor and also calculates the peak cladding temperature in the dry storage though spent fuel module. To predict accurately the axial and peak cladding temperature in the dry storage, COBRA-SFS is used to reflect the geometry of dry storage cask. Westinghouse assembly (WH 15 x 15) and TN-24P dry cask were used. The major specifications provide in Table 1 and Table 2.

Table 1. WH 15 x 15 Major specifications

Description	Value
Cladding outer diameter	10.71 (mm)
Cladding thickness	0.62(mm)
Total (active) fuel length	3658 (mm)
Fuel U-235 enrichment	3.2 (a/o)
Cladding type	Zry-4

Table 2. TN-24P Major specifications

Description	Value
Cask outer diameter	2281(mm)
Cask length	5063(mm)
Loaded Weight	100(ton)
Basket length	4121(mm)
Basket material	Aluminum
Backfill	Helium

2.1.1 Cladding Temperature. The cladding temperature is calculated by COBRA-SFS with the burnup information which was calculated from FRAPCON-4.0. FRAPCON-4.0 can calculate the axial burnup distribution and the average burnup. The axial burnup distribution is the important factor to predict the axial cladding temperature because it depends on operation. So, FRAPCON-4.0 and COBRA-SFS were connected for calculation.

2.1.2 Hoop stress. In FRAPCON-4.0, The cladding hoop stress, σ, is calculated according to eq[1].

$$\sigma = \frac{r_i P_i - r_o P_O}{t} \quad (1)$$

The outer diameter of the cladding is changed along with cladding oxidation. It can reduce Zircaloy metal thickness. Ratio of a oxide thickness to Zircaloy metal consumption is 1.56. But, FRAPCON-4.0 uses multiplying related to ratio.

To calculate the hoop stress in dry storage, burned fuel information such as rod internal pressure, axial cladding temperature, hoop stress is used. It was calculated with ideal gas equation.

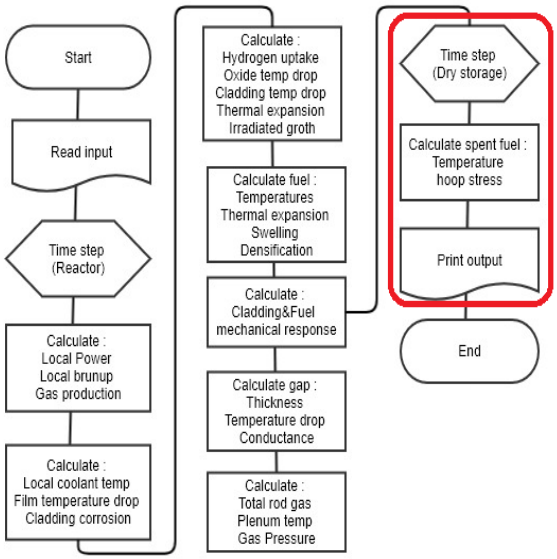

Fig. 1. Flowchart of analysis methods.

2.2 Results

Fig. 2 shows the peak cladding temperature at 53GWD/MTU. The peak cladding temperature decreased sharply before the storage time of about 40year. Fig.3 shows the axial cladding temperature. The axial temperature distribution depends on storage time. It is nearly uniform after 40year. Fig.4 shows axial hoop stress.

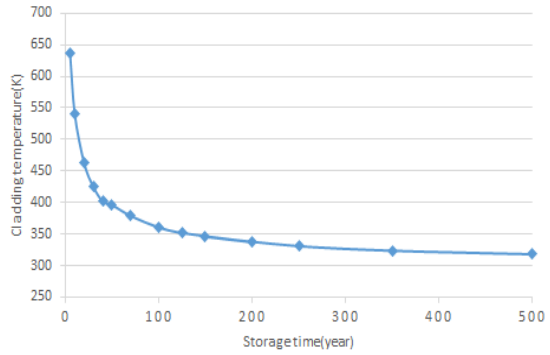

Fig. 2. Peak Cladding Temperature.

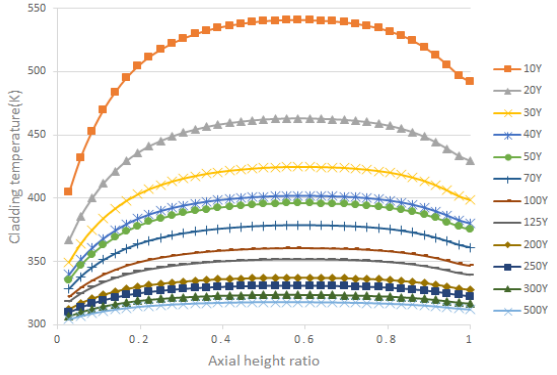

Fig. 3. Axial Cladding Temperature.

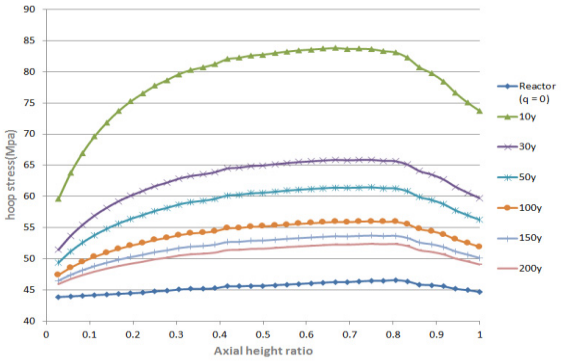

Fig. 4. Axial Hoop Stress.

3. Conclusion

To predict the cladding temperature and hoop stress of spent fuel is very important for integrity evaluation during the dry storage. The axial temperature and hoop stress during dry storage will give information such as the weakest location. If the locations of the maximum temperature and hoop stress are same, it will be weaker than other location.

REFERENCES

[1] FRAPCON-4.0: A Computer Code for the Calculation of Steady-State, Thermal-Mechanical Behavior of Oxide Fuel Rods for High Burnup.

[2] COBRA-SFS: A THERMAL-HYDRAULIC ANALYSIS CODE FOR SPENT FUEL STORAGE AND TRANSPORTATION CASKS.

[3] David J. Richmond, “FRAPCON analysis of cladding performance during dry storage operations”, Nuclear Engineering and Technology (2018).

[4] F. Feria, L.E. Herranz, J. Penalva “On the way to enabling FRAPCON-3 to model spent fuel under dry storage conditions: The thermal evolution”, Annals of Nuclear Energy (2015).

Numerical Simulations of the Flow Field in a Vacuum Chamber for the Drying Test Equipment of Spent Fuel

Ju-Chan Lee, K.S. Bang, S.H. Yu, S.S. Cho, and W.S. Choi
Korea Atomic Energy Research Institute, Daedeok-daero989ben-gil 111,Yuseong-gu, Daejeon, Republic of Korea
sjclee@kaeri.re.kr

1. Introduction

Drying equipment is being developed for the dry storage of spent fuel. There are two types of drying system, vacuum and forced helium drying [1]. The vacuum drying process depends on the reduced pressure to evaporate moisture from the spent fuel cask. CFD analyses were performed to simulate the flow field in a vacuum chamber for the drying test equipment.

2. Flow Field for Vacuum Analysis

At a low pressure such as a vacuum chamber, the gas behaves differently from standard conditions. To distinguish the flow regimes, the Knudsen number(K_n) is defined as follows.

$$k_n = \frac{\lambda}{L} \quad (1)$$

$$\lambda = \frac{k_B T}{\sqrt{2}\pi d^2 P} \quad (2)$$

Where,

λ : mean free path [m]
L : characteristic length of chamber [m]
K_B : Boltzmann's constant [J/K]
T : temperature [K]
P : pressure [Pa]
d : diameter of molecule [m]

Based on the Knudsen number, the kinetic gas flow can be classed into three regimes[2].

- Viscous flow : Kn < 0.01
- Transient flow : 0.01 < Kn < 1
- Free molecular flow : Kn > 1

Table 1 shows some typical values for air at different pressures of room temperature [3]. K_n is calculated with the mean free path and the chamber length of 0.5 m.

The pressure of the vacuum chamber is expected to be within about 400 Pa(3 Torr). In this low vacuum pressure, the K_n is estimated to be about 2.0E-04. Therefore, the viscous flow can be applied for the CFD analysis of the vacuum chamber.

Table 1. Mean free path and Knudsen numbers

Vacuum rage	Absolute P.(Pa)	Mean free path(m)	Knudsen number(K_n)
Atmosphere	1.0E+05	6.8E-08	1.4E-07
Low Vacuum	1.0E+04	2.5E-07	5.0E-07
	1.0E+02	1.0E-04	2.0E-04
Medium Vacuum	1.0E+01	1.0E-03	2.0E-03
	1.0E+00	1.0E-02	2.0E-02
High Vacuum	1.0E-02	1.0E+00	2.0E+00
	1.0E-03	1.0E+01	2.0E+01

3. Flow Analysis Model

Three dimensional CFD analysis model was constructed for a vacuum chamber as shown in Fig. 1. The outer diameter and internal length of the chamber are 406 mm, 500 mm, respectively. The internal volume of the chamber is 51.8 liter.

W2V60 vacuum rotary vane pump is connected to the suction port of the canister. The pumping speed is 600 liter/min. The suction port of the pump is NW 40 with inner diameter of 32 mm. The velocity at the suction port is calculated with 12.4 m/s in the atmospheric pressure. Fig. 2 shows the performance curve for the vacuum pump. The pumping speed is rapidly decreasing as the pressure drops below 1.0E-03 Pa.

Velocity inlet boundary condition is considered in the suction port. Velocities in the port are considered with constant value of 12.4 m/s and P-V(Pressure-Velocity) curve utilizing Fluent's User Defined Functions(UDF). The P-V curve is obtained from the pump's performance curve.

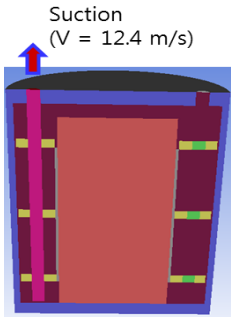

Fig. 1. CFD model.

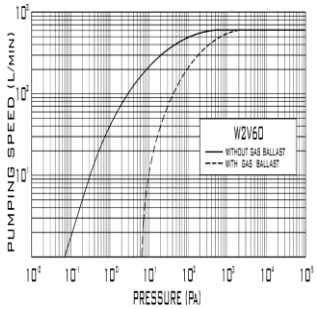

Fig. 2. Performance curve.

4. Results and Discussion

CFD analyses for the vacuum chamber were performed under the evacuation velocities at the constant and P-V curve. Fig. 3 shows the pressure and velocity distributions in the chamber according to the evacuation time. Fig. 4 shows the pressure and density contours for the P-V curve velocity condition.

At the constant velocity condition, the internal pressure dropped more rapidly than the P-V curve velocity condition. As the internal pressure decreases, the performance of the vacuum pump decreases and velocity also decreases. Therefore, P-V curve velocity should be considered to for the vacuum process.

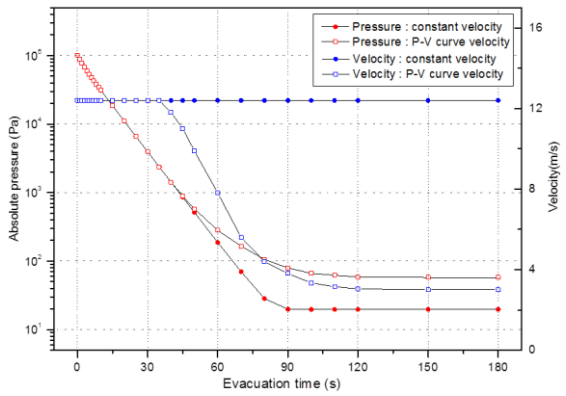

Fig. 3. Pressure and velocity distributions.

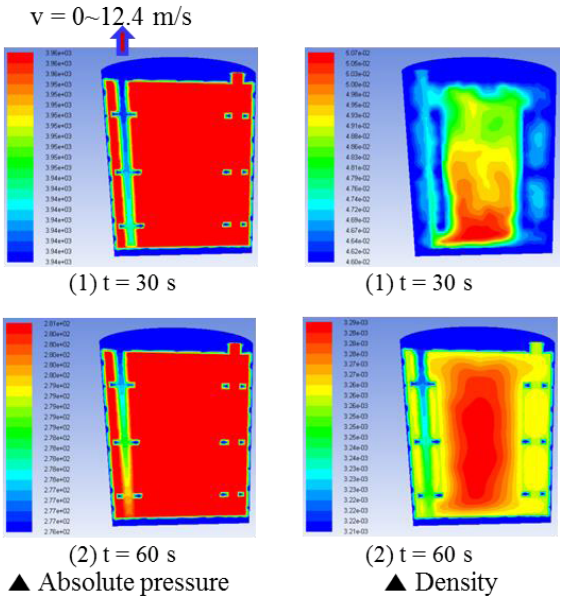

Fig. 4. Pressure and density contours.

5. Conclusion

The Knudsen number was estimated to distinguish the flow state for the vacuum chamber, and the viscous flow can be applied for the CFD analysis. The internal pressure dropped more rapidly at the constant velocity than the P-V curve velocity. The results of this study can be used as the basic data for the design and test of the vacuum drying equipment.

REFERENCES

[1] ASTM C-1553-16, “Standard Guide for Drying Behavior of Spent Nuclear Fuel, ASTM, 2016.

[2] Oerlikon Leybold Vacuum, Fundamentals of vacuum technology, 2007.

[3] Brunglinghaus, Marion, “Mean free path”, European Nuclear Society, Retrieved 2011.11.8.

Design of an Actuation Module for a Cathode Basket Lifting Mechanism

Doyeon Kim*, Dongseok Ryu, and Seungnam Yu
Korea Atomic Energy Research Institute, 989-111 Daedeok-Daero Yuseong-Gu, Deajeon, Republic of Korea
*doyeon1301@kaeri.re.kr

1. Introduction

Pyroprocessing, a method to recycle spent fuels, has been studied to reduce down high radiation waste. The facilities such as PRIDE and ACPF have been constructed to perform engineering scale experiments at KAERI (Korea Atomic Energy Research Institute). In order to maintain systematic operation and stable performance of the process equipment, a way to automation should be considered in process operation.

The PAVM (Pyroprocessing Automation Verifying Mockup) was proposed to provide the experimental space dedicated to the mechanical feasibility of equipment, including automation function [1].

In this study, an actuation module for a basket lifting mechanism of equipment in PAVM is discussed.

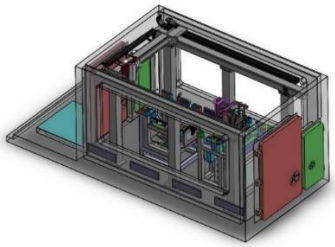

Fig. 1. PAVM (Pyroprocessing Automation Verifying Mockup).

2. Actuation module for cathode basket lifting mechanism

2.1 Automation concept of basket lifting module

Pyroprocessing is composed of several sub-processes, including an electrolytic reduction process.

The purpose of the electrolytic reduction process is to turn the uranium oxides to uranium metals. The oxides fuels are loaded at cathode in molten LiCl containing Li_2O so as to dissolve oxide ions. The basket-shaped cathode should be replaced at each batch of the oxide reduction process [2].

The repeated operations of basket to immerse into and put out of molten salt are difficult and dangerous. Only with the manual remote operation, it is not reliable and safe. Some dedicated mechanism is desirable.

For simple and convenience handling of the cathode basket, the basket lifting module was proposed. It was designed as an assembly of four modules, a testing basket, a basket socket, a fork lift module, and an actuation module, as shown in Fig. 2.

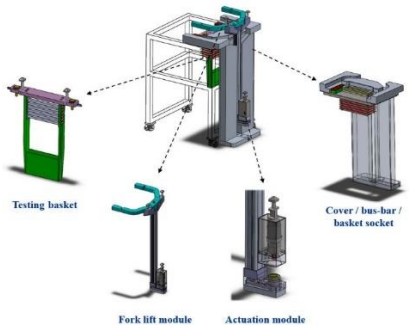

Fig. 2. A modular design of the basket lifting mechanism.

The mechanism is modularized and the basket automatically moves by lifting module.

2.2 Design of the actuation module

The actuation module in basket lifting mechanism

is designed to meet two requirements. The first is easiness of combine, and the second is simultaneous electric connection when the module is mechanically combined. To meet the first requirement, tapered guide faces are shaped on the contact surfaces. A mechanical coupler for torque transmission is compliant for convenience in attachment. For the second requirement, the spring loaded pins were utilized. Spring loaded pin, acting as a connector, contacts provide a reliable electrical and mechanical connection. As a feature of the spring loaded pin, the electrical power and signals to actuation module are keep connected reliably in the cases of uneven mating surfaces, different floating heights, or even exposure to extreme vibration. The figure 3 shows the spring loaded pin.

Fig. 3. Spring loaded pin.

Due to the electrical integration by the spring loaded pins, as a power source, the mechanical connection of the actuator and the basket lifting module is activated. And then, a motor gear is engaged to drive the belt and actuate the lift module.

The actuator are designed as modules which have a docking knob is attached on the top of the actuation module, considered to be easily maintained by using the automated handling device [3].

When the actuation module is simply loaded on the assembly, the tapered faces guide and align the actuation modules to the exact position. The weight of the actuation modules pushes the spring loaded pins to keep contact electrically.

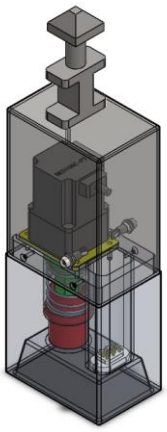

Fig. 4. Mechanical and electrical integrated connection actuation module.

3. Conclusion

The actuation module for basket lifting mechanism was designed in this research. The main concept of actuator is to utilize a spring loaded pin embedded in the module as a connector. After the pin is electrically connected, the motor is activated to move the fork lift module. In terms of maintenance, a docking knob was designed on the top of the actuator to make it easy to handle automated device.

REFERENCES

[1] Dongseok Ryu, et al. "Needs and Goals of Pyroprocessing Automation Verification Mock up," Proc. of Korea Radioactive Waste Society 2017 Spring, pp. 53-54, 2017.

[2] Eun-young Choi, et al. "Scale-up of electrochemical reduction process," Proc. of KECS 2013, pp. 15, 2013.

[3] Dongseok Ryu, et al. "Example Operating Procedure for an Automation Concept of Electrochemical Process," Proc. of KRWS 2017 Spring, pp. 151-2, 2017.

Hydrogen Content Effects on Delayed Hydride Cracking in Zircaloy-4 Cladding

Wooyong Choi and Kwangheon Park *

Nuclear Engr. Department, Kyung Hee Univ., 1732 Deogyeong-daero, Giheung-gu, Yongin-si, Gyeonggi-do, Republic of Korea

kpark@khu.ac.kr

1. Introduction

Since Delayed Hydride Cracking (DHC) is observed from pressure tubes of Zr-2.5Nb alloy, there have been lots of studies of DHC. Recently, spent nuclear fuel dry storage period is getting longer in many countries. So, DHC is re-considered as a possible mechanism for the degradation of zirconium alloy fuel cladding. Also, because of long period operation, burn-up of spent nuclear fuel and hydrogen contents of cladding is getting higher. For that reason, the relation between hydride content in zircaloy-4 cladding and delayed hydride cracking was evaluated experimentally in this paper.

2. Delayed Hydride Cracking Experiment

2.1 Specimen

Zircaloy-4 tube was used as a specimen. For hydrogen charging, 150 mm Zircaloy-4 tubes were located in an electric furnace and heated up to 400℃ with hydrogen gas. After hydrogen charging, the specimens were sealed in vacuumed quartz and treated at 400 ℃ for 24 hours to homogenize hydrogen distribution in the specimens. To confirm hydrogen content, hot vacuum extraction method was used and the hydrogen content of each specimens are shown in Table 1.

Table 1. Hydrogen content of specimens

	S1	S2	S3	S4
Hydrogen content (wppm)	173.3	247.0	304.0	599.3

2.2 Experiment equipment

Experiment was conducted by Pin Loading Test method developed in Studsvik. Pin loading fixture, shown in Fig. 1, was prepared and located at the center of equipment. To control the temperature of specimen, heater was set up, surrounding the specimen. At the bottom of the bar, connected to PLT fixture, weight disk was hanged.

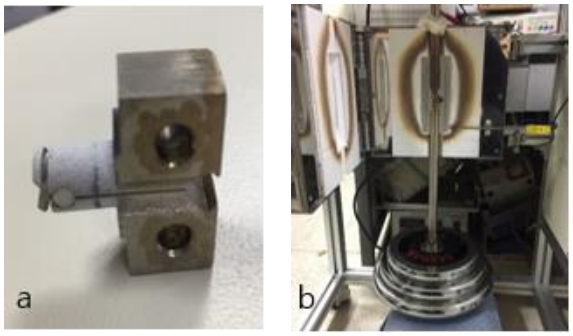

Fig. 1. (a) Pin Loading Test fixture, (b) Heater and Tensioning Tester.

2.3 Experimental condition

Experimental condition is described in Fig. 2. The temperature was increased from room temperature to 400℃. After an hour holding 400℃, the temperature decreased to test temperature which was 250℃. To minimize temperature fluctuation, the temperature

was held for 30 minutes before loading. After loading weight, the condition of experiment was maintained for 20 hours. Different hydrogen content specimens were experimented same as above.

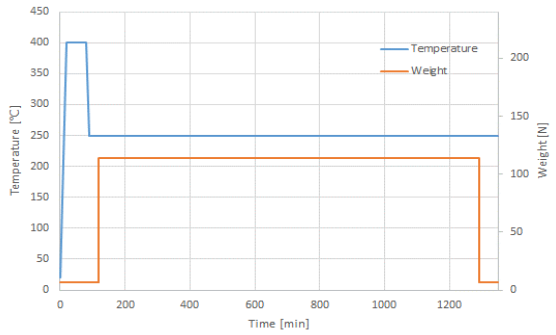

Fig. 2. The experimental condition of temperature and weight.

2.4 Experiment result

Firstly, relation between hydrogen content and delayed hydride crack initiation weight was tested. When the loading weight was 89.2 N, DHC wasn't occurred at S1 specimen but DHC was occurred at S2 and S3 specimens. Even, when S4 specimen was tested, DHC was occurred with lower weight which was 79.4 N. It means that DHC occurring weight was lower when hydrogen content was higher.

Also, DHC crack growth rate was tested when the loading weight was increased. The result showed that DHC growth rate was faster when the loading weight was increased.

Table 2 shows the result of crack growth rate and stress intensity factor at the different hydrogen content specimens. From the result, it is possible to estimate K_I threshold range for each hydrogen content specimens.

Table 2. DHC crack growth rate and stress intensity factor of different hydrogen content specimens depending on loading weight

	Weight [N]	**Crack growth [mm]**	**Crack growth rate [m/s]**	**K_I [MPam$^{1/2}$]**
S1	89.2	0	0	6.12
	113.7	0.18	2.50E-09	8.83
	138.2	0.583	8.10E-09	
S2	79.4	0	0	5.58
	89.2	0.059	8.19E-10	6.27
	113.7	0.478	6.64E-09	
	138.2	0.611	8.49E-09	
S3	79.4	0	0	5.41
	89.2	0.088	1.22E-09	6.07
	113.7	0.611	8.49E-09	
	138.2	0.644	8.94E-09	
S4	69.6	0	0	5.06
	79.4	0.18	2.5E-09	5.17
	89.2	1.15	1.6E-08	
	113.7	1.05	1.46E-08	
	138.2	1.06	1.47E-08	

3. Conclusion

In this study, hydrogen content effects on DHC was estimated by using PLT specimen. According to experiment result, when the hydrogen content was higher, DHC occurring load was lower and when the loading weight was increased, DHC growth rate was faster. It means that high burn-up spent nuclear fuel is less safe from DHC than low burn-up spent nuclear fuel during spent nuclear fuel dry storage.

REFERENCES

[1] IAEA, "Delayed Hydride Cracking of Zirconium Alloy Fuel Cladding", IAEA-TECDOC-1649, 2010.

Development of Forced Helium Dehydration (FHD) Test System for Spent Fuel Canister

Kyung-Wook Shin, Gyung-Sun Chae, Byeong-Mok Park, Suk-Nam Lim, and Jae-Seok Park
SAE-AN ENGINEERING CO., 184, Gasan digital 2-ro, Geumcheon-gu, Seoul, Republic of Korea
and9211@sae-an.co.kr

1. Introduction

The Spent Nuclear Fuel (SNF) in the domestic NPP's is to be stored in dry storage instead of wet storage according to national radioactive waste management plan. The process of transferring SNF from the wet storage facility to the dry storage facility in the same site is called the short-term loading operations, which includes the drying, backfilling with inert gas, transfer of the cask to the storage pad [1]. Drying is one of the main processes for the prevention of corrosion and hydration of cladding during dry storage and transportation of SNF. There are two commercialized drying methods; vacuum drying and forced gas dehydration. Vacuum drying is very simple in the system, while FHD has advantages of keeping the SNF cladding safe during drying and shortening drying time, etc.

Accordingly, the development of FHD is required. Data for development a commercial grade FHD will be acquired by operation of the FHD test system.

2. FHD Test System

2.1 General information

The test system consists of a drying skid, chiller skid, reduced model canister and real size model SNF; drying skid circulates the process gas through the canister to remove the remaining moisture, and a chiller skid provides drying skid refrigerant for cooling the process gas. The size and weight of each skid are shown in Table1 and shown in Fig. 1.

Table1. Dimension and Weight

No	Length (mm)	Width (mm)	Height (mm)	Weight (kg)
Drying skid	2,500	1,600	1,952	1,320
Chiller skid	2,900	1,000	1,952	660

Fig.1. Left: drying skid / right: chiller skid.

2.2 Configuration of the test system

The configuration and arrangement of the test system is as following Fig. 2.

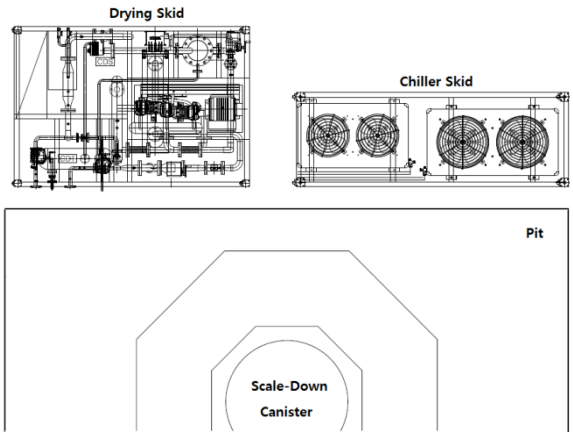

Fig. 2. The test facility layout.

This test system is defined by series connected each module. Heated process gas is moved to canister by a pipe line connected to vent line of canister. The Drain line of canister is in turn connected to the condenser and the freezer. Outlet of freezer is connected to suction of circulating pump. The process gas from the circulating pump is heated in the heater and flows into the canister through flow control. Configuration features of test system are; heater can operate steadily because heater is located after flow controller and flow fluctuation can be minimized. Process gas is supplied through vent line for maximizing evaporation rate. First cooled process

gas again is strongly frozen for further removing residual moisture. The chiller skid is connected to the condenser and the freezer in the drying skid to supply refrigerant as a cooling source for removing moisture in the process gas.

Drying test system is designed and manufactured with appropriate skid size, ease of transportation and safety and operational convenience. The test system installed at the test site is shown in Fig. 3.

Fig. 3. The site placement.

2.3 Instrumentation and control

The test system performs logic processing of the input signal sequentially by the program, and controls the external device by the programmable logic controller (PLC) used for the sequential control using the output. The PLC is connected to the Human Machine Interface (HMI) touch panel, and is capable of monitoring all operation status of the drying test system, and be set operational parameters and controlled all component such as the gas circulation pump, condenser and freezer on and off, the opening and closing of automatic valve. Also all data such as pressure, temperature, dew point flow rate are acquired. Information on component operating states is indicated on the touch screen

Major operation variables are recorded and stored in the portable memory in real time. In the event of loss of power, the main equipment and the control power signal of the drying test system are shut down. UPS) is installed for supplying essential power to instrument and control device.

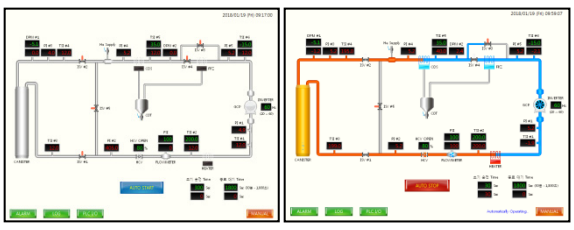

Fig. 4. HMI main screen.

2.4 Operation mode

There are two operation mode; manual operation mode and automatic operation mode. Automatic operation mode consists of the initial operation, the automatic operation and the termination waiting operation. Automatic operation control logic is shown in Fig. 5.

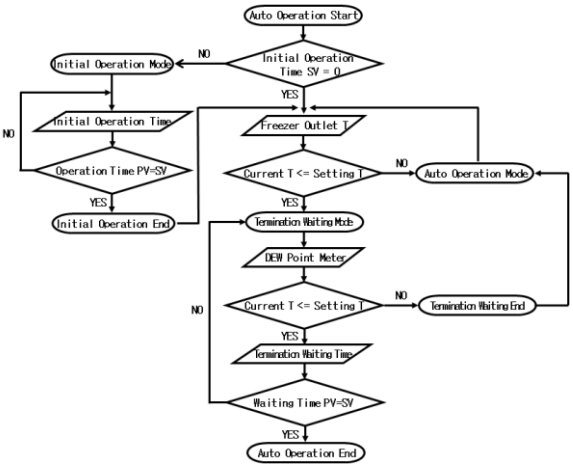

Fig. 5. Automatic operation control flow chart.

3. Conclusion

The test system is intended to test the removal of residual moisture in the canister during SNF transportation and dry storage. The data generated by the test confirm the drying performance of the test facility and produce design data for the development of commercial forced gas dehydration. Also it is expected to contribute not only establish the operation procedure of the drying process, but also to produce the data necessary for dry safety evaluation.

Acknowledgement

This work was financially supported by Korea Institute of Energy Technology Evaluation and Planning (KETEP) grant funded by Ministry of Trade, Industry & Energy (20161720200930).

References

[1] NUREG-1536 Revision 1 “Standard review plan for spent nuclear fuel dry storage system at a general license facility”.

[2] ASTM C1553-16, “Standard Guide for Drying Behavior of Spent Nuclear Fuel[1]”, ASTM, 2016.

Design of a Basket Lifting Mechanism for Pyroprocessing Automation Verifying Mockup

Dongseok Ryu*, Jongkwang Lee, and Seungnam Yoo
Korea Atomic Energy Research Institute, 989-111 Daedeok-Daero Yuseong-Gu, Deajeon, Republic of Korea
*sayryu@kaeri.re.kr

1. Introduction

The equipment in a hot cell should be simple and easy to operate, because the human operator is not allowed to access inside and executes all operation by using remote devices. Pyropocessing, one methods to recycling spent fuel, has been studied, and the related equipment should be considered in view of remote operation. To enhance the operability and reliability of the developing equipment, a new non-radioactive experimental space, the PAVM (Pyroprocessing Automation Verifying Mockup) was planned.

In this research, a basket lifting module for simplifying some operations of the testing equipment in PAVM is discussed.

2. Basket Lifting Module for Oxide Reduction Process

2.1 needs for the basket lifting module

One of the key process of the Pyroprocessing is the oxide reduction. A vessel is enclosed by a heater, and the vessel is kept warmed as 600 degree Celsius to melt the LiCl salt. Anode and cathode are installed in the molten salts, and high current is engaged. The cathode is designed as a basket shape to Uranium oxide (UO_2), and the UO_2 in the Cathode are reduced when the current is engaged. The separated Oxygen turns to gas and exhausted off at the Anode.

The cathode basket should be replaced after each batch of the oxide reduction process, and the mechanical replacing operation is annoying and physically difficult.

The Fig. 1 shows the basic concept for the oxide reduction, and installing operation of cathode basket.

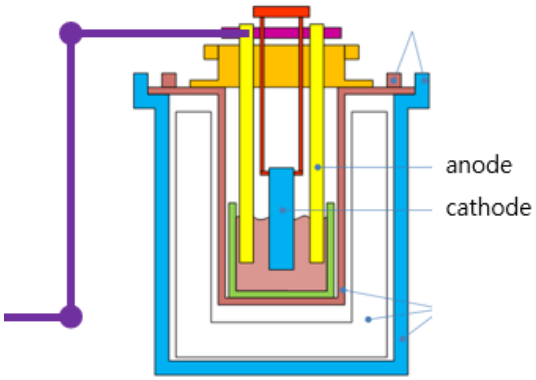

Fig. 1. Concept of oxide reduction, and replacing cathode basket.

A dedicating mechanism for replacing cathode basket was discussed to simplify the operation, and the design requirement was deduced as below.

◆ The cathode basket lifting module
- The basket is automatically lifted by the mechanism
- The capacity of the list is 50kg or more
- The lift is controlled as 3 positions (top, middle, and bottom position)
- Bus-bar is connected at the bottom position
- The mechanism is modularized.

2.2 Design of the basket lifting module

The basket lifting module was designed by four different modules, testing basket, basket socket, fork lift module, and actuation module, as shown in Fig. 2.

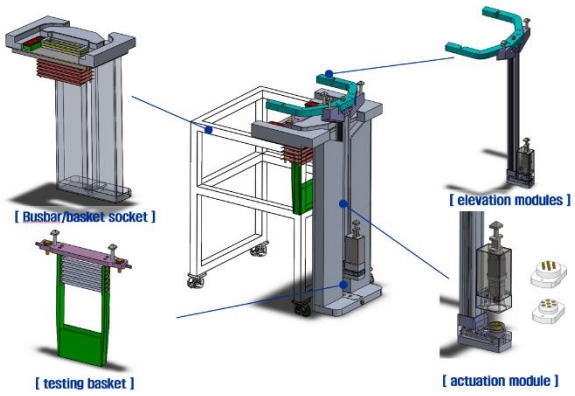

Fig. 2. modularized design of the basket lifting module.

Basically the testing basket is loaded on the fork lift module, and the fork lift module is controlled as three different positions, top, middle, and bottom. A ball screw is installed in the fork lift module enough to elevate 50kg load. A commercial high current bus-bar connector was embedded on the testing basket and the basket socket. When the basket is lowered down to the bottom position, the bus-bar connector is physically connected by the weight of the basket. Oppositely, the connector is departed when the basket is lifted up. The Fig. 3 shows the applied commercial bus-bar connector.

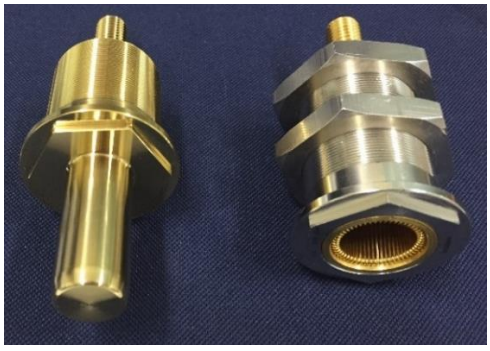

Fig. 3. 750 A high current commercial connector.

The reason why the basket lifting mechanism is designed by an assembly of multiple modules is for the convenience in maintenance. The modules are able to be assembled and disassembled by crane and master slave manipulator. Classically, the power plug or signal connectors should be inserted after mechanical attachment. The electric connection by remote operation is annoying job for human workers and bring troubles. In the proposed mechanism, spring loaded pins are utilized instead of the classic connectors, so that the modules are electrically connected when those are mechanically assembled.

3. Conclusion

The basket lift mechanism was designed for Pyroprocessing automation verifying mockup (PAVM). The remote operation of basket replacing is difficult due to high pay load and interference at the entrance of the basket socket. The proposed mechanism dedicated to the basket replacing operation. In existing operation manual, the bus-bar connection was separate task after basket replacing task. The proposed basket lift mechanism is able to connect the bus-bar, when it replace the basket.

REFERENCES

[1] Dongseok Ryu, et al. "Needs and Goals of the Pyroprocessing Automation Verifying Mockup," Proc. of KRWS 2017 Fall, pp. 53-4, (2017).

[2] Dongseok Ryu, et al. "Example Operating Procedure for an Automation Concept of Electrochemical Process," Proc. of KRWS 2017 Spring, pp. 151-2, (2017).

Construction of Dry Room for Pyroprocessing Automation Verification Mock-up

Jonghui Han*, Byungsuk Park, Jaehoon Lim, Dongseok Ryu, and Seungnam Yu
Korea Atomic Energy Research Institute, 989-111 Daedeok-daero, Yuseong-gu, Daejeon, Republic of Korea
*jhan@kaeri.re.kr

1. Introduction

Recently, KAERI has designed a mock-up for verifying the automation of pyroprocessing equipment [1]. In this mock-up, the reliability and the operability of automated process equipment in high temperature or molten salt environment are going to be studied. The mock-up will not use any radioactive material, and its atmosphere will be maintained at low moisture to prevent from corrosion by salt. To support these objectives, the mock-up has four subsystems: dry room, drying system, remote systems and process equipment. This paper addresses the design and construction of the dry room.

2. Design of Dry Room

2.1 Design Specification

The dry room is mainly comprised of the process room and the auxiliary room. These rooms should have low leak rate to maintain the humidity of the room and they should also have the structural resistance against pressure up to a certain level. The process room should have an enough size so that two equipments could be operated. The main design specifications are listed in Table 1 [1].

Table 1. Design specification of dry room

Dew point	-40℃
Temperature	25 ~ 30 ℃
Pressure	50 ㎜H_2O
Leak rate	1 CMH
Size	5.2 x 4.1 x 4.45 m
Level difference	< 1 ㎜

2.2 Design and Modification

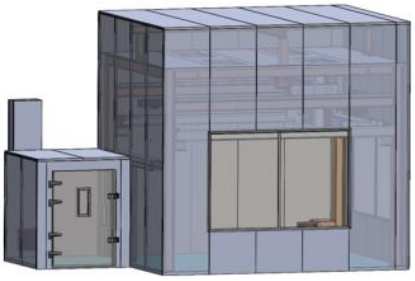

Fig. 1. Design of Dry Room for Mock-up.

Fig. 1 shows the designed dry room. As shown, the wall of the room is constructed with panels, and it has a gas tight door and two windows. Inside of the process room, there is a structure for remote handling equipment such as crane and gantry robot. Since vibration during the operation of the automated handling systems can deteriorate the sealing performance of the wall, the design was modified so that the structure was separated with the wall. In addition, support bars were considered to reinforce wall structure and a transfer port for gantry maintenance was added.

3. Construction of Dry Room

3.1 Construction Procedure

To build the dry room, floor, wall, double ceiling and handling systems are constructed. Since the structure of handling systems and wall are separated, the structure should be installed before the ceiling is constructed. In addition, in the middle of construction, several tests about floor level and welding quality were accompanied. The rough procedure was as follows: 1) Anchoring for handling system structure, 2) reinforcement and leveling of floor (check for welding and level), 3) construction of wall panel, 4) install of handling system structure and crane, 5) covering of double ceiling, 6) install of windows, door, and ports, 7) caulking of the room, and 8) reinforcement of the dry room wall.

3.2 Construction of the Dry Room

The dry room was constructed following the procedure. Followed figures are photos during the construction.

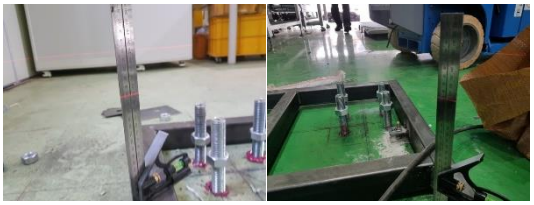

Fig. 2. Installation of Anchor.

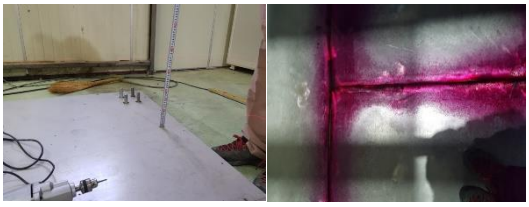

Fig. 3. Floor Construction and Test.

Fig. 4. Installation of Wall Panel.

Fig. 5. Installation of Crane Structure and Utility Ports.

Fig. 6. Constructed Dry Room.

4. Conclusion

A dry room for pyroprocessing automation verification mock-up has been designed and constructed. A drying system will be installed and connected with this room in the future. Then the automation of pyroprocess equipment will be verified.

REFERENCES

[1] J. H. Lim, et al., “Design of Dry Room for Process Automation and Salt Test”, Proc. of the SAREK 2017 Winter Annual Conference, Nov. 2017.

15 m Drop Analysis for Spent Nuclear Fuel Transport Cask

JaeHoon Lim[1, *], Sang Soon Cho[1], Yun-young Yang[1], Kiseog Seo[1], Woo-seok Choi[1], and Daesik Yook[2]

[1]Korea Atomic Energy Research Institute, Daedeok-daero989ben-gil 111,Yuseong-gu, Daejeon, Republic of Korea

[2]Korea Institute of Nuclear Safety, 62, Gwahak-ro, Yuseong-gu, Daejeon, Republic of Korea

[*]jhlim85@kaeri.re.kr

1. Introduction

It is expected that when the spent nuclear fuel cask is transported at a nuclear power plant, a dropping accident can occur at a height of fifteen meters without the impact limiter which are beyond the regulatory hypothetical accident conditions.

Therefore, in this study, transient impact structural analysis model simulating one-third scaled cask is dropped into concrete at a height of fifteen meters without the impact limiter is developed and analyzed.

2. Analysis Model

In the present transient impact analysis model, the cask has an initial vertical velocity of 17.16 m/s, which is the speed at the time of collision to the concrete floor to simulate the dropping from the 15 m height to the concrete floor.

The developed overall analysis model is shown in Fig. 1. The concrete and cask are also modeled as finite elements.

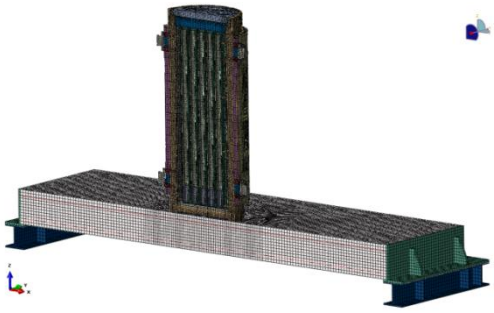

Fig. 1. Overall analysis model.

Inside the cask, there is a fuel assembly model including surrogate fuel rods as shown in the Fig. 1. The fuel assembly model consists of top nozzle, middle grid, bottom nozzle, three surrogate fuel rods and five guide tubes. Since this model is a one-third model, additional mass is added to the top of the fuel rod to apply appropriate impact load on fuel rods.

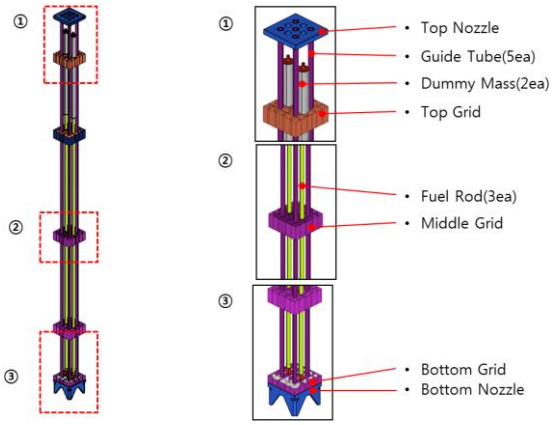

Fig. 2. Analysis model for fuel assembly.

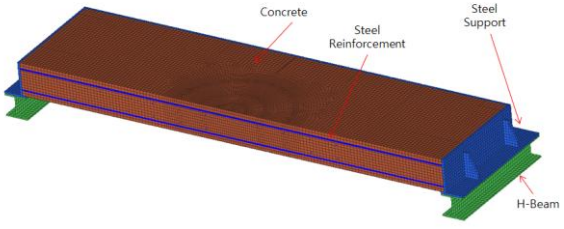

Fig. 3. Analysis model for concrete and support structures.

The concrete has a reinforced structure and supported by steel support at two ends as shown in Fig. 3.

3. Analysis Results

The energy diagram is shown in Fig. 4. Maximum displacement occurred at 0.175 sec after collision with minimum kinetic energy. The displacement at that time is shown in Fig. 5. As shown in the figure, it is observed that the concrete is deflected approximately 140 mm.

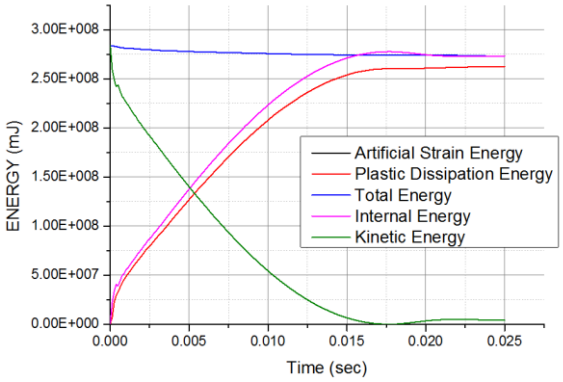

Fig. 4. Energy variation with respect to time.

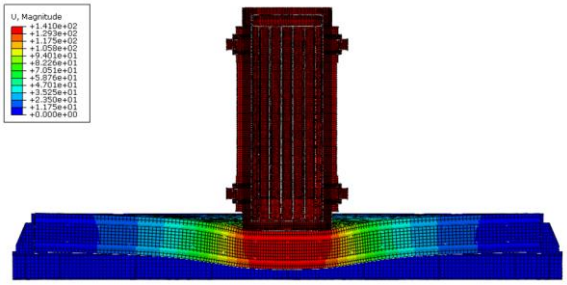

Fig. 5. Maximum displacement after collision.

It was also observed that no plastic deformation occurred in the fuel rods. That is due to that concrete behaves as a shock cushion by absorbing the impact as it deflected.

4. Conclusion

A fifteen meter dropping analysis of the one-third model of spent nuclear fuel transport cask was performed. As a result, the integrity of fuel rod is maintained. That is due to that the concrete behaves as shock cushion like impact limiter. It is expected that more accurate and reliable analysis results can be obtained when the effect of scabbing, spalling and cracking of the concrete is implemented.

Radiation Shielding Evaluation for Spent Fuel Storage Pool According to Burnup

Young-Hwan Choi*[1], Jae-Hun Ko[1], and Ki-Young Kim[2]

[1]Korea Nuclear Engineering & Service, #5, Hyundai Plaza, 798-1, Yuseong-daero, Daejeon, Republic of Korea

[2]KHNP Central Research Institute, 1312-70, Yuseong-daero, Yuseong-gu, Daejeon, Republic of Korea

*Sarn2000@kones21.com

1. Introduction

The spent fuel pool is equipped with storage racks designed to hold the spent fuel assemblies removed from the reactor and is typically 12 meters or more deep to keep radiation levels below acceptable levels. Therefore, the spent fuel storage pool is shall secure the radiological safety for a person working around the storage pool through the analysis for the capacity and specifications of the stored spent fuel.

This paper addresses the radiation dose rate at the water surface of the spent fuel pool were addressed by considering storage capacity and burnup for the spent fuel pool of the HANUL unit 3.

2. Shielding Evaluation of Spent Fuel Pool

2.1 Acceptance Criteria

Spent Fuel Storage Pool is classified as nuclear fuel facilities under the domestic nuclear safety act, must comply with the Nuclear Safety Commission Regulation No. 19. Therefore, the radiation dose rate on the water surface of the pool should not exceed 25μSv/hr.

2.2 Specification of Spent Fuel

The evaluated spent fuels were selected from spent fuels released from reactor of HANUL unit 3, and the source term was evaluated according to the burnup rates. The specifications of the evaluated spent fuels were assumed to be of various burnups up to maximum 60,000MWD/MTU and 5.0wt% enrichment. Table.1 shows the specifications of the spent fuels applied in the source term evaluation.

Table 1. Specification of Spent Fuel

Fuel Type	Enrichment [wt%]	Burnup [MWD/MTU]
CE Type PLUS7	5.0	50,000
		55,000
		60,000

2.3 Radiation Source

In general, radiation source term in the spent fuel storage pool is calculated considering a number of spent fuels stored in the storage racks (region II) and one fuel assembly in transit from region I to region II. Primary gamma rays and neutrons generated from spontaneous fission and (α, n)reaction of fissile materials were calculated considering the burnup and cooling time of the spent fuel using the ORIGEN-ARP modules of SCALE 6.0 computer code[1]. But the effects of radiation dose rates by neutron and secondary gamma excluded in this evaluation because they are relatively very small compared to dose rate by primary gamma source.

Fig. 1 shows the gamma spectrum according to energy of the spent fuel with a typical burnup of 60,000 MWD / MTU. The blue line and red line of the Fig. 1 mean gamma sources for a spent fuel which cooling time is 150hr, and the average value of 1,232 spent fuels stored in the region II.

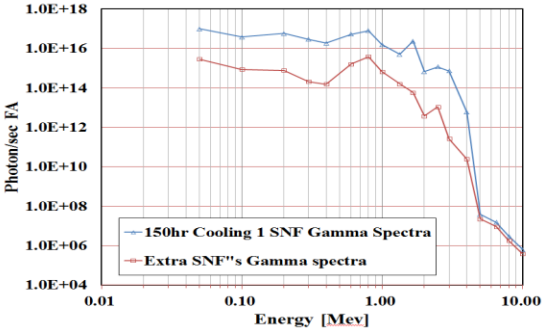

Fig. 1. Gamma spectrum of the Spent Fuel.

2.4 Radiation Shielding Evaluation

The spent fuel storage pool of the HANUL unit 3 is the concrete structure filled with water with the inside of the 12 m height. The storage rack consists of Region I, which 177 fuels for emergency storage of nuclear fuel of the reactor, and Region II, where 1,232 spent fuels is stored. MCNP6 computer code was used for shielding evaluation of spent fuel storage pool. MCNP6 computer code calculates transport equation for photons, neutrons and electrons, etc. using the three-dimensional Monte Carlo method[2].

To calculate dose rates at the various locations on external surface of the spent fuel storage pool, eight virtual tallies were placed. Fig. 2 shows shielding evaluation model of the spent fuel storage pool.

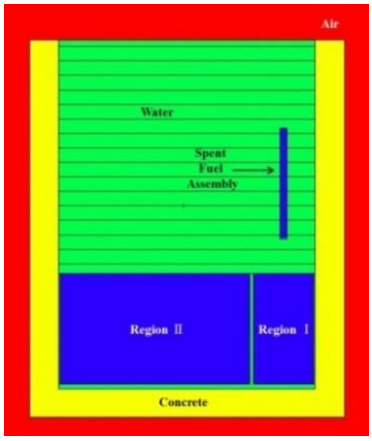

Fig. 2. Shielding Evaluation Analysis Model.

3. Result

Table 2 shows the radiation dose rate on the external surface of a spent fuel storage pool according to burnup, and it shows the largest radiation dose rate among the eight virtual tallies. Relative errors of these virtual tallies are showed 0.06~0.1. Fig. 3 shows the distribution of the radiation dose rate according to various positions and the dose rate of a virtual tally located in the center of the Region Ⅰ shows the largest. Table 3 shows the dose rates according to the presence or absence of fuel assembly in transit. This is the result of the dose rate at the maximum burnup of 60,000 MWD / MTU. As the result, we confirmed that the dose rate of a fuel assembly in transit is dominant in this analysis.

Table 2. Dose Rates Result

Burnup [MWD/MTU]	External Surface [μSv/hr]	
	Result	Limit
50,000	23.1	25
55,000	23.8	
60,000	24.4	

Table 3. Dose Rates with(or without) a FA in transit

Condition	External Surface [μSv/hr]
With a FA in transit	24.3
Without a FA in transit	9.2×10^{-5}

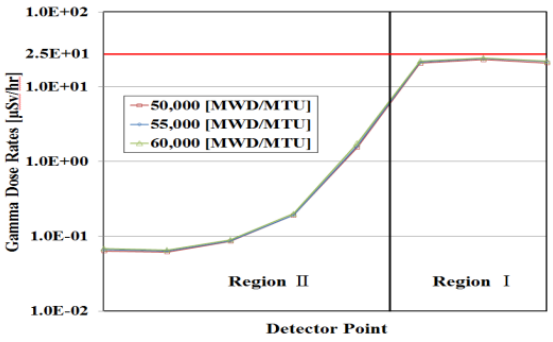

Fig. 3. Distribution of Dose Rates.

4. Conclusion

Radiation shielding evaluation of spent fuel storage pool in NPP was performed. As can be seen from the evaluation results, the radiation dose rate on the external surface of the spent fuel storage pool meets the acceptance criteria even though the spent fuel is burned up to 60,000 MWD/MTU. Also, we confirmed that the radiation dose rate of a fuel assembly in transit is dominant.

REFERENCES

[1] Scale: A Comprehensive Modeling and Simulation Suite for Nuclear Safety Analysis and Design, Version 6.1 (2011).

[2] Los Alamos National Laboratory, “A General Monte Carlo N Particle Transport Code, Version 6.0”, MCNP6, Rev.0 (2013).

Dynamic Optimization of the PWR SF Transportation With Constraints on Storage Capacity and SF Movement

Hong Jang* and Hyo On Nam
Korea Atomic Energy Research Institute, Daedeok-daero989ben-gil 111,Yuseong-gu, Daejeon, Republic of Korea
*janghong@kaeri.re.kr

1. Introduction

Most countries including Korea where the national policy for the spent fuel (SF) is "wait and see" are now faced with a big problem in wet storage capacity of the nuclear power plant (NPP). One temporary solution for this situation is to construct additional on- or off-site dry storages [1]. Assumed a single dry storage with a fixed capacity per each site in Korea, this work estimates the required construction times of on- and off-site dry storages from dynamic optimization of the PWR SF transportation.

2. Korean Phase-out Scenario

Based on current national policy on the nuclear power, total 29 NPPs (25 PWRs and 4 PHWRs) are expected to be operated until their lifetime without lifetime extension or addition of new fleets (Fig. 1). According to this, the accumulated SFs generated from PWRs are expected to reach about 27,000 tHM.

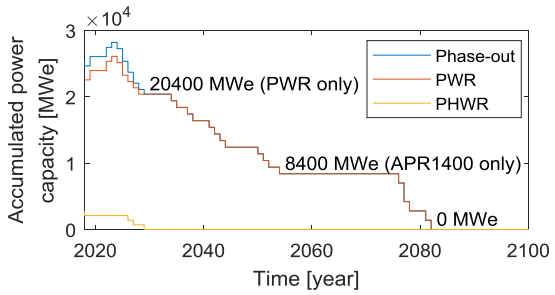

Fig. 1. Accumulated power capacity in phase-out scenario.

In the Basic Plan on High-level Radioactive Waste Management (draft) [2], the saturation times of wet storages in all sites and the plan for establishing an off-site dry storage (until 2035) are specified. But since the plan is based on the 7th Basic Plan on Electricity Demand and Supply [3], it is necessary to re-establish a construction plan for additional dry storages under the phase-out scenario (that is consistent with the 8th Basic Plan on Electricity Demand and Supply (draft) [4]). In addition, realistic limitations on the storage capacity and SF movement should be considered in the estimation of the required construction times for on- and off-site dry storages.

3. Dynamic Optimization

Assumed that a single dry storage per each site, the required construction times of on- and off-site dry storages are estimated by using dynamic optimization. It is assumed that there is no additional installation of the compact rack for existing wet storages. And the on-site transportation of PWR SFs between NPPs is simplified by aggregating NPPs as a single fleet.

The optimization problem is to minimize the SF transportation to a new storage, which can be formulated as follows,

$$\min_{m_k \forall k=t_0,\ldots,T} \sum_{k=t_0}^{T} |x_{s,k}| \quad (1)$$

subject to,

$$0 \le x_{r,k} \le x_{r,k}^u \quad (2)$$

$$0 \le m_k \le m_k^u \quad (3)$$

$$x_{r,k} = x_{r,k-1} - m_k + g_k,\ g_k = \frac{p_k \times CF \times 365}{\varepsilon \times BU} \quad (4)$$

$$x_{s,k} = x_{s,k-1} + m_k \quad (5)$$

where $x_{s,k}$ is accumulated SFs at time k in the new storage s, $x_{r,k}$ is accumulated SFs at time k in the existing storage r, $x_{r,k}^u$ is the upper boundary of $x_{r,k}$, m_k is the amount of SF transportation at time k, m_k^u is the upper boundary of m_k, g_k is the amount of SFs generated by PWR at time k in the site, p_k is accumulated power capacity at time k in the site, CF is the capacity factor, ε is the efficiency, BU is the burn-up, t_0 is the current time, and T is the final time. Limitations on the storage capacity and SF movement are set by $x_{r,k}^u$ and m_k^u.

All constraints are included in the on-site SF transportation problem (from wet storages to new dry storages) with 500 tHM/yr for m_k^u in the constraint (3). But the constraint (3) is excluded in the off-site SF transportation problem (from on-site storages to an off-site dry storage) because it doesn't affect the estimated construction time of the off-site dry storage. Time-varying upper boundaries, $x_{r,k}^u$, in the constraint (2) are described in Fig. 3 with red lines.

As shown in Fig. 2, the required construction time of the off-site dry storage is expected to 2032. And the required construction times for the on-site dry storages are indicated in Fig. 3. It can be seen from the result that, tight constraints on the on-site dry storage capacity and SF movement could pull the required construction time for the off-site dry storage.

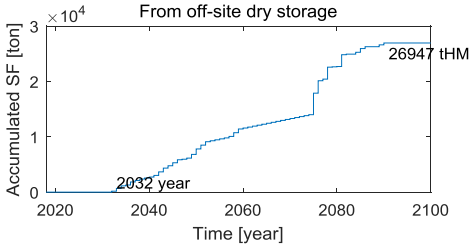

Fig. 2. Accumulated SF from the off-site dry storage.

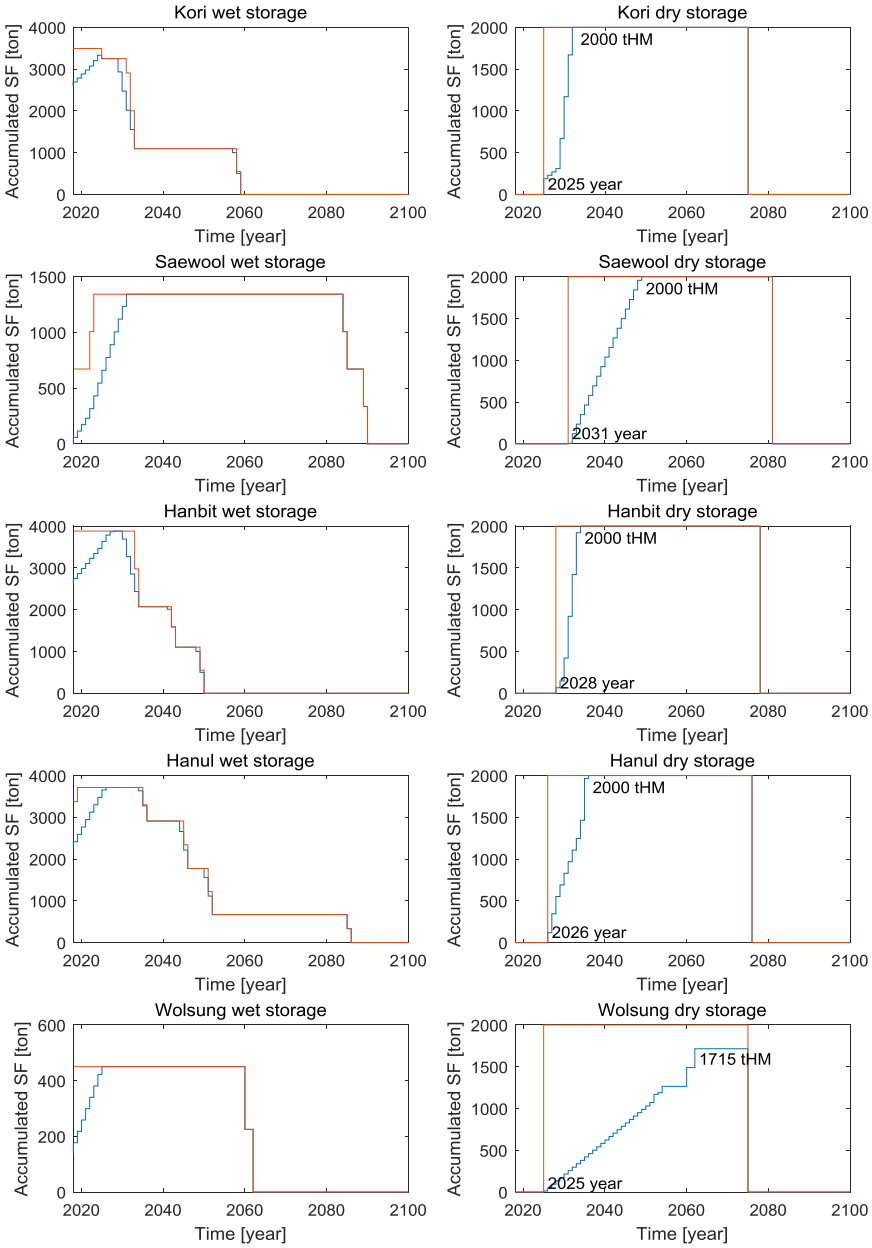

Fig. 3. Accumulated SFs of on-site wet and dry storages (blue line: accumulated SFs, red line: upper boundary).

4. Conclusion

Under the national nuclear phase-out policy, the required construction times of on- and off-site dry storages for PWR SFs were estimated by solving a dynamic optimization problem. In particular, tight constraints on the storage capacity and SF movement were applied to see the effect on the estimated construction times of the dry storages. As a next step, the effect of various limitations on the storage capacity and SF movement will be analyzed.

REFERENCES

[1] MIT Nuclear Fuel Cycle Study Advisory Committee, The Future of the Nuclear Fuel Cycle: An Interdisciplinary Study, MIT, Boston, MA, US, 2011.

[2] MOTIE, Basic Plan on High-level Radioactive Waste Management (Draft), MOTIE, Seoul, Korea, 2016.

[3] MOTIE, The 7th Basic Plan on Electricity Demand and Supply (2015~2029), MOTIE, Seoul, Korea, 2015.

[4] MOTIE, The 8th Basic Plan on Electricity Demand and Supply (Draft), MOTIE, Seoul, Korea, 2017.

Application of Likelihood Evaluation Method for an Integrated Safety Analysis

Seok-Jun Seo*, Woojin Jo, Siwan Noh, Hongrae Jeon, Gil-Sung You, Jeong-Hoe Ku, and Seung Nam Yu
Nuclear Fuel Cycle Strategy Division, Korea Atomic Energy Research Institute,
989-111 Daedeok-daero, Yuseong-gu, Daejeon, Republic of Korea
*sjseo@kaeri.re.kr

1. Introduction

One of the most significant issues in South Korea is management of spent fuels (SFs) due to relatively narrow territory and low public acceptance on safe and reliable controls on radioactive wastes. Currently, a low- and intermediate-level radioactive waste (LILW) disposal facility in Gyeongju province has been operated since 2015. However, high-level radioactive wastes such as PWR SFs have been temporarily stored in SF pools with active cooling systems in nuclear power plant (NPP) sites. In addition, a shortage of the temporary storage capacity is anticipated by 2024 for Hanbit and Kori NPPs. In order to recycle the valuable materials in SFs and to reduce the amount of wastes, Korea Atomic Energy Research Institute (KAERI) has been developing a pyroprocess technology as a dry process compared to a wet process.

In a pyroprocess, it is essential to ensure safety of operations due to the high radiological consequences of radioactive materials on facility workers as well as public and the environment. U.S. Nuclear Regulatory Commission (NRC) requests conducting integrated safety analysis (ISA) for fuel cycle facilities to identify potential accident sequences and to designate items relied on for safety (IROFS) for prevention and mitigation of the accidents[1]. In a risk matrix of 3 by 3, three types of consequences and likelihoods, respectively, are divided based on 10 CFR 70.61. In this study, a likelihood evaluation method is applied by distinguishing failure frequency index numbers and failure probability index numbers according to f-type and p-type events, respectively.

2. Methodology

2.1 Consequence category, likelihood category, and risk index matrix[1]

Table 1. Consequence Category

	Workers	Offsite Public
Category 3: High Consequence	RD > 1Sv CD > AEGL-3, ERPG-3	RD > 0.25Sv 30 mg sol U intake CD > AEGL-2, ERPG-2
Category 2: Intermediate Consequence	0.25 Sv (25 rem) < RD < 1 Sv AEGL-2, ERPG-2 < CD < AEGL-3, ERPG-3	0.05 Sv (5rem) < RD < 0.25Sv AEGL-1, ERPG-1 < CD < AEGL-2, ERPG-2
Category 1: Low Consequence	Accidents with lower radiological and chemical exposures than those above in this column	Accidents with lower radiological and chemical exposures than those above in this column

Table 2. Likelihood Category

	Likelihood	Range
3	Not Unlikely	More than 10^{-4}/yr
2	Unlikely	10^{-4}/yr ~ 10^{-5}/yr
1	Highly Unlikely	Less than 10^{-6}/yr

Table 3. 4x4 Risk Index Matrix

		Likelihood of Occurrence		
		Highly Unlikely	Unlikely	Not Unlikely
		[1]	[2]	[3]
Conseq-uence	High [3]	Acceptable 3	Not Acceptable 6	Not Acceptable 9
	Interme-diate [2]	Acceptable 2	Acceptable 4	Not Acceptable 6
	Low [1]	Acceptable 1	Acceptable 2	Acceptable 3

Acknowledgement

This work was supported by National Research Foundation of Korea (NRF)

REFERENCES

[1] NUREG-1520, Standard Review Plan for Fuel Cycle Facilities License Applications, U.S. Nuclear Regulatory Commission (2015).

A Study on the Improvement of Process Operation Through Logistics Control

Hun Suk Im, Hong Jang, and Hyo Jik Lee
Korea Atomic Energy Research Institute, Daedeok-daero989ben-gil 111,Yuseong-gu, Daejeon, Republic of Korea
ihs95@karei.re.kr

1. Introduction

Pyroprocessing technology has been developed at Korea Atomic Energy Research Institute (KAERI) as an alternative for management of spent nuclear fuel [1-2]. Each fundamental unit process of pyroprocessing has been developed successfully up to the lab-scale so far [3-4], while treatment performance, duration and organic operation between unit processes for massive fuel have not been investigated up to now. Thus modeling and simulation studies for integrated pyroprocessing have been challenged up to now[5-6] and the prototype model IOMP(Integrated Operation Model for Pyroprocessing) was finally developed. This model implements the current flowsheet of pyroprocessing and covers the up-to-date process operation schedules.

2. IOMP

IOMP had been introduced at the previous conference[Fig. 1]. This program has been invented with ExtendSim, being implemented with model file(.mox), library file(.lib) and EXCEL import file for user-defined conditions. At the previous study it gave the basic information such as the concentration behavior of high-heating nuclear element in the molten salt and the bottle-neck points over the whole processes, and waste streams. Because IOMP includes a calculator based on the chemical reaction for tracking mass. Thus it can track the dynamic concentration variation according to the feed material.

The objective of this study is to analyze logistics of products and wastes, total operation days according to the WIP (Work In Process) control for establishing optimization strategy. However the safeguards restriction condition was not applied except for the head-end cell.

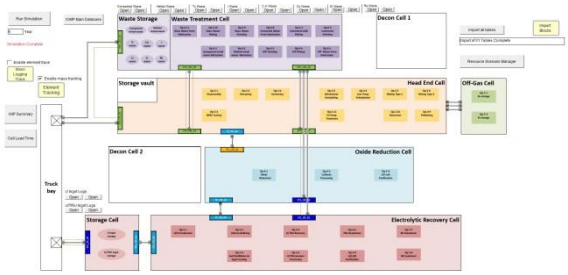

Fig. 1. Conceptual diagram of the pyroprocessing.

3. Assumption

3.1 Assumptions

The assumed amount of fuel is 70 assemblies per SF conditioning year. Here 1 SF (Spent Fuel) conditioning year does not mean the real 365 days, but the duration for consuming the total 70 assemblies. Simulation starts from charging procedure of spent fuel. After being satisfied with accountancy condition at the head-end cell, the fuels can be transferred into the next oxide reduction process. WIP (Work In Process) exists between individual unit process. The initial capacity of WIP is set to unlimited. The main process parameters and procedures are based on the flowsheet of Pyroprocessing[7].

4. Result and Conclusion

In order to check the transient duration the long-term simulation (over 10 years) was operated and the result shows the trend of operation days[Fig. 2]. SF

conditioning year means that the 1 year is defined as the operation days to treat spent fuel 70 assemblies.

Fig. 2 shows that even though operation year increases in the beginning (up to 4th year), it converged to a slight larger value (~ 1.2 times) under the unlimited WIP conditions. The cause of the increase is presumably due to accumulated fuel in the WIP or storage point.

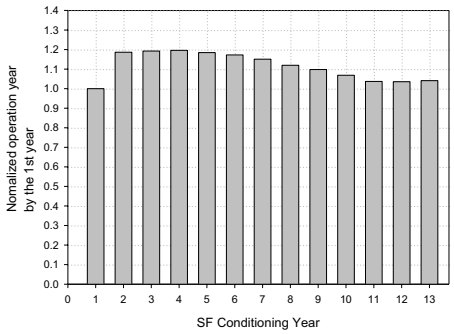

Fig. 2. Normalized operation year by the 1st SF conditioning year.

Fig. 3 shows the distribution of WIP amount compared to each own process batch size in the waste treatment cell. "1" is defined as the batch capacity. The case of less "1" means that WIP maintains the amount of products under the batch size. On the other hand WIP can accumulate products up to 8~9 times more than the batch size under the unlimited WIP condition.

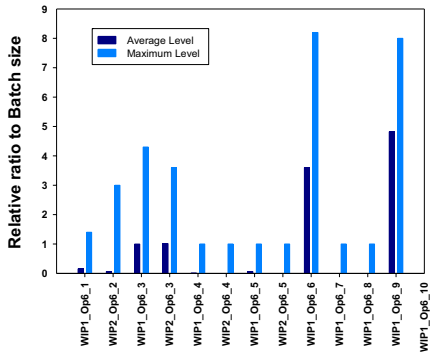

Fig. 3. Relative WIP size ratio to Batch size.

The effect of these unbalanced distribution on the WIP balance has not been identified clearly so far. However it is predicted that WIP can be built up due to the long waiting time for the next process or transfer into the next cell. Study for efficient configuration of WIP size have to be investigated.

In addition to WIP size, many parameters affect process operation and a phased approach is also required. All organic and coherent analysis would be induced from the unified operation model including design requirements for unit process and operation.

The analysis results would be reflected into the strategies of the advanced operation model. Several scenario of operation model based on the separation ratio, process capacity and WIP capacity can be simulated as well and it helps to find the optimized operation strategy. Various database related to mass flow according to the individual scenario will be accumulated and used for highly reliable operation as well. We will propose strategies forward for optimization of process operation and material flow through stepwise computer simulation

REFERENCES

[1] H. S. Lee et al, "Pyroprocessing technology development at KAERI," Nuclear Engineering and Technology, 43, 4, 3171(2011).

[2] D. H. Ahn et al, "Development of Pyroprocess Technology for the Management of Spent Nuclear Fuel," News & Information for chemical engineers, 34, 3, 249 (2016).

[3] J. M. Hur et al, "Electrochemical reduction of uranium oxide in the Li2O-LiCl molten salt," Seventh information exchange meeting on actinide and fission products partitioning and tramsmutation,

[4] H. S. Lee et al, "Current status of Pyroprocessing development at KAERI," Science and Technology of Nuclear Installations, 2013.

[5] F. M. LAST, The Title of the Book, page or chapter numbers, Publisher, City (year).

[6] www.extendsim .com

[7] Flowsheets (v.5.1) of Pyroprocessing (KAERI/TRU-6847/2017).

Evaluation of Spent Fuel Damage in Actually Happenable 15 m Drop Accident Test

Woo-seok Choi[1]*, Sangsoon Cho[1], Yun-young Yang[1], Sanghyeok Han[2], Jae-hoon Lim[1], and Daesik Yook[3]

[1]Korea Atomic Energy Research Institute, Daedeok-daero989ben-gil 111,Yuseong-gu, Daejeon, Republic of Korea

[2] Sungshin ENG.

[3] Korea Institute of Nuclear Safety, Gwahak-Ro 62, Yuseong, Daejeon, Republic of Korea

*wschoi@kaeri.re.kr

1. Introduction

As we construct a safety case of transport cask and spent fuel, there are actually happenable accident conditions in the life-cycle, which are beyond the regulatory hypothetical accident conditions. To ensure the safety of spent fuel transportation, it is necessary to select the accident conditions for the safety evaluation based on the analysis of accident scenarios and to perform a safety assessment under these actual accident conditions.

2. Test plan for 15m drop accident conditions

2.1 Evaluation of actual accident conditions

Actual operation scenarios of spent fuel handling and transportation were derived by analyzing spent nuclear fuel storage facilities, transport systems and transport procedures in domestic nuclear power plants.

Among them, it was analyzed that there could be a possibility of a drop of nuclear fuel due to the shortage of the crane cables, the damage of the fuel handling device, or the operator's mistake during withdrawal, movement and loading of the fuel in the spent fuel wet storage tank.

In case of underwater fall, the maximum drop height was estimated to be about 5 m. The nuclear fuel would be damaged, but no radioactivity or radiation leakage would occur. In addition, when the cask is moved from the decontamination tank to the transportation vehicle, it is possible to cause a drop of 9.5 ~ 14 m due to the various reason described above.

One of the worst accident conditions in which the cladding of the spent nuclear fuel assemblies is damaged is dropping of cask from the high height without the impact limiter which is shock absorbing component. Therefore, it is necessary to evaluate the safety of the actual accident condition when the cask without impact limiter drops down from 15 m height.

In this study, structural integrity of cask, nuclear fuel assemblies, cladding tubes and support grids is evaluated when a transport cask without shock absorbers drops down to concrete pad at a maximum of 15 m.

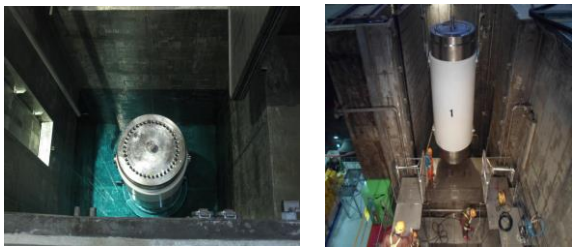

Fig. 1. Cask transportation w/o lid bolt fastening (Loading pit -> Decon. pit).

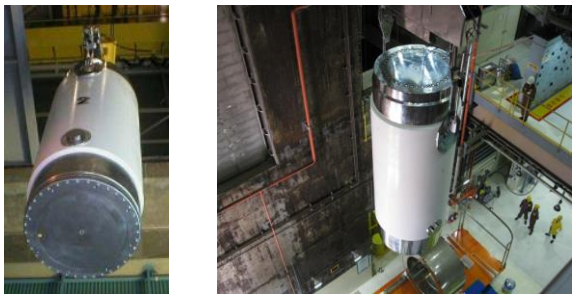

Fig. 2. Cask transportation w/o impact limiters (Decon. pit -> Truck bay).

2.2 Test plan simulating actual accident condition

To assess the actual accident conditions, KAERI conducted a non-absorbing drop test with a drop height of 15 m.

The scenario we want to simulate is to drop cask without impact limiter onto a concrete pad, which represent the second floor of a building. Therefore, we will construct the concrete pad laid over the ground through reinforcement work on the empty space of test facility. The protecting structure will be installed to prevent accidents caused by the rebound of the transport cask after the impact. We decided to use a portable heavy car crane to lift the cask to a

height of 15 m and to drop it. A lot of budget was required for the series of works such as modifying of test facility, performing drop test, and restoration of facility after test. The preparation and layout for the test are shown in Fig. 3.

Fig. 3. Preparation for drop test.

2.3 Test results

A number of accelerometers and strain sensors were attached to the outer cask and internal fuel assemblies for impact test. The changes in acceleration and strain measured before and after the test are discussed in the following paper. In this paper, we focus on the deformation pattern of the simulated fuel assembly and the damage of the concrete pad as a result of the test.

Additional concentrated masses were attached with at the top end of the fuel rod to simulate the mass of the original length of fuel rod. After the test, the welding part of the concentrated mass was broken and hit the spacer grid at the below. We observed that the spacer grid was pushed down to the next spacer grid. However, buckling was not observed at the bottom span of the fuel rod, and it was found that the lateral deformation was small. The shape of the fuel assembly before and after the drop impact test is shown in Fig. 4.

On the other hand, concrete pads were observed to be considerably damaged. If it were not for the reinforcing bars in the concrete pads, it would probably have been penetrated. The deformed shape of the damaged concrete is shown in Fig. 5.

It was found that no leakage occurred in the leak test performed after the drop test. It is considered that most of the impact energy was absorbed by the concrete pad and the cask was not subjected to large impact energy.

Fig. 4. Damage and deformation of concrete pad.

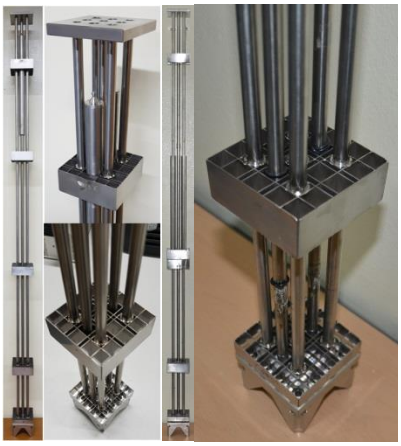

(a) Before drop (b) After drop

Fig. 5. Displacement and velocity time history.

3. Conclusions

The actually happenable drop accident conditions beyond regulatory accident conditions were evaluated. Among them, preliminary structural integrity evaluation was carried out for the actual drop accident condition in which the transport cask without impact limiter drops at a maximum of 15 m. As a result, it was estimated that the deformation of claddings, supporting guide tube, bottom nozzle were small. But spacer grids had some deformation. The concrete pad had considerable damage. The cask was observed to be safe and no leakage occurred after the drop test.

The test condition of 15 m drop without impact limiter onto the concrete pad is less severe that the hypothetical accident condition, which is 9 m drop with impact limiter onto unyielding surface. However, the severe damage of concrete pad should be considered for the safety of cask manipulating area.

Factors Affecting Spent Nuclear Fuel Rod Resistance Against Impact

Sanghoon Lee[1], Belal Almomani[2], and Dongchan Jang[2]

[1]Keimyung University, 1095 Dalgubeol-daero, Dalseo-gu, Daegu, Republic of Korea

[2]Korea Advanced Institute of Science and Technology, 291 Daehak-ro, Yuseong-gu, Daejeon, Republic of Korea

shlee1222@kmu.ac.kr

1. Introduction

This paper discusses various uncertain factors that affect the structural integrity of spent nuclear fuel rod during a horizontal drop case. Due to the stochastic nature inside the reactor, the spent fuel rods are subject to various types of uncertainty in material properties, interfacial conditions, and so on. They affect the resilience of spent fuel rod against rupture during an impact accident but their relative importance has not been discussed much. In this work, a detailed numerical model of a single fuel rod and structural parts of spent fuel assembly was built and dynamic explicit simulations are performed to calculate structural behavior of fuel rod under impact. Then, the effects of uncertain factors are studied using design of experiments.

2. Numerical analyses of spent fuel rod

2.1 Finite Element Model of Fuel Rod

The fuel rod was modelled with the actual dimensions of 350 fuel pellets in a 4.094-m-long fuel cladding referred to CE16x16 Plus 7 fuel type, as well as 2 end plugs, 2 insulating pellets, 2 guide tubes, top/bottom nozzles, and 12 SGs (see Fig. 1) were all modelled to investigate the interaction of fuel rod against the supporting components. This model is designed in a way to provide useful results that can be transferred to fuel assembly level model in a cask-loaded condition.

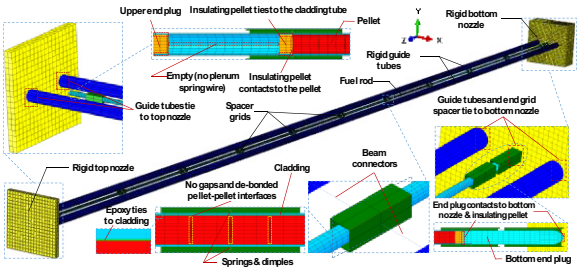

Fig. 1. Finite element model of a single fuel rod.

2.2 Analysis Condition

The fuel rod assembly model is drop from a height to measure the maximum plastic strain on the cladding. The threshold plastic strain for fuel rod rupture is set as 0.1 % which is known to be a typical value for high burnup fuels. The critical drop height which results in the threshold strain value is found by trial and error. The target surface is modeled as a rigid body.

3. Factor Effect Study Using DOE

3.1 Factors to be studied

The four factors of which affects are studied are the material property of cladding, interfacial condition between the pellets and cladding, fuel rod internal pressure, and the stiffness of dimple and spring of spacer grid. Those are some of the uncertain factors that possibly affect the integrity of spent fuel rods during accidents.

3.2 Design of Experiments and Results

The effects of uncertain factors are studied using the full factorial design of experiments. For interfacial condition, 3 levels are selected as, fully bonded, partially bonded, fully debonded. The other factors have 2 levels, each. For material property, a soft and ductile stress-strain relationship with a hard and brittle stress-strain relationship are selected as two bounding cases.

Fig. 2 is the main effect and interaction diagram of those factors on the critical drop height. It is seen that the material property of cladding and the pellet-cladding interaction (PCMI) are those two dominating parameters of critical drop height.

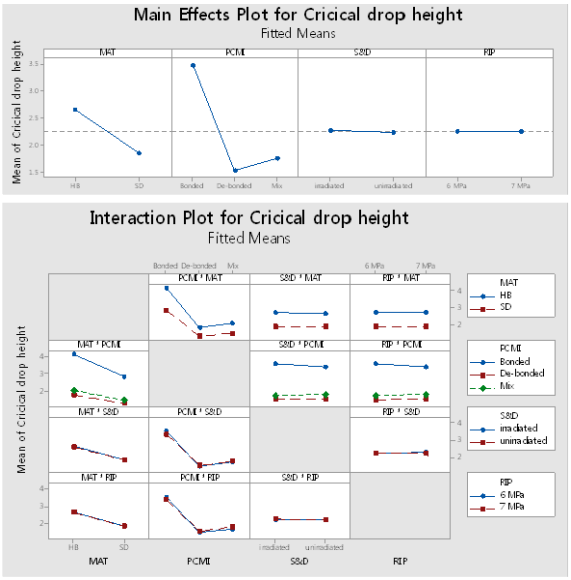

Fig. 2. Main effect and interaction diagram.

It is seen that the fuel rod internal pressure and the spring and dimple stiffness degradation do not have significant effects on the critical drop height of spent fuel rod. It is interesting to see that the difference between the fully bonded case is much bigger than that between partially bonded and fully debonded case. There are no significant interaction effects among factors. Thus the effects of those parameters can be analyzed by one factor at a time basis.

4. Conclusions

Due to its stochastic nature, the structural integrity of spent nuclear fuel is hardly quantifiable. In this work, some important factors that results in the variation of structural performance of spent fuel rods are studied using a sophisticated finite element analysis and design of experiments. It was revealed that the PCMI and the material properties are important factors that determine the impact resistance of spent fuel rod against rupture during impact.

This work considered only horizontal drop case, and the results for vertical drop case will be presented in the future.

REFERENCES

[1] Adkins, H. et al. Used Nuclear Fuel Loading and Structural Performance under Normal Conditions of Transport— Demonstration of Approach and Results on Used Fuel Performance Characterization, US DOE, 2013.

A Simulation Study for Galvanic Reduction of Metal Chloride From LiCl-KCl Eutectic Salt

Kwang-Rag Kim*, Sung-Ki Kim, Hun-Suk Im, and Hyo-On Nam
Korea Atomic Energy Research Institute, Daedeok-daero989ben-gil 111,Yuseong-gu, Daejeon, Republic of Korea
*krkim1@kaeri.re.kr

1. Introduction

Pyrochemical processing based on molten salt electrolysis is preferred over the conventional wet process for treating spent nuclear fuels in view of several advantages such as its simplicity and less secondary wastes, etc. [1]. This process also includes TRU and rare-earth drawdown steps in order to completely recover the fission products from the LiCl-KCl eutectic salt. The small amount of actinides remaining in the salt used in the electrowinning process is treated by a drawdown step to remove it from the salt before being transferred to the salt purification process.

A residual actinide recovery (RAR) process has been developed by combining the electrolysis and oxidation in the molten salt contacting with immiscible Cd phase [2]. This process is also useful to control TRU/RE ratio for SFR fuel composition.

An alternative drawdown process recently proposed is to employ a galvanic reduction for between the metals which have different redox potentials in the salt. Galvanic reduction is a spontaneous electrochemical process using an active metal as the reductant in the LiCl-KCl eutectic salt.

In this study, a modeling approach for studying an analysis of a galvanic reduction system was used to investigate whether the selective metal reduction is theoretically possible to be an alternative drawdown process.

2. Theory

2.1 Redox reaction

To recover the residual actinides from the salt waste, using chemically active rare earth metal as the reductant directly in the LiCl-KCl eutectic salt is the unique aspect of the galvanic reduction process. The galvanic reduction of actinide chloride ($AcCl_3$) is reduced by contacting the rare earth (RE) metal in the salt phase:

$$RE + AcCl_3 = Ac + RECl_3 \quad (1)$$

Nernst equation can be employed to calculate the equilibrium potential by the RE/$RECl_3$ redox reaction, in which the reduced species are at unit activity:

$$E_{RE}^{eq} = E_{RE/RECl_3}^{0} + \frac{RT}{nF} ln\left(a_{RECl_3}\right) \quad (2)$$

For reduction reaction of actinide chloride, an equilibrium equation is given by:

$$E_{Ac}^{eq} = E_{Ac/AcCl_3}^{0} + \frac{RT}{nF} ln\left(a_{AcCl_3}\right) \quad (3)$$

where E^{eq} is the equilibrium half-cell potential, E^0 is the standard potential, R is the gas constant (8.314 J/K mol), T is the absolute temperature (K), n is the number of electrons transferred, F is the Faraday constant (96,487 coulomb/equiv.), and a is the activity of oxidized or reduced species. The Tafel relationship between reaction rate (i) and overvoltage

(η_a) for activation polarization is:

$$\eta_a = \frac{RT}{nF} ln\left(\frac{i}{i_0}\right) \quad (4)$$

2.2 Numerical model

Binary galvanic reaction (1) depends on the redox potential difference between two redox systems. For a multispecies system, the competing reduction reactions proceed with the potential difference (driving force) for a given oxidation of metal reductant.

For *j* species in a given reduction system, the variation of the partial and total current density (*I*) with overpotential are given by:

$$i_j(E^{eq}) = i_j(\eta_a) \quad (5)$$

$$I = \sum i_j \quad (6)$$

A set of these equations is simultaneous nonlinear system and can be solved by iteration process. .

3. Results and discussion

The use of rare earth metals to recover actinide metals has been proposed [3]. In this case, reduced metal accumulated at the bottom of molten salt bath as a precipitate as schematically shown in Fig. 1. The oxidation of the rare earth metal to form ions in the salt phase will proceed at potentials slightly less negative than the equilibrium redox potential for the metal contact with the salt. On the other hand, actinides have a reduction potential more positive than that of the rare earths. Thus, actinides are precipitated as metal from the salt without use of an electrical power supply. In association with this technology possibility, a simulation study was performed to investigate the multispecies reduction behaviors of spontaneous galvanic system.

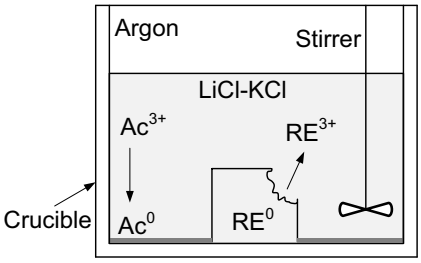

Fig. 1. Conceptual schematic of galvanic reduction system.

4. Conclusion

An analysis of a galvanic reduction system was carried out to investigate whether the selective metal reduction is theoretically possible.

REFERENCES

[1] OECD NEA, "Spent Nuclear Fuel Reprocessing Flowsheet," NEA/NSC/WPFC /DOC, Paris, 15 (2012).

[2] H. Lee et al., "Koran Pyrochemical Process R&D Activities," Energy Procedia, 7, 391-395 (2011).

[3] J. B. Shim et al., "Uranium Recovery Tests Using Rare Earth Metals in LiCl-KCl Molten Salt," International Pyroprocessing Research Conference, Sept. 21-23, 2016, Jeju, Korea.

Technical Review of Force-Reflecting Telemanipulator System

Seungnam Yu*, Jongkwang Lee, and Byungsuk Park
Korea Atomic Energy Research Institute, 111, Daedeok-daero 989beon-gil, Yuseong-gu, Daejeon, Republic of Korea
*snyu@kaeri.re.kr

1. Introduction

In a broad sense, teleoperation encompasses all techniques that allow a human operator to replicate or manipulate from a remote position based on his ability to act on objects in real time through sensory feedback (vision, touch, motion and so on). In the nuclear industry, teleoperation is used to handle objects located either in inaccessible zones or dangerous areas (nuclear cells, sub-sea, and human body). Over the last several decades, the nuclear industry has remarkably contributed to the development of the useful tools for teleoperation. In the most general case of teleoperation system, a master system is handled by the operator and a slave one located in the remote area replicates the movements of the master. The first mechanical Master Slave Manipulator (MSM) was developed in 1948 by R. Goertz at Argonne National Laboratories. In MSM system, a mechanical connection using rod and cable is applied for force and movement transmission between the master and the slave workstations. However, this mechanism intrinsically has limitation of distance between the master and slave arm. To overcome this issue, servo-type manipulators were designed [1, 2], and the master-and-slave units which have the same kinematics are driven by electrical motors. Practically, a bilateral joint control is established to the servo manipulator: i.e. each movement of master arm is perceived and instantly mimic by the slave one. The level of control algorithm and operational reliability of such systems are now highly improved. This has been proven during the long-term evaluation of maintenance programs of experimental target facilities such as the Joint European Torus in the UK [3, 4] or the Spallation Neutron Source in the US [5]. Meanwhile, a computer-assisted teleoperation systems proposed in the late 90's and it was new evolutions focused on increasing the control sensitivity and interoperability between the equipment. Consequently, requirements for such type of systems were to develop an improved controller [6] that could address both master and slave systems even designed with different kinematics and actuation technologies [7,8,9]. Due to the different type of kinematics between master and slave arm, the control strategy for these systems in computer assisted teleoperation systems is generally performed in the Cartesian space (i.e. bilateral control between a reference tool-frame attached to the slave arm and a control grip-frame attached to the master arm). This scheme is generally applied in industrial nuclear hot cells [9] and finally recent developments introduced Virtual Reality (VR) techniques and supervisory control systems in an attempt to improve the efficiency of entire processes through the introduction to the programmed motions and assistances for the operator. In this regard, this paper presents the technical review of the force-reflecting manipulators widely used in the teleoperation systems of nuclear facilities.

2. Design Requirements for Force-Reflecting Telemanipulator

Table 1 shows the comparison of characteristics between a force-reflecting telemanipulator and industrial robot based on the generally accepted performances in each individual domains. Table 2 shows the design requirements for force-reflecting performance of a telemanipulator system and technical selections of transmission type for each parameter of force-reflecting performance.

Table 1. Comparison of performances between force-reflecting manipulator and industrial robot

Parameters	Force-Reflecting Manipulator	Industrial Robot
Friction	1~5 % of capacity	30% or larger
Backlash	Low to medium	No backlash
Input device	Master (Replica)	Teach pendant, keyboard
Deflection	2.5~5 cm at full load	No deflection
DOF	6 DOF arm with end effector	4~6 DOF arm with end effector

Controller	Bilateral force reflection with operator in the loop	Force reflection with direct sensing
Inertia	Relatively low (for minimum fatigue)	High (for high stiffness designs)
Kinematics	Approximately similar to human arm	Mission dependent
Accuracy and repeatability	Not important	Important
Total weight/ payload ratio	< 3	10 ~ 40
End effector	Universal	Interchangeable

Table 2. Design requirements of the force-reflecting manipulator

Requirements	Force-reflecting manipulator	Transmission	
		Wire	Gear
		Manipulator	Robot
Maximum speed (No load)	> 1 m/sec, > 6.28 rad/s (360 deg/s)		O
Joint index speed			
Maximum acceleration	1 g (unloaded) 0.5 g (loaded)		O
Damping (Load)			O
Backdrivability*	1~5 % of capacity	O	
Backlash	Low to Medium	O	
Deflection (Load)	2.5~5 cm at full load		O
Motion coupling	< 1 mm		O
Arm gravitational balance	< 0.4 kgf		
Payload/Weight ratio	0.1~0.25 (1/10~1/4)	O	

* Backdrivability means that a force applied at the end-effector will be reflected on the actuators.

3. Conclusions

This paper covers the technical review of performance of force-reflecting telemanipulator to understand the design concept and purpose of the considered system. As a future work, it is required to standardize the effective handling capacity with the corresponding static and dynamic safety factors. It is important in the nuclear facilities because the various kinds of customized telemanipulators could be considered for the target facility and those systems have to be compared with each other more quantitatively. Furthermore, up-to-date telemanipulator systems and their innovative applications need to be surveyed even the teleoperation systems in nuclear areas generally have a tendency to stick to the traditional approaches for safety and reliability.

REFERENCES

[1] R.C. Goertz, W. M. Thompson, “Electronically Controlled Manipulator”, Nucleonics, Vol. 12 N. 11. pp. 46-47, 1954.

[2] C.R. Flatau, J. Vertut, “Ma22 a compact bilateral master slave manipulator”, Proceedings of Conference on Remote Systems Technology, ANS, 1972.

[3] A.C. Rolfe,P. Brown, P. Carter, R. Cusak, A. Gaberscik, L. Galbiati, B. Haist, R. Horn, M. Irving, D. Locke, A. Loving, P. Martin, S. Mills, R. Minchin, J. Palmer, S. Sanders, S. G. Sanders, R. Stokes, “A report on the first remote handling operations at JET”, Fusion Engineering and Design, Vol. 46, No. 2-4, pp. 299-306, 1999.

[4] A.C. Rolfe, “A perspective on Remote Handling Techniques”, Fusion Engineering and Design, Vol. 82, No. 15-24, pp. 1917-1923, 2007.

[5] M.J. Rennich, T.W. Burgess, “Remote handling in the Spallation Neutron Source target facility”, Nuclear news, pp. 32-36, 2006.

[6] P. Gicquel, C. Andriot, F. Lauture, Y. Measson, P. Desbats, “TAO2000: a generic control architecture for advanced computer aided teleoperation systems”, Proceedings of ANS 9th Topical Meeting on Robotics and Remote Systems, Seattle, 2001.

[7] O. David, Y. Measson, C. Bidard, C. Rotinat-Libersa, F. X. Russotto, “Maestro: a hydraulic manipulator for maintenance and decommissioning application”, Transactions of the European Nuclear Conference, September 2007, Brussels, Belgium.

[8] P. Garrec, F. Geffard, Y. Perrot, G. Piolain, A.G. Freudenreich, “Evaluation tests of the telerobotic system MT200-tao in areva- nc/La Hague hot cells”, Transaction of the European Nuclear Conference, September 2007, Brussels, Belgium.

[9] G. Piolain, F. Geffard, A. Coudray, P. Garrec, J-F. Thro and Y. Perrot, “Dedicated and Standard Industrial Robots used as Force-Feedback Telemaintenance Remote Devices at the AREVA Recycling Plant”, Proceedings of the 1st IEEE international Conference on Applied Robotics and for the Power Industry (CARPI), October 2010.

Electrochemical Formation of RE-Mg Alloy in LiCl-KCl-$RECl_3$ Molten Salt

Gha-Young Kim* and Sung-Jai Lee

Korea Atomic Energy Research Institute, Daedeok-daero 989-111, Yuseong-gu, Daejeon, Republic of Korea

*gkim@kaeri.re.kr

1. Introduction

Pyroprocessing is considered as a potential option for an innovative nuclear fuel cycle to attain the sustainable use of nuclear energy [1]. The spent oxide nuclear fuel is reduced through electrolytic reduction process and then the fuel components (U and TRU) are recovered from the reduced fuel at electrorefining process. After the recovery of U and TRU, there are abundant amounts of rare earth elements (RE) in the salt. The molten salt needs to be recycled to minimize the secondary generation of radioactive waste and the amount of radioactive waste and, for this purpose, the RE remained in the salt should be removed.

The molten salt electrolysis method is an efficient method to produce and/or recover rare earth metals. In this work, we observed the electrochemical formation of RE-Mg alloy in a LiCl-KCl-$RECl_3$ molten salt at 773 K by potentiostatic electrolysis.

2. Experimental

All the experiments were performed in a glove box with an Ar(g) atmosphere (H_2O < 1 ppm; O_2 < 3 ppm). A mixture of LiCl-KCl eutectic salt (99.99%purity, Sigma-Aldrich) and $RECl_3$ (RE: Dy and Gd, 99.99%purity, Alfa-Aesar) was prepared in an alumina crucible. The CV measurements were conducted with Mo wire (1 mm diameter) and Mg plate (2 mm×5 mm) as a working electrode and a glassy carbon rod (3 mm diameter, Alfa-Aesar) as a counter electrode, and a Ag/1 mol%AgCl as a reference electrode. Electrochemical experiments were carried out by Bio Logic SP-300 potentiostat/galvanostat. The cross-sectional morphology of the RE-deposited Mg was observed with scanning electron microscopy (SEM) (Hitachi, S-8010).

3. Result and discussion

Fig. 1 shows the CV results using Mo wire and Mg electrode in LiCl-KCl-$DyCl_3$-$GdCl_3$ at 773 K. At Mo electrode, the reduction peaks of Dy^{3+} to Dy and Gd^{3+} to Gd were observed at -1.90 V and -2.06 V vs. Ag/AgCl, respectively (Fig. 1a). However, these reduction peaks were not clearly found at Mg electrode and it was due to the formation of RE-Mg alloy. The formation potentials of Dy-Mg and Gd-Mg alloy were assumed about -1.88 V and -1.94 V vs. Ag/AgCl, respectively. According to the phase diagram, one Dy-Mg alloy (DyMg) and four Gd-Mg alloys ($GdMg_n$, where n = 1, 2, 3, 5) can be obtained at 773 K [2], but only one peak of Gd-Mg alloy formation was found in Fig. 1b.

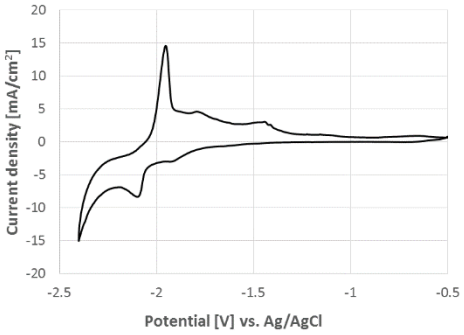

(a)

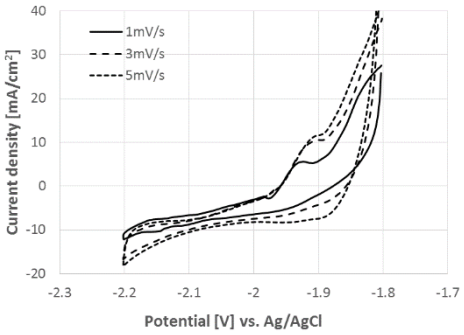

(b)

Fig. 1. Cyclic voltammetry measurement of (a) Mo and (b) Mg electrode in LiCl-KCl-$DyCl_3$-$GdCl_3$ at 773 K (scan rate: (a) 100 mV/s, (b) 1, 3, 5 mV/s).

To confirm the electrochemical formation of RE on Mg electrode, potentiostatic electrolysis was conducted in LiCl-KCl-$DyCl_3$(0.15wt%)-$GdCl_3$(0.59wt%) at -1.9 V for 12 h at 773 K. The RE deposit on Mg electrode was visually examined and the deposited RE layer was confirmed by the analysis of cross-sectional area of the RE-posited Mg electrode.

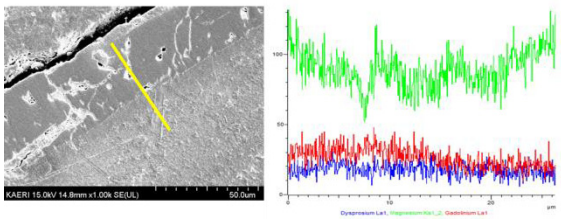

Fig. 2. The cross-sectional image and elemental analysis of RE-deposited Mg electrode.

4. Conclusions

In this study, we reported the electrochemical formation of RE-Mg alloy in LiCl-KCl-$RECl_3$. CV result showed formation of RE-Mg alloys and the electrodeposition of RE on Mg electrode was confirmed by employing potentiostatic electrolysis.

ACKNOWLEDGEMENT

This work was supported by a National Research Foundation of Korea (NRF) grant funded by the Korean government (MSIP) (No.2017M2A8A5015079).

REFERENCES

[1] J.J. Laidler, J.E. Battles, W.E. Miller, J.P. Ackerman, E.I. Carls, “Development of pyroprocessing technology”, Progress of Nuclear Energy, 31, 131-140 (1997).

[2] T.B. Massalski (Ed.), Binary alloy phase diagrams, ASM Metals Park, Ohio, 1986 (ISBN 0-87170-261-4).

3분과

고준위폐기물처분 (Oral)

Modelling of Sulphide Induced Copper Corrosion in Deep Geologocial Repository With Expected Condition

Nakkyu Chae[1], Sungyeol Choi[1], and Heui-Joo Choi[2]

[1]Department of Nuclear and Quantum Engineering, Korea Advanced Institute of Science and Technology, Daejeon, KS015, Republic of Korea

[2]Department of Radioactive Waste Disposal Research, Korea Atomic Energy Research Institute, Daejeon, KS015, Republic of Korea

coskrrb2002@kaist.ac.kr

1. Introduction

Deep geological repository is an important issue in Korea and world. Recently, the land and environmental court in Nacka, Sweden, concluded that the KBS-3 model is not safe enough due to corrosion problems. In Korea and other countries have a similar concept as KBS-3 model. We have to concentrate on the corrosion problems on canisters in the deep geological repository. Hence, in this work we focus on the copper corrosion with sulphide in the deep geological repository with an expected condition (anaerobic). We calculated the expect corrosion depth with several scenarios.

2. Method

2.1 Model description

Deep geological repository is located in 500m depth of underground. After the deep geological repository closed, condition expected to be anaerobic condition [1]. Sulphide could be only exist in sulphide ions (HS^-) without oxygen conditions (O_2 < 0.001 ppb) [1]. During the anaerobic condition, the sulphide ions (HS^-) will be the dominant corrosion specie. The overall reaction of sulphide ions with copper is equation (1).

$$2Cu+HS^- +H_2O \rightarrow Cu_2S+H_2+OH^- \quad (1)$$

In this study, we assumed the fully saturated condition in bentonite and transport is rate determining step of corrosion. We use COMSOL Multiphysics (Numerical analysis program use Finite Element Method, PDE module) to predict the corrosion depth until 10,000 years.

2.2 Kinetic and Transport-rate determining step

In deep geological repository system with fully saturated bentonite and anaerobic condition, copper corrosion rate will be determined by transport rate of sulphide (HS^-). Various literatures relate with copper corrosion with sulphide suggest that transport rate of sulphide (transport) is much slower than sulphide and copper reaction rate (kinetic) [1]. Hence, overall rate determining step of copper corrosion with sulphide is transporation of sulphide (diffusion in bentonite). We used the assumption in our model by equation (2). Equation (3) is steady state analytic solution that will be compared with COMSOL results.

$$\frac{\partial C}{\partial t} = \nabla \cdot (D \nabla C) \quad (2)$$

$$C(r)=\frac{C_1\ln(\frac{b}{r})+C_2\ln(\frac{r}{a})}{\ln(\frac{b}{a})} \qquad (3)$$

2.3 Scenario

Bentonite and Host rock interface is sulphide (HS^-) source for copper corrosion. Upper and bottom are impermeable conditions. Sulphides are immediately react with copper at the canister surface as they are transported.

3. Case results

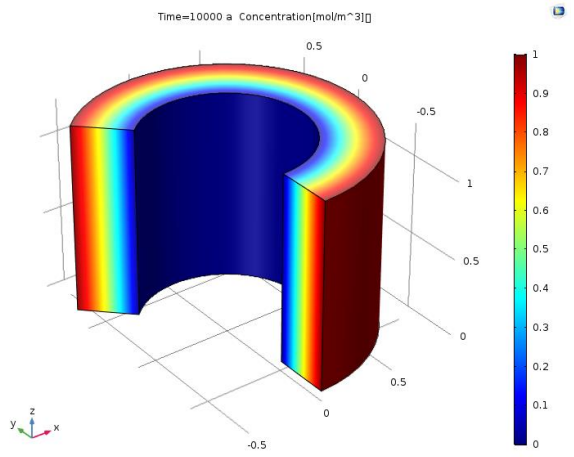

Fig. 1. Result of sulphide concentration in bentonite.

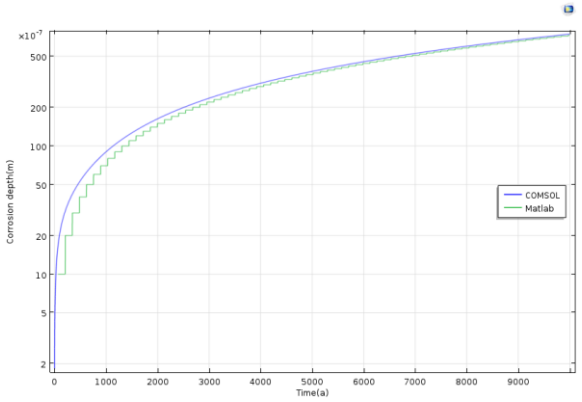

Fig. 2. Result of copper corrosion depth compare between COMSOL (transient state) and Matlab(steady state with analytical solution).

4. Conclusion

The result of transient state with COMSOL is similar to analytical solution calculated by Matlab. We saw the possibilities of COMSOL to solve the transient state. The maximum corrosion depth after 10,000 years with COMSOL is 7.4466 x 10^{-5}[m] and analytical solution is 7.2698 x 10^{-5}[m]. From this model we will develop our model for copper corrosion in anticipated condition.

REFERENCES

[1] F. King et al., “An Update of the State-of-the-art Report on the Corrosion of Copper under Expected Conditions in a Deep Geological Repository.”, 246, 2012.

[2] Smith, J.M., “The Corrosion and Electrochemistry of Copper in Aqueous, Anoxic Sulphide Solutions, PhD thesis, University of Western Ontario.”, 2007.

Performance Evaluation of Novel Emplacement Device

Minsoo Lee*, Jong Yul Lee, and Sung-Hoon Ji
Korea Atomic Energy Research Institute, Daedeok-daero989ben-gil 111,Yuseong-gu, Daejeon, Republic of Korea
*minm@kaeri.re.kr

1. Introduction

DBD (Deep borehole disposal) of high level radioactive waste at the depth of 3~5 km is under discussion nowadays [1]. The one of key devices in DBD operations is the joint device between a disposal canister and emplacement rig. J-slot joint is well known device for this purpose [2], and has been used in oil & gas industry. But J-slot joint can be connected only to drill pipe, and the recombining is impossible after disconnecting.

In this study, a new joint concept was suggested to overcome the problems of the existing joint device for DBD process. New joint device can be applied to various emplacement rigs such as drill pipe, wireline, coiled tubing, and etc. And it also makes the emplacement rig to be connected or disconnected to the disposal canister only by the mechanical operations.

For demonstration of the new joint concept, a joint device, a twin canister string, and a test water tube were manufactured through the detailed designs of them in 1/3 scale. And the deployment mud was prepared in two forms of Ca-type and Na-type bentonite.

2. Design

The novel joint device was designed to seize the wedge on top of a canister string, and move down through a borehole. When it arrives at the bottom of a borehole, the joint releases the wedge by compressive action. The novel device can recombine with the canister string by placing it onto the settled canister string. This recombination can be achieved by the movable sliding hook box in the joint device. If the joint device lifting is faster than the falling speed of the hook box, disconnection occurs. And if it is slower, the wedge on the canister string is seized by the hooks again. The joint device can be equipped to various emplacement jigs.

3. Manufacturing

The novel joint device(Φ110 mm, H148 mm), the twin canister string (Φ140 mm, H1,105 mm), and the water tube (Φ150 mm, H1,500 mm) as a substitute for the borehole were manufactured in 1/3 scale through the detailed designs. And the deployment muds were prepared to fill in the water tube with Na-type bentonite (MX-80) and Ca-type bentonite (GJ-II) respectively.

4. Experiment

The joint device was equipped in a crane hoist, and a twin canister string was dipped in the water tube filled with deployment mud. The connecting, lifting, going down, and releasing tests were performed. The novel joint device exhibited good operations in Na and Ca-type muds with a moving speed of 10 m/min of a crane hoist.

5. Conclusion

The novel joint device was designed for the emplacement & retrieval of a disposal canister in DBD process. And the novel device showed good performance in the simulation test. Therefore, it was concluded that the novel joint device can be used for the emplacement & retrieval of a disposal canister in DBD process.

Acknowledgement

This work was supported by the Ministry of Science, ICT and Future Planning within the framework of the national long-term nuclear R&D program (NRF-2017M2A8A5014858).

REFERENCES

[1] Kristopher L. Kuhlman, "Deep Borehole: from Disposal Concept to Field Test", Sandia National Laboratories Presentation, SAND2015-3116 PE (2015)

[2] Tim Harrison, Very deep borehole; Deutag's opinion on boring, canister emplacement and retrievability, SKB Report, R-00-35, May (2000)

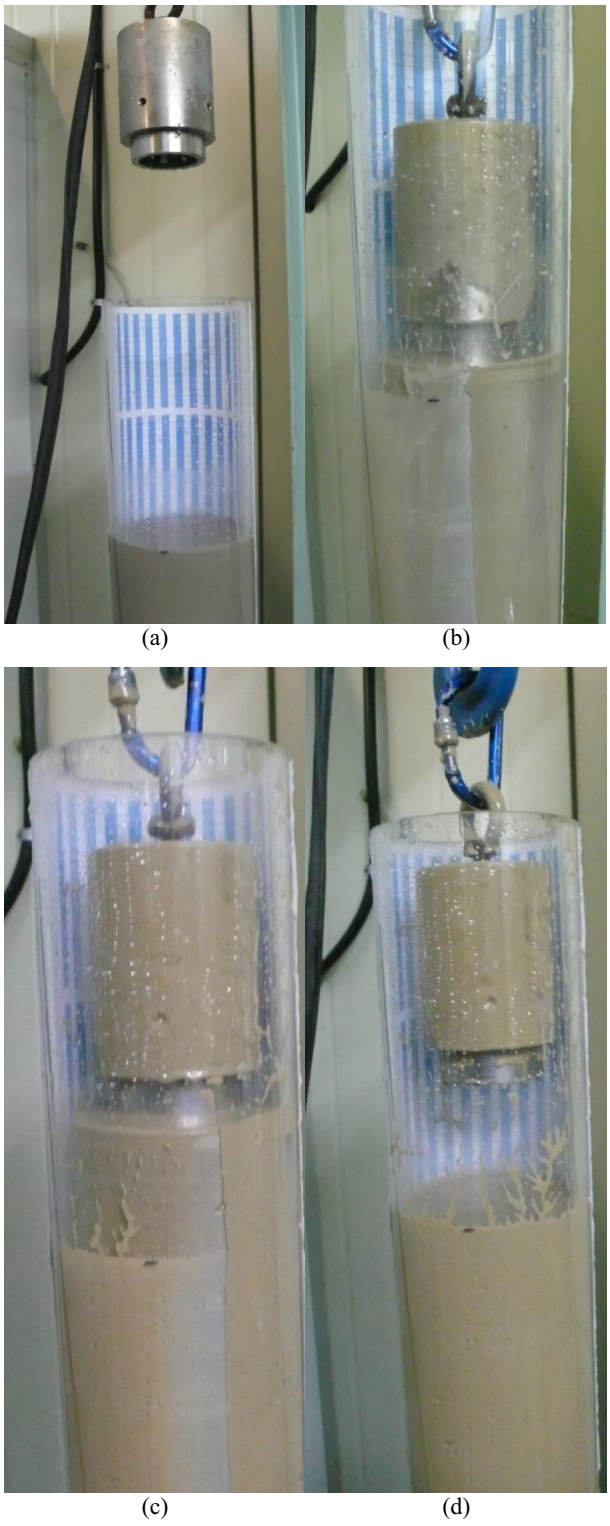

(a) (b)

(c) (d)

Fig. 1. Performance testing of the novel emplacement joint in Na & Ca bentonite mud; (a) setting for the test, (b) lifting a canister in Na bentonite mud, (c) lifting a canister in Ca bentonite mud, and (d) releasing a canister in Ca bentonite mud.

Preliminary Analysis on the Domestic Applicability of Deep Borehole Disposal

Jong-Youl LEE*, Min-Soo LEE, Heui-Joo CHOI, Kyung-Su KIM, and Dong-Keun CHO
Korea Atomic Energy research Institute, 989-111, Daedeok-daero, Yuseong-gu, Daejeon, Republic of Korea
*njylee@kaeri.re.kr

1. Introduction

There are lots of methods to isolate the radioactive waste from human beings. For the spent fuels or high level radioactive waste, a deep geological disposal (DGD) concept is considered as the safest method with the best available technology at present time to isolate them from the biosphere. But as an alternative to the deep geological disposal technology which is considered as a reference concept and currently under the stage of licensing, a deep borehole disposal(DBD) concept to dispose of high level radioactive waste or spent fuels at the depth of 3 to 5 km in crystalline rock that is more stable in geological and geo-hydrological conditions(Fig. 1.) has been studied in the USA and some European countries.

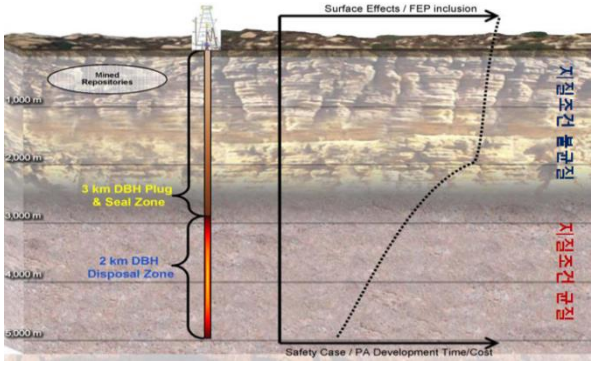

Fig. 1. Geological Condition for DBD[1].

In order to apply the deep borehole disposal concept, it is necessary to secure the drilling and investigation technology for deep borehole with large diameter. With this technology, the geological and geochemical conditions at the depth of 5 km underground should be confirmed to be suitable for deep borehole disposal[2]. Also, the technology for a deep borehole disposal concept and safety assessment should be developed and the technologies are actually demonstrated and proved.

In this paper, the analyses on the applicability of deep borehole disposal in Korea were carried out in technical point of view. The results of this study can be used as an engineering data for establishment of the national policy on spent fuel management, and the information necessary for the stakeholders who are interested in the DBD technology.

2. Technical Applicability for DBD

2.1 Deep borehole drilling and investigation technology

The current status of domestic and foreign deep borehole drilling technology was reviewed and the possible deep borehole drilling technology suitable for deep borehole disposal(diameter, depth) was analyzed. The rotary drilling, the air hammer drilling and the water hammer drilling techniques were reviewed and the applicability to the deep borehole disposal technology was analyzed. The drilling experience and the possibility are shown in Fig. 2[3].

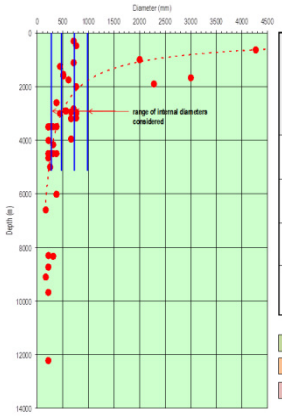

a. Drilling experience(depth : diameter)

Depth (km)	Diameter (mm)			
	300	500	750	1000
2	G	G	G	O
3	G	G	O	O
4	G	O	O	R
5	G	O	R	R

G Possible with current technology
O Possible in the near future
R Impossible in the near future

b. Drilling possibility

Fig. 2. Drilling Experience and the Possibility.

As a part of the site suitability assessment for deep borehole disposal, the evaluation method with the geophysical exploration and the site characterization method based on geological and geo-hydrological data from geothermal industry were analyzed. In addition, the evaluation methods using the deep borehole investigation equipment owned by other institute and industry were reviewed.

2.2 Development of preliminary DBD concept

The literature survey data and the investigation data of geothermal drilling site (Pohang, Seokmodo,

Gwangju/Naju) were reviewed and the characteristics of bedrock in Korean peninsula including geothermal, age, geochemistry were analyzed.

Based on the domestic environment, the concepts of deep borehole/casing, disposal container and it's handling/operation system and preliminary borehole sealing were derived. With these unit module concepts, a preliminary reference deep borehole disposal concept was established(Fig. 3.).

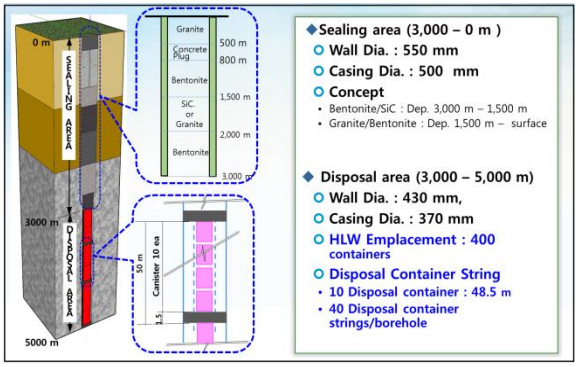

Fig. 3. Preliminary DBD Concept.

Through the preliminary thermal analysis for the established deep borehole disposal system(Fig. 4.), the distance between the deep boreholes was determined. With these results, the deep borehole disposal system layout was derived and compared with the deep geological disposal concept in terms of disposal area. In addition, a graphic disposal environment was constructed and a computer graphical simulation for the deep borehole disposal process was performed.

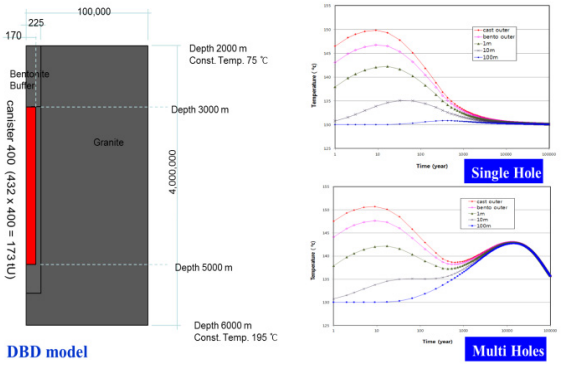

Fig. 4. Thermal Analyses for the DBD Concept.

2.3 Preliminary DBD System Evaluation

The legal basis and the basic requirements for the safety of the deep borehole disposal were analyzed and the thermal/structural stability assessment method of the disposal container and disposal system in the disposal environment was established. The basic test of granite powder melting for the evaluation of the borehole sealing performance was carried out. In addition, preliminary criticality analysis of disposal container and disposal systems was performed, and preliminary safety assessments using the result of thermal - hydraulic calculation of deep borehole disposal system were conducted.

3. Concluding Remarks

Based on the results of analysis on domestic nuclear environment, geology and industrial environment, preliminary analyses on applicability of deep borehole disposal technology including domestic geological environment, deep borehole drilling and investigation technology, concept development technology and safety assessment technology were carried out. Although the concept of deep borehole disposal is considered to be advantageous in terms of safety and economic feasibility due to disposal method and depth, it is absolutely necessary to demonstrate the key technologies and safety for practical application.

The results of this study can be used as an input data for establishment of national policy on spent fuel management, and can be used as the information necessary for the various stakeholders who are interested in the deep borehole disposal technology

ACKNOWLEDGEMENT

This work was supported by the Ministry of Science and ICT within the framework of the national long-term nuclear R&D program (NRF-2017M2A8A5014856).

REFERENCES

[1] Patrick V. Brady, Bill W. Arnold, Geoff A. Freeze, Peter N. Swift, Stephen J. Bauer, Joseph L. Kanney, Robert P. Rechard, Joshua S. Stein., Deep Borehole Disposal of High-Level Radioactive Waste, SAND2009-4401, SNL, Albuquerque, NM (2009).

[2] B. W. Arnold, P. V. Brady, S. J. Bauer, Courtney Herrick, Stephen Pye, and John Finger, Reference Design and Operations for Deep Borehole Disposal of High-Level Radioactive Waste, SAND2011-6749, Sandia National Laboratories, Albuquerque, NM (2011).

[3] Beswick, J. Status of Technology for Deep Borehole Disposal. Report for the Nuclear Decommissioning Authority by EPS International, Contract No. NP01185 (2003).

Correlations Among Fracture Distribution, in Situ Stress States and Hydraulic Conductivity of Fractured Rock Mass

Yeonguk Jo*, Kyung-Woo Park, and Sung-Hoon Ji
Korea Atomic Energy Research Institute, Daedeok-daero989ben-gil 111,Yuseong-gu, Daejeon, Republic of Korea
*joy@kaeri.re.kr

1. Introduction

It is an important issue to investigate groundwater flow in fractured bedrock, in a wide range of rock engineering, such as deep geological radioactive waste disposal. The fluid flow in fractured rock mass tends to be influenced by geometrical features of fractures and their distributions. The KURT is located in a crystalline bedrock, which is fairly homogeneous, but intermittently fractured, and the results of site characterization works indicate that the hydraulic characteristics of the KURT site were affected by presence of permeable structures and its distributions [1].

One of known factors controls permeability of a fracture is that intrinsic shape of fracture in terms of aperture size and types (open or closed). The open-type fracture showing relatively wide aperture and loosely closed due to infilling materials such as weathered rock fragments, is considered as a dominant permeable structure.

It is also proposed that the hydraulic conductivity of fractured rock domain can be altered by in situ stress states, because the aperture of fracture can be changed due to stress condition leading to variation of its permeability. Therefore, the influence of stress on permeability should be properly investigated.

In this context, we attempt to compare the hydraulic conductivity in part of KURT research area, with fracture distribution and stress states there, in order to understand how the fracture distributions and stress conditions influence the hydraulic characteristics of fractured rock mass.

2. In-Situ borehole tests

2.1. Borehole Image Loggings

We identified natural fractures and its distributions which cross the boreholes using a borehole acoustic televiewer (BHTV). We classified the types of individual fractures into open, semi-open, and closed, based on the reflected amplitude and travel time. The spatial distributions of fracture frequency are defined as number of fractures at a 10 m interval. The natural fractures are ubiquitously distributed with depths, but intermittently highly concentrated at several sections.

2.2. Constant Head Injection Tests

The hydraulic conductivity was determined by constant head injection tests, using a double-packer system with an interval length of ~10 m [1]. There are two methods, what we used, to estimate hydraulic conductivity from the test results: Moye [2] and Horner [3] to steady state and transient phase, respectively.

The determined hydraulic conductivities from two individual interpretations, are qualitatively comparable, and have a range between 10^{-8} and 10^{-10} m/sec, representing general value for granitic rock, and a log-normal distribution.

2.3. Stress estimations

The states of in-situ stress were evaluated using hydraulic fracturing tests and borehole wall stress indicators [4]. Local stress condition at KURT research site represents the S_{Hmax} orientation of ESE-WNW, averaging N97ºE, with prevailing lateral compression, indicating thrust-faulting favored stress regime.

3. Influence of fracture distribution and stress states on permeability of fracture

3.1. Relationship between fracture distribution and hydraulic conductivity

The relationship between fracture distribution and hydraulic conductivity shows that some intervals, where natural fractures, especially open-type fractures, are relatively abundant (i.e., high frequency

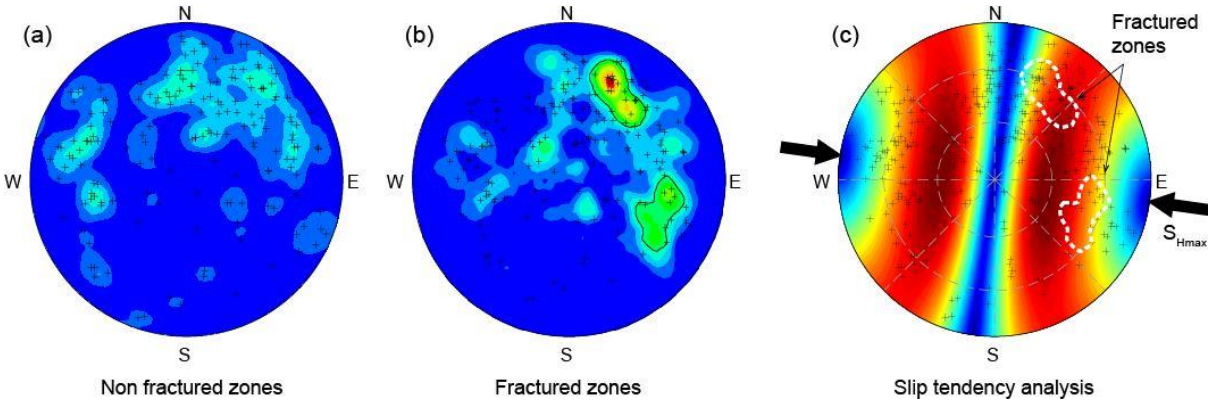

Fig. 1. Streonets representing pole of natural fractures in non-fractured zones (a) and fractured zones (b). All natural fractures are quite randomly oriented. But the fractures in fractured zones tend to be clustered in area of where slip tendency is relatively high (c).

of the fracture), are relatively highly permeable. It suggests that the presence of open-type fracture has a proper relation with hydraulic conductivity, as we expected. There are, however, relatively high conductivity intervals, although no distinct permeable structure exists.

3.2. Influence of stress states on fracture water conductivity

In some boreholes, we observed somewhat unexpected correlations between the fracture distribution and hydraulic conductivity. Several intervals, where no open-type fracture crosses there but fracture frequency is relatively high due to presence of numerous closed-type fractures, show relatively high hydraulic conductivity.

To understand the origins of this phenomenon, we analyzed slip tendency of the structures. All natural fractures have significantly different slip potential depending on their orientations. But some fractures in the concentrated zones have relatively high slip tendency under in situ stress states of KURT site.

It is reported that stress condition (especially, shear stress) on the fracture plane can derive dilation of fracture aperture due to slip, which leads to not only increase in permeability of the individual fractures, but also channeling effects [5]. Thus, we interpret that the high water conductivity zone where no open-type fracture exists is influenced by in situ stress.

4. Conclusion

In the present study, we consider both the fracture distributions and in situ stress states as influence factors on permeability of fractures. The relationship between stress and permeability suggests that the stress condition can significantly affect groundwater flow in fractured bedrock.

Acknowledgement

This work was supported by the Ministry of Science, ICT and Future Planning within the framework of the national long-term nuclear R&D program (NRF-2017M2A8A5014858).

REFERENCES

[1] K.-W. Park and D.-S. Bae, “Analysis of correlation between hydraulic conductivity and fracture charateristics observed by Televiewer logging,” *J. Geol. Soc. Korea*, 41(2), 269–285 (2005). (Korean with English abstract)

[2] D. G. Moye, “Diamond Drilling for Foundation Exploration,” *Civ. Eng. Trans.*, 95–100 (1967).

[3] D. R. Horner, “Pressure Build-up in Wells,” *3rd World Petroleum Congress*. World Petroleum Congress, The Hague, the Netherlands (1951).

[4] Y. Jo, C. Chang, K.-W. Park, S.-H. Ji, and C. Lee, “In situ stress estimation in KURT site,” *J. Geol. Soc. Korea*, 53(5), 689–701 (2017). (Korean with English abstract)

[5] K.-B. Min, J. Rutqvist, C.-F. Tsang, and L. Jing, “Stress-dependent permeability of fractured rock masses: a numerical study,” *Int. J. Rock Mech. Min. Sci.*, 41(7), 1191–1210 (2004).

Studies on Excavation Damage by Blasting in Underground Research Laboratories

Seung-Hoon Park and Sangki Kwon*

Department of Energy Resources Engineering, Inha University, 100, Inha-ro, Nam-gu, Incheon, Republic of Korea

*kwonsk@inha.ac.kr

1. Introduction

For the deep geological disposal of high-level radioactive waste(HLW) in deep underground, the validation and demonstration of HLW disposal system in underground research laboratories(URL) are essential. To construct an URL in deep underground by blasting, it is inevitable to have an excavation damaged zone(EDZ) around the tunnels. In the EDZ various rock properties including permeability, elastic modulus, rock strengths, and thermal conductivity are changed. The size and characteristics of EDZ are dependent on the original rock properties, rock conditions, blasting design, depth, discontinuities, and tunnel geometry. Lots of studies for investigating the characteristics of EDZ and possible influence of EDZ in many URLs in foreign countries.

2. Excavation damaged zone

An EDZ is developed by blasting impact as well as stress redistribution after excavation. EDZ is defined as a zone that has suffered permanent irreversible changes in the rock properties, and a disturbed zone that is dominated by a change in states, such as stress and pore pressure, and the changes are insignificant or reversible(Fig.1). Table 1 lists the EDZ extents measured at different URLs. In the EDZ, various rock properties are changing from its original properties. In the case of elastic modulus, it was reduced 19~82% in the EDZ compared to its original value.

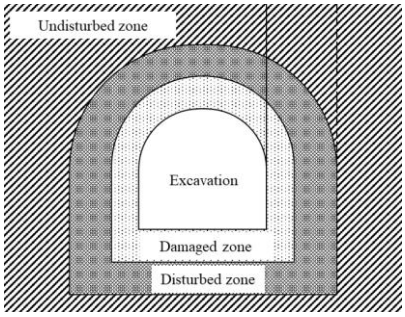

Fig. 1. EDZ around an underground tunnel.

Table 1. EDZ size in crystalline rock

Experiment site (Country)	Depth (m)	EDZ extent(m)
ASPO-access tunnel (Sweden)	80	1~1.7
ASPO-ZEDEX(Sweden)	420	0.3-0.8
ASPO-TASQ(Sweden)	450	0.3
ASPO-TASS(Sweden)	450	0.25
Stripa(Sweden)	340	~0.8
URL-Room2009(Canada)	240	0.3
URL-Mine by tunnel(Canada)	420	0.2~0.3
URL-tunnel sealing(Canada)	420	~1.0
URL-blast damage(Canada)	240	~0.6
Onkalo(Finland)	500	0.3
GTS(Switzerland)	450	~2.0
Mizunami(Japan)	500	1.0
Kamaishi mine(Japan)	250	1.0
KURT(Korea)	100	0.6~1.5

3. Prediction of excavation damaged zone

In order to investigate the possible influence of different parameters such as excavation methods, explosives, initiation system, time delay, and pre-existing fractures on the development of EDZ, studies had been carried out. Fig.2 shows the

blasting design for investigating the influence of time delay between perimeter blast holes on the fracture length developed by blasting.

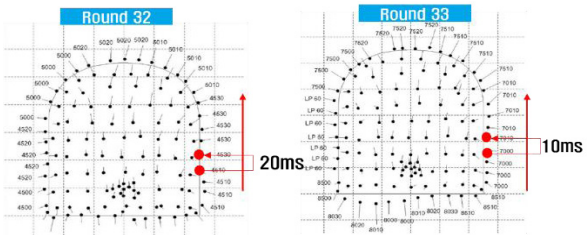

Fig. 2. Blasting to check the influence of time delay between blast holes in Sweden ASPO[1].

From the studies, it was found that mechanical excavation and controlled blasting can significantly reduce the extent of EDZ. Shorter time delay between perimeter blast holes could reduce EDZ size. Water can enhance the crack extension. For predicting the extent of EDZ, an empirical equation, Eq.1, was used in Onkalo. Fig.3 shows the predicted possible extent of fractures(R_c) from blasting[2]

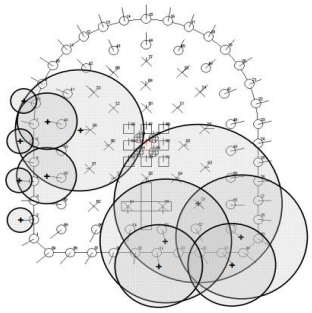

Fig. 3. Prediction of EDZ from blasting design[2].

$$R_c = R_{co} \times F_h \times F_t \times F_v \times F_b \qquad (1)$$

where, R_{co} is uncorrected crack length, F_h, F_t, F_v, F_b are factors for hole spacing, delay time, water content, and rock condition, respectively.

In this study, the ground vibration equation was used to predict the extent of EDZ(D_{EDZ}).

$$D_{EDZ} = \left(\frac{K E}{\sigma_t V_p}\right)^{\frac{1}{1.5}} \sqrt[3]{W} \qquad (2)$$

where, K is site specific constant, σ_t is tensile strength, V_p is P wave velocity, E is Young's modulus, and W amount of explosive. Fig.4 shows the comparison between the prediction using Eq.2 and the measurement at KURT.

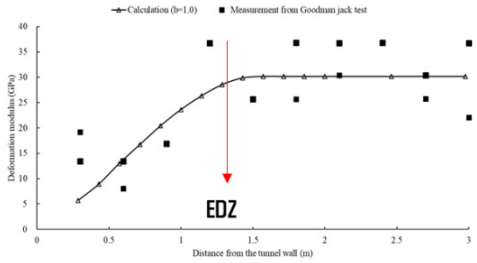

Fig. 4. Predicted EDZ using ground vibration equation.

4. Conclusion

It is inevitable to have EDZ around an underground tunnel. In this study, the studies from foreign URLs were review and derived conclusions about the influence of different parameters such as blasting method, delay time, blasting design, etc. Furthermore, a new way for predicting the extent of EDZ based on ground vibration equation was suggested.

Acknowledgement

This research was supported by NRF (NRF-2016R1D1A1B03933268).

REFERENCES

[1] Olsson, M., Niklasson, B., Wilson, L., Andersson, C.,2004,a Experiences of blasting of the TASQ tunnel. SKB, TR-04-73.

[2] Mustonen, S., Norokallio, J., Mellanen, S., Lehtimaki, T., Heikkinen, E., 2010, EDZ09 Project and Related EDZ Studies in ONKALO 2008–2010, Posiva,WR-2010-27.

Groundwater Flow Modeling Based on the Site Descriptive Model Around KURT

Kyung-Woo PARK*, Su-Lim Jung, and Sung-Hoon Ji

Korea Atomic Energy Research Institute, 989-111 Daedeokdaero, Yuseong, Daejeon, Republic of Korea

*woosbest@kaeri.re.kr

1. Introduction

Korea Atomic Energy Research Institute Underground Research Tunnel (here after KURT) is a research tunnel for high level radioactive waste disposal in Korea. Several geo-environmental studies related to the site characterization such as geological, hydro-geological and geochemical investigations had been carried out around KURT site since 2007 [1]. Recently, the site description model for KURT was finally built from the results of various geo-environment studies [2, 3]. In this study, we would like to introduce the site descriptive model of KURT area such as the geological model and the hydrogeological model, and the groundwater flow modeling results based on the site descriptive model.

2. Site descriptive model around KURT

2.1 Geological model

We synthesized the site characteristics obtained by various types of site investigations to construct the geological model around KURT site. From the geological investigations at the surface and boreholes, four geological components such as subsurface weathered rock, upper fractured rock, lower fractured rock and fracture zones were defined for the construction of geological model. In addition, the three-dimensional geometries of these geological components were analyzed for the model (Fig. 1).

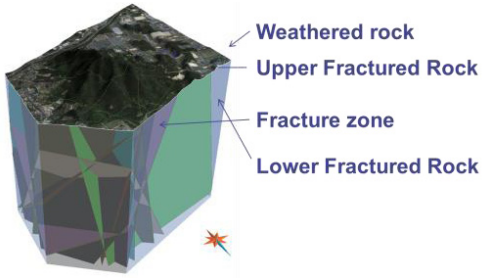

Fig. 1. Geological model around KURT.

2.2 Hydro-geological model

The geological model was used to construct the hydro-geological model (hear after HG model) around KURT site. Hundreds of in-situ hydraulic field tests had been carried out to obtain the hydrogeological properties of geological components around KURT site.

As a result, four geological components such as weathered rock, upper fractured rock, lower fractured rock and fracture zones were identified Hydraulic Soil Domain (HSD), Upper Hydraulic Rock Domain (UHRD), Lower Hydraulic Rock Domain (LHRD) and Hydraulic Conductor Domain (HCD) of the HG model, respectively (Fig. 2).

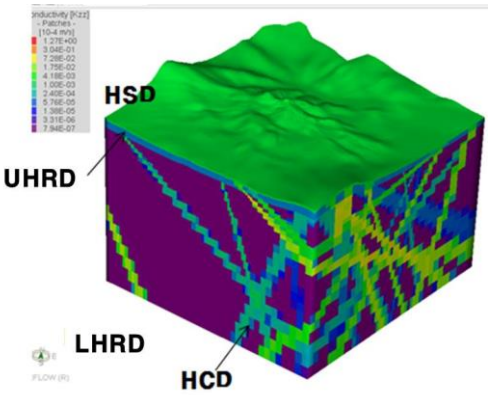

Fig. 2. Hydrogeological model around KURT.

2.3 Groundwater(GW) flow modeling

The model domain for groundwater flow modeling was constructed based on the HG model. The domain for modeling had total 30 layers, which the 1st layer was for HSD, the 2nd and 3rd layer were for UHRD and the below layers of the 3rd layer were for LHRD. The HCDs were located inside the LHRD with the estimated hydraulic conductivities from in-situ hydraulic tests.

The boundary conditions used in groundwater flow modeling were the constant head boundaries for side walls of the domain, which was obtained from lager scale model (local scale model), and the flux boundary was assigned to the upper surface as recharge boundary (Fig. 3). The groundwater flow model was calibrated by adjusting the recharge rate to minimize the difference between the observed and simulated hydraulic heads, and the calibrated recharge rate was 12.7% of annual precipitation around KURT area.

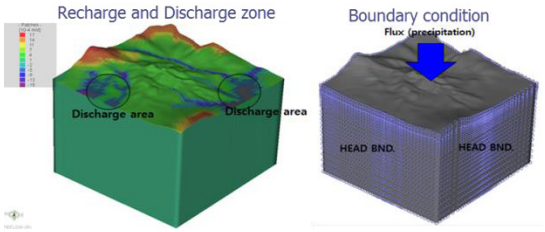

Fig. 3. Recharge rate and boundary condition used in groundwater flow modeling.

3. Results of GW flow modeling

The results of groundwater flow model could explain the artesian condition of southern area of KURT, which was one of the most important hydrogeological properties around KURT site. Also, we could understand that the groundwater flow of the deep environment of KURT was mainly affected by HCDs. To validate groundwater flow modeling around KURT area, the results from modeling are compared with the results of in-situ hydraulic tests (i.e. long term interference test). The validation results show that our groundwater flow model described the long term interference tests well.

4. Conclusion

Groundwater flow modeling was carried out around KURT area. Before the groundwater flow modeling, the geological model was constructed after geological investigation. Then, in-situ hydraulic tests to characterize the hydrogeological properties of the geological components around KURT were conducted, and the HG model was constructed. In the geological model, there were four model units, which were weathered rock, upper fractured rock, lower fractured rock and fracture zone in the geological model although HSD, UHRD, LHRD and HCDs in the HG model. The HG model was used for the input parameters for groundwater flow modeling, and the results indicated that the fracture zones were very influential on deep groundwater flow around KURT area.

Acknowledgement

This work was supported by the Ministry of Science, ICT and Future Planning within the framework of the national long-term nuclear R&D program (NRF-2017M2A8A5014858).

REFERENCES

[1] Kim, K.S. et al, A Safety Case of the Conceptual Disposal System for Pyro-processing High-Level Waste Based on the KURT Site (AKRS-16): Safety Case Synthesis Report, KAERI/TR-6726/2016 (2016).

[2] Park, K.W., Koh, Y.K., Kim, K.S., Choi, J.W., Construction of the Geological Model around KURT area based on the surface investigations, Journal of nuclear fuel cycle and waste technology, v7(4),191-205 (2009).

[3] Park, K.W., Koh, Y.K., Jung, S.L. Site descriptive model in granitic area (Geologic model), KAERI/TR-6025/2015 (2015).

Application of Complementary Indicators for the Performance Assessment of Disposal Facility in Korea

Yongheum Jo, Sol-Chan Han, and Jong-Il Yun*

Department of Nuclear and Quantum Engineering, KAIST, 291 Daehak-ro, Yuseong-gu,

Daejeon, Republic of Korea

jiyun@kaist.ac.kr

1. Introduction

In order to assess the safety of disposal system for radioactive waste in terms of dose to human, the simulation of biosphere is required to illustrate exposure pathways. However, due to the altering properties of biosphere over times, the approach related to ecosystem has a relatively high uncertainty in long-term safety assessment. Therefore, the robustness of the safety assessment of a repository should be reinforced by the introduction of complementary indicators alongside primary safety indicators (dose and risk).

This work discussed the practical use of complementary indicators (radiotoxicity flux and radiotoxicity concentration in natural water) with the safety assessment for the rock-cavern type low- and intermediate-level waste (LILW) disposal facility of Korea.

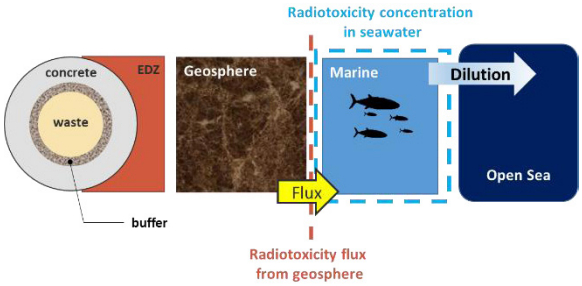

Fig. 1. Conceptual illustration of radiotoxicity flux and concentration in natural water.

2. Methods

2.1 Concentration measurement of natural radionuclides in groundwater and seawater

The concentrations of ^{40}K, ^{226,228}Ra, ^{232}Th, and ^{234,235,238}U in groundwater samples taken from three sites in Gyeongju were assayed by mass spectrometry. In seawater collected near the shoreline, only ^{40}K content was measured. Based on our measurements, the reference levels for complementary indicators has been derived by dose conversion factors [1] and equations given in the previous study [2].

2.2 Modeling

The Goldsim model has been developed for the calculation of radioactive flux from the geosphere and the radiotoxicity concentration in seawater from the rock-cavern type LILW repository. The model consists of engineered barrier, geosphere, and biosphere based on the conceptual design of silo-type disposal system. Details on the modeling are presented in elsewhere [3].

3. Results and Discussions

The natural radiotoxicity in groundwater varied between 1.18×10^{-4} Sv/m^3 and 1.00×10^{-3} Sv/m^3

depending on the sampling sites. The ^{40}K radiotoxicity in seawater was 6.95×10^{-5} Sv/m^3. These measurements were utilized for the determination of yardstick for the complementary indicators related to radiotoxicity flux and radiotoxicity concentration. The safety of disposal system was assessed by comparing simulation results from our model with reference values determined by the natural system.

REFERENCES

[1] International Commission on Radiological Protection (ICRP), “Compendium of Dose Coefficients based on ICRP Publication 60”, ICRP Publication 119, Ann. ICRP 41(Suppl.) (2012).

[2] D.-A. Becker, J.-L. Cormenzana, A. Delos, L. Duro, J. Grupa, J. Hart, J. Landa, J. Marivoet, L. Orzechowski, T.J. Schröder, A. Vokal, J. Weber, E. Weetjens, and J. Wolf, “Safety and Performance Indicators”, Deliverable 3.4.2 of the European Commission, PAMINA Project (2009).

[3] S.-C. Han, “Interdependent Safety Assessment of Integrated Low-and Intermediate Radioactive Waste Disposal System in the Republic of Korea”, Master's Thesis (2015).

Numerical Analysis of Upward Movement of Dummy Canister at Engineered Barrier Emplacement Experiment

Changsoo Lee, Jaewon Lee, and Geon Young Kim

Korea Atomic Energy Research Institute, Daedeok-daero989ben-gil 111,Yuseong-gu, Daejeon, Republic of Korea

leecs@kaeri.re.kr

1. Introduction

DECOVALEX-2019 was started with 14 funding organizations in 2016. Since then, seven tasks have been carried out in the project. Korea Atomic Energy Research Institute joined the project as one of funding organizations and participates as a research team for Task A and D. This paper contains the main results of the coupled numerical analyses performed by KAERI within the framework of the DECOVALEX-2019 Task D deals with the coupled interactions in buffer materials [1].

2. Numerical model for EB experiment

The first task is numerical modeling of engineered barrier emplacement experiment (EB) in the DECOVALEX-2019 Task D. The large scale EB experiment was performed at the Mont Terri Underground Laboratory (Fig. 1). The EB experiment is isothermal test to investigate the HM interactions and it was performed for 10.7 years [2]. KAERI research team used TOUGH2-MP/FLAC3D (Fig. 2) to conduct the numerical simulations for the EB experiment.

In this study, 2D dimensional analysis was performed in 20 m wide and 40 m height domain. Initial pore pressure of host rock was set to 1.2 MPa. And sxx and syy were set to 2.5 and 6.0 MPa, respectively. The initial saturation was set to 1.0 at the rockmass. And relative humidity on the tunnel surface was assumed by 93 % and 9.6 MPa suction was assigned on the surface after the excavation. And pore pressure was fixed by 0.1 MPa on the tunnel surface. Based on the information in the Task D description [1], initial suction of pellets and bentonite block are about 450 MPa and 125 MPa, respectively. Therefore, initial Rh of pellets and bentonite block were set to 3.5 % and 40 %, respectively.

Main parameters of hydraulic model are listed in Table 1.

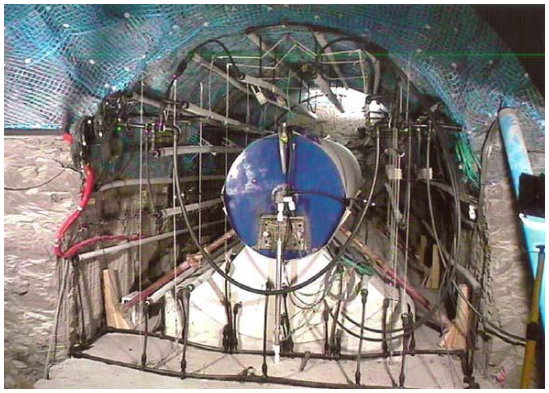

Fig. 1. Pre-conditions of the GBM emplacement [1].

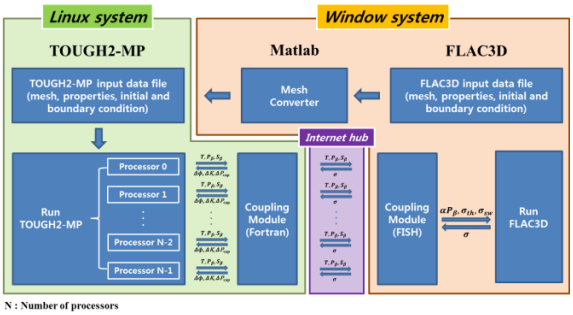

Fig. 2. TOUGH2-MP/FLAC3D coupling module algorithm.

Table 1. Hydraulic parameters of main materials

Parameters	GBM	Bentonite Block	Host rock
Density (kg/m^3)	2,700	2,700	2,700
Porosity (-)	0.496	0.374	0.162
Permeability (m^2)	2.0E-18	5.0E-21	5.0E-20
Relative permeability	$S^{1.9}$	$S^{4.64}$	$S^{3.0}$
λ in van Genuchten model	0.217	0.32	0.401
P0 in van Genuchten model	0.95	30.0	18.0

In this study, generalized power law was used for the consideration of relative permeability (Eq. 1). And van Genuchten model is adopted in this

modeling. For the mechanical analysis, Barcelona Basic Model (BBM) was used for granular bentonite material (GBM) and bentonite block and the used BBM parameters are listed in Table 2.

Table 2. Mechanical parameters for Barcelona Basic model

Parameters	GBM	Bentonite Block
$M\ (-)$	1.5	1.5
$k_s\ (-)$	0.1	0.1
$\kappa_{ps0}\ (-)$	0.06	0.027
$\alpha_{ps}\ (MPa^{-1})$	-0.0015	-0.003
$\kappa_{sp0}\ (-)$	0.05	0.052
$\alpha_{sp}\ (-)$	-0.13	-0.12
$\alpha_{ss}\ (MPa^{-1})$	-0.016	-0.007
$\lambda_{ps0}\ (-)$	0.17	0.18
$R_\lambda\ (-)$	0.6	0.75
$\beta_\lambda\ (MPa^{-1})$	0.05	0.05
$P_0^*\ (MPa)$	1.0	14.0
$P^c\ (MPa)$	0.075	0.1

3. Displacement

Modeling results are plotted with results of in-situ experiment at section A1 in Fig. 3. An upward movement of 10.6 mm was measured in the section A1, because higher swelling potential of bentonite block compared with the lighter pellets. The phenomenon was modeled well in the BBM. And the calculated upward displacement show good agreement with measured data. The upward movement of 11.6 mm was calculated in the modeling.

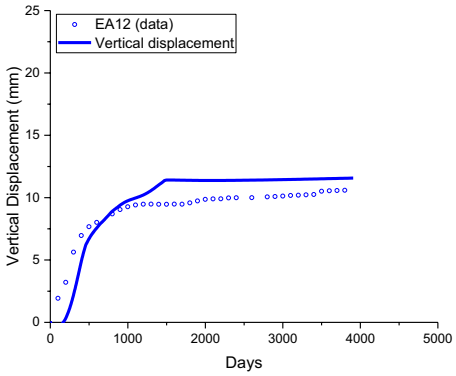

Fig. 3. Vertical displacement of the canister at section A1.

4. Conclusion

TOUGH2-MP/FLAC was used to perform numerical modeling of EB experiment. BBM was used to calculate displacement. Calculated displacement shows good agreement with measured data.

ACKNOWLEDGEMENT

This research was supported by the Nuclear Research and Development Program of the National Research Foundation of Korea (NRF-2017M2A8A5014857) funded by the Minister of Science and ICT.

DECOVALEX is an international research project comprising participants from industry, government and academia, focusing on development of understanding, models and codes in complex coupled problems in sub-surface geological and engineering applications; DECOVALEX-2019 is the current phase of the project. The authors appreciate and thank the DECOVALEX-2019 Funding Organisations Andra, BGR/UFZ, CNSC, US DOE, ENSI, JAEA, IRSN, KAERI, NWMO, RWM, SÚRAO, SSM and Taipower for their financial and technical support of the work described in this paper. The statements made in the paper are, however, solely those of the authors and do not necessarily reflect those of the Funding Organisations.

REFERENCES

[1] A. Gens, DECOVALEX-2019 Task D description: HM and THM interactions in bentonite engineered barriers (INBEB) - Stage 1: Operational period of the EB experiment (2016).

[2] J.C. Mayor et al., Engineered barrier emplacement experiment in Opalinus Clay for the disposal of radioactive waste in underground repositories. in P. Bossart and C. Nussbaum (editors) Mont Terri Project - Heater Experiment, Engineered Barriers Emplacement and Ventilation Tests, p. 115-179 (2007).

3분과

고준위폐기물처분 (Poster)

Shearing Analysis of Disassembly Machine in HeadEnd

Younghwan Kim*, Yungzon Cho, and Youngsoon Lee
Korea Atomic Energy Research Institute, Daedeok-daero989beon-gil 111,Yuseong-gu, Daejeon, Republic of Korea
Yhkim3@kaeri.re.kr

1. Introduction

Mechanical head-end processing of SF (Spent Fuel) disassembly and shearing nuclear fuel rods (tube+pellet) shall be performed in advance as the head-end process of the pyro-process for the recycling of SF. Also, for oxidation treatment of the nuclear fuel, a device is required to shear the SF rods generated from the nuclear plant. In this paper, we tried to calculate the optimal shearing force of the light water reactor rods (PWR 16x16), and design the nuclear fuel rods shearer reflecting this. For this, simulated SF shearer (Prototype-1) and simulated nuclear fuel rods were made and the shearing stress formula was derived to carry out the basic device test. Also, using the shearing formula the calculated value of the shearing stress of the aluminum pellet and the experiment value using the device were compared. As a result, the degree of maintaining the original form of the cross section of the rods after the shearing was relatively nice, and the aluminum shearing force theory and the average experiment value almost matched. Also, using the derived shearing force formula, the shearing forces of the zircaloy hull and the spent fuel pellet were calculated, and SF shearer design plan was made. Using the shearing force formula calculated with the diameters of the hull and the pellet as the process variables, you can get the shearing forces of various PWR spent fuel rods.

2. Main Contents

2.1 Summary of the rods shearer

Prototype-1 is the 2^{ND} device to derive the data and to design SF rods shearer by testing with nuclear fuel rods that simulated 16x16 PWR SF rods. The basic device is composed to shear 1 rod each time, and it is fixed to prevent shaking during the shearing process. Main composition largely includes shearing part, frame part, hydraulic part, clamping part, and load cell, etc.

2.2 Experiment method

As in figure 1-a, a Prototype-1 with the maximum capacity of the load cell of 2 ton is made. Also, as in figure 1-b, Zircaloy (Zry-4) hull was used, aluminum and cement were inserted in the form of pellet to make the simulated rods, and the shearing test was carried out. For this, first the shearing stress formula was derived and the basic device test was carried out. Also, the calculated value of the shearing stress of the aluminum pellet using the shearing formula and the experiment value using the device were compared. Using the derived shearing force formula, the shearing forces of Zry-4 hull and the pellet, which is the SF, were calculated. Based on the above data, PWR 16x16 SF shearer design was made.

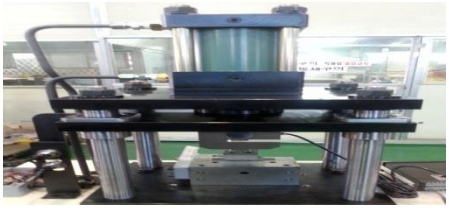

(a) Pototype-1

(b) Rods

Fig.1. Prototype-1 device and rods for sharing test.

2.3 Rods shearing formula derivation

To calculate the optimal shearing stress of PWR 16x16 rods (hull+pellet), the shearing formula (1) and formula (2) were used to design new device, and the Prototype-1 of figure 1-a was used to get the value of the experiment shearing force. Also, τ_1 of the aluminum material using the formula (1) and formula (2), the calculated τ_2 value of the zircaloy material, and the experiment value were compared.

$$w_1 = \frac{\pi}{4}(x_2{}^2 - x_1{}^2)\tau_1 \qquad (1)$$

$$w_2 = \frac{\pi}{4} dx_1{}^2 - \bullet\, \tau_2 \qquad (2)$$

(τ_1: pellet shearing stress, τ_2: hull shearing stress, w_1: pellet shearing force, w_2: hull shearing force, d_2: hull diameter, d_1: pellet diameter)

2.4 Experiment result and device design

As in figure 2-b, the degree of maintaining the original form of the sheared cross section was relatively good. As in figure 2-a, the aluminum shearing force was 1120 kgf. Also, the theoretical value of the uranium (UO_2) pellet, which is SF, was 879 kgf. Among the rod-cut shearing forces, cement was 1750 kgf. Figure 2-c is a newly designed shearer.

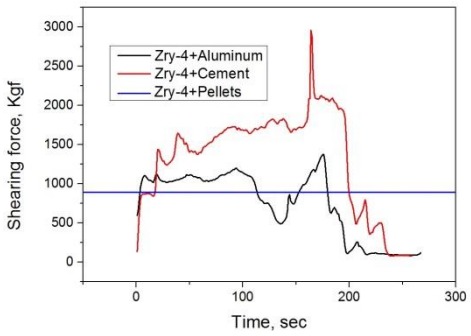

(a)Results

(b)sheared rods

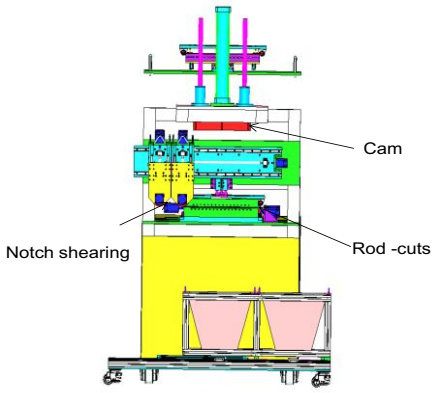

(c)New design

Fig.2. Theoretical, experimental results and new design.

3. Conclusion

The shearing stress formula was derived, and the basic device test was carried out. Also, the calculated shearing force value of the aluminum pellet using the shearing formula and the experiment value using the device were compared. As a result of the shearing test, the degree of maintaining the original form of the sheared rod was relatively good, The shearing formula was used to indirectly get the shearing force of the hull and the pellet of the actual SF, and the data was obtained to be used in the design of the head-end process shearer for SF recycling. Also, you can get the shearing forces of various PWR spent fuel rods using the calculated shearing force formula with the diameters of the hull and the pellet as the process variables.

ACKNOWLEDGEMENTS

This paper is the study carried out with the 2013 funding of the Ministry of Education, Science and Technology and the support from National Research Foundation of Korea (Nuclear Energy Technology Development Project, No. 2012M2A8A5025 696).

REFERENCES

[1] B. D. Cul, R. H. Hunt, "Advanced head-end processing of spent fuel," 2004 ANS Winter Meeting, Washington DC, Nov. 16, 2004.

Thermal Conductivity Investigation of Korean Bentonite Buffer Materials

Seok Yoon*, Wanhyoung Cho, Changsoo Lee, and Geonyoung Kim

Korea Atomic Energy Research Institute, Daedeok-daero989ben-gil 111,Yuseong-gu, Daejeon, Republic of Korea

*syoon@kaeri.re.kr

1. Introduction

The concept of an engineered barrier system (EBS) is suggested to dispose high level waste (HLW). EBS is composed of a disposal canister with packed spent fuel, a buffer material, backfill material, and near field rock mass. A buffer material is very essential to guarantee the disposal safety of HLW, and play a very important role to protect the waste and canister against any external mechanical impact. Furthermore, it requires high thermal conductivity to release as much decay heat as possible from the spent fuel. The thermal conductivity of the buffer material is a crucial property that determines the temperature change owing to decay heat from spent fuel. There have been many researches to investigate the thermal conductivity of bentonite buffer materials or many types of soils. However, there is a lack of research on the overall evaluation of the thermal conductivity of Korean bentontonite buffer materials. Therefore, this paper investigated and analyzed previous researches on the thermal conductivity of the Korean bentonite buffer materials produced in Kyeongju.

2. Results and discussion

In Korea, Ca bentonite buffer materials have been produced in Kyeongju by CLIRIANT KOREA. Ca bentonite is named as KJ-I produced before 2015, and KJ-II after 2015 [1]. There have been several researches investigating thermal conductivity of KJ-I [2-4] considering various affecting factors such as the degree of saturation, dry density and temperature variation. Yoon et al. (2017) [5] also investigated thermal conductivity of KJ-II and suggested the prediction model considering various factors. Table 1 shows a quantitative analysis for KJ-I and KJ-II in order to analyze the mineral composition, and Table 2 shows the variation of thermal conductivity with respect to the degree of saturation and dry density.

Table 1. Quantitative analysis for KJ-I and KJ-II bentonite

Bentonite Type	KJ-I				KJ-Ⅱ			
Sample No.	1	2	3	Avg.	4	5	6	Avg.
Montmorillonite	60.0	67.4	62.1	63.2	63.4	61.7	60.5	61.9
Albite	27.2	22.2	27.5	25.6	19.4	22.8	20.4	20.9
(λ=1.96 W/mK)	(68.0%)	(68.1%)	(72.6%)	(69.6%)	(53.0%)	(59.5%)	(51.7%)	(54.9%)
Quartz	5.0	4.8	5.0	4.9	5.8	4.9	5.3	5.3
(λ=7.69 W/mK)	(12.5%)	(14.7%)	(13.2%)	(13.3%)	(15.8%)	(12.8%)	(13.4%)	(13.9%)
Cristobalite	3.6	1.8	3.5	3.0	4.0	4.5	3.7	4.1
(λ= 6.15 W/mK)	(9.0%)	(5.5%)	(9.2%)	(8.2%)	(10.9%)	(11.8%)	(9.4%)	(10.8%)
Calcite	2.4	2.0	2.0	2.1	4.3	3.3	6.8	4.8
(λ=3.59 W/mK)	(6.0%)	(6.1%)	(5.3%)	(5.7%)	(11.7%)	(8.6%)	(17.2%)	(12.6%)
Heulandite	1.8	1.7		1.8	3.0	2.7	3.3	3.0
(λ=1.09 W/mK)	(4.5%)	(5.2%)	(- %)	(4.9%)	(8.2%)	(7.1%)	(8.4%)	(7.9%)

Table 2. Thermal conductivity of KJ-I and KJ-II bentonite

	Saturation (%)	Dry density (kg/m³)	Thermal conductivity (W/mK)
KJ-1	0~100	1200~1800	0.301~1.249
KJ-2	0~100	1527~1803	0.627~1.345

The thermal conductivity of the bentonite buffer materials was proportional to the degree of saturation and dry density (Fig. 1). As shown in Table 1, the composition of montmorillonite was almost similar between KJ-I and KJ-II. However, KJ-II has more minerals with high thermal conductivity such as Quartz, Cristobalite, and Calcite than KJ-I, and it is thought that the thermal conductivity of KJ-II was higher than that of KJ-I.

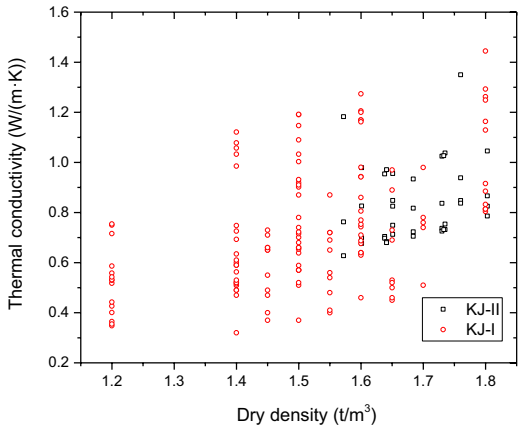

(a) Thermal conductivity *vs* dry density

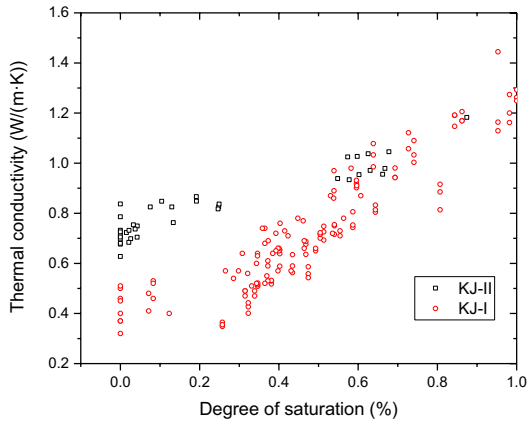

(b) Thermal conductivity *vs* degree of saturation

Fig.1. Thermal conductivity variation.

3. Conclusion

This paper summarized the thermal conductivity of the Kyeongju bentonite buffer materials. The thermal conductivity of KJ-II was higher than that of KJ-I because KJ-II has more minerals with high thermal conductivity such as Quartz, Cristobalite, and Calcite than KJ-I. Therefore, it is thought that KJ-II has more benefit for the buffer materials in terms of the thermal properties.

ACKNOWLEDGEMENT

This research was supported by the Nuclear Research and Development Program of the National Research Foundation of Korea (NRF-2017M2A8A5014857), funded by the Ministry of Science and ICT.

REFERENCES

[1] You, M., Choi, H.J., Lee, M.S., Lee, S.Y., Chemical and mineralogical characterization of domestic bentonite for a buffer of an HLW repository, KAERI/TR-6182(2015).

[2] Lee, M.S., Choi, H.J., Lee, J.O., Lee, J.P., Improvement of the thermal conductivity of a compacted bentonite buffer, KAERI/TR-5311(2013).

[3] Cho, W.J., Lee, J.O., Choi, H.J., Thermal conductivity of domestic compacted bentonite and bentonit-sand mixture, KAERI/TR-5561 (2014).

[4] Lee, J.W., Choi, H., Lee, J.Y., Thermal conductivity of compacted bentonite as a buffer material for a high-level radioactive waste repository, Ann Nucl Energy 94, 848-855 (2016).

[5] Yoon, S., Lee, M.S., Kim, G.Y., Lee, S.R., Kim, M.J., A prediction of thermal conductivity for compacted bentonite buffer in the high-level radioactive waste repository, J. Korean Geotech Soc 32, 55-64 (2017).

Nuclide Transport Behavior in the Fracture Around a Conceptual German HLW Repository

Youn-Myoung Lee[1] and Thorsten Schaefer[2]
[1]Korea Atomic Energy Research Institute, Daedeok-daero989ben-gil 111,Yuseong-gu, Daejeon, Republic of Korea
[2]Karlsruhe Institute of Technology, INE, Hermann-von-Helmholtz-Platz 1, 76344, Eggenstein-Leopoldshafen, Germany
ymlee@kaeri.re.kr

1. Introduction

After Fukushima NPP accident, Germany has decided to gradually abrogate nuclear power generation. By 2018 more than 28,000 cubic meters of high-level radioactive waste are expected to be stored when all the NPP and research facilities are finally decommissioned.

Currently radioactive waste is placed in interim storage facilities, with spent nuclear fuels mostly stored at reactor sites. Most German used fuel is reprocessed overseas, from which vitrified HLW arises (for the part of contracts signed up to 1989) is stored in surface facilities at Gorleben and Ahaus.

According to a draft national radioactive waste disposal program proposed by environment ministry and adopted by the German cabinet in 2015, for the final disposal of radioactive waste, the former iron ore mine, Konrad is proposed exclusively for LILW waste, and for HLW another site which will be determined in 2022 around when the last NPP is shut down.

In 2016, another report that provides a recommended method for the disposal of waste in a geologic repository was prepared. According to the report, the safest site is to be sought in a three-phase process and defined by federal law. The site selection should be accompanied by extensive nationwide public participation. And the rock in which repository will be placed could be such various rock type of clay or crystalline over salt.

The research project, ENTRIA[1] is disposal options currently being considered in Germany in cooperation with 11 institutes at German universities and research facilities as well as one Suisse partner for radioactive residues which requires interdisciplinary analyses and development of evaluation principles.

For analyzing radioactive waste management subjects from the viewpoint of all involved academic disciplines such as natural sciences, engineering, and possible whatever, ENTRIA is engaged in finding options for the disposal of HLW, which actually means heat generating radioactive waste in Germany.

Past discussions in decades throughout the society and feedback on recent political events have clearly shown that this kind of complex issues may never be solved from solely pure technical, academic, or natural science viewpoints through research and development. That is the reason ENTRIA combines technical and social aspects of the following three most important radioactive waste management options: 1) Final disposal in deep geological formations without retrieval (maintenance-free), 2) Disposal in deep geological formations with monitoring and retrieval option, and 3) Simple surface storage.

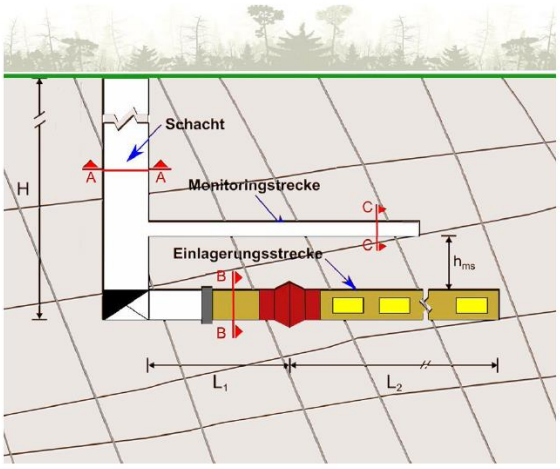

Fig. 1. An ENTRIA HLW disposal concept.

Working independently from politics, any specific consideration of sites and their qualification studies for a repository is excluded in the project.

Through this study we have tried to technically assess a limited far-field part of the hypothetical repository (Fig. 1.) in the crystalline geological rock medium, which is conceptually being considered for

ENTRIA as a candidate among possible other rock media, in which HLW is supposed to be disposed of.

Two physical sensitivities of travel distance and matrix diffusion perpendicular to the wall of the fracture associated with nuclide transport in the fractures were investigated in view of safety assessment of the repository.

2. Results

Along the fracture zone in the crystalline rock medium with a higher hydraulic conductivity than the near-field area and through which nuclides that are released from artificial barriers, a fast nuclide transport is anticipated with advection dominated as well as the dispersion and rock matrix diffusion. Two separate results, one of which is from probabilistic assessment for sensitivity of the travel length variation, and the rest of which is from a deterministic comparative evaluation to see the effect of the matrix diffusion are shown in turn. All the data used are found in the report. [2]

2.1 Travel Length

In order to observe the behavior of the nuclide flux released from the fracture in accordance with varying travel lengths in the fracture, a hypothetical pdf following a triangular distribution for the stochastic travel lengths were introduced.

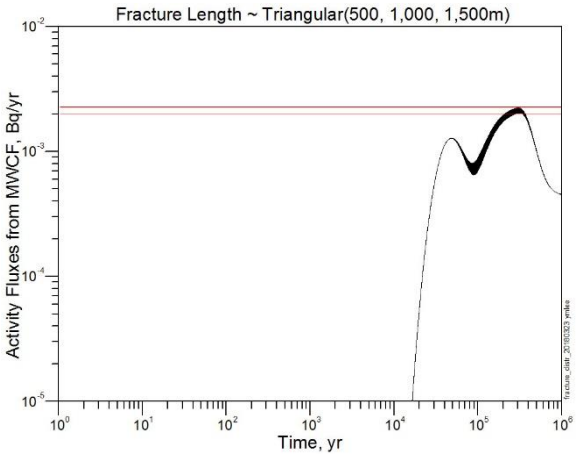

Fig. 2. Sensitivity of the travel distances for selected nuclides to their released rates from the fracture, based on a (Tri(500, 1000, 1500m)) distribution of all travel lengths.

Breakthroughs for selected nuclides from a probabilistic calculation with several thousand Latin hypercube sampling for the travel length is shown in Fig. 2. A rather broad band of the second peak values are found in the figure, showing rather high sensitivity of the travel length to the nuclide flux.

2.2 Matrix Diffusion

Behavior of nuclide fluxes from the fracture was also observed and compared with each other in Fig. 3, when matrix diffusion into the rock matrix takes place or not.

As seen in the figure some nuclides such as ^{241}Am and ^{243}Am which have relatively high degree of retardation show their large difference in their peak fluxes are found.

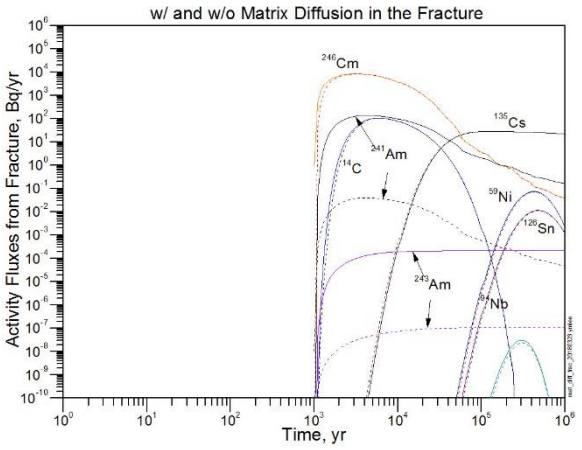

Fig. 3. Breakthroughs in case of no matrix diffusion (solid), compared to the case of matrix diffusion (dashed).

REFERENCES

[1] Joachim Stahlmann et al., Generische Tiefenlagermodelle mit Option zur Rückholung der radioaktiven Reststoffe: Geologische und Geotechnische Aspekte für die AuslegungInstitut für Grundbau und Bodenmechanik TU-Braunschweig, ENTRIA-Arbeitsbericht-03, (2014).

[2] Youn-Myoung Lee and Dong-Keun Cho, A GoldSim Model for Performance Assessment of a Horizontal-Type ENTRIA Repository, KAERI/TR-7189/2018.

Numerical Evaluation for In-Situ Tests Investigating a Local Hydraulic Property on a Borehole

Nak-Youl Ko* and Sung-Hoon Ji

Korea Atomic Energy Research Institute, 111, Daedeok-daero 989 beon-gil, Yuseong-gu, Daejeon, Republic of Korea

*nyko@kaeri.re.kr

1. Introduction

Deposition holes emplacing canisters can be damaged by changing stress conditions induced from excavation of the holes or other processes. In this study, previous researches for investigating local damages or fractures at boreholes were examined and numerical simulations were performed for evaluating the existing characterization methods.

2. Method

Previous works on single borehole tests, which can be applicable for estimating local properties of the vicinity or wall of boreholes were reviewed. Then, applicability of the analysis methods suggested in the reviewed works was determined by conducting a case study. A hypothetic groundwater flow system was assumed, and a single borehole test was simulated. With the simulation results, the hydraulic property of the system was estimated using the analysis methods from the previous works, and compared to the assumed one of the hypothetical groundwater flow system.

3. Results

3.1 Dipole Flow Test

From the reviewed single borehole tests, the dipole flow test (DFT), which makes groundwater flow circulate between multiple intervals of a test borehole and has been used to estimate a hydraulic property and anisotropy ratio at a local part of the borehole [1, 2], were considered as an available hydraulic test methods for in-situ conditions. In addition, the dipole flow tracer test (DFTT), which is a tracer test based on the DFT, was also examined to determine properties of solute transport such as dispersivity.

3.2 Numerical Simulations for Hypothetical DFT

From evaluating applicability of the test by numerical simulations, the analysis methods suggested in the previous studies were available for estimating a hydraulic property based on in-situ field tests. The methods were applied to results of numerical simulations with a hypothetical aquifer. From the analysis, the estimated horizontal hydraulic conductivity of the hypothetical aquifer had the same order (= 10^{-7} m/s) as the assumption.

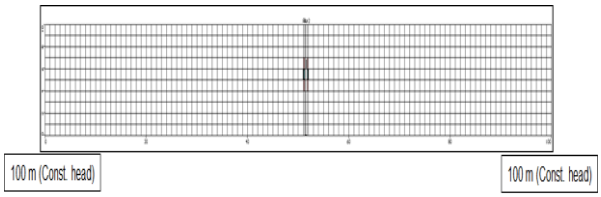

Fig. 1. Hypothetical aquifer and a test borehole.

Table 1. Parameters for Hypothetical aquifer

Parameters	Value
Horizontal hydraulic conductivity	10^{-7} m/s
Vertical hydraulic conductivity	10^{-8} m/s
Aquifer thickness	10 m
Boundary condition for both ends	100 m
Anisotropic ratio	3.16

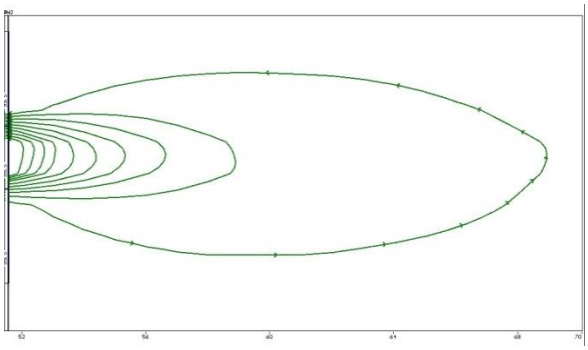

Fig. 2. Groundwater flow path simulated with the hypothetical aquifer.

4. Conclusions

To investigate locally damaged areas or discontinuity in a borehole, DFT was examined and tested in a hypothetical aquifer condition. It is thought that DFT is applicable to characterization of local structures in the vicinity of boreholes. Besides, it may be contributed to designing in-situ hydraulic test plans. The results of this study can be used for practical application to a deep geological disposal of high-level wastes.

Acknowledgement

This work was supported by the Ministry of Science, ICT and Future Planning within the framework of the national long-term nuclear R&D program (NRF-2017M2A8A5014858).

REFERENCES

[1] Z.J. Kabala, “The dipole-flow test: a new single-borehole tests for aquifer characterization”, Water Resources Research, 29(1), 99–107 (1993).

[2] M.S. Hantush, Hydraulics of Wells, Advances in Hydroscience, edited by Ven Te Chow, Academic Press, New York, 281-442 (1964).

Development of Modeling Interface for a Process-Based Total System Performance Assessment of a Geological Disposal System

Jung-Woo Kim*, Jaewon Lee, and Dong-Keun Cho
Korea Atomic Energy Research Institute, 111, Daedeok-daero 989beon-gil, Yuseong-gu, Daejeon, Republic of Korea
* jw_kim@kaeri.re.kr

1. Introduction

Until recently, only a system-level safety assessment model was generally used for the safety assessment of a geological disposal system in Korea. For instance, KAERI developed K-PAM (KAERI Performance Assessment Model), a system-level safety assessment model [1], and used it for the safety assessment in its safety case [2].

The system-level safety assessment is a kind of conservative approach and has the advantage of short computation time. However, it has limitations to reflect short- and long-term evolution of the disposal system and to realistically simulate thermal, hydraulic, mechanical, and chemical complex phenomena. Because many important processes are highly abstracted in the system-level models, the advanced knowledge from state-of-the-art researches is seldom applied into the safety assessment. In addition, it is impossible or very difficult to verify the total system models owing to the absence of the system-scale experimental data.

To cope with the limitations of the total system models shown above, the US has been trying to use high-performance computational codes to move the total system model closer to the process model level [3], and the EU has developed and been using a multiphysics simulation framework by coupling COMSOL Multiphysics and PHREEQC [4]. Although the process-based total system performance assessment requires a lot of computational resources and computation time, the computational efficiency can be improved through parallel computation that takes advantage of recent high-performance computers.

To keep up with the trends, KAERI has also recently proposed developing a process-based total system performance assessment model for a geological disposal system (APro). As the first step of development of the model, the modeling interface was designed in this study.

2. APro

APro stands for "**A**dvanced **Pro**cess-based total system performance assessment framework for a geological disposal system". APro employs a bottom-up approach unlike a system-level model which uses top-down approach. APro was basically designed to be able to simulate all the processes that can be occurred in a geological disposal system including thermal, hydraulic, mechanical, chemical, and radiological processes. The flowchart of APro is depicted in Fig. 1.

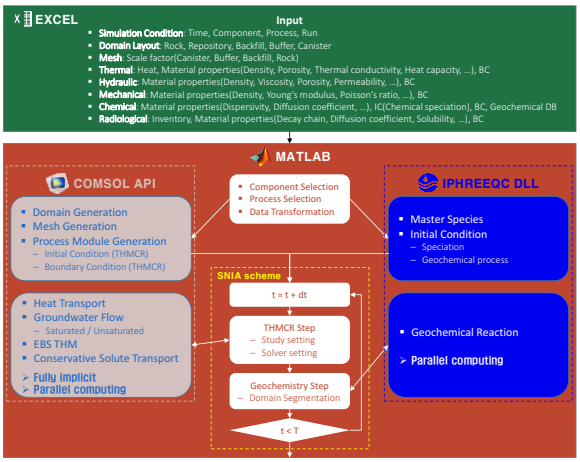

Fig. 1. Flowchart of APro.

2.1 Input

All input data are defined in an EXCEL file. The input EXCEL file consists of "Simulation Condition", "Domain Layout", "Mesh", "Thermal", "Hydraulic", "Mechanical", "Chemical", "Radiological" sheets.

2.1.1 Simulation Condition. From "Simulation Condition" sheet, time-related parameters, components and processes to be considered in the simulation, and output options are defined.

2.1.2 Domain Layout. The target repository considered in APro is typical KBS3-type including both vertical- and horizontal types. From "Domain Layout" sheet, the numbers of repositories, tunnels, boreholes and canisters, and dimensions of them can be defined.

2.1.3 Mesh. From "Mesh" sheet, the scale factors for each components are defined to control mesh size.

2.1.4 Thermal. From “Thermal” sheet, the input data related to the thermal process, such as heat source, density, porosity, thermal conductivity, heat capacity, etc., are defined. Each parameter can be defined as not only a constant but also a function of time or temperature.

2.1.5 Hydraulic. From “Hydraulic” sheet, the input data related to the hydraulic process, such as water density, viscosity, porosity, permeability, etc., are defined. Each parameter can be defined as not only a constant but also a function of temperature.

2.1.6 Mechanical. From “Mechanical” sheet, the input data related to the mechanical process, such as density, Young’s modulus, Poisson’s ratio, etc., are defined with respect to the linear elastic model.

2.1.7 Chemical. From “Chemical” sheet, the input data related to the geochemical process, such as dispersivity, diffusion coefficient, initial condition, boundary condition, thermodynamic DB, etc., are defined. The initial and boundary conditions and thermodynamic DB are defined as separated PHREEQC files which should be in a subfolder.

2.1.8 Radiological. From “Radiological” sheet, the input data related to the radiological process, such as inventories for each repository, radioactive decay properties, diffusion coefficients and solubilities of radionuclides, etc. are defined.

2.2 Computation Procedure

The overall computation is mainly managed in MATLAB workspace by controlling COMSOL API and IPHREEQC DLL.

Firstly, input data are loaded and rearranged in MATLAB workspace. Secondly, model domain and mesh are constructed using COMSOL based on the selected components. Thirdly, COMSOL physics are defined based on the selected processes. In case of the “Chemical” process, the chemical speciation of the initial and boundary conditions is calculated by IPHREEQC DLL and transferred to the COMSOL physics. Finally, the computations are iterated with COMSOL API and IPHREEQC DLL for each time step.

In each time step, heat source, radionuclide inventory, etc. are updated, and THMC process including heat transport, groundwater flow, EBS THM, non-reactive transport, etc., are computed by COMSOL. And then, radioactive decay is computed in MATLAB workspace, and the geochemical reactions for each mesh nodes are computed in parallel by using PHREEQC DLL.

3. Conclusion

As the first step of development of a process-based total system performance assessment model, APro, the modeling interface was designed in this study. After configuring the interface, each specific processes as module-type will be embedded into the overall framework step by step, and the coupled effects will additionally be evaluated. In the future, APro is expected to contribute to improving the reliability of the safety assessment in combination with the system-level safety assessment model (e.g., K-PAM).

ACKNOWLEDGEMENT

This work was supported by the Nuclear Research and Development Program (No. 2017M2A8A5014856) of the National Research Foundation of Korea (NRF) funded by the Ministry of Science, ICT and Future Planning (MSIP).

REFERENCES

[1] J.-W. Kim et al., “Model Development for Risk-Based Safety Assessment of a Geological Disposal System of Radioactive Wastes Generated by Pyroprocessing of Pressurized Water Reactor Spent Fuel in Korea”, Nuclear Technology, DOI: 10.1080/00295450.2018.1426331 (2018).

[2] J.-W. Kim et al., “A Safety Case of the Conceptual Disposal System for Pyro-processing High-Level Waste Based on the KURT Site (AKRS-16): VII. Post-Closure Safety Assessment”, KAERI/TR-6733/2016 (2016).

[3] R.T. Mills et al., “Simulating Subsurface Flow and Transport on Ultrascale Computers using PFLOTRAN”, Journal of Physics: Conference Series, 78, 012051 (2007).

[4] A. Nardi et al., “Interface COMSOL-PHREEQC (iCP), an efficient numerical framework for the solution of coupled multiphysics and geochemistry”, Computers & Geosciences, 69, 10-21 (2014).

Statistical Approach of the Geochemical Mobility of Geogenic Uranium in Groundwater of KURT

Jihye Jeong*, Jang-Soon Kwon, Yong-Kwon Koh, and Jae-Kwang Lee
Korea Atomic Energy Research Institute, Daedeok-daero989ben-gil 111,Yuseong-gu, Daejeon, Republic of Korea
* yz0201@kaeri.re.kr

1. Introduction

For the high-level radioactive waste disposal facilities, it is important to evaluate the mobility of radionuclides in groundwater and the geochemical factors that control its behavior in case of unplanned leakage of radionuclides to groundwater. So far, a number of studies have been conducted to investigate hydrochemical and biogeochemical properties of the groundwater in the KAERI Underground Research Tunnel (KURT) [1]–[4], but statistical approach of mobility and transport of natural nuclides in the groundwater have not been carried out. The purpose of this study is to evaluate geochemical characteristics of groundwater in DB-1 (500m in depth) within KURT and to statistically identify factors that affect uranium mobility in the KURT groundwater.

2. Results and Discussions

2.1 Hydrochemical characteristics of KURT groundwater

Analytical results of the samples acquired on a quarterly in 2015 and 2016 in the KURT DB-1 borehole have been used for evaluation of hydrochemical characteristics. The interval of the borehole is divided into six sections (i2, i3, i4, i5, i6 and i7) with the depth. The groundwater chemistry with depth in DB-1 shows the changes from Ca-HCO_3 to Na-HCO_3 (exclude i5 section) which is common trend in granitic aquifers.

2.2 Hydrochemical type with depth

The i3 section (91.7 ~ 114.7 m) shows relatively high Eh, DO and PCO_2 values. Moreover the uranium concentration is the highest in the section (mean value: 720.34 μg/L).

The i5 section (199.7 ~ 228 m) shows considerably higher pH, K, SO_4, and CO_3 values. This section may have the potential for a grouting effect, and the water quality in the section is classified as an anthropogenic (not natural) interval.

The i7 section (246.7 ~ 299.7 m) shows a Na-HCO_3 water type due to a relatively long residence time. Therefore, this section shows high pH, EC, F, Na and HCO_3 values while Eh and DO are low.

2.3 Geochemical mobility of uranium

The uranium concentration in each section showed a statistical difference through the analyses of Variance (ANOVA) test was performed (p<0.05). The uranium concentration in the KURT groundwater is the highest in the i3 section under oxidized condition. Uranium mobility shows the increases in the groundwater with higher oxic-alkaline condition and PCO_2. The main factors affecting uranium mobility in groundwater are pH, DO (ORP) and partial pressure of carbon dioxide (PCO_2) [5]. The statistical result confirmed that uranium mobility is higher under the pH 8.0 - 9.5, DO>0.5 and high PCO_2 conditions. The Eh-pH

diagram for uranium species in the KURT groundwater showed that major specie of uranium existed as $UO_2(CO_3)_3^{4-}$ which is a high mobile one in a solution.

3. Conclusions

The water quality of DB-1 groundwater in KURT is evolving from Ca-HCO_3 to Na-HCO_3 with depth. The concentration of uranium is the highest in the i3 section (around 100 m), and the DO, Eh, and PCO_2 values are also high in the section. The i5 section (around 200 m) is likely to have a grouting effect. The i7 section (around 300 m) is characterized the Na-HCO_3 type with relatively high EC, pH, F, and Na values because of long residence time. Geogenic Uranium in the KURT groundwater within granite bedrock demonstrated statistically different existence and mobility in each section (depth). Uranium mobility in groundwater generally depends on the pH, DO (Redox), and PCO_2, and its mobility in the KURT groundwater is increased under oxic-alkaline and high PCO_2 conditions.

Acknowledgement

This work was supported by the Ministry of Science and ICT within the framework of the national long-term nuclear R&D program (NRF-2017M2A8A5014859).

References

[1] J.-H. Ryu, J.-S. Kwon, G.-Y. Kim, and Y.-K. Koh, "Geochemical Characterization of Rock-Water Interaction in Groundwater at the KURT Site," *J. Nucl. Fuel Cycle Waste Technol.*, vol. 10, no. 3, pp. 189–197 (2012).

[2] N.-Y. Ko, K. W. Park, K. S. Kim, and J. W. Choi, "Groundwater Flow Modeling in the KURT site for a Case Study about a Hypothetical Geological Disposal Facility of Radioactive Wastes," *J. Nucl. Fuel Cycle Waste Technol.*, vol. 10, no. 3, pp. 143–149 (2012).

[3] J.-H. Lee, H. Jung, E. Lee, and S. Kim, "Estimation of groundwater level fluctuation of the crystalline site using time series analyses in south Korea," *J. Nucl. Fuel Cycle Waste Technol.*, vol. 11, no. 3, pp. 179–192 (2013).

[4] S. Y. Lee, Y. Roh, and J. T. Jeong, "Changes of the Oxidation/Reduction Potential of Groundwater by the Biogeochemical Activity of Indigenous Bacteria," *Econ. Environ. Geol.*, vol. 47, no. 1, pp. 61–69 (2014).

[5] P. L. Smedley, B. Smith, C. Abesser, and D. Lapworth, "Uranium occurrence and behaviour in British groundwater", 2006.

Characteristics of KyungJu-II Bentonite Heated With Different Potassium Concentrations

Wan Hyoung Cho *, Ji-Hun Ryu, and Jae Kwang Lee
Korea Atomic Energy Research Institute, Daedeok-daero989ben-gil 111,Yuseong-gu, Daejeon, Republic of Korea
cho0714@kaeri.re.kr

1. Introduction

Buffer is the major component of engineering barrier with canister in high-radioactive waste disposal. Bentonite is considered as a buffer material, because it has properties such as high swelling potential, low hydraulic conductivity and high thermal conductivity. But bentonite lost its major functions by long-term exposure to the decay heat from high-radioactive wastes and geochemical conditions of groundwater [1]. This study carried out heating experiments of KJ-II bentonite at high temperature condition with different potassium concentrations.

2. Methods

2.1 Samples

Table 1. The list of bentonite Samples

	Sample No.	Mixed solution
Type-1	Ca-1	D.I. water
	Ca-2	0.005M KCl-solution
	Ca-3	0.05M KCl-solution
	Ca-4	0.1M KCl-solution
Type-2	Na-1	D.I. water
	Na-2	0.005M KCl-solution
	Na-3	0.05M KCl-solution
	Na-4	0.1M KCl-solution

The material used in this study was KyungJu (KJ)-II bentonite. Two sets of samples were prepared by two different pretreatments (table 1). For type-1, KJ-II bentonite was washed with D.I. water. The fine particles of the bentonite were collected after centrifugation. For type-2, the bentonite was saturated with 1M NaCl, then the samples were washed with D.I. water to remove Cl^{-}. The fine particles of KJ-II bentonite were collected after centrifugation. The collected samples were completely dried using the freeze-dry method.

2.2 Experiment procedure

The samples(type-1 and type-2) were mixed D.I. water and KCl-solutions of 0.005M, 0.05M and 0.1M at a ratio of 1(0.5 g) : 2(10 mL), respectively. The mixed samples were agitated to get homogenized at 120rpm for 20mins and heated in furnace at 150℃ for 24hours (Fig. 1).

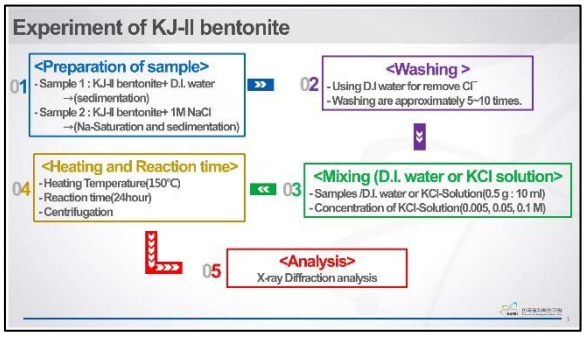

Fig. 1. The bentonite Experiment procedure.

3. Results and Discussion

The results of XRD indicated major constituent minerals of KJ-II bentonite were smectite, albite, orthoclase, quartz, cristobalite and calcite (Fig. 2). The slight difference in the intensity was identified at Ca-1 and Ca-2 as well as Na-1 and Na-2, which were heated with D.I.water and 0.005M KCl-solution, respectively. But, the results of XRD from Ca-3 and Na-3 samples (reacted with 0.05M KCl-solution) as well as Ca-4 and Na-4 samples (reacted with 0.1M KCl-solutions) showed the inflected 2-theta of smectite which was confirmed approximately 7.16.

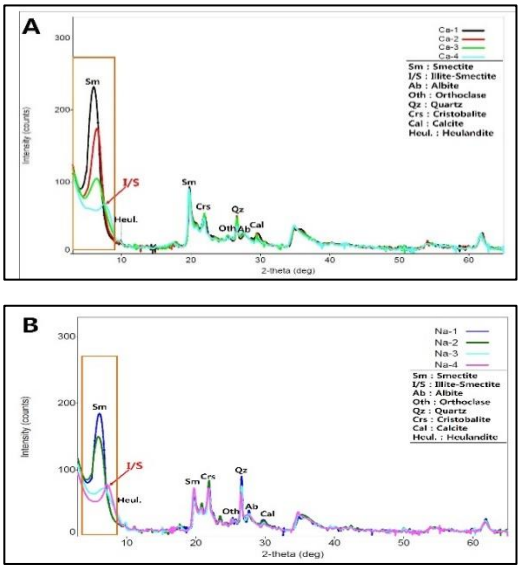

Fig. 2. X-ray diffraction patterns from the samples heated with D.I. water and various KCl-solutions([K+]= 0.005M, 0.05M, 0.1M). A: Type-1, B: Type-2.

In general, d(0,0,1) value of smectite was 15 Å. The values of d(0,0,1) of Ca-1and Ca-2 were similar with that of Na-1 and Na-2, which were approximately 14.71~14.55 Å. But, Ca-4 and Na-4 samples showed a decreased in d(0,0,1) values, which were approximately 12.34 Å. The results showed that dehydration occurred between the interlayers and the ion exchange of potassium and cation, by reaction with high-concentration KCl-solutions at 150℃.

4. Conclusion

The slight difference in the intensity was identified between Ca-1 and Ca-2(heated with D.I. water) as well as Na-1 and Na-2(heated with 0.005M KCl-solution). But, Ca-3 and Na-3 samples (heated with 0.05M KCl-solution), and Ca-4 and Na-4 samples (heated with 0.1M KCl-solutions) showed the variation in 2-theta and d values compared to that of smectite. It indicated that dehydration occurred between the interlayers and the ion exchange of potassium and cation, by heating with high KCl concentration solutions at 150℃. The result indicated that smectite transforms into illite at high temperature with high concentration potassium.

ACKNOWLEDGMENTS

This research was supported by National Research Foundation of Korea (NRF) funded by the Minister of Science, ICT and Future Planning (The nuclear research and development program No. 2017M2A8A5014859)

REFERENCES

[1] J.W. Lee, and W.J. Cho, “Hydrothermal behaviors and long-term stability of bentonitic buffer material”, J.of the Korean Radioactive Waste society, v. 5(2), p.145-154(2007).

[2] L.C. Carniel, R.V.Conceicao, N. Dani, V.F. Stefani, N.M. Balzaretti, R.D. Reis, “Stuctural changes of potassium-saturated smectite at high pressures and high temperatures: Application for subduction zones”, Applied clay Sience, v.102, p.164-171 (2014).

Preliminary Evaluation of Rare Earth Effect on Burnup Limit in TRU Fuel

Byoung Oon Lee*, Chan Bock Lee, June Hyung Kim, Jin Sik Cheon, Jeong Yong Park, and Sung Ho Kim
Korea Atomic Energy Research Institute, Daedeok-daero989ben-gil 111,Yuseong-gu, Daejeon, Republic of Korea
*bolee@kaeri.re.kr

1. Introduction

The U-TRU-RE-Zr metal fuel is being developed in combination with the pyro-processing. Since RE (Rare Earth) will be included in the metal fuel, it is necessary to evaluate the effects of RE on burnup limit. In this paper, preliminary penetration rate model of RE to the cladding was developed based on the available data. The evaluation of burnup limits according to RE contents was carried out using the code with the developed model.

2. Preliminary penetration rate model of RE to the cladding according to the RE contents

One of the main issues that may limit burnup in metal fuel is FCCI (Fuel Cladding Chemical Interaction) due to reaction of REs with the cladding.

In order to develop the penetration rate model of RE to the cladding, the concept of penetration model developed using EBR-II DB was used [1].

In the existing model considering EBR-II DB, the coefficients such as activation energy and a diffusion coefficient were adjusted to match the penetration depths for the metal fuels with 0 wt.% RE.

In this paper, the activation energy in the model was evaluated and derived for the development of penetration rate model according to RE contents,

When RE content was 0 wt.%, the activation energy (Q) was set by applying EBR-II DB results [1].

In addition, the activation energies related to 100wt. % and 5wt. % RE were evaluated and derived using diffusion couple test data [2] and U-10Zr-5Ce HANARO irradiation data (Refer to Fig. 1) [3] .

Based on the THERMO-CALC code and the OECD DB [4], the activity of Ce-Fe was evaluated to establish the activation energies for other RE content.

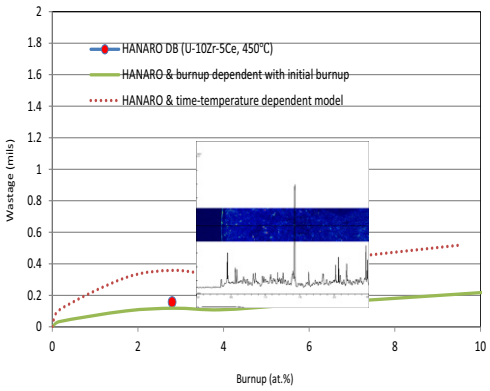

Fig. 1. Comparison of HANARO DB and calculated penetration depth.

It was analyzed that the diffusion would occur rapidly when the RE concentration reached a certain level.

The activity values for RE contents were determined considering the threshold that leads to rapid diffusion, as shown in Table 1.

Table 1. Derivation of activation energy by RE contents

RE contents (wt. %)	Activation energy, Q (kJ/mol)
0	48.227
1	47.344
3	45.616
5	43.938
100	33

The diffusion coefficient D_0 was also adjusted to be equal to the U-Pu-Zr data at 580℃ in EBR-II irradiation, because the diffusion rate of U-Pu-Zr was faster than that of U-Zr.

3. Evaluation of RE effects

3.1 Code and irradiation history for performance evaluation

In order to evaluate the bunup limit due to the RE

contents, the LIFE-METAL code [5] developed jointly with ANL (Argonne National Laboratory) was used.

Since the irradiation history for the TRU core has not yet been established, the history of the U core was applied.

Fuel rods of the U core consist of U-10Zr / FC92, and the diameter and length of the fuel slug are 5.54 mm and 900 mm, respectively. The outer diameter and thickness of the cladding are 7.4 mm and 0.5 mm respectively. The core inlet temperature of the coolant is 390℃, PICT (Peak Cladding Inner Temperature) is 650℃, and EFPD (Effective Full Power Day) of the inner / outer core is 1160 and 1450, respectively.

Fuel slug for the TRU core is assumed to be U-24TRU-RE-10Zr and the other conditions are same as the U core.

The design methodology for evaluating the burnup limits applies the specific design methodology established in the fuel rods for PGSFR.

3.2 Burnup limit evaluation according to the RE contents

In this paper, CDF (Cumulative damage fraction), which is one of fuel design criteria, was evaluated in order to evaluate the burnup limit due to the RE contents.

The burnup above the CDF limit of 0.05 were calculated. Fig.2 shows the calculated results of the burnup limit for 0, 1, 3 and 5 wt.% of RE.

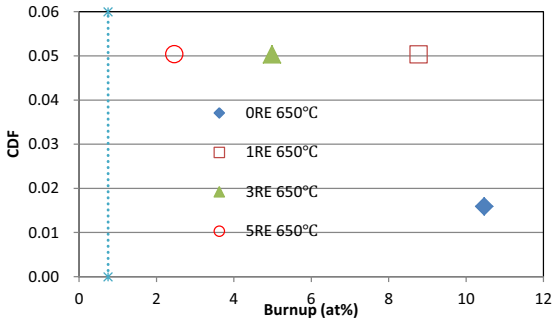

Fig. 2. Calculated results of the burnup limit for 0, 1, 3 and 5 wt.% of RE.

When the RE content was 0 wt.%, it was calculated that the CDF limit was satisfied above 11 at% of burnup.

In the case of 1, 3 and 5 wt.% of RE, however, burnup limits were calculated as 8.7, 4.9 and 2.45 at%, respectively.

Therefore, in the case of high RE contents in the metal fuel, the use of a barrier cladding is considered to be essential because a high RE earth content has a great influence on the integrity of the fuel rod.

4. Conclusion

In order to evaluate the effects of the RE content, preliminary penetration rate model was developed according to the RE contents.

Activation energies according to the RE contents were derived by considering EBR-II DB, HANARO DB, diffusion couple tests data and OECD DB.

The burnup limits according the RE contents were evaluated by applying the code and irradiation history.

It was calculated that a high RE content has a great effect on the burnup limit and the integrity of the fuel rod.

The use of a concept of barrier cladding is needed if the metal fuel has a high RE content.

ACKNOWLEDGEMENT

This work has been carried out under the National Nuclear R&D program supported by the Ministry of Science and ICT. The authors would like to express their appreciation to the members of OECD TAF ID for the establishment of thermodynamic database.

REFERENCES

[1] Personal communications with ANL.
[2] J. H. Kim et al, Journal of Nuclear Materials 479 (2016).
[3] J.S. Cheon et al, Korean Nuclear Society Spring Meeting, Jeju, Korea, May (2014).
[4] C. Guéneau et al., MMSNF (2017).
[5] M. C. Billone, et al., Proc. ANS Conf. Reliable fuels for LMRs, Tucson, (1986).

Effects of Microbial Activity on the Biochemical Alteration of KJ-II Bentonite Under Alkaline-Reducing Conditions

Hyo-Jin Seo*, Seung Yeop Lee, Jae-Kwang Lee, and Wan Hyoung Cho

Korea Atomic Energy Research Institute, Daedeok-daero989ben-gil 111,Yuseong-gu, Daejeon, Republic of Korea

*hjseo@kaeri.re.kr

1. Introduction

Bentonite has been considered as a buffer material for deep geological disposal of high-level radioactive wastes. Various kinds of microbe were found in pores of the bentonite. Sulfate-reducing bacteria (SRB) are one of representative native microbes that reduce sulfate (SO_4^{2-}) to sulfide (S^{2-}) in the bentonite. Such a microbial activity might make bentonite altered, affecting the behavior of radionuclides.

Bentonite can be affected by cement materials used as the construction for the repositories during the long-term disposal process. The cement can lead the environment to be alkaline. The pH of the cementitious condition is higher than that of the surrounding environment in which microbe can live. It has been reported that some microbes can survive and metabolize in an extreme environment like high temperature. However, it has not been known if indigenous microbes in the bentonite can survive in high alkaline conditions.

In this study, we investigated effect a microbial on the biochemical alteration of KJ-II (Gyeongju) bentonite by its indigenous microbe under alkaline-reducing conditions.

2. Materials and methods

2.1 Materials

The bentonite used in this study was taken from Gyeongju. We named it as “KJ-II bentonite”. It is a Ca-type bentonite with its ratio of CaO : Na_2O as 5.5:1, containing montmorillonite with > 65% in its total amount [1].

2.2 Methods

2.2.1 Bentonite. Distilled water sterilized was added to the KJ-II bentonite to make a solid-liquid ratio (S/L) to be 1g/30ml in a centrifuge tube of 50 ml. To remove some oxygen in the bentonite, it was saturated and shaken for 3 days (120 rpm, 30°C). Finally, the supernatant was removed after centrifugation (10,000 rpm, 5 minutes), then the centrifuge tube was placed in a glove box filled with N_2 gas.

2.2.2 Solutions. Under the clean bench, solutions were prepared by adding reagents into water. Before addition of the reagents, they were sterilized by 0.20 μm filtration (ADVANTEC). To investigate some microbial effects occurring in the KJ-II bentonite, some aqueous conditions such as 1) distilled water, 2) distilled water+10mM Na-lactate, and 3) distilled water+10mM Na-lactate+2mM sulfate were prepared respectively. All solutions were purged with N_2 gas for 40 minutes to remove oxygen in the solution and then moved to the glove box.

2.2.3 Experiments. All experiments were carried out in the glove box filled with N_2 gas (anaerobic condition). The prepared solutions were poured into centrifuge tubes with bentonite. NaOH solution was used to adjust the pH of the media as 9, 10, and 11, respectively (Table 1). The experiments were carried out for 5 months.

Table 1. Experimental solutions prepared for the study

Case	Solutions	pHs
1	distilled water	9, 10, 11
2	distilled water + 10mM Na-lactate	9, 10, 11
3	distilled water + 10mM Na-lactate + 2mM sulfate	9, 10, 11

3. Results and discussion

3.1 Color changes of bentonites

Initial color of the bentonites had not changed

easily at any cases. However, a specific bentonite was changed to black at the pH 10 and 11 after 1 month for the case 3. A sample in the case 3 was completely blackened after 2 months at pH 9 (Fig. 1). It was assumed that this phenomenon was caused by the indigenous bacteria that were alive in the bentonite, if some electron donors (e.g., lactate) were supplied. The sulfate that was initially injected into the solution can be reduced to sulfide, which color is black as combined with metals (e.g., Fe). However, cases 1 and 2 showed a different color of light gray. It is assumed that it might be difficult to form sulfides due to the lack of sulfate for the cases 1 and 2.

The concentrations of sulfate in the natural groundwater are generally higher than about several tens ppm (mg/L) in Korea. In addition, it is reported that the sulfate concentrations in the groundwater near the sea shore are much higher. The repository sites could be placed near the sea shore in Korea, so the case 3 could be an example to study an effect of sulfate. According to a report, there are more than four kinds of SRB in the KJ-II bentonite [2]. In this study, the indigenous bacteria in the KJ-II bentonite were survived even in the strong alkaline conditions.

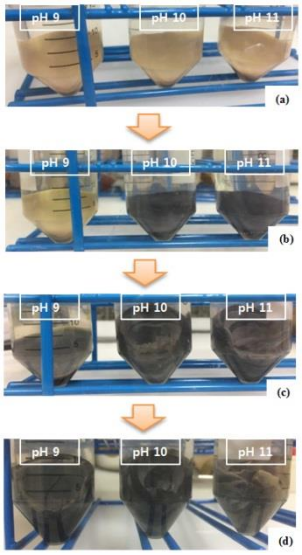

Fig. 1. Alteration of KJ-II bentonites in different pHs for the Case 3; (a) 1 week, (b) 1 month, (c) 2 months, and (d) 5 months.

3.2 Changes of chemical compositions

The supernatant of bentonite was extracted and analyzed to determine the concentrations of Al, Si and Ca using ICP-MS (inductively coupled plasma mass spectrometer). The result shows that the concentration of Ca increased at pH 11 for 2 month in all cases, and then decreased after that. Ca ions released from the bentonite by Na ions from the NaOH that was added for the pH adjustment. The concentration of Si increased steadily for 4 months at pH 11. It was 120~200 times higher than those of other samples. Finally, it also decreased after 4 months. The decreases of Ca and Si concentrations at pH 11 seemed that the ions may be combined to form a new mineral. In contrast, the concentrations of Al were lower than 0.1 mg/L in all cases. The dissolution of Si was superior to that of Al under our alkaline conditions.

4. Conclusion

The effect of microbial activity under alkaline-reducing conditions was investigated experimentally. In this study, the color of bentonite was changed by the activity of indigenous bacteria that are alive in the bentonite. It means that the indigenous microbe of KJ-II bentonite could survive under alkaline condition. In addition, the chemical compositions of bentonite supernatant were changed due to the chemical alteration of KJ-II bentonite.

The bentonite solid samples were analyzed by XRD (X-ray diffraction) to detect secondary minerals produced by the alteration of bentonite.

Acknowledgement

This research was supported by National Research Foundation of Korea (NRF) funded by the Ministry of Science, ICT and Future Planning (The nuclear research and development program No. 2017M2A8A5014859).

REFERENCES

[1] Y. Malgobalgaebitnala, et al., “Measurement of Properties of Domestic Bentonite for a Buffer of an HLW Repository”, JNFCWT, 14(2), 135-147 (2016).

[2] Ji Young Lee, et al., “Existence and Characteristics of Microbial cells in the Bentonite to be used for a Buffer Material of High-Level Wastes”, J. Korean Radioact. Waste Soc., 11(2), 95-102, (2013).

Introduction of the IAEA URF Network and Role of the KAERI

Geon Young Kim*, Kyungsu Kim, Min-Hoon Baik, and Young-Chul Choi
Korea Atomic Energy Research Institute, Daedeok-daero989ben-gil 111,Yuseong-gu, Daejeon, Republic of Korea
*kimgy@kaeri.re.kr

1. Introduction

IAEA Member States operating a nuclear power plant, or planning to establish future use of nuclear power, must implement solutions for the back end management of resulting intermediate level waste, high level waste and/or spent nuclear fuel. Geological disposal offers an internationally accepted solution for safe and sustainable management of such waste. All URFs (Underground Research Facilities) play an important role in the development of deep geological repository systems for the disposal of long lived and high level radioactive waste, both from a scientific and technological point of view and for building public confidence [2]. The IAEA Underground Research Facilities Network (URF Network) was formally initiated in 2001 to address the needs of all Member States involved in the development of civilian nuclear technologies. The URF Network provides its members with a platform to assess and share best practices in developing, evaluating and implementing geological disposal solutions. This paper reports on current status of the IAEA URF Network and role of the KARTI and KURT (KAERI Underground Research Tunnel) which is currently the only URF in Korea.

2. Current Status of the URF Network

2.1 Role of the URF Network

A URF or URL is an underground facility in which site characterization and testing activities are carried out along with technology development and demonstration activities in support of the development of deep geological repositories for radioactive waste [2]. The URF Network establishes a community of practice and learning for geological disposal. At its inception in 2001, the Network focused on the role of URFs in supporting geological disposal developments. After over a decade of operation, the URF Network has reassessed its role to deliver support to Member States needing solutions to the back end management of intermediate level waste, high level waste and spent nuclear fuel [3].

2.2 Scope of the URF Network

The scope of the Network is to provide and maintain a:

- Community of practice and learning for geological disposal.
- Platform to assess and share best practices in developing, evaluating and implementing geological disposal solutions.
- Platform which emphasises the role and use of URFs to support successful geological disposal implementation.

Best practices begin with understanding of high-level requirements (safety, security, safeguards, intergenerational equity and sustainability) and the resulting governance needs to achieve successful disposal. Network activities focus on methods and technologies to site, design, and license a disposal facility that meets these high-level requirements, as well as prepare for its implementation. This includes consideration of viable approaches in establishing national policies, strategies, and gaining and maintaining project acceptance by relevant stakeholders. Relevant information on construction and operation becomes increasingly important as some Network members progress toward commissioning a disposal facility [3].

The URF Network organizes an annual meeting, whose primary purpose if to tailor and plan the URF Network activities to meet timely Network members' needs. The actual delivery of the URF Network programme of activities to meet the Network members' needs is then subject to discussion with all attendees of the annual meeting. Implementation can be through workshops, meetings, scientific visits and fellowships, and developing information support, as e.g. reports, presentations at international meetings,

or short articles published online [3].

2.3 Members

The Network is open to accession by organizations with specific responsibilities related to establishing, developing, providing the scientific and technical basis for, and/or implementing deep geological disposal projects for radioactive waste [3]. Accession to the Network by any such organizations is formalized through a letter of intent addressed to the Director of the IAEA Division of Nuclear Fuel Cycle and Waste Technology. At present, the URF Network members are from Argentina, Armenia, Brazil, Belgium, Bulgaria, Canada, Chile, China, Croatia, Czech Rep., Finland, France, Germany, Hungary, India, Japan, Kazakhstan, Korea Rep., Lithuania, Mexico, Netherlands, Pakistan, Philippines, Poland, Romania, Russian Federation, Slovakia, Slovenia, South Africa Sweden, Switzerland, Ukraine, United Kingdom, and USA. The contact person for each organization is informally communicated to the IAEA Network Secretary, and serves as information point for all correspondence related to the Network.

3. Role of the KAERI and KURT in the URF Network

Korea Atomic Energy Research Institute (KAERI) was assessed as a member of the URF Network in 2013. The 13th annual meeting of the URF Network was hosted by the KAERI and held in Daejeon, from 17 to 21 November 2014. During the meeting site visits were conducted to KURT and Gyeongju which will be organized by Korea Radioactive Waste Agency (KORAD). KAERI has been participating in projects of “Roadmap to developing DGR and how URFs can support this” and “Compendium of RD&D results carried out at URFs for Geological Disposal” under the URF Network. Especially, KURT is an important part of information sheet on existing URFs in these projects.

Fig. 1. Website of the IAEA URF Network [3].

ACKNOWLEDGEMENT

This research was supported by the Nuclear Research and Development Program of the National Research Foundation of Korea (NRF-2017M2A8A5014857), funded by the Ministry of Science and ICT.

REFERENCES

[1] IAEA, “The use of scientific and technical results from underground research laboratory investigations for the geological disposal of radioactive waste”, IAEA-TECDOC-1243, 1-7 (2001).

[2] OECD/NEA. “Underground Research Laboratories (URL)”, NEA/RWM/R(2013)2, 9-11 (2013).

[3] IAEA, “Underground Research Facilities Network for Geological Disposal-Terms of Reference”,https://nucleus.iaea.org/sites/connect/URFpublic.

Modelling Transport of Radionuclides Observed in In-Situ Tracer Tests Based on Microstructure Characterization

Dong Kyu Park* and Sung-Hoon Ji
Korea Atomic Energy Research Institute, Daedeok-daero989ben-gil 111,Yuseong-gu, Daejeon, Republic of Korea
*dkpark@kaeri.re.kr

1. Background

The SKB Task Force is a forum for the international organizations supporting the Äspö Hard Rock Laboratory (HRL), Sweden, in the area of conceptual and numerical modelling of groundwater flow and solute transport in fractured rock. The 9th task of this forum was intended to increase realism in modelling of solute transport for the respective in-situ tracer tests performed at the Äspö HRL and the ONKALO underground rock characterization facility (URCF) in Finland. For the 2nd and 3rd steps of this task (called Task 9B and 9C), in particular, the inverse and predictive modelling works have been carried out based on the experimental data and results from the LTDE-SD test and the TDE test, respectively.

2. The in-situ tracer tests

2.1 The LTDE-SD test

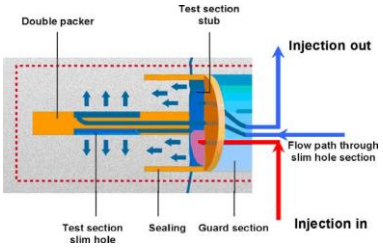

Fig. 1. The schematic diagram of the LTDE-SD test.

The LTDE-SD test was performed in a borehole installed at the Äspö HRL during 198 days. The fracture surface and the slimhole wall within the experimental section of the borehole were simultaneously exposed to the cocktail mixed with 22 radioactive tracers (Fig. 1). One of the main results from this test was the penetration profiles of ^{137}Cs having two slopes. In particular, the flat slope of tail in the profiles implies that the sorbing tracer migrated much deeper into the rock matrix than that expected from assuming homogeneous diffusion. The objective of Task 9B was to reproduce this anomalous observation from this test and to reinterpret its mechanisms.

2.2 The TDE test

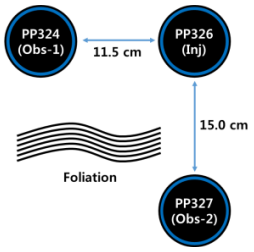

Fig. 2. The schematic diagram of the TDE test.

As a part of the REPRO project performed at the ONKALO URCF, this in-situ tracer test is still ongoing. Three parallel boreholes were installed as a right-angled triangle (Fig. 2): one injection borehole (PP326) and two observation boreholes (PP324 and PP327). Each pair of them is placed along or across the foliation existing in the bedrock and changes in concentrations of tracers injected have been monitored in each borehole. Thus, this test is to understand the migration of radionuclides depending on the foliation in rock matrix. The Task 9C aims at prediction of experimental results from this test.

3. Modelling procedure

We presumed that rock heterogeneity would be the most probable reason for the experimental results from both the in-situ tests. To prove this, it was incorporated into the model domains based on the microstructure characterization on the rock samples taken from the respective test sites, using mineral staining technique and ^{14}C-PMMA autoradiography (Fig. 3). In particular, for the LTDE-SD test, planar or linear types of model components were delineated along the geometries of mineral grains and micropores characterized with both the techniques. For the TDE test, due to the highly complicated geometries of minerals and micropores in the rock sample, a mapping technique for raster images was applied to incorporate them into the model.

For both the tests, it was assumed that the transport of radionuclides occurred in rock matrix were governed by diffusion along and sorption on its microstructures. In particular, the selective sorption

of Cs on the biotite and the micropore network composed of porous minerals, vein, and microfractures were considered. For the LTDE-SD test, considering disturbance near the fracture surface or borehole wall, increased porosity and sorption capacity were assumed to the minerals located at the rock surface.

For the LTDE-SD test, the transport parameters for the respective microstructures were determined for the experimental results of ^{137}Cs and ^{22}Na through the curve-fitting procedures. For the TDE test, the concentration change of non- or sorbing tracers in the injection and observation boreholes for 10 years were predicted. To focus on effects of foliation, the distances from the injection borehole to each observation borehole were assumed to be identical in the modelling.

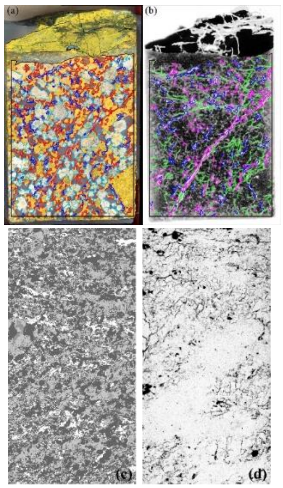

Fig. 3. Microstructure characterization on the LTDE-SD (a, b) and the TDE (c, d) rock samples: using mineral staining (a, c) and ^{14}C-PMMA autoradiography (b, d).

4. Results and discussion

For the LTDE-SD test, the determined parameters well reproduced the penetration profiles and the concentration changes of ^{137}Cs and ^{22}Na in tracer cocktail observed in this test. Sensitivity analysis demonstrates the effects of the respective microstructures on the migration of tracers occurred during this test. These results show that the strong sorption of Cs on the disturbed biotite grains located at the rock surface would lead to the peak and the drastic decrease in concentration of the profiles. They also show that through the vein and microfractures the sorbing tracers would migrate into the biotite grains located in deep region of rock matrix and, as a result, such long tails seem to be created.

The foliation existing in the rock sample from the TDE test site was observed as the arranged biotite grains through the mineral staining image, while was not shown clearly in the ^{14}C-PMMA autoradiograph. Therefore, its effects predicted for this test would be the results from the selective sorption of tracers on such arrangement of biotite grains. As a result, the concentration changes of non-sorbing tracers in the boreholes seem to be irrelevant to the direction of foliation. When the distribution coefficient of a tracer on biotite was assumed to 0.01 m^3/kg, however, the concentration in observation borehole placed parallel to the foliation increased more rapidly than that in the vertical one.

5. Conclusion

Understanding retention mechanisms of radionuclides in bedrock must be important for safety and performance assessment of a geological repository. However, the experimental results from the in-situ tests have shown that with only conventional approaches it is difficult to account for the realistic transport of radionuclides in rock matrix and, as a result, its safety and performance cannot be assessed appropriately. From the modelling results shown here, it is concluded that the experimental results from the in-situ tracer tests may result from the interactions among various microstructures existing in the rock matrix, or rock heterogeneity. This conclusion highlight the importance of considering roles of microstructures in transport of radionuclides in rock matrix. In other words, a careful characterization of rock microstructures needs to precede in estimation of retention parameters of bedrock in a repository for safety and performance assessments.

Acknowledgement

This work was supported by the Ministry of Science, ICT and Future Planning within the framework of the national long-term nuclear R&D program (NRF-2017M2A8A5014858).

The State-of-the Art of the Geological Evolution Research to Verify the Long-Term Safety of Disposal Site

Soolim Jung* and Sung-Hoon Ji

Korea Atomic Energy Research Institute, Daedeok-daero989ben-gil 111,Yuseong-gu, Daejeon, Republic of Korea

*sljung@kaeri.re.kr

1. Introduction

Disposal facilities for radioactive waste should be sited to provide isolation from the accessible biosphere for several hundreds to thousands of years after closure. For safety assessments of the repository, the long-term natural evolution and possible events of the site, which can cause disturbances to the facility over the period of interest, should be considered. Understanding the history of paleo-geological evolution is one of the key factors to verify long-term safety of the given area.

2. Nations investigated

The cases of Finland, Sweden and Japan were investigated. Finland and Sweden are the most advanced nations for geological research on disposal sites. Both nations had launched radioactive waste disposal project for over 30 years using their own deep Underground Research Laboratories (URL). The host rock types of the two countries were crystalline rocks. Japan is a neighboring country to Korea, and a geologically active region. Relatively strong tectonic events and fast plate movement shall affect the researches in Japan. The host rock type of Mizunami URL in Japan is granitic rock, which is being considered as the most safe rock type for geological disposal in Korea.

3. Researches on tectonic evolution

Research on history of tectonic evolution and possibility of consequent events, which can cause disturbances to the repository, is one of the fundamental procedures to verify the long-term safety of the site.

Technologies for the research were nearly same for most of nations. Surface-based lithological investigations were performed to increase accuracy of the evolution history. Borehole geophysical surveys have been performed to collect geological information of the deep underground, and the drilling core samples were taken for structural analyzing and age dating. Brittle and ductile deformation histories were evaluated using structural analysis data from the field works, geophysical surveys and drilling core investigations.

On the other hand, visualizing ways of the results were varied by country. Sweden used detailed age-dating data for constructing each deformational history with a graphic chart. Finland indicated the evolution of paleostress, several tectonic events, and age-dating data at the same chart.

4. Future geological evolution

To produce more precise and specific results, the nuclear advanced nations have constructed quantitative models for future geological evolution. Each nation applied different approaches and

techniques to estimating long-term geological evolution of the disposal site, which were developed suitably for their site characteristics. Finland and Sweden, countries located high latitude area, constructed climate and glacial estimating model, whereas hydraulic evolution with geographic changes was applied to the Mizunami site composed of granitic body and active tectonic regime.

5. Conclusion

From the results, it is suggested that the development of Korean own techniques for long-term geological evolution and its safety assurance depending on Korean geological characteristics should be conducted in near future. The advanced methodologies for understanding geological evolutions and evaluating long-term safety can contribute to develop Korean own technologies.

Acknowledgement

This work was supported by the Ministry of Science, ICT and Future Planning within the framework of the national long-term nuclear R&D program (NRF-2017M2A8A5014858).

REFERENCES

[1] I. Aaltonen et al., “Geology of Olkiluoto”, Posiva Oy, Posiva Report 2016-16 (2016).

[2] H. Saegusa and T. Matsuoka, “Final Report on the Surface-based Investigation Phase (Phase 1) at the Mizunami Underground Research Laboratory Project”, Japan Atomic Energy Agency, JAEA-Research 2010-067 (2011).

[3] Söderbäck B (ed), “Geological evolution, paleoclimate and historical development of the Forsmark and Laxemar-Simpevarp areas - Site descriptive modelling (SDM-Site)”, SKB R-08-19 (2008).

Numerical Modelling of Gas Injection Experiment Using Damage Model

Jaewon Lee, Changsoo Lee, and Geon Young Kim

Korea Atomic Energy Research Institute, Daedeok-daero989ben-gil 111,Yuseong-gu, Daejeon, Republic of Korea

jwl@kaeri.re.kr

1. Introduction

In the case of a repository for radioactive waste, corrosion of ferrous materials under anoxic conditions lead to the formation of hydrogen, carbon dioxide, hydrogen sulphide and methane [1]. If the gas production rate exceeds the gas diffusion rate in the pores of the engineering barrier, the pressure of the gas continuously increases and sudden gas flow occurs when the specific pressure is reached. Since the concept of the porous medium considering the existing two-phase flow is inadequate to simulate this phenomenon, it is necessary to develop a new numerical model for gas migration in the low permeability layer. Therefore, in this study, we developed a gas migration model using mechanical damage model and compared the results of laboratory gas injection experiment and numerical analysis.

2. Numerical model

2.1 Mechanical damage model

In order to model the gas migration phenomena, we adopted elastic damage model by Tang et al. [2]. In this model, the elastic modulus of the element may degrade gradually as damage progresses, and the elastic modulus of the damaged element is defined as follows:

$$E = (1 - D)E_0 \tag{1}$$

where D represents the damage variable, and E and E_0 are the elastic moduli of the damaged and undamaged elements, respectively.

2.2 Gas injection experiment

BGS conducted a 1D gas flow test on pre-compacted bentonite subject to a constant volume boundary condition. Fig. 1 shows schematic view of gas injection experiment. The test is comprised of a two stages; sample hydration and gas injection. Gas was injected with constant flow rate, so gas pressure gradually increased. After gas breakthrough, the injection pump was stopped and the pore water pressures decreased substantially.

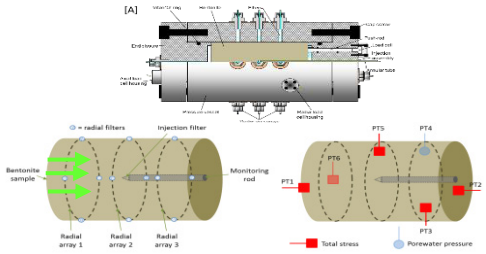

Fig. 1. Schematic view of 1D gas injection experiment [3].

2.3 Properties

Table 1 shows properties of bentonite. Elastic modulus, Poisson ratio, porosity, and permeability are given properties. Other mechanical and hydraulic properties are issued by references except damage model properties.

Table 1. Properties of bentonite

Properties		Bentonite
Elastic model	Elastic modulus (Pa)	3.07E+08
	Poisson ratio	0.4
Damage model	Tensile strength (Pa)	1.00E+06
	Residual tensile strength (Pa)	2.00E+05
	Compressive strength (Pa)	1.20E+6
	Residual compressive strength (Pa)	3.00E+6
	Tensile strain limit	5.00E-03
Biot coefficient		0.862
Porosity (-)		0.44
Intrinsic Permeability (m^2)		3.40E-21

3. Results

Fig. 2 shows pore pressure evolution at injection filter and back pressure filter. Pore pressure increase dramatically due to the damage of bentonite. The trend of peak and post-peak pressure is well matched, however, timing of increase to the peak is different because damage of bentonite is occurred gradually from injection filter to backpressure filter.

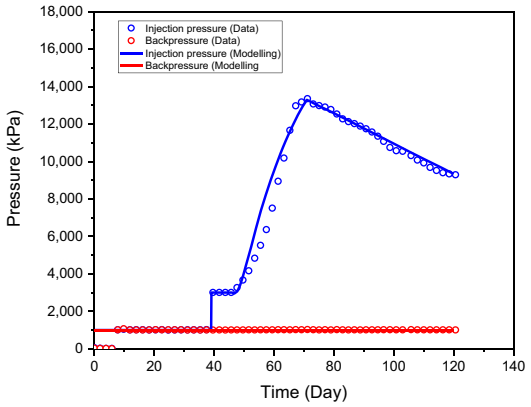

Fig. 2. Pore pressure evolution at injection filter and back pressure filter.

Fig. 3 shows damage evolution. Damage evolves from injection filter to backpressure filter. Increase of pore pressure induces decrease of effective stress. If effective stress is less than the tensile strength, damage is occurred. Damage is not observed near the stainless steel tube because stainless steel tube has relatively high elastic modulus.

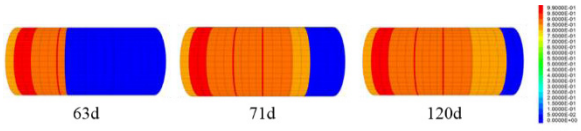

Fig. 3. Damage evolution.

4. Conclusion

For modelling about gas migration, we developed a gas migration model using mechanical damage model and compared the results of laboratory gas injection experiment and numerical analysis. In general, Pore pressure results are well matched. The trend of peak and post-peak pressure is well matched, however, timing of increase to the peak is wrongly predicted. Damage evolves from injection filter to backpressure filter similar with pore pressure increase.

ACKNOWLEDGEMENT

This research was supported by the Nuclear Research and Development Program of the National Research Foundation of Korea (NRF-2017M2A8A5014857) funded by the Minister of Science and ICT.

DECOVALEX is an international research project comprising participants from industry, government and academia, focusing on development of understanding, models and codes in complex coupled problems in sub-surface geological and engineering applications; DECOVALEX-2019 is the current phase of the project. The authors appreciate and thank the DECOVALEX-2019 Funding Organisations Andra, BGR/UFZ, CNSC, US DOE, ENSI, JAEA, IRSN, KAERI, NWMO, RWM, SÚRAO, SSM and Taipower for their financial and technical support of the work described in this paper. The statements made in the paper are, however, solely those of the authors and do not necessarily reflect those of the Funding Organisations.

REFERENCES

[1] J.F. Harrington, C.C. Graham, R.J. Cuss, and S. Norris, “Gas network development in a precompacted bentonite experiment: Evidence of generation and evolution”, Applied Clay Science, 147, 80-89 (2017).

[2] C.A. Tang, L.G. Tham, P.K.K. Lee, T.H. Yang, and L.C. Li, “Coupled analysis of flow, stress and damage (FSD) in rock failure”, International Journal of Rock Mechanics & Mining Sciences, 39, 477-489 (2002).

[3] J.F. Harrington, and S.T. Horseman, “Gas migration in KBS-3 buffer bentonite: Sensitivity of test parameters to experimental boundary conditions”, SKB Report TR-03-02, Stockholm, Sweden (2003).

Recent Suction and Temperature-Controlled Tests for Measuring the Mechanical Properties of Unsaturated Bentonite Buffer

Jaw Owan Lee and Geon Young Kim
Korea Atomic Energy Research Institute, Daedeok-daero989ben-gil 111,Yuseong-gu, Daejeon, Republic of Korea
jolee@kaeri.re.kr

1. Introduction

The mechanical properties of bentonite buffer are essential for the performance assessment and design of engineered barrier system (EBS). The mechanical properties have been measured mostly for saturated bentonite buffers, whereas measurements for unsaturated bentonite buffers have been performed recently and, for that reason, generalized measurement method and device are not established. Especially for unsaturated bentonite buffer, they are complicated and different depending on different investigators. Those difficulties are attributed to the problem of considering the swelling and high suction of unsaturated compacted bentonite and the elevated temperature due to decay heat of radioactive waste. The purpose of this study is to review the measurement methods (mainly for oedometer test and triaxial cell test) of the mechanical properties of unsaturated porous medium (soil, bentonite, etc.) reported in literature and, based on the review results, to suggest measuring systems which are suitable for the mechanical properties of unsaturated bentonite buffer for a Korean HLW repository.

2. Oedometer and Triaxial Cell Tests

2.1 Basic test concept

Consolidation is the removal of water and air from the pores of porous medium. An oedometer test is a geotechnical test to measure the consolidation properties of the porous medium during one-dimensional loading. The loading condition results in vertical strain without lateral strain in response to a change in effective stress during drying/wetting. A triaxial cell test is to measure the consolidation properties of the porous medium allowing independent control of the loading (stress) in three perpendicular directions. The three dimensional loading produces a total volume change (strain) of the porous sample during drying/wetting. Both the oedometer test and tri-axial cell test have several variations: Consolidated Drained (CD), Consolidated Undrained (CU), Unconsolidated Undrained (UU).

2.2 Suction Control

For the unsaturated porous medium, the void ratio and specific volume are different depending on the suction when a loading acts on the sample. Because of this, suction-controlled apparatus for the oedoemter test and triaxial cell test is needed to measure the consolidation properties of the unsaturated porous medium. There are two types of suction control method: axial translation (AT) method and vapor equilibrium (VE) method. The AT method is the most widely used suction control method. It is based on the fact that the liquid phase in a porous medium undergoes an increase in pressure equal to that of the gaseous phase. The AT method, which controls the matric suction $(\mathrm{s} = u_a - u_w)$of the porous medium, is applicable in the suction range of less than 1.5 Mpa, because water cavitation may occur in a higher value of matric suction. The VE method overcomes the limitation of the AT method which can not be applied to the higher suction >1.5 MPa. The VE method controls the relative humidity and thus total suction (including the effect of capillary action, osmotic force, and sorptive forces)

in the porous medium. It assumes vapor transfer and equilibrium with pore water in the porous medium. The thermodynamic relationship between total suction and relative humidity is based on Kelvin's law:

$$s = -10^{-6}\,(RT/V_w)\ln(RH/100) \qquad (1)$$

where s is total suction [MPa], R is universal gas constant [8.3143 J/K mol], T is absolute temperature, V_w is molar volume of water [1.8 x 10^{-5} m^3/mol]. This suction control method is applied especially to unsaturated bentonite with higher suction value >1.5 MPa.

2.3 Temperature Control

The consolidation properties of unsaturated bentonite buffer are affected not only by suction but also by temperature change due to radioactive decay heat. In most studies, the temperature-control has been performed by installing a water bath and heating coil in the suction-control test apparatus.

3. Discussion and Conclusions

The oedometer and triaxial cell tests are used for measuring the mechanical (i.e., consolidation) properties of unsaturated porous medium including bentonite buffer. They require suction control because the unsaturated medium has different consolidation properties depending on the moisture content. If temperature control is required, the oedometer and triaxial cell test apparatuses should be installed in a water bath or with heating coil to keep a constant temperature. The suction and temperature-controlled oedometer and triaxial cell test apparatuses are suitable for measuring the mechanical properties of unsaturated bentonite buffer for an HLW repository. As the unsaturated bentonite buffer has total suction and the suction value is high, it is reasonable to use VE method instead of AT method for the suction control of unsaturated bentonite buffer [Fig. 1 and 2].

The results of this study can be utilized to build a measuring system for the mechanical properties of unsaturated bentonite buffer which are affected under thermal-hydro-mechanical(THM) condition, and the mechnical properties determined using this system will improve the reliability of EBS performance assessment and design.

References

[1] Alonso, E.E., Hoffmann, C., Romero, E., "Pellet mixtures in isolation barriers," J. of Rock Mech. and Geotech. Eng. 2(1), 12-31(2010).

[2] Cai, G., Zhao, C., Li, J., Liu, Y., "A new triaxial apparatus for testing soil water retention curves of unsaturated soils under different temperatures," J. of Zhejiang Uni.-Sci. A (Applied Phy. & Eng.) 15(5), 364-373 (2014).

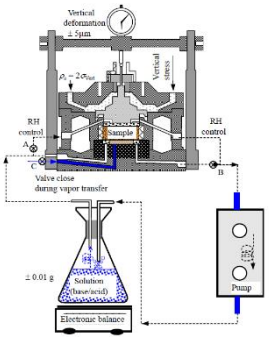

Fig. 1. Schematic diagram of oedometer test apparatus based on VE suction control [1].

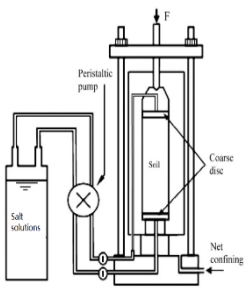

Fig. 2. Schematic diagram of triaxial cell test apparatus based on VE suction control [2].

Application of Mazars Damage Model to KURT Rock Under Thermo-Hydro-Mechanical Coupled Conditions

Jin-Seop Kim, Young-Chul Choi, Seok Yoon, and Geon-Young Kim
Korea Atomic Energy Research Institute, 111, Daedeok-daero 989beon-gil, Yuseong-gu, Daejeon, Republic of Korea
kjs@kaeri.re.kr

1. Introduction

The coupled thermo-hydro-mechanical (THM) behaviors in a geological formation is one of the key issues from the perspective of a nuclear waste disposal. The damage evolution and its evaluation are prominent with regard to the long-term performance assessment.

While, most of damage models have been developed based on the experiments, primarily carried out in dry and room temperature conditions. These are far away from the in-situ real condition of a waste disposal.

The objective of this study is, therefore, to apply the damage model (Mazars) to KURT (KAERI Underground Research Tunnel) rock under THM (Thermo-Hydro-Mechanical) coupled conditions to investigate the time-dependent deformation and failure process of rock. This information will be used as a primary input parameter in the development of coupled THMD (Thermo-Hydro-Mechanical Damage) model in KAERI.

2. Approach & Experiments

Mazars' damage model is described by two different evolution laws under tension and compression.

$$D = \alpha_t * D_t + \alpha_c * D_c \quad (1)$$

$$D_t = 1 - \frac{(1-A_t)\varepsilon_{d0}}{\varepsilon_{eq}} - A_t e^{B_t(\varepsilon_{eq}-\varepsilon_{d0})} \quad (2)$$

$$D_c = 1 - \frac{(1-A_c)\varepsilon_{d0}}{\varepsilon_{eq}} - A_c e^{B_c(\varepsilon_{eq}-\varepsilon_{d0})} \quad (3)$$

Where D is the total damage, D_t and D_c indicate tensile and compressive damages. A_t, B_t, ε_{d0}, A_c, and B_c are material parameters which can be determined by experiments.

With regard to determination of constants in Mazars damage model, the uniaxial compression and indirect tensile tests were performed under a simulated THM coupled condition (Fig. 1). Simultaneously, acoustic emission (AE) was also monitored during the test to compare the degree-of-damages predicted from the damage model and physically measured from AE detection.

Fig. 1. Experimental apparatus and DAQ system.

Target temperature were 15, 21, 45, and 75 ◦C which were determined from the numerical study (the maximum temperature at the interface between buffer and rock mass was predicted as 70 ℃).

Table 1. Test conditions and sample numbers in use

Tests		Notations	Temp.	Cond.	Sample no.	AE meas.	Strain meas.
Material Properties		UCS, E, ν, n, γ	21℃	Dry	27	X	X
Uniaxial compression test	M test	Mc-AE	21℃	Dry	3	O	O
	TM test	TMc(L)-AE	15℃	Dry	3	O	O
		TMc(M)-AE	45℃	Dry	3	O	O
		TMc(H)-AE	75℃	Dry	3	O	O
	HM test	HMc-AE	21℃	Sat.	3	O	O
	THM test	THMc(L)-AE	15℃	Sat.	3	O	O
		THMc(M)-AE	45℃	Sat.	3	O	O
		THMc(H)-AE	75℃	Sat.	3	O	O
Indirect tensile test	M test	Mt-AE	21℃	Dry	3	O	O
	TM test	TMt(L)-AE	15℃	Dry	3	O	O
		TMt(M)-AE	45℃	Dry	3	O	O
		TMt(H)-AE	75℃	Dry	3	O	O
	HM test	HMt-AE	21℃	Sat.	3	O	O
	THM test	THMt(L)-AE	15℃	Sat.	3	O	O
		THMt(M)-AE	45℃	Sat.	3	O	O
		THMt(H)-AE	75℃	Sat.	3	O	O

* c: compression test, t: tensile test, T: thermal test, H: hydraulic test, M: mechanical test, L: at 15℃, M: at 45℃, H: at 75℃

3. Main Results

From the HM test at a room temperature, the initial damage threshold (ε_{d0}) was determined within the range of 85~140 με. The tensile parameters A_t and B_t showed the values of 0.20~0.25 and 1996~3156 respectively. Compressive material parameters A_c and B_c showed a distribution of 19~23, and 1962~2789 respectively.

In case of THM(H) test, ε_{d0} was determined within a range of 90~125 με. A_t and B_t were 0.20~1.30 and 3268~5883 and A_c and B_c were 8~14 and 1475~1992.

Among the various test results, the representative stress-strain relations measured for THM test at 15◦C test is presented in Fig. 2.

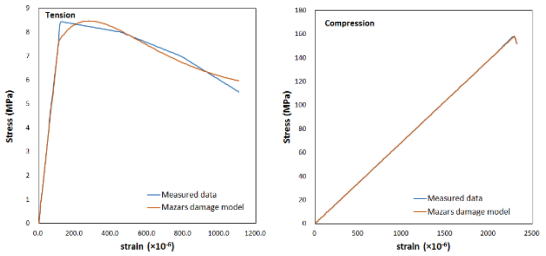

Fig. 2. Predicted and measured stress-strain relation for THM(L) test.

Table 2. Mazars damage model parameters under coupled test conditions

Test Name		Specimen ID	Damage model parameters				
			ε_{d0} (με)	Tension		Compression	
				A_t	B_t	A_c	B_c
M test		M-3	170	0.55	2349	12	1242
TM test	15℃	TM(L)-3	210	0.35	2346	8	1011
	45℃	TM(M)-3	155	0.37	2729	18	1555
	75℃	TM(H)-3	155	0.45	2885	7	1206
HM test		HM-3	85	0.25	3156	23	1962
THM test	15℃	THM(L)-3	110	0.30	3595	25	2065
	45℃	THM(M)-3	115	0.25	3342	28	2133
	75℃	THM(H)-3	110	0.20	3268	14	1992

4. Conclusion

Mazars damage model was successfully obtained under the simulated THM condition of a geological waste disposal. The development of damage evolution model can contribute to the better prediction of in-situ rock behaviors in a nuclear waste repository.

REFERENCES

[1] J. Mazars, “A description of micro-and macroscale damage of concrete structures”, Engineering Fracture Mechanics, 25(5/6), 729-737 (1986).

[2] R.W. Lewis and B.A. Schrefler, “The finite element method in the static and dynamic deformation and consolidation of porous media”, John Wiley & Sons, England (1998).

4분과

중저준위폐기물관리 (Oral)

Newly Developed Technology Introduction: Radioactive Spent Resin Treatment System Using Combined Dewatering Hopper

JongSeo Choi*, Sung-Hyun Heo, Yun Jae Lee, and Gi-Ho Park
DAEWOO E&C, 75, Saemunan-ro, Jongno-gu, Seoul, Republic of Korea
*jongseo.choi@daewooenc.com

1. Introduction

The ion exchange process is well-developed and very effective to treat a large volume of radioactive liquid into a small volume of solid [1]. At the end of its life, spent ion exchange resin has to be replaced, transferred, provisionally stored and packaged and/or conditioned safely and efficiently. Regarding this, the present paper deals with a more simple and economic treating system using the Combined Dewatering Hopper which is to provide functions of dewatering, storing and evacuating spent resin in one body newly developed by DAEWOO E&C.

2. Technology Background and Application

There may be a number of technologies which has been studied, applied and improved from long before are available to treat spent resin; dewatering is effectively used as one of the conditioning method without immobilization together with volume reduction [2, 3].

In Korea, in some cases, spent resin was often dealt with cartridge type contained inside a steel pressure vessel (column) in the past. Though this method has the merit to simply replace it using a crane, there is a large possibility that a worker is exposed to the radiation emitted during a replacing operation of the cartridge. Thus, this method requires a crane for handling and storing the cartridge, an exclusive transfer cask for shielding.

In some nuclear power plants, spent resin has been sluiced from columns by hydraulic pressure and stored in some big tanks; after then evacuated, dewatered and/or dried and packaged. Because of remotely transferring and handling spent resin, this method may allow the worker to easily work and reduce the possibility of the radiation exposure. However, to perform container packaging or solidification treatment of the radioactive spent resin accommodated in the spent resin tank, a separate discharging and drying system capable of taking spent resin out of the tank and/or drying are needed. Although this is appropriate for treating a high activity level and a large amount of radioactive spent resin, this method may be inefficient to treat a relatively lower activity level and smaller amount of spent resin in consideration of the subsidiary facility and installation area [4].

As the developed treating method of the existing dewatering technology, this system is considered to transfer spent resin by hydraulic pressure and to dewater, store and evacuate spent resin into a package such as High Integrity Container (HIC) using the combined dewatering hopper in one; therefore, a separate spent resin discharge system and/or drying/solidification one are unnecessary and smaller space could be considered. This technology was applied as purpose-built design to Jordan Research Reactor and already commissioned expertly in 2016.

3. System Arrangement

Fig. 1 represents a system block diagram showing a brief configuration for treating spent resin using combined dewatering hopper.

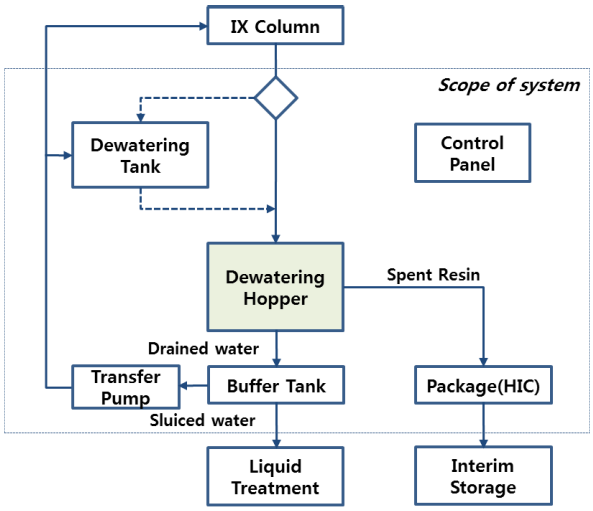

Fig. 1. Brief System Block Diagram.

Spent resin contained in an ion exchanger(IX) column which is comprised of a nuclear facility's purification system is fluidizing, pressurizing by

transfer pump(and/or with compressed air) and then evacuating by opening the control valve in system; the mixture of spent resin and water is sluiced into the combined dewatering hopper. Only water is passed through the screen and introduced into the buffer tank which is a water source of transferring spent resin. After evacuating work of spent resin from an ion exchanger is finished, water in buffer tank can be drained to liquid treatment system or recycled as fit for purpose. When the separation process on spent resin and water is completed in the hopper, evacuation process may be performed that spent resin is discharged into the package such as HIC etc. after a certain period of decay storage time.

In different with combined dewatering hopper in atmospheric operation, dewatering tank is designed additionally so that it performs pressurization in consideration of a long distance transfer.

4. Configuration of Dewatering Hopper

In Fig. 2, a schematic diagram of combined dewatering hopper is illustrated.

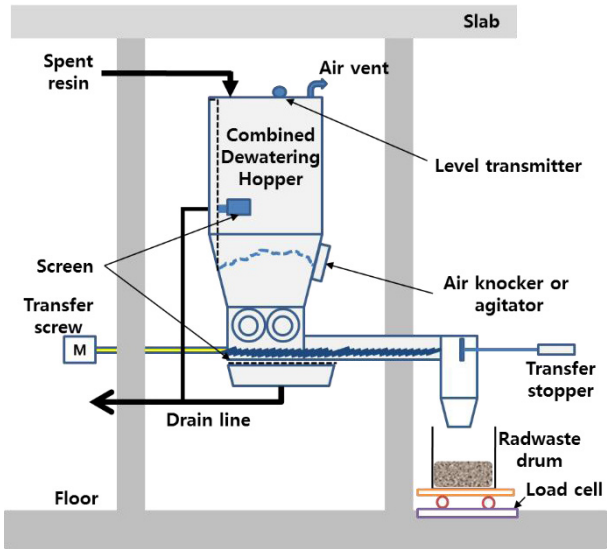

Fig. 2. Schematic Diagram of Dewatering Hopper.

The concept of this hopper is to reasonably combine the existing proven technologies such as transferring/dewatering spent resin hydraulically and screw discharging method etc.

This hopper is arranged at a shielded room and is mainly comprised of a housing customized by design capacity, screen of filter-type and/or plate-type for separating spent resin from sluicing water, a stirring agitator and/or a knocker as a bridge breaker, discharge unit for evacuating resin into a package which is equipped with a load cell.

Based on the research results using the pilot plant, it is estimated that free-standing water mixed in spent resin inside a hopper is removed less than 0.5 percent of the waste volume as free-standing water within 2 months in case of 1.2 m^3 of spent resin in a hopper in accordance with ANS 55.1 methodology; namely, free-standing water could be drained below the regulatory limit during decay storage by natural drainage [5].

5. Concluding Remark

This paper deals with a more simple and economic treating system using the Combined Dewatering Hopper which is to provide functions of dewatering, storing and evacuating spent resin in one body.

Although this technology has been currently applied only to research reactor, it is expected that it can be used in various forms of treating method for comparatively smaller amount and lower level of spent resin in the future such as small and medium sized reactors, small scale liquid radwaste treatment facilities etc.

REFERENCES

[1] IAEA, “Application of Ion Exchange Processes for the Treatment of Radioactive Waste and Management of Spent Ion Exchangers”, Technical Reports Series No. 408 (2002).

[2] IAEA, “Management of Spent Ion-Exchange Resins from Nuclear Power Plants”, IAEA-TECDOC-238 (1981).

[3] IAEA, “Treatment of Spent Ion-Exchange Resins for Storage and Disposal”, Technical Reports Series No. 254 (1985).

[4] PCT/KR2014/000189, “System for Transferring and Treating Radioactive Spent Resin, and Method for Transferring and Treating Radioactive Spent Resin using the same”, (2014).

[5] DAEWOO Institute of Construction Technology, “Assessment of Behavior of Waste Resin in Solid Radwaste System”, (2014)

Development of the PHWR Spent Resin Treatment Technology to Secure Disposal Safety

Kyu-Tae Park*, Jung-Min Yoo, Hyeon-Oh Park, and Young-Ku Choi
Sunkwang T&S Co.,Ltd, Sunkyung Officetel 20F, #3, Gongwon-ro, Guro-gu, Seoul, Republic of Korea
Paradoxno1@hanmail.net

1. Introduction

The annual average amount of spent resin, generated by domestic PHWR (Pressurized Heavy Water Reactor) NPPs, is 72,520L for Wolsong NPP #1, and 52,040L for Wolsong NPP #2. As of December 2017, 362,600L and 260,200L of spent resin is stored in Wolsong NPP #1 and Wolsong NPP #2 respectively.

AS the currently stored spent resin has a high concentration of C-14, it is classified as intermediate-level radioactive waste, and must be disposed of in a rock cavern. As the total radioactivity of C-14 in the spent resin is about 10 times higher than the total limit of the underground repository cavern, however, C-14 in the spent resin must be removed to dispose of spent resin.

In this study, development of the spent resin mixture separation and C-14 removal technology for the currently stored spent resin to treating. And the method of recycling it was researched.

2. PHWR spent resin treatment technology

2.1 Spent resin treatment process development

The spent resin mixture, stored in the PHWR NPP, was divided into spent resin and other mixtures. The validity of disposal and deregulation of the other mixtures with relatively low radioactivity was reviewed. And then, C-14 was removed from the spent resin, classified as intermediate-level radioactive waste, and disposal suitability was secured.

The validity of recycling the removed C-14, which is an expensive resource, by adsorbing it and turning it into a labeled compound ($Ba^{14}CO_3$), which is used in the industry, was reviewed.

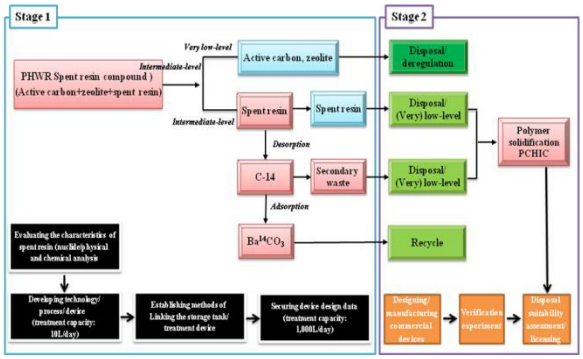

Fig. 1. PHWR spent resin treatment process.

2.2 Developing the spent resin mixture separation technology

Currently the spent resin, stored in the storage tank of the NPP is stored as a mixture of zeolite, active carbon and resin along with the stored liquid waste. Also, the mixture in the repository is solidly fixated depending on location.

The fixated parts are crushed with a crushing machine, and transferred to the buffer tank through the resin outlet.

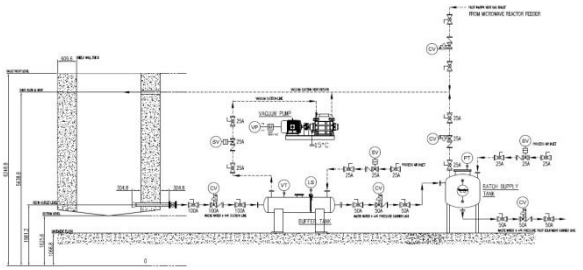

Fig. 2. Spent resin storage tank and transfer device.

10L of the spent resin mixture in the buffer tank is transferred at a time by the spent resin separating and sorting device. The transferred spent resin mixture goes through the multi-level mesh together with the supplied water, and is separated into zeolite and active carbon at the top, and spent resin at the bottom. The zeolite and active carbon at the top will return to the mixture recovery tank, and be contained in the disposal vessel. The separated spent resin at the bottom will be transferred to the resin supply tank at the top and stored there.

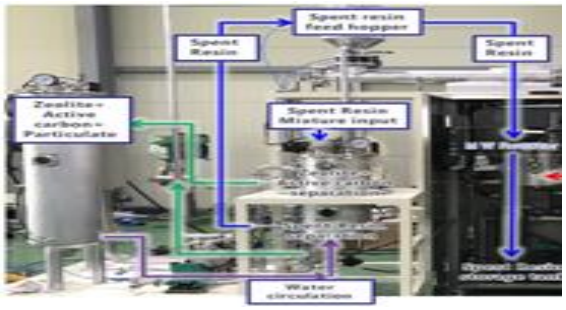

Fig. 3. Spent resin mixture separating and sorting device.

2.3 Developing the technology for desorbing /adsorbing the C-14 in the spent resin

2kg of spent resin is transferred from the spent resin supply tank to the microwave reactor at a time, and C-14 is desorbed. The hot gas, containing the C-14 generated after reaction will circulate the closed circuit, and the moisture is removed by the cooling tower in the downstream and passes the first multi-level adsorption tower, and is adsorbed by the charged adsorbent. This process is operated in a close-circuit circulation mode to increase the efficiency of adsorption. The C-14 gas, which remains after the circulation process, is stored in the compression tank in the downstream, and sent to the secondary multi-level adsorption tower for circulation.

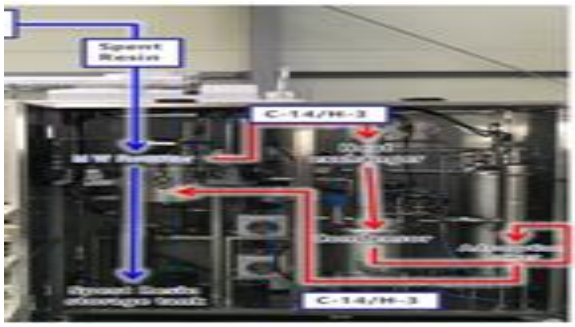

Fig. 4. A device for desorbing/adsorbing C-14 in the spent resin.

3. Verification experiment for the PHWR spent resin mixture treatment device

The PHWR spent resin mixture treatment devices, which was developed by this study, was used to conduct the verification experiment. The sample was the 20L of spent resin mixture collected from #2 tank of Wolsong NPP #1. It was used to separate the mixture and desorb/adsorb the C-14 in the spent resin. The experiment was conducted a total of 4 times under the conditions in Table 1. The optimal mixture separation and C-14 desorption/ adsorption conditions using the microwave were derived by conducting basic performance tests in the field before the verification experiment.

Table 1. Operating conditions by batch

Classification	Target specimen	Amount of injected mixture	Reactor injection
BATCH 1	manhole	7 L	2 kg
BATCH 2	manhole	4 L	2 kg
BATCH 3	manhole	4 L	2 kg
BATCH 4	testhole	2 L	2 kg

4. Securing a method of recycling the removed C-14

The C-14 labeled compound is mainly used as a tracer in educational researches and new drug development. Currently domestic companies, i.e. Curachem, Inc. and KRCC, Inc. are importing $Ba^{14}CO_3$, hich is made by irradiating neutrons on C-13 to meet the quantities they need. The recycling standard for C-14 as a labeled compound is commercial 50 mCi/mmol.

A porous alkaline earth adsorbent, suitable for the process in the spent resin disposal scenario, will be developed to test/verify the adsorption process with the most efficient porous BaO adsorbent.

Also, the C-14 adsorption efficiency of the developed adsorbent will be increased, and thus the import substitution of the labeled compound raw material can be expected.

5. Conclusion

For final disposal of the spent resin generated in the PHWR NPP, the treatment process and device were developed, and they were used to conduct verification experiments in Wolsong NPP #1.

The results of the verification experiments showed that more than 94.4% of the C-14 in the spent resin was desorbed, and the desorbed C-14 was adsorbed using the calcium-based adsorbent.

The authors are planning to enhance the technology for desorbing the C-14 in the spent resin, and use the barium-based adsorbent for the recycling of C-14 to improve the adsorption rate.

ACKNOWLEDGEMENT

This work was supported by a Korea Institute of Energy Technology Evaluation and Planning (KETEP) grant funded by the Korean government (No. 20151520302120).

Consequence Analysis on the Transportation Accident of Spent Resin Waste From a Heavy Water-Cooled Reactor to the Gyeongju Disposal Facility

Ki Joon Kang[a], UkJae Lee, Jaeseong Min, and Hee Reyoung Kim

School of Mechanical, Aerospace and Nuclear Engineering, Ulsan National Institute of Science and Technology, Ulsan 44919, Republic of Korea

roffl1234@unist.ac.kr[a]

1. Introduction

The radiological safety is one of the important issues concerning accidents in transporting radioactive spent resin wastes from a heavy water-cooled reactor. Ion exchange resins are used to filter radionuclides in Wolsung nuclear power plant. The plant has storage with a capacity of (354.9 m^3). However, the amount of radioactive waste is expected to exceed it within 10 years. Therefore, the radioactive waste needs to be transferred from the Wolsung receiving area to the Gyeongju radioactive waste disposal facility. Once transported, 50 drums with a capacity of 200 L are carried on trucks, which is a large quantity, hence the radiation safety for accidents that may occur during transportation are essential. In this paper, the radiological safety assessment for the hypothetical accident is performed by evaluating the radiation effects after calculating the Total Effective Dose Equivalent (TEDE) using the HotSpot Code, which was developed by the Lawrence Livermore National Laboratory.

2. Materials and Methods

2.1 Input Parameters

The TEDE of cement solidification and dry spent resins are evaluated for radioactive waste. Cement solidification and dry spent resin are divided into 1% exposure and 10%. For the evaluation of atmospheric dispersion, 1% leakage is assumed to be a small value and 10% leakage is assumed to be a large value. Each case is divided into low-level waste (LLW) and intermediate-level waste (ILW) depending on whether it is lower than 10^{-3} Sv/yr. The HotSpot Code can set radioactive nuclides, meteorological and geological conditions, and can set the degree of radiation leakage (1%, 10%) and the duration of leak. The nuclides, which are ^{3}H, ^{14}C, ^{55}Fe, ^{58}Co, ^{60}Co, ^{59}Ni, ^{63}Ni, ^{90}Sr, ^{94}Nb, ^{99}Tc, ^{129}I, ^{137}Cs, and ^{144}Ce are used according to the notification of the Nuclear Safety and Security Commission in Korea. The air condition is set to be very stable because it is most similar with the stable state since precipitation is high in July and the effect of atmospheric dispersion is the least, and wind direction and wind speed are set to NW and 4.7 m/s. The precipitation is set at 5.42mm, which is the average of precipitation in July of Gyeongju, accident site. Because July has a highest precipitation during the year. It is assumed that the radioactive waste would leak for 10 minutes in case of an accident. The location of the accident was set at an arbitrary midpoint on the path from the Wolsung receiving area to Gyeongju radioactive waste disposal facility in Google map. Gaussian plume

model is used as diffusion model.

2.2 Total Effective Dose Equivalent

The TEDE contour plots according to distance is as follows. The doses of 1.0×10^{-11} Sv, 5.0×10^{-12} Sv, and 1.0×10^{-12} Sv shown in Fig. 1 indicate the dose when the leakage from the source to the atmosphere reaches the ellipse. The inner value 1.0×10^{-11} Sv is lower than 1.903×10^{-8} Sv, equivalent to 10 minutes effective dose of the annual effective dose.

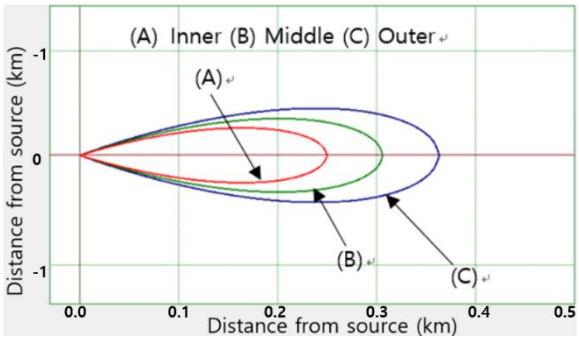

Fig. 1. TEDE contour plots of the cement solidification drum accident scenarios with 10% release of ILW (Inner: 1.0×10^{-11} Sv, Middle: 5.0×10^{-12} Sv, Outer: 1.0×10^{-12} Sv).

3. Conclusion

Among the eight cases, 10% leakage of the ILW dry spent resin showed the highest dose as 1.4×10^{-3} Sv during 10 minutes at a distance of 0.03 km from the hypothetical accident site. This dose is 140% of the annual effective dose of 10^{-3} Sv/yr. Therefore, additional measures are thought to need for radiological protection of nearby residents in case of radioactive waste transportation accidents.

REFERENCES

[1] Jeong, J., Baik, M. H., Kang, M. J., Ahn, H. J., Hwang, D. S., Hong, D. S., ... & Kim, K. (2016). Radiological Safety Assessment of Transporting Radioactive Wastes to the Gyeongju Disposal Facility in Korea. Nuclear Engineering and Technology, 48(6), 1368-1375.

[2] Hotmann, S., & Fernando, A. (2013). Hotspots Health Physics Codes Version 3.0 Users Guide. National Atmospheric Release Advisory Center Lawrence Livermore National Laboratory, Livermore. CA, 94550

[3] Yang, H. Y. (2006). Development of nuclear power plant spent resin treatment technology (removal of C-14). Korea Hydro & Nuclear Power CO.

Radiological Safety Analysis in Transportation for Radioactive Wastes Disposal

Woo Nyun Choi and Hee Reyoung Kim
Department of Nuclear Engineering, Ulsan National Institute of Science and Technology, 50, UNIST-gil, Eonyang-eup, Ulju-gun, Ulsan, Republic of Korea
Chldnsus95@unist.ac.kr

1. Introduction

The resin mixture containing the radioactive materials will be transported to the radioactive waste disposal facility in Gyeongju after disposal. When transporting for disposal, radioactive wastes should undergo a radiological safety assessment of the process of transportation. In this study, radiological safety assessment is conducted using RADTRAN ver 6 code [1]. For using RADTRAN code, parameters such as the specification of the container, dose rate, and surrounding population are required.

2. Method

2.1 Packaging container

PC-HIC (Polymer Concrete High Integrity Container) drums are used for packaging. The height of PC-HIC drum is 1,260 mm, the diameter is 1,200 mm and the thickness of outer concrete is 65 mm.

The resin mixture consists of zeolite, activated carbon and spent resin. They will be separated during the treatment process and transported in a PC-HIC packaging container with the internal volume of 860 L. Since radionuclides have different radioactivity concentrations at different sampling locations where Manhole 1,2 and 3 located in Wolseong NPP (nuclear power plant) Unit 1's spent resin storage tank #3, they were evaluated for each sampling locations.

Dose rates were calculated by using the Microshield version 10 which is the commercial code [2]. The dose rate was calculated at 1 m outside of the PC-HIC packaging containers.

2.2 Transportation route and population density

It was assumed that truck which transports radioactive materials travels at a speed of 30 km/h and drives 4.7 km from Wolseong NPP to radioactive waste disposal facility in Gyeongju.

Subjects that are exposed to radiation outside the vehicle during transport are divided into truck drivers, on-link and off-link public. On-link public are considered in vehicles that are on the move and off-link public are considered to be next to the road while on the move.

Population density was obtained as the 54.5 persons/km^2 per area [3]. And the accident probability was calculated as the 8.31-E-08 accidents/veh-km [4].

2.3 Loading and unloading operation and driver

When the waste drums were loaded and unloaded, the number of workers was set as 4 and the working time 1 hour. The average distance between the drums and the workers was entered as 0.1 m.

Conservatively, it was assumed that two people boarded the truck.

2.4 Assumptions of accident scenarios

The accident scenarios were assumed that the exposure of radioactive nuclides to the public was

caused by accidents during truck transportation. And conservatively, it was assumed that the accident caused 0.1 % of the total radioactivity leakage. Also, it was assumed that all leaked radionuclides like ^{3}H, ^{14}C, ^{60}Co, ^{134}Cs, ^{137}Cs, etc., were aerosolizing and leaking into respirable form.

Atmospheric stability was set as the most frequent weak stability (E) of the atmospheric stability distribution of Wolseong Nuclear Power Plant site [5].

3. Result and Discussion

As shown in Table 1, the individual doses of truck driver, off-link and on-link in normal transportation were 6.10E-03 mSv, 1.59E-04 mSv and 1.96E-06 mSv, respectively. All of these did not reach the individual dose limit.

Tables 2 shows collective and individual doses of the loading and unloading workers in normal transportation of spent resin and the public at the time of truck accident at Manhole 3. The highest dose value was 11.2 mSv.

Table 1. Collective and Individual Doses in Normal Transportation

Object		Collective Dose (man·mSv)	Individual Dose (mSv)	Individual Dose Limit (mSv/year)
Truck driver		1.22E-02	6.10E-03	12
Public	on-link	2.77E-02	1.59E-04	1
	off-link	7.50E-04	1.96E-06	1

Table 2. Collective and Individual Doses of Loading and Unloading Workers and Public at the Time of Accident

Object	Manhole 3		Individual Dose Limit (mSv/year)
	Collective Dose (man·mSv)	Individual Dose (mSv)	
Worker	4.48E+01	1.12E+01	50
Public	1.55E-10	2.09E-15	1

4. Conclusion

In the case of disposal of spent resin, zeolite and activated carbon in a waste disposal container of PC-HIC, the maximum dose received value was 11.2 mSv. This value dose not reach the maximum dose limit of 50 mSv/year of radiation workers.

Doses were below the limit at all routes, objects and sampling locations. Therefore, it was evaluated that radiological safe in transportation for radioactive wastes disposal.

REFERENCES

[1] Ruth F. Weinner, D. Hinojosa, T. J. Heames, C. O. Farnum and E. A. Kalinina, “RADTRAN 6/Radcat 6 User Guide”, Sandia National Laboratories, 2013.

[2] Grove Software, “MicroShield User’s Manual”, 2007.

[3] Gyeonju-si, “Statistical Yearbook of Gyeongju”, 2015.

[4] Road Traffic Authority, Accident Analysis System and Traffic Volume Information System, 2015.

[5] Korea Hydro & Nuclear Power, “Report of Environmental Radiation Survey and Evaluation”, 2015.

Potential Management Options of Radioactive Large Metallic Components From NPPs in Operation and Decommissioning

Jin-ho Park, Jae hak Cheong*, and Joo-ho Hwang

KyungHee University, 1732, Deogyeong-daero, Giheung-gu, Yongin-si, Gyeonggi-do, Republic of Korea

*jhcheong@khu.ac.kr

1. Introduction

Today, in Korea, large component generated by replacement during operation from nuclear power plant is stored in the temporary storage facility. Also, as the dismantling of the nuclear power plant progresses, a larger amount of metal radwaste will be generated. However, the management option of large component generated in this way has not been decided. Therefore, it is necessary to derive a transport scenario for selecting the optimum treatment/disposal plan.

2. Management scenario

2.1 Current state of treatment/disposal of large component

The domestic steam generator generated by the replacements during the operation, although there are transporting experiences inside the NPP, it is actually not yet transported outside.

There is a case that has been brought the original form to the disposal facility if overseas, and there were cases in which large component was temporarily stored/disposed after cutting or melting treatment. The method of treatment/disposing of international large component can be seen by seeing Table 1 below.

Table 1. Current state of treatment/disposal of large component abroad

Country	Material	Radwaste form	Transport mode
U.S.A	RPV SG PZ	Original shape, Cutting	Truck+barge, Truck+Rail
Germany	RPV SG PZ	Original shape, Cutting, Melting	Truck+rail, Private ship
Sweden	SG	Melting	Private ship

2.2 Scenario selection factor for large component transport

2.2.1 Transport method. Transport methods can basically be distinguished as land and marine. In the case of land, it can be divided into railroads, trucks and the like. In the case of sea, it can be classified as dedicated vessel or barge.

2.2.2 Transport form and treatment facility. Large component is bulky and heavy, so it can be transported in its original shape, but it may take a lot of restrictions. Depending on the situation, the shape can be deformed through work such as cutting or melting through the treatment facility, and the volume can be reduced or the weight can be reduced and conveyed.

2.3 Large component transport scenario

In the transport scenario of large component, it

was divided into two routes, land and sea. Truck in the case of land transport, only the method using the private ship on the sea was considered.

2.3.1 Transport form and treatment facility. Schematic diagrams of land and sea scenarios are the same as in Fig. 1 below. In the case of the treatment facility, it was classified into the on-site facilities of NPP and off-site facilities of NPP, and selected for transport to the disposal site.

2.3.2 Transport form and treatment facility. The transport scenario was the same as in Fig. 2, and a total of 11 scenarios were selected, separated by land and sea.

3. Conclusion

In this paper, we selected a scenario for treatment/disposing of large component. Based on this scenario, we expect to be able to derive the optimal scenario for large-scale metal waste disposal/disposal when risk assessment and economic analysis etc. are additionally executed.

REFERENCES

[1] Consultation on the Site for Interim Storage of ILW - Supporting Information on RPVs and RPV store, Nov., 2014.

[2] AEN NEA, The management of large components from decommissioning to storage and disposal, 2012.

[3] Disposal of steam Generators from Decommissioning of PWR Nuclear Power Plants, IYNC 2008.

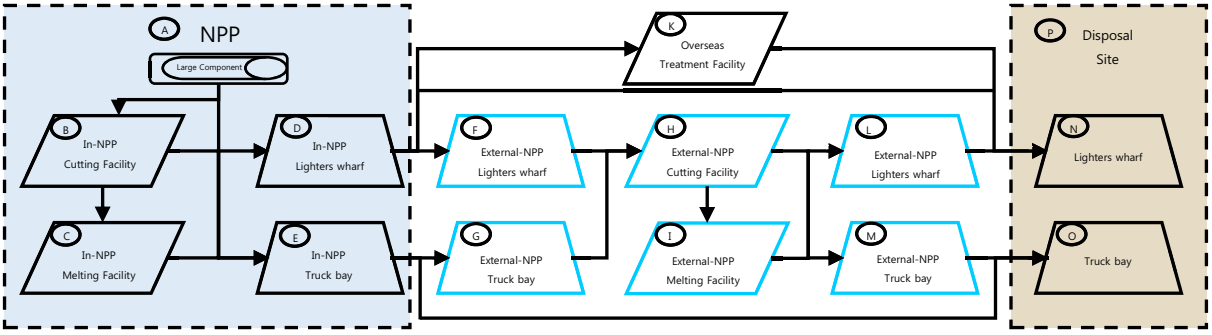

Fig. 1. Schematic diagrams of land and sea scenarios.

Scenario #	Overland transport	Scenario #	Marine transportation
#1	A → E → O → P	#6	A → D → N → P
#2	A → B → E → O → P	#7	A → B → D → N → P
#3	A → B → C → E → O → P	#8	A → B → C → D → N → P
#4	A → E → G → H → M → O → P	#9	A → D → F → H → L → N → P
#5	A → E → G → H → I → M → O → P	#10	A → D → F → H → I → L → N → P
		#11	A → D → K → N → P

Fig. 2. Transport scenario.

Probabilistic Safety Assessment for LILW Silo Repository in Earthquake Scenario Using Domestic Earthquake List

Sol-Chan Han and Jong-Il Yun*
Dept. of Nuclear and Quantum Eng., Korea Advanced Institute of Science and Technology,
291 Daehak-ro , Yuseong-gu, Daejeon, Republic of Korea
jiyun@kaist.ac.kr

1. Introduction

To understand and examine the safety of disposal facility, we developed the safety assessment model with the Monte Carlo based simulation frame, Goldsim, and analyzed both the radio-biological effects and the sensitivity of various input parameters [1]. From our previous studies, it was observed that the safety of repositories in a normal scenario is highly achievable. The robustness in safety, meanwhile, should be guaranteed for various abnormal scenarios as well.

In this work, the safety assessment model is newly modified to evaluate the safety of disposal facility under the earthquake scenario, and the domestic earthquake list was adopted for site-specific assessment. Simultaneously, we developed an earthquake analysis program with the template of MATLAB to reinforce the utilization of the research results.

2. Model Description

2.1 Development of the domestic earthquake list analysis program

The earthquake occurrence characteristics highly depend on the geological domain of interest. Therefore, hypothesized earthquake data could increase the uncertainty of safety assessment results. To enhance the reliability of results, we applied the domestic earthquake list to safety assessment model.

In general, the cumulative number of earthquake events according to their magnitude is described following the Gutenberg-Richter (G-R) relation,

$$\log_{10} N(M) = a - bM \quad (M > M_c) \qquad (1)$$

where N(M) is the number of earthquake events, which have the magnitude greater than M. The M_c is the threshold of the magnitude, which indicates the smallest magnitude that the G-R relation is applied to the particular earthquake list.

The annual occurrence rate of an earthquake was estimated by MATLAB-based earthquake list analysis program with the G-R relation. In addition, the distribution of the distance between repository and epicenter and the probabilistic distribution function for the magnitude of earthquakes were obtained by using analysis program.

2.2 Performance assessment module for an earthquake scenario

The figure below shows a schematic diagram of the newly developed earthquake scenario module. Most of other modules (i.e. silo repository module and biosphere module) are basically identical to the model used in the previous study [1].

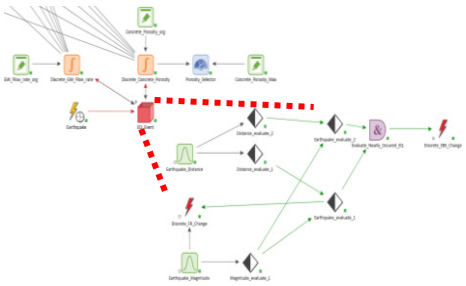

Fig. 1. Schematic diagram of earthquake scenario module.

The yellow thunder shape element in Fig. 1 is the ‘timed event element’. In the Goldsim program environment, this element was employed to estimate the time intervals between events (earthquakes), and the Poisson distribution, which is usually used to predict the occurrence of an earthquake [2, 3], was implemented in this element.

Similar to previous studies [4, 5], not only the magnitude of an earthquake but also the distance from epicenter to the repository were utilized to select the ‘valid’ earthquake among all events. The assumption for this process are listed in Table 1.

Table 1. Assumption of earthquake scenario

Criterion	Threshold	Effect
Distance from epicenter to repository	≤ 8 km	Increase the groundwater flow rate
	≤ 3 km	Increase the porosity of EBS (concrete barrier)
Magnitude	≥ 4	Increase the groundwater flow rate

3. Modeling Result

For the probabilistic safety assessment, 1,000 earthquake scenarios are simulated as shown in Fig. 2, which shows the annual dose rate of all cases. Within a few centuries, no significant difference among the scenarios was observed. The maximum annual dose rate within the 1,000 simulations was reached to 2.34×10^{-5} mSv/yr, which is negligible compared to the safety limit for the normal scenario, i.e. 0.1 mSv/yr.

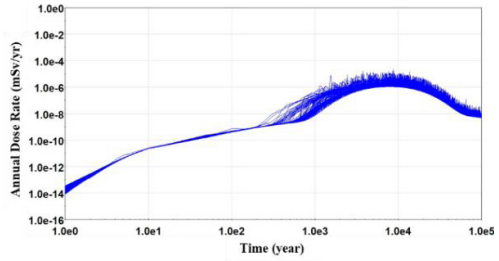

Fig. 2. Annual dose rate obtained from 1,000 simulations.

In addition, the risk for the earthquake scenario was calculated based on the 1,000 simulations, and the risk assessment results are depicted in Fig. 3. The maximum risk of 5.81×10^{-11} yr^{-1} as well as the annual dose rate were much smaller than the safety limit.

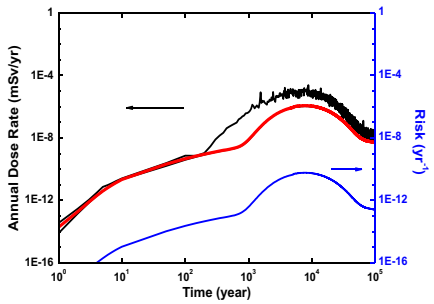

Fig. 3. Risk assessment results of earthquake scenario.

4. Conclusions

From the multiple earthquake scenario simulations, it was deduced that the repository provides a robust safety against for the seismic effect, and no simulation case exceeds the safety limit. In particular, the maximum risk of 5.81×10^{-11} yr^{-1} calculated from this work corresponds to 0.006% of the regulatory criterion of 10^{-11} yr^{-1}.

5. Acknowledgement

This work was supported by the Nuclear Safety Research Program through the Korea Foundation Of Nuclear Safety(KOFONS), granted financial resource from the Nuclear Safety and Security Commission(NSSC), Republic of Korea (No. 1305032)

REFERENCES

[1] S. C. Han and J.-I, Yun, “Sensitivity Analysis for Major Input Parameters in LILW Repository Safety Assessment Model”, Proc. of the KRS 2016 Autumn Conference, 14(2), October 12-14, 2016, Jeju.

[2] C. A. Cornell, “Engineering Seismic Risk Analysis”, Bulletin of the Seismological Society of America, 58, 1583-1606 (1968).

[3] R. M. Allen, “Earthquake hazard Mitigation: New Directions and Opportunities”, 4(4.21) ed., Elsevier (2007).

[4] Y.-M. Lee and H.-J. Choi, “An evaluation of nuclide release from a trench-type LILW repository”, Progress in Nuclear Energy, 88, 95-103 (2016).

[5] J.-W. Kim, D.-K. Cho, N.-Y. Ko and J. Jeong, “Characterization of Domestic Earthquake Events for the Safety Assessment of the Geological Disposal System”, Journal of Nuclear Fuel Cycle and Waste Technology, 13(2), 87-98 (2015).

Solidification of HyBRID Waste Using Geopolymer Waste Form

Jinmo Ahn[1], Won-Seok Kim[1], Seongye Kwon[1], Seonbyeong Kim[2], Wangkyu Choi[2], and Wooyong Um[1,*]

[1]Division of Advanced Nuclear Engineering, POSTECH, 77, Cheongam-ro, Nam-gu, Pohang, Korea

[2]Decontamination and Decommissioning Research Division, Korea Atomic Energy Research Institute, Daedeok-daero989ben-gil 111,Yuseong-gu, Daejeon, Republic of Korea

wooyongum@postech.ac.kr

1. Introduction

The hydrazine based reductive metal ion decontamination (HyBRID) process with sulfuric acid is recently developed and considered as an attractive process consisting of hydrazine, copper ion, and sulfuric acid without any organic chelates. The target radionuclides such as Cobalt and Cesium are separated through HyBRID process from the primary system decontamination and subsequently present in HyBRID wastewater containing high contents of sulfate ion. This HyBRID wastewater is then converted to HyBRID sludge waste through a precipitation process.

The HyBRID sludge, which has the high contents of sulfate ion, makes cement waste form defective due to the potential formation of Ettringite mineral [$Ca_6Al_2(SO_4)_3(OH)_{12}\cdot 26H_2O$] [1]. Therefore, the geopolymer waste form was proposed to immobilize the HyBRID sludge waste with the waste loading (>10%).

2. Geopolymer waste forms

2.1 materials and methods

Kaolin was obtained from Sigma Aldrich and calcined at 750 °C for 4 h to transform to the MK. The chemical compositions of MK and HyBRID sludge using X-ray fluorescence (XRF) are shown in Table 1.

Metakaolin (MK) was used as geopolymer precursor and the alkaline activator was prepared by mixing sodium silicate solution (Na_2O=10%, SiO_2=30%, H_2O=60% in mass) and sodium hydroxide solution (~19M). Geopolymer precursor and the alkaline activator were mixed using planetary centrifugal mixer. Subsequently, all paste samples were poured into cylindrical mold (23 mm in diameter x 46mm in height) with a cap. The sealed geopolymer pastes were placed in the clean bench at 20°C for 7 days to cure.

Table 1. Chemical compositions of metakaolin and HyBRID sludge waste (wt%)

	SiO_2	Al_2O_3	BaO	SO_3	LOI*
MK	54.8	39.5	-	-	4.89
HyBRID sludge	45.8	2.04	28.9	13.8	4.42

*LOI: loss of ignition

2.2 Geopolymer synthesis with varying conditions

Geopolymer waste forms were formulated with desired ratio of Si/Al (1.7-2.1) with varying waste loadings [2]. Geopolymer waste forms were successfully synthesized to meet the acceptance criteria (>3.45 MPa). Geopolymers formed with Si/Al molar ratio of 1.7, 1.9, and 2.1 and it achieved the compressive strength of 7.13, 21.7, and 38.0 MPa, respectively. With increasing Si/Al ratio, the final compressive strength also increased.

The result of FT-IR spectra of each geopolymer waste forms is shown in Fig. 1. The absorbance band at 976, 973, and 964 cm^{-1} indicated the vibrations of Si-O-Si and Si-O-Al groups of the geopolymer gel network [3]. The band at 1211 cm^{-1} which indicated the amorphous silica disappeared as Si/Al ratio increased.

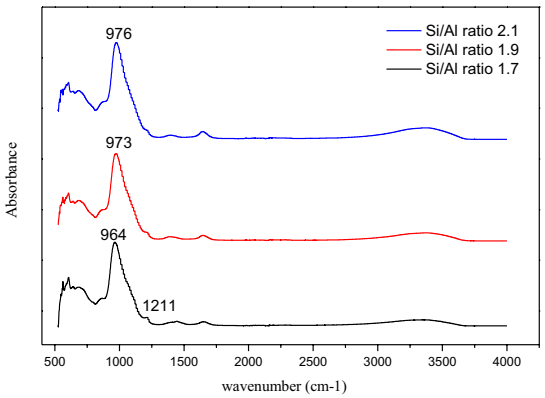

Fig. 1. FT-IR spectra of geopolymer depending on Si/Al ratio.

3. Conclusions

Geopolymer waste form was proposed to immobilize the HyBRID sludge waste with high sulfate content. Geopolymer waste forms with HyBRID sludge have met the acceptance criteria. The compressive strength of the geopolymer waste forms was 37.95MP with 16 wt% of HyBRID sludge. The FT-IR result revealed the presence of residual amorphous silica at low Si/Al ratio (Si/Al=1.7). The Si/Al ratio affected the compressive strength of geopolymer in that Si-O-Si absorbance band increased.

ACKNOWLEDGEMENT

This work was supported by the Korea Atomic Energy Research Institute (KAERI) granted financial resource (NRF- 2018M2A8A5024109).

REFERENCES

[1] M.S.H. Khan, O. Kayali, and U. Troitzsch, “Effect of NaOH activation on sulphate resistance of GGBFS and binary blend pastes”, Cement and Concrete Composites, 81, 49-58 (2017).

[2] RP Williams and A Van Riessen, “Determination of the reactive component of fly ashes for geopolymer production using XRF and XRD”, Fuel, 89(12), 3683-3692, (2010).

[3] N. K. Lee, Hammad R. Khalid, H.K.Lee, “Adsorption characteristics of cesium onto mesoporous geopolymers containing nano-crystalline zeolites”, Microporous and Mesoporous Materials, 242, 238-244 (2017).

A Study on the Proper Amount of $Ba(OH)_2$ for the Wastewater Treatment From the SP-HyBRID Decontamination Process

J.Y. Jung[a,b], H.C. Eun[a], S.Y. Park[a,*], H.J. Won[a], J.S. Park[a], S.B. Kim[a], B.K. Seo[a], and S.J. Park[b]
[a]Korea Atomic Energy Research Institute, 989-111 Daedeok-daero, Yuseong-gu, Daejeon, Republic of Korea
[b]Department of Applied Chemistry and Biological Engineering, Chungnam National University, 99 Daehak-ro Yuseong-gu, Daejeon, Republic of Korea
[*]nsypark@kaeri.re.kr

1. Introduction

SP-HyBRID, which has been developed in KAERI, is a new decontamination process for the primary coolant system of PWR. This SP-HyBRID process does not contain any organic chemicals in the decontamination solution[1]. Therefore a wastewater generated from the SP-HyBRID process only contains inorganic chemical included in the decontamination solution and dissolved from oxide at the inner surface of RCS. Among those, various metal ions as well as sulfate ions are removed by precipitation method using $Ba(OH)_2$ instead of ion-exchange method to reduce the secondary waste volume[1]. Sulfate ions react with barium ions, and then are precipitated as a form of barium sulfate. pH in the wastewater increases by the added $Ba(OH)_2$, and metal ions are precipitated as a form of metal hydroxide[2,3]. Most of the metal ions in the wastewater can be separated, and the use of ion exchange resins for purifying the wastewater can be minimized. However, if an excess amount of $Ba(OH)_2$ is used to remove sulfate ions completely in the wastewater, a certain amount of barium ions can be residual in a purified wastewater, and cause a problem to need an additional treatment process. It is necessary to determine a proper amount of $Ba(OH)_2$ for purifying the wastewater.

In this study, precipitation tests of sulfate and metal ions in a wastewater surrogate were conducted to derive a required amount of $Ba(OH)_2$. A proper amount of $Ba(OH)_2$ was determined by removal tests of sulfate ions in a solution without metal ions changing a $Ba(OH)_2$ injection amount. And a removal performance of sulfate and metal ions in a wastewater surrogate was evaluated at the determined use of $Ba(OH)_2$. The drinking water quality standards expressed in Table 1 were utilized to evaluate these test results.

Table 1. Drinking water quality standards

Species of ions	Concentration [ppm]
SO_4^{2-}	< 200
Ba	< 0.7
Cu	< 1
Fe	< 0.3
Cr	< 0.05
Ni	< 0.01
Mn	< 0.05
Zn	< 3

2. Experimental Methods

2.1 Determination of a proper use of $Ba(OH)_2$

A solution containing only sulfuric acid and hydrazine without metal ions was prepared to determine a proper use of $Ba(OH)_2$. Theoretical mole ratio of the reaction between sulfate and barium ion is 1:1 as shown in the Eq. (1). The molar ratio was determined at 0.8 ~ 1.05 of barium ion over sulfate ion. Test solutions were mixed at 200rpm under room temperature in a 500ml solution. After the mixing for 1 h, a sample was taken from the solution, and then filtered to analyze concentrations of sulfate and barium. The concentrations of sulfate and barium were analyzed using UV-vis spectroscopy and ICP-OES, respectively.

$$SO_4^{2-} + Ba^{2+} = BaSO_4 \quad (1)$$

2.2 Removal of sulfate and metal ions

A wastewater surrogate was prepared to conduct removal tests of sulfate and metal ions as shown in the Table 2. The composition of metal ions in the wastewater surrogate used in this study were chosen to be as close to those values expected in a real primary coolant decontamination wastewater as

possible. The amount of added $Ba(OH)_2$ was determined by the results obtained through section 2.1. The removal tests of sulfate and metal ions in the wastewater surrogate were performed in 1L solution. The test conditions and analyzing methods were same with tests described in section 2.1

Table 2. Composition of wastewater surrogate used in this study

	Concentration of compositions [ppm]
SP-HyBRID	$KMnO_4$ 1000, H_2SO_4 3630, N_2H_4 1856, $CuSO_4$ 80
Dissolved metal ions	Fe, Cr, Ni, Cu, Zn, Co (50, 75, 100 respectively)

3. Results

In the determination test of a proper $Ba(OH)_2$ use, when $Ba(OH)_2$ was injected at a higher molar ratio than 1, barium ions in the tested solution were greatly increased as shown in Table 3. When $Ba(OH)_2$ was injected in the range of 0.95 to 1, the concentrations met the drinking water quality standards. Since the standard of barium ion is very low comparing with sulfate ion, in determining the amount of $Ba(OH)_2$, emphasis was on low barium ion concentrations. Considering the results in Table 3 and the drinking water quality standards, 0.975 was determined as a proper molar ratio. In the precipitation test of sulfate and metal ions in the wastewater surrogate using this molar ratio of $Ba(OH)_2$ injection, it was confirmed that concentrations of sulfate and metal ions in the purified wastewater surrogate also meet the standards. Concentration of sulfate ion in solution was below 0.5ppm. Barium ion remain below 0.4ppm. The dissolved metal ions in Table 2 were not detected on ICP-OES. (Limit detection : 0.01ppm)

Table 3. Concentration of residual sulfate and barium ions in the tested solution after the determination test of a proper $Ba(OH)_2$ use

Molar ratio	SO_4^{2-} [ppm]	Ba^{2+} [ppm]
0.8	531	0.3
0.9	256	0.4
0.925	225	0.48
0.95	79	0.22
0.975	39	0.18
1	2	0.32
1.05	0	87.32

4. Conclusion

To meet the drinking water quality standards about the concentrations of sulfate and metal ions in a purified wastewater after purifying a wastewater from the SP-HyBRID decontamination process, an proper use of $Ba(OH)_2$ was at 0.975, and it was confirmed that the removal of sulfate and metal ions was effective. This result can be utilized to reduce an overdose of $Ba(OH)_2$ during the purification of the wastewater treatment process, and contribute to the reduction of final waste.

ACKNOWLEDGE

The authors would like to express their appreciation to the National Research Foundation of Korea (NRF) for the award of a grant funded by the Ministry of Science and ICT (MSIT) of the Republic of Korea, in support of the authors' work through the Nuclear Research and Development Program (NRF-2017M2A8A5015144).

REFERENCES

[1] S.Y. Park, H.J. Won, M.S. Choi, S.B. Kim, W.K. Choi, and J.K. Moon, Waste Minimization of HyBRID Decontamination Process, WM2017 Conference, March 5-9, Phoenix, Arizona, USA (2017).

[2] M. M. Pourbaix, "Atlas of electrochemical equilibria in aqueous solutions", National Association of Corrosion Engineers (1974).

[3] Tomasz Suponik "ENSURING PERMEABLE REACTIVE BARRIER EFFICACY AND LONGEVITY", Environmental Engineering of the Polish Academy of Sciences (2010).

4분과

중저준위폐기물관리 (Poster)

Radiation Shielding Evaluation for IP-2 Transport Container Including Activated Cutting Waste of KORI Unit 1 RV/RVI

Jae-Hun Ko[*1], Duk-Woon Jung[1], Dong-Kyu Lee[1], and Young-Hwan Hwang[2]

[1]Korea Nuclear Engineering & Service, #5, Hyundai Plaza, 798-1 Yuseong-daero, Daejeon, Korea

[2]KHNP Central Research Institute, 1312-70 Yuseong-daero, Yuseon-gu, Daejeon, Korea

[*]kojh4@kones21.com

1. Introduction

In order to secure safety and to improve economics for disposal of VLLW/LLW, radioactive cutting wastes generated during decommissioning of the RV/RVI are should considered for characteristics of waste, site conditions, transportation and the temporary storage. Therefore it is essential to secure packaging technology these radwaste. Most of the RV/RVI cutting waste is classified as LLW and VLLW, and in the case of KORI unit 1, it accounts for about 65% of the activated RV/RVI radwaste. Accordingly in Korea, where nuclear power plant decommissioning has been actively researched, has been developing packaging containers for cut radwaste of KORI unit 1 RV/RVI, recently. In this paper, the calculation of the dose rate under the normal transportation conditions of the IP-2 transport package for transporting the packaging containers for the RV/RVI cutting waste currently under development to the disposal facility was performed.

2. Shielding Evaluation of IP-2 container

2.1 Dose Rates Criteria

There are several regulations related to radioactive waste transport in the domestic and international laws. Under the Normal transport condition, dose rate at the surface of the IP-2 transport container is limited to 2mSv/hr and one at any point 2m away from the container is limited to 0.1mSv/hr.

2.2 Source Terms

According to previous evaluation for radioactive nuclide inventory of the KORI unit 1 RV/RVI, LLW/VLLW accounts for about 65% of the activated RV/RVI radwaste. The region with the highest radioactivity level in LLW is the upper core plate of reactor vessel internal. The cut of the upper core plate is filled in only 50% of the volume inside the package, and the remaining space is grouted with cement for immobilization, therefore calculated weight of this inside the container is 7.88tons. Table 1 shows specific activity and radioactivity considered weights of the upper core plate.

Table 1. Radioactivity of Upper Core plate

Nuclides	Specific Activity [TBq/g]	Activity [Bq]
Fe-55	1.91E-06	1.28E+13
Co-60	7.51E-09	5.03E+10
Ni-59	1.78E-08	1.19E+11
Ni-63	1.88E-06	1.26E+13

2.3 LLW Package for cut RV/RVI

The dimensions of the container for packaging the LLW of the RV/RVI are 1.46m(W) x 1.46m(L) x 0.95m(H) and thickness of it is 0.3cm. In the inside of the packaging container there is a steel-ridge for fixing and draining the contents, and the grouting using the cement is filled between the inside of the steel-ridge and the packaging container. External dimensions of the IP-2 transport container are 1.6m(W) x 3.4m(L) x 1.2m(H) and thickness of it is 0.12cm. The IP-2 transport packaging contains two LLW packaging containers. Fig. 1 shows IP-2 transport container with decommissioning waste that is LLW such as upper core plate.

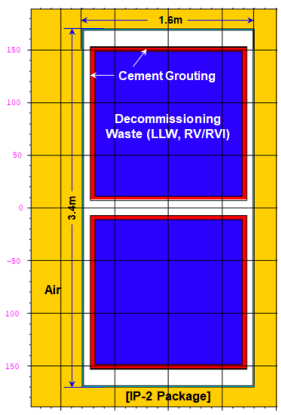

Fig. 1. Shielding Evaluation Model.

2.4 Shielding Evaluation

MCNP5 computer code using the three-dimensional Monte Carlo method was used to analyze to calculation dose rates at the various desired location of the IP-2 transport container [1]. It calculates photon flux which can be converted into dose rates by the use dose conversion factors. The dose conversion factors used in this calculation was taken from ICRP-74(1996) [2].

3. Shielding Evaluation Results

In this MCNP calculation, virtual detectors are placed at the considering points to obtain the information for dose rate. 15 detectors are respectively placed at external surface and 2m position of the IP-2 transport container. Table 2 and Fig. 2 show respectively maximum dose rates at all position and dose rates at considered points for the top and side of the IP-2 transport container. Relative errors of these detectors are showed 0.03~0.05.

Table 2. Dose Rates Results for IP-2 Container

[Unit : mSv/hr]

Cal. Point	External Surface		2m from the Surface	
	Results	Limit	Results	Limit
Front	0.288	2.0	0.023	0.1
Side	0.301		0.043	
Top	0.408		0.073	
Bottom	0.299		0.058	

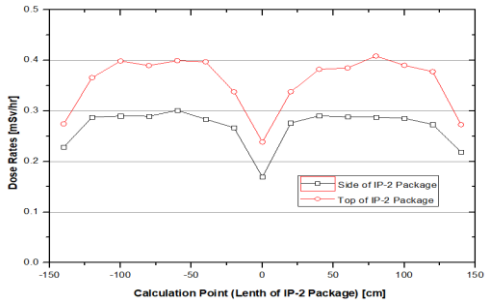

(a) Dose rates at External Surface

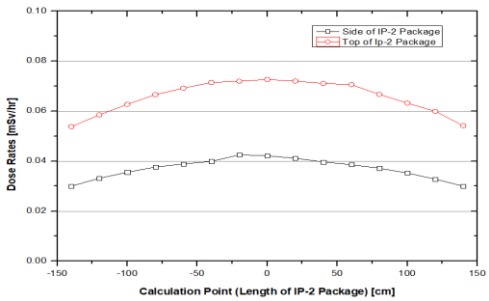

(b) Dose rates at 2m form the Surface

Fig. 2. Results of Shielding Evaluation.

4. Conclusion

Recently, containers for RV/ RVI cut contents packaging are being conceptually designed, radiation shielding evaluation was performed to IP-2 transport container with decommissioning waste that is LLW such as upper core plate. IP-2 transport container including RV/RVI of Low-Level Waste radioactive waste satisfies radiation dose limits under normal transport condition.

ACKNOWLEDGEMENT

This work was supported by the Korea Institute of Energy Technology Evaluation and Planning (KETEP) generated financial resource from the MOTIE, Republic of Korea. (No.20161510300430)

REFERENCES

[1] Los Alamos National Laboratory, MCNP –A General Monte Carlo N particle Transport Code, Ver.5, Release 1.40 (2005).

[2] ICRP, Conversion Coefficients for Use in Radiological Protection Against External Radiation, ICRP-74 (1996).

Radionuclide Inventory of Past Radioactive Waste in NPPs

HeeJin Ahn* and HongJoo Ahn
*Korea Hydro Nuclear Power, 70, 1312-gil, Yuseong-daero, Yuseong-gu, Daejeon, Republic of Korea
Korea Atomic Energy Research Institute, 111 Daedeok-daero-989, Yuseong-gu, Daejeon, Republic of Korea
*cowahn61@khnp.co.kr, ahjoo@kaeri.re.kr

Dry active waste arising from PWR- and PHWR-type NPPs have to be shipped to a permanent disposal facility. For permanent disposal of LILWs, the radionuclide inventories should be evaluated using the scaling factor, which was determined between 2004 and 2008. Therefore, it is necessary to examine the applicability of the scaling factor to the dry active waste (DAW) drums generated prior to 2004. The samples that were assayed were obtained from DAW drums generated prior to 2004, and were pretreated to make-up a 20 ㎖ solution, separated radiochemically, and counted by radiation counters. In addition, using the database, the applicability of the scaling factor to the old DAW drums generated before 2004 was examined through a comparison between the measured radioactivity for a specific β-emitting radionuclide in the past DAW drums and the estimated radioactivity by the scaling factor. As a result, the radioactivity ratios of specific radionuclides were distributed within the identified data ranges of the scaling factor, which showed great significance at a 95% confidence level.

1. Introduction

Since the completion of a disposal site, the Korean Radioactive Waste Agency (KORAD) has accepted approximately 7,000 waste drums each year. It is necessary to quickly develop and secure technologies and facilities that can prove the compliance of the waste acceptance criteria for permanent disposal. This is to prevent a shortage of drums disposed of at the disposal site owing to the delay of the current technological development. To permanently dispose of the waste drums to the disposal site, it is necessary to comply with the disposal regulations based on the KORAD "Waste Delivery Criteria" and the Korea Atomic Energy Agency Notice "Waste Acceptance Criteria". In the case of all waste drums that have been generated during the past (prior to 2004), it must be verified whether the Waste Delivery/Acceptance Criteria for the drums is satisfactory. Therefore, the validity of the scale factor must be quickly verified through the establishment of a "Radionuclide inventory DB" for the past waste drums. The past waste drums are being stored in an interim storage of each Nuclear Power Plant site and currently reach approximately 55,000 drums [1].

In this study, the samples to be assayed were obtained from DAW drums generated prior to 2004, and were analyzed through radiochemical pretreatment and radionuclide separation [2]. Using the “database, the applicability of the scaling factor to the past DAW drums was examined through a comparison between radionuclide concentrations analyzed directly in the past DAW drums and radionuclide concentrations estimated by the scaling factor.

2. Experimental

2.1 Sampling of the past waste drums

The samples of the super compressed dry active waste were transferred to the Radioactive Waste Form Examination Facility (RWFEF) in the Korea Atomic Energy Research Institute (KAERI) from the Hanul NPP site. RWFEF is a facility used to identify the inventory of the specific radionuclides. In order to analyze the concentrations of some radionuclides, the RWFEF opened each drum to get representative samples, and sent to the radionuclide analysis laboratory.

2.2 Radiochemical analysis of the radionuclides

The samples, which were weighed and ashed in a furnace, were put into a 125 ㎖ digestion vessel. The ashed samples were dissolved completely using a HNO_3/HCl/HF mixed solvent. Subsequently, they were placed in a microwave oven (Ethos PLUS Milestone Microwave Digestion), and irradiated with a maximum energy of 400 W for 20 to 50 minutes in order to be dissolved in the mixed solvent. A representative sampling is very important to reduce the sampling error from the inhomogeneous distributions of the nuclides. Sequentially, a single portion of the digested sample was sequentially used throughout the procedures before the γ-spectroscopic measurement. The samples were classified into volatile difficult-to-measure (DTM) nuclides such as ^{3}H, ^{14}C, ^{99}Tc, and non-volatile nuclides. ^{3}H and ^{14}C in the radwastes were extracted into gaseous $^{14}CO_2$ and liquefied HTO through a wet oxidation and distillation method simultaneously [3]. ^{99}Tc was separated and purified with an ion exchange resin and counted by Gas flow Proportional Counter. ^{55}Fe from the completely dissolved samples were separated using an ion exchange resin and extraction chromatography [4].

2.3 Application of Scaling Factor

A scaling factor is a general method to estimate DTM nuclides in the waste drums. In order to develop the scaling factor, analytical samples were extracted representatively among the LILWs generated from the PWR and PHWR-type NPPs between 2004 and 2008. Eventually, the first scaling factor was derived through a radiochemical and statistical analysis. The applicability of the scaling factor to the past DAW drums generated prior to 2004 was examined through a comparison between the measured radioactivity for a specific β-emitting radionuclide in the past DAW drums and the estimated radioactivity by the scaling factor.

3. Results and Conclusions

In the past drums, the radionuclide concentrations of ^{60}Co and ^{137}Cs showed wide radioactivity distributions in the ranges of 2.1E-1 to 1.4E+3 Bq/g and 2.9E+0 ~ 1.3E+4 Bq/g, respectively. The concentration distributions of those radionuclides in the PWR-type NPP was over ten-fold higher than the case of the PHWR-type NPP. Among the target beta emitting radionuclides, ^{3}H and 14C radionuclides were distributed within the ranges of 6.6E+0 ~ 1.2E+3 and 6.6E-2 to 3.3E+0 Bq/g, respectively. ^{55}Fe and ^{99}Tc radionuclides as representatives of activation and fission products were distributed within concentration ranges of 1.2E+2 ~ 2.5E+2 and 1.9E-2 ~ 4.7E-2 Bq/g, respectively.

From these radiochemical analysis results, the applicability of the scale factor was confirmed through a comparison of the radioactivity ratio of the target radionuclide to the key radionuclide between the scaling factor results and radionuclide concentration results generated prior to 2004. As a result, both radioactivity ratios of ^{3}H, ^{14}C, ^{55}Fe, and ^{99}Tc were distributed within the identified data ranges, which had great significance at a 95% confidence level.

REFERENCES

[1] http://www.khnp.co.kr

[2] 2012 Nuclear energy yearbook published in Korea Atomic Industrial Forum (2012).

[3] H. J. Ahn, H. N. Lee, and S. H. Han, "Simultaneous assay of ^{14}C and ^{3}H in evaporator bottom by chemical oxidation method", J. Kor. Rad. Waste Soc., 3, 193 (2005).

[4] C. H. Lee, M. Y. Suh, K. S. Choi, K. Y. Jee, and W. H. Kim, "Sequential separation of ^{99}Tc, ^{94}Nb, ^{55}Fe, ^{90}Sr and $^{59/63}Ni$", J. Radioanal. Nucl. Chem., 272, 187-194 (2007).

5-Bromo-Ph4-BTPhen Ligand for Selective Removal of Strontium and Cobalt From Water

Jiseon Jang[a], Laurence M. Harwood[b]*, Joe Cowell[b], Ashfaq Afsar[b], and Dae Sung Lee[a]*

[a]Department of Environmental Engineering, Kyungpook National University, 80 Daehak-ro, Buk-gu, Daegu, Republic of Korea

[b]Department of Chemistry, University of Reading, Whiteknights, Reading RG6 6AD, United Kingdom

daesung@knu.ac.kr

Abstract

In this study, 5-bromo-2,9-bis(5,6-diphenyl-1,2,4-triazin-3-yl)-1,10-phenanthroline (5-bromo-Ph4-BTPhen) was synthesized and evaluated for its ability to remove major radionuclides (Cs^{+}, Sr^{2+}, and Co^{2+}). The synthesized ligand removed both Sr^{2+} and Co^{2+} from 1 mg L^{-1} aqueous solutions with extraction efficiencies of up to 99% at neutral and alkaline pH. The Sr^{2+} and Co^{2+} removal efficiencies decreased as a consequence of the higher bonding strengths of competing metal ions to the N-donor atoms in the cavity of the ligand; competing divalent ions affected the Sr^{2+} and Co^{2+} removal efficiencies more than monovalent ions.

Keywords: BTPhen, radioactive wastewater, distribution coefficient, radionuclides, ligand

Treatment of Radwastes From Medical Radioisotope Production

Seung-Kon Lee*, Suseung Lee, Myunggoo Kang, Kyungsoek Woo, and Junsig Lee
Division of Radioisotope Research, Korea Atomic Energy Research Institute, 111, Daedeok-daero 989beon-gil, Yuseong-gu, Daejeon, Republic of Korea
*seungkonlee@kaeri.re.kr

1. Introduction

Molybdenum-99 (Mo-99) and its daughter isotope technetium-99m (Tc-99m) has been the most commonly used medical radioisotope which covers 85% of overall nuclear diagnostics. Currently, majority of Mo-99 supplied in the market is fission-based Mo-99 produced by the fission of U-235 in research reactors. In spite of substitutive production schemes, reactor-based fission Mo-99 (FM) exhibits significant advantages with higher specific activity (~10^4Ci/g) with lower production cost. [1]

Historically, the most FM producers have been used highly enriched uranium (HEU) targets. However, to limit the use of HEU in private sector for non-proliferation, all producers are being forced to convert their HEU-based process to use low enriched uranium (LEU, 19.75% U-235 enrichment) targets by 2018.

Consequently, overall cost for the production of the FM increased significantly. It is not only because of the 50% less yield, but also because of the radioactive waste increase by 200%. Therefore, designing optimal radwaste treatment system for FM production is becoming more important. [2, 3]

2. Fission Mo-99 Production

2.1 Fission Mo-99 Target

Today, all industrial-scale FM producers use dedicated uranium targets optimized for the alkaline digestion. KAERI developed plate-type LEU target composed of UAl_3/UAl_4 meat dispersed in Al-6061 cladding. Each target plate contains 14.95g LEU and uranium density of the meat is 2.6 g U/cm^3. The targets are irradiated in the reactor, then transferred from the FM production facility for processing after cooling for 24 hrs.

2.2 Fission Mo-99 Process

The irradiated targets are dissolved in sodium hydroxide solution for processing. Fission products other than Mo-99 are removed from the solution using multiple separation steps, as shown in the Fig. 1. Then Mo-99 is eluted and purified to meet standard for international pharmacopoeia. [4, 5, 6]

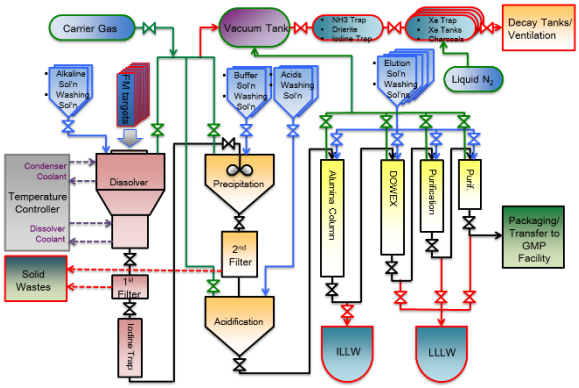

Fig. 1. Scheme for the FM process.

3. Radwastes in FM Production

As shown in the Fig. 1, solid, liquid and gaseous radwastes in various activity levels are produced during the FM production. In terms of radionuclides, isotopes of iodine, xenon, krypton, technetium and uranium are the major components in the waste stream.

3.1 Solid Radwastes

Uranium aluminide dissolved in the alkaline solution transforms to the insoluble oxide forms. The most of uranium and insoluble impurities containing transition metals, part of alkaline earth metals and transuranium elements forms colloidal particles. In alkaline solution, aluminum metal forms soluble sodium aluminides. But eventually, it transformed to insoluble aluminum oxides. Columns and consumables used in the separation and purification stages are also an origin of solid wastes.

3.2 Liquid Radwastes

Intermediate level liquid wastes (ILW) containing various fission products is generated from the separation of Mo-99 after alkaline dissolution of targets. KAERI developed new technology to facilitate waste treatment by converting sludge-type waste, which is difficult to handle, into independent solid and liquid wastes. Using this scheme, salt concentration in the ILW can be reduced significantly to make cementation much easier.

In the FM process with caustic digestion, most iodine remains in the liquid phase as negatively charged iodide form. Therefore, iodine can be separated using a dedicated column from to the ILW.

Low level liquid wastes produced during elution and washing for purification step can be treated by combination of ion-exchange and evaporation.

3.3 Gaseous Radwastes

Radioisotopes of xenon (Xe) and krypton (Kr) are generated from the fission of Uranium. Emission of radioxenon from the medical radioisotope production is controlled via delayed release through large charcoal beds.

KAERI developed compact xenon adsorption module with chilled carbon column to meet 5 GBq/day of CTBTO recommendation. It can satisfy the guideline with only 8.5 kg charcoal, instead of 32 tons of conventional system.

4. Conclusion

To achieve production objective (2,000 Ci/week) of Mo-99 in KJRR, KAERI is developing the FM production process with dedicated facility. Weekly production of 2,000 Ci (100,000 Ci/yr, 6-day calibration) Mo-99 will cover 100% domestic, as well as 20% of international demand. Every year, 3,000 L of ILW and 10 kg of spent uranium is expected to be treated.

Therefore, development of radwaste treatment program for the FM production is one of the most essential piece for the successful construction, licensing and operation of the new research reactor (KJRR), which is being constructed in Gijang, Busan, Korea.

ACKNOWLEDGEMENT

This work was supported by the National Research Foundation of Korea (NRF), funded by the Ministry of Science and ICT (NRF-2012M2A2A6009866).

REFERENCES

[1] International Atomic Energy Agency, “Non-HEU Production Technologies for Molybdenum-99 and Technetium-99m”, IAEA Nuclear Energy Series No. NF-T-5.4 (2013).

[2] International Atomic Energy Agency “Fission Molybdenum for Medical Use”, IAEA-TECDOC-515 (1989).

[3] International Atomic Energy Agency, “Management of Radioactive Waste from 99 Mo Production”, IAEA-TECDOC-1051 (1998).

[4] M. V. Wilkinson, A. V. Mondino, A. C. Manzini, J. Radionanl. Nucl. Chem., 256, 413 (2003).

[5] R. Muenze, G. J. Beyer, R. Ross, G. Wagner, D. Novotny, E. Franke, M. Jehangir, S. Pervez, A. Mushtaq, Sci. and Tech. of Nuclear Installations, 932546, 9 (2013).

[6] S. Dittrich, Sci. and Tech. of Nuclear Installations, 514894, 9 (2013).

Study on Predictive Models for Leaching Behavior of Waste Glasses Based on Machine Learning Algorithms

Jae Hwan Yang
Korea Atomic Energy Research Institute, Daedeok-daero989ben-gil 111,Yuseong-gu, Daejeon, Republic of Korea
yjh98@kaeri.re.kr

1. Introduction

Radioactive waste produced from spent nuclear fuel reprocessing or operation of nuclear power plants has been converted to borosilicate glasses. These glasses are destined to be disposed of in repositories over ten thousands of years. The leaching behavior of waste glasses is essential to reasonably predict the long-term stability of the glasses. In this regard, many studies have been performed to produce data related to glass leaching behavior. Empirical data is made by experiments that simulate the repository environments. Theoretical works has revealed the various mechanisms of glass dissolution. Computational studies are also contributing to the understanding of glass alteration behavior. However, the current phase of glass leaching research is still far from the level of the prediction of glass leaching characteristics for sufficiently long time. In this study, efforts are focused on the examination of predictive models of glass leaching behavior based on machine learning algorithms.

2. Methods

2.1 Input data manipulation

Modeling by machine learning requires many data to find a reasonable model for prediction. Herein, data on glass properties and leaching rates were obtained from a published report [1]. The leaching rates were produced by Product Consistency Test (PCT) and data on B, Li, Na, Si were provided. Feature (sometimes called parameter) selection was followed. Glass leaching could be affected by several factors such as glass composition, melting temperature, cooling method, and testing environment. All glasses were described to be melted at 1150 °C and quickly cooled glasses were only considered. In addition, PCT data obtained by a test at 90 °C were used. Therefore, it is considered that glass composition is the only substantial feature to affect the leaching rates in this research. Among 61 components presented in the report, ones with higher than 0.5 wt% and ones that are told to be related to the leaching property were selected and 42 components were finally chosen as features. As a result, total 1207 PCT data were used as training, cross-validation, and testing dataset. The purpose of this study is to develop a basic predictive model that classifies the durability of glasses based on leaching rates. Therefore, data were labeled to indicate the durability level: 1, 2, and 3 means poor, normal, and good durability.

2.2 Machine learning modeling

Support vector machine (SVM) algorithm, a representative classification algorithm, was used to

develop a model. Source codes necessary for the model were obtained from the famous libraries of scikit-learn [2]. As a first step, parameter optimization was performed by adjusting kernel parameters (C, γ) with cross-validation. Then, the model with the optimized parameters was trained by training dataset. Finally, the predictive accuracy was performed by using test dataset.

3. Results and discussion

Fig. 1 shows the result of grid search to find the optimal parameter combination. Gamma and C factors were varied from 0.001 to 100 and the mean scores of 5-fold cross-validation were written in each box. As seen in the heat map, most scores remain 0.75 even after parameter adjustment. The best score is shown in the brightest box which corresponds to (C, γ)=(10, 100). This score means that the prediction accuracy is 87% after parameter optimization.

The accuracy score is not enough to validate model performance. Error matrix was calculated to see how precise the model predicts for each label. As indicated in Fig. 2, the number of precise prediction for the label 1, 2, and 3 is 25, 149, 7, respectively. The accuracy score for the label 1, 2, and 3 is 0.81, 0.89, and 0.88, respectively. This result indicates that the classification into low durable glass group by using the current model is relatively inaccurate. Further research should be performed to modify the performance of the model. Machine learning based models are thought to suggest the optimized glass compositions that improve the stability of the glass.

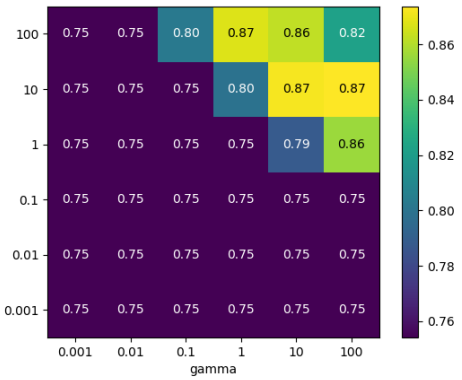

Fig. 1. Result of grid search for parameter optimization.

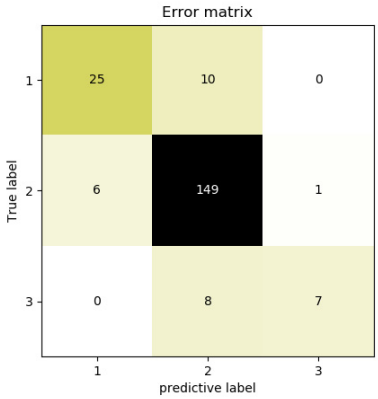

Fig. 2. Error matrix of the predictive model.

REFERENCES

[1] J. Vienna, D. Kim, P. Hrma. “Database and Interim Glass Property Models for Hanford HLW and LAW Glasses”, PNNL-14060, Pacific Northwest National Laboratory, (2002).

[2] http://scikit-learn.org/stable/

A Comparative Study on Domestic and Overseas WTS for Implementation of the Integrated Radioactive Waste Tracking System

Sun Il Kim, Hak Yun Lee, Ki Tae Yang, and Jong Soon Song*

Chosun University, 309 Pilmun-daero, Dong-gu, Gwangju, Republic of Korea

jssong@chosun.ac.kr

1. Introduction

To efficiently manage information on domestic radioactive waste, it is necessary to build and operate a comprehensive national database (DB) to which the latest information technology (IT) is applied. Recently major advanced countries in nuclear power are digitalizing various safety regulation data and disclose it to the general public through the communication network.

Currently, domestic nuclear power plants, Korea Atomic Energy Research Institute and Korea Nuclear Fuel Company, Ltd. developed their own radioactive waste tracking systems, but these management systems are implemented only for classification and recording information at the basic level.

2. Main Title

2.1 Key radioactive waste management systems in Korea

2.1.1 DREAMS (Digital Realtime Enterprise Management System). Korea Hydro & Nuclear Power Co., Ltd.'s enterprise resource planning (ERP) includes the RAdiation Management (RAM) system for managing the workers' history management function and the radiation work permit system, and the Rad-Waste Management (RWM) system for managing the solid radioactive waste management function and the liquid/gaseous radioactive waste discharge permit and result function.

2.1.2 WACID (WAste Comprehensive Information Database). It is an integrated information system that Korea Institute of Nuclear Safety developed to objectively and accurately manage safety management information regarding domestic radioactive waste and spent nuclear fuel. Depending on the characteristics of the data, KINS developed individual database modules, such as low and intermediate-level waste, spent nuclear fuel, liquid/gaseous radioactive effluent and decommissioning waste.

2.2 Key foreign radioactive waste management systems

2.2.1 NMMSS (Nuclear Material Management & Safeguard System). It is an integrated system that the US DOE is using for nuclear materials inventory and cycle management, related reporting function, data collection transaction module, and safe management of material balance.

2.2.2 WWIS (WIPP Waste management Information System). It is used for history management and nuclide information management related to the disposal of the waste, collected, loaded and treated by the US DOE and the TRU waste, and it is designed to transfer related data and information to NMMSS.

2.2.3 IWTS (Integrated Waste Tracking System). This system has a radio network system, and uses a wireless scanner so that workers can scan the barcode on the drum and view and enter the history of the database. (excluding applications related to spent nuclear fuel and high-level waste)

2.2.4 MIMS (Manifest Information Management System). INEEL of the US DOE uses this web-based information disclosure system for organizing, searching and viewing the types of low-level waste, the concentration of nuclides, the disposal history of each disposal site by period

2.2.5 Low-Track. It is implemented as a submodule of MIMS, and it has the 2-D bar code module, the data transfer function and the regular reporting function with regard to waste management.

2.2.6 ReVK (RevkRestoff-Verfolgung und Kontrolle). This system traces the material flow of decommissioning waste. It was developed to efficiently provide the information required by operators and regulatory agencies.

Table 1. Key domestic and foreign radioactive waste management systems

System Name	Nation	Function
DREAMS -RAM,RWM	KOREA	-Inventory management -Waste Tracking System -Safety management -Print the report -ERP system
NMMSS	USA	-Inventory, Material balance management - track material flow - Data transaction
WWIS	USA	-Inventory management -waste information input/output -Data transfer function -Print the report -Waste Rating
MIMS	USA	-Waste information input/output -Search history by repository -Print the report(web)
Low-Track	USA	-Search for disposal waste information -Search history by repository -Print the report(web)
IWTS	USA	-Real-time waste information input/output -Inventory management -bar-code
ReVK	Germany	-Dismantled waste information / print -Inventory management -bar-code

3. Conclusion

Different waste-generating organizations, e.g. Korea Nuclear Fuel Company, Ltd., NPP sites and Korea Atomic Energy Research Institute have different radioactive waste tracking systems. Currently the Korea Radioactive Waste Agency, which accepts radioactive waste, manages only the final data of organizations generating radioactive waste, and as it does not adequately manage all process data necessary for waste certification, repeated or periodical monitoring is required.

This paper analyzed the characteristics of the domestic and overseas waste management systems that is required before implementation of the waste tracking system of organizations which accept radioactive waste. If the above analysis results, the classification standards and characterization standards, prescribed in existing international standards and guidelines are used, it will be helpful to the building of the waste lifecycle database.

REFERENCES

[1] “Establishment Of Database System for the Management of KAERI Wastes”, KAERI.

[2] “Establishment of an Integrated Information Management System for Safe Management of Radioactive Waste”, KINS.

An Experimental Study on the Pelletization of Powdered Radioactive Waste Using the Roll Compaction System

Jongsoon Song, Minyoung Jung, and Sanghyun Lim*

Chosun University, 309 Pilmun-Daero, Dong-Gu, Gwangju, 501-759, Republic of Korea

1991sanghyun@naver.com

1. Introduction

Among radioactive waste unfit to be disposed of, powdered radioactive waste can be solidified using various mixing methods and solidification agent. But the mixed solidification process has a greater volume than the existing solidification process. To solve this problem, we can propose a method of turning them into disposable forms by compression-forming powdered radioactive waste into pellets to reduce the volume, and filling them with liquid solidifying materials like epoxy to solidify them.

This study tries to reduce the volume of powdered radioactive waste as much as possible by pelletizing it.

2. Experimental

2.1 Experimental materials

The bentonite, used for the pelletization experiment, is the Active Bentonite, sold by Company L, whose particle size is 85~100 ㎛ Active Bentonite. As a high-adhesion polymer, which can adjust the viscosity of the solution when the solidification agent is made, and tightly fasten the pellets after hardening, was needed, Company K's YD-128-epoxy, G1034-hardener and LGE-diluent were selected.

2.2 Experimental equipment

To form particulate fine powder into pellets, the Roll Compaction System, shown in Table 1, was selected. The conditions for system selection are intended to ensure the integrity of volume reduction and compact, and usability in nuclear facilities, and the high-volume-reduction forming device, including this system, is as shown in Fig. 1.

Table 1. Conditions for selecting the Roll Compaction System

No	Item
1	Possibility of forming pellets without using forming agent
2	Whether the pellet size is uniform
3	Possibility of forming high-density pellets (high volume reduction)
4	Whether it is possible to make it with a size and structure making it easy to install and maintain
5	No ancillary device should be necessary before and after pelletization.

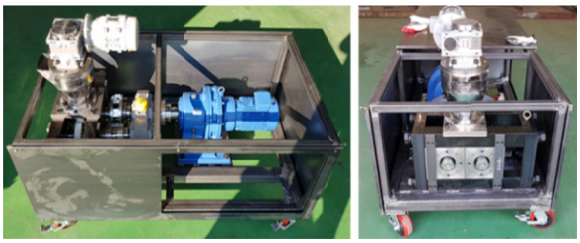

Fig. 1. Pellet forming device – side (L), front(R).

2.3 Pellet making experiment

The high-volume-reduction forming device was used to form the bentonite into rectangular pellets. At a constant powder feed rate and roll speed, the compressive force was increased to measure the gap distance and pellet compaction as illustrated in Fig. 2. As the forming compressive force increased, the gap decreased, and the compaction of the pellets was very good.

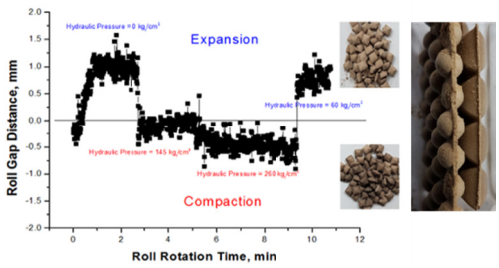

Fig. 2. Gap distance and compaction depending on the compressive force.

Secondly, the operating standards of the device were determined, and changes in the mass of the pellets were measured when operating parameters like the roll rpm (a), the powder feed rate (b) and the forming compressive force (c) were changed as shown in Fig. 3.

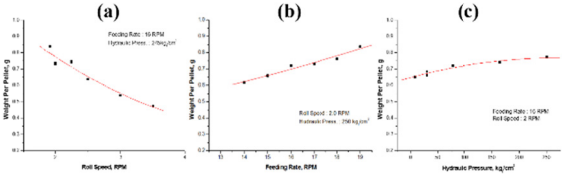

Fig. 3. Changes in the weight of the pellets depending on changes in the operating parameters.

The best forming conditions for making pellets were roll speed 2 rpm, powder feed rate 14.0 rpm, and forming compressive force 245 kg_f/cm^2.

2.4 Comparison of the standard volume reduction rate of the powder and the solidification agent

The weight of each formed pellet was 0.4739 g ~ 0.8644 g. From the conservative viewpoint, which maintains the shape of the pellet and has a constant strength, the weight of one pellet was 0.5847 g, and it was used for evaluating the volume reduction rate. To calculate the volume reduction rate of the powder, the pellet density of one pellet was divided by the density of the powder as shown below.

Volume reduction rate of the powder

$$\frac{\boldsymbol{Density\ of\ the\ pellet}(\mathbf{2.00\ g/cm^3})}{\boldsymbol{Density\ of\ the\ powder}(\mathbf{0.87\ g/cm^3})} = \mathbf{2.30}$$

To evaluate the volume reduction rate of the final solidification agent, the powder polymer solidification agent, mixed in the normal way, and the pellet polymer solidification agent were made, and the volume reduction rate was evaluated. The pellet and the powder polymer solidification agent look as shown in Fig. 4, and details of each solidification agent are shown in Table 2.

Fig. 3. Powder Solidification agent(L) and Pellet Solidification agent(R).

Table 2. Technical specifications by type.

Sample Type	Sample Size (mm)	Weight(g)			Sample volume(cm^3)
		powder	Epoxy	Total	
Pellet Solidification agent	H=100.03 D=49.90	228.41	85.74	314.15	195.52
Powder Solidification agent	H=104.59 D=50.23	56.75	161.99	218.74	207.15

When the solidification agent volume reduction rate is evaluated, the weight ratio of the powder itself and the pellet, which was injected for the same solidification agent volume, can be viewed as the volume reduction rate, and the formula is as shown below:

Volume reduction rate of the solidfication agent

$$\frac{\boldsymbol{Weight\ of\ the\ powder\ in\ the\ pellet\ solidification\ agent}(\mathbf{228.41\ g})}{\boldsymbol{Weight\ of\ the\ powder\ in\ the\ powder\ solidification\ agent}(\mathbf{53.56\ g})} = \mathbf{4.26}$$

3. Conclusion

The results of the experiment show that the volume reduction rate of the powder was 2.3 times higher, and the volume reduction rate of the solidification agent was 4.26 times higher. The authors will contribute to solving the problem related to the excessive waste disposal cost and disposal of inadequate waste by conducting additional experiments, e.g. measuring the mixing ratio of epoxy, changes in the form of pellets, thermal properties and strength of the solidification agent.

Acknowledgements

This paper is a research project funded by Ministry of Commerce, Industry and Energy, which was conducted with the help of the Korea Institute of Energy Technology Evaluation and Planning. (No. 20171520101630)

REFERENCES

[1] Radwaste Acceptance Criteria, LILW –Operation-Radiation-028, Korea Radioac tive Waste Agency.
[2] Solidification Radwaste structural soundness verification of examination, LILW-Operate-Radiation-048, Korea Radioactive Waste Agency.
[3] Johanson, J.R, 1965. A rolling theory for granular solids. J. Appl. Mech. 32, 842-848.

Implementation of Waste Tracking System (WTS) for Solidification Process and Management

Sungjong Kim*, Changhwan Cho, Jawon Jeng, and Wooseok Heo
MIRAEEN Co. Ltd., 72, Techno Jungang-ro, Yuseong-gu, Daejeon, Republic of Korea
*sungjong.kim@mirae-en.co.kr

1. Introduction

Low and intermediate level of radioactive waste should be solidified to be accepted and delivered to Korea Radioactive Waste Agency (KORAD). This paper provides the design and implementation of WTS (Waste Tracking System), which primarily includes the characteristics testing results and historical data of solidified specimen and its treated drum of sludge-type of radioactive waste from nuclear fuel manufacturing cycle.

2. Requirement of WTS [1]

2.1 The generation and collection of wastes

All the wastes has been collected in a collected drums with identification. This drums will have radioactive waste management process in Fig. 1. All the data acquired in the generation and collection of wastes should be logged into WTS also, which should have function of input, search, retrieval and report generation including visualization like trend, graph and any other mean to indicate the statistical data.

2.2 Treatment of radioactive wastes

Theoretically the treatment process has various sub-processes and technologies such as solidification, vitrification, incineration and etc. In this project, the treatment of solidification using solidification agent [5] is hired and its specimen and treated drums are tested to verify if those results of characteristics testing for solidified radioactive waste meet the acceptance criteria of KORAD.

Unexpectedly the information generated from this treatment process is relatively huge, which should be kept in WTS for internal as well as external utilization to maintain the traceability of wastes.

2.3 Characteristic testing

This process performs the characteristics testing that requires compressive strength, thermal cycling, leaching and immersion, free standing water, and test analysis necessary to identify the chemical and radiological features. The result of all kind of these tests should meet the acceptance criteria [3].

2.4 Disposal and delivery

The specimen and its relative treated drum should pass the conformity test. Also WTS should generate certificate and reports.

This WTS as part of KNFC Manufacturing Execution System (MES) has linked with review and approval function for these consecutive tests.

3. Implementation of WTS

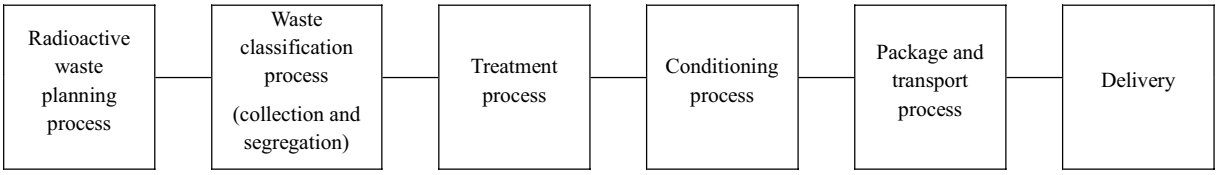

Fig. 1. Radioactive waste management process (ISO TC 85 SC5 proposal).

3.1 Development environment

This project expands the legacy MES to have capability to keep and manage the bulky data generated through the radioactive waste treatment and characteristics testing partly described in Section 2.2.

Thus legacy of client and server environment and the utilization of commercial 3rd party tools based on .NET infra has been maintained.

3.2 Database design and implementation

Legacy radioactive information system in KNFC uses the Oracle-based database management system. Thus the new database necessary to manage the process data also has been designed and implemented using Oracle DBMS and its relative tools such as Toad and others.

New database and query design is truly based on the analysis information acquired from the ongoing solidification and characteristics testing activities, and database normalization to get rid of an anomalies of insertion, deletion, update and retrieval.

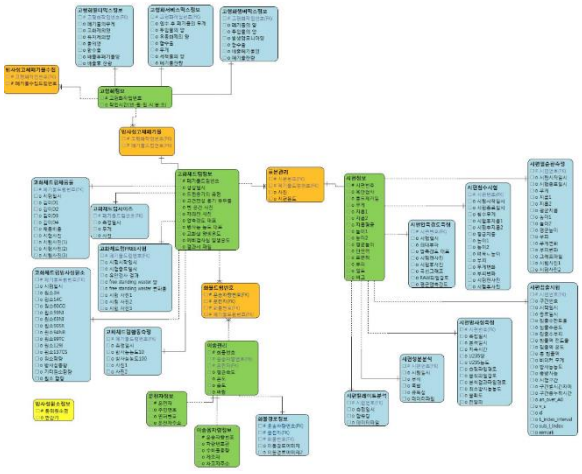

Fig. 2. Logical ERD.

According to the solidification batch, the relation between collected drum and treated drum, and its relative test specimens are established for logical schema and physical schema of database, which is indicated in Entity-Relationship Diagram (ERD) of Fig. 2.

3.3 Query, MMI and SDLC design

Query design of WTS is conducted based on the User Interface (UI) requirements such as primarily report generation and data visualization like graph and trend based on the secure coding guide [4].

This WTS implements the UI requirements in Section 3.3 and the requirements of user who operates this WTS in order to enhance the accessibility and efficiency.

All of the design and implementation activities described so far is adhered to the Software Development Life Cycle (SDLC) in order to software verification and validation [2] that could be conducted in final testing and evaluation phase.

4. Conclusion

An automatic data acquisition and upload is necessary with the support of industrial Internet of Thing (IoT). It is highly expected that Waste Certification Program (WCP) by independent 3rd party is activated reliably for simplification of waste inspection and delivery.

REFERENCES

[1] Request for Proposal for Establishment of Radioactive Waste Tracking System, 2017.05

[2] IEEE 1012: 2010 Software Verification and Validation

[3] Safety Analysis Report for LILW disposal facilities (SAR)

[4] Ministry of the Interior and Safety, guide of Software Development Security

Characteristics Testing of Solidified Radioactive Waste From Nuclear Fuel Manufacturing

Sungjong Kim[a*], Changhwan Cho[a], Seunghoon Han[b], Youngjong Ju[b], Hyunkyu Kang[b], and Jungwoo Lee[b]
[a]MIRAEEN Co. Ltd., 72, Techno Jungang-ro, Yuseong-gu, Daejeon, Republic of Korea
[b]KEPCO NF, Daedeok-daero 989beon-gil, Yuseong-gu, Daejeon, Republic of Korea
[*]sungjong.kim@mirae-en.co.kr

1. Introduction

The sludge-type of radioactive wastes generated from the nuclear fuel manufacturing cycle should be solidified using solidification agent for physically and chemically safe deliverable to disposal site. This is accomplished through the solidification methods and its process.

To deliver these kind of treated radioactive waste, waste generator should show that this solidified radioactive wastes should have physical integrity by ensuring the results of consecutive tests such as compressive strength, leaching and immersion, thermal cycling and free standing liquid, which should be implemented based on the test plan and procedure–

2. Test criteria and methods

To test the treated solidified radioactive wastes, instead of deliverable drum, the multi number of test specimens are prepared for their own unique test during the process of solidification.

This specimen has a size of 1:2 for diameter and height, and this should be cured more than 28 days after preparation. The details of specimen preparation is left out.

3. Physical integrity test

3.1 Compressive strength test

The primary objective of compressive strength test is for making sure of physical and mechanical robustness of solidified radioactive waste in the event of incident. .

Compressive strength in KS F 2405[1] of test method and criteria for concrete compressive strength', requires more than 3.44 MPa. In the lab., the specimen meets the this criteria.

Fig. 1. Compressive strength test of specimen (before/after).

3.2 Immersion and leaching

When radioactive waste is exposed to rain or groundwater, there is a possibility of dispersion of radionuclide and/or corrosion of an internal of container. To protect this at best, the immersion and leaching test has been done to show that this symptom is not assumable.

Leaching test has been done based on the ANS 16.1[5], and immersion test has been done by verifying the status of specimen such as weight and the change of volume through visual inspection. After this immersion and leaching, additionally compressive strength test is conducted again to show mechanical integrity.

Container and holders used for test should use the material of HDPE (High Density Polyethylene), which eliminate the chemical reaction with leachant and specimen.

In order to calculate the leaching index, initial radioactivity and the leachate radioactivity of each leaching interval are measured through HPGe.

Fig. 2. Immersion and leaching test.

3.3 Thermal cycling test

The solidified radioactive wastes maintained in temporary and permanent storage for long time can experience the environmental change especially temperature and humidity. Thermal cycling test has been done to evaluate and show that this solidified radioactive waste can endure the environmental changes [4]

3.4 Free standing liquid

Standard requires test of free standing water because free standing liquid inside the drum can increase the liquidity of radionuclides, which can cause adverse impact to safety.

Free standing liquid test is done by lifting the drum and rotate 180 degree, and watching 24 hours to see if free standing liquid is less than 0.5% from the deliverable drum.

Fig. 2. Free standing water test.

4. Conclusions

The series of test requirements of standards is established a couple of decade ago primarily guidance for cement based solidified radioactive waste. However today there are various solidification agent and immobilization technologies like paraffin and vitrification and etc. is being developed and available in laboratory level. Thus it is recommended that all the testing required for solidified radioactive waste be discussed for confirmation.

Also a serious of independent test such as compressive strength, immersion and leaching, thermal cycling, voidage, irradiation and other chemical characteristics testing should be reviewed and upgraded for solidified radioactive waste, and its relationship and interoperability among tests should be discussed. For example, the merge of leaching and immersion could be acceptable in some kind of aspect.

REFERENCES

[1] KS F2405: 2010 (Standard test method for compressive strength of concrete)

[2] 10CFR61 (Waste Classification and Waste Form Requirements)

[3] NRC Technical Position on Waste Form, Rev.1

[4] ASTM B553-79(Standard Test Method for Thermal Cycling of Electroplated Plastics, Withdrawn 1991)

[5] ANSI/ANS 16.1-2003(Measurement of the Leachability of Solidified Low-level Radioactive Wastes by a Short-term Test Procedure)

Leaching Test of Lime Precipitate Radioactive Waste Containing Uranium

Changhwan Cho[a*], Sungjong Kim[a], Seunghoon Han[b], Youngjong Ju[b], Jungwoo Lee[b], and Jeongmyeong Kim[b]
[a]MIRAEEN Co. Ltd., 72, Techno Jungang-ro, Yuseong-gu, Daejeon, Republic of Korea
[b]KEPCO NF, Daedeok-daero 989beon-gil, Yuseong-gu, Daejeon, Republic of Korea
[*]changhwan.cho@mirae-en.co.kr

1. Introduction

Homogenous radioactive wastes (condensate waste, spent resin, sludge) should be solidified for delivery through acceptance by KORAD (Korea Radioactive Waste Disposal), which encompasses the acceptance tests such as compressive strength, leaching test, immersion test, thermal cycling, irradiation test, and free standing water test to meet the acceptance criteria of solidified radioactive wastes.

In this paper, it provides the leaching characteristics of sludge type of radioactive waste according to the ANSI/ANS 16.1[1] that contains uranium. This test should show the leachability index of solidified radioactive waste in the face of water like rain or ground water.

2. Leaching Test Methods and Results

This section provides the test methodology and results that is performed based on the ANSI/ANS 16.1[1]

2.1 Test Methods

2.1.1 Test Equipment. For leachability test, demineralized waster of leachant with electrical conductivity of less than 5[μmho/cm] at 25 ℃ is used, and leach test vessel and its specimen holder is a material of high density polyethylene that does not cause chemical reaction.

2.1.2 Specimen Preparation. The specimen of sludge type of lime precipitate is solidified using Calcium Aluminate Cement (CAC) agent is prepared in the shape of cylinder as indicated in Table 1.

Table 1. Dimension of specimen

Specimen No.	Diameter [mm]	Height [mm]	Surface Area [cm^2]	Height-to-Diameter Ratio
LS-2017042912-LC	49.950	97.995	192.968	1.962
LS-2017042934-LC	49.820	98.195	192.677	1.971

2.1.3 Activity measure of specimen. To conduct the leaching test, initial activity (A_o) of U-235 of the specimen is measured using the HPGe (High-Purity Germanium) detectors as in Table 2.

Table 2. A_o measurement

Specimen No.	Activity of U-235 [Bq]
LS-2017042912-LC	1.3407E+4
LS-2017042934-LC	1.3323E+4

2.1.4 Leaching test. The Fig. 1 shows a leaching test cut. The specimen is fixed with holder in leach test vessel containing leachant for leaching test.

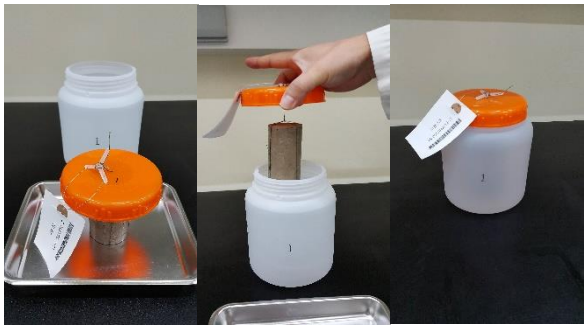

Fig. 1. Process of leaching test.

When replacing leachant, the demineralized water to collect the U-235 by rinsing the surface of the specimen and leach test vessel is mixed with leachate together and measure total weight of rinsing water and leachate.

Some of these is put in marinelli beaker and measure weight of leachate in it. Also activity concentration of U-235 of leachate in marinelli beaker is measured using the HPGe (High-Purity Germanium) detectors in each leach interval.

2.2 Test Results

2.2.1 Leachate's activity of U-235 in each leach interval. Leachate's activity of U-235(a_n, where leach interval n = 1, 2,...,10) in each leach interval is calculated based on the leachate's activity concentration of U-235 and the its weight.

The test results of each specimen are described in Table 3.

Table 3. Leachate's activity in each leach interval.

Leach Interval (n)	LS-2017042912-LC		LS-2017042932-LC	
	Activity Concentrations of U-235 [Bq/g]	Activity of U-235 [Bq]	Activity Concentrations of U-235 [Bq/g]	Activity of U-235 [Bq]
1	9.22E-04	2.43964	4.1825E-4*	1.04923
2	5.46E-04	1.36655	6.02E-04	1.53783

3	2.8258E-4*	0.72304	6.21E-04	1.63465
4	3.2075E-4*	0.83354	5.14E-04	1.39682
5	5.50E-04	1.4506	5.59E-04	1.52514
6	6.45E-04	1.64331	5.07E-04	1.36975
7	4.57E-04	1.18797	3.1250E-4*	0.82854
8	1.08E-03	2.67381	7.6720E-4*	2.0453
9	7.5370E-4*	1.89801	7.6571E-4*	2.00519
10	7.16E-04	1.93304	5.58E-04	1.44714

* Activity concentration of U-235 is measure to 0 (zero), therefore the activity concentration of U-235 is determined MDA (Minimum Detectable Activity) value.

2.2.2 Analysis of leaching test result. This test is conducted through standard and extended leach interval to acquire the effective diffusivity (D) and leachability index (L), and test result of each leach interval is summarized in Table 4 and 5.

Table 4. Analysis result of LS-2017042912-LC

Leach Interval	Leaching Time [S] Incremental $(\Delta t)_n$	Leaching Time [S] Cumulative $t = \sum(\Delta t)_n$	Incremental Fraction Leached a_n/A_o	Incremental Leaching Rate [fraction/s] $(a_n/A_o)/(\Delta t)_n$	Effective Diffusivity (D_n) [cm^2/s]	Leach-ability Index (L_n)
1	7,210	7,210	1.81967E-4	2.52382E-8	3.6082E-10	9.4
2	18,000	25,210	1.01928E-4	5.66267E-9	1.5116E-10	9.8
3	61,200	86,410	5.39303E-5	8.81214E-10	1.2635E-11	10.9
4	86,400	172,810	6.21722E-5	7.19586E-10	2.0701E-11	10.7
5	86,400	259,210	1.08197E-4	1.25228E-9	1.0648E-10	10.0
6	86,395	345,605	1.22571E-4	1.41873E-9	1.9228E-10	9.7
7	86,400	432,005	8.86082E-5	1.02556E-9	1.2945E-10	9.9
Results of Standard Test Leachability Index(L) : 10.1 Confidence Range : 8.9 to 11.3 Correlation Coefficient : -0.09						
8	1,209,600	1,641,605	1.99434E-4	1.64876E-10	8.1092E-12	11.1
9	2,419,200	4,060,805	1.41569E-4	5.85188E-11	2.9539E-12	11.5
10	3,715,200	7,776,005	1.44181E-4	3.88084E-11	2.7305E-12	11.6
Results of Extended Test Leachability Index(L) : 10.5 Confidence Range : 8.3 to 12.6 Correlation Coefficient : 0.74						

Table 5. Analysis result of LS-2017042932-LC

Leach Interval	Leaching Time [S] Incremental $(\Delta t)_n$	Leaching Time [S] Cumulative $t = \sum(\Delta t)_n$	Incremental Fraction Leached a_n/A_o	Incremental Leaching Rate [fraction/s] $(a_n/A_o)/(\Delta t)_n$	Effective Diffusivity (D_n) [cm^2/s]	Leach-ability Index (L_n)
1	7,205	7,205	7.87536E-5	1.09304E-8	6.7835E-11	10.2
2	18,067	25,272	1.15427E-4	6.38882E-9	1.9326E-10	9.7
3	61,267	86,539	1.22694E-4	2.00261E-9	6.5570E-11	10.2
4	86,400	172,939	1.04843E-4	1.21346E-9	5.9108E-11	10.2
5	86,400	259,339	1.14474E-4	1.32493E-9	1.1962E-10	9.9
6	86,395	345,734	1.02811E-4	1.19001E-9	1.3575E-10	9.9
7	86,405	432,139	6.21890E-5	7.19738E-10	6.3970E-11	10.2
Results of Standard Test Leachability Index(L) : 10.0 Confidence Range : 9.6 to 10.5 Correlation Coefficient : 0.07						
8	1,209,600	1,641,739	1.53517E-4	1.26915E-10	4.8203E-12	11.3
9	2,419,200	4,060,939	1.50506E-4	6.22130E-11	3.3489E-12	11.5
10	3,715,200	7,776,139	1.08620E-4	2.92366E-11	1.5544E-12	11.8
Results of Extended Test Leachability Index(L) : 10.5 Confidence Range : 8.4 to 12.6 Correlation Coefficient : 0.88						

The following Fig. 2 indicates the trend of cumulative fraction leached in each leach interval, showing that the leachability in the beginning increase constantly, then stabilized after leach interval 7.

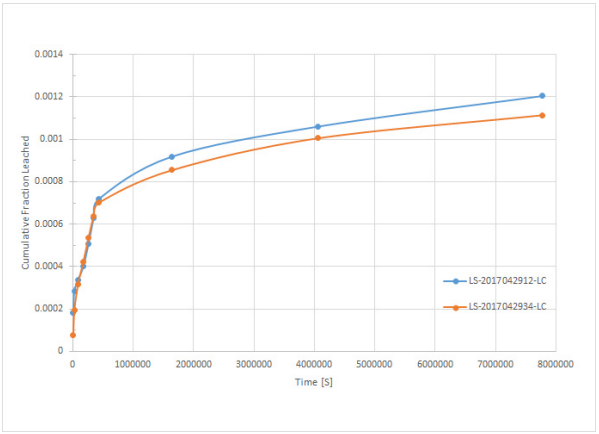

Fig. 2. Trend of cumulative fraction leached.

3. Conclusions

After the leaching test, it is identified that the leachability index of solidified radioactive waste containing uranium is more than 6 that is acceptable for waste disposal.

Also it is found that the leachability after leach interval 7 is abruptly decreased and stabilized, which means that standard interval for leaching test is enough to get the reliable leachability index without performing extended interval.

REFERENCES

[1] ANSI/ANS 16.1-2003, 'Measurement of the Leachability of Solidified Low-level Radioactive Wastes by a Short-term Test Procedure', 2003.

[2] ASTM C1308-08, 'Standard Test Method for Accelerated Leach Test for Diffusive Releases from Solidified Waste and a Computer Program to Model Diffusive, Fractional Leaching from Cylindrical Waste Forms', 2008.

[3] K.h Kim, 'Evaluation of Standard Leaching Tests in Cemented Waste Forms Incorporated Borate Waste', Transactions of the KNS Spring Meeting, 2004.

Evaluation of Structural Stability for Cement Waste Form of Lime Waste

Jong Sik Shon*, Gi Yong Kim, Ki-baek Shin, Junhyuck Im, and Dae Seok Hong
Korea Atomic Energy Research Institute, Daedeok-daero989ben-gil 111,Yuseong-gu, Daejeon, Republic of Korea
* njsshon@kaeri.re.kr

1. Introduction

Lime waste was generated in the AUM (Ammonium Uranyl Carbonate) process, which is a wet manufacturing process of UO_2 powder and storage in KAERI (435 drums, 200L drums). Lime waste is no longer generated because of the closure of the research facility. It is important to safely dispose [1] of low-and intermediate level radioactive waste from operation of the research facility. One of the efficient way to treat radioactive waste is cement solidification. The cement solidification method is cheap and simple than other solidification method. Portland cement (Type I) has been used for a long time as solidification material and has proven technically safer and more convenient. This Portland cement has an initial setting time of about 4 hours, which is advantageous in ensuring sufficient working time for fast curing speed and high calorific value [2]. The purpose of this study is to evaluate the simple process for permanent disposal and the structural stability of the Lime cement waste form. In addition, Lime cement waste form meets the waste acceptance or satisfy the waste acceptance criteria for final disposal facility in several tests such like compressive strength, immersion, leaching test, and thermal cycling test.

2. Methods and Results

2.1 Materials

Portland cement was purchased from SSangyong. The components of lime waste are deduced from NH_4NO_3, $NaNO_3$, $Ca(NO_3)_2$, $CaCo_3$ and $Ca(OH)_2$ [3]. The real image of lime waste and XRD patterns are shown in Fig. 1.

As shows in Table 1, radionuclides concentration of lime waste. Lime waste is estimated to be extremely low level waste.

Table 1. Characterization of lime waste

Radioactive concentration [Bq/g]	Main component	pH
U-238 : 55.4 Cs-137 〈 0.200	$CaCO_3$ $Ca(NO_3)_2$	8.2

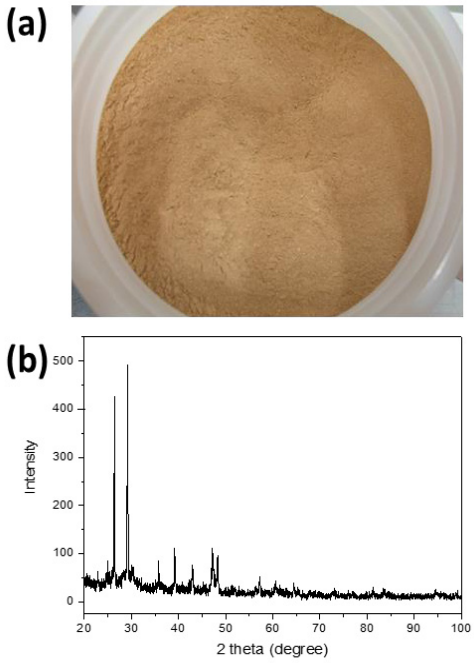

Fig. 1. (a) Real image of lime waste powder and (b) XRD patterns.

2.2 Manufacture of lime cement waste form

The Lime cement waste form were manufactured in accordance with the Korean Industrial Standard (KS-L-5109) [4]. The mechanical mixer was purchased from Jl-206 (Jeil Precision, Korea). And Lime cement waste form solidified while under curing at room temperature with relative humidity of 40 to 60 % for 28 days. After 28 days, the uniformity of the Lime cement waste form was visually confirmed.

Lime cement waste form were made to find the optimal mixing rate (W/C, where W is water and C is cement) from 1.8 to 2.3. The operating range was

determined by workability, free-standing water test, and water immersion test (90 day).

2.3 Operation range of lime cement waste form

In preliminary tests, the maximum lime waste content of the cement waste is 80 wt.%. For stability and reliability, lime cement waste form of lime waste content was selected at 75 wt.%, the content of portland cement as 25 wt.%. Therefore, the volume increase of Lime cement waste form material is estimated to be less than 10% considering the density of cement (3.16 g /cm^3). When the W/C ratio is less than 1.80, the mixture (lime waste, cement, water) has no fluidity, but W/C ratio is higher than 2.40, the lime cement waste form has free-standing water. Therefore, the optimal mixing rate is 1.85 to 2.20. Fig. 2 shows the operating range the W/C ratio of the lime cement waste form.

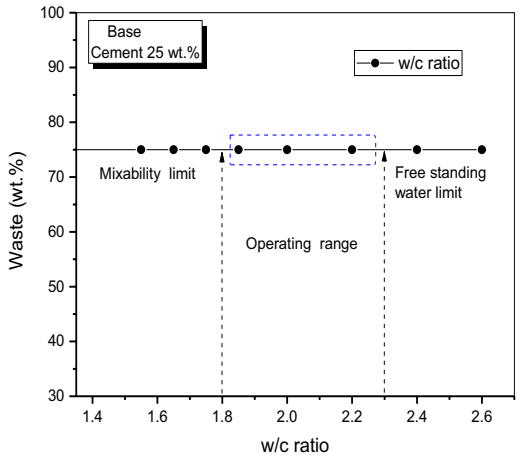

Fig. 2. Operating range of Lime cement waste form.

2.4 Stability evaluation of lime cement waste form

The stability evaluation of lime cement waste form was determined by the acceptance criteria such as compressive strength, thermal cycling test, immersion, and leaching test [1].

As shown in Fig.3, compressive strength result of the lime cement waste form. The compressive strength is 55 ~ 76.3 kgf/cm^2, which satisfied the acceptance criteria of 35.2 kfg/cm^2 (3.44MPa). And, all experiment groups were satisfied with the final disposal facility.

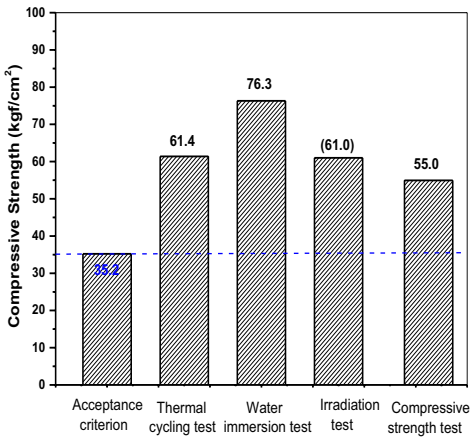

Fig. 3. Compressive strength test of Lime cement waste form.

3. Conclusions

1. Cement solidification method is a recognized technology, the lime waste content of lime cement waste form is 75 wt.% and volume increase is less than 10%.

2. The operating range of lime cement waste form is estimated to be between 1.80 and 2.30 W/C ratios.

3. Optimum condition is W/C ratio is 1.85 ~ 2.20 and lime cement waste form meets the waste acceptance and satisfy the waste acceptance criteria for final disposal facility.

REFERENCES

[1] Korea Radioactive Wastes Agency, “Safety analysis report of Low-and intermediate-Level Radioactive Waste Disposal Facility”, (2008).

[2] Soroka, I, et al., "Portland Cement Paste and Conctret”, 1st edn, Chemical Publishing, NY, (1980)

[3] D. S. Hwong, et al., “Dissolution Characteristic of Lagoon Sludges Generated form the Uranium Conversion Plant”, Applied Chemistry, 6 (2002).

[4] W.H. Jang, et al., "A Study on Operating Range of Cement Solidification for Final Disposal of Radioactive Soil”, Journal of Korea Society of Waste Management, 34 (2017).

The Applicability of Core Sampling to Treatment of ITER Type B Radwaste

Sunggeun Kim*, Myungchul Park, Wanho Oh, and Sangbok Ahn
Korea Atomic Energy Research Institute, Daedeok-daero989ben-gil 111,Yuseong-gu, Daejeon, Republic of Korea
*sg316@kaeri.re.kr

1. Introduction

Type B radwaste (intermediate level and long lived radioactive waste) generated from the vacuum vessel of the ITER Tokamak building are to be treated and stored in the hot cell building. Sampling is the one of treatment processes, which is used to obtain small pieces of samples from metallic Type B radwaste components in order to evaluate the tritium content. In addition, sampling has to be carried out without the use of any liquid coolant to avoid the spread of contamination. In this study, core sampling is suggested as one of the sampling techniques.

2. Core sampling

Core sampling is applied to take core samples from materials using a broach cutter (Fig. 1) as a core drill bit under dry conditions. During the core sampling, compressed air is supplied continuously to reduce the drilling temperature of the drill bit and workpiece, and remove the cutting chips, which damage on the drill bit.

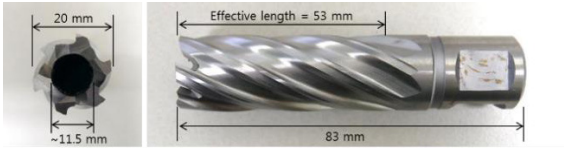

Fig. 1. Core drill bit used in core sampling.

3. Experiment

3.1 Sampling

Core sampling experiments for SS316L and CuCrZr materials, both of which have a 50 mm thickness, were conducted. Experimental conditions are presented in Table 1, and obtained SS316L and CuCrZr core samples of 50 mm in length are shown in Fig. 2.

Table 1. Sampling conditions of core sampling

	SS316L	CuCrZr
Spindle speed (rpm)	150	150
Feed rate (mm/min)	5	5
Traverse speed (mm/min)	150	150
Depth of cut (mm)	0.5	1.0

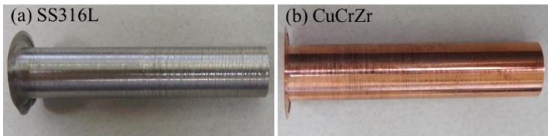

Fig. 2. Core sample: (a) SS316L (b) CuCrZr.

3.2 Measurement of Temperature Variation

The goal of sampling is to take samples without tritium loss. Because tritium release is generally affected by temperature, it is essential to know the temperature distribution into the core sample and the cutting zone during the sampling process. To measure the temperature of the core sample, a K-type thermocouple was used. Based on the fact that

tritium is concentrated near the surface of Type B radwaste, a thermocouple was embedded 5 mm below the surface at the center of the core sample. Experiments were performed to a depth of 30 mm, and the temperature values were recorded in real time. Fig. 3 shows the measured core center temperature for SS316L and CuCrZr. The maximum temperatures were 44.5 ºC and 32.8 ºC (initial temperature=25 ºC), respectively.

The temperature distribution in the cutting zone was recorded by infrared (IR) camera during core sampling. Fig. 4 shows the analysis results of IR images captured at the beginning of the sampling. The maximum temperatures were 76.1 ºC for SS316L and 14.5 ºC for CuCrZr, which increased approximately 73 ºC and 12 ºC compared with initial temperature, respectively.

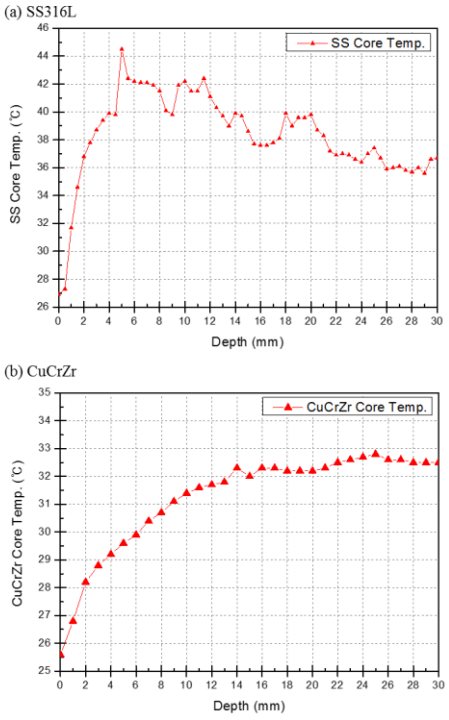

Fig. 3. Temperature variation measured at the center of core sample during drilling for (a) SS316L and (b) CuCrZr.

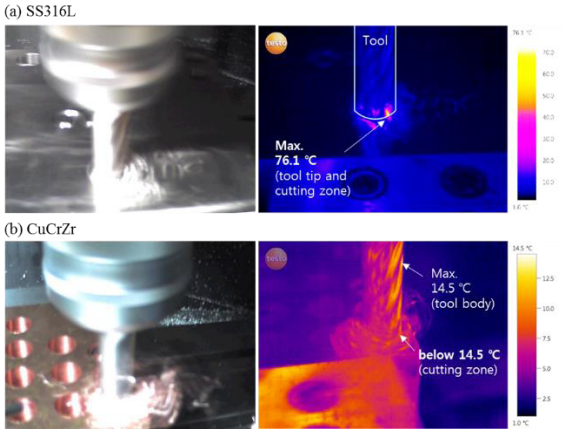

Fig. 4. Cutting zone temperature (a) SS316L and (b) CuCrZr.

4. Conclusion

Core sampling, which is a candidate sampling technique to be applied to the ITER hot cell, is available for thin (less than 50 mm) metallic Type B radwaste, SS316L and CuCrZr, without the use of a coolant. According to the results of a temperature measurement, it can be stated that the temperature of the core sample and cutting zone for SS316L and CuCrZr will be below 100 ºC during the core sampling under the applied conditions. These cutting temperatures are considered to be much lower than the tritium releasing temperature of Type B radwaste. Thus, it can be affirmed that heat generation during core sampling will have no significant effect on the tritium release.

REFERENCES

[1] D. Torcy et. al. “Technical specification of Type B radwaste processing and treatment equipment development”, EGVZ3J(ITER Document), 08 Jul. 2015.

The Homogeneity Test and Analysis for Solidified Specimen of Low and Intermediate Level of Radioactive Wastes

Jawon Jeng[a*], Sungjong Kim[a], Seunghoon Han[b], Youngjong Ju[b], Jungwoo Lee[b], and Jeongmyeong Kim[b]
[a]MIRAEEN Co., Ltd. 72, Techno Jungang-ro, Yuseong-gu, Daejeon, Republic of Korea
[b]KEPCO NF, Daedeok-daero 989beon-gil, Yuseong-gu, Daejeon, Republic of Korea
[*] jawon.jeng@mirae-en.co.kr

1. Introduction

Homogeneity test and proof for the solidified specimen of low and intermediate level of radioactive wastes, which is required for safe radioactive waste management by regulation and KORAD, is one of the acceptance criteria for conformity assessments for waste disposal.

In order to show the homogeneity in this study, the uranium-contained specimen that is solidified using Calcium Aluminate Cement (CAC) solidification agent for sludge type of precipitate in KNFC was used. The homogeneity of these specimens based on radioactivity was conducted based on ANOVA (Analysis of Variance) in KS A ISO GUIDE 35 [1].

2. Radioactivity measure

2.1 The preparation of specimen

The total specimens of 30 out of 37 prepared from drum of NF-2017-B01-0009, NF-2017-B01-0010, and NF-2017-B01-0011 for conformity test in Apr. 29th, 2017, excluding specimens for thermal cycle test, leaching test and immersion test, are used, and those are solidified according to the TPI-34-52 [3].

2.2 Radioactivity concentration measurement

The total radioactivity concentration is gained by dividing U-235 specimen's activity by weight.
HPGe(High-Purity Germanium detector) was used to measure the radioactivity for specimen containing U-235 as in Fig. 1.

Fig. 1. HPGe.

3. Homogeneity and variance assessment

3.1. The selection of group

For ANOVA analysis, more than 2 groups of specimens are prepared. Thus, 30 specimens prepared in Section 2.1.2 are allocated into 3 groups of 10 specimens as in Table 1 and 2 just as manufacturing order.

Table 1. Grouping for Specimen No.

Group 1	Group 2	Group 3
LS-2017042901-C	LS-2017042914-C	LS-2017042924-LC
LS-2017042902-C	LS-2017042915-C	LS-2017042925-S
LS-2017042903-C	LS-2017042916-C	LS-2017042926-C
LS-2017042904-C	LS-2017042917-C	LS-2017042927-C
LS-2017042906-C	LS-2017042918-C	LS-2017042928-C
LS-2017042907-C	LS-2017042919-S	LS-2017042929-C
LS-2017042908-C	LS-2017042920-C	LS-2017042930-C
LS-2017042909-C	LS-2017042921-C	LS-2017042931-C
LS-2017042910-C	LS-2017042922-C	LS-2017042932-C
LS-2017042913-S	LS-2017042923-TC	LS-2017042935-S

Table 2. Grouping for Concentration Activity [Unit : Bq/g]

Group 1	Group 2	Group 3
9.6514E+00	1.0231E+01	1.0339E+01
9.8950E+00	1.0585E+01	1.0205E+01
9.9829E+00	1.0647E+01	1.0518E+01
9.8752E+00	1.0465E+01	1.0215E+01
1.0564E+01	1.0251E+01	1.0104E+01
1.0471E+01	1.0782E+01	1.0269E+01
1.0324E+01	1.0377E+01	1.0275E+01
1.0528E+01	1.0501E+01	1.0562E+01
1.0671E+01	1.0539E+01	1.0468E+01
1.0562E+01	1.0489E+01	1.0465E+01

3.2 The analysis of variance

The homogeneity of radioactivity concentration among 3 groups are identified by assessing if the average and distribution of the measured radioactivity concentration values of 3 groups are same or similar.

a) Hypothesis establishment
- Null hypothesis: the average and distribution of 3 groups is the same (the concentration of radioactivity is homogeneous)
- Alternative hypothesis: the average or distribution of 3 groups is not the same (the

concentration of radioactivity is not homogeneous)

b) Hypothesis testing

The established hypothesis calculates the F ratio, F critical value and P-value

Total variance of SST(ST) is calculated through formula-1.

$$SST(S_T) = \sum_{i=1}^{k}\sum_{j=1}^{n}(y_{ij} - \overline{y})^2 \quad (1)$$

Where,

y_{ij} : measured value (i: group number, j: number within group)

$\overline{y}$: total average

k : the number of groups

n : the number of data element within group

Thus summarizing the total variance of SST(ST) can be expressed as the sum of the variation between group (SSA(SA)) and the variation within group (SSE(SE)).

$$SST(S_T) = \sum_{i=1}^{k}\sum_{j=1}^{n}(y_{ij} - \overline{y_i})^2 + \sum_{i=1}^{k}\sum_{j=1}^{n}(y_{ij} - \overline{y})^2$$

$$= \text{SSE(SE)} + \text{SSA(SA)} \quad (2)$$

The degree of freedom (DF) of variation is defined as follows;

DF for total variation: $\Phi_T = kn - 1$

DF for variation between groups: $\Phi_A = k - 1$

DF for variation within groups: $\Phi_E = k(n-1)$

The F ratio is calculated through dividing the average for variation between groups (VA) by the average for variation within groups (VE) as in formula-3.

$$F_{ratio} = \frac{V_A}{V_E} \quad (3)$$

Where,

$V_E = \frac{SSE(S_E)}{\Phi_E}$, $V_A = \frac{SSE(S_A)}{\Phi_A}$

We can find the F critical value in F-table for α=0.05 using the DF for variation within groups and DF for variation between groups

In this study, the F critical value is 3.35 because DF for variation between groups is 2 and DF for variation within groups is 27 in 95% of confidence interval of 3 groups that have 10 elements. Using F ratio, F critical value and P-value based the analysis above, one of the null and alternative hypothesis is selected. If F ratio is less than F critical value, and P-value is bigger than 0.05, them null hypothesis is selected. And if F ratio is bigger than F critical value, or P-value is less than 0.05, then alternative hypothesis is selected.

3.3 The assessment of analysis

If null hypothesis is selected, assessing that specimens prepared during the solidification process is homogeneous in the concentration of radioactivity. And if alternative hypothesis is selected, assessing that specimen prepared during the solidification process is not homogeneous in the concentration of radioactivity.

Using the radioactivity measurement values of 3 groups of homogeneity test specimen in 3.1, Microsoft excel's statistical analysis tool for the analysis of variance is used to analyze one-way ANOVA. The Table 3 shows summary of calculation, and Table 4 shows the results of one-way ANOVA.

Table 3. Summary of Calculation (Group 1, 2 and 3)

Groups	Count	Sum	Average	Variance
Group 1	10	102.5245	10.25245	0.133431821
Group 2	10	104.867	10.4867	0.028772011
Group 3	10	103.42	10.342	0.023527778

Table 4. One-way ANOVA results

Source of Variation	Between Groups	Within Group	Total variation
Sum of square	0.279434517	1.671584485	1.951019002
DF	2	27	29
Mean square	0.139717258	0.061910536	
F ratio	2.256760582		
P-Value	0.124080129		
F critical value	3.354130829		

4. Conclusions

As a result of One-way ANOVA using the radioactivity measurement values of 3 groups of homogeneity test specimen, F ratio (2.256760582) is less than F critical value (3.354130829), and P-value (0.124080129) is bigger than 0.05.

Thus null hypothesis is conclusively selected to assess that the test specimens solidified during solidification process are homogeneous.

REFERENCES

[1] KS A ISO GUIDE 35: 2010, Certification of reference materials - General and statistical principles

[2] KS Q ISO 13528: 2014, Statistical methods for use in proficiency testing by interlaboratory comparisons

[3] TPI-34-52, The plan and procedure for solidification of sludge type of radioactive waste from fuel manufacturing (KNFC internal)

Solidification of Spent Resin for Safe Storage

Won-Seok Kim[1]*, Jaehyuk Kang[1], Taeho Jung[1], Mi-suk Jang[2], Jong-seon Jeon[2], and Wooyong Um[1]
[1]Division of Advanced Nuclear Engineering (DANE), Pohang University of Science and Technology (POSTECH), 77 Chungam-ro, Nam-gu, Pohang, Republic of Korea
[2]Nuclear Engineering Service & Solution Co. (NESS), Daejeon Business Agency #705, 96 Gajeongbuk-ro, Yuseong-gu, Daejeon, Republic of Korea
*wkim23@postech.ac.kr

1. Introduction

Spent ion-exchange resins from nuclear power plant are considered to be problematic waste so that, in many case, it requires special approaches and precautions during their solidification to meet the acceptance criteria for disposal. Because the radioactive materials can be released form spent ion-exchange resin during treatment, the selection of treatment options for spent ion-exchange resins must consider their physical, chemical, and radiological characteristics. Direct immobilization method, producing a stable end product by using cement, bitumen, polymer or high integrity containers, was proposed to be considered. In addition, in an environment without final disposal options and limited interim storage capacity, volume reduction is an essential criterion.

The overall objective of this study is an investigation of the solidification of spent ion-exchange resin waste. The specific objective of this research is looking for the optimal condition for solidification of spent ion-exchange resin waste in order to stable store to repository. The solidification ingredients for spent ion-exchange resin should be characterized advance and compare to make waste form with spent ion-exchange resin.

2. Materials and methods

The solidification ingredients, mortar and Epoxy (polyester) were investigated. The mortar was prepared with slag, fly ash, sand, and Portland (Type I) cement. The mortar sample was analyzed to investigate the characteristic by XRD (X-ray diffraction), FT-IR (Fourier Transform Infrared Spectroscopy), SEM-EDS (Scanning Electron Microscopy with Energy Dispersive Spectroscopy), and XRF (X-ray fluorescence). The polyester epoxy was prepared to compare with mortar for solidification of spent ion-exchange resin (Fig. 1).

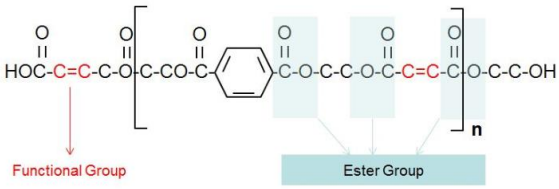

Fig. 1. Polyester Epoxy.

In this study, the GRAVEX GR 3-16 N (mixed bed) resin was used as spent ion-exchange resin. The characteristic of GRAVEX GR 3-16 N is shown in Table 1. Cation (GR 2-0 NG) and anion (GR 1-9 NG) exchange resin was mixed by 1 to 2 as volume ratio.

The solidifications of resin waste which formulated with (1) mortar, (2) mortar with epoxy, and (3) epoxy were formed and compared for compressive strength to meet the acceptance criteria for repository.

Table 1. The characteristics of GRAVEX GR 3-16 N

Resin	GR 2-0 NG Cation-exchange	GR 1-9 NG Anion-exchange
Interacting ion	H^+	OH^-
Functional group	$-SO_3H$	$-CH_2N(CH_3)_3OH$
Ion exchange capacity	>2.4eq/L (H^+)	>1.2eq/L (OH^-)
Average diameter	1.188mm (95%)	1.188mm (95%)
Water contents	36-42%	53-59%
Volume ratio	1	2

3. Results

The XRD patterns of mortar are shown in fig. 2 (a), and the FT-IR spectra of mortar are shown in fig. 2 (b). The XRD analysis shows SiO_2 as the most dominant phase in mortar, and the FT-IR peaks are consistent with the silicate and carbonate [1, 2]. In addition, the characteristics of polyester epoxy were investigated for solidification of resin waste. The resin waste was prepared by cobalt and cesium adsorption, and the compressive strength of solidifications of resin waste was tested, which meet the acceptance criteria.

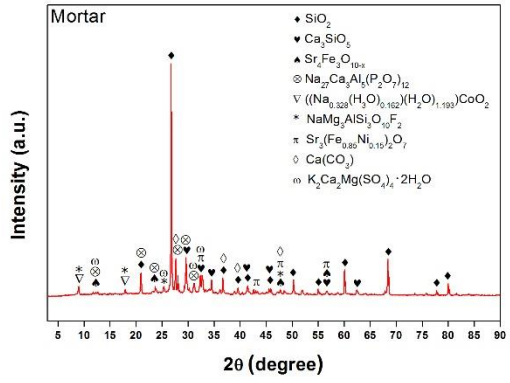

(a) XRD

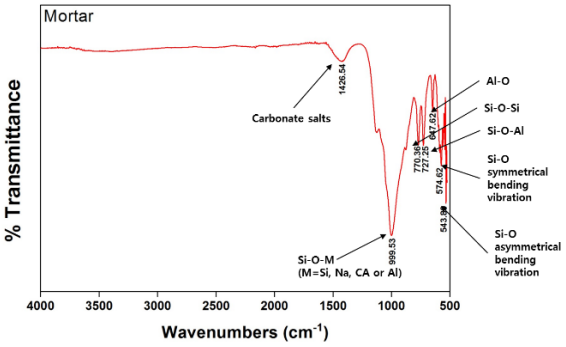

(b) FT-IR

Fig. 2. The (a)XRD and (b)FT-IR results of mortar.

4. Conclusion

The solidifications of mortar and polyester epoxy were tested for resin waste. In order to optimize the solidification of resin waste for acceptance to repository, the solidification ingredients should be characterized for the final formulation condition.

ACKNOWLEDGEMEMT

This work was supported by the Korea Institute of Energy Technology Evaluation and Planning (KETEP) granted financial resource from the Ministry of Trade, Industry & Energy, and Republic of Korea (No. 20171520000410).

REFERENCES

[1] J. Hlavay, K. Jonas, S. Elek, J. Inczedy, "Characterizaion of the particle size and the crystallinity of certain minerals by ir spectrophotometry and other instrumental metohds: II, Investigations on quartz and feldspar", Clays and Clay Minerals, 26(2), 139-143 (1978).

[2] H. Xu, J.S.J. Van Deventer, "The effect of alkali metals on the formation of geopolymeric gels from alkali-feldspars", Colloids and Surfaces A: Physicochem. Eng. Aspects, 216, 27-44 (2003).

A Study on Characteristic for Manufacturing Immobilization of Green Body for Moist Particulate and Sludge-Type Radioactive Waste

[1),*] Yongho Hong, [1)] Minsu Kim, [1)] Heekyung Kim, [1)] Hyoungmin Park, [1)] Dongchul Kim, [1)] Taekyu Lee, [2)] Byunggu Lee, [2)] Seonghun Yoon, and [2)] Jeongsu Kim
[1)] ACT Co., Ltd., 406, IT Venture Town, 35, Techno 9 Ro, Yuseong-gu, Daejeon
[2)] TAEKWANG Co., Ltd., 68, Bugok-ro, Nam-gu, Ulsan
hyh@actbest.com

1. Introduction

It is study of the process for manufacturing a green body for the moist particulate and sludge-type radioactive waste for disposal in domestic industry. The radioactive waste should be volume-reduced and satisfied with the requirements of radioactive waste delivery regulations for preventing the spread of contamination in radiation accident. In this study, it is aimed to derive the optimum molding pressure condition by observing the change of the height of green body and the apparent density by manufacturing a large size compression molding equipment.

2. Main Title

2.1 Process of manufacturing green body

As shown in Table 1, it is a comparison of composition between original radioactive waste samples and the simulated samples.

Table 1. Comparison of composition analysis between original samples and simulated samples(ppm)

	Si	Sb	Mo	Fe	Al	Cu	Zn	P	Ca	Mg	B	Ti
O.S*	22.3	2.58	332	27.04	35.21	-	1.33	2.27	698.7	21	61.85	0.38
S.S**	34.2	3.39	839.6	37.76	97.8	70.9	2.24	61.86	1704	52.9	123.7	1.69

*O.S : Original Sample **S.S : Simulated Sample

Fig. 1 shows the process of producing the dried powder sample. First of all, the simulated samples are dried in a large dryer for at least 6 hours to remove moisture in the molding process and put into a Super-Mixer to make a homogeneous powder. Then, the calculated amount of boron oxide and cerium(IV)oxide are injected into the powder.

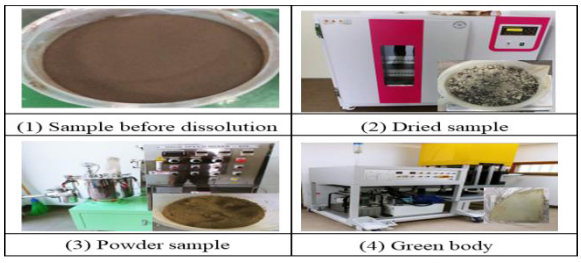

Fig. 1. Process for Manufacturing Powder Sample. The role of additives in the mixed sample is to maintain the state of glass ceramic compound and the shape of structure during the process of heat treatment.

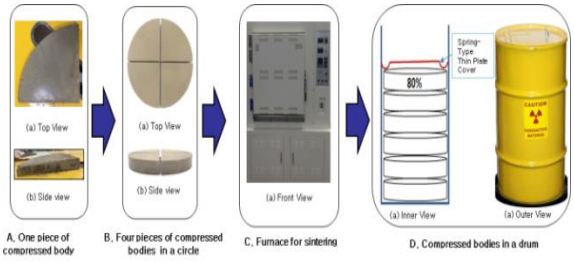

Fig. 2. The manufacturing process of green body.

2.2 Design and manufacturing the compression molding equipment

The shape of the mold is a fan shape which is 20 cm diameter with 200 ton maximum pressure.

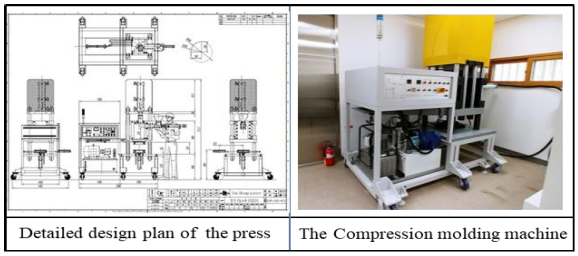

Fig. 3. Compression Molding Equipment.

2.3 Manufacturing Green Body

4kg dried powder sample was injected into the inside of the mold and flatting the surface of the sample before the compression. As shown in Table 2, the molding pressure was gradually set from 30 to 60 MPa, so sufficient molding pressure can be performed in consideration of the state of the green body.

Table 2. Pressure applied value per unit area

Diameter (cm)	Area ($A = \pi r^2$)	1/4 Area(cm^2)	Ton	MPa
40	1,256	314	96	30
			128	40
			160	50
			192	60

2.4 The Characteristic of Green Body according to Pressure

As shown in Fig. 3, it was measuring the height of the green body according to changing the pressure by

using the Vernier calipers.

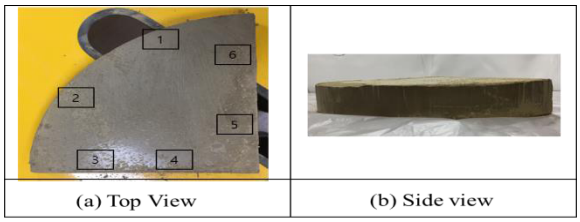

Fig. 4. Measurement of green body.

As a result, it was found that the height of the green body was lowered and the apparent density was increased according to the increased pressure as shown in the Table 3 & 4

Table 3. Variation of the height of the green body by pressure increase

Point Pressure	1	2	3	4	5	6	Avg. Height (cm)
30	5.201	5.188	5.205	5.214	5.245	5.170	5.203
40	5.132	5.130	5.133	5.144	5.158	5.250	5.158
50	5.097	5.045	5.066	5.032	5.057	5.05.3	5.059
60	5.045	4.987	5.018	5.050	4.944	4.938	4.997

Table 4. Variation of apparent density according to pressure increase

Weight (g)	Pressure [MPa]	r(cm)	H(cm)	V(cm^2)	Apparent Density (g/cm^3)	Relative Density
4,000	30	20	5.203	163.45	0.0244	0.960
	40		5.158	162.04	0.0247	0.969
	50		5.058	158.92	0.00252	0.988
	60		4.997	156.99	0.0255	1

As the representative value of the height for the green body by increasing the pressure from 30 to 60 MPa, it is obtained with the Lagrange third degree polynomial by using the simplest interpolation of Eq (1) and the result of third degree polynomial is Eq (2).

$$f(x) = \sum_k \left(\prod_{j\neq k} \frac{x-x_i}{x_k-x_j}\right) y_k \quad (1)$$

$$f(x) = p_1x^3 + p_2x^2 + p_3x^3 + p_4 \quad (2)$$

p_1 = 3.12E-07 $\quad p_2 = -8.89E-05$

$p_3 = -1.14E-03 \quad p_4 = 5.32E+00$

As using Eq (2), it could predict the height of the green body by more than designed pressure of the pilot-scale equipment. Fig. 4 is the estimated graph by using MATLAB program. As a result, it was confirmed that the optimum pressure value of the pilot-scale equipment is 60 MPa, which is the maximum value of the designed value.

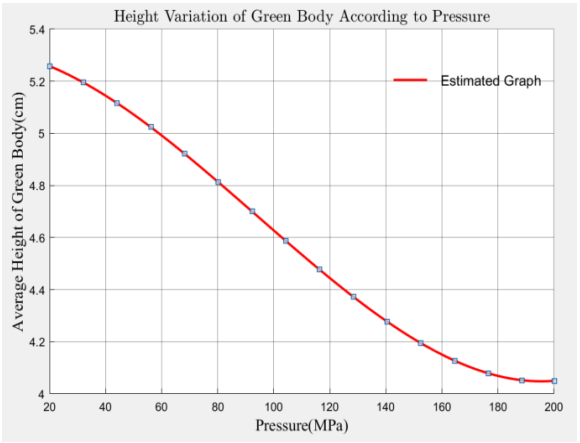

Fig. 5. Height Variation of Green Body by Using Lagrange Interpolation.

3. Conclusions

As a result of evaluating the characteristics of the compression green body of a large size, it was confirmed that the larger the pressure, the smaller the volume. In addition the apparent density was increased and the shape of green body had a smooth appearance. Based on the results of this study, it will be established with a suitable method of manufacturing a green body and study the appropriate to height of the green body. As the results of this study, it will be expected to be applied to the design basis of commercial compression molding equipment.

ACKNOWLEDGEMENT

This research is the result of the technical transfer of the Korea Atomic Energy Research Institute to carry out the task of "Research service for ensuring requirements of radioactive waste delivery" by Tae Kwang Industrial Co., Ltd.

REFERENCES

[1] KARIE, Patent Publication(10-2017-0089622)
[2] KARIE, Patent Publication(10-2017-0125984)
[3] KARIE, Development of Technology for Volume Reduction of Depleted Uranium Waste (2017).
[4] ACT co., Ltd.., Development of Technology for Volume Reduction of Depleted Uranium Waste (2017).

Mixing Treatment of Radioactive Wastes and Structural Stability Evaluation of Solid Waste Form From the FMPP

Jong Sik Shon*, Junhyuck Im, Gi Yong Kim, Dong-Ju Lee, and Dae-Seok Hong
Korea Atomic Energy Research Institute, Daedeok-daero989ben-gil 111,Yuseong-gu, Daejeon, Republic of Korea
*njsshon@kaeri.re.kr

1. Introduction

KJRR (Kijang Research Reactor) will include the Fission Moly Production Process (FMPP) and the Radioactive Wastes Treatment Facility (RWTF). In KJRR's FMPP, solid waste such as spent uranium cake, aluminum cake (Al_2O_3 residue) and Intermediate level liquid waste (ILLW) are generated. The ILLW of FMPP requires a minimum of two years storage period to allow short half-life radionuclides generated from FMPP to decay naturally. RWTF is designed to store ILLW for 5 years and the nuclide affecting the radioactivity concentration after storage is Cs-137 (half-life 30.17 years) [1].

The amount of generated waste such as spent uranium cake (precipitates), aluminum cake and ILLW is 220 L/year, 3,200L/year and 3,000 L/year, respectively. The purpose of this study is to evaluate both the effective mixing process of the wastes from FMPP and the structural stability of the solid waste by acceptance criteria of disposal facilities.

2. Experimental Methods

2.1 Characteristics of Wastes from FMPP

The main chemical composition of ILLW is NaCl and Na_2SO_4, and the salt concentration is 170.81 g/L. Therefore, at room temperature (20 °C), there is no precipitates in a completely dissolved state. The nuclide with the highest radioactivity concentration is Cs-137, so, ILLW is classified as intermediate-level according to Korea's Atomic Energy Act [3]. Aluminum cake is easily dissolved in water due to having 1.23 wt. % water. The radioactivity concentrations of Cs-137 and Co-60 in aluminum cake are estimated to be low-level according to the Korean Atomic Energy Act [2, 3].

2.2 Experimental Methods and Evaluation

The cement used for solidification was portland cement (type I). The wastes used in the experiment were the liquid waste and aluminum cake generated from the simulation of FMPP. The range of operation was based on 30 wt. % of aluminum cake and the mixing ratio of portland cement and liquid waste was varied from 0.45 to 0.75 w/c.

Specimens for the acceptance test were prepared with optimum conditions (Aluminum cake 30 wt. %, w/c ratio 0.6) derived from the operating range experiment. Three solid specimens were prepared for each test items and mean values were used for the evaluation. Test items, methods and procedures according to acceptance criteria of disposal facilities are applied for the structural stability evaluation of cement solidification [4].

3. Results and discussion

3.1 Operating Range and Optimum Condition

In this study, the w/c ratio is defined as the liquid waste/cement ratio. Fig. 2 shows that the operating range is between 0.50 and 0.60 w/c ratio, and the salt

content (salt/cement weight ratio) of solid wastes is 8.54 ~ 10.25 wt. %. The optimal operating condition considering the economic efficiency is 0.60 w/c ratio, and in this case, the salt content of solid wastes is 10.25 wt. %.

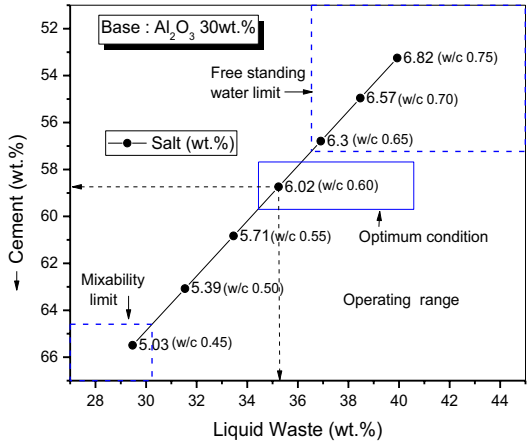

Fig. 1. The operating range and optimum conditions for cement solidification of liquid waste and aluminum cake.

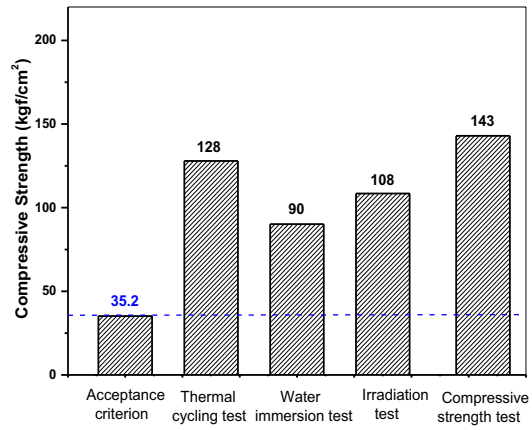

Fig. 2. Structural stability evaluation according to acceptance criteria of disposal facilities.

3.2 Structural Stability Evaluation of Solid Wastes

The solidified specimens for the structural stability evaluation were fabricated with the optimum operating condition, w/c ratio 0.60. Compressive strength on the solidified specimens was measured at ambient and after thermal cycling test, water immersion test, and irradiation test were completed. The specimens were also broken and subjected to free standing water test. After each test, the compressive strength is 90 ~ 143 kgf/cm^2, satisfying the acceptance criteria of 35.2 kgf/cm^2 (3.44 MPa). Fig. 2 shows the results of the acceptance criteria evaluation for the cement waste of mixed wastes from FMPP.

4. Conclusions

The main results of this study are summarized as follows;

1. The operating range is between 0.50 and 0.60 w / c ratio, in which case the solids content (salt / cement weight percentage) is 8.54 ~ 10.25 wt. %.

2. Optimum condition considering economic efficiency is w / c ratio 0.60. In this case, the solid waste content is 40.25 wt. % (salt 10.25 wt. % + aluminum cake 30 wt. %).

3. The structural stability of solid bodies satisfies the criteria for acceptance of repositories.

4. Mixing treatment of waste liquid (intermediate-level) and aluminum cake (low level, 30 wt. %) is considered to be an efficient method due to the dispersion effect of bulkiness and mid-range nuclides.

REFERENCES

[1] Martin W. A. Stewart, “Immobilization of Higher Activity Wastes from Nuclear Reactor Production of 99Mo”, Science and Technology of Nuclear Installations, 2013.

[2] S.K. Lee, G.J. Beyer and J.S. Lee, “Development of Industrial-Scale Fission 99Mo Production Process Using Low Enriched Uranium Target”, Nuclear Engineering and Technology 48, 613, 2016.

[3] Atomic Energy Act of Korea, Notification 2014-003.

[4] KORAD, “Safety analysis report for the inter- and low-level radwastes disposal facility”, 2008.

Collection of Samples for Periodically Validating the Scale Factor

Bong-Ki Ko, Kyung-Ho Kim, Myoung-Ju Yoo, and Young-Ku Choi
Sunkwang T&S Co.,Ltd,, Sunkyung Officetel 20F, #3, Gongwon-ro, Guro-gu, Seoul, Republic of Korea
kobongkea@naver.com

1. Introduction

Low and intermediate-level radioactive waste, generated by NPPs, are classified by pollution source, generation process and radiological characteristics. To send the low and intermediate-level radioactive waste to disposal facilities according to the low and intermediate-level radioactive waste acceptance criteria (Nuclear Safety and Security Commission Notification No. 2015-4), the concentration of the radionuclide, which accounts for more than 95% of the total radioactivity contained in the waste, investigated. For final disposal of radioactive waste in all NPPs, the scale factor for the low and intermediate-level radioactive waste, generated between 2004 and 2007, was developed. The scale factor was periodically validated every 2 years starting with the first validation in 2010 ~ 2011. The 5th periodical validation was conducted for the DAW (Dry Activity Waste), CBP (Concentrate Boric Powder), SRH (Spent Resin High) and ST (Stainless Steel) waste, generated between 2015 and 2016.

This study analyzed the waste generation of NPPs by waste type to collect the samples for the 5th periodical validation of the scale factor, and compared the radionuclide concentration of the waste to be sampled.

2. Main Subject

2.1 Waste generation

The waste, generated by NPPs, can be divided into waste generated during normal operation and waste generated during overhaul. The samples for periodical validation of the scale factor are collected from the relatively highly contaminated waste generated during overhaul from the conservative standpoint. The waste, generated by each NPP between 2015 and 2016, is as shown in Table 1.

Table 1. Radioactive waste drums (200L), generated by each NPP during normal operation and overhaul between 2015 and 2016

Classification		DAW	CBP	SRH	ST
KR	Normal Operation	675	22	22	0
	Overhaul	224	4	4	0
SKR	Normal Operation	233	0	0	0
	Overhaul	58	0	0	0
WS	Normal Operation	742	0	0	0
	Overhaul	223	0	0	0
YK	Normal Operation	924	132	21	225
	Overhaul	189	0	0	0
UJ	Normal Operation	721	181	34	0
	Overhaul	223	33	0	0

The waste generation varies, and it can be confirmed that YK NPP generated ST waste. The samples for periodical validation of the scale factor were collected from the waste generated during overhaul, and samples were collected from 292 drums as shown in Table 2.

Table 2. Radioactive waste drums (200L) of each NPP from which samples were collected

Classification	DAW	CBP	SRH	ST
KR	24	6	6	0
SKR	24	0	0	0
WS	36	0	0	0
YK	36	6	6	100
UJ	36	6	6	0

2.2 Specific radioactivity of labeled nuclides

To take out the collected samples, nuclide analysis was conducted at the site. Fig. 1 shows the specific radioactivity of ^{60}Co and ^{137}Cs by waste type.

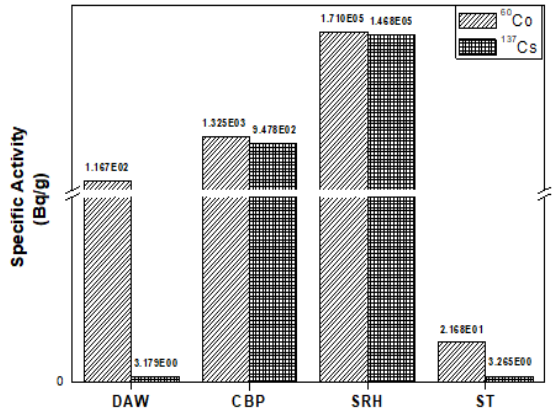

Fig. 1. Mean specific radioactivity of ^{60}Co and ^{137}Cs by waste type.

The specific radioactivity of the labeled nuclide of CBP and SRH is high, whereas the specific radioactivity of ^{137}Cs nuclide of DAW is low. Most of the ^{60}Co and ^{137}Cs nuclide are melted in the coolant system, and CBP and SRH are waste generated in the liquid treatment system. On the other hand, DAW is generated in the nuclear reactor building and auxiliary building, and ^{137}Cs nuclide is unlikely to be detected. Also, ^{137}Cs nuclide detection of DAW waste varies between existing NPPs and new NPPS. Fig. 2 illustrates the specific radioactivity of ^{137}Cs nuclide in old NPPs and new NPPs.

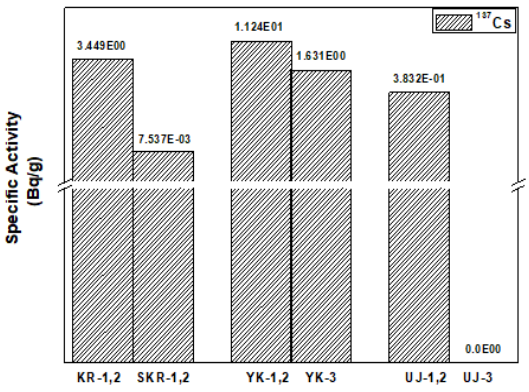

Fig. 2. Specific radioactivity of ^{137}Cs of DAW waste in old NPPs and new NPPs.

In old NPPs, not new NPPs, defective fuel is generated and corrosion products are eluted due to the damage of the fuel cladding. Due to these defects of old NPPs, ^{60}Co and ^{137}Cs nuclide are more likely to be detected in DAW waste including decontamination paper in old NPPS than in new NPPs.

3. Conclusion

Radioactive waste, generated in all NPPs between 2015 and 2016, was analyzed, and the specific radioactivity of labeled nuclides was compared. The specific radioactivity of ^{137}Cs nuclide of DAW in old NPPs and new NPPs was compared. In new NPPs, labeled nuclides were hardly detected.

4. References

[1] Sung-Wook Hong, et al 'Determination of Radionuclide Concentration Limit for Low and Intermediate-Level Radioactive Waste Disposal Facility II: Application of Optimization Methodology for Underground Silo Type Disposal Facility' Korea Radioactive Waste Society spring conference (2017).

[2] Ki-Ha Hwang, et al 'Development of Radionuclide Inventory Declaration Methods Using Scaling Factors for the Korean NPPs' Korea Radioactive Waste Society spring conference (2004).

Developing the Process of Collecting Samples of the Waste Filter for NPP Waste

Kyung-Ho Kim, Bong-Ki Ko, Dong-Je Lee, and Young-Ku Choi
Sunkwang T&S Co.,Ltd Sunkyung Officetel 20F, #3, Gongwon-ro, Guro-gu, Seoul, Republic of Korea
kyungho0121@naver.com

1. Introduction

The annual average amount of low and intermediate-level radioactive waste, generated by domestic NPPs, is 1,200 or so drums (200L), and as of December 2017, about 89,180 drums are stored in the waste repositories of NPPs. [1] Among the NPP waste generated before 2004, 709 drums of waste filters are stored, and among them, 522 drums are stored in PWR and 187 drums are stored in PHWR. PWR and PHWR waste filters are stored in different ways, and they are different types too. PWR waste filters are stored in specially made vessels (F, SH drum), and PHWR waste filters are stored in the lattice structure in the basement of temporary repositories. For final disposal of stored waste filters, nuclide analysis, required by the radioactive waste acceptance criteria, must be conducted before disposal.

This study developed the process of collecting samples for nuclide analysis to evaluate the nuclide inventory for final disposal of waste filters, generated by PWR before 2004.

2. Main subjest

2.1 Types and storage status of filters

Filters are used in various systems during operation of NPPs. In PWR NPPs, 6 systems are using filters to purify liquid waste as illustrated in Fig. 1.

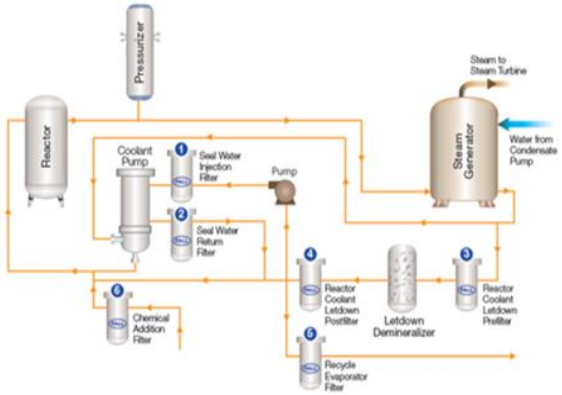

Fig. 1. Utilization of PWR filters.

Waste filters to be sampled are filters for purifying coolants, and there are many types as shown in Table 1 and Fig. 2.

Table 1. Dimensions of PWR

Filter type		Size	Volume(㎥)
RC	Reactor Coolant	6¾" OD X 20"	0.012
SI	Seal Injection	2¾" OD X 20"	0.0029
EC	Clean-up	6¾" OD X 30"	0.017
BA	Boric Acid	6¾" OD X 20"	0.012

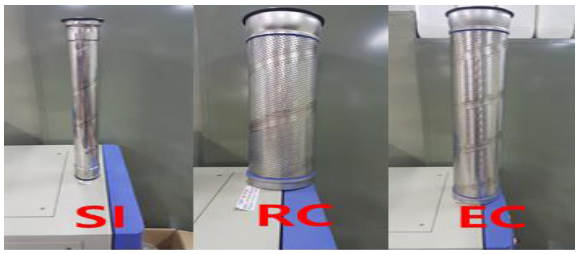

Fig. 2. Images of the PWR filter.

Filters are stored in specially made vessels (F[2], SH[3]drum), and they are made of concrete except for the inside of the vessels. The dimensions of the specially made vessels are illustrated in Fig. 3.

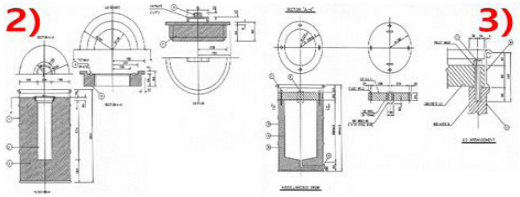

Fig. 3. Dimensions of the F drum and the SH drum.

2.2 Sampling plan

The information and storage status of selected drums are checked, and a presentation is given at the NPP where waste filters will be selected. The doses and surface doses are checked when drums are generated, and the radiation protection plan for minimizing the radiation exposure of workers is established.

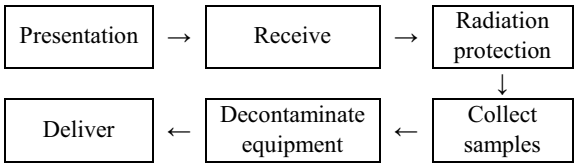

Fig. 4. Sampling procedure.

2.3 Selecting target drums and collecting samples

2.3.1 Simulation. The dimensions of the F drums, actually used in NPPs, were secured, and internal simulation samples were made. The core drill and hole cutter were used to collect samples, and a device for preventing the spread of contamination due to the cement dust, generated in the collection process, was installed as shown in Fig. 5.

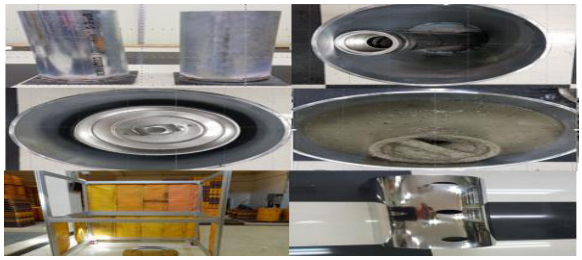

Fig. 5. Internal simulation samples and a device for preventing the spread of contamination.

2.3.2 Collecting samples. The sample waste filters for nuclide analysis included 9 from KR NPP 2, which were generated before 2004, and 1 from YK NPP 1. Samples were collected from the waste filter storage drums selected for the sampling as shown in Table 2.

Table 2. Selected waste filter drum number

Classification	Selection No.	Date generated
KR NPP 2	K20-1987-F03-0001	1987.04.14
	K20-1987-F03-0002	1987.04.14
	K20-1987-F03-0015	1987.10.25
	K20-1987-F03-0017	1987.11.03
	K20-1988-F03-0002	1988.02.16
	K20-1988-F03-0007	1988.05.23
	K20-1988-F03-0008	1988.05.23
	K24-1988-F03-0002	1988.06.12
	K23-1988-F03-0001	1988.07.08
YK NPP 1	Y1-1999-F03-0003	1999.12.30
	Y1-1999-F03-0011	1999.12.30
	Y1-1999-F03-0016	1999.12.30

Sample were collected according to the method described in Fig. 6.

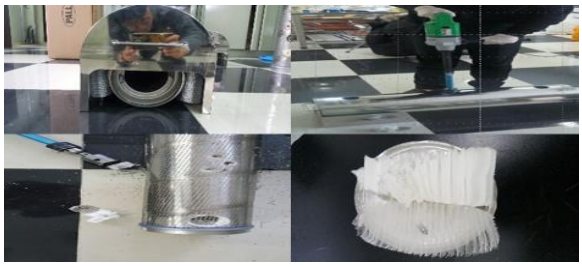

Fig. 6. Sampling procedure.

1) Establish the radiation controlled area.
2) Move the selected drums to the controlled area.
3) Install the device for preventing the spread of contamination.
4) Move the selected drums to the unit to preventing the spread of contamination.
5) Open the cap of the moved drum and measure the dose.
6) Use a breaker to remove concrete and measure the dose.
7) Opening the drum inner cap and dosimetry using automatic impact wrench and pipe wrench 8) Check inside the drum.
9) If both cement and waste filters are stored together in the drum, use the sampling device to cut the waste filter.
10) If only the waste filters are stored, use a hook to lift up the waste filter.
11) Use the core drill and hole cutter to collect samples from three locations of the waste filter.
12) Separate the collected waste filter samples from the concrete.
13) Pack the separated waste filter samples in sealed vinyl, and measure the surface dose.
14) Storage using radioactive material transport container

3. Conclusion

The simulation for collecting samples of waste filters stored in F drums and SH drums was conducted, and based on the results, the sampling procedure for preventing the spread of contamination and minimizing the exposure of workers was established.

Based on this, samples were collected from 9 waste filters in KR NPP 2 and 3 waste filters in YK NPP 1.

REFERENCES

[1] www.kins.re.kr
[2] Gwang-seop Choi, et al ‘Waste filter volume reduction method’ Korea Radioactive Waste Society spring conference (2013).
[3] Yeong-yong Ji, et al ‘Current status of waste filters stored by KAERI and their treatment plan’ spring conference (2007).

Evaluation on Glass Mold Integrity of Cold Crucible Induction Melter for Discharging Glass Melt

Sunghoon Hong[a*], Seok-Ju Hwang[a], Cheon-Woo Kim[a], and Toshiro Oniki[b]
[a]KHNP CRI, 70, 1312-gil, Yuseong-daero, Yuseong-gu, Daejeon, Republic of Korea
[b]IHI Yokohama Engineering Center, Kanagawa 235-8501, Yokohama-shi, Isogo-ku, Shin-Nakahara-cho, Japan
[*]sunghoon.hong@khnp.co.kr

1. Introduction

Vitrification using the CCIM (Cold Crucible Induction Melter) is considered as one of promising radioactive wastes treatment technology [1]. Vitrification technology is to incorporate radioactive nuclides in the stable glass matrix as radioactive wastes are fed on the molten glass. Accordingly, release of radioactive nuclides to the environment at the disposal site can be fundamentally prevented.

Currently, in the KHNP CRI, with CCIM with 85 cm diameter, vitrification demonstration test has been conducted to confirm the possibility of treatment of liquid wastes. Also, the various operation parameter which produced by the demonstration test are analyzed for the design data of commercial facility. Among of the various operation parameter, glass mold of temperature including cooling rate is one of the vital value to form the glass structure on the vitrification process. Also, the temperature could induce diverse problems such as thermal deformation, thermal degradation and etc. of the glass mold.

Therefore, in this study, the temperature recording system is installed to continuously measure the glass mold temperature during the glass melt discharge. The temperature measured is discussed in view of the integrity of glass mold.

2. Experimental

2.1 System of vitrification plant of KHNP CRI

The virtification process developed by the KHNP CRI consists of loading glass, startup for melting glass, feeding and vitrifying and draining as shown in the Fig. 1. The CCIM with 85 cm diameter is a water-coolded melter in which electrical currents are directly induced in the glass melt from an external high frequency generator (HFG). The HFG with Metal Oxide Semiconductor Field Effect Transistor (MOSFET) invertor provides induction power of up to 600 kWe at a nominal frequency of 250 kHz [2].

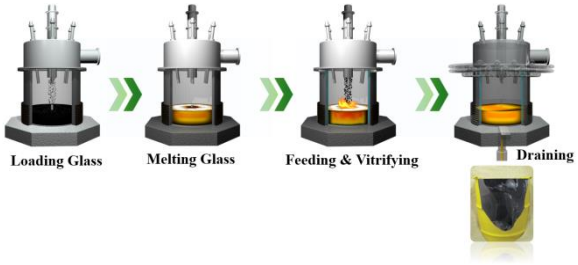

Fig. 1. Vitrification process by using CCIM [2].

2.2 Operation data of demonstration test

The operation data of demonstration test using a slurry feed is summarized as shown in Table. 1. The Slurry and glass frit were fed into CCIM and a borosilicate glass melt was formulated and discharged.

Table 1. Operation data of demonstration test

Time	Event	Remarks
11:16	HTF on	
11:26	Start the ignition of Ti-ring	3 'o clock direction
13:46	Temp. of glass melt - Upper : 1141 ℃ - Middle : 840 ℃ - Bottom : 558 ℃	
14:00~ 14:30	Slurry feed rate @ 20 ℓ/hr	Amount of feed -Liquid waste : 390 ℓ -Glass frit : 107 kg
14:30~ 15:00	Slurry feed rate @ 50 ℓ/hr	
15:00~ 18:00	Slurry feed rate @ 85 ℓ/hr	
18:00~ 19:00	Slurry feed rate @ 100 ℓ/hr	
19:00~ 19:20	Mixing glass melt	
19:28~	Start the discharge	Amount : 224 kg
19:48	HFG off	

2.3 Specification of glass mold

Glass mold which made of stainless steel 304 is used for discharging. To measure the history of temperature during glass discharging, eight of thermocouple guides (bottom: 2, side: 6) were

attached as shown in the Fig. 2. For good contact between thermocouple and glass mold surface, regardless of thermal expansion, the guide applies the spring fixing method as shown in the Fig. 3. Also, K-type thermocouple is used with the temperature recorder GL240 (GRAPHTEC Co.).

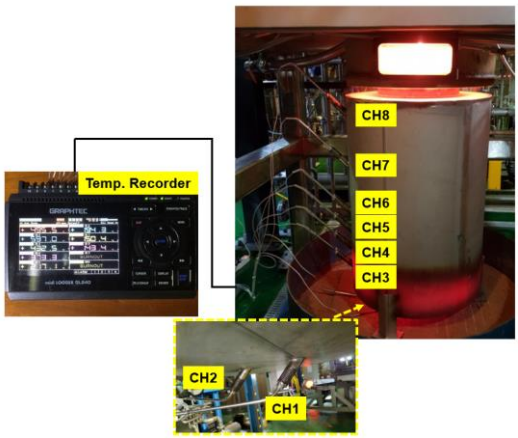

Fig. 2. Temperature recording system for the glass mold.

Fig. 3. The spring guide for fixing thermocouple.

3. Result and Discussion

During the glass melt discharge, the temperature of glass in the mold is continuously measured by the temperature recording system. The system receives signals from eight of channels where two are on the bottom (CH1, 2) and the others are on the side (CH3, 4, 5, 6, 7, 8).

Fig. 4 shows the temperature profile of glass mold for discharge. Molten glass is drained for 20 min (started at 07:28 pm and finished at 07:48 pm). The maximum temperature of glass mold is about 700 °C at the bottom center (CH1) after 30 minutes of discharge. Accordingly, the integrity of glass mold could be maintained (melting point of stainless steel 304 : 1400 ~ 1450 ℃).

Table. 2 summarized the temperature history which the temperature was cooled down by room temperature (~25 ℃). The time to spend from maximum temperature to room temperature is 2751 minutes (47 hr 51 min).

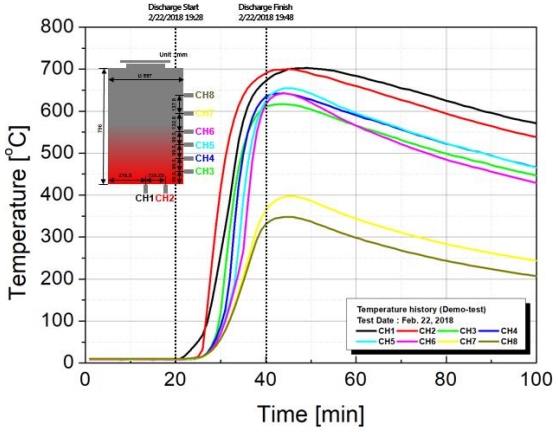

Fig. 4. Temperature history of mold for glass discharge.

Table 2. Temperature history at CH1 (bottom center of mold)

Time	Mold surface Temp. at CH1	ΔTime (min)	Remarks
19:28	8.7 ℃	0	Start discharge
19:48	662.7 ℃	20	Finish discharge
19:58	703.2 ℃	30	Max. Temp.
20:37	600 ℃	69	
21:22	500 ℃	114	
22:32	400 ℃	184	
00:25	300 ℃	295	
04:10	200 ℃	520	
12:55	100 ℃	1045	
10:21	30 ℃	2331	
17:51	25 ℃	2781	Cool down completely

4. Conclusion

The temperature profiles were measured at eight different positions of STS mold. The glass mold shown the excellent integrity, i.e., no deformation and degradation during the glass melt discharge. Additionally, the glass produced is being investigating in view of the micro-structure.

REFERENCES

[1] C.W. Kim, et al., “Chemically Durable Iron Phosphate Glasses for Vitrifying Sodium Bearing Waste (SBW) Using Conventional and Cold Crucible Induction Melting (CCIM) Techniques”, Journal of Nuclear Materials (2003).

[2] C.W. Kim, “Vitrification Technology for Radioactive Waste Treatment”, Korea Atomic Industrial Forum (2011).

Cost-Benefit Analysis for Regulatory Clearance of VLLW Metal Radwastes at KAERI

Ki-baek Shin[1], Dae-seok Hong[1], Il-sik Kang[1], Gi Yong Kim[1], and In Ho Kim[2*]

[1]Korea Atomic Energy Research Institute, 111, Daedeok-daero 989beon-gil, Yuseong-gu, Daejeon, Republic of Korea

[2]Chungnam National University, 220 Gung-dong, Yuseong-gu, Daejeon, Republic of Korea

[*]ihkim@cnu.ac.kr

1. Introduction

In Korea, the first regulatory clearance was conducted in 1994. Since then, regulatory clearance has been conducted for radwastes from numerous nuclear facilities.

At Korea Atomic Energy Research Institute (KAERI), nuclear facilities have generated diverse metal radwastes that have extremely low levels of radioactivity. Thus, reducing the amount of metal radwastes by regulatory clearance has become one of important tasks for radwaste management. The total amount of metal radwastes was about 40 tonnes, all of them were cleared by regulatory clearance in 2015.

In this study, the cost for the clearance and the disposal cost saving were analysed, and, based on that, the economic efficiency of the regulatory clearance was discussed.

2. Procedure of Regulatory Clearance

The metal radwastes such as spent ventilation filter frame, rebar within concrete, dismantled radwastes of exhaust fan at radiation field and parts of hot cell equipment were generated during the operation of nuclear facilities at KAERI. For regulatory clearance, radioactive contamination was monitored for all these radwastes, and then they were washed and rinsed with pressurized water. They were cut and stored at a designated area in Radioactive Waste Treatment Facility (RWTF) at KAERI.

Fig. 1. VLLW Metal Radwastes cleared in 2015.

After a series of processes, samples were taken for radioactivity analysis. This analysis results showed that the major radionuclides in radwastes were Co-60, Cs-137 or U-238. The radiological doses were assessed based on a clearance scenario. A scenario for the regulatory clearance was set up using RESRAD-RECYCLE Code, and default parameter values of this code were used for the assessment.

After permission from a regulatory body in Korea, the metal radwastes were cleared by committed disposal for recycling.

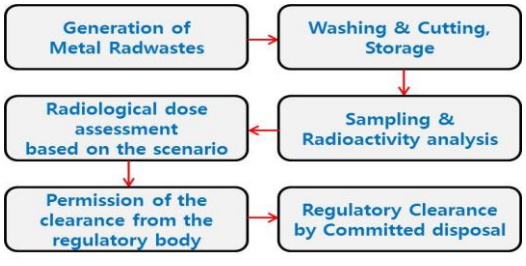

Fig. 2. Procedure of Regulatory Clearance for Metal Radwastes.

3. Cost-benefit Analysis

3.1 Cost Estimation

Until now, all the activities for the regulatory clearance were explained. These activities were accompanied with time, labor, and costs. Some parts of the activities were outsourced.

In total, the regulatory clearance costs about 50 Thousand US dollars and spans two years. Because a discount rate is not applied in the cost estimation, the present value is somewhat underestimated. Among the several cost terms, the labor cost due to outsourcing accounts for about 60 %, and secondary wastes accounts for about 15 %.

3.2 Benefit Estimation

In Korea, the final disposal of low and intermediate level radioactive waste costs about 12 Thousand US dollars per 200 L Drum. So, due to the regulatory clearance, a disposal cost of about 1 million US dollars for about 80 drums was saved.

3.3 Cost-benefit ratio

A cost-benefit analysis result shows that the regulatory clearance costs about 50 Thousand US dollars while saving about 1 million US dollars.

Therefore, it can be concluded that the regulatory clearance of 80 drums of VLLW metal waste shows a cost-benefit ratio more than 20.

4. Conclusion

There have been recent increases in the type and amount of radwastes considered for regulatory clearance in Korea. Metal radwastes account for most of the primary radwastes subject to regulatory clearance. At KAERI, a variety of metal radwastes with extremely low radioactivity were generated from nuclear facilities. The metal radwastes about 40 tonnes were cleared by regulatory clearance in 2015. The regulatory clearance was conducted in the form of committed disposal for recycling. By use of regulatory clearance, the disposal costs for radwastes were greatly saved. Additionally management of radwaste became more efficient in view of storage capacity.

REFERENCES

[1] K.B Shin, et al., “Procedure of regulatory clearance for metal radwastes at the KAERI”, Global 2015 Conference, Paper 5149, P2156~2163.

[2] K.B Shin, et al., “Application of Mass-to-surface Ratio for Regulatory Clearance of VLLW Metal Radwastes at KAERI”, IAEA Conference, CN-242, No. 149.

[3] Atomic Energy Act of Korea, notification No. 2014-003.

Safety Analysis of Radwastes Storage Buildings in KAERI : Earthquake Case

Jongjin Kim*, Hong Rae Jeon, Dong Ju Lee, Jeong-guk Kim, and Dae-Seok Hong
Korea Atomic Energy Research Institute, Daedeok-daero989ben-gil 111, Yuseong-gu, Daejeon, Republic of Korea
kjj@kaeri.re.kr

1. Introduction

Safety concerns for radioactive waste storage have increased. And the Nuclear Safety Commission (NSC) is asking nuclear agencies to conduct a safety evaluation for their radwastes storages under disasters such as fire and earthquake.

Korea Atomic Energy Research Institute, Korea Hydro & Nuclear Power Co., Korea Nuclear Fuel Co., Ltd., and KORAD are conducting safety evaluations for their respective storages.

In this paper, we discuss the method and results of the safety evaluation of the radioactive waste storage at the Korea Atomic Energy Research Institute for earthquake situation.

2. Safety Analysis Method

The accident analysis of the storage consists of three steps. In the first stage, Hazard Definition is used to identify potential hazards that could lead to an accident. In the second stage, Hazard assessment of unmitigated event, which includes event selection process, is performed. In the third step, the accident scenarios were established for the high-risk events identified in the non-audit audit potential risk assessment, and a quantitative accident assessment was conducted accordingly.

Generally, the potential exposures due to radioactive waste of the storage can be broadly categorized as on-site workers and out-of-bounds boundaries. However, in this study, the decision-maker for the accident impact assessment is defined as an individual at the boundary of the storage restricted area.

The internal effective dose by breathing can be calculated using following equation 1.

$$H_{th} = X/Q \times Br \times \sum(Q_i DCF_{thi}) \quad (1)$$

Where, X/Q is atmospheric dispersion factor for 2hrs at the boundary of restricted area (sec/m^3), and Qi is the amount of released radio nuclide i for 2 hrs (Bq), and DCF_{thi} is the dose conversion factor of radio nuclide i(mSv/Bq), and Br is breathing rate, NRC usually used 3.47E-04m^3/sec for average individual breathing rate after 0~8hrs after accident.

The effective dose by external exposure can be calculated by equation 2.

$$H_{ed} = X/Q \times \sum(Q_i DCF_{edi}) \quad (2)$$

Where, X/Q is atmospheric dispersion factor for 2hrs at the boundary of restricted area (sec/m^3), and Qi is the amount of released radio nuclide i for 2 hrs (Bq), and DCF_{edi} is the dose conversion factor of external exposure from semi-finite radioactive source (mSv/Bq).

The radioactive source can be calculated using equation (3)

$$\mathrm{Q} = \mathrm{MAR} \times \mathrm{DR} \times \mathrm{ARF} \times \mathrm{RF} \times \mathrm{LPF} \quad (3)$$

Where :

MAR = Material at Risk, DR = Damage Ratio

ARF = Airborne release fraction

RF = Respirable Fraction

LPF = Leakpath factor

The material at risk is the amount of radioactive material (in grams or curies of radioactivity for each radionuclide) available to be acted on by a given

physical stress. The damage ratio is the fraction of the material at risk impacted by the actual accident-generated conditions under evaluation. The airborne release fraction is the coefficient used to estimate the amount of a radioactive material that can be suspended in air and made available for airborne transport under a specific set of induced physical stresses. It is applicable to events and situations that are completed during the course of the event. The respirable fraction is the fraction of airborne radionuclides as particles that can be transported through air and inhaled into the human respiratory system and is commonly assumed to include particulate matter less than or equal to 10 micrometers in diameter.

We used average value of destructive analysis results of operational radwastes with gaseous radioactive nuclides and average concentration values for decommissioning radwastes with gaseous radioactive nuclides. KAERI has 3 storage builds for operational radwastes and 2 for radwastes from decommissioning. The maximum storage capacities are 11,010, 1,404 and 3,320 drums for operational radwastes storage, 2,250 and 2067m^3 for decommissioning, respectively.

We assumed the radwastes were fully stored as maximum capacity and multiply 5 for conservative evaluation. The damage ratio is 10% for earthquake case and ARF*RF is 0.001. The LPF usually 1 for conservative evaluation.

For the internal dose conversion factor [1], we adopted the value from ICRP publication 119[2] “Compendium of Dose Coefficients based on ICRP Publication 60”. For external dose coefficients, we adopted from EPA parameters.[3] And we used 7.38E-02 as the atmosphere dispersion factor (50m, 2hrs)

3. Results and Discussion

The analysis results are summarized in table 1 and 2

Table 1. Results of operational radwastes storage

Storage	1	2	2-1
Effective Dose (mSv)	6.22E-04	3.32E-05	2.52E-05
% vs 25mSv	2.49E-03	1.33E-04	1.01E-04

Table 2. Results of decommissioning radwastes storage

Storage	1	2
Effective Dose (mSv)	1.75	1.92
% vs 25mSv	7.0E+00	8.2E+00

4. Conclusion

We performed safety analysis for the radwastes storage buildings at KAERI for the earthquake case. All calculation performed with conservative assumption and expectation. The results of operational radwastes storage shows much lower effective dose than regulation criteria. (less than 1E-04%). While, the effective dose of the decommissioning radwastes storage higher than that of operational radwastes but still lower than regulation criteria. Thus, all storage buildings in the KAERI are safe in case of earthquake. The direct exposure will be considered for the further safety analysis.

REFERENCES

[1] H. Smith, Age-Dependent Doses from Intake of Radionuclides, ICRP 72, 1997.

[2] C. H. Clement, Compendium of Dose Coefficients based on ICRP Publication 60, 119, 2012.

[3] K. F. Eckerman and J. C. Ryman, External Exposure to Radionuclides in Air, Water, and Soil. EPA-402-R-93-08, 1993.

Waste Characteristics Evaluating Strategy of KRR1&2 Reclassified Wastes by Applying the IAEA TECDOC 1537 (Strategy and Methodology for Radioactive Waste Characterization)

JeongWook Moon*, GuenHo Kim, JeongGuk Kim, JongJin Kim, JongWon Choi, and DaeSeok Hong
Korea Atomic Energy Research Institute, 989-111 Daedeok-daero, Yuseong-gu, Daejeon, Republic of Korea
*jwmoon@kaeri.re.kr

1. Introduction

TRIGA MARK-2 & 3 was dismantled at the research site of Gongneung-dong, Seoul, and some wastes were reclassified due to the change of the some regulation policy in 2014. These reclassified wastes have historical specificity and extremely low-level wastes. While, even they are extremely low, still it needs to perform same process to disposal but it would be inefficient for these wastes. Therefore, it is believed that establishing a strategy for characterization evaluation in accordance with the IAEA report will help to carry out similar types of decommissioning waste disposal in the future.

2. Characterization of KRR reclassifying the waste

2.1 Waste Occurrence history

In the past, the wastes had been classified as clearance level wastes under 0.4Bq/g and stored, but after 2014 Notice (No.2017), they had to be reclassified as low-level wastes.). Since then, low levels waste between 0.1-0.4Bq/g based on gamma radioactivity have been additionally reclassified. Fig. 1 shows the distribution of Co-60, the representative nuclear species of decommissioning wastes.

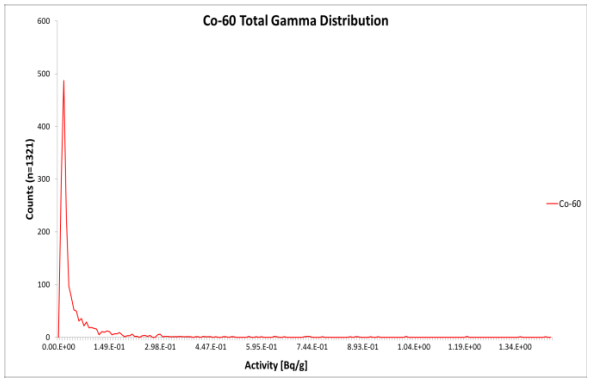

Fig. 1. Total distribution of Co-60 (Reclassified waste).

2.2 Consideration of dividing waste stream

KRR(Korea Research Reactor) basically have various characteristics same as common decommissioning wastes.

At the IAEA Report, it is referred to as “If partitioning is achievable, it will undoubtedly result in easier to manage streams and reduced treatment and disposal costs.” As a result, the feasibility of the separation about waste stream was examined through the results of nuclide analysis of KRR(Korea Research Reactor) Concrete waste disposal in the past.

2.2.1 Co-60 distribution by KRR1&2 stream.

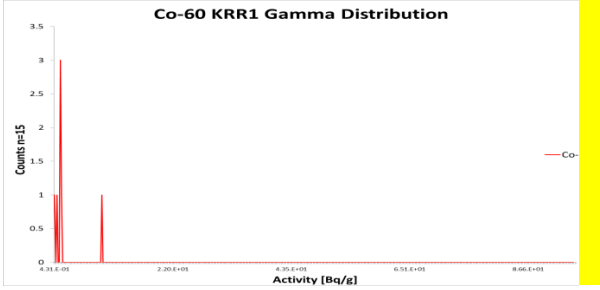

Fig. 2. KRR1 Concrete Co-60 Distribution (Past disposed waste).

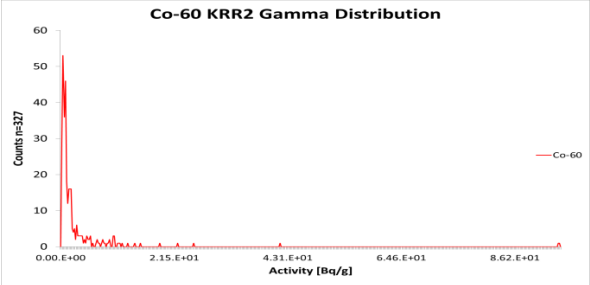

Fig. 3. KRR2 Concrete Co-60 Distribution (Past disposed waste).

2.2.2 Co-60 distribution by total stream.

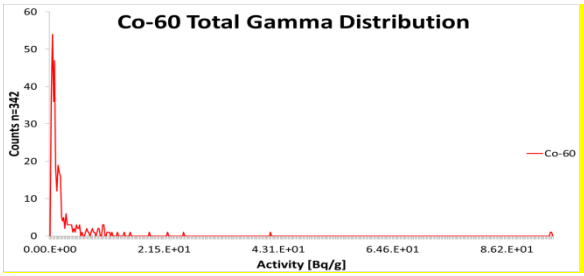

Fig. 4. KRR1&2 Concrete Co-60 Distribution (Past disposed waste).

For this, the decision of reclassification waste stream cannot identify practical meaning for very low levels waste.

3. Waste Characteristics Evaluating Strategy in KRR

KRR reclassification wastes generated before the revision of the past law, so it is not easy to track the waste stream through various deconstruction processes. The application of the scaling factor also cannot have practical meaning at present. In the IAEA report, fully detailed inspection or conservative limit values are recommended for waste characterization. But full inspection cannot be used because of the huge amount of decommissioning cost. The use of conservative limits is assessed as appropriate for use in reclassified wastes stored at the KRR.

4. Discussion and Conclusion

In the case of reclassification process in the KRR, it has very low level activity limit.

In addition, classification by stream has no actual meaning in the past history of waste disposal by KRR

Based on these findings, it is necessary to classify the characteristics evaluation groups for securing as many specimens as possible in order to evaluate the characteristics of KRR reclassified wastes. Using conservative limits for Waste Acceptance Criteria satisfaction will be a way to identify adequate and cost effective characterization requirements.

REFERENCES

[1] INTERNATIONAL ATOMIC ENERGY AGENCY, “Strategy and Methodology for Radioactive Waste Characterization”, IAEA-TECDOC-1357, IAEA, Vienna (2007).

[2] INTERNATIONAL ATOMIC ENERGY AGENCY, Characterization of Radioactive Waste Forms and Packages, Technical Reports Series No. 383, IAEA, Vienna (1997).

A Study on the Application of the Reactor Power Cutback System to WH 1000 Type Nuclear Power Plant

Beyongho Yi and Jongsoon Song*
Chosun University, 309 Pilmun-daero, Dong-gu, Gwangju, Republic of Korea
godot21@naver.com

1. Introduction

The reactor shutdown of WH1000 type NPPs is inevitable during the secondary system transients, such as the loss of the total load, while OPR1000 NPPs are designed to prevent shutdown the reactor by the operation of the reactor power cutback system(RPCS). In this study, it is proved that the NPPs can be improved economically through preventing the unnecessary reactor shutdown by applying RPCS to the WH1000 type NPPs.

2. Main title

2.1 Analysis on cause of shutdown for NPP type

The analysis on the causes of unplanned shutdown of the nuclear reactor at the Hanbit1 power plant(WH1000 type), 55% of the cases were caused by the secondary system, whereas in the case of the OPR1000 type was 27%, about half of WH1000 type.

2.2 Necessity of R & D

To prevent the reactor shutdown of WH1000 NPPs in case of a secondary abnormal such as loss of total load, it is necessary to secure enough main steam dump capacity such as Hanul1 power plant or to apply RPCS like OPR1000 type. If a reactor shutdown occurs due to a failure or an accident, the NPPs will take a long time to analyze the cause of the shutdown and perform the safety assessment in order to obtain approval for restarting the reactor due to conservative decision making. As a result, the utilization rate is lowered and economic costs are increased according to the inspection. Therefore, reducing the number of reactor shutdowns in NPP operation is essential not only for economic improvement, but also for securing public confidence.

2.3 Steam dump system by NPP type

Comparison of characteristics and operating mechanisms of the WH1000 type and OPR1000 type power plant for the steam dump system used in the event of high power output from the reactor system caused by sudden loss of loads with the secondary system.

2.3.1 The steam dump system of WH1000 is designed to remove 64% of steam via the condenser and atmospheric in order to eliminate surplus thermal energy generated by the reactor when the turbine load is rapidly reduced or lost. But reactor shutdown cannot be avoided even if the steam dump system is operated when the turbine load is rapidly reduced or lost at 100% power operation.

2.3.2 The steam dump capacity of OPR1000 type is 55%, which is rather smaller than that of WH1000 type. The remaining surplus output is controlled by RPCS and the reactor control system. The plant

maintains equilibrium energy and the reactor does not shutdown.

2.4 Application of WH1000 type RPCS

In the case of the WH1000 type NPPs, if two main feedwater pumps are lost, a turbine runback occurs and turbine power is maintained at 45%. Because the reactor output cannot be reduced quickly, the turbine-reactor output is mismatched, and the low level of the steam generator causes the reactor shutdown due to the shortage of water supply. Otherwise reactor shutdown occurs by primary system overheating (pressurizer high pressure, OTΔT). In order to prevent the reactor shutdown according to the above mechanism, it is necessary to apply RPCS to the WH1000 NPPs. The RPCS drops the selected control rods into the core to reduce reactor power and through the steam dump system quickly stabilizing the reactor output and turbine output.

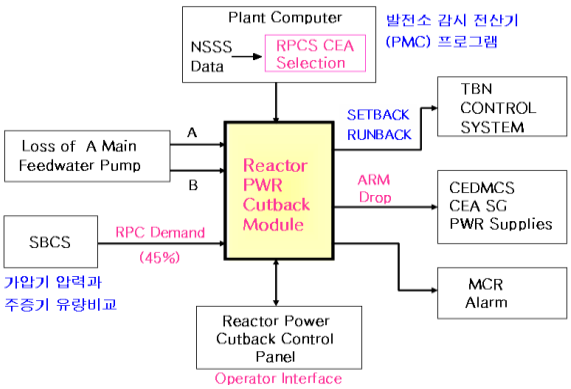

Fig. 1. Diagram of OPR1000 RPCS.

2.5 Simulation of the RPCS WH1000

A simulation model of the Hanbit 1 power plant was developed using the performance analysis code based on the Advanced Continuous Simulation Language (ACSL). Assuming that the secondary system has lost at the full loads. The comparative variables are reactor power, etc. When not applying the RPCS, the reactor coolant temperature was continuously increased from 588°F to 596°F due to the inability to properly cool the reactor coolant. The pressurizer pressure was increased and the reactor shutdown by the OTDT occurred at about 21 seconds after the total load loss. On the other hand, in the case of the RPCS applying model, part of the control rod was inserted into the core by the RPCS actuating and the reactor output was rapidly reduced to 40% and stabilized.

3. Conclusion

This study conceptually introduced the application of RPCS to the WH1000 NPPs to prevent reactor shutdown by the turbine stop or large secondary system transients. Applying this concept to the field, this will drastically reduce the frequency of unexpected shutdown at the existing Westinghouse1000 type NPPs.

REFERENCES

[1] CRI, KHNP(2012), Improvement of success rate for WH type full load dropout

[2] KHNP(2016), Hanbit unit 5,6 system manual

5분과

제염해체 (Oral)

Performance Evaluation of Decontamination Foam According to the Characteristics of Surface Contamination

Wangkyu Choi*, Seungeun Kim, Chonghun Jung, Seonbyeong Kim, and Bumkyoung Seo
Korea Atomic Energy Research Institute, 111, Daedeok-daero 989beon-gil, Yuseong-gu, Daejeon, Korea
*nwkchoi@kaeri.re.kr

1. Introduction

Foam decontamination process has a potentially wide application in the removal of contaminants from large components with complex shapes or large area or large volumes. This process can be applied to any direction regardless of walls, floors and ceilings, and basically it has the advantage of generating less secondary wastes[1]. However, there is a disadvantage that the decontamination factor (DF) is relatively low only by one batch application[2]. In order to improve the DF of the foam decontamination process, many attempts have been made to introduce various chemical decontamination agents into the foam and enhance the contact time of the foam between the chemical decontamination agent and the contaminated surface by introducing a viscosifier to improve the stability of the foam[1,3].

In this study, the effects of periodically supplied new decontamination foam on the decontamination performance was investigated. In addition, the decontamination performance of the foams containing various chemical components was evaluated according to the characteristics of surface contamination.

2. Materials and Methods

2.1 Preparation of Decontamination Foam

The decontamination foams used in this study were prepared by combining surfactants, silica nanoparticles, inorganic acids such as HNO_3 and HF, and oxidizing agents such as Ce(IV).

In order to evaluate the decontamination performance of the contaminated specimens, various decontamination foams prepared are summarized in Table 1.

2.2 Performance Test with Decontamination Foam

Decontamination performance tests were carried out by applying various decontamination foams as shown in Table 1 to the simulated specimens contaminated with non-fixed particles and oil, and the specimens with fixed corrosion oxide films.

Table 1. Composition of Various Decontamination Foams

Foam Type	Chemical Composition
F-1	1 wt% EM100[1] + 1 wt% M-5[2]
F-2	1 wt% EM100 + 1 wt% M-5 + 2M HNO_3
F-3	1 wt% EM100 + 0.5M HF + 2M HNO_3
F-4	1 wt% TBS[3] + 1 wt% M-5 + 0.1~0.5M Ce(IV) + 2M HNO_3

1) ELOTANT Milcoside 100, C08-10 alkyl polyglucoside
2) CAB-O-SIL® M-5 Fumed Silica Nanoparticle
3) Zonyl® TBS, Anionic fluorosurfactant,

Particulate contaminated specimens and oil contaminated specimens were prepared as non-fixed contaminated specimens. Simulated particulate contamination specimens were prepared by coating a mixture of Eu_2O_3 and fluorescent powders on a 20x20 mm stainless steel surface. Simulated oil contamination specimens were prepared by coating a mixture of TBP as an oily contaminant with the fluorescent power on the stainless steel surface. Specimens coated with $NiFe_2O_4$ and $FeCr_2O_4$ were used as fixed contamination specimens. The $NiFe_2O_4$ coated specimens having a thickness of 500 nm were prepared using the E-beam evaporator system. Specimens with $FeCr_2O_4$ film having a thickness of *ca.* 10 μm formed on the surface of stainless steel 304 were prepared in an autoclave.

The decontamination performance test was carried out in an experimental apparatus consisting of a foam solution make-up tank, a decontamination foam generator and a foam filling column. After the simulated contaminated specimens were placed in the foam filling column followed by filling with the decontamination foam through the foam generator. As the drainage is continuously generated from the liquid film of the filled foams, the solution accumulated at the lower end of the filling column at intervals of 20 minutes is recirculated to the foam solution make-up tank and a new decontamination foam prepared via a

foam generator was fed to the bottom of the foam filling column. As a result, the dry foam at the top of the filling column is pushed out and filled with new foam. This is called 'push-blowing' cyclic foam filling process.

The decontamination performance of the particulate and oil contaminated specimens was evaluated by analyzing the state of the surface and the removal of the contaminants using the UV lamp before and after applying the decontamination foam to the specimens. Similarly, the decontamination performance of the corrosion oxide film contaminated specimens was evaluated by measuring weight loss before and after decontamination.

3. Results and Discussion

The decontamination performance was improved by keeping the physicochemical properties of the decontamination foam substantially constant by applying 'push-blowing' cyclic foam filling process.

In the removal of contaminants from the simulated specimens by the decontamination foam, non-fixed contamination consisting of a mixture of Eu_2O_3 particles, TBP oil and fluorescent powder was completely removed within 4 hours by neutral decontamination foam, F-1 containing no acids or oxidants.

For the removal of the fixed contaminants, the $NiFe_2O_4$ film coated on the stainless steel specimen at 500 nm thickness was completely removed within 2 hours by acid decontamination foam, F-3 mixed with nitric acid and hydrofluoric acid. On the other hand, only *ca.* 3% of the $NiFe_2O_4$ was removed during the same time period by acid decontamination foam, F-2 containing only nitric acid as shown in Fig. 1.

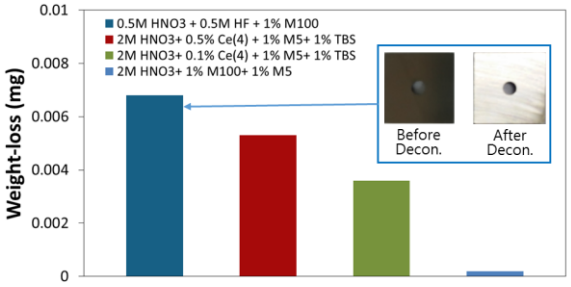

Fig. 1. Comparison of Foam Decontamination Performance of $NiFe_2O_4$ coating specimens.

$FeCr_2O_4$ film with a thickness of 10 ㎛ produced in the autoclave was completely removed within 2 hours by oxidative decontamination foam, F-4 containing Ce(IV) as an oxidant, but almost not by acidic decontamination foam, F-3 as shown in Fig. 2. It was found that the corrosion oxide film containing chromium can be removed by the oxidative decontamination foam while it was difficult to remove by the acidic decontamination foam.

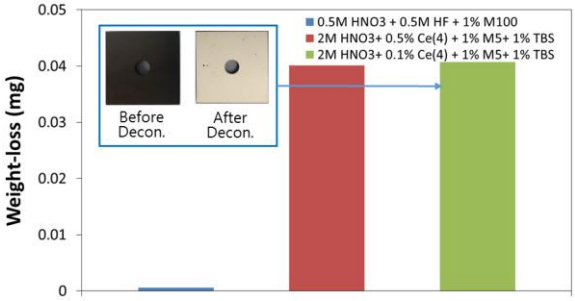

Fig. 2. Comparison of Foam Decontamination Performance of $FeCr_2O_4$ coating specimens.

4. Conclusion

The foam decontamination performance was improved by applying 'push-blowing' cyclic foam filling process. It was found that the application of the appropriate decontamination foam is required depending on the characteristics of contamination. Further study is needed to optimize the condition of foam decontamination process.

ACKNOWLEDGEMENT

This work was supported by the Nuclear R&D Program (2017M2A8A5015144) funded by Ministry of Science, ICT & Future Planning.

REFERENCES

[1] C. Dame, C. Fritz, O. Pitois, and S. Faure, "Relations between physicochemical properties and instability of decontamination foams", Colloids Surf., A, 263, 210-218 (2005).

[2] EUNDETRAF II, "European nuclear decommissioning training facility", project N°: FI6OCT-2003-509070, SCK·CEN, Belgium (2006).

[3] I.H. Yoon, C.H. Jung, S.B. Yoon, S.Y. Park, J.K. Moon, and W.K. Choi, "Effect of silica nanoparticles on the stability of decontamination foam and their application for oxide dissolution of corroded specimens", Ann. Nucl. Energy, 73, 168-174 (2014).

Study of Chemical Separation Methods for the Treatment of a Uranium Containing Process Effluent

Maeng-Kyo Oh[1,2], Keun-Young Lee[2*], Richard I. Foster[2], Kwang-Wook Kim[2], and Chang-Ha Lee[1*]
[1]Yonsei University, Department of Chemical and Biomolecular Engineering, Seoul, Republic of Korea
[2]Korea Atomic Energy Research Institute, Daedeok-daero989ben-gil 111,Yuseong-gu, Daejeon, Republic of Korea
* lky@kaeri.re.kr, leech@yonei.ac.kr

1. Introduction

A chemically-complex solid uranium waste awaits a management and disposal strategy. A process has been proposed for the treatment of such a waste.[1] However, owing to the chosen treatment process, a large volume of secondary liquid waste is generated. The treatment of this secondary waste forms the focus of this study.

The effluent contains approximately 400 ppm uranium which must be removed to below free release level. The effluent also contains a range of impurities, the most significant of which is Si at 24,000 ppm. The difference in solubility between silicon and uranium complexes could be used for the mutual separation of silicon from solution by precipitation as silica (SiO_2). Separation of the in-active silicon would reduce the final volume of secondary wastes requiring final disposal. A second removal step for the removal of residual uranium contained in the liquid waste from the first stage is also required. The addition of peroxide to form insoluble uranium peroxide precipitates offers promise. If UO_4 precipitation can be used to effectively remove uranium from the process effluent to less than 1 ppm, then the effluent can be safely discharged.

2. Materials and Methods

2.1 Si-U Separation experiment.

All experiments were conducted with samples of the real process effluent. For the purpose of selective silicon precipitation uranium was retained in solution as the soluble uranyl-peroxo carbonate ($UO_2(O_2)(CO_3)_2^{4-}$) species.[2] Sodium carbonate solution was added to the effluent before pH adjustment by H_2SO_4 to pH 12. Hydrogen peroxide was then injected in excess; this was followed by the further addition of H_2SO_4 in-order to reduce the pH to below 9 thus inducing selective silicon precipitation as SiO_2. The precipitates were separated from solution, washed and then dried for 24hrs. Residual uranium activity was analyzed using gamma and alpha spectrometry. In the event of a uranium activity higher than the free release level, the silica was re-dissolved and re-precipitated.

2.2 Uranium peroxide precipitation experiment

Initially a simulated process effluent solution was used. A volume of uranium solution, uranyl nitrate hexahydrate ($UO_2(NO_3)_2{\cdot}6H_2O$; UNH) was added to a sodium nitrate solution resulting in uranium concentrations of 1000 ~ 10 ppm. Hydrogen peroxide (H_2O_2, 30%) was injected into the simulated solution to reach a 1M followed by pH adjustment to 3~4. Optimized process conditions were applied to the real effluent. Uranium concentrations were analyzed by ICP-MS and UV-spectrophotometry. Solid analysis was done using SEM, TEM-EDS and XRD.

3. Result and discussion

3.1 Si-U separation experiment

Fig. 1 shows the residual radioactivity of the silica. A single purification step reduces the activity by 46% to below 1Bq/g. Additional purification steps reduces the activity further, however, achieving only an additional 20% reduction after five purification cycles is not deemed economical.

In order to reduce the residual activity further, while limiting the number of purification cycles, different washing conditions were tested to remove residual uranyl ions from the silica surface. If an acidic solution is used for washing, the residual activity is reduced to levels akin to four purification cycles (Fig. 1 & 2). This is credited to a change of the silica surface zeta potential as H^+ concentration rises releasing bound UO_2^{2+}.

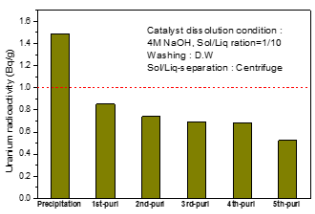

Fig. 1. Uranium radioactivity of precipitates after application of existing method.

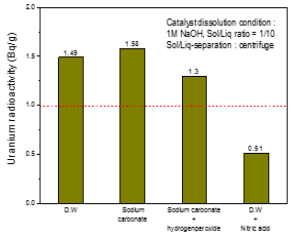

Fig. 2. Uranium radioactivity of precipitates with different washing solution.

3.2 Uranium peroxide precipitation experiment.

Fig. 3 shows the change in uranium concentration with and without mixing after setting initial uranium concentrations in the simulated effluent. The higher initial uranium concentration, the faster UO_4 precipitated. The residual uranium concentration in solution was confirmed to be less than 1 ppm. However, at lower initial uranium concentrations, about 10ppm, the precipitation of UO_4 hardly occurred. At every concentration tested the precipitation rate was faster while stirring. When the initial concentration is high or the solution is mixed, the number of particle collisions increases, so nucleation rapidly occurs leading to particle growth and thus effective removal of uranium.

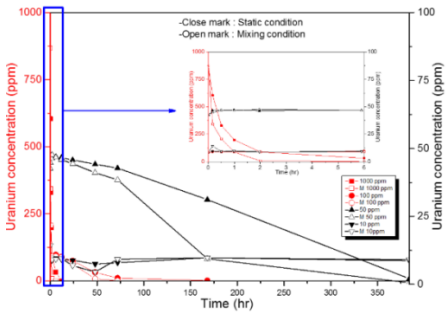

Fig. 3. Variation of residual uranium concentration with different initial concentrations.

The uranium concentration in the real process effluent was about 100 ppm. Impurities such as Si, Sb, Fe were measured at several ppm. The rate of UO_4 precipitation from the real process effluent was 2~3 times faster than simulated experiment. Fig. 4 shows the results of solid phase and particle size analysis of the formed particles using SEM-EDS and a particle size analyzer. The pure UO_4 precipitate formed spherical and very small particles, but UO_4 particles formed in the real process effluent were larger and not perfectly spherical. In addition, the result of EDS analysis showed that Si, Fe, Sb and other impurities in solution were co-precipitated together with UO_4 particles. Thus the particle size and precipitation rate were affected by the presence of the impurities.

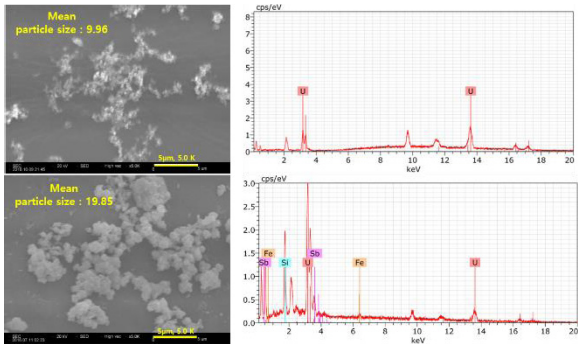

Fig. 4. PSA and SEM-EDS results of precipitated UO_4 particles.

4. Conclusion

This study has established the feasibility of chemical separation methods for the treatment of a uranium containing effluent. Separation of inactive silicon reduces the final volume of secondary wastes requiring disposal. A single purification cycle followed by acid washing reduces residual activity to below environmental release level. A second step by peroxide addition, leading to the formation of insoluble uranium peroxide, is shown to effectively remove uranium from the process effluent allowing discharge the environment.

5. Acknowledgement

This work was supported by the National Research Foundation of Korea grant (No. NRF-2017M2A8A5015147) funded by Ministry of Science and ICT.

REFERENCES

[1] K.W. Kim, M.K. Oh, J.M. Kim, M.J. Kim, R.I. Foster, K.Y. Lee, “Volume reduction of uranium catalyst waste used for production of acrylonitrile”, MRS2017-Sci. (90), Oct 12, 2017, Sydney.

[2] K.W. Kim, E.C. Jung, K.Y. Lee, H.R. Cho, E.H. Lee, D.Y. Chung, “Evaluation of the behavior of uranium peroxocarbonate complexes in Na−U(VI)−CO3−OH−H2O2 solutions by raman spectroscopy”, J.Phys. Chem. A, 116, 12024−12031, (2012).

[3] K.Y. Lee, M.K. Oh, J.M. Kim, E.H. Lee, K.W. Kim, D.Y. Chung, J.K. Moon, J.W. Choi, “Effect of impurity ions on the precipitation property of uranyl peroxide”, 6th asia-pacific symposium on Radiochemistry, Sep 17-20, 2017, Jeju

Dismantling Scenario of Reactor Vessel (RV) in KORI 1

Kwang-Soo Park*, Hae-Woong Kim, Gyu-Ho Jang, Hee-Dong Sohn, and Jin-Woo Choi
Doosan Heavy Industries & Construction, 22, Doosan-Volvo-ro, Seongsan-gu, Changwon, Gyeongnam, Republic of Korea
*kwangsoo.park@doosan.com

1. Introduction

Kori 1 has not been operated since it was shut down in 2016. The contaminated components in reactor building will be dismantled after 2022 or 2023. The dismantling of Kori 1 is the first to be dismantled in Korea. Also there is no dismantling experience. So we need to develop core dismantling technology.

In order to solve the problem, we are performing the dismantling technology development of RV using the government fund. We has developed dismantling scenario of RV in Kori 1.

2. Dismantling scenario for RV of Kori 1

2.1 RV of Kori 1

The main dimensions of RV in Kori 1 shows in table 1. The outer diameter of RV is 3994mm. The maximum thickness is 480mm. Due to this thickness of RV, a suitable cutting method is required. The weight of RV is 180 ton. The inside wall and the flanges are clad in stainless steel and its thickness is about 6mm.

The RV is installed in cavity, which is concrete structure. The Fig. 1 shows the installed state.

Table 1. The main dimensions of RV

Items	Size (mm)
Height	9718.1
Outer diameter of shell	3525.3
Inner diameter of shell	3352.8
Max. thickness	480
Radius of bottom head	1685.8

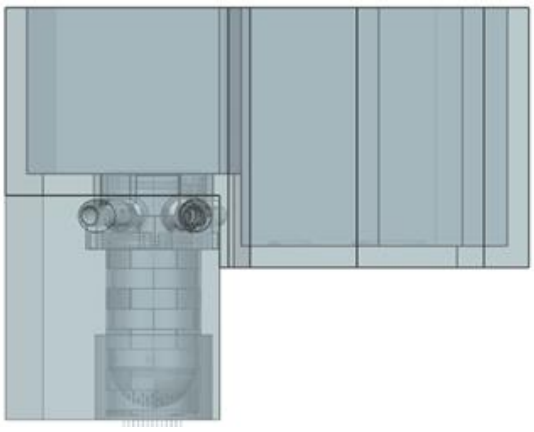

Fig. 1. Reactor and Cavity.

2.2 Dismantling Scenario of RV in Kori 1

The developed Kori 1 RV dismantling scenario is basically to cut by raising the RV in the air environment using the thermal cutting method. This dismantling of RV in an air environment is a proven technology. In overseas application, there are Zion[1], Stade[2] NPP etc.

The process of RV dismantling for Kori 1 shows in Fig. 2.

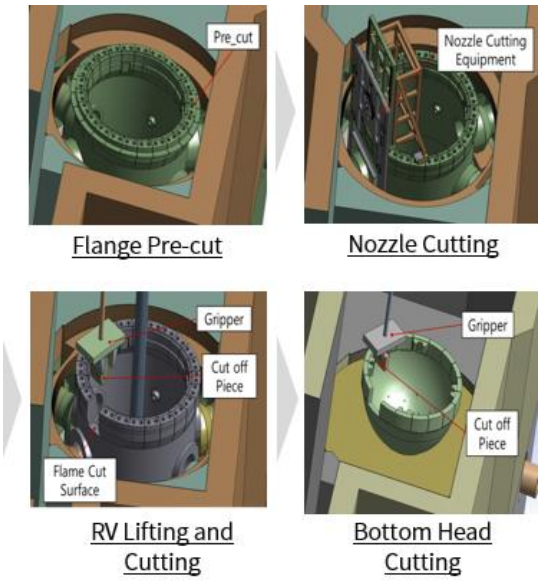

Fig. 2. Process of RV Dismantling.

The pre-cut process using the mechanical cutting method is for cutting the stainless steel cladding on the flange of RV. And then nozzle cutting of RV is performed using the mechanical cutting method. Once the preparations for lifting the RV are completed, dismantling of RV shell is performed using the thermal cutting method. When the RV shell dismantling is finished, the rigging tool is disassembled and the RV bottom head is dismantled. Finally, the insulation structure is dismantled using the mechanical cutting method.

2.3 Review the Risk of RV Dismantling Process

We reviewed the risk factors in the developed process. The risks are radiological, chemical, physical & biological factor. The chemical & biological risks are expected to be absent in the developed process. Therefore we should consider radiological & physical hazards.

The physical hazards are expected to follow the industrial safety regulations. However radiological hazards must take into account the effects on the public as well as the operators. So the consideration is the diffusion of aerosol during the thermal cutting. In order to prevent the condition, the special ventilation equipment is required, and this should be connected to the NPP ventilation system.

3. Conclusion

We has developed dismantling scenario of RV in Kori unit 1. This dismantling scenario for RV of Kori unit 1 is proven technology and method. In the course of developing the dismantling scenario, we considered safety aspects such as ventilation, process simplification and so on.

In the future, we plan to upgrade dismantling process by reviewing safety aspects while the developing technology. Also for the safety reasons, when the operation of ventilation system is stopped, thermal cutting operation is stopped at the same time.

REFERENCES

[1] A.Loeb, D.Stanke, “Decommissioning of the reactor pressure vessels by remote controlled thermal cutting segmentation facilities of the Zion nuclear plant at Zion”, WM2016 Conference, 2016.

[2] A.Loeb,D.Stanke, “Decommissioning of the reactor pressure vessel and its peripheral facilities of the nuclear power plant in Stade”, WM2011 Conference, 2011.

Characteristics of and Implications From Radioactive Discharge Data Before and After Post-Shutdown of Nuclear Power Plants in the United States

Na Yoon Choi and Jae Hak Cheong*
Kyung Hee Univ, Engineering, Deokyoung Daero 1732, Giheong gu, Yongin si, Gyeonggi do, Republic of Korea
*jhcheong@khu.ac.kr

1. Introduction

Nuclear power plants after permanent shutdown no longer use nuclear fuel, so It has a different composition in radioactive effluents than operation phase. US NRC (United States Nuclear Regulatory Commission) Regulatory Guide 1.184 revision 1 provides the regulatory position on decommissioning of nuclear power plants. It is recommended that radiological impacts - including radioactive effluents - should be evaluated for nuclear power plants in transient and decommissioning phase [1]. In addition, the OECD / NEA Radioactivity Characterization and Decommissioning Group has mentioned that during transient phase, nuclear power plants should be assessed for the radiological impacts in performing decommissioning activities caused by radioactive effluents for normal and accidental conditions in its report [2]. In general, the radioactive effluents of a nuclear power plants under operation is monitored at all times by Sampling & Monitoring with radioactivity alarm set points for each radionuclide and in US, it should be reported in the Annual Radioactive Effluents Release Report (ARERR) by 10 CFR 50.36a (a) (2) and Technical specification for each nuclear power plants [3]. This is also valid after permanent shutdown [3]. Before the decommissioning is completed, appropriate monitoring systems should be established to assess the radiological impacts, such as the offsite dose and the radioactivity concentration of the radioactive effluents the that composition is changed by performing the decommissioning activities. In addition, to reduce the risk of activity after a permanent shutdown, the characteristics of the changed radioactive effluents after the permanent shutdown should be identified early. This can be effected as a factor in determining decommissioning activity. In this study presents the implications by analyzing the annual characteristics of the radioactive effluents for the three nuclear power plants which is under the transient/decommissioning phase in US

2. Method

Annual release rate and concentrations and the resulting doses of commercial nuclear power plants in US, can be found in ARERR. In this study, analyzing the characteristics of radioactive effluents before and after the permanent shutdown by using ARERR data of transient/decommissioning phase NPPs and suggesting the implications for decommissioning activities after the permanent shutdown of nuclear power plants perspective in radioactive effluents.

The NPPs to be evaluated are San Onofre Unit 2 & 3, Kewaunee, and Crystal River Unit 3 in the US. The radioactive effluent to be evaluated is the gas and liquid effluent released from NPPs. The evaluation period is from 2006 to all years after the permanent shutdown of each NPPs.

The evaluated subject NPP and its permanent shutdown dates are mentioned in Table 1.

Table 1. Subject Reactor and Shutdown Date

No.	Reactor Name	Unit	Shutdown Date
1	Crystal river	3	2009
2	Kewaunee		2013
3	San Onofre	2&3	2013

3. Results

3.1 Analysis the Aspect of Gaseous Radioactive Effluents of Undergoing Decommissioning NPPs

The gaseous radioactive effluents of the Crystal River Unit 3, Kewaunee and San Onofre Unit 2 & 3 nuclear power plants are plotted in Fig. 1. Tritium emissions are not significantly affected by permanent shutdown, but large amounts are continuously released. However, in the case of Fission Product or Activation Product gas, it is seen that the amount is rapidly decreased due to the fact that the fuel is not irradiated after the permanent shutdown. Particulates gas shows a variety of emission patterns or not emitted after permanent shutdown.

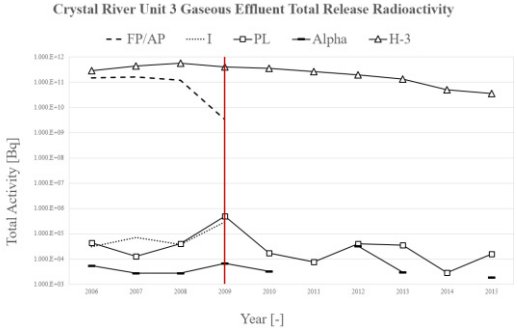

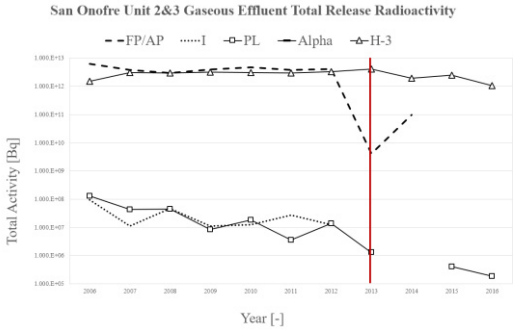

Fig. 1. Total Radioactivity Release Data from 2006 of for Crystal River Unit 3 and San Onofre Unit 2&3 Gaseous Radioactive Effluents.

3.2 Analysis the Aspect of Liquid Radioactive Effluents of Undergoing Decommissioning NPPs

The liquid radioactive effluents of the Crystal River Unit 3, Kewaunee and San Onofre Unit 2 & 3 nuclear power plants are plotted in Fig. 2. Liquid radioactive effluents show more variation than gas effluents. In the case of Tritium, unlike Tritium in gas effluents, emissions continue to decrease after permanent shutdown. The Fission product and Activation product also tends to reduce emissions after a permanent shutdown due to the fact that the fuel is not irradiated.

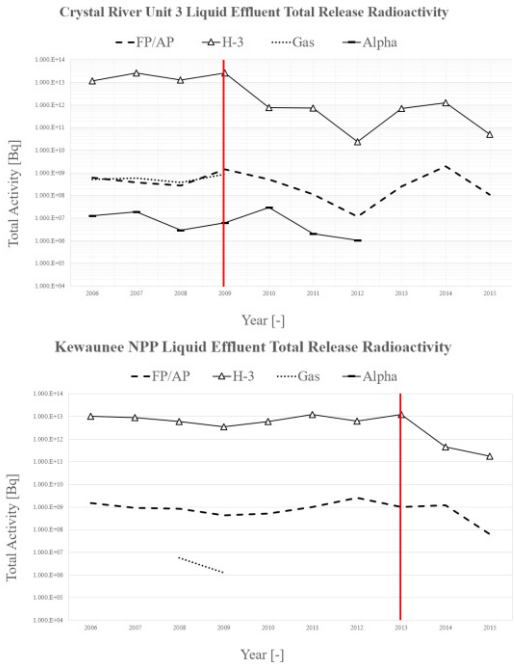

Fig. 2. Total Radioactivity Release Data from 2006 of for Crystal River Unit 3 and Kewaunee Gaseous Radioactive Effluents.

It can be predicted that it will reduce the amount of annual radioactivity release rate of liquid radioactive effluents by for such reasons. Also, it can be expected that the dilution water flow rate for diluting the radioactive effluent will also decrease. As a result of analyzing the flow rate, dilution water flow rate and dilution factor value of the three nuclear power plant, the discharge flow rate of the radioactive effluent decreased after the permanent shutdown. Dilution water flow rate and dilution factor also decreased. There are two reasons why the dilution water flow rate decreases. First, intentional activity can be expected to reduce the dilution water flow in anticipation of a decrease in annual radioactivity emissions of the radioactive effluent. Secondly, it can be expected that the provided dilution water flow rate is reduced. In most cases, the flow rate of the cooling water in the condenser is in charge of the dilution water flow rate. The cooling water in condenser system is decreased by the unnecessary of cooling the system after permanent shutdown. So, the dilution water flow rate can be decreased. Monitoring alarm set point is determined by the value of effluent flow rate and dilution water flow rate. Therefore, the value of the monitoring alarm set point of the radioactive effluent in the NPP during operation may not be able to applicable after the permanent shutdown.

4. Conclusion

In this study, analyzing the annual radioactive effluent trends for three permanent shutdown NPPs (Kewaunee, San Onofre Unit 2 & 3, Crystal River Unit 3) in US. Fission product and Activation product decreases for both gaseous and liquid radioactive effluents. In the case of Tritium, almost constant amount is released regardless of the permanent shutdown in gaseous radioactive effluent. But for liquid radioactive effluents, it shows a decreasing trend, similar with the Fission product and Activation product. The flow rate and the dilution water flow rate of the liquid radioactive effluent decrease after the permanent shutdown. As a result, there is a possibility that the value of the monitoring alarm set point of the radioactive effluent in the NPP during operation is cannot be applicable after the permanent shutdown. Therefore, it may be necessary to establish monitoring alarm settings that take into account the information of the gaseous and liquid radioactive waste management system which is different with the operation phase.

REFERENCE

[1] U.S. NRC, Decommissioning of Nuclear Power Reactors, Regulatory Guide 1.184, Revision 1, October 2013.

[2] OECD/NEA, Ivan Rehak, Radiological Characterisation for Decommissioning of Nuclear Installations, September 2013.

[3] U.S. NRC, Domestic Licensing of Production and Utilization Facility, Code of Federal Regulations Title 10, part 50, 2015.

Establishment of DF(Decontamination Factor) Target for Kori-1 Full System Chemical Decontamination

Dooho Lee
KHNP Central Research Institute, 1312-70, Yuseong-daero, Yuseong-gu, Daejeon, Republic of Korea
dooho.lee@khnp.co.kr

1. Introduction

Full system decontamination (FSD) will be conducted in preparation for decommissioning and dismantling Kori-1. This paper deals with DF (Decontamination Factor) target for Kori-1 FSD campaign based on the recent contact dose rate measurements.

2. Methodology

2.1 Radiological Survey

Contact dose rates at 21 points of Kori-1 were measured by Teletector (Model No. 6112) on August 3, 2017. In addition to the contact dose rate measurement, relative radiological contributions of radionuclides to dose rates were assessed by gamma spectrometry detector at the same time.

2.2 Prediction of Future Dose Rate Trends

Dose rate trends of Kori-1 were predicted by the equation below. In this prediction, no additional source term for radionuclides was assumed because Kori-1 is now in the permanent shutdown phase.

$$D_i(t) = D_0\left(\sum \frac{C_n}{100} e^{-\lambda_n t}\right) \quad (1)$$

Where, $D_i(t)$: Predicted Dose Rate (mSv/hr)
D_o : Measured Dose Rate (mSv/hr)
C_N : % Contribution to Dose Rate of Radionuclide N
λ_n : Decay Constant (day^{-1})
t : Time (day)

3. Result

The measured contact dose rates are presented in Table 1. During the measurement, all the systems except pressurizer spray line were filled with water. At the same time with measurement of contact dose rates, radiological contributions to measured dose rates at each location were also assessed. In this assessment, as expected, the Co-60 was found to be the main contributor to measured dose rates at the time of measurement.

Based on the relative contribution to dose rate of main radionuclides, future dose rates were projected assuming that Kori-1 FSD campaign will be performed in the first quarter of 2019. The predicted dose rates are also given in the Table 1 (The target date to prediction is set to January 1, 2019)

Table 1. Measured and Predicted Dose Rate

Survey Point		Dose Rate (uSv/hr)	
		Measured	Predicted
Loop 1	HL1	800	454
	CL1	700	397
	C2	1,000	542
	C5	250	158
	S1	120	68
	S2	70	40
Loop 2	HL1	700	397
	CL1	1,000	567
	C2	600	343
	C5	200	126
	S1	60	34
	S2	50	28
PZR	Surge	500	333
	Spray	800	481
CVCS	Letdown	900	379
	Charging	30	12
	Orifice	700	421
RHR	Piping	150	75
	Piping	100	50

The goal of FSD is normally defined by establishing a DF target. In order to comply with Nuclear Safety Act Amendments of Korea, radiation exposure of plant workers should be limited to 100 mSv during 5 years. So FSD target for Kori-1 campaign is established to restrict the radiation exposure to allowable limits in a conservative way.

For this purpose, we assume that annual working hour of plant workers be 2,080 hours.

The overall DF target is set up by just averaging DF values at each surveyed point to comply with limits specified in the Nuclear Safety Act of Korea based on the projected dose rate values (namely, 9.6 uSv/hr). From this calculation, we establish the target of DF for Kori-1 FSD campaign to be 30 on the whole.

4. Conclusion

The following conclusions can be made from this study.

1) Contribution of Co-60 to measured dose rate is verified to be dominant at this time of Kori-1.
2) Large variations in the surface isotopic composition were observed from different points in Kori-1.
3) The DF target of 30 was reasonably established for Kori-1 FSD campaign based on the projected dose rates.

Formation of Meta-Ankoleite for the Decontamination of Uranium Bearing Effluents: From Laboratory to Pilot Plant

Richard I. Foster*, Kwang-Wook Kim, Maeng-Kyo Oh, Min-Jeong Kim, and Keun-Young Lee
Korea Atomic Energy Research Institute, 111, Daedeok-daero 989beon-gil, Yuseong-gu, Daejeon, Republic of Korea
*rifoster@kaeri.re.kr

1. Introduction

In a number of recent publications, we have characterized a uranium containing spent catalyst waste and detailed a process for the treatment of this waste.[1-3] As part of the process the formation of Meta-Ankoleite ($KUO_2PO_4.4H_2O$), during one of two precipitation steps, is used to remove uranium and decontaminate the effluent. Previously, our Meta-Ankoleite precipitation studies have focused on laboratory scale testing (10 – 100 mL).[3] In this paper, we wish to communicate the steps taken and results obtained since going from the Laboratory to Pilot Plant (1000 L), via Bench Scale (1 – 3 L), and discuss the problems and challenges faced. A full description of the waste, steps taken for treatment and proposed Meta-Ankoleite formation method can be found in pervious publications.[1-3]

2. Experiment

2.1 Materials

All materials were used as received. For laboratory and bench scale tests, mono-potassium phosphate (MKP, KH_2PO_4, 99.5%) was obtained from SHOWA, KOH (85%) from JUNSEI. For the Pilot Plant, MKP (90%) and KOH (90%) were used. In all cases nitric acid (65%) was obtained from Merck. All ICP dilutions were performed with deionised water (18 MΩ). Full details of the target effluent are in ref 1-3.

2.2. Method

To a known volume of effluent MKP was dosed while being mixed resulting in a total [PO_4^{3-}] of between 1 – 4 mM. The solution was then adjusted to the target pH by the addition of KOH. Stirring was maintained throughout the experiment. The resulting suspended Meta-Ankoleite was removed via a filter press. The solution was then passed through a pleated filter before "final release". Solution analysis took place before and after precipitation and after both filters. Analysis consisted of ICP-OES, TSS, NTU, PSA, pH, EC and ORP measurements. SEM/EDS, XRD and XRF analysis of the formed solids were also performed.

3. Results and discussion

3.1 Optimal laboratory conditions

At the outset of this project phosphate was dosed in the form of MH_2PO_4 (M = Na, K or NH_4). According to reported solubilities, the NH_4 counter ion should yield the greatest uranium removal, followed by K and Na. This was confirmed to be the case although the difference between the lowest [U] was only 11, 18 and 38 ppb for NH_4, K and Na, respectively, at pH 6. Due to concerns with the decomposition of $NH_4(UO_2)(PO_4)$ during thermal solidification the K form, Meta-Ankoleite, was chosen. Dosage and kinetics measurements confirmed a concentration of 1 mM for a period of 60 minutes was sufficient for the removal of uranium (Table 1).[3]

Table 1. Optimized laboratory conditions for Uranium removal

pH	Ion	Dosage	Stir speed	Time	Final [U]
6.25	K^+	1 mM	100 rpm	60 min	20 ppb

3.2 Bench scale testing and process refinement

The transition to bench scale was not without its problems. Initial tests revealed that the optimized laboratory conditions traversed well. However, the effluent used had aged which was unrepresentative of the real system which does not allow for a prolonged aging period (> 24 hr). Subsequent tests with fresh effluent revealed a slower rate of kinetics. It has been concluded that effluent aging allows for the formation of particulate Sb-oxides which aid in the rapid removal of uranium via seeding. Regardless, all test conditions lead to a removal of uranium to below the release limit; although an increase of phosphate dosage to 2mM was found optimal.

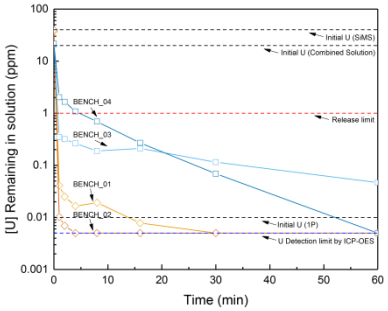

Fig. 1. Uranium removal kinetics at bench scale. Bench_01 and Bench_02 performed with aged effluent at a [PO_4^{3-}] of 1 and 2 mM, respectively. Bench_03 and Bench_04 performed with fresh effluent at a [PO_4^{3-}] of 1 and 2 mM, respectively.

3.3 Pilot Plant

3.3.1 Meta-ankoleite formation. Regulatory restrictions prohibited the use of the real waste catalyst during pilot scale tests. In order to test the whole process a simulant was proposed for the silica precipitation stage; the resulting effluents were to be

treated at the phosphate precipitation stage (**Table 2**). A 1000 L stainless steel tank with a two tier quad-bladed stirrer was used. The incoming effluent totaled approx. 220 L, containing 28 ppm U.

Table 2. Pilot plant simulant effluent (ppm)

Contaminant:	U	Si	Sb	Mo	Fe	Al	Mg
Initial simulant	200	20,000	1800	300	30	30	20
Effluent	28	107	38	44	6	4	20

A total phosphate concentration of 2 mM was used. The pH was adjusted to 6.2 which drifted only slightly to 6.4 over 1 hour. The formation of lemon-yellow precipitates, also indicated by a change in turbidity, was almost instantaneous. The formed precipitates were confirmed to be meta-ankoleite by XRD and chemical analysis (**Table 3**). The analysis results matched well with the previous smaller scale tests, thus indicating that the process can be scaled.

Table 3. Meta-ankoleite chemical analysis

	U	K	P	Si	Sb	Mo	Fe	Al	LE
Pure	58.8	9.6	7.7	-	-	-	-	-	23.7
Simulant	14.5	7.7	1.2	2.7	15.5	-	1.1	-	40.0

The precipitates were allowed to settle for one hour before filtration, although settling was seen to have occurred within 10 min by visual inspection. While the particles are small, approx. 10 µm [3], they possess a high density resulting in fast settling times.

3.3.2 Filtration. Working at pilot scale gave rise to the opportunity to test a number of filtering scenarios. Filtering was done with a filter press, with and without a filter aid, and also via a pleated filter. While the use of no filter aid afforded the fastest filtration rates these quickly retarded due to filter membrane blockages. The use of a filter aid affords greater filtration rate consistency. Opting to only filter the supernatant yielded the best filtration rate. Results indicate a single pass through a pleated filter is sufficient (**Table 4**). Allowing the particles to settle prior to supernatant filtering is the preferred method.

Table 4. Summary of effluent U concentrations after filtration.

		Time (minutes)					
Filter Press		**1**	**2**	**4**	**8**	**16**	**30**
Without filter aid	Bulk	5.8	2.7	0.9	0.2	0.1	0.09
	Supernatant	1.2	1.2	0.8	0.8	-	-
Filter aid	Bulk	2.8	1.8	0.7	0.4	0.4	0.07
	Supernatant	0.4	0.3	0.3	0.3	-	-
Pleated filter		1st		2nd	3rd		4th
	Supernatant	0.12		0.10	0.07		0.06

3.3.3 Process comparisons. The physical and chemical properties of the treated effluents and solids are summaries in table 5. **Green** values meet release criteria while **Red** values need to be addressed further. **Black** values have no direct regulatory consequence. Principally, all three experimental scales meet the release requirement with regard to uranium. All other parameters are similarly comparable indicating a consistency in the process. A removal method for the residual TSS and [PO_4^{3-}] is required with both precipitation, by $FeCl_3$, or ion-exchange, for PO_4^{3-}, being actively considered.

Table 5. Summary of solution and solid analysis

	Measurement	Lab scale	Bench scale	Pilot Plant
Solution	[U] Initial (ppm)	20	20	28
	[U] Final (ppb)	**20**	**5**	**63**
	DF[1]	1111	4000	444
	[P] Final (ppm)	**16**	**18**	**50**
	TSS[2] (ppm)	**282**	**194**[3]	-
	Turbidity (NTU)	**0.2**	**0.5**[3]	**0.5**[3]
	Particle size (µm)	63.1	53.8	10.0
	pH	**6.00**	**6.19**	**6.4**
	EC[4] (mS/cm)	-	58	-
	ORP[5]	-	**514**	-
Solid	Floc volume (mL/L)	16.7	12.5	-
	Solid volume (mL/L)	0.08	0.10	-
	VRF[6]	12540	10000	-

4. Conclusions

Over three experimental scales the removal of uranium via meta-ankoleite formation has been tested. Both laboratory and bench scale tests made use of the real effluent which was effectively decontaminated. Due to regulator restrictions the real waste could not be used at the pilot plant, thus limiting the pilot plant tests to a simulant. Nonetheless, the results were in good agreement with previous smaller scale tests. It was therefore accepted that the removal of uranium via the formation of meta-ankoleite was successful over all three tested experimental scales. The complete process is now in the process of being up-scaled to a commercial scale plant. A PO_4^{3-} removal method is still required, with $FeCl_3$ dosing preferred.

ACKNOWLEDGEMENTS

This work was supported by the National Research Foundation of Korea (NRF) grant (No. NRF-2017M2A8A5015147) funded by Ministry of Science and ICT.

REFERENCES

[1] K. W. Kim *et al.*, "Development of a Treatment Process and Immobilization Method for the Volume Reduction of Uranium-Bearing Spent Catalysts for Final Disposal", In Press, (2018).

[2] K. W. Kim *et al.*, "Volume reduction of uranium catalyst waste for final disposal", Eurasia 2018 Waste Management Symposium Proceeding, Istanbul, (2018).

[3] R. I. Foster *et al.*, "The Removal of Uranium via Phosphate Addition for the Treatment of Uranium Laden Effluents", In Press, (2018).

Development of Testbed for Advanced Remote Dismantling System

Dongjun Hyun*, Ikjune Kim, Sungmoon Joo, Jonghwan Lee, and Shin Young Kang
Korea Atomic Energy Research Institute, 989-111 Daedeok-daero, Yuseong-gu, Daejeon, Republic of Korea
*dongjunn@kaeri.re.kr

1. Introduction

The advanced remote dismantling system is a remote dismantling system incorporating advanced technologies such as spatial perception based teleoperation technology and high payload robot arms and underwater laser cutting technology. In the field of nuclear dismantling, conventional equipment had to be replaced at every time a target structure was changed during the process stage. The replacement work has been a major cause of increased time, cost and risk of dismantling processes. However, thanks to advanced technologies mentioned above, the advanced remote dismantling systems could handle all the processes without equipment replacement. A seamless remote system was proposed by the author et al. with a similar concept [1].

This paper proposes a testbed to develop spatial perception based teleoperation technology and control framework. The testbed consists of a 3d scanner, robot arms and various computer systems to acquire and process 3d data as well as to build a control framework. Spatial perception based teleoperation technology and control framework developed by this testbed will be integrated with the currently being developed high payload robot arms and underwater laser cutting technology to complete the advanced remote dismantling system.

2. Objectives of testbed

Objectives of the testbed are to study algorithms related to spatial perception and teleoperation of robot arms, and to develop an integrated control framework governing various computer systems, PLCs, local controllers and sensor networks.

2.1 3D perception based teleoperation technology

3D perception based teleoperation technology is a key technology that enables robot arms to devote to nuclear dismantling because excessively difficult remote manipulation has become an obstacle to the dismantling of nuclear facilities by robot arms.

In this study, researched are being conducted on the problem of remote manipulation by spatial perception and interaction technology. Interactive Robotics Division under CEA List is conducting research by approaching force feedback technology With regard to teleoperation technology of robot arms in the nuclear field [2].

2.2 Integrated control framework

The integrated control framework is a set of governing logic and data structures, and a testbed capable of emulating a target system is needed to develop the integrated control framework. The target systems is the advanced remote dismantling system which consists of various computer systems, PLCs, local controllers and sensor networks.

3. Configuration of testbed

The hardware and control framework is developed to be compatible with the concept of the Smart Factory for future scalability. The hardware of the testbed consists of three layers of actuator/sensor layer, controller/PLC layer, and process controller layer. The framework of the testbed is implemented to include the OPC server, which can collect all data from the control system and link data with the virtual commissioning system and nuclear dismantling simulation system.

3.1 Hardware setup of testbed

As shown in Fig. 1, the hardware configuration of the testbed with three layers could be assumed to be a prototype of the advanced remote dismantling system.

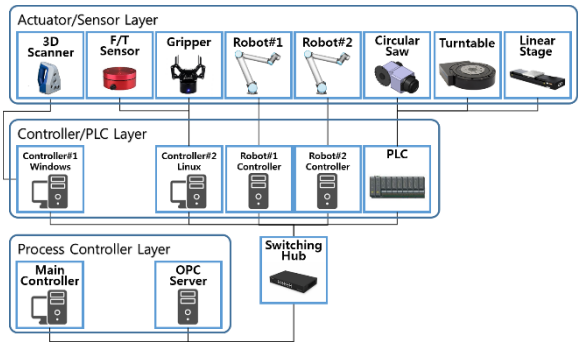

Fig. 1. Hardware configuration of testbed.

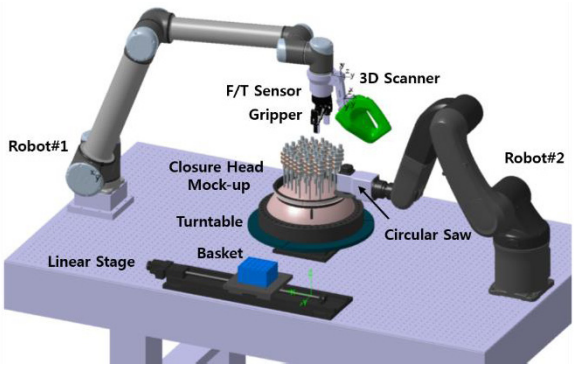

Fig. 2. Digital mockup of testbed.

As shown in Fig. 2, the testbed can perform cutting, gripping and transferring processes using two robot arms, a gripper, a circular saw, a turntable and a linear stage.

3.2 Control framework of testbed

The control framework of the testbed controls the basic processes in the order of 3d scanning, 3d registration, dynamic replanning and calibrated process generation. All actuator and sensor data are collected through the OPC server and transferred to the graphic update module and other module.

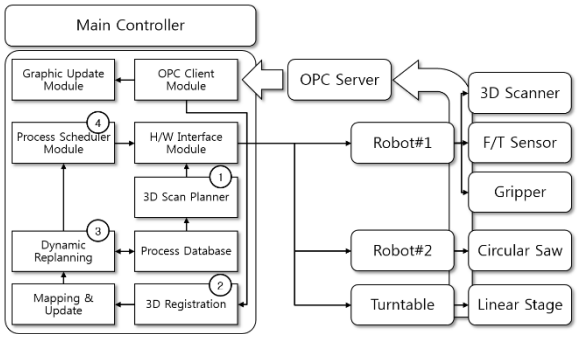

Fig. 3. Control framework of testbed.

4. Task running on testbed

In this testbed, the primary objective of the robot arm is to deliver an end-effector to the target position in the absolute coordinate system by only 3D scanning, not teaching. To achieve the objective, coordinate system configuration, calibration of the 3D scanner, and kinematic calibration of the robot arm are being performed.

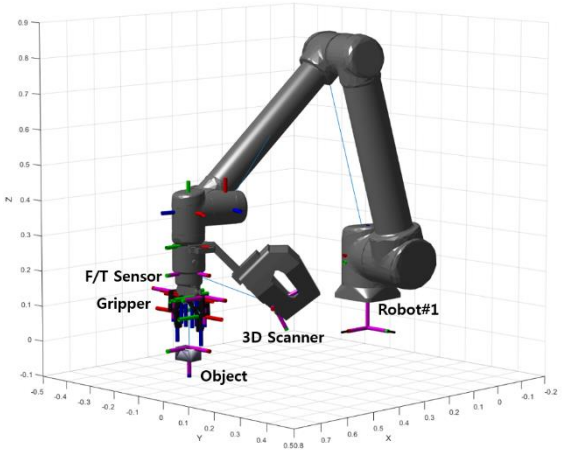

Fig. 4. Coordinate system of testbed.

5. Conclusion

The proposed testbed achieves previously mentioned goals capable of demonstrating spatial perception algorithms and control framework.

Acknowledgements

This work was supported by the nuclear research and development program (2017M2A8A5015146) through the National Research Foundation of Korea, funded by the Ministry of Science and ICT, Republic of Korea.

REFERENCES

[1] Hyun, D., Lee S., Seo Y., Kim G., Lee J., Jeong K., Choi B., Moon J., “Seamless remote dismantling system for heavy and highly radioactive components of Korean nuclear power plants”, Annals of Nuclear Energy, 73, 39-45 (2014).

[2] Philippe Garrec, Yann Perrot, “Force feedback nuclear telerobotics in France: R&D results and industrial achievements”, PURESAFE Final Conference Jan., 2015, Geneva.

Preliminary Evaluation for the Nuclide Inventory of the RCP Suction Leg for Decommissioning of Kori Unit 1

Jonghoa Kim*, Homin Jeon, Yongsik Kim, Jaejoon Song, Kyeongho Han, and Jangsoo Seo
Sae-An Engineering Co., Ltd, 184 Gasan Digital 2-ro, Geumcheon-gu, Seoul, Korea
*jhkim4198@sae-an.co.kr

1. Introduction

The methods for evaluating the gamma nuclide inventory present on the inner surface of component subject to decommissioning Nuclear Power Plant are LABSOCS (Laboratory SOurceless Calibration Software) that indirectly measures a sample that can demonstrate the representativeness of component subject to decommissioning, ISOCS (In Situ Object Counting System) that measures directly from the surface of a component subject to decommissioning, and MicroShield® computer program that estimates the nuclide inventory on the inner surface of component using the dose rate of component subject to decommissioning and the radioactivity of the sample[1,2,3,4].

In this study, ISOCS was used to evaluate the direct nuclide inventory for the RCP Suction Leg B of Kori unit 1. The contact dose rate was calculated by MicroShield® ver. 10.03 computer program and compared with the direct measurement by Teletector.

2. Materials and Methods

2.1 ISOCS

Unlike fixed semiconductor detectors, ISOCS does not use standard calibration sources for calibration. ISOCS performs the efficiency calibration by modeling the measurement object with the source. ISOCS can evaluate nuclides and radioactivity quantitatively regardless of the size of the target. The ISOCS detector used in this study is a high purity germanium detector manufactured by CANBERRA. The detector relative efficiency is 20% and the energy resolution is 1.8 keV at ^{60}Co of 1.33 MeV[1, 2].

2.2 MicroShield Computer Program

The MicroShield® computer program uses 16 fixed geometry models for radiation shielding evaluation of point sources, line sources, and volume sources using the Point Kernel method. The basic concept of the Point Kernel method is to divide the volume source into a large number of small point sources and regard each as a point source, and add up the respective contributions. The fixed geometry model approach reduces the effort required to express the geometry numerically for shielding evaluation, and can be applied to most problems, except when an accurate evaluation of complex geometry is required[3,4].

2.3 RCP Suction Leg B

The length of the RCP Suction Leg B measured by ISOCS is 184 cm, the radius is 39.25 cm, the thickness is 7.62 cm, and the material is carbon steel. The inside of the pipe is 100% drained and the inside is filled with air.

2.4 Measurements Methods

The contact dose rate of RCP Suction Leg B was estimated to be 2 mSv/h at maximum, and the detector was located 254 cm from the surface of RCP Suction Leg B as shown in Fig. 1 to satisfy dead time within 10%. And an absorber of 3.95 cm (lead: 2.75 cm, stainless steel: 1.2 cm) was placed in front of the detector and measured for 1,000 seconds.

Fig. 1. Measurement position of ISOCS.

3. Results and Discussions

The nuclide inventory of RCP Suction Leg B measured by ISOCS were ^{58}Co 3.87×10^{9} Bq, ^{60}Co 3.19×10^{10} Bq, and ^{65}Zn 3.01×10^{9} Bq. And the spectrum is shown in Fig. 2.

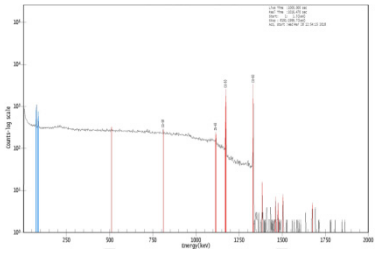

Fig. 2. Spectrum of RCP Suction Leg B.

The contact dose rate of the RCP Suction Leg B nuclide inventory was estimated to be 2.85 mSv/h using a MicroShield computer program. Therefore, the relative error of 2 mSv/h directly measured by Teletector was 0.43.

When the contact dose rate of RCP Suction Leg B was 2 mSv/h, the radioactivity of ^{60}Co single nuclide was evaluated by MicroShield computer program as 2.36×10^{10} Bq. Therefore, the relative error to 3.19×10^{10} Bq directly measured by ISOCS was 0.26.

4. Conclusion

In this study, the stock of nuclide stocks was evaluated by ISOCS and MicroShield ver. 10.03 computer program for Kori Unit 1 RCP Suction Leg B. The ^{60}Co radioactivity evaluated by ISOCS and MicroShield is 3.19×10^{10} Bq and 2.36×10^{10} Bq. Therefore, the relative error was 0.26. On the other hand, since the components subject to decommissioning have complicated shape and various materials, optimal modeling for this is important. In addition, for accurate error range and applicability, it is necessary to verify the validity of ISOCS and LABSOCS by performing radioactivity measurement and mutual comparison and analysis.

Acknowledgments

This study was conducted as part of the "Development of Decontamination Technology of Reactor Coolant System and Dismantled Equipment foe NPP Decommissioning" project supported by the MOTIE (Ministry of Trade, Industry and Energy) and the KETEP (Korea Institute of Energy Technology Evaluation and Planning (Project Number: 20141510300310).

REFERENCES

[1] CANBERRA, In-Situ Object Counting Systems, 2012.
[2] CANBERRA, Genie 2000 Spectroscopy Software Operation Manual, 2013.
[3] Grove Software, "MicroShield ver. 10.03", 2015.
[4] Grove Software, "MicroShield® User's Manual", 2015.

5분과

제염해체 (Poster)

The Main Issues of Large Components From Decommissioning to Storage and Disposal of a Nuclear Facility

KwanSeong Jeong *, SeungKook Park, and BumKyung Seo

Korea Atomic Energy Research Institute, Daedeok-daero989ben-gil 111,Yuseong-gu, Daejeon, Republic of Korea

*ksjeong1@kaeri.re.kr

1. Introduction

This paper is intended to facilitate the review of the issue at stake through a case-by-case approach, addressing all intermediate steps, such as treatment and conditioning, transportation and relevant decision-making parameters, in order to determine the overall relevancy of potential management routes depending upon given circumstances.

2. The relevant issues of managing large components

2.1 Main relevant actors in the technical process of managing large components

Managing radioactive waste involves many actors at various stages, including operators, regulators and a range of stakeholders. The actors are considered as the operator of the nuclear facility, the decommissioning organization, the transportation organization, the treatment of storage organization, and the operator of the disposal facility.

2.2 Management stages for large disused components

In order to assess the relevancy of a waste management option for large disused components, different aspects have to be investigated such as technical aspects, regulatory aspects, stakeholder aspects, and economic aspects. Those aspects must be considered at every stage throughout the management of disused large components such as decommissioning, transportation, waste treatment or storage, either performed at or away from the decommissioned site, and disposal.

3. Interdependency of activities and overall optimization

The assessment may be performed on the basis of an evaluation matrix that is described as shown in Table 1~5. Such an approach itself and the existing situation in the decommissioning facility, but also on the storage or disposal opportunities, the assessment results may vary. The evaluation matrix considers main issues such as regulatory and licensing issues, technical and operational issues, safety and ALARA issues, economic and schedule issues, and public-acceptance and stakeholders issues.

Table 1. Evaluation matrix considering the regulatory and licensing issues

Stages/ Processes	Decommissioning	Transportation	Waste treatment/Interim storage	Disposal
Parameters	Prior references for similar projects	Waste classification	Free release limits and processes	Need to develop for special licensing process for non-standard packages, including the preparation of specific safety cases
	'First-of-a-kind' issues (processes, containers, etc.)	Acceptability of industrial packages	Conditional clearance limits and processes	Need to develop dedicated acceptance criteria for non-standard package
	Overall D&D project ALARA compliance	Licensed packages	Treatment and conditioning process for disposal	
	Required changes in waste acceptance criteria and/or processes and facilities of disposal site	Regulatory exemptions (e.g., transport without packaging)	Interim-storage licensing	
	Applicability of free release/clearance criteria			

Table 2. Evaluation matrix considering the technical and operational issues

Stages/ Processes	Decommissioning	Transportation	Waste treatment/Interim storage	Disposal
Parameters	Availability of mature and tested technologies for the proposed concept	Number of expected expeditions	Evaluation of applicable waste-treatment techniques/processes (decontamination, segmentation, volume reduction, etc.)	Evaluation of modifications required at the disposal site for handling large non-standard packages

	Previous references in similar projects	Packaging issues (e.g., external shielding, shock absorbers, etc.)	Need for new ancillary facilities	Need to design new dedicated storage cells for large non-standard packages
	Feasibility/ease of deployment	Handling issues (availability and flexibility of handling means)	Minimization of secondary waste	Need to develop a new conditioning process at the disposal site in order to accommodate large non-standard packages
	Use of original plant systems and load-handling means	Required changes in transport infrastructure	On-site handling issues	Need to develop new characterization strategies for large non-standard packages
	Number and extent of required plant modifications			
	Primary and secondary waste disposal policy			

Table 3. Evaluation matrix considering the safety and ALARA issues

Stages /Processes	Decommissioning	Transportation	Waste treatment/Interim storage	Disposal
Parameters	Expected external and internal workers exposure	Compliance with transport dose limits	Expected doses to the workers due to treatment processes	Need to re-evaluate conventional and radiological risks for handling, conditioning and disposal non-standard packages
	Expected public exposure	Transport security and waste retrievability issues	Potential new risks/hazards (e.g., chemical, aerosols, etc.)	Expected doses to workers from the handling, conditioning and disposal of waste packages
	On-site radiological risks (irradiation contamination, etc.)	Optimization of waste itinerary (road, railway, and sea options)	Doses resulting from waste handling	Validity evaluation of the disposal site's performance assessment for large non-standard packages, including human-intrusion scenarios
	Off-site radiological risks (uncontrolled activity release)			
	On-site conventional risks			

Table 4. Evaluation matrix considering the economic and scheduling issues

Stages/ Processes	Decommissioning	Transportation	Waste treatment/Interim storage	Disposal
Parameters	Total project schedule duration	Container cost	Cost-benefit analysis (reduction of transport, storage and disposal costs vs treatment costs)	Overall disposal costs, including design, licensing, new process development and investment in new facilities
	Total project cost	Containers design, testing, and licensing costs	Potential risk schedule in case of treatment contingencies	Use of disposal space
	Potential internal risks for schedule and cost	Timely procurement of containers	Costs of interim-storage facilities	Potential internal risks for schedule and cost (e.g., design and test delays, analyses uncertainties, etc.)
	Potential external risks for schedule and cots	Impact on schedule of transport-related contingencies (e.g., road blockage, weather, etc.)		Potential external risks for schedule and cost (e.g., licensing delay, intervener action, etc.)
		Liabilities, cost of insurance		

Table 5. Evaluation matrix considering the public acceptance and stakeholder issues

Stages/ Processes	Decommissioning	Transportation	Waste treatment/Interim storage	Disposal
Parameters	Overall project risk perception by public	Number and visibility of off-site expeditions	Need to justify the need for interim storage to public	Public involvement in disposal site re-licensing (if required)
	Waste minimization via recycling/ clearance	Avoidance of large population areas	Public positive perception on the reduction of waste for disposal	
		Impact of transport route restriction		

4. Conclusions

The optimization process should be discussed with respective regulators and the acceptability of the management option to regulators is an integral part of the successful delivery of the project in some cases, that may lead to the specific approval of all or part of the decommissioning plan. Good practice includes making the process and decisions readily available to stakeholders.

ACKNOWLEDGEMENT

This work was supported by the Nuclear Research and Development Program through the National Research Foundation of Korea funded by the Ministry of Science and ICT.

A Study on the Effect of Internal Exposure of Worker due to Radioactive Aerosols Generated During NPP Dismantling Process

Sun Il Kim, Hak Yun Lee, and Jong Soon Song*
Chosun University, 309 Pilmun-daero, Dong-gu, Gwangju, Republic of Korea
jssong@chosun.ac.kr

1. Introduction

Radioactive aerosols are generated during the cutting and melting processes of the nuclear power plant decommissioning. These aerosols can infiltrate into the body of the worker through the respiratory system and they are the main factors inducing internal exposure. The infiltrated radioactive aerosols accumulate in different parts of the respiratory system depending on the size of the particles. Generally, aerosols between the size of 10 and 15um deposit on the mouth and nose while those between 5 and 10um and those between 1 and 5um deposit on the upper bronchus and the alveoli, respectively. Particularly, radioactive aerosols deposited on the alveoli are absorbed into the blood vessel due to osmotic action, resulting in whole-body irradiation. This study evaluated the internal exposure of workers by utilizing the production and size distribution of radioactive aerosols during the melting processes of the nuclear power plant decommissioning.

2. Main Title

2.1 Internal Exposure Evaluation Code and Selection of Input Data

This study used BiDAS (Bioassay Data Analysis Software) whose reliability was verified by verifying the results values using IMBA and IMIE. The BiDAS Code was developed by KAERI (Korea Atomic Energy Research Institute) in 2009.

2.1.1 Respiratory Rate. The respiratory rate of workers is directly related to the intake of particles in the air. This study believed that it is difficult to define the actual intensity of work of workers, and applied 1.20m^3/hr, the average respiratory rate of male adults during the simple work suggested by ICRP-66. Table 1 shows the average respiration rate of workers in ICRP-66.

Table 1. The average respiration rate of workers according to type of activity

Activity	Spent Time	Respiratory Rate(m^3/hr)
Occupational Work	Minor Work	1.20
	Intense Work	1.68

2.1.2 Work Time. This study also believed that it is difficult to define the work time like the respiratory rate, and applied 8 hours a day on average and 5 days a week, the general work time in Korea.

2.1.3 Quantity of Aerosols by Nuclide. The nuclide data, collected in the melting process conducted by the Kozloduy PMF (Plasma Melting Facility), was used as the generation data of each nuclide to be applied to assessment of internal exposure. The concentration of each nuclide is shown in Table 2.

Table 2. Radionuclides Concentration of Radioactive Aerosols Collected from PMF

Radionuclides	Concentration(MBq)
^{54}Mn	0.362
^{59}Fe	0.181
^{58}Co	0.0603
^{60}Co	3.44
^{134}Cs	0.362

2.1.4 Particle size of the Radioactive Aerosol. The quantity of aerosols, collected in the melting process conducted by the Kozloduy PMF (Plasma Melting Facility), was not measured by particle size. Accordingly, the aerosol quantity data by particle size in the melting process (Figure 1) conducted in

other studies was used as the input data for the BiDAS Code

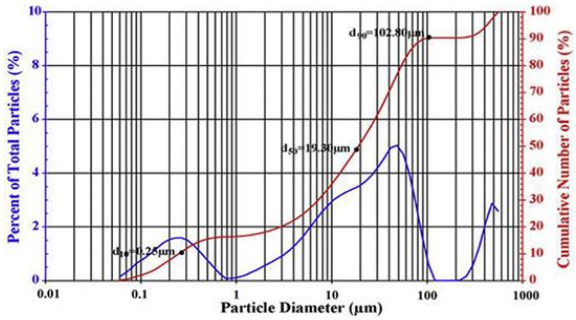

Fig. 1. Particle Size Distribution of EAF (Electric Arc Furnace).

3. Conclusion

The committed effective dose of workers was assessed using the BiDAS Code, and the results are as follows. 1.18×10^{-3} for ^{54}Mn, 4.03×10^{-4} for ^{59}Fe, 5.31×10^{-4} for ^{58}Co, 7.02×10^{-2} for ^{60}Co, and 5.16×10^{-3}mSv for ^{134}Cs.

It is about 0.0016% of Korea's annual maximum permissible dose of 50mSv, and it is about 0.39% of the 5-year average of 20mSv. These figures can be said to be insignificant compared to the annual permissible dose. There is no concern about overexposure due to radioactive aerosols generated in the melting process.

In addition, in the assessment of the internal exposure by nuclide and particle size to understand the difference in the committed effective dose (CED) by particle size, it accounted for 58.5% of the total dose at 0.1um or less and 25% at 3um or more in case of ^{134}Cs. In case of other nuclides excluding ^{134}Cs, it accounted for 76.5% of the total dose at 0.1um or less.

REFERENCES

[1] KAERI, "A State-of-the Art on the Dismantling Techniques for the KRR-1 & 2 Decommissioning", KAERI/AR-609/2001.

[2] Annotation of the Investment Proposal-Activities and Technologies, Environmental Impact Assessment Report for the Decommissioning of Units 1 to 4 at Kozloduy Nuclear Power Plant, P16Del109Rev02_EIA_R (2013).

[3] X. Lin, Z. Peng, J. Yan, Z. Li, J. Yang Hwang, Y. Zhang, G. Li, T. Jiang, "Pyrometallurgical Recycling of Electric Arc Furnace Dust", Journal of Cleaner Production 149 1079-1100 (2010).

Review of the Practical Cost Estimations for Decommissioning of Nuclear Facilities

KwanSeong Jeong *, SeungKook Park, DaeSeo Koo, InHye Hahm, JaeHyun Ha, SangBum Hong, and BumKyoung Seo
Korea Atomic Energy Research Institute, Daedeok-daero989beon-gil 111,Yuseong-gu, Daejeon, Republic of Korea
*ksjeong1@kaeri.re.kr

1. Introduction

Decommissioning cost estimation is not a new practice and in fact has been ongoing since the early 1970s. Only recently have efforts been made to standardize cost estimation formats to facilitate reviews and ensure completeness. The cost for decommissioning of nuclear facilities is no longer a simple arithmetic calculation based on power and size, but has been based on the actual inventories of materials and radioactivity for each unit together with a realistic project organization and planning. This paper is intended to discuss from a literature point of view and facilitate the cost estimation for decommissioning of nuclear facilities.

2. The current practices of cost estimation for decommissioning of nuclear facilities

2.1 Approaches to cost estimation

Figure 1 shows the categorized approaches to cost estimating. The activity-dependent costs are complemented by period-dependent costs. Collateral costs are included. All costs are adjusted for industrial standard contingencies to achieve a best estimation.

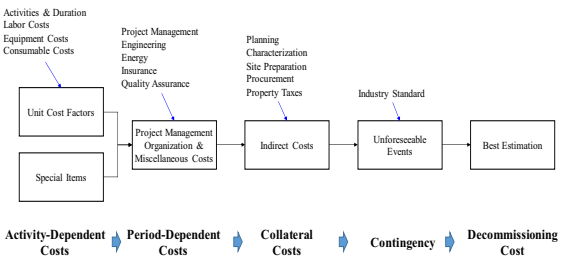

Fig. 1. A schematic flow for decommissioning estimation.

2.2 Elements of cost estimation

There are four basic elements to a cost estimation: basis of estimation, structure of estimation, work breakdown structure and schedule and uncertainty analysis.

2.3 Elements of cost estimation

There are four basic elements to a cost estimation: basis of estimation, structure of estimation, work breakdown structure and schedule and uncertainty analysis.

2.4 Schedule of cost estimation

The duration of a decommissioning project affects its cost importantly through the period-dependent costs and the selected technology for the activity-dependent work. The project schedule is an integral part of a detailed cost estimation. These two interrelated elements must be maintained in balance when preparing an overall cost and schedule estimation.

3. Major drivers of decommissioning costs

3.1 Major cost drivers

There are categorized cost drivers from literature: general circumstances, basic project assumptions, cost estimation model, assumptions for waste management, and technical assumptions.

3.2 Observations on completeness

A basic attribute of any estimation is that it is a complete representation of the work to be performed. Decisions regarding the adequacy of funds to pay for decommissioning can only be based on a sound, comprehensive cost and schedule analysis. While all estimators attempt to deal with absolute values related to the planned activities to be performed and the anticipated schedule to be met, the reality of the situation is that the work involves some uncertainty. Some of the uncertainty within the defined project scope can be accounted for by allowances based on best available information. Other uncertainties within the defined scope can be accounted for by contingency funds that are fully expected to be incurred and spent. Uncertainties dealing with probabilistic events are best handled within a risk analysis based on experienced judgement of the lowest, most likely, and highest cost of each item of the baseline cost. The risks analysis allows the estimators to visualize the importance of the major drivers through the sensitivity analysis.

3.3 Observations on accuracy

No estimation can be 100% accurate since the estimator is attempting to anticipate virtually every planned activity, problem area and potential resolution for issues that can change from numerous external causes. Allowances, contingencies and risk analyses are sued to account for these potentially changing conditions to ensure sufficient funds will be available to safely perform the work. Most countries accept this fact and allow form periodic updates every three to five years not only to account for inflation, escalation and regulatory changes, but also to incorporate new technologies and techniques to improve the safety and cost effectiveness, and to shorten the schedule.

ACKNOWLEDGEMENT

This work was supported by the Nuclear Research and Development Program through the National Research Foundation of Korea funded by the Ministry of Science and ICT.

Review of Operating Conditions for Full System Decontamination Operation Procedure Development of Kori-1 Nuclear Power Plant

Hak-Soo Kim* and Cho-Rong Kim

KHNP Central Research Institute, 7, 1312-gil, Yuseong-daero, Yuseong-gu, Daejeon, Republic of Korea

*hskim0071@khnp.co.kr

1. Introduction

The Kori-1 nuclear power plant (NPP) operated for approximately 40 years in Korea, was permanently shut downed on June 18, 2017. Kori-1 NPP will be performed with the full system decontamination to reduce worker exposure to radiation by reducing the dose rate in the system before starting main decommissioning activities. In order to successfully complete system decontamination, it is very important not only how to efficiently remove the corrosion oxide film deposited on the inner surface of system, but also how to operate the plant. The operation of system decontamination is very different from the operating NPPs. The major differences from the operating NPP are that there is no need for various the operating variables such as temperature, pressure, interlocking signal, etc., applied to the NPP because there is no fuel in the reactor core and that some facilities in the system are removed or changed to maximize the decontamination effect. This paper deals with the results of the review of the circulating flow supply method and the decontamination operation temperature/pressure control method in operating conditions of Kori-1 NPP for the development of the system decontamination operating procedure.

2. Methods and Results

2.1 Concept of System Decontamination Operation

The principal goal of the decontamination is to re`duce the radiation exposure in fields to which the decommissioning workers will be exposed. The concepts of system decontamination operation for Kori-1 NPP are as follows [1].

- Decontamination Factor (DF): > 30
- Implement ALARA
- Minimization of secondary radioactive waste generation
- Utilization of plant facilities as much as possible
- Application of organic-acid based chemical process
- System decontamination temperature: ~95℃
- Decontamination scope: PRV, PZR, SG, CVCS, RHRS and RCS piping
- Decontamination facility connecting location: Residual Heat Removal System

● Circulating Flow Supply Method

System decontamination is known to have a close relation to the decontamination effect of the circulating flow formed in the range of system decontamination [2]. There are a variety of ways to provide the circulating flow for system decontamination as shown in Table 1 [3, 4]. In case of Kori-1 NPP system decontamination, RCP operation was considered to provide adequate the circulating flow to the decontamination scope, especially in SG U-tubes.

Table 1. System Decontamination operation in NPPs decommissioning

NPPs	Maine Yankee	Connecti-cut Yankee	Jose Cabrera
Decontamination Technology	DfD	HP CORD	DfD
Decontamination Scope	RCS, PZR, CVCS, RHRS (Excl. RPV & SG)	RCS, PZR, SG, CVCS, RHRS (Excl. RPV)	RCS, PZR, SG, CVCS, RHRS, RPV
Driving Force	Vendor's Pump	RHRS Pump	RCP

The RCP startup conditions are required to operate RCP as follows [5].

- Pressure in RCS: > 22.4 bar
- Differential Pressure of RCP Seal #1: > 14 bar
- Temperature of Seal Water: < 54.4 ℃
- Seal Leakage of RCP Seal #1: within the allowable flow rate
- Supply the Component Cooling Water

The oxidation step during the decontamination process has been reported to have a negative impact on the RCP seal. Figure 1 shows the schematic diagram of RCP seal. Manganese dioxide which is a solid material produced in the oxidation step has a negative effect on the RCP seal #1 and the chemical injected in the oxidation step also has a negative effect on RCP seal #2&#3 containing Cr component

[6]. Therefore, a separate approach is needed to protect the RCP seal.

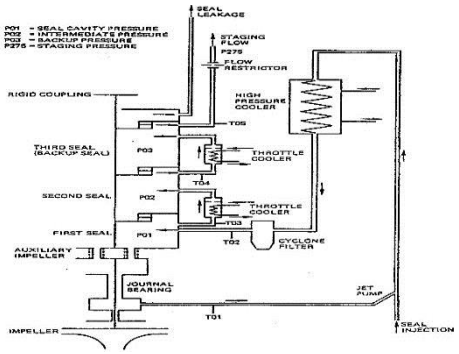

Fig. 1. Schematic Diagram of RCP Seal.

● Control of Temperature and Pressure

The heat sources for increasing RCS temperature are RCS pumps and PZR heaters. For normal operation (NOT & NOP) of NPPs, the operation temperature is maintained by RCS pumps and PZR heaters, and the pressure is controlled by vapor formed in upper portion of the PZR. The temperature and pressure requiring for system decontamination is 95℃ and 25~26 bar. The decontamination operating temperature is the same as the temperature control method during normal operation of NPP, but the decontamination operating pressure is adjusted by injecting and exhausting nitrogen gas into the upper portion of the PZR. The system decontamination operating pressure is associated with RCP NPSHR (Net Positive Suction Head Required) and LTOP (Low Temperature Ove Pressure) setpoint. Figure 2 shows the RCP performance characteristic of Kori1-1 NPP [5].

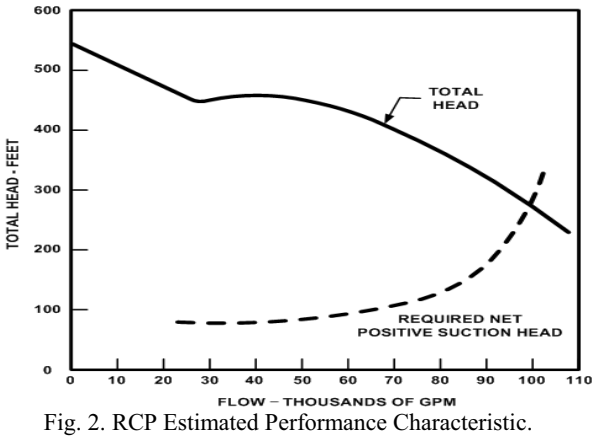

Fig. 2. RCP Estimated Performance Characteristic.

As shown in Fig.2, the RCP is operated at a pressure that satisfies the NPSHR. In case of no fuel in core, the requiring NPSH is about 200 psig but 300 psig considering the NPSH margin [7]. The components in RCS have the characteristic of being broken when the high pressure is formed at low temperature condition. It is called LTOP. The RCS in Kori-1 NPP is equipped with a release valve to prevent overpressure under low temperature. The LTOP setpoint of Kori-1 NPP is 450 psig. The release valve should be maintained below 405 psig as it opens at 90% of the LTOP setpoint. Therefore, the system decontamination operating pressure range will be 300 ~ 405 psig (20.7 ~ 27.9 bar). The system decontamination operating pressure should be controlled by solid operation or nitrogen gas because the vapor is not formed under the operating temperature of system decontamination. The operating pressure will be 370 psig slightly higher than the medium value of pressure range. This operating pressure is not enough margin with LTOP setpoint, so it is difficult to carry out the solid operation. Additionally, the pressure in the solid operation will change suddenly because the frequent pressure fluctuation is expected for system decontamination due to additional chemical injection, temperature change, and demineralized water injection. It is likely to be a burden on the operators. Therefore, it is desirable to control the pressure fluctuation by injecting/exhausting of nitrogen gas in the upper of the PZR

3. Conclusions

It was evaluated that a separate approach such as a demineralized water supply equipment is needed to protect the RCP seal because the oxidation step has been reported to have a negative impact on the RCP seal during the system decontamination operation, and that the temperature control is not much difficult compared with the normal operation and the pressure control was advantageous to pressurize the nitrogen gas in the upper of the PZR.

ACKNOWLEDGMENTS

This work was supported by the Korea Institute of Energy Technology Evaluation and Planning(KETEP), granted financial resources from the Ministry of Trade, Industry & Energy(No. 20141510200310)

REFERENCES

[1] H.S. Kim, et al., Development of Decontamination Technology of reactor Coolant System and Dismantled Equipment for NPP Decommissioning, Annual Report, 2016
[2] EPRI, Decontamination Handbook, TR-112352, 1999
[3] EPRI, Evaluation of the Decontamination of the Reactor Coolant Systems at Maine Yankee and Connecticut Yankee, TR-112092, 1999
[4] EPRI, Jose Cabrera Nuclear Power Plant Full System Chemical Decontamination Experience Report, TR-109230, 2009
[5] KHNP, Final Safety Analysis Report of Kori Unit 1, 2014
[6] EPRI, PWR Full RCS Decontamination Engineering Evaluations and Reactor System Operating Procedures, TR-103431, Jan. 1994
[7] ANSI/HI 9.6.1-2000, Centrifugal and Vertical Pumps for NPSH Margin

Underwater Laser Cutting Experiment of Stainless Steel Plate Using Supersonic Conical Nozzle for Nuclear Decommissioning

Seong Y. Oh, Jae Sung Shin, Sangwoo Seon, Taek Soo Kim, Hyunmin Park, Lim Lee, Chin-Man Chung, and Jonghwan Lee

Korea Atomic Energy Research Institute, Daedeok-daero989beon-gil 111,Yuseong-gu, Daejeon, Republic of Korea

syoh73@kaeri.re.kr

1. Introduction

Laser cutting technology is based on the concept that local area of specimen is melted by incident high-powered laser beam and simultaneously auxiliary gas with high speed is discharged to remove the resultant melts. Cutting is accomplished along the path of the kerf generated through the removal of the resultant melts. Unlike other cutting tools, laser cutting technology has a distinguishable mark: the production of a small amount of debris. This mark meets significant decommissioning requirement. Furthermore, the use of optical fiber for the purpose of transmitting high-powered laser beam enhances remote controllability. Laser cutting technology coupled with fiber laser can be suitable dismantling tool at a nuclear decommissioning site. [1]

Dismantling works at underwater environment can contribute to the significant reduction of nuclear contaminants spreading outward the atmosphere. [2] However, laser cutting in underwater environment tends to be more difficult than in atmosphere environment because of higher absorption rate of laser beam by water, significant reduction of thermal conductivity, the possibility of water penetration into laser cutting head, and so on. In this study, we have investigated cutting performance of stainless steel plate with 30~50mm thickness in underwater environment.

2. Experiment

2.1 Experimental Setup

Underwater laser cutting system contains 6kW fiber lasers (IPG, YLS 6000, 1070 nm), laser cutting head, and water-filled tank. The high-powered laser beam is fed into laser cutting head via 25-m-long optical process fiber. The cutting head consist of a few of optics to effectively focus laser beam toward the specimen: collimation lens (f: 160mm), parabolic focusing mirror (f: 600mm), reflection mirror, widows. The end part of cutting head is connected to the high-pressure gas pipe to introduce compressible air of 10.0 bar gauge pressure. The supplied compressible air and focused laser beam are coaxially passed through the nozzle with small diameter. The throat diameters of supersonic nozzle used in the experiment was 3mm and the flow rates were about 860L/min. The stainless steel block (SUS 304L) was immersed in the water tank.

3. Result and Discussion

The underwater cutting experiment of stainless steel plate (SUS 304L) with 50mm thickness was carried out using conical supersonic nozzle. The supersonic conical nozzle has a convergent-divergent shape. Fig. 1 presents the underwater laser cutting scene of 50-mm-thick stainless steel.

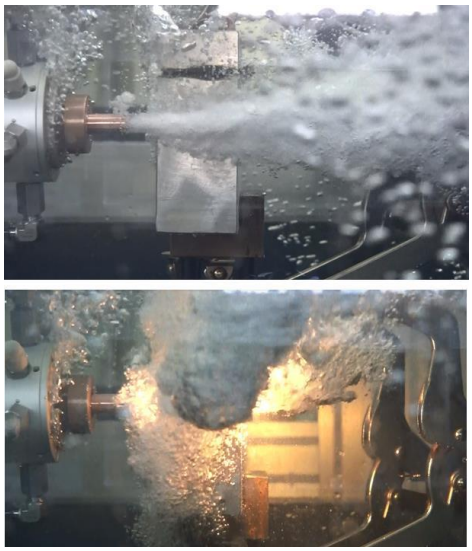

Fig. 1. Underwater laser cutting of stainless steel plate.

The cutting head is initially placed initially in the atmosphere, and then it is submerged into water tank according to relative motion X-Y-Z axis stage in order to cutting the immersed specimen. The entire cutting length was 40mm. The underwater cutting speed was initially set at 5 mm/min until after 10mm had been cut, after which, the cutting speed was increased to 20 mm/min until 30mm had been cut.

The stand-off distance was sequentially increased from 7.5mm, 10mm, up to 13 mm. The stand-off distance refers to the distance between the nozzle tip and the top surface of the steel plate. Fig. 2 shows the front, rear views of stainless steel after underwater cutting.

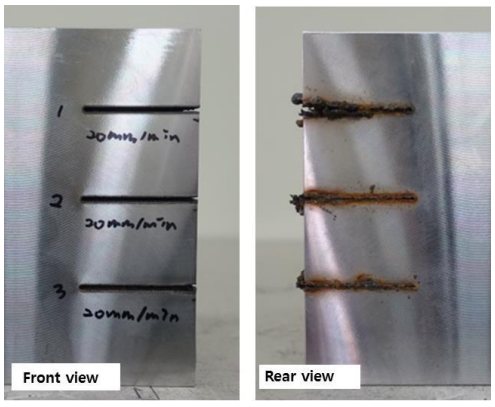

Fig. 2. Underwater laser cutting of 50-mm-thick stainless steel. Stand-off distance (1) 7.5mm, (2) 10mm, (3) 13mm.

4. Conclusion

We observed that it is possible to completely cut a 50-mm-thick stainless steel plate in the underwater environment under the condition of over 7.5mm stand-off distance.

REFERENCES

[1] K. Tamura, R. Ishigami, and R. Yamagishi, “Laser cutting of thick steel plates and simulated steel components using a 30 kW fiber laser”, Journal of Nuclear Science and Technology, 53, 916-920 (2016).

[2] D Paul Hilton and Ali Khan, “New developments in laser cutting for nuclear decommissioning”, WM2014 Conference Proceeding, Phoenix (2014).

Risk Informed Economic Assessment for the Decommissioning Project

Younggook Kim, Taesik Yun, and Hyunmin Kim*
Decommissioning Technology Team, Central Research Institute, KHNP
70, Yuseong-daero 1312beon-gil, Yuseong-gu, Daejeon, Republic of Korea
* hyunmin.kim@khnp.co.kr

1. Introduction

The purpose of the economic assessment of a project is to see if it is feasible to move on to the next stage. By the way, the methodologies so far we have used are just to demonstrate the net present value of the project is greater than or equal to "0". With this methodology, the value could be calculated with a fixed discount rate and capacity factor reflecting all the risks in the course of the project life. Hence, risks brought up in the life of the project have not be considered in a proper manner.

In this article, we introduce the methodology to embrace the risks as expenses factors on top of capital, maintenance and operation costs. In order to assess the project value with regard to risks in a different manner, it is essential to know what the risk management are.

2. Risk Management

Risk management is a series of process to minimize the impact of unfortunate events or to maximize the realization of economic values such as identification, evaluation, prioritization and coordination. Thus it is necessary to consider the integrated approach to maximize risk reduction (ISO 31000). In this article, we extract risks which can be brought about in the course of decommissioning process and suggest how to reflect those risks as cost factors.

3. Decommissioning Risks

Generally decommissioning consists of four periods: Preparation for decommissioning activities, Safe Storage, Decontamination and Dismantlement (D&D), and Site Restoration before final operation license termination. There are so many risks in each period. We extract a few risks as examples to demonstrate the risk informed economic assessment.

3.1 Preparation for decommissioning activities

Plant systems, structures, and components (SSCs) were investigated in a comprehensive manner to identify if they are needed to support plant operations (e.g., Spent Fuel Pool cooling). In this process, although the SSCs are not required to support plant decommissioning, they should be further evaluated whether to be included in the plant lay-up program in case of potential future use during plant decommissioning. In this stage, the risks below can be happened

- *Spent fuel storage on site or interim equipment, etc.*
- *Estimation of decommissioning cost and schedule*
- *Mobilization of quality human resources*

3.2 Decontamination and dismantlement

Approximately 12 to 18 months before the start of decontamination and dismantlement (D&D) activities, the administrative and engineering organization should be mobilized. Some activities should be carried out during the first several months of D&D period; there are some risks below we have to consider,

- *Mobilizing administrative and engineering organization*
- *Preparation of engineering specifications and procedures, etc.*

4. Risk Informed Economic Assessment

4.1 Current NPV(Net Present Value) methodology

Traditionally, we have used the NPV in consideration of Free Cash Flow of Firm (FCFF) on the basis of the Earning Before Interest and Tax (EBIT).

$$\text{NPV} = \sum_{n=1}^{N} \frac{FCFF_n}{(1+k_0^L)^n} - IC$$

$$FCFF = EBIT(1-tax) - NIFA - AWC$$

$$EBIT = Revenue - O\&M\ Cost - Deprecialtion$$

$$k_0^L = k_e^L \frac{S}{V} + k_d(1-t)\frac{B}{V}$$

$$\beta_S^L = \beta_S^U \left\{1 + (1-t)\frac{B}{S}\right\}$$

$$k_e^L = R_f + \left[E(R_m) - R_f\right]\beta_S^L$$

where, *NIFA* is the Net Investment to the fixed Asset and *AWC* is Additional Working Capital and IC is investment costs. β refers to the risks the incumbent project has.

In the risk informed economic assessment, the calculation of *FCFF* should consider risks and their probabilities.

Example: Risk informed cost Table

Risks	Cost (USD)	Probability (%)	Expected cost(USD)
Mobilization of quality human resources	1000	10	100
Comprehensive final radiation survey	500	5	25
Total	1500	15	125

$$FCFF = EBIT(1-tax) - RIC - NIFA - AWC$$

where, *RIC* is the risk informed cost

5. Conclusion

The risk informed economic assessment we suggest is a new horizon to calculate the value of the project. On the other hand, the traditional way has its limit to assess the value in a reasonable way as long as it skips the risks informed cost. We will continue to develop the methodology of the risk informed costs assessment to value the project as practically as possible.

REFERENCES

[1] Pierre et al, Introduction to Corporate Finance, Wiley Online Library, Dec. (2015).

[2] IAEA, “Risk management: A tool for improving NPP performance, IAEA-TECDOC-1209, April (2001).

Suggestion of Safeguards Regulatory Framework for Decommissioning

Junghee Son*, Seungmin Lee, and Chul Heo
Korea Institute of Nuclear Nonproliferation and Control, 1534, Yuseong-daero, Yuseong-gu, Daejeon, Republic of Korea
*jhson@kinac.re.kr

1. Introduction

In the field of decommissioning nuclear facilities, there is lack of discussions or studies on safeguards and nuclear nonproliferation. However, the government of ROK is regulated in the area of safeguards. Therefore, Korea needs to establish a regulation framework of safeguards for nuclear decommissioning.

This paper examines the decommissioning regulation and the cases of overseas cases from the perspective of IAEA safeguards, and discusses the safeguards in the decommissioning of nuclear power plants in Korea.

2. Safeguards for Decommissioning

2.1 Decommissioning Concept and requirements

In Nuclear Safety Act, "decommissioning" means all activities for exempt from the application of this Act by dismantling facilities and sites, or by removing radioactive contamination. Consequently, in order to complete the decommissioning of the facility, the facility or site concerned must not only secure radiological safety, but also be completely excluded from the obligation of safeguards such as the management and reporting of nuclear material and the inspection required by the Nuclear Safety Act. Therefore, if there are any undeclared production or process of nuclear materials in decommissioning facility, it should be detected.

The IAEA provides verification of appropriate safeguards and security as one of the factors to consider in the transitional process from facility operation to decommissioning. [1]

2.2 Decommissioning phase in safeguards

From the standpoint of safeguards, dismantling is divided into two phase: Shutdown and Closed down. The shutdown phase means that the reactor has been shut down, but there is nuclear material in the facility and the reactor can re-start operation in a short period of time. The close down phase means that the reactor has been shut down and all nuclear material has been removed from the facility. From the safeguards point of view, when the facility enters the Decommissioning phase, the government of ROK needs to provide the IAEA with facility information to identify each phase. The range of information to be provided for each decommissioning phase is distinguished. [2]

3. Safeguards requirements

3.1 Provision of information

Based on the ‘Agreement between ROK-IAEA for the application safeguards(INFCIRC/236)’ article 8, The government of ROK already provided the Design Information Questionnaire (hereinafter

referred to as ‘DIQ’) to describe the feature of facilities and nuclear material relevant to the application of safeguards in sufficient details. And the DIQ need to be updated base on ‘the agreement’ article 45 when design information related safeguards is modified in advance including operation states likes decommissioning. The IAEA can be known the facility states by providing the updated DIQ. And the IAEA requests the modified DIQ including a decommissioning schedule and the essential equipment removal or inoperability schedule.

3.2 Concept of essential equipment and ending point of decommissioning

The essential equipment is equipment to product a nuclear material at the reactor such as a reactor, a fuel handling machine, a control rod assembly, a reactor coolant pump, and etc. And the IAEA carries out periodic design information verifications(DIVs) to ascertain the physical condition of facilities and essential equipment. The status of removal or inoperability of essential equipment is used to support the evaluation of the decommissioned status of a facility for safeguards purposes.

Before a facility can be considered by the IAEA to be decommissioned, all nuclear material and a sufficient portion of the essential equipment must be removed from the facility such that re-activation of the facility would require an effort equivalent to or greater than the effort to build a new facility or retrofit other similar structures to reconstitute its former capabilities. When a sufficient portion of essential equipment is removed or rendered inoperable at a facility, the IAEA carries out a final DIV to verify the facility as decommissioned for safeguards purposes.

4. Conclusion

In order to complete the decommissioning from the viewpoint of safety measures, it is necessary to plan appropriately the time and method of transfer of nuclear materials and essential equipment on site. Therefore, a safeguards regulatory framework for decommissioning facilities is required

In addition, cooperation between government, regulatory agencies, IAEA, and operators is essential for ensuring safeguards during the decommissioning period.

REFERENCES

[1] 1. IAEA, TRS 420 Transition from Operation to Decommissioning of Nuclear Installations, Austria: IAEA (2004).

[2] IAEA, Safeguards During Decommissioning, IAEA (2017).

Remote Sample Taking Techniques From a Large Metallic Radwaste

Kwonpyo Hong*, Sanghee Jung, Myungchul Park, Sunggeun Kim, and Wanho Oh
Korea Atomic Energy Research Institute, 111, Daedeok-daero 989, Yuseong-gu, Daejeon, Republic of Korea
kp8452@gmail.com

1. Introduction

In order to investigate the inventory of a certain radioactive materials, taking samples from mother materials is usually required. However, if the mother material is large and rigid such as dismantled reactor vessel then it is not easy to take specimen by remote operation.

In this paper our study results of several sample taking techniques are introduced, which techniques could be applied in dismantling field of nuclear reactors for radwaste inventory evaluation.

2. Sample Taking Process

2.1 Sample taking environment

The target object for sampling is assumed to be large(e.g. a few meters in size), heavy(e.g. a few tonnes in weight), metallic(such as stainless steel), and highly radioactive(at least medium level). So, it should be handled in a hot cell or similar shielded facility. Remote handling systems such as manipulators or cranes are also needed for remote operation of sample taking equipment.

The target object would be fixed in hot cell and the sampling tool is remotely moved. The tool usually has 6 degrees of freedom to enable sampling at any situation.

2.2 Core-drilling

Core drilling sample could be obtained from metallic thick plate by completely penetrating the mother material. The maximum penetrating thickness seems about 10 cm for stainless steel. The increased temperature due to drilling is about 25~30 degrees without using coolant [1].

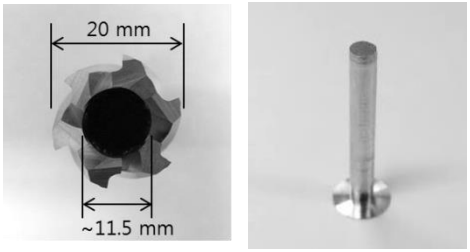

Fig. 1. Core drill bit and obtained specimen.

2.3 Drilling chips

Drilling chips generated in the process of drilling have almost same inventory rate with the mother material except a part of volatile elements. So, it can be a good candidate for inventory evaluation method after finding the inventory correlation between mother material and drilling chips. Following figure shows a usual drill chip of stainless steel.

Fig. 2. Chips specimen by normal drilling.

2.4 Laser ablation

At high flux of pulsed laser the laser-irradiated object is evaporated or converted to plasma. Collecting the ablated dust or gaseous samples the inventory can be evaluated for the surface of radwaste material. However as the collection of gaseous samples is not easy and the amount of obtained sample is too small (~ 10^{-5} cc), it seems not a good sampling method

unless the equipment is an elaborate system.

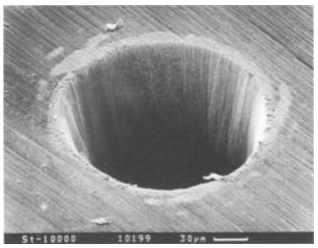

Fig. 3. Ablated hole by femtosecond laser [2].

2.5 Circular saw cutting

3 or 4 times of slope cuttings with a wheel such as side milling cutter can make a wedge type specimen from the surface of mother material [3]. There is no limit on the thickness of object. As the temperature increase due to cutting is about 30 degrees the heat affection to the sample is negligible. Following is a wedge sampling experimental result from Cu alloy.

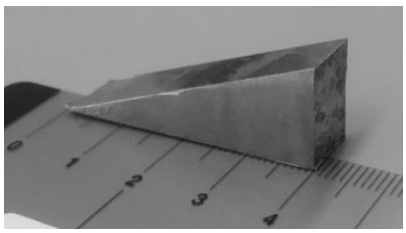

Fig. 4. Wedge specimen by circular saw slope cutting.

2.6 EDM

From the plate type conductor material a specimen can be obtained using electrical discharge machining. This technique is useful in speedy sampling and remote operation, but it should use of liquid insulator so that 2nd liquid radwaste would be produced.

Fig. 5. Specimen taking by EDM.

2.7 Laser cutting

By all around cutting with slope laser beam a conical or disk sample can be obtained rapidly. But in case of thick material if it doesn't fully penetrate the target object, the melting dross wouldn't be discharged. So it has a limit on thickness of target object.

Fig. 6. Laser slope cutting.

3. Conclusion

Several kinds of sample taking techniques from a bulky, metallic, and highly radioactive radwaste were studied. In that case the proper sample taking method seems to be the wedge sampling or the chips sampling. They are relatively easy to take samples and relatively low heat affection to the samples.

These studies are expected to be applied in the field of decontamination and dismantling of nuclear reactors or any highly radioactive heavy metallic objects.

REFERENCES

[1] S. G. Kim, et. al. "Development of core sampling technique for ITER Type B radwaste", Proc. of KNS 2016 Autumn Meeting, Oct. 27-28 (2016)

[2] B.N. Chichkov, Appl. Phys. A 63, 109 (1996)

[3] Kwonpyo Hong et. al. "Development of wedge sampling technique by slope cutting", Proc. of the KRS 2016 Spring Conference, May 25-27, 2016, Mokpo.

Cutting Process Update Method to Simulate the Nuclear Facility Decommission

Ikjune Kim*, Dongjun Hyun, Jonghwan Lee, Shinyoung Kang, and Sungmoon Joo
Korea Atomic Energy Research Institute, Daedeok-daero989ben-gil 111,Yuseong-gu, Daejeon, Republic of Korea
* ikjunekim@kaeri.re.kr

1. Introduction

In the previous study, we have developed the cutting simulation software framework to simulate the nuclear facility decommission [1, 2]. However the software is difficult to update the cutting process due to lack of remaining information of related device model and target model of the cutting, after creating the process. To solve the problem, in this study, we proposed the cutting process update method.

2. Cutting process update method

2.1 Data structures

In the cutting process modeling procedure of existing cutting simulation software, a user selects the models of the cutting and carrier devices from the resource list and selects the cut target product in the product list as input of a cutting process creation. The selected cutting device model has a pre-defined cutter profile and cutting depth. And the user creates moving path using the carrier device. Based on the created moving path and cutter profile, the cutting volume is created to cut the target model.

The cutting process is able to store information about the movement of the carrier and cutter device and post visual process which hide target product and show cut result product, as shown in Fig. 1. However, the cutting volume is no longer available after cutting procedure is finished. Therefore to update the specific cutting process, user needs to recreate the cutting volume and the cutting process manually.

To automate the procedures we add a new data structure as a sub element of the cutting process item as shown in Fig. 1. Using the data structure we record the cutting device and carrier device, target product and cutting option to recreate the cutting volume.

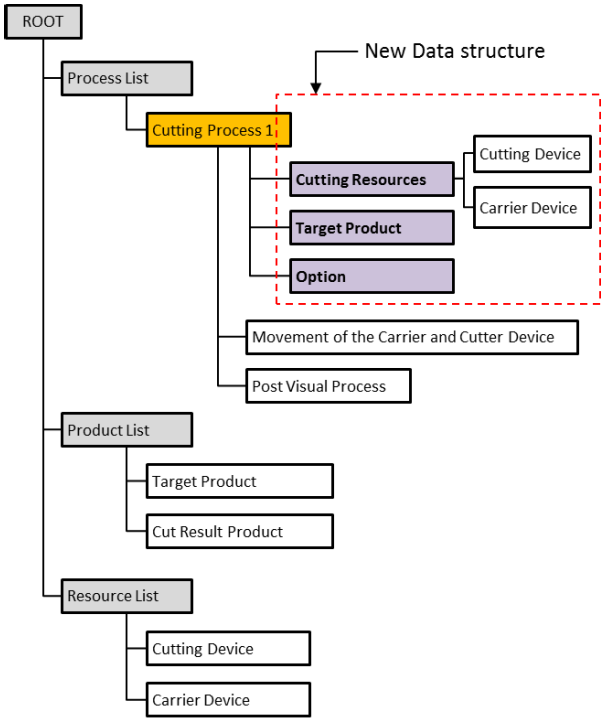

Fig. 1. Data Structure.

2.2 Cutting process update

In case of cutting resources has changed or the target product and cutting option has changed, the cutting process should be updated. We duplicate the

cutting process which will be updated, and recreate cutting volume using cutting resources and create cutting process by cutting the target product based on stored data in the proposed new data structure. And finally delete the original cutting process and create process flow to new cutting process to be able to simulate using the updated cutting process.

3. Conclusion

In this study, we proposed the cutting process update method in the cutting process simulation software. We define the new data structure to enable the cutting process update feature. And we describe the general cutting process update scenario. This method helps reducing the process modeling time when modeling the cutting process of the nuclear facility decommission.

ACKNOWLEDGEMENT

This work was supported by the nuclear research and development program through the National Research Foundation of Korea, funded by the Ministry of Science and ICT, Republic of Korea (Grant Code: 2017M2A8A5015146).

REFERENCES

[1] I. Kim, B. Choi, D. Hyun, J. Moon, J. Lee, K. Jeong, et al., A framework for a flexible cutting-process simulation of a nuclear facility decommission, Annals of Nuclear Energy, vol. 97, pp. 204-207 (2016).

[2] I. Kim, et al., Cutting Method of the CAD model of the Nuclear facility for Dismantling Simulation, Transactions of the Korean Nuclear Society Spring Meeting, Jeju, Korea, May 7-8, 2015 Journal of Nuclear Fuel Cycle and Waste Technology, 1(1), 1-10 (2015).

Electrolytic Reduction of Palladium in DBSO/Ionic Liquid System

Iksoo Kim*, Dongyong Chung, and Keunyoung Lee

Korea Atomic Energy Research Institute, Daedeok-daero989ben-gil 111,Yuseong-gu, Daejeon, Republic of Korea

*niskim@kaeri.re.kr

1. Introduction

This research is to develop a source technology for a treatment of radioactive and decontamination waste produced from the nuclear fuel cycle process by using ionic liquids. Ionic liquids easily dissolve organic or inorganic compounds, therefore feasibility studies on ionic liquids application for high level wastes treatment was conducted. Ionic liquids are being evaluated as an alternative to the conventional diluent, n-dodecane, in aqueous reprocessing, and as a substitute to the traditional high-temperature molten salts in the non-aqueous reprocessing of spent nuclear fuels [1].

As a part of the research to recover platinum group metals from nitric acid, the extraction and electrolytic reduction of palladium was studied using dibutyl sulfoxide (DBSO) as an extractant in the ionic liquid, 1-butyl-3-methylimidazolium bis(trifluoromethane-sulfonyl)imide (C_4mimTf_2N). The feasibility of the Extraction and Electrodeposition (EX-EL) process was demonstrated.

2. Experimental

2.1 Chemicals and equipment

All the chemicals and reagents used in the study were of analytical grade and used without further purification. Ionic liquid, C_4mimTf_2N, and DBSO were procured from Sigma-Aldrich. To remove the water and volatile impurities, C_4mimTf_2N was dried under a reduced pressure at 373 K, and the residual water concentrations measured using a Karl Fisher moisture content meter (Metrohm 831 KF Coulometer) were below 100 ppm.

2.2 Experimental method

The extraction experiment was carried out by equilibrating the organic phase (0.03~1 M DBSO in C_4mimTf_2N) and the aqueous phase (1,000 ppm of palladium in the desired HNO_3 concentration) with a phase ratio of 1:1 at 298 K. After equilibration, Pd concentration in the aqueous phase was determined by ICP-OES (Model No. PQ 9000 Elite), and the distribution ratio of palladium (D_{Pd}) was calculated.

All electrochemical experiments were carried out in a three-electrode cell. For cyclic voltammetric measurements, a glassy carbon (cylindrical, SA = 0.07 cm^2) and a platinum wire were used as a working electrode and a counter electrode, respectively. As a quasi-reference electrode, a platinum wire was used. Cyclic voltammograms of the ionic liquid solutions were recorded using ZIVE SP2 (WonA Tech) equipped with Smart Manager program.

3. Results and discussion

The distribution ratio of palladium in solutions of 0.03 to 1 M DBSO/C_4mimTf_2N as a function of concentration of nitric acid is shown in Fig. 1. The extraction mechanism of palladium into C_4mimTf_2N can be best represented by a cation exchange reaction.

A plot of log D_{Pd} vs. DBSO concentration results in straight lines with a slope 2.3 from 0.05 M nitric acid feed and 1.0 from 5 M nitric acid feed.

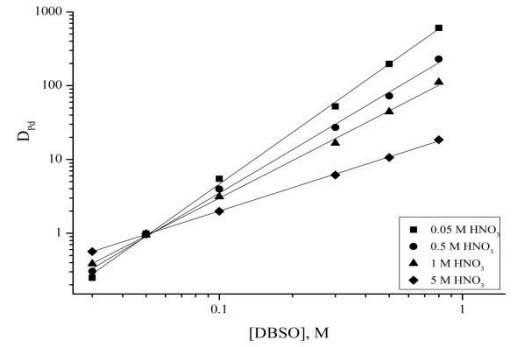

Fig. 1. Distribution ratio of palladium at varying DBSO concentrations extracted from HNO_3 feed into C_4mimTf_2N.

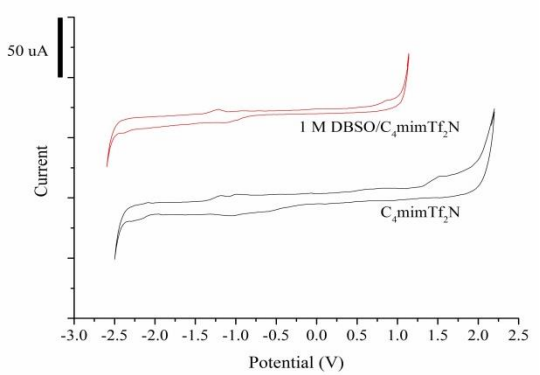

Fig. 2. Cyclic voltammogram of C_4mimTf_2N and 1 M DBSO/C_4mimTf_2N at 298 K.

The results indicate that, in high acidity, palladium is coordinated with 1.0 DBSO molecules, compared with 2.3 molecules in low acidity, due to competition between palladium and hydrogen ions.

The cyclic voltammogram (CV) of C_4mimTf_2N at 298 K on glassy carbon electrode is shown in Fig. 2. C_4mimTf_2N exhibits a window of 4.5 V. The CV of 1 M DBSO/C_4mimTf_2N is also shown in the same figure. Although the addition of DBSO shifts the peak potential anodically with a cathodic stability up to -2.5 V, it is sufficient for enabling the reduction of metallic ions into metal state.

30 mM of palladium ion was extracted from 0.5 M nitric acid using 1 M DBSO/C_4mimTf_2N. The CV for the reduction of Pd(II) in this solution on glassy carbon working electrode at the scan rate of 10 mV/s is shown in Fig. 3. The CV consists of a reduction wave occurring at a peak potential of -1.1 V, and oxidation wave occurring at peak potential of -0.7 V. The results from the CV experiments at various scan rates and temperatures indicate that a reduction of Pd(II) takes place through a quasi-reversible single-step two electron transfer reaction.

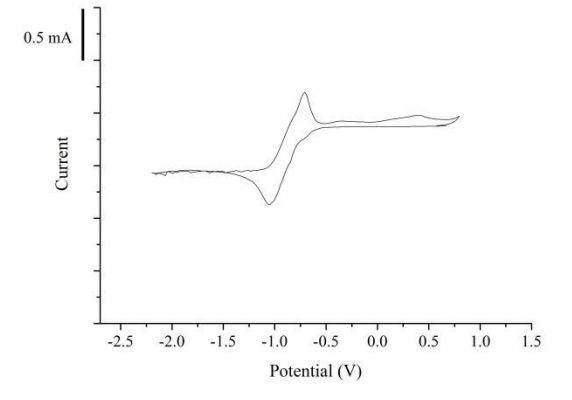

Fig. 3.Cyclic voltammogram of 1M DBSO/C_4mimTf_2N containing 30 mM $PdCl_2$ after extraction.

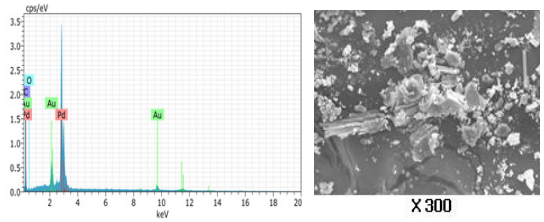

(a) (b)

Fig. 4. (a) EDS Analysis, (b) SEM photograph.

The cathodic peak current (i_p^c) depends linearly on square root of scan rate ($\nu^{1/2}$), which confirms that the reduction of Pd(II) is diffusion controlled.

Electrodeposition experiments of Pd ions extracted from 0.5 M nitric acid using 1 M DBSO/C_4mimTf_2N were carried out at -1.0 V potential. The current response for the potentiostatic electrolysis was stable throughout, and black and dense particles were deposited on the glassy carbon electrode. The XRD pattern and EDS of such deposit confirmed the palladium deposited in metallic form (Fig. 4.).

4. Conclusion

The extraction and electrochemical behavior of palladium in the new media, 1 M DBSO/C_4mimTf_2N, were investigated, and the feasibility of the Extraction-Electrodeposition (EX-EL) process was demonstrated. Lower distribution coefficient was obtained from higher acidity, and palladium ion formed a complex with less DBSO molecules in higher acidity.

The redox potential of palladium was obtained from DBSO/C_4mimTf_2N containing palladium either dissolved or extracted. The result of potentiostatic electrodeposition showed palladium recovery process using ionic liquid was feasible.

ACKNOWLEDGEMENT

This work was supported by the Nuclear Research and Development Program through the National Research Foundation of Korea funded by the Ministry of Science and ICT.

REFERENCES

[1] X.Q. Sun, H.M. Luo and S. Dai, Ionic liquids-based extraction: A promising strategy for the advanced nuclear fuel cycle, Chemical Reviews 112, 2100-2128 (2012).

Comparison of Radiolytic Decomposition of Oxidation Decontamination Solutions

N.O. Chang[1,2], H.J. Won[1*], S.Y. Park[1], S.B. Kim[1], and Y.S. Kim[2]
[1]Korea Atomic Energy Research Institute, 111, Daedeok-daero 989beon-gil, Yuseong-gu, Daejeon, Korea
[2]Department of Nuclear Engineering, Hanyang University, 222Wangsimri-ro, Seongdong-gu, Seoul, Korea
[*] nhjwon@kaeri.re.kr

1. Introduction

Before decommissioning, it is necessary to remove the radionuclides in the primary system of NPP. To remove it, HyBRID(Hydrazine-Base Reductive metal Ion Decontamination) chemical decontamination process developed by KAERI can be used. It consists of SP or SP(Cu) oxidizing and reducing process. In each process, the control of $KMnO_4$ or N_2H_4 concentration is important for removing oxide layer. However, permanganate ion and hydrazine decompose under the high radiation field during the decontamination. In this study, the radiolytic products of $KMnO_4$ are analyzed. Also, the results are compared with results of N_2H_4.

2. Methods and Results

2.1 Sample preparation and γ-ray irradiation

SP oxidizing decontamination agent was prepared with 6.33 mM $KMnO_4$ and 3.25 mM H_2SO_4. SP(Cu) agent was made of 6.33 mM $KMnO_4$, 3.25 mM H_2SO_4, and 0.5 mM $CuCl_2$. The absorbed doses of the samples were 0, 5, 10, 20, 40 and 80 kGy, respectively by using low-dose γ-ray irradiator of jeongeup.

2.2 Comparison of radiolytic decomposition Between SP and SP(Cu)

To analyze concentration of [$KMnO_4$], UV analysis method(UV spectrometer DR5000 of Hach Co.) was used. The amount of MnO_2 was calculated using relation of concentration of total manganese and [$KMnO_4$]. AA analysis(AAnalyst 400 of Perkin Elmer Co.) was used to analyze [Mn^{2+}]. The concentration change of each species against absorbed dose is shown in Fig. 1.

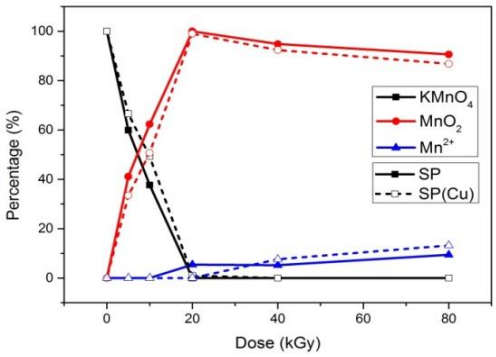

Fig. 1. Concentration change of $KMnO_4$, MnO_2, and Mn^{2+}.

As shown Fig. 1, it can be explained that [$KMnO_4$] decreases due to the reaction between MnO_4^- and radiolysis products of the water($\dot{O}H$, e_{aq}^-, etc.). After this reaction, MnO_4^{2-} is produced. MnO_4^{2-} reacts with H^+ rapidly and generates MnO_2 because it is unstable in acidic condition. After $KMnO_4$ is completely decomposed, MnO_2 reacts with e_{aq}^- and produce Mn^{2+} and OH^- [1]. However, as listed in Table 1, $KMnO_4$ in the SP agent decomposes but it remains in the SP(Cu) at 20 kGy. This can be explained by the eqs. (1) and (2) [2].

$$H^+ + Cu^{2+} + \dot{O}H \rightarrow Cu^{3+} + H_2O \quad (1)$$

$$e_{aq}^- + Cu^{2+} \rightarrow Cu^+ \quad (2)$$

As Cu^{2+} ion reacts with H^+ or e_{aq}^- in an acidic condition, the probabilities of reaction between MnO_4^{2-} and H^+, and MnO_2 and e_{aq}^- decrease. Thus,

SP(Cu) agent is expected to be more stable than SP agent in the radiation field.

Table 1. Percentage change of $KMnO_4$

Absorbed dose(kGy)	$KMnO_4$ in SP(%)	$KMnO_4$ in SP(Cu)(%)
0	100.0	100.0
5	59.0	66.6
10	37.7	49.3
20	0.0	1.0
40	0.0	0.0
80	0.0	0.0

2.3 Comparison of radiolysis between oxidizing and reducing decontamination agent

In the previous study, it is founded that radiolysis of N_2H_4 depends on existence of Cu^{2+} ions [3]. The result is shown in the Fig. 2.

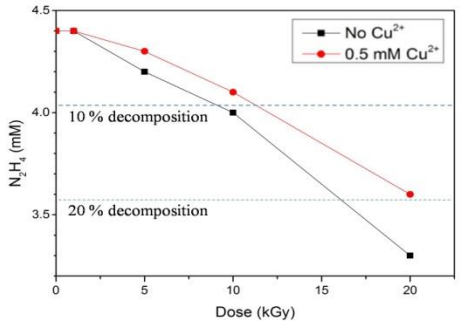

Fig. 2. Decomposition of [N_2H_4] under varied doses [3].

As shown in the Fig. 2, when Cu^{2+} ions are added, less N_2H_4 decomposes at the same absorbed dose. This phenomenon is similar to the [$KMnO_4$] change in the oxidizing decontamination agent.

3. Conclusions

$KMnO_4$ in the oxidizing decontamination agent decomposes during the γ-ray irradiation. SP(Cu) agent has higher stability than SP under the radiation field. The reason is explained by the reaction between Cu^{2+} ions and H^+ or e_{aq}^-. This phenomenon also occurs in the reducing decontamination agent N_2H_4. However, when high absorbed dose is irradiated, $KMnO_4$ decomposes completely regardless of presence of Cu^{2+} ions. Thus, it is necessary to estimate the absorbed dose of $KMnO_4$ during the decontamination and to decide the application times. It is also necessary to study the effect of other metal ions on the radiation stability of $KMnO_4$.

ACKNOWLEDGMENT

This work has been carried out under the Nuclear R&D Program (NRF-2017M2A8A5015144) funded by Ministry of Science and ICT.

REFERENCES

[1] R. Puspalata et al, "Gamma radiation induced formation and characterization of the nano-oxides of manganese", Radiation Physics and Chemistry, 85, 142-160 (2013).

[2] Paul Y. Feng et al, "High-Intensity Radiolysis of Aqueous Ferrous Sulfate-Cupric Sulfate-Sulfuric Acid Solutions", The Journal of Physical Chemistry, 74(6), 1221-1227 (1970).

[3] Wang-Kyu Choi et al., "Development of Advanced Decontamination Technology for Nuclear Facilities", KEARI/RR-3964/2014 (2015).

Effective Cross Section Estimation of ^{36}Cl and ^{41}Ca in Concrete of Kori Unit 1

Mee Jang, Hyunchul Kim, Chang Jong Kim, and Jong Myoung Lim
Korea Atomic Energy Research Institute, Daedeok-daero989ben-gil 111,Yuseong-gu, Daejeon, Republic of Korea
mjang@kaeri.re.kr

1. Introduction

The radionuclide inventory prediction of a nuclear power plant can help establish decommissioning plan by providing information of radiation environment. Accumulated radionuclide in reactors and related facilities after reactor shutdown can be divided into neutron activated materials and contaminated materials. Usually, the steps to calculate the radionuclide inventory are consist of two steps as follows: (1) calculating the neutron flux and (2) estimating induced radioactivity throughout the reactor. The neutron activated materials are generated in different amounts depending on the neutron flux and effective cross section.

In this study, we calculated the neutron flux and estimated the effective cross section of ^{36}Cl and ^{41}Ca in bio concrete of Kori Unit 1. These two radionuclides are important from the viewpoint of disposal because of its long half-life.

2. Methods and Results

2.1 Activation Products in Bio Concrete

Unlike metallic materials, which are specified in the technical standards of the American Society of Mechanical Engineers (ASME), concrete has no limit on the content of constituents. The composition of the bio concrete without impurity as shown in Table 1. [1] The type and content of impurities of concrete can be changed according to the factors such as manufacturing process and added aggregate. Therefore it is necessary to evaluate the amount of ^{36}Cl and ^{41}Ca produced depending on the impurities. The physicochemical characteristics of ^{36}Cl and ^{41}Ca are shown in Table 2.[2]

Table 1. Composition of the bio concrete without impurity

Element	Weight Fraction (%)
H	0.55
O	49.83
Si	31.57
Ca	8.26
Na	1.70
Mg	0.26
Al	4.55
S	0.13
K	1.91
Fe	1.23

Table 2. Physicochemical characteristics of ^{36}Cl and ^{41}Ca

Parent	^{35}Cl	^{40}Ca
Nuclear Reaction	n, γ	n, γ
Daughter Nuclide	^{36}Cl	^{41}Ca
Principal Emission	β-(β+, EC)	EC
Half-life(y)	301000	103000

2.2 Neutron Flux

To evaluate the effective cross section of ^{36}Cl and ^{41}Ca in bio concrete, it is necessary to calculate average neutron flux in each zone of reactor. In this research, we simplified the geometry of Kori Unit 1

as shown in Fig. 1 and consists of 8 zones as follows: (1) Baffle (2) Barrel (3) Bypass (4) Thermal Shield (5) Downcomer (6) RPV (7) Air (8) Bio Concrete. We calculated the averaged neutron flux in each zone using MCNPX code and the results are shown in Table 3.

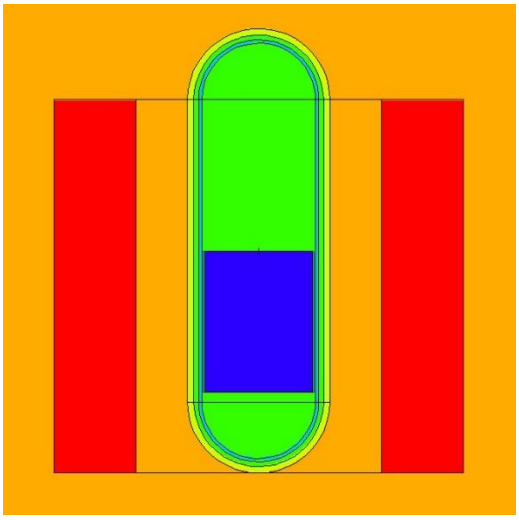

Fig. 1. Simplified geometry of Kori Unit 1.

Table 3. Neutron flux in each region of Kori Unit 1

	Zone	Neutron Flux(#/cm^2-s)
1	Baffle	7.79E+12
2	Barrel	4.41E+11
3	Bypass	2.79E+10
4	Thermal shield	3.59E+10
5	Downcomer	1.40E+10
6	RPV	6.73E+08
7	Air	2.75E+08
8	Bio concrete	1.39E+07

2.3 Effective Cross section in Bio Concrete

Using the calculated neutron flux, we estimated the effective cross section of ^{36}Cl and ^{41}Ca and the results are shown in Table 4.

Table 4. Effective Cross Section of ^{36}Cl and ^{41}Ca

Radionuclide	^{36}Cl	^{41}Ca
Reaction Rate	2.31E+08	2.24E+06
Effective Cross Section(barn)	1.794E+01	1.740E-01

3. Conclusion

In this research, we estimated the effective cross section of ^{36}Cl and ^{41}Ca using the averaged neutron flux in each region of Kori Unit 1. This results can be used the inventory of ^{36}Cl and ^{41}Ca using activation calculation code such as ORIGEN2.

REFERENCES

[1] International Atomic Energy Agency, “Radiological Characterization of Shut Down Nuclear Reactors for Decommissioning Purposes”, Technical Reports Series No. 389 (1998).

[2] Gil Yong Cha, Soon Young Kim, Jae Min Lee and Yong Soo Kim, “The Effects of Impurity Composition and Concentration in Reactors Structure Material on Neutron Activation Inventory in Pressurized Water Reactor”, Journal of Nuclear Fuel Cycle and Waste Technology, 14(2), 91-100 (2016).

The Applicability of pH Measurement as an Indicator for Estimation of Oxalic Acid Concentration

Jin-Hee Kim[1]*, Hyun-kyu Lee[1], Won-Zin Oh[1], and Sang-June Choi[1,2]
[1]Research Institute of Advanced Energy Technology, 80, Daehakro, Bukgu, Daegu, Republic of Korea
[2]Kyungpook National University, 80, Daehakro, Bukgu, Daegu, Republic of Korea
*Kimjinhee33@knu.ac.kr

1. Introduction

The key factor is less radioactive waste in applying the chemical decontamination method to remove the corrosion oxide film on the surface of NPP system. For this, the oxalic acid($H_2C_2O_4$) is widely used as a reducing agent, and thus oxalic acid waste liquid is generated[1]. To decompose the oxalic acid, a method of applying advanced oxidation processes(AOPs) has been studied, and UV/H_2O_2 treatment has been generally applied[2].

In the UV/H_2O_2 treatment, excessive H_2O_2 dose causes a scavenge effect that consume OH radicals[3], and thus an appropriate H_2O_2 dose estimate is required depending on the concentration of the treated target. However, during decomposing the oxalic acid by UV/H_2O_2 treatment, it is difficult to measure the concentration of oxalic acid immediately. Therefore, a measure for immediate concentration estimation is needed to estimate the appropriate amount of H_2O_2 dose depending on the concentration of oxalic acid.

In this study, pH was selected as an indicator to estimate the concentration of oxalic acid. To determine suitability as an indicator, it was confirmed that the pH depending on the concentration of oxalic acid with ferrous ion was appropriately fitted with the concentration of hydrogen ion according to the acid dissociation constant(pKa) of the oxalic acid. In addition, it was confirmed that pH in the decomposition of oxalic acid by UV/H_2O_2 was fitted with this model to assess whether it is applicable in the actual decomposition process.

2. Experiments

2.1 Fitting of pH depending on the concentration of oxalic acid

The oxalic acid has acid dissociation equilibrium as shown in the following equation, and it can estimate the concentration of hydrogen ion depending on the oxalic acid concentration.

$$H_2C_2O_4 \leftrightarrow HC_2O_4^- + H^+ \qquad pKa_1 = 1.25 \qquad (1)$$

$$HC_2O_4^- \leftrightarrow C_2O_4^{2-} + H^+ \qquad pKa_2 = 4.14 \qquad (2)$$

We confirmed how well the hydrogen ions concentration depending on the oxalic acid concentration(from the above equation) fitted the pH value of the mixed solutions of various concentration oxalic acid with 2 mM $FeCl_2$. The oxalic acid concentration was set as 5, 10, 15, 20, 25, 30 mM and MATLAB was used for pH calculation.

2.2 Applicability in oxalic acid decomposition process

In order to confirm the applicability of the model formula to the actual oxalic acid decomposition process, pH of the oxalic acid containing ferrous ion was measured over time in the UV/H_2O_2 treatment. The solution was prepared by mixing 2 mM ferrous chloride and 30 mM oxalic acid. For the UV/H_2O_2 treatment, 120 W amalgam lamp was used. After injection of 30 mM H_2O_2, the UV lamp was operated with 200 mL/min circulation using the peristaltic pump. The decomposition was carried out for 1 hour, and the change behavior of oxalic acid concentration and pH over time was observed. To investigate decomposition behavior of oxalic acid, Total Organic Carbon(TOC) was measured using TOC analyzer(TOC-V CPH, SHIMADZU, JAPAN)

3. Results

Fig. 1 shows that the comparison of pH by calculated from the acid dissociation constant and pH by measurement of the mixed solutions of various concentration oxalic acid with 2 mM $FeCl_2$. The results show that there is no significant difference between the pH calculated from the acid dissociation constant of pure oxalic acid and pH by measurement of the mixed solutions although 2 mM $FeCl_2$ is present. Also, as shown in Fig. 2, the pH calculated from the oxalic acid concentration over time in UV/H_2O_2 and the measured pH were not significantly different. However, there was a difference at the low concentration, which is considered to be the influence of residual Cl^- ion after decomposition.

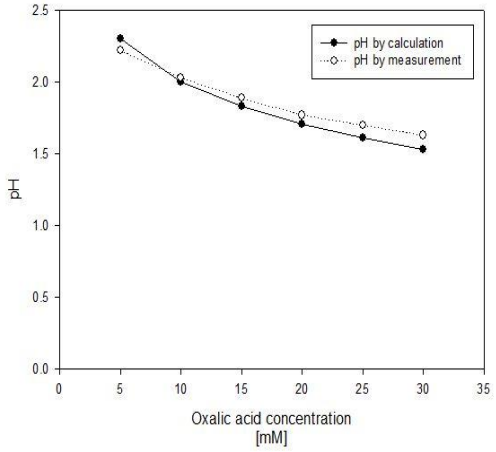

Fig. 1. Comparison of pH by calculation and by measurement depending on oxalic acid concentration.

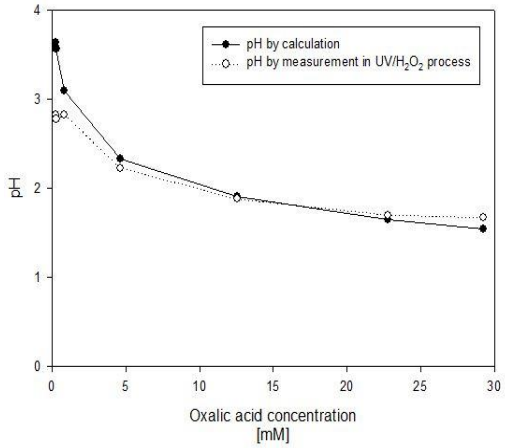

Fig. 2. Comparison of pH by calculation and by measurement in UV/H_2O_2 process.

4. Conclusion

It was investigated whether pH is suitable as an indicator for estimation of oxalic acid concentration. We obtained the following conclusion from the experimental results:

1. The oxalic acid containing Fe^{2+} ion follows hydrogen dissociation behavior similar to the acid dissociation equilibrium of pure oxalic acid
2. In the UV/H_2O_2 process to decompose oxalic acid, immediate concentration estimation is possible by measuring pH at concentration range above 5 mM.

5. Acknowledgement

This work was supported by the Korea Institute of Energy Technology Evaluation and Planning (KETEP) and the Ministry of Trade, Industry & Energy (MOTIE) of the Republic of Korea (No. 20141510300310).

REFERENCES

[1] Nagase, Makoto, et al., “Low corrosive chemical decontamination method using pH control, (I) basic system”, Journal of nuclear science and technology, 38(12), 1090-1096 (2001).

[2] Quici, Natalia, et al., “Oxalic acid destruction at high concentrations by combined heterogeneous photocatalysis and photo-Fenton processes”, Catalysis today, 101(3-4), 253-260 (2005).

[3] Wang, G. S., et al, “Characteristics of natural organic matter degradation in water by UV/H_2O_2 treatment”, Environmental technology, 27(3), 277-287 (2006).

Trend and Current State of Decommissioning Waste Quantity and Cost in Korea

Jae Yong Oh* and Taesik Yun

Decommissioning Technology Team, CRI, KHNP, 70, Yuseong-daero 1312beon-gil, Yuseong-gu, Daejeon, Korea

*jaeyongoh@khnp.co.kr

1. Introduction

Korea Hydro and Nuclear Power (KHNP) made a decision for permanent shutdown (PS) of Kori-1 on June 18th, 2015, which, finally, has been shut down since June 19th, 2017. Thus, decommissioning has emerged a matter of main concerns in Korean nuclear power industry.

Separately, KHNP has periodically evaluated decommissioning cost to comply with the Radioactive Waste Management Act and the corresponding government notices in Korea. Thus, it is necessary to calculate precise cost with the application of the regulation, guideline and site-specific characterization results or assumptions, since the feasibility study plays an important role in the decommissioning process. For this sake, estimation of decommissioning waste quantity and cost for Korean NPP are mainly described in this paper.

2. Methodologies & Results

Decommissioning cost can be regarded as all the cost for the decommissioning with regard to technical and administrative activities to allow the removal of the regulatory requirements from the decommissioning preparation to the site restoration [1]. In order to achieve the accuracy and details of decommissioning cost, Bottom-up approach is utilized based on Unit Cost Factors (UCF). UCF is defined as the simplified units for cost estimation of decommissioning activities for a number of Structure, System and Components (SSCs) including manpower, expenses [2].

2.1 Decommissioning Period and Assumptions

2.1.1 Decommissioning Period. The initial first two years are for planning of decommissioning preparation before PS of the NPP. With PS of the NPP, a transition period should be needed around 5 years. At the end of the transition period, approximately 8.5-year Decontamination and Dismantling (D&D) phase follows. The final phase of decommissioning is the site restoration which would be conducted at least two years. Fig.1 depicts the outline of decommissioning project phases and schedule.

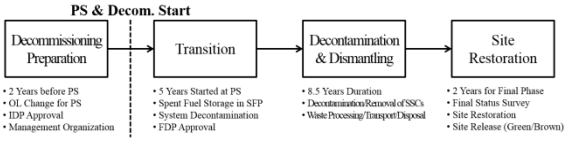

Fig. 1. Outline of decommissioning schedule.

2.1.2 Main Assumptions. According to the strategies generally suggested, NPP decommissioning will be carried out by the immediate dismantling known as DECON. Some of the scenarios of

decommissioning are listed in Table 1.

Table 1. Assumptions for decommissioning scenarios

Scenarios	Assumptions
Alternatives	Immediate Dismantling (DECON)
Decom. Operator	Utility (KHNP)
Decontamination	In Decommissioning Site
Final Site Status	Brown Field

2.2 Plant Inventory and Waste Quantity

SSCs should be surveyed by a sort of data to generate Plant Inventory (PI) DB. After the construction of PI DB, PI DB is going to be converted to waste quantity. By using this method, Ministry of Trade, Industry and Energy (MOTIE), in Korea expected the waste quantity in a range of 14,500~18,850 drums.

2.3 Decommissioning Cost Estimation

In pursuance of decommissioning cost estimation, a series of UCF are altered from PI DB as input data to a cost computation program. Decommissioning cost estimation are carried out as shown in Fig. 2.

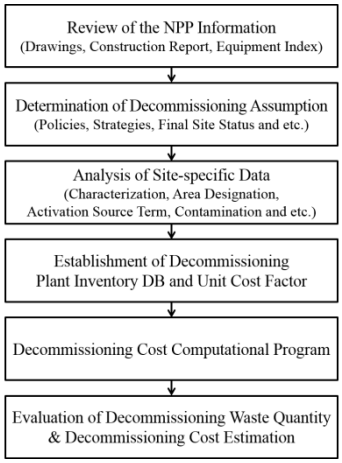

Fig. 2. Flow diagram of decommissioning cost estimation.

2.4 Updates of Decommissioning Cost in Korea

Decommissioning cost is periodically updated as demonstrated in Table 2 to observe the relevant regulations in Korea. The cost consists of project management and removal, waste disposal and contingency [3].

Table 2. Trend of Decommissioning Cost in Korea

Year / Cost(M$)	2003	2012	2014	2016
Project Mngmt.	69.4	291.3	359.8	383.9
Waste Mngmt.	241.4	232.3	231.3	239.8
Contingency		43.7		
Total	310.8	567.3	591.1	623.7

3. Conclusions

Since there is no real radiological characterization and site-specific data for Korean NPP, to date, decommissioning cost is limited to the preliminary analysis. It is noted that discrepancies might be presented between future actual cost and current estimated cost. In this regards, to make up for the deficiency of data should be key factor to calculate decommissioning cost in an accurate manner.

REFERENCES

[1] Nuclear Energy Agency, Improving Nuclear Regulation, NEA No. 6275, OECD (2009).

[2] Thomas S. L., etc., Guidelines for Producing Commercial Nuclear Power Plant Decommissioning Cost Estimates, AIF/NESP-036, Volume 1 (1986).

[3] Notice of Ministry of Trade, Industry and Energy, 2017-195 (2017).

Kori-1 Decommissioning Project Expense Evaluation

Jae Yong Oh*, Jihwan Yu, Younggook Kim, Gilim Kim, Hyejin Jung, and Wook Sohn
Decommissioning Technology Team, CRI, KHNP, 70, Yuseong-daero 1312beon-gil, Yuseong-gu, Daejeon, Korea
*jaeyongoh@khnp.co.kr

1. Introduction

In Korea, a general decommissioning cost per one unit has been estimated (623.7 million US dollars). However, to undertake the decommissioning project for a specific unit in a reliable way, it is necessary to evaluate a decommissioning project expense using site-specific information. Furthermore, in order to manage the project in a detailed and economic manner, decommissioning project expense is based on decommissioning waste quantity and cost estimation similar to those of construction expense. Therefore, this paper describes the methodologies for the evaluation of the project expense for Kori-1, the first commercial Nuclear Power Plant in Korea.

2. Methods & Current States

To evaluate the decommissioning project expense for Kori-1, decommissioning cost computation program is used, which calculates Project Expense for Kori-1 based on decommissioning waste by incorporating Plant Inventory (PI) database and other information as shown in Fig. 1.

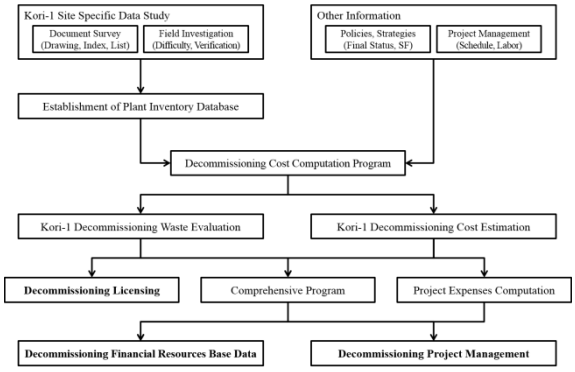

Fig. 1. Process and Applications of Decommissioning Cost.

2.1 Kori-1 Site-specific Plant Inventory Study

2.1.1 Document Survey. Site-specific document survey should be conducted for PI establishment the same as erstwhile decommissioning cost estimation. For Kori-1, some of the essential materials for PI study are depicted in Table 1.

Table 1. List of essential materials for PI study

Type	Essential Materials
Kori-1 Specific Data	Drawings, Construction Report, Indices, Lists, Non-radiological & Radiological Survey data
Other Information	Final Status of Site Release, Schedule & Process, Standard of Construction Estimate

2.1.2 Field Investigation. Field investigation is one of the most important activities that Kori-1 decommissioning project expense differentiated from the existing decommissioning cost in Korea. Main targets of Kori-1 field investigation are listed in Table 2.

Table 2. Targets of Kori-1 field investigation for PI study

Category	Main Target of Field Investigation
Structures	Building (Reactor, Auxiliary, Service, Miscellaneous, etc.), Yard, Structural Steel
Systems	NSSS, CVCS, Reactor Cooling, Main Steam, Feedwater, Fire Protection
Components	Reactor Vessel, Steam Generator, Turbine, Generator, Condenser, Pump, Pipe, Valve, Tank

2.2 Decommissioning Cost Computation Program

Computation program is utilized to process a lot of input and output data as shown in Fig. 2 for Kori-1 decommissioning cost estimation [2]. Investigated Kori-1 site-specific materials and surveyed other information are used as input data in computation program. The computation results, decommissioning waste quantity and cost, reflect to licensing, project expense and etc.

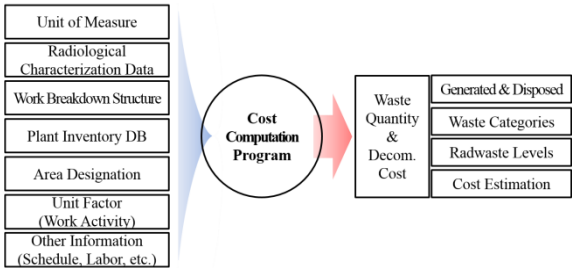

Fig. 2. Input and output in Cost Computation Program.

2.3 Decommissioning Project Expense Evaluation

Differentiated from decommissioning cost, project expense is going to stand on the basis of Cost Breakdown Structure (CBS), a kind of Work Breakdown Structure (WBS). CBS based expense is evaluated with the purpose of easy project management such as fund accounting and service design.

2.4 Conceptual Design on Waste Quantity, Cost and Process Comprehensive Program

KHNP has developed the 3D-based decommissioning waste quantity estimation program using Building Information Modelling (BIM) for Kori-1 [3]. Comprehensive program, linked with cost and process, is being improved from waste estimation program.

3. Conclusions

Different from decommissioning cost, Kori-1 decommissioning project expense is not easily evaluated due to the lack of precedents analysis. However, KHNP tries its best to progress the project expense evaluation in a variety of fields and methods. The ultimate result of project expense evaluation can contribute to the safe and reliable decommissioning for Kori-1. Applications of this investigation are expected to acquire licensing, appropriate service order to supply chains, and effective project management.

REFERENCES

[1] Notice of Ministry of Trade, Industry and Energy, 2017-195 (2017).

[2] Kim, H.; Park, J., Development of Computer Program for Estimating Decommissioning Cost, 2011 ICEM, Sep. 28.

[3] Kim, J.; Min, B., Development of 3D-based Nuclear Power Plant Decommissioning Waste Quantity Estimation Program, Proc. of the 2016 Autumn Conference, 14(2), Oct. 12-14, Jeju.

Risk Assessment Method for the Decommissioning Activities by Using Risk Matrix

Hyung-Woo Seo, Kwang-Ho Jo, and Kun-Man Kwon

Korea Hydro & Nuclear Power (KHNP) Central Research Institute, 70, 1312-gil, Yuseong-daero, Yuseong-gu, Daejeon, Republic of Korea

1. Introduction

One of the important parts of NPP (Nuclear Power Plant) decommissioning preparation is to secure the safety associated with planned activities. Various approaches have been used to evaluate safety for NPP decommissioning. Methodologies such as HAZOP (HAZard and OPerability analysis) for identification of possible deviations form planned activities, or risk matrix for risk rating have been used for a safety evaluation. In particular, in using the risk matrix, setting the levels such as radiation exposure, consequences, and likelihood for each axis will be a crucial factor to be resolved. Therefore, in this study, we introduce a risk rating methodology using the risk matrix for decommissioning activities.

2. Methods

2.1 The main steps of safety assessment

In the safety assessment, relevant items to be performed at the initial stages are the characterization of the site and systems to be decommissioned. The use and handling of nuclear fuels are known as the main content of the safety assessment during the operation of NPP, while the radioactivity and systems, structure, and components (SCCs) are the main subject during the decommissioning. In summary, the safety assessment of a NPP identifies potential events in decommissioning activities and, therefore, assesses its impact during normal decommissioning or in the event of an accident. It is a series of processes that compares the evaluation results with the safety standards and implements controls to safely manage risks that do not meet the criteria. The main steps of safety assessment can be listed [1]: (1) safety assessment framework; (2) description of the facility and decommissioning activities; (3) hazard identification and screening; (4) hazard analysis; (5) engineering analysis; (6) evaluation of results and identification of safety control measures; (7) independent review by the operator and/or regulator prior to implementation of the controls in practice.

2.2 Risk matrix for risk assessment

As a methodology for assessing safety, risk matrix has been used to rank various risks in order of importance. The risk matrix consists of the elements of two axes; in order to determine the rankings, the risk is determined by multiplying the values of two elements of the axis by the level values. The risk matrix shown in Fig. 1 would be an example.

Consequence	Injury	Level of likelihood				
		1	2	3	4	5
		< 10%	10% ~ 25%	25% ~ 50%	50% ~ 75%	> 75%
5	> 1 yr or death	5	10	15	20	25
4	3 mon ~ 1 yr	4	8	12	16	20
3	1 mon ~ 3 mon	3	6	9	12	15
2	1 week ~ 1 mon	2	4	6	8	10
1	No injuries	1	2	3	4	5

Fig. 1. Example of risk matrix.

The safety assessment of the decommissioning activities is largely divided into works associated with radiological hazards and non-radiological hazards. The likelihood will be used as input values as one axis for both radiological hazards and non-radiological hazards, and the other axis will be the radiation exposure and the consequence.

2.3 The levels of consequences and likelihood

In general, the risk matrix may be a 3 × 3 cells, 5 × 5 cells, 5 × 7 cells, or more cells matrix depending on the levels of radiation exposure, consequences, and likelihood as elements of axes. And the frequency and severity of accidents are determined by scaling down or raising the levels depending on the scale of activities and processes being evaluated [2]. Therefore, in applying the risk matrix for decommissioning NPPs, appropriate application shall be made to the levels of risk consequence and likelihood.

3. Results & discussion

3.1 The Level of consequence

Table 1 demonstrates the severity of consequences for the activities to assess the radiological and non-radiological risks associated with the decommissioning work.

Table 1. Levels of consequence

Level	Description	Radiation Dose [3]	Injury or Disease [3]
1	Insignificant	< 0.1 mSv	No injuries
2	Minor	0.1-1 mSv	1 week-1 mon
3	Moderate	1-20 mSv	1-3mon
4	Major	20-100 mSv	3mon-1yr
5	Severe	>100 mSv	>1yr or one death

3.2 The Frequency evaluation table

The frequency of occurrence is usually determined by taking into account recent industrial accidents, disasters, and anticipated risks in a similar situation. Therefore, in this study, the frequency is assumed consisting of 5 levels as shown in Table 2.

Table 2. Frequency evaluation table

Level	Description	Decision Criterion
1	None	- Not expected to occur. - Less than 1 occurrence in 5 years.
2	Attention	- Very unlikely. - Less than 2 occurrences in 5 years or 2~3 in a similar situation.
3	Caution	- Unlikely. - Less than 3 occurrences in 5 years or 4~5 in a similar situation.
4	Warning	- Likely. - Less than 5 occurrences in 5 years or 6~7 in a similar situation.
5	Danger	- Very likely. - More than 5 occurrences in 5 years or more than 7 in a similar situation.

3.3 Risk evaluation

The risk of decommissioning activities can be ranked in accordance with the classified consequences and frequency, and the risk assessment table can be depicted as Fig. 2 based on proposed levels of radiation dose, injury, and likelihood. Depending on the risk rating, the red area will not be allowed to work, and it will be possible to classify activities requiring a stepwise conditional acceptance or management measures.

Consequence	Radiation Dose	Injury or Disease	Level of likelihood				
			1	2	3	4	5
			None	Attention	Caution	Warning	Danger
5	> 100 mSv	> 1 yr or death	5	10	15	20	25
4	20 - 100 mSv	3 mon ~ 1 yr	4	8	12	16	20
3	1 - 20 mSv	1 mon ~ 3 mon	3	6	9	12	15
2	0.1 - 1 mSv	1 week ~ 1 mon	2	4	6	8	10
1	< 0.1 mSv	No injuries	1	2	3	4	5

Fig. 2. Risk evaluation table.

4. Conclusion

In this paper, we reviewed the level of consequences and likelihood that should be established to determine the activities in order of importance for the safety assessment of NPP decommissioning. Each level can be defined in terms of the nature and scale of the work, and we set the criteria by referring to the existing risk assessment method for the general industry and materials related to safety management in NPP operation. The classified detailed level of the risk matrix of this study can be more expanded in the future to enhance the reliability of the safety assessment and to be used as a reference for evaluation of the safety of NPP decommissioning.

REFERENCES

[1] IAEA, Safety Assessment for Decommissioning, International Atomic Energy Agency Safety Reports Series No. 77, 2013.

[2] KOSHA, Guidelines for risk assessment of machinery and equipment manufacturing, Korea Occupational Safety and Health Agency, G-84-2012, 2012.

[3] Kwan-Seong Jeong, Kune-Woo Lee, Hyeon-Kyo Lim, Risk Assessment on hazards for decommissioning safety of a nuclear facility, Annals of Nuclear Energy, 2010.

Design of the Advance Remote Dismantling System Framework

Jonghwan Lee*, Sungmoon Joo, Dongjun Hyun, and Ikjune Kim

Korea Atomic Energy Research Institute, 111, Daedeok-daero 989beon-gil, Yuseong-gu, Daejeon, Republic of Korea

*jhl@kaeri.re.kr

1. Introduction

The dismantling process of core equipment for high radioactivity in nuclear power plants is a complex process that requires various technologies and equipment, while considering economy and safety [1]. The basic concept of the advanced remote dismantling system under development is to optimize the disassembly process in real time through 3-dimensional process simulation based on the design data and on-site environment data, and to perform the dismantling process safely and efficiently with the robot remotely. This paper introduces the framework of advanced remote dismantling system set up for this purpose.

2. Module configuration of the system

The main components of the advanced remote dismantling system are environmental information acquisition module, environmental information feedback module, and a number of remote operation modules for cutting and transporting and so on. The environmental information acquisition module acquires the on-site environment information of the dismantling process as point cloud data through three-dimensional space scanning and obtains the as-built drawing using the obtained point cloud data. The environmental information feedback module compares the measured drawings with the existing design drawings, updates the design drawings when differences are found, or detects changes in the progress of cutting operations and reflects them in the work plan. Remote operation modules is a module for performing remote cutting and transfer operations through pre-simulation such as multi-axis robot manipulator capable of remote or autonomous control, vertical rail for conveying the manipulator, and gantry crane.

3. Design of the system framework

Since each module composing the advanced remote dismantling system must interoperate with each other in real time during operation, its system framework should be constructed considering simplification of communication network and load distribution of unit system. The requirements for the modules of the advanced remote dismantling system include a number of functional requirements for

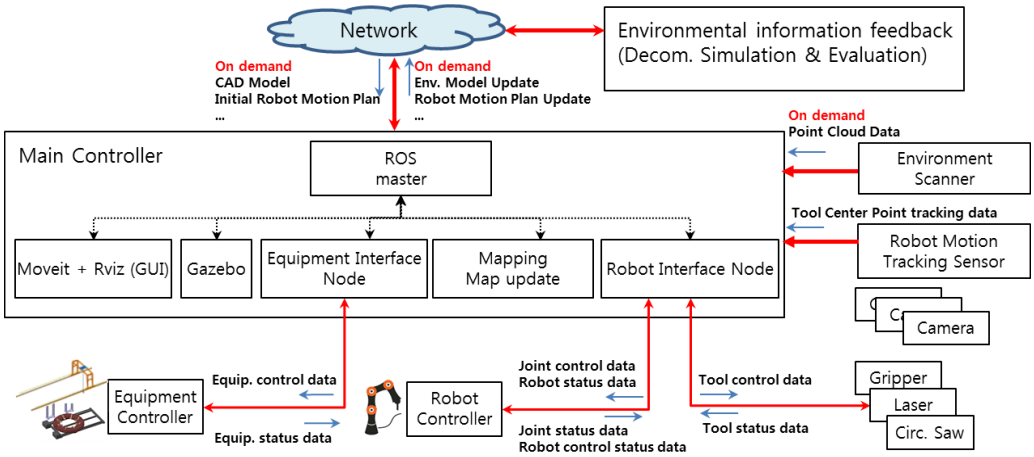

Fig. 1. System framework of the advanced remote dismantling system.

master controller, command generation, three-dimensional geometry mapping & update, dynamic re-planning, interactive remote control and so on. Figure 1 shows the overall system framework for interoperating modules based on these functional requirements. This framework links each component based on ROS-based master controller including sub-functional elements such as Mapping & Update part, Robot interface node, Equipment interface node, etc., and allows each component to exchange necessary information according to the derived functional requirements.

4. Conclusion

The designed framework will be continuously improved through ongoing research and will be validated through virtual commissioning technology. The advanced remote dismantling system to be developed through this framework is expected to provide an innovative way to economically and safely dismantle nuclear facilities with high radioactivity.

ACKNOWLEDGEMENT

This work was supported by the nuclear research and development program (2017M2A8A5015146) through the National Research Foundation of Korea, funded by the Ministry of Science and ICT, Republic of Korea.

REFERENCES

[1] J. Lee, G.-H. Kim, I. Kim, D. Hyun, K.S. Jeong, B.-S. Choi and J. Moon, “Establishment of the framework to visualize the space dose rates on the dismantling simulation system based on a digital manufacturing plat-form”, Annals of Nuclear Energy, 95, 161-167 (2016).

Establishment of Technology Requirements for Environmental Information Feedback to Dismantle Core Facilities of Nuclear Power Plants

Jonghwan Lee*, Ikjune Kim, Sungmoon Joo, Dongjun Hyun, and Shin Young Kang
Korea Atomic Energy Research Institute, 111, Daedeok-daero 989beon-gil, Yuseong-gu, Daejeon, Republic of Korea
*jhl@kaeri.re.kr

1. Introduction

The dismantling process of nuclear facilities with high radioactivity is a complex process requiring various technologies and equipments while being economical and safe. Lack of dismantling site information causes process inefficiency in dismantling process [1]. If the environmental information of the dismantling site is linked to the remote cutting system in real time and reflected directly to the planned dismantling process, the process can be corrected and supplemented in a short time, and the economical efficiency and efficiency of the dismantling process can be further improved. This study explains the requirements of environmental information feedback technology to reflect environmental information instantly on dismantling site in dismantling process.

2. Preprocessing for dismantling environmental information feedback

In general, data for optically acquiring surface coordinate information and related attributes of an object is stored in the form of a point cloud having three-dimensional coordinates. In the case of a large object such as a nuclear core facility, in order to scan the entire surface optically, the position and orientation of the scanner are changed and scanned at various positions and angles. The three-dimensional point cloud data corresponding to the scenes scanned at different positions and angles need to be transformed into a single coordinate system and merged. Since the point cloud created through this process is a set of simple three-dimensional points, it must be modeled again as a three-dimensional geometry using a manual or appropriate (automatic

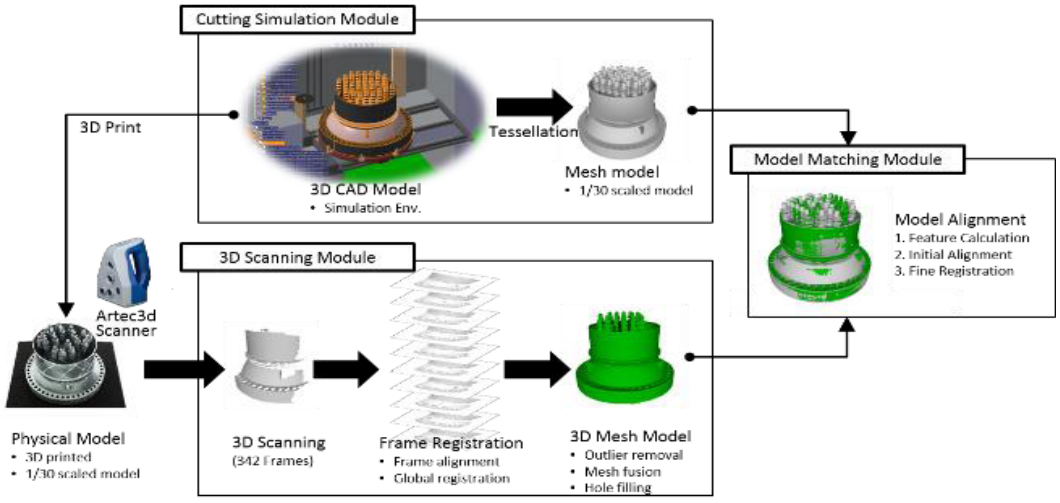

Fig. 1. Overall configuration of the software test bed for the environmental information feedback system.

or semi-automatic) algorithm for comparison analysis with the design information of the dismantling target.

3. Establishment of technology requirements with environmental information feedback test bed

Even if a three-dimensional model with high accuracy is obtained by acquiring the environmental information of the dismantling site, it is necessary to analyze the deviation by comparing it with the three-dimensional model of the dismantling process simulation in order to reflect it in the dismantling process simulation. If necessary, the three-dimensional model of the existing simulation should be updated again based on the three-dimensional environment information obtained from the dismantling site. This process needs to deal with not only simple shape information but also semantic information. The goal of the test bed for the environment information feedback is to set the technical requirements for feedback of the dismantling environmental information by performing a matching test between the scan model of the actual mockup and the CAD model of the simulation environment. Figure 1 shows the overall configuration of the software test bed for the environmental information feedback system. The technical requirements of the environmental information feedback system derived from the multiple tests with the actual mockup output by the 3D printer using this test bed are as follows.

- Consider the local feature description method for feature calculation because the scan model does not have perfect shape.
- Both models require sampling of the same resolution dataset for improved matching accuracy.
- In CAD model, point sampling is needed not only in vertex coordinates but also in face.
- Diversification of future feature extraction method according to the shape of the model

4. Conclusion

The environmental information feedback system will be continuously improved through the test bed based on the derived technical requirements. This technology is one of the key technologies for the advanced remote dismantling systems and is expected to provide a new approach for economical and safe dismantling of high radioactivity core facilities.

ACKNOWLEDGEMENT

This work was supported by the nuclear research and development program (2017M2A8A5015146) through the National Research Foundation of Korea, funded by the Ministry of Science and ICT, Republic of Korea.

REFERENCES

[1] J. Lee, G.-H. Kim, I. Kim, D. Hyun, K.S. Jeong, B.-S. Choi and J. Moon, “Establishment of the framework to visualize the space dose rates on the dismantling simulation system based on a digital manufacturing plat-form”, Annals of Nuclear Energy, 95, 161-167 (2016).

Strategy of the Kori-1 Final Decommissioning Plan Base on IAEA Safety Assessment Methodology

Kwang-Ho Jo*, Hyung-Woo Seo, and Kun-Man Kwon

Korea Hydro & Nuclear Power Central Research Institute, 70, Yuseong-daero 1312beon-gil, Yuseong-gu, Daejeon, Republic of Korea

*kwangho.jo@khnp.co.kr

1. INTRODUCTION

Kori unit 1, the Korean oldest commercial NPP, was permanently shut down in 2017 without a second extended operation. Within five years after its shutdown, KHNP, the licensee, should submit a final decommissioning plan (FDP) to the regulator with incorporating the results of the public hearings in order to get approval for decommissioning.

The safety assessment is one of essential part of the PDP because it describes how exposures of workers and the public are kept as low as reasonably achievable (ALARA) below the relevant limits during decommissioning. However, there is no specific assessment guideline for FDP yet. For this sake we have carried out the review and analysis of IAEA safety assessment methodology and its exposure pathway to apply to the FDP.

In this article, the IAEA approach for safety assessment is reviewed taking into accounts the requirement of the related regulatory notice. Also, potential radiological exposure pathways are investigated for analysis of exposure doses of workers and the public due to normal decommissioning activities.

2. DEVELOPMENT OF THE FDP

2.1 Relationships with Regulatory Requirements

Fig. 1 shows the relationships between the regulatory requirements and the IAEA approach related to the safety assessment. For example, HAZARD Identification and Screening, the third step of the IAEA process where existing and future hazards (both radiological and non-radiological) under normal and accident conditions during decommissioning are identified and estimated matches with the regulatory requirements 2), 5) and 6).

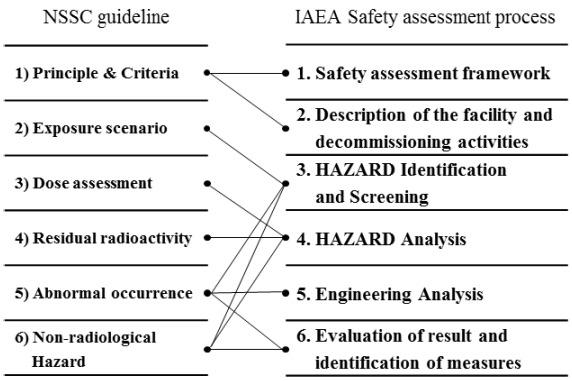

Fig. 1. Comparison of the NSSC with IAEA.

2.2 Practical considerations

To identify hazards, method(s) appropriated for a specific facility should be selected among HAZOP, checklist, and brainstorming [2]. Then, the hazard is analyzed in terms of the severity of risk.

Since the dismantlement of a facility may include various activities, risks for workers and the public should be assessed based on the dismantlement activities in question. For example, for cutting activities, the risk from airborne particles should be assessed in an appropriate manner by taking into accounts work time, distance and the number of worker. Generally, the risk assessment requires that parameters, which are not available, be assumed reasonably.

3. EXPOSURE PATHWAY

3.1 Pathways to Workers and the Public doses

Decommissioning is different from operation in terms of causes for doses incurred. For instance, decommissioning includes cutting of radioactively contaminated materials in which radioactive dusts and gas are dispersed into work space. Thus, for the safety assessment, it is necessary to estimate the

amount of radionuclides released under the assumed normal conditions by considering residual radioactive inventory, dismantling activities and schedule of decommissioning

The radiological waste disposal strategies are under the established through collaboration with KEPCO E&C. In accordance with the IAEA methodology, the assumed exposure pathway is developed [3]. The dismantled wastes will be temporarily stored in the building which was not designed for waste storage, that is, the concrete wall and ceiling of the building do not have sufficient shieling effects. Fig. 2 shows a variety of exposure pathways resulting from the release of radionuclides and radiation during dismantling activities.

3.2 Airborne particles modeling approaches

The kerf volume and the kerf area of components of interest are important factors for dose evaluation, because radioactive contamination is limited to the material surface in contaminated components, and activated products are uniformly distributed in the activated components. The kerf width is actually decided by the choice of the cutting tool applied. The kerf length depends on the type of the container in which the component will be stored. Shapes of components such as piping and ducts also affect the kerf lengths. Therefore these factors need to be considered during decommissioning activities.

4. FUTURE WORK

For the sake of decommissioning in a safe manner reasonable assumptions are very important to evaluate the dose of workers and the public. The assumptions required for the evaluation of each activity shall be reviewed as well as analysis methods for each activity should be developed. Furthermore, practical waste management strategy should be established.

REFERENCES

[1] Nuclear Safety and Security Commission, Regulations of Nuclear Facilities Decommissioning Plan, Notice 2015-8.

[2] Safety Assessment for Decommissioning, IAEA Safety Report Series No.77.

[3] Safety Assessment for Decommissioning of a Nuclear Power Plant, IAEA Safety Report Series No.77. Annex I, Part A

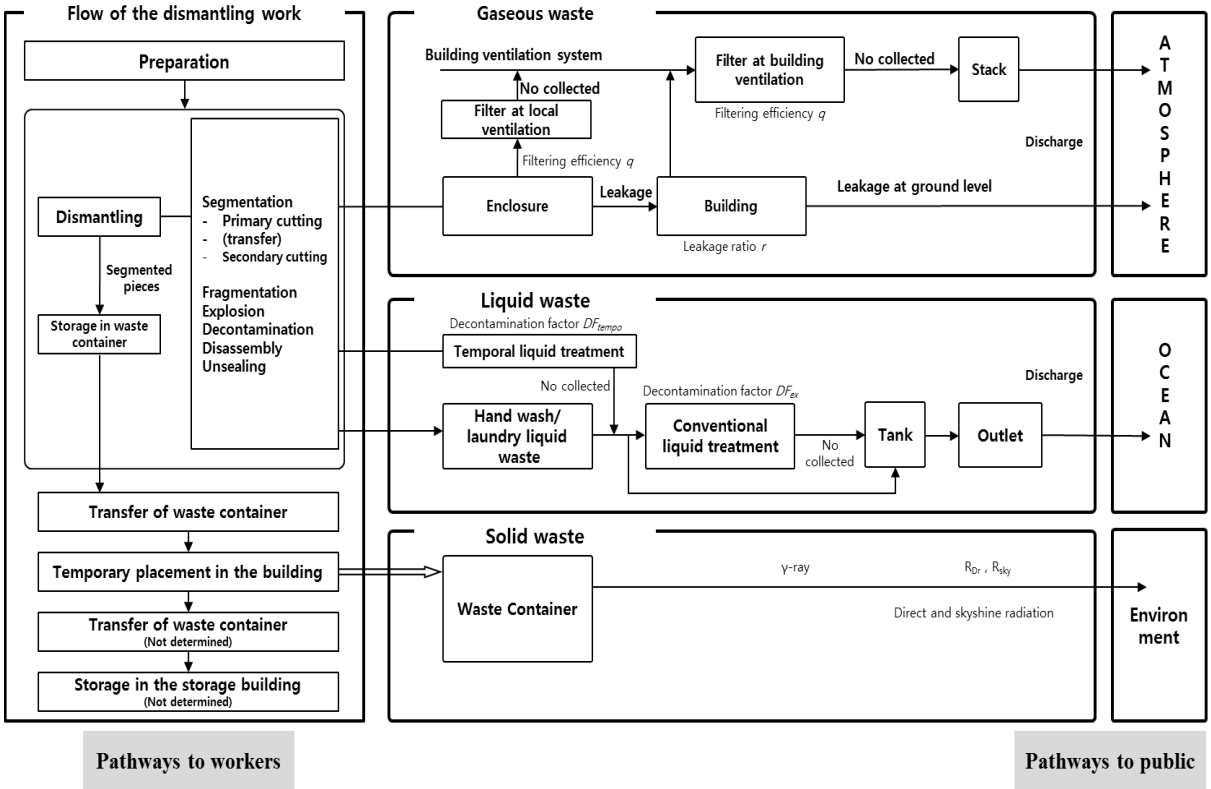

Fig. 2. Relationship of dismantling processes and pathways.

Measurement of Minimum Detectable Activity for Clearance Level

Min-Seung Ko*, Jae-Yong Lee, Kyung-Min Kim, and Yong-Soo Kim
Dept. of Nuclear Engineering, Hanyang Univ., 222 Wangsimni-ro, Seongdong-gu, Seoul, Republic of Korea
*hjgo2003@hanyang.ac.kr, chungooc@hanyang.ac.kr, nuclearphy@hanyang.ac.kr, yongskim@hanyang.ac.kr

1. Introduction

Many decommissioning wastes are generated during decommissioning NPP. In particular, very low level wastes occur mostly. Table 1. shows that by the year 2090, the very low level radioactive waste among the total 616,000 drums is the largest with 413,336 drums (67.1%) [1].

Table 1. Occurrence of Domestic Decommissioning Waste by 2090

Classification	Number of Drums (rate, %)
Intermediate Level Waste	25,872 (4.2)
Low Level Waste	176,792 (28.7)
Very Low Level Waste	413,336 (67.1)
Total	616,000 (100)

Therefore, if it is possible to accurately classify and dispose that are very low level wastes and general wastes, economic and environmental benefits will be gained.

In Korea NPP, clearance level for radionuclide of IAEA is followed [2]. Therefore, it is necessary to be able to measure less than the clearance level of radionuclide. Very low level waste has a wide variety of shape and characteristics. There is a need for technologies that can accurately measure the characteristics of various wastes.

In this study, we conducted to evaluate the factors that can affect the MDA (Minimum Detectable Activity) research using the standard source and designed box.

2. Methods and Result

2.1 Experiment

To measure the change of MDA according to time and background count, the experimental equipment was configured as shown in Fig. 1.

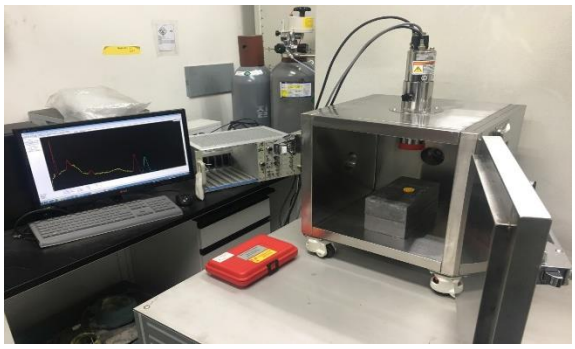

Fig. 1. Detection system composed of NaI(Tl) Scintillator and genie-2000.

As shown in Table 2., NaI(Tl) scintillation was fixed in the measurement box and the standard source was measured with Genie-2000 software. Co-57, Co-60, and Cs-137 were selected for the standard source to measure from low energy to high energy.

Table 2. NaI(Tl) Scintillation

Model	Efficiency	Voltage	Range	Number of channel
Canberra 802-2*2	7.5%	1100V	2MeV	1024

The measurement time and the background count were set as variables to measure changes in the MDA value.

As the thickness of the shield increases, the background count decreases. To measure the reduction of MDA due to shielding, measurements were conducted for 200s at the lead 0mm (air), lead 3mm (measurement box) and lead 50mm (lead brick). We also measured the change in MDA from 50s to 1000s.

2.2 Result

As a result of the experiment with lead thickness of 0mm, 3mm, and 50mm at the measurement time of 200s as shown in Fig. 2., MDA decreased during increasing the thickness of the lead and decreasing the background count.

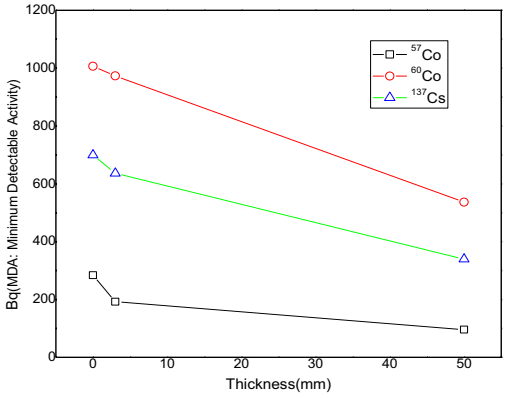

Fig. 2. MDA values varying with shield thickness at 200s.

As shown in Fig. 3., the MDA value decreased in the entire energy range as measurement time increases at the lead 50 mm.

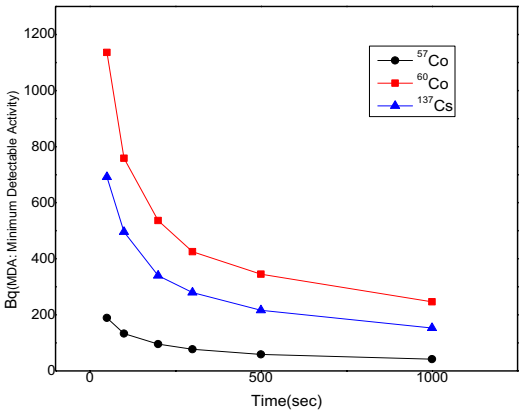

Fig. 3. MDA value that varies with measurement time at lead 50mm.

3. Conclusion

In this paper, we conducted a basic study to measure below clearance level in actual decommissioning wastes.

There is a need to set the appropriate measurement time and shielding thickness when measuring very low level waste after NPP decommissioning.

A measurement box was constructed to measure very low level waste of various shapes. Also, it is necessary to develop the technology for the clearance level by increasing the reliability of measured values through MCNP simulation.

REFERENCES

[1] Korea Radioactive Waste Agency, Analysis of scenario for management of decommissioning waste, KORAD/TR/2013-24 (2013).

[2] Nuclear Safety and Security Commission, NSSC Notice No. 2014-003 (2014).

Comparison Study of MARSSIM and EURSSEM Methodology for Final Status Survey

Inhye Hahm*, Sang Bum Hong, and Bum-Kyoung Seo
Korea Atomic Energy Research Institute, Daedeok-daero989ben-gil 111,Yuseong-gu, Daejeon, Republic of Korea
*hih@kaeri.re.kr

1. Introduction

After decommissioning of nuclear facilities, the residual radiation and radioactivity survey method are required for performing regulatory clearance of decommissioning sites. Methods and guidance have been developed for evaluating environmental and facility radiological surveys conducted to demonstrate compliance with a dose- or risk-based regulation. This study compares the Multi-Agency Radiation Survey and Site Investigation Manual (MARSSIM) [1] developed by the multi US agency workgroup and European Radiation Survey and Site Execution Manual (EURSSEM) [2] developed by European Community.

2. Comparison of MARSSIM and EURSSEM

2.1 Background and Target Scope

The MARSSIM is a standardized approach for final status radiological survey for demonstrating compliance developed collaboratively by four Federal agencies having authority and control over radioactive materials: Department of Defense (DOD), Department of Energy (DOE), Environmental Protection Agency (EPA), and Nuclear Regulatory Commission (NRC). MARSSIM targets building surface and surface soil. We cannot apply MARSSIM to subsurface (>15cm) soil contamination.

The first edition of EURSSEM is not an abbreviation for the current European Radiation Survey and Site Execution Manual but for the European Radiation Survey and Site Execution Manual. It develop by “Co-ordination Network on Decommissioning of Nuclear Installations Project (2008-2008)” funded by the European Community. [3]

EURSSEM is a much wider range of manuals that closely matches MARSSIM with regard to the final status survey about surface soil. But it contains not only final status survey but also remediation, reuse, short-term and long-term stewardship on radioactively contaminated and potentially radioactively contaminated sites and/or groundwater. The remediation and reuse of site and groundwater is described on generic level. Most of the content related to characterization of radioactively contaminated sites is described in Chapter 3.

2.2 Data Quality Objectives (DQOs)

Both MARSSIM and EURSSEM are based on the Data Quality Objectives (DQOs) process. This is important concept in both manuals, minimizing the costs associated with data collection by eliminating redundant or overly precise data. In order for the collected data to be of sufficient accuracy and quantity, it is necessary to establish the criteria in advance and design the data collection process based on this. The development of such an efficient data collection design is called the DQOs process and has the following seven steps.

Table 1. The data quality objectives process

No	Step
1	State the Problem
2	Identify the Decision
3	Identify the Inputs to the Decision
4	Define the Boundaries of the Study
5	Develop a Decision Rule
6	Specify Limits on Decision Errors
7	Optimize the Design for Collecting Data

2.3 Sampling

When site characterization is performed the design of the site investigation procedures must be followed systematic review and strategy.

MARSSIM presents a statistical approach to detect a certain size of "hot spot" with a certain level of confidence. [1] If no contamination is present, it is assumed that there is no hot spot at least a certain size. In other words this means more sampling is needed for higher confidence.

The basic method is similar to MARSSIM, but EURSSEM uses more rigorous approach. The area to be sampled should be partitioned into regular sub-areas. Each sub-area should carry only one sampling point. Sampling points should be systematic and should not be aligned to improve detecting hot spot ability. Therefore we cannot use square grid in EURSSEM because sampling points are aligned. A herringbone pattern is considered to be the optimum type of non-targeted grid pattern in EURSSEM. [2]

2.4 Statistical Tests

Final status survey is performed to demonstrate that residual radioactivity in each survey unit satisfies release criteria. When the data clearly show that a survey unit meets or exceed the release criteria, the result is often obvious without performing statistical analysis. When we perform statistical tests the null hypothesis is set to baseline condition. MARSSIM assumes the residual radioactivity exceeds the release criteria as a null hypothesis. In contrast the null hypothesis recommended for use in EURSSEM is that the residual radioactivity in the survey unit does not exceed the release criteria.

3. Conclusion

A comparison study of MARSSIM and EURSSEM Methodology for final status survey was conducted. MARSSIM is the most widely used method and the related studies are being conducted in Korea. Since no actual cases of EURSSEM has been reported a comparative analysis with MARSSIM for application methods should be performed in the future. We would like to use this study as one of reference material for domestic application by comparing the other final status survey methods.

REFERENCES

[1] NUREG-1575, Rev1. EPA 402-R-97-106, Rev1. DOE/EH-0624, Rev1. "Multi-Agency Radiation Survey and Site Investigation Manual (MARSSIM)", August 2000.

[2] Co-ordination Network on Decommissioning, "European Radiation Survey and Site Execution Manual (EURSSEM), June 2009.

[3] Leo van Velzen, "European Radiation Survey and Site Execution Manual (EURSSEM)", ASME 2009 12th International Conference on Environmental Remediation and Radioactive Waste Management, October 11-15, 2009.

A Study on the Conceptual Design of Package for the RV/RVI Cutting Wastes During Decommissioning of Kori Unit-1 NPP

Duk-Woon Jung [1*], Hyosub Kim [1], Dong-gyu Lee [1], and Kyu-Sub Choi [1], and Young- Hwan Hwang [2]

[1] Korea Nuclear Engineering & Service, #5F, IL-Heung Bldg., Myeongdal-ro, Seocho-gu, Seoul, Republic of Korea

[2] KHNP CRI, 1312-70 Yuseong-daero, Yuseong-gu, Dajeon, Republic of Korea

[*] dwjung@kones21.com

1. Introduction

Recently, a R&D project has been conducted for segmentation of RV/RVI and packaging technology of those radioactive wastes to prepare for the upcoming issue regarding decommissioning of Kori-1 NPP. The main issue for the decommissioning of Kori-1 NPP is the management of RV/RVI which is categorized as a LLW/VLLW. In addition, the design of RV/RVI cutting waste packaging container should meet the safety requirements for transportation, storage and disposal as well as WAC (Waste Acceptance Criteria) for the repository at Kyeongju [1].

In this paper, the concept of the design for the RV/RVI cutting waste package of Kori-1 NPP is presented.

2. Consideration

2.1 Domestic radioactive waste management

The process of wastes from operation and maintenance in Republic of Korea is packaging the radioactive waste in standard steel 200 or 320 L drums. For instances, 8 drums (200 L) were loaded on the IP-2 type transport container (8 drums per one container) and transported to LILW repository at Kyeongju(silo type facility).

The used transportation containers can be reused after unloading the drums, and those drums are repacked and disposed of in the concrete disposal container (16 drums per one container).

2.2 Waste characteristics

In case of RV/RVI waste of Kori unit 1, approximately 66 tons of ILW and 128 tons of LLW and VLLW are expected to be generated during the future decommissioning activity.

Table 1. Waste classification of RV/RVI from Kori-1 NPP

COMPONENT		Total Activity [Bq]	Classification	Weight [ton]
RV		6.17E+15	LLW, VLLW	185
RVI	Upper Support Assembly	3.56E+08	VLLW	42
	Upper Core Plate	5.85E+12	LLW	
	Guide Tube	2.65E+10	VLLW	
	Upper Support Column	7.72E+10	VLLW	
	Lower Core Plate	1.21E+12	LLW	
	Core Support Assembly	1.26E+10	VLLW	
	Thermal Shield	8.21E+15	ILW	66
	Barrel	3.54E+16	ILW	
	Baffle Plate	3.06E+16	ILW	
	Baffle Former	5.85E+14	ILW	

2.3 Assumptions

2.3.1 Radioactive waste management system. Considering the uncertainty on the stability of the management and regulatory requirements in case of the RV/RVI cutting wastes from Kori-1 NPP, it would be an effective way to make the most of the current infrastructure or to add an additional waste management system from the existing systems.

2.3.2 Packaging. In order to minimize the number of RV/RVI cuttings, the larger the packing unit is, the more favorable it is. However, according to the KORAD's waste acceptance criteria, the maximum size of the package is less than 10 tons of concrete packages, whose size is 1.5 m (L) × 1.5 m (W) × 1.5 m (H).

2.3.3 Transportation. The package is designed to be transported by the IP-2 type container which can let us utilize the current waste handling system. This container was designed to be disposed of at the vault-type near-surface facility of phase II under construction at Kyeongju.

3. Conceptual design

The package for the RV/RVI cutting wastes for Kori unit-1 is a container for both packaging and disposal purposes, in the form of a square box-shaped steel container

The body and cover are made of carbon steel, and there is a small hole for the grouting work in the lid of the package. Also stillage which is located inside the package is used for fixing the materials inside and improved radiation shielding performance. Figure 1, 2 below shows the schematic design of the package and IP-2 including the package.

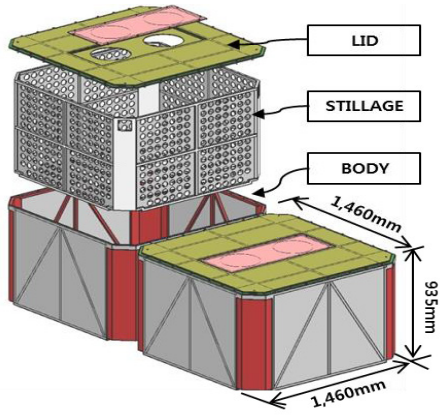

Fig. 1. Conceptual design of waste package.

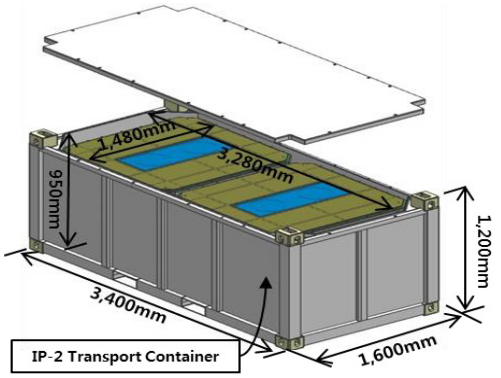

Fig. 2. Scheme of IP-2 including conceptual package.

The packages are designed to pack a maximum 5.9 tons of wastes (total package weight limit: max. 9.4 tons). (Change of the transportation container design is necessary since the transportation weight limit is 18.8 tons.) The evaluation of structural analysis of IP-2 container including the package will be conducted in the future.

4. Conclusion

The conceptual design of the package for the management of RV/RVI wastes from Kori-1 NPP was presented. This conceptual package was designed considering the compatibility with the current domestic radioactive waste management system and the near-surface disposal facility at Kyeongju.

ACKNOWLEDGEMENT

This work was supported by the Korea Institute of Energy Technology Evaluation and Planning (KETEP) granted fund by MOTIE, Republic of Korea. (No.20161510300430)

REFERENCES

[1] Jaesol Lee, et al., “Development of Multi-Purpose Containers for Managing LLW/VLLW from D&D”, JNFCWT, Vol.14, No.2, pp.157-168, 2016.

Spontaneous Reductive Decomposition Behavior of Permanganic Acid Depending on Initial Concentration and Reaction Temperature for the Chemical Decontamination of NPP

Hyun-Kyu Lee[1*], June-Hyun Kim[2], Jin-Hee Kim[1], Wonzin Oh[1], and Sang-June Choi[1,2]

[1]Research Institute of Advanced Energy Technology, 80, Daehakro, Bukgu, Daegu, Republic of Korea

[2]Kyungpook National University, 80, Daehakro, Bukgu, Daegu, Republic of Korea

[*]lhk7933@knu.ac.kr

1. Introduction

Permanganic acid ($HMnO_4$) is used as an oxidizing agent to dissolve chromium oxide (Cr_2O_3) [1]. However, because $HMnO_4$ is unstable, MnO_4^- reacts with H^+ in a 1:1 molar ratio and spontaneously decomposes to form MnO_2, as shown in the following equation [2]:

$$4MnO_4^- + 4H^+ \rightarrow 4MnO_2 + 3O_2 + 2H_2O \quad (1)$$

The spontaneous reductive decomposition characteristics of MnO_4^- have not been studied under chemical decontamination conditions, such as the HP CORD process, using $HMnO_4$.

In this study, the spontaneous reductive decomposition behavior of $HMnO_4$ was investigated within the range of concentrations and temperatures used in the HP CORD process.

2. Experimental details

All experiments were performed in a 500 mL glass reaction vessel equipped with a reflux condenser, thermometer, and an electric heating stirring mantle (MS-DMSB, Misung Scientific Co. Ltd., Korea).

The effect of the initial $HMnO_4$ concentration on its spontaneous reductive decomposition was evaluated at 95 °C for 360 min with initial $HMnO_4$ concentrations varying from 1 to 6 mM. To evaluate the effect of the reaction temperature, 3 mM of $HMnO_4$ solution was heated to 40, 60, 80, and 95 °C for 360 min.

3. Results and discussion

It was experimentally determined that the two-step reaction of the spontaneous reductive decomposition of $HMnO_4$ was judged to follow the characteristics of the MnO_2 nucleation and crystal growth. Based on the experimental results and classical nucleation theory, the following mathematical model was applied to prediction of the spontaneous reductive decomposition behavior of $HMnO_4$.

$$X(\mathrm{t}) = \omega e^{-k_n t_n} + (100 - \omega) e^{-k_c t_c} \quad (2)$$

where X represents the residual fraction (%) of MnO_4^-, t is the reaction time (min), ω and $100 - \omega$ denote $X_n(t)$ and $X_c(t)$ respectively, and k_n and k_c are the rate constants of MnO_2 nucleation and crystal growth, respectively.

The experimental data for the spontaneous reductive decomposition of MnO_4^- as a function of initial $HMnO_4$ concentration and reaction temperature were fitted by Eq. (2), and the results are shown in Fig. 1 and 2, respectively. The coefficient of determination of the curve fitting by the model

was estimated to be ≥ 0.96 at all concentrations and temperatures. Therefore, it was confirmed that the proposed model accurately reproduces the experimental data.

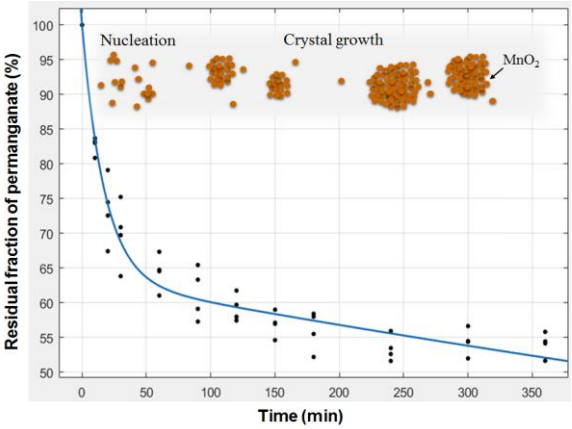

Fig. 1. Results of the mathematical model estimation of the $HMnO_4$ decomposition at 95 °C for initial $HMnO_4$ concentrations of 1, 2, 3, and 6 mM (dots are experimental data, solid line is a nonlinear least square fit).

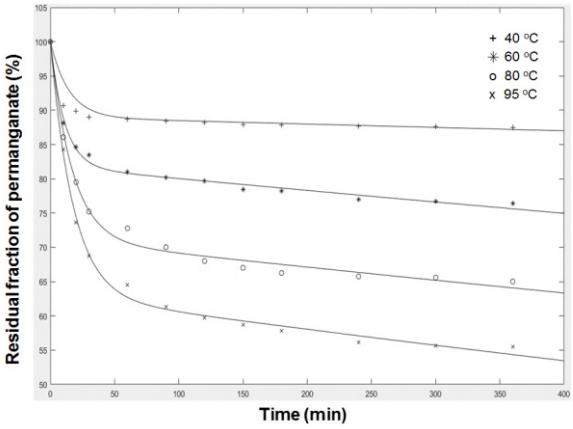

Fig. 2. Results of the mathematical model estimation of the $HMnO_4$ decomposition at 3 mM $HMnO_4$ at 40, 60, 80, and 95 °C (dots are experimental data, solid line is a nonlinear least square fit).

4. Conclusions

The proposed mathematical model consisting of two first-order reactions accurately predicted the spontaneous reductive decomposition behavior of $HMnO_4$. This behavior was dependent on the residual $HMnO_4$ concentration and reaction temperature within the experimental error range as follows:

$$X(\mathrm{t,T}) = \omega e^{-k_n t_n} + (100-\omega)e^{-k_c t_c} \qquad (3)$$

where $k_n = 5.3\times10^{-5}T^2 - 0.038T + 6.92$, $k_c = 7\times10^{-6}T - 0.002$, $\omega = 0.48T - 140$, X (%), ω (%), t (min), and T (K).

Based on the good fit of the experimental data with the proposed model, k_n and ω accurately simulate the nucleation step, and k_c and 100-ω accurately reproduce the crystal growth step.

ACKNOWLEDGEMENT

This work was supported by the Korea Institute of Energy Technology Evaluation and Planning (KETEP) and the Ministry of Trade, Industry & Energy (MOTIE) of the Republic of Korea (No. 20141510300310).

REFERENCES

[1] W.K. Choi et al., “Chemical decontamination of a primary coolant system using hydrazine based solutions”, presented at WM2015 Conf., March 15-19, 2015, USA.

[2] J.W. Ladbury et al., “Kinetics and mechanism of oxidation by permanganate”, *Chemical Reviews*, 58(2), 403-438 (1958)

Scenarios of Effective Treatment Process of Decommissioned Radioactive Metal Waste

Daeseo Koo*, Seung-Kook Park, Kwan Seong Jeong, Jea Hyun Ha, In Hye Hahm, Sang Bum Hong,
Bum Kyoung Seo, and Kook-Nam Park.
Korea Atomic Energy Research Institute, Daedeok-daero989ben-gil 111,Yuseong-gu, Daejeon, Republic of Korea
*ndskoo@kaeri.re.kr

1. Introduction

Radioactive treatment and disposal also requires significant costs. For effective management of decommissioned radioactive waste, the quantity of radioactive waste will be diminished using several selective combinations of decontamination and treatment [1-2]. Such requirement will be fulfilled for the effective management of decommissioned waste.

In this study, the characteristics of decommissioned radioactive waste are investigated. For the safe management and effective treatment of decommissioned radioactive metal waste, selective treatment process scenarios are presented. The results of these scenarios on the decommissioning of radioactive metal waste are also discussed.

2. Scenarios of effective management of decommissioned radioactive metal waste

2.1 Characteristics of decommissioned radioactive waste

Table 1 shows the estimated quantity of decommissioned radioactive waste. Radioactive waste makes up <5% of all waste generated, and non-radioactive waste makes up >95%. According to IAEA data, the types of decommissioned radioactive waste include metal (stainless steel, carbon steel, aluminum, lead, etc.) at about 60%, and concrete (contamination, activation) at about 30%. The remaining decommissioned radioactive waste is combustible waste, waste resin, waste filter, and sludge, at about 10%. Decommissioning radioactive waste per a reactor unit is about A drums.

Table1. Estimated Quantity of Decommissioned Radioactive Waste

Nuclear Installation (country)	Reactor Type	Output Power [MWe]	Radioactive Waste Amount[t]	Non-Radioactive Waste Amount[t]
Barseback1 (Sweden)	BWR	600	5370	177310
Rinhals 3 (Sweden)	PWR	1000	5260	207860
Tokai 1 (Japan)	GCR	160	18200	174000

2.2 Scenarios of effective treatment of decommissioned radioactive metal waste

2.2.1 Estimated quantity of decommissioning metal waste. If the amount of decommissioned radioactive metal waste generated from the decommissioning of a nuclear power plant is about 0.6A(0.6 X A) drums and (A=A1+A2+A3) drums, all decommissioned metal waste is as follows to be classified according the characteristics of contamination, and shape of the decommissioned metal waste. The amount of plate type radioactive metal waste is about (0.6A1drums). The amount of curved/cracked type radioactive metal waste is about (0.6A2drums). The amount of activated type radioactive metal waste is about (0.6A3drums).

2.2.2 Scenarios of treatment process of decommissioning radioactive metal waste. Fig. 1 shows several selective treatment processes of decommissioned radioactive metal waste. By performing a surface decontamination process on plate type decommissioning radioactive metal waste, they will be reused by 0.6A1 drums according to the tolerance concentration of self-disposal under completion of surface decontamination. By conducting an ultra-high compression process on the activated decommissioning radioactive metal waste, the quantity of the activated decommissioning radioactive metal waste will be reduced by (1/7 X

0.6A3)drums. By melting the curved/cracked type decommissioning radioactive metal waste, a large ingot will be created and a small amount of slag will be created. Fig. 2 shows the scenarios of the melting process of decommissioned radioactive metal waste. When the curved/cracked type decommissioning radioactive metal waste (0.6A2drums) and additive are melted according to the melting temperature of the material, a large ingot and a small amount of slag are also created by (0.6 X 0.95A2)drums, (0.6 X 0.05A2)drums respectively [1-2].

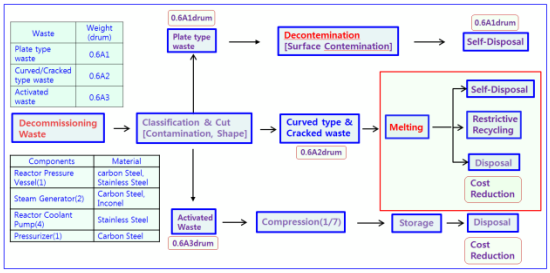

Fig. 1. Scenarios of Treatment Process of Decommissioned Radioactive Metal Waste.

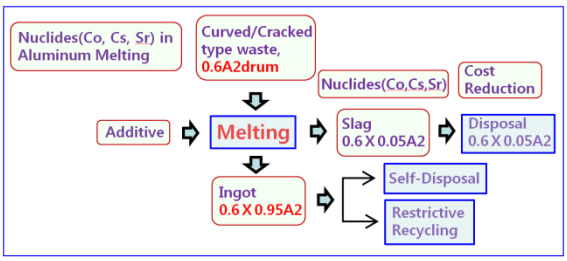

Fig. 2. Scenarios of Melting Process of Decommissioned Radioactive Metal Waste.

2.3 Result and Discussion

Table 2 shows the results of the treatment process scenarios of decommissioned radioactive metal waste. If the amount of decommissioned radioactive metal waste generated from the decommissioning of a nuclear power plant is about 0.6A drums, the amount of decommissioned radioactive metal waste is to be reduced by about (0.6 X 0.05A2+1/7 X 0.6A3)drums using several selective treatment processes. The ingot is to be reused or recycled by (0.6 X A1+0.6 X 0.95A2) drums based on the tolerance concentration of self-disposal. The slag is to be disposal of according to the disposal requirements.

Table 2. Results of the Scenarios of Treatment Process of Decommissioned Radioactive Metal Waste

Waste	Weight (Drum)	Treatment Process	Result
Plate Type Waste	0.6A1	Surface Decontamination	Self-Disposal:0.6A1*
Curved/ Cracked Type Waste	0.6A2	Melting	Ingot:0.6 X 0.95A2** Slag:0.6 X 0.05A2**
Activated Waste	0.6A3	Compression	Volume Reduction Ratio(1/7): 1/7 X 0.6A3***
Total	0.6A		Self-disposal + Restrictive Recycling:(0.6 X A1+0.6 X 0.95A2) Disposal:(0.6 X 0.05A2+1/7 X 0.6A3)

* condition: completion of surface decontamination

** ref(1), ref(2)

*** application of an ultra-high compression

3. Conclusion

Scenarios for the effective treatment of decommissioned radioactive metal waste are to be conducted and discussed. If the amount of decommissioned radioactive metal waste generated from the decommissioning of a nuclear power plant is about 0.6A drums, all decommissioned radioactive metal waste is to be reduced by about (0.6 X 0.05A2+1/7 X 0.6A3) drums using several selective treatment processes.

Acknowledgement

This work is supported by the Ministry of Science and ICT(No. 2017M2A8A5015143) of the Republic of Korea.

REFERENCES

[1] Byung-Youn Min, Pyung Seob Song, Jun-Hyung Ahn, Wang Kyu Choi, Chong-Hun Jung, Won Zin Oh and Yong Kang, “Melting Characteristics for Radioactive Aluminum Wastes in Electric Arc Furnace”, Journal of the Korean Radioactive Waste Society, 4(1), 33-40 (2006).

[2] REN Xinwen, LIU Wencang, ZHANG Yuan, “Melt Refining of Uranium Contaminated Copper, Nickel, and Mild Steel”, China Institute for Radiation Protection, pp. 110-117.

A Fundamental Study for Development of Radioactive Waste Content and Solidifying During the Dissolution of Concrete in Decommissioning Nuclear Power Plant

Youngbum Mun*, Hyunkook Choi, Jaeyoung Kim, and Donghee An

Sungshin Cement Co., LTD, 48-37 Bugang oecheon-ro, Bugang-myeon, Sejong, Republic of Korea

*heromyb@sscem.com

1. Introduction

It is a concrete waste that occupies the largest amount of waste produced in the process of decommissioning a nuclear plant. In the concrete of the radioactive elements of the paste (the curing of the cement and water) is present in most cases, selectively separating the parts of the radioactive concrete waste volume can be greatly reduced.

The purpose of this study is to obtain the basic data necessary for the development of the solidification technology for radioactive waste disposal by restoration of hydration ability by through firing the paste part contaminated with radioactivity among radioactive concrete wastes.

2. Experiments

2.1 Materials

The paste was made W/B = 40% and cured for 28 days. For making the paste as the sample powder of solidification agent, crashed to a size of several millimeters using jaw-crasher. And they were dried at 100 °C to remove un-acted water. Also it was ground as same particle size to cement using ball mill.

2.2 Experiment methods and items

In order to sift the waste portion of the concrete and the sand, the fluorescence X-ray analysis method by the analysis of the XRF(x-Ray-Fluorescence, Rigaku, Japan, ZSX primus Ⅱ) analysis device was used, In order to analyze the correlation between chemical composition of paste and sand, each 10% was mixed at a constant ratio.

In order to be used as a solidifying, the hydration of the cementitious materials is required. Therefore, the calcination temperature of the previous 500 to 900℃ calcination temperature test results based on the thermal decomposion mechanism, the method for recovering the reactive hydration was carried out by 600℃.

Mortar compressive strength was measured according to KS L ISO 679 for evaluation of strength development.

2.3 Result of Paste Content calculation

The results of the XRF analysis for chemical composition according to the volume of paste and sand are expressed in table 1. Cao ingredients can be seen that the paste contains a large amount of SiO_2 in the sand, and the presence of 10% content at a certain rate.

Table 1. XRF analysis of Samples

No	Mixture ratio(%)		Chemical composition(%)		
	Paste	Sand	CaO	SiO_2	Al_2O_3
0	100	0	70.3	18.3	2.8
1	90	10	69.0	20.0	2.8
2	80	20	67.2	21.8	2.8
3	70	30	63.0	26.4	2.7
4	60	40	58.2	31.7	2.6
5	50	50	52.1	38.6	2.4
6	40	60	43.6	48.0	2.2
7	30	70	34.1	59.0	2.0
8	20	80	24.5	70.1	1.6
9	10	90	11.6	85.2	1.0
10	0	100	0.1	98.8	0.4

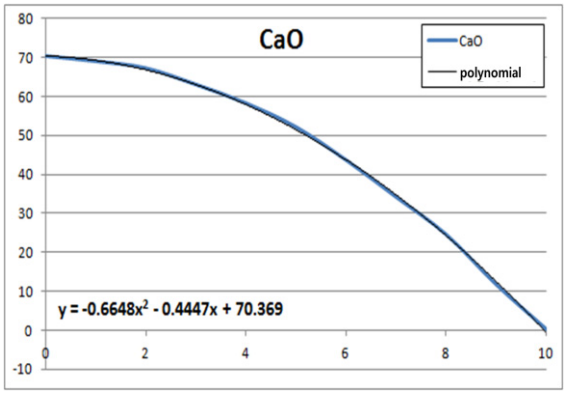

Fig. 1. Calculation of paste content.

The result according to an estimated formula based on the CaO ingredient that contains a large amount of waste is shown in Fig. 1. If you apply it by analyzing the CaO content of the recycled concrete, it is judged to be able to easily predict the content of the waste paste.

2.4 Result of compressive strength and Heat

Based on Table 1, the compressive strength of 28 days is shown in Fig. 2. 0, 1, 9, and 10 were analyzed and excluded from the results of this experiment to a very low value. If only a paste or sand exists, the strength was very low. In this experiment, the strength of the high-intensity standard is over 3.44MPa, and the formulation satisfying the strength criteria appeared in 2 ~ 6. The contents of the adequate paste should be more than 40%, and the paste content increases, the higher the compressive strength can be confirmed.

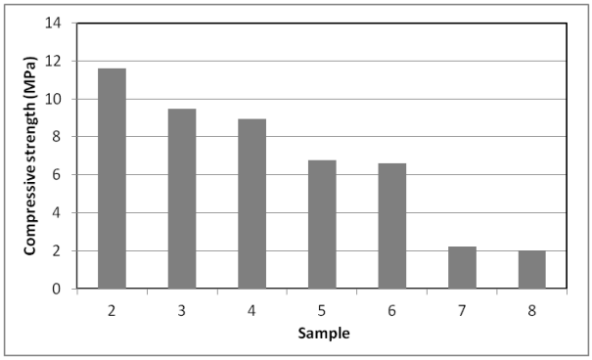

Fig. 2. Compressive strength of Solidifying.

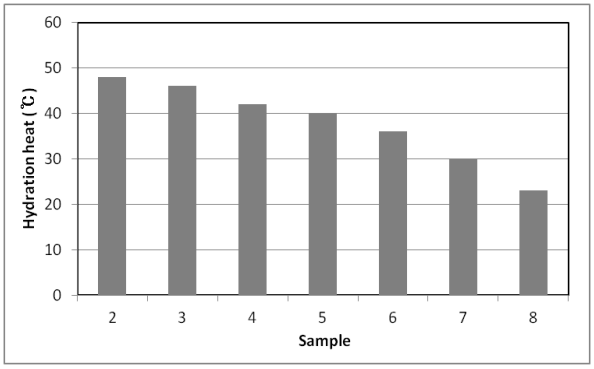

Fig. 3. Hydration heat of Solidifying.

3. Conclusion

Fig. 3 is a graph showing the temperature of the hydration heat of the compressive strength experiment. The higher the paste content was analyzed to increase the hydration heat, and in the second batch of experiments, a very high heat generated at 48℃, and the future of the paste Recycling study also considered necessary for the occurrence of hydration heat.

Acknowledgement

This work was supported by the Energy Technology Program of the Korea Institute of Energy Technology Evaluation and Planning(KETEP) granted financial resource from the Ministry of Trade, Industry & Energy, Republic of Korea (No. 20161510300420)

REFERENCES

[1] Jang Jong-Ho, “A Study on the Fundamental Properties and Application as Cementious Admixture by heating Temperature of Recycled Powder”, Proceeding of Korea Concrete Institute, May 12, 635-40, (2001).

[2] Ahn JC, Lee JH, Kang BH, “Properties of Recycle Cement made of Cementitious Powder from Concrete Waste by Conditions of Burning”, Journal of Architectural Institute of Korea, Nov,19(11):109-12, (2013).

Preliminary Study on Virtual Waste Package Concept Associated With Consolidated Configuration Management for Decommissioning of Nuclear Power Plant

Jae Min Lee, Na Yoon Choi, Ji Woo Lee, Jae Hak Cheong*, and Joo Ho Whang
Department of Nuclear Engineering, Kyung Hee University, 1732, Deogyeong-daero, Giheung-gu, Yongin-si, Gyeonggi-do, Republic of Korea
*jhcheong@khu.ac.kr

1. Introduction

Configuration management (CM) in nuclear power plants (NPP), is process of ensure that the construction, operation and maintenance in NPP comply with design standards for safe opearation. CM has been emphasized minimizing a nuclear accident, such as nuclear breakdown, corruption and the problem of the complement system in the meantime in Korea. However, the CM that intended to pursue in Korea does not consider decommissioning of NPP. IAEA recommands that CM of NPP is important not only for the operation but also for the decommissioning. Therefore, this study proposed the concept of Consolidated CM and the concept of Virtual Waste Package that considers from design to decommissioning for safe operation and decommissioning of nuclear power plant.

2. Configuration Management of Decommissioning

2.1 Application of Configuration Management in Nuclear Power Plant (IAEA)

IAEA specifies the goal of CM is to understand and maintain the design basis consistent with licensing basis. In addition, decommissioning plan should be created based on the design and operational requirements at that time. Consequently, it is important to track the information through CM from the time it was first designed to the point of decommissioning.

2.2 Concept of Consolidated Configration Management

Operator of NPPs, KHNP Co., Ltd in Korea is being construct CM system. EMD is managed as part of CM, and is managed by 7 items as shown in Table 1 below. Each item is divided into detailed items, all of which are tracked for safe operation of the NPP.

Table 1. Contents of Equipment Master Data (EMD)

Information		Basic information management items
1. Basic	→	1.1. Feature Location
2. Quality		1.2. Feature importance decision
3. Production		
4. Department		1.3. Location
5. Size		1.4. Radiation Location Information
6. BOM		1.5. Blue print
7. Etc.		1.6. Maintenance

The IAEA recommends that the CM of NPP be maintained from design to decommissioning. However, CM for decommissioning is different from that of operation management in that it is

specified as a special challenge. Items to be managed for disposal as radioactive waste in EMD management items are not considered. Items to be managed to dispose of radioactive waste are physical, chemical, and radiological information and can be identified through the Waste Acceptance Criteria. There is a need to consolidate the CM list for operation management and the CM list for disposal waste management for complete CM, and present it as a concept of consolidated CM.

3. Virtual Waste Package Concept

If the physical, chemical, and radiological characteristics of the NPP are analyzed in addition to the EMD, the decommissioning waste inventory can be estimated more accurately when the NPP is dismantled. Therefore, concept of virtual waste package (VWP) is proposed in this study. The concept of VWP can consider of decommissioning at the design and operation stage. It analyzes the design data of NPP to predict the amount of radioactive waste generated during decommissioning. When using VWP concept, it is possible to predict radionuclides inventory either by using data from FSAR or code modeling. In order to apply VWP more practically in decommissioning, CM should be performed well in operation stage. Moreover, if the data is continuously maintained, more safe and economical decommissioning will be possible.

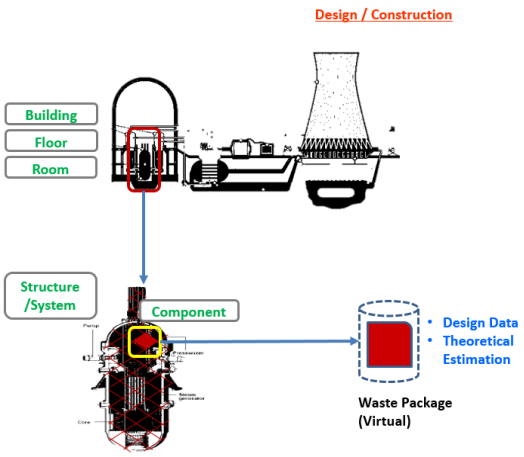

Fig. 1. Virtual Waste Package Concept.

4. Conclusion

In order to apply efficient consolidated CM, it is necessary to decide when to apply configuration management for disposal waste management, and determine the level of depth to apply CM. It is also necessary to determine the extent of application of disposal waste management. Through the VWP concept in this study, the decommissioning planning through design and operation information will be more accurate.

REFERENCES

[1] KINS, Study on Establishment of Regulation Policy for the Reinforcement of Configuration Management and Application in Nuclear Power Plants, KINS/GR-546 (2013).

[2] IAEA, Application of configuration Management in Nuclear Power Plants, IAEA. SRS. No. 65 (2010).

Performance Shaping Factors for the Human Reliability in Decommissioning Activities

Byung-Sik Lee * and Hyun-Jae Yoo
Dankook Univ., 119, Dandae-ro, Chunan, Chungnam, Republic of Korea
* bslee@dankook.ac.kr

1. Introduction

In recent years, technological developments of redundancy and protection, which have made systems more reliable, has reduced accidents due to technical failures. However, it is impossible to say that the system is reliable without monitoring the failure rate of all system components, especially the impact of one of the components, human errors, on the system. Although valid values are difficult to obtain, estimates agree that errors committed by man are responsible for 60–90% of the accidents [1, 2, 3]. Human reliability analysis (HRA) is required to reduce the cause of human errors [1].

The purpose of a human reliability analysis is 'to assess the contribution of operator to the system reliability' and, more accurately predict the 'human error rate' and to determine the associated human-machine system to assess the performance degradation of the system and to evaluate other systems and human characteristics that may affect system behavior [4].

2. HRA Methods

Human activities are a fundamental factor that weakens the industrial system, so HRA investigates the human factors that the worker has on the industrial activities [1]. Nominal human error probability (HEP) is calculated on the basis of operator's activities. To obtain a quantitative estimate of HEP, many HRA methodologies use performance shaping factors (PSF), because it provides numerical criteria for characterizing important aspects of human error and adjusting the nominal HEP levels. The PSFs are environmental factors, activities that are personal, or have potential to affect performance in a positive/ negative way. The key step in HRA is therefore to identify and quantify the impact PSF. Another key step is to interpret and simulate human behavior, which is a dynamic process driven by cognitive and behavioral rules, and is also influenced by physical and psychological factors. It is clear from the literature that the complexity of the human behavioral model to satisfy this is because it prefers to numerically represent the error probability to predict and prevent unsafe behavior. For this reason, the research on human reliability must solve a complex problem between psychology, ergonomics, engineering, reliability analysis, and system analysis [3].

3. Task Analysis

Task analysis (TA) is the task of analyzing task objectives, methods, contents and procedures to grasp task characteristics, vulnerabilities and suitability.

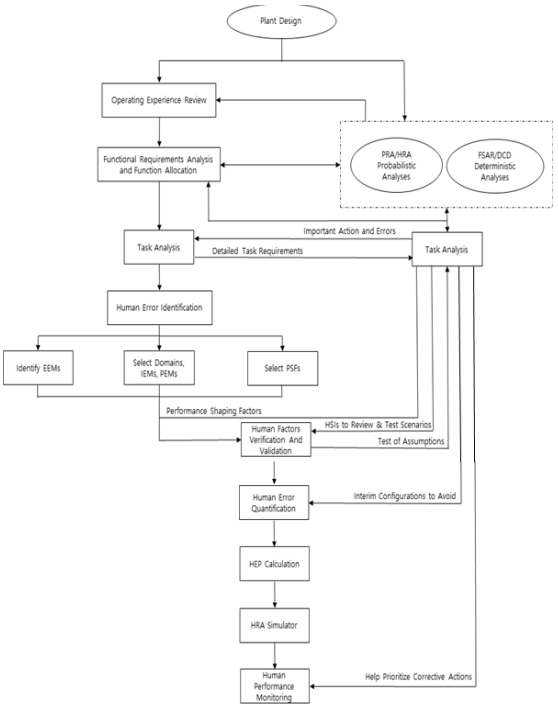

Fig. 1. The role of human actions and procedure in the HRA.

The scope of task analysis, the content of necessary information, and the method of collecting information vary according to the purpose of task analysis. In addition to detailed information on task, task analysis also provides a variety of information on tasks that are useful for error prediction and prevention. There is considerable redundancy between task analysis and HRA. The HRA method generally uses the results of the TA as a starting point to examine what aspects of the task can contribute to human error. Therefore, the combination of TA and HRA methods will be the most suitable form of analysis.

HTA (Hierarchical Task Analysis) is one of suitable TA method, which is a systematic and detailed task analysis method, and which grasps detailed tasks and conditions and expresses complex task steps in a hierarchy. Based on the results of HTA, PHEA (Predictive Human Error Analysis) is used to identify the error and the probability of occurrence and develop a reduction strategy in the TA. Therefore, analysis is performed in the form of a combination of HTA and PHEA.

A TA is begun with detailed narratives of what personnel have to do, which is sufficiently detailed to define the alarms, information, controls, and task

support needed to accomplish the task. The detailed topics to be analyzed in the TA are listed in Table 1.

Table 1. Detailed topics to be performed in TA

Task	Title
Task information	• Working parameters (cutting size, cutting number, precision, etc.) • Output requirements • Feedback needed to indicate adequacy of action taken • Alarms and warnings
Job description	• Activities • Equipment (type, size, constraints….) • Frequency and accuracy of task • Physical position (stand, sit, squat etc) • Movement (Lift, push, turn, pull, etc.) • Required force
Working time	• Unit work time considering activities • Additional hours taking into account of working environment
Teamwork & communi-cation	• Coordination needed between the teams • Personnel communication for monitoring information or taking control actions
Workload	• Cognitive, Physical • Overlap of task requirements (serial vs. parallel task elements)
Operation Support	• Special and protective clothing • Jon aids, procedures or reference materials needed • Tools and equipment needed
Workplace Factors	• Ingress and egress paths to workplace • Workspace needed to perform the task • Typical environmental conditions (ex, lighting, temperature, noise, etc.) • Breaks taking into account "work environment factors"
Hazards	• Identification of hazards involved such as potential personal injury
Expected Performance Shaping Factors	• Stress • Time pressure (in the critical path activity) • Extreme environmental conditions • Reduced staffing

Based on the Table 1, the TA of the decommissioning activities in nuclear power plants has been performed on the reactor pressure vessel internal (RPVI) cutting process. This segmentation process consists of four main tasks and 13 sub-tasks ranging from control rod guide tube cutting to core barrel cutting.

4. Performance Shaping Factor

The PSF is a factor affecting the performance of the task. It is derived from the Task Analysis's lowest level of task. This PSF will reasonably deal with the range of human impacts affecting the decommissioning of nuclear power plants.

The PSF is divided into 3 levels, and Level 1 can be divided into 5 groups as Human, System, Task, Organization and Environment.

First, Human Factor refers to the factors related to the psychological, physical status and ability of the worker, and System Factor is a factor related to H/W system and physical characteristics of decommissioning workplace. Task Factor is the factors related to task characteristics required for the worker and the procedures and information required for decommissioning. Organization Factor is the factors related to team and organization characteristics and communication, and Environment Factor refers to factors related to physical work environment.

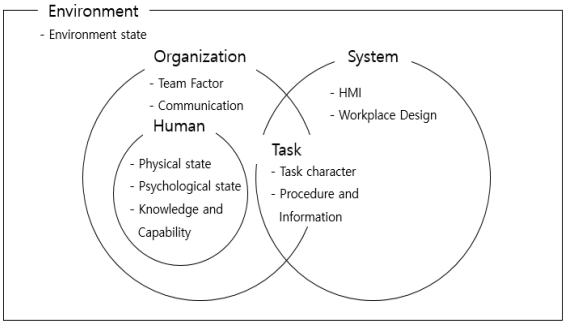

Fig. 2. The classification of PSFs Level 1, 2.

The standard set of PSFs for cutting activities has been derived for the RPVI cutting process.

5. Further Study

Current PSFs require its quantification through algorithms in computer software to ensure consistent interpretation of similar PSFs, and to objectively evaluate them, in particular through various methods for NPP decommissioning activities. And it is required to develop a tool, which is used to select optimal PSFs considering the subjected activities.

Within HRA community, there is a widely recognized need for an improved HRA methodology with a more robust scientific basis, in the decommissioning of the nuclear power plants.

Acknowledgments

This work was supported by the National Research Foundation of Korea (NRF) grant funded by the Korean government, Ministry of Science, ICT and Future Planning (No.2017M2A8A5015148 and No.2016M2B2B1945086).

REFERENCES

[1] Valentina Di Pasquale, et al.: An overview of human reliability analysis techniques in manufacturing operations. Chapter 9, INTECH, 2015.

[2] Griffith, C.D., Mahadevan, S.: Inclusion of fatigue effects in human reliability analysis. Reliability Engineering & System Safety, 96 (11), 1437–1447 (2011).

[3] Hollnagel, E.: Cognitive Reliability and Error Analysis Method CREAM (1998).

[4] Cacciabue, P.C.: Modelling and simulation of human behaviour for safety analysis and control of complex systems. Safety Science, 28 (2), 97–110 (1998).

Evaluation of Oxide Removal Rate by Oxidation/Reduction Continuous Process Based on Permanganic acid-Oxalic acid

Chorong Kim* and Hak-Soo Kim

KHNP Central Research Institute, 70, 1312-gil, Yuseong-daero, Yuseong-gu, Daejeon, Republic of Korea

*chorong.kim@khnp.co.kr

1. Introduction

Nuclear power plant widely applied dilute chemical solvent to remove deposited radioactivity and thereby lower exposure of plant personnel to radiation[1]. The oxide film layer formed on the surface of the structural material of the Light-Water-Reactor was composed of metal oxides of iron, nickel and chromium. The chromium oxide was dissolved by the oxidizing process(alkaline permanganate and nitric permanganate) and iron and nickel in metal oxides were dissolved by the reduction reaction(oxalic acid, citric acid et al)[1].

In this study, oxide removal rate and surface change of specimen were evaluated by decontamination process based on permanganic acid-oxalic acid.

2. Methods

This study evaluated the surface change of the test specimen and the oxide removal rate through continuous decontamination process. The experiment was carried out under the following conditions.

- Test specimen type : SUS304, SA508, Alloy600
- Consecutive times: 1~3cycles
- Test equipment : System decontamination process equipment (Fig. 1)
- Oxidation / reduction process conditions

	Agent	Concentration	Time	Temperature
Oxidation	$HMnO_4$	300ppm	5hr	95℃
Reduction	$C_2H_2O_4$	2000ppm	4hr	

The surface of the specimens was carried out using videoscope and the weight of the test specimens before and after decontamination was measured to evaluate the oxide removal rate and decontamination factor(DF).

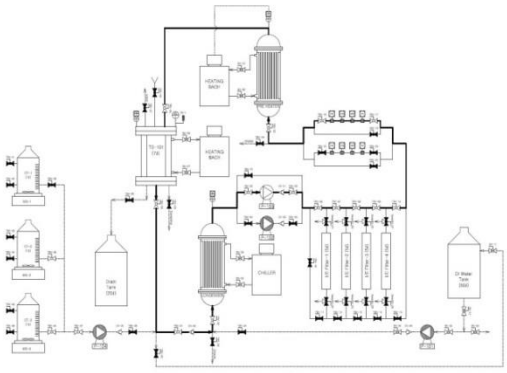

Fig. 1. Schematic Diagram of system decontamination process equipment.

3. Results and Discussion

3.1 Surface analysis of the specimen

For analyzing the surface of the specimen before and after decontamination, videoscope was used. The results of videoscope analysis were shown in Fig. 2.

The pre-decontamination specimens were confirmed that black oxide layer was formed. After the third decontamination, the oxide film of SUS304 was completely removed. In case of SA508, an iron oxide was formed on the surface, and local corrosion and pitting occurred[2]. The oxide film of Alloy 600 was partially removed[3].

Fig. 2. Videoscope analysis of test specimen surface(x60).

3.2 Evaluation of oxide removal rate by oxidation/reduction process

The removal rate of oxide film on the surface of test specimens was evaluated through a continuous decontamination process based on permanganic acid-oxalic acid. Table 1 and Fig. 3 show the oxide removal rates after the contamination process. In the case of SUS304, it was confirmed that the oxide film was completely removed when the decontamination process was performed for 3cycles. For SA508, the removal rate of the oxide film was more than 100% after 2cycles. The oxide films of Alloy 600 were partially removed after 3cycles. As the decontamination process was repeated for the three specimens, the removal rate of oxide film increased.

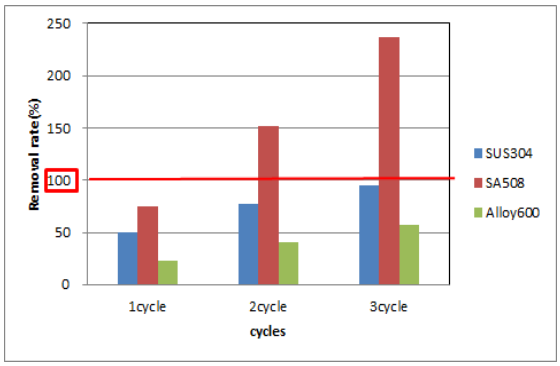

Fig. 3. Removal rate of oxide film of specimen according to the number of continuous decontamination process.

Table 1. The weight of the test specimens before and after decontamination

Type	Before	1cycle		2cycle		3cycle	
		%	DF	%	DF	%	DF
SUS304	0.327	50	2	78	4.5	95	21
SA508	0.993	75	4	152	-	237	
Alloy690	0.208	22	1.3	40	1.7	57	2.3

4. Conclusions

In this study, the removal rate of the oxides film on the test specimen was evaluated. From the experiment result, it was confirmed that the removal rate of the oxide film increased as the decontamination process was repeated. When the continuous process was repeated three times, SA508 removed not only the oxide film but also the base material. Oxide film of Alloy 600 was partially removed. As a result, in case of SUS304 and SA508, decontamination process should be performed 2~3times to remove the oxide film. For Alloy 600, decontamination process should be performed more than 3 times to remove oxide film.

ACKNOWLEDGMENTS

This work was supported by the Korea Institute of Energy Technology Evaluation and Planning (KETEP), granted financial resources from the Ministry of Trade, Industry & Energy, Republic of Korea (Number 20141510300310)

REFERENCES

[1] Decontamination Handbook, EPRI, TR-112352 (1999).

[2] Jun-Young.Jung et al., Crevice Corrosion Properties of PWR Structure Materials Under Reductive Decontamination Conditions, JNFCWT, 12, 199-209 (2014).

[3] Wenjun Kuang et al., The mechanism of oxide film formation on Alloy 690 in oxygenated high temperature water, Corrosion Science, 53, 3853-3860 (2011).

The Cost Estimation for Decommissioning of a Nuclear Fuel Cycle Facility Using CERREX Based on ISDC Structure

JaeHyun Ha*, KwanSeong Jeong, SeungKook Park, DaeSeo Koo, InHye Hahm, SangBum Hong, and BumKyoung Seo

Korea Atomic Energy Research Institute, Daedeok-daero989beon-gil 111,Yuseong-gu, Daejeon, Republic of Korea

*jhha78@kaeri.re.kr

1. Introduction

CERREX(Cost Estimation for Research Reactors in Excel) was developed in line with the IAEA recommendations for decommissioning costing and fully implements ISDC(International Structure for Decommissioning Cost) structure and costing methodology. The purpose of this work is to calculate the decommissioning cost of a nuclear fuel cycle facility by using CERREX based on ISDC structure.

2. ISDC

The ISDC was developed as a common platform of systematized typical decommissioning activities that cover all types of activities identified in any decommissioning project for any type of nuclear installation, regardless of its size, composition/complexity of systems and structures and radiological conditions. The typical representative decommissioning activities are composed of 11 sections. Special features of the ISDC-based costing is that the ISDC cost categories(labor cost, investment cost, expense and contingency) are calculated at the level elementary decommissioning activities and aggregated at upper level as shown on Fig. 1.

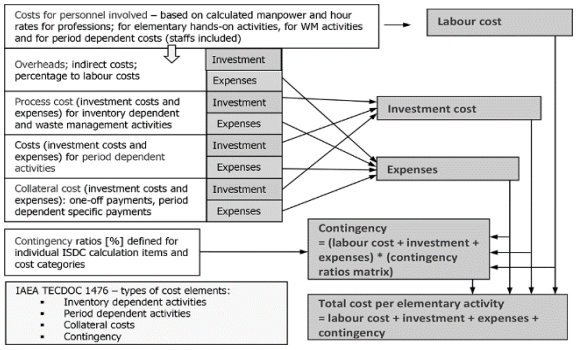

Fig. 1. The principle of ISDC cost calculation methodology.

3. CERREX

The CERREX is short for cost estimation for research reactors in excel and is a simplified costing model for research reactors. One of the IAEA missions is the support for decommissioning of research reactors around the world. The target users of CERREX are countries with limited experience in decommissioning costing and its purpose is to estimate the preliminary cost for research reactors. The cost calculation structure of CERREX is the generic ISDC definition. As shown in Fig. 2., the principles of definition of waste streams for processing in CERREX are partitioned with inventory items and historical/legacy waste items in presented as Fig. 3.

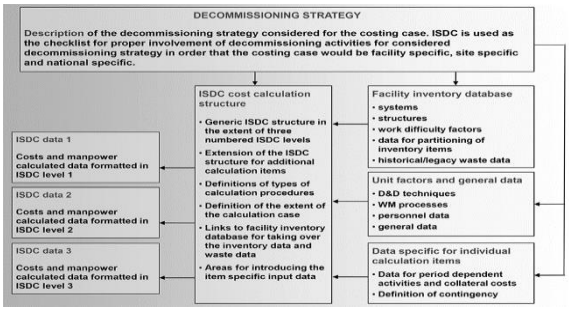

Fig. 2. The principal scheme of CERREX.

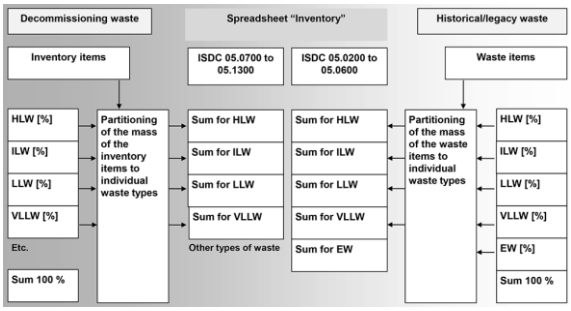

Fig. 3. The waste streams of CERREX.

4. The cost calculation for decommissioning of a RWTF using CERREX

Fig. 4 shows the decommissioning cost calculation of RWTF (Radioactive Waste Treatment Facility). As shown in Fig. 4, the workforce of RWTF decommissioning is about 176,677 man/hour and the decommissioning cost is about 11 M(USD) including its labor cost is about 5.4 M(USD), its investment cost is about 0.63 M(USD), its expense cost is about 2.5 M(USD), and its contingency is about 2.5 M (USD).

© CERREX-D_Cost Estimation for Research Reactors in Excel; Version R; 8-11-2013						Currency	USD
Case:	Sae-bit Fuel Science Building						
Reactor:		Total calculated data		Calculated cost categories			
Operation:	Radioactive WasteTeratment Facility	Workforce	Costs	Labour costs	Investment	Expences	Contingency
© International Atomic Energy Agency		[man.h]	[USD]	[USD]	[USD]	[USD]	[USD]
ISDC No.	ISDC Name	176,677	11,033,148	5,421,916	626,168	2,438,953	2,546,111
01	Pre-decommissioning actions	24,750	1,635,161	967,551	0	290,265	377,345
02	Facility shutdown activities	0	0	0	0	0	0
03	Additional activities for safe enclosure or entombment	0	0	0	0	0	0
04	Dismantling activities within the controlled area	6,754	323,526	188,448	2,533	57,885	74,660
05	Waste processing, storage and disposal	74,596	5,466,423	2,296,822	483,032	1,425,086	1,261,482
06	Site infrastructure and operation	0	0	0	0	0	0
07	Conventional dismantling and demolition and site restoration	70,577	3,608,038	1,969,095	140,603	665,716	832,624
08	Project management, engineering and support	0	0	0	0	0	0
09	Research and development	0	0	0	0	0	0
10	Fuel and nuclear material	0	0	0	0	0	0
11	Miscellaneous expenditures	0	0	0	0	0	0

Fig. 4. The decommissioning cost calculation of a RWFT using CERREX.

5. Discussion

The CERREX has a disadvantage of data reliability about the cost calculation results according to waste types, materials, and processes. That is why grouping functions of waste types, materials, and process do not automatically work in the CERREX and users input in detail the data into the CERREX.

ACKNOWLEDGEMENT

This work was supported by the Nuclear Research and Development Program(No. 2017M2A8A5015143) through the National Research Foundation of Korea funded by the Ministry of Science and ICT.

A Study on the Development of Interview Procedure for HSA at Kori Unit 1

Donghee Lee*, Wook Sohn, Sukbon Yoon, and Suhee Lee
Central Research Institute Korea Hydro and Nuclear Power Co. LTD,
1312-70 Yuseon-daero, Yuseong-gu Deajeon, Republic of Korea
donghee.lee@khnp.co.kr

1. Introduction

For Kori unit 1 to be finally released after completion of site restoration, the licensee (KHNP) should demonstrate that the level of residual radioactivity at the site meets the criteria for site release. This demonstration can be accomplished by implementing the Radiation Survey and Site Investigation (RSSI) process. Historical Site Assessment (HSA), the first step of the RSSI, uses two methods in order to investigate the history of a radiological contamination from siting to permanent shutdown: 1) collection and assessment of documents and data produced during the operation period and 2) interview of persons who know undocumented events resulting in radiological contamination. Among the two methods mentioned above, this paper describes how the procedure of the interview including questionnaires was developed to obtain "tacit knowledge" [1] for Kori unit 1.

2. Purpose of Interview

The purpose of the HSA interviews or questionnaires is to obtain "tacit knowledge" regarding undocumented events resulting in radiological contaminations. Usually, it consists of unique capabilities, skills, and knowledge. Interviews with current or previous employees allow the collection of first-hand information from a site or facility. Interviews cover general topics, such as radioactive waste handling procedures. Results of early interviews are used to guide subsequent data collection activities [2].

3. Development of Interview Procedure[3]

3.1 Interview type & methods

3.1.1 Type of interview. The interview can be grouped into two types. First, direct interviewing is a method where an interviewee meets an interviewer in a face-to-face interaction. If the interviewee is working, the interviewer visits him/her in the office and proceeds with the interview. If not (retired employees), the interviewer arranges the schedule and place for interviews. The second method, indirect interviewing, is using other means in situations where direct interviewing is not possible. Examples include mail, e-mail, telephone, and fax.

3.1.2 Methods of interview. Several different interviewing approaches may be used to gather information. These approaches should be tailored to best meet the site needs. One common approach is a single interviewer and a single interviewee. The advantage of this approach is that it is less intimidating to the interviewee and may be viewed as a more confidential way of gathering information. However, a limitation of this approach is that the interviewer must continually split the focus between asking questions and documenting the obtained responses. Another approach is two interviewers and a single interviewee. This format allows one interviewer to ask questions, while the other one notes the responses. However, while eliminating the potential concerns with adequate recording of the interview responses, the interviewee may view two interviewers with some concern, hence using this approach might potentially result in less openness and potentially less information. A third approach is group interviews with multiple interviewees at a time. In this case, it is essential that at least two interviewers gather information. The advantage of this approach is that information may can be gathered faster than when only one interviewer or one interviewee is involved.

3.2 Questionnaire development

The questionnaire should be structured in a way so that it allows for obtaining undocumented contamination information among all the produced

data during the operation of a facility for the purpose of the interview. In addition, questionnaires should be developed according to the implementation method, because it can vary in time, content, etc. depending on how interviews are conducted. There are four types of questions with a questionnaire being able to simultaneously employ two or more of those types of questions:

- Open type: The questions do not have a predefined response format, so that respondents can reply in a free form.
- Choice type: The type of choose an answer from a prepared question.
- Dichotomy questions: Respondents can answer "yes" or "no".
- Multiple choice type: Respondents are provided with choices to answer a question.

The questionnaire developed referred to the questionnaires of overseas decommissioning plants, and was revised to determine details. At this point, the details were determined according to the purpose of the questionnaire, accuracy, and needs of information. Finally, the questionnaire should be easy to understand considering the interviewee's position, avoiding ambiguous expressions and two or more questions on one question. In addition, indirect expressions should be used in questions asking about potentially sensitive issues.

3.3 Selection of interviewee

The interviewer should select a person (current / retired) who has worked for at least 5 years in Kori unit 1 related departments and partner companies or add through an existing interviewee introduction. In particular, the interviewer should give priority to those who have worked in a department related with operations, maintenance, and radiation management (radiation protection, health physics, radioactive waste management, etc.).

3.4 Implementation of interview

Interview schedules are determined through coordination with the interviewee, and the schedule was discussed at least seven days in advance. After scheduling, the questionnaire was sent to the interviewee at least three days in advance to shorten the interview time. In the case of a direct interview, an independent location for the interview should be decided and a voice recorder should be used if necessary. After the interview, the final questionnaire should be collected and, if the interview results are not sufficient, additional interviews should be performed.

4. Result & Conclusion

This paper describes the interview procedure with current or previous employees to collect undocumented information about the site or facility and to verify or clarify information gathered from the existing records. Interviews can vary according to the type and method, and the contents of the questionnaire should be prepared in accordance with the purpose of the interview. The questions should be easy to understand for interviewees. The undocumented contamination information obtained from the interview results is used in classifying an area as a potential contaminated area.

Kori unit 1 is the first nuclear power plant in Korea to which the HSA applies. Results from the interviewing which is an important process of the HSA can affect the level of characterization effort. Therefore, interviews using systematic procedures are useful for performance of HSA at Kori unit 1, and they are expected to play an even greater role for site release criteria at Kori unit 1 in the future.

REFERENCES

[1] NRC, “Multi Agency Radiation Survey and Site Investigation Manual (MARSSIM) Revision1”, NUREG-1575, 2000.
[2] EPRI, “Capturing Historical Knowledge for Decommissioning of Nuclear Power Plants”, 1009410, 2004.
[3] KHNP, Interview Procedure of Historical Site Assessment for Decommissioning NPPs, 2017.

Study on the Common Ion Effect on Cs^+ Extraction by Using Ionic Liquid

*Hayeon Ryu, Seungyeon Cho, Jungweon Choi, Wonzin Oh, and Sang-june Choi
Kyungpook National University, 80, Daehakro, Bukgu, Daegu, Republic of Korea
*hayeon0420@knu.ac.kr

1. Introduction

The radioactive substance, cesium (Cs^+), is the main fission product. It is long half-life and water-soluble.

As a method for removing cesium, there is a method of cation exchange of cation and cesium ions of an Ionic liquid to extract cesium as organic solvent.

In this study, we applied a new extraction method "common ion effect" which extracts cesium ions by combining the common ion and the Cs^+ comparing with conventional extraction method.

2. Experimental details

2.1 Material

1-Ethyl-3-methylimidazolium bis(trifluoromethylsulfonyl) imide ($[C_2mim][Tf_2N]$) was used as an Ionic liquid and Lithium Bis(trifluoromethanesulfonyl)imide ($[Li][Tf_2N]$) was used as the common ion that is same as ionic liquid's anion. Dicyclohexano-18-crown-6 (DCH18C6, 98%, Sigma-Aldrich, Germany) was used as extractant. Cesium nitrate ($CsNO_3$, 99%, Sigma-Aldrich Chemical Co. Korea) was used as a simulated waste solution.

2.2 Method

$CsNO_3$ simulated waste solution was prepared at 0.3, 0.6, and 1.2 mmol concentration. And then 0.6 mmol of $LiTf_2N$ were dissolved to simulated solution, $CsNO_3$. The 0.6 mmol DCH18C6 was dissolved in 2 mmol C_2mimTf_2N. These mixtures of aqueous phase and organic phase was mixed for 2 hours (25 °C, 250 rpm). After extraction, the mixture was centrifuged at 3000 rpm for 10 minutes and filtered aqueous phase using 0.2 μm nylon filter.

An inductively coupled plasma spectrometer (ICP-OES, Optima 2100 DV, Perkin Elmer, USA) was used to measure the residual Cs^+ concentration.

The conventional extraction method is the same process except for common ion ($LiTf_2N$).

3. Results

As you can see, Table 1 shows the distribution coefficient and removal according to Cs^+ concentrations when using the common ion effect method.

Distribution coefficient Cs^+ (D_{Cs}) of generally larger than 10 (D_{Cs} >10) is efficient extraction system. In the common ion effect system, D_{Cs} is much larger than 10, so this is an efficient extraction system.

Table 1. Distribution coefficient and removal of Cs^+ extraction efficiency using common ion effect method.

Cs^+ [mmol]	D_{Cs}	R_{Cs} (%)
0.3	9428.78	99.21
0.6	8957.43	99.14
1.2	84.25	52.02

Following Table 2 shows the distribution coefficient and removal efficiency according to Cs^+ concentrations when using the conventional extraction method.

D_{Cs} is higher than 10 at all concentrations, so it shows high efficient extraction system. However, at 0.6 mmol of Cs^+ concentration, it is slightly lower than the common ion effect method.

Table 2. Distribution coefficient and removal of Cs^+ extraction efficiency using conventional extraction method.

Cs^+ [mmol]	D_{Cs}	R_{Cs} (%)
0.3	20928	99.63
0.6	1453.43	94.91
1.2	82.55	51.51

4. Conclusions

The following conclusions were obtained through this study

1) Conventional cation exchange mechanisms cannot regenerate ionic liquids because cation exchange of ionic liquid and Cs^+ occurs. However, using the common ion effect method of this study, ionic liquid can be regenerated because there is no ionic change of ionic liquid during extraction.
2) Since the selectivity of cesium is higher than that of lithium, the common ion effect method can be effectively separated by the use of a selective extractant for Cs^+.

We will study about “common ion effect” further, using various ionic liquids and extractants to show higher efficiency and commercialize.

ACKNOWLEDGEMENT

This work was supported by the Korea Institute of Energy Technology Evaluation and Planning (KETEP) and the Ministry of Trade, Industry & Energy (MOTIE) of the Republic of Korea (No.20141510300310).

REFERENCES

[1] Jungweon Choi., “A study of Cs+ selective extraction and solid-liquid separation technology in radioactive liquid waste using ionic liquids”, Kyungpook National University, (2016).

[2] Su-Min Kwon et al., “A novel method for separating Cs+ from liquid radioactive waste using ionic liquids and a selective extractant”, Journal of Radioanalytical and Nuclear Chemistry, 311(3), 1605-1611 (2017).

Change of Adsorption/Desorption of Cesium on Illite Depending on the Ionic Strength of Ion Exchange Electrolyte

Sung Man Kim[1,2], Chan Woo Park[1], Il-Gook Kim[1], Kune-Woo Lee[1], So-Jin Park[2], and In-ho Yoon[1*]

[1] Decommissioning Technology Research Division, Korea Atomic Energy Research Institute, 111, Daedeokdaero 989, Yuseong-gu, Daejeon, Republic of Korea

[2] Department of Chemical Engineering and Applied Chemistry, Chungnam National University, Daehakro 99, Yuseong-gu, Daejeon, Republic of Korea

*ihyoon@kaeri.re.kr

1. Introduction

Cs is known to selectively adsorb strongly to 2: 1 type clay minerals. Radioactive cesium is adsorbed on interlayer and weathered edges in clay minerals and on the outer surface of clay. Generally, frayed edge sites are formed by weathering llite, which is highly selective for Cs.

In this study, it was collapsed due to K^+ in the interlayer, so that other cation exchange ions were hardly adsorbed and other cation exchange electrolyte were adsorbed on illite because Cs desorption was difficult. In other words, we intend to confirm the adsorption / desorption and structural change of Cs by $Ca^{2+,}$ Na^+, K^+ adsorption, Ca^{2+} with high hydration energy and de-collapse between layers through ion exchange electrolyte at high concentration and increase CEC capacity.

2. Materials and Method

2.1 Materials

The clay used in the experiment was purchased from clay mineral society as an illite. Cesium chloride used for Cs contamination, Oxalic acid dehydrate for removing Cs from clay, Calcium chloride dehydrate used as an ion exchange electrolyte, Sodium chloride, Patassium Chloride was purchased from Sigma-Aldrich.

2.2 Preparation of ion exchange electrolyte adsorbed illite

Ion exchange electrolyte 0.01M is mixed with each electrolyte solution (50ml) in illite (5g), and electrolytic solution (20ml) is mixed with illite (2g) in 0.5M and shaked at 25 ℃ for 1day. After separating the solid and liquid, discard the supernatant and dry the solid sample.

2.3 Sorption experiment

CsCl solution (35ml) was added to the sample which was adsorbed to Illite (0.35g) in the previous step stirred at 30mM, 3 mM, 0.3 mM and 0.03 mM concentration at 25 ℃ for 7 days in a shaking incubater and adjusted to pH 7.0. In addition, the desorption experiment using oxalic acid was carried out in a shaking water bath at 80 ° C for 3 days at a concentration of 0.015, 0.15, and 1.5M of oxalic acid on a sample adsorbed at the previous stage and adsorbed with CsCl (3 mM). Analysis was performed by inductively coupled plasma mass spectroscopy (ICP-MS; ELAN DRC II, PerkinElmer, USA) for filtering(0.45 μm) the supernatant.

3. Results and Discussion

3.1 Adsorption characterization of ion exchange electrolytes

As shown in Fig. 1, the change of adsorption characteristics according to the ion exchange electrolyte was not significant. However, adsorption amount was adsorbed in order of Na^+, K^+, Ca^{2+}. The adsorption amount of Ca^{2+} decreased due to the largest hydration radius.

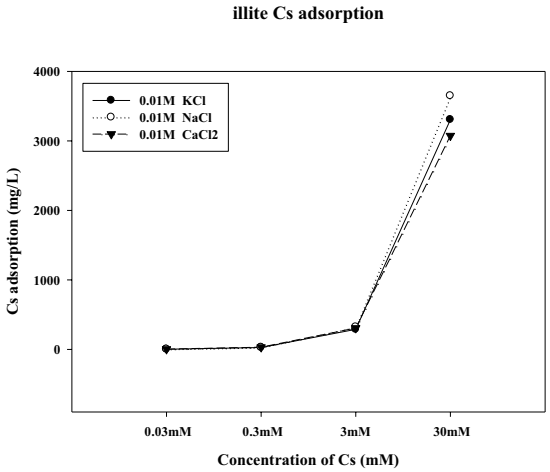

Fig. 1. Cs adsorption behavior on illite adsorbed ion exchange electrolyte(K^+, Na^+, Ca^{2+}).

3.2 Cesium desorption of illite by ion exchange electrolyte

The change of Cs desorption of oxalic acid in illite adsorbed ion exchange electrolyte was studied. As shown in Fig. (2), desorption rate increased with increasing desorbent concentration. However, there was not increase in CEC and desorption rate due to Ca^{2+} treatment, and the desorption rate of Na^+ was the largest.

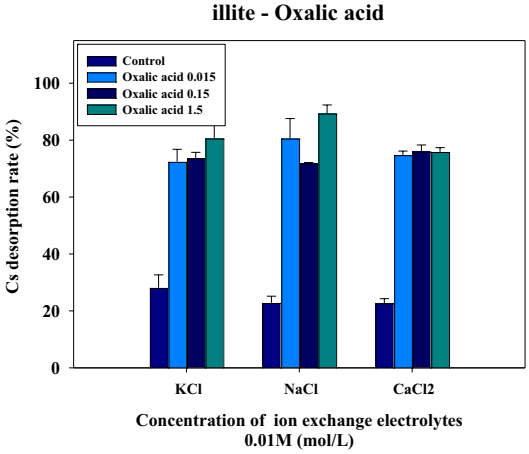

Fig. 2. Desorption characteristics of Cs by Oxalic acid treatment on illite adsorbed ion exchange electrolyte (K^+, Na^+, Ca^{2+}).

4. Conclusion

We have experimented to changes of adsorption and desorption depending on Na^+, K^+, Ca^{2+} ionic strength. However, as a result of experiments, we could not confirm the large change according to the ionic strength. it was considered that one of the reasons why the concentration used for desorption of Cs was fixed at a low concentration of 3mM and could not be changed. Fortunately, we have found a good desorption effect on oxlic acid in 2:1 non-expandable clay.

ACKNOWLEDGMENTS

This work was supported by the National Research Foundation of Korea(NRF) grant funded by the Korean government(Ministry of Science and ICT) (No. 2017 M2A8A5015148)

Suggestion of Kori-1 Decommissioning Target Facilities

Hyunmin Kim*, Hyejin Jung, and Wook Sohn
Decommissioning & Spent Fuel Technology Center, KHNP CRI, 70, Yuseong-daero 1312beon-gil, Yuseong-gu, Daejeon, Republic of Korea
*hyunmin.kim@khnp.co.kr

1. Introduction

On June 19, 2017, Kori-1 was permanently shut-down for decommissioning. To start its decommissioning, the utility is required to submit a FDP (Final Decommissioning Plan) to the regulator by Nuclear Safety and Security Commission Notice 2015-8 [1]. Chapter one of the FDP document, which consists of twelve chapters, should describes a summary of decommissioning project, decommissioning target facilities, and facility operating history including accident & radioactivity leakage.

This article provides results of technical reviews for overseas PDF in order to suggest the Kori-1 decommissioning target facilities for the preparation of the FDP.

2. Overseas cases

2.1 IAEA SRS (Safety Reports Series)-45[2]

IAEA SRS-45 provides a brief overview of how to describe the decommissioning target facilities such as buildings, major components and ancillary equipment. Then, subsection also provides building drawings that indicate areas within the buildings that will be included in the decommissioning process. During decommissioning, engineering schematics and system layout drawings should be given sufficient to provide a overall knowledge of the systems and major components.

2.2 YNPS DP(Yankee nuclear power station decommissioning plan)[3]

YNPS DP classifies the facility description into 58 categories that comprise general description, major systems, buildings and components. Each category provides a brief description of the target facility's major functions, structure, materials and decommissioning configuration. In addition, detail engineering schematics are explained in the next section "decommissioning activities and planning".

2.3 BNFL: Zorita PWR Decommissioning Study[4]

Zorita PWR Decommissioning Study gives a brief overview of the plant description that has plant basic descriptions, such as Zorita NPP (nuclear power plant) buildings description. The description of buildings are Reactor Building, Turbine Building, Auxiliary Building, Evaporator Building, Radioactive Waste Temporary Storage Buildings and other Plant Buildings. Each Building provides a brief description with regard to major functions, structure, materials and drawing,

3. Kori-1

In overseas cases, the operator considered a single unit of NPP, but we must consider the presence of Kori-1 & Kori-2 together. So, consideration shall be given to some common facilities of Kori-1 and Kori-2 under the operation.

Fig. 1. Kori-1&2 satellite picture.

In the FDP, Decommissioning target facilities shall refer to all buildings associated with Kori-1. So, I suggest the decommissioning target facilities based on the Kori-1&2 arrangements. The Kori-1 buildings and common facilities that are visible in the Kori-1&2 arrangements must be classified and the systems included in each building should be added.

Table 1 shows visible buildings and common facilities:

Table 1. classified Kori-1 decommissioning target facilities

Building	**Common Facility**	**Storage Tank**
Reactor	C.W. Pump	Cond. WTR
Turbine	Demi WTR Storage TK	Fresh WTR
Auxiliary	Demi WTR Transfer PP	Rad Waste
Service	CPP Reg.	Aux BLR F.O
EDG	Emergency WTR Storage TK	EDG F.O
CC S.W.	H_2SO_4 Storage TK	ETC.
STM HDR HVAC	NaOH Storage TK	
Workshop	ETC. Storage House	
MTr A/B room		

4. Conclusion

This article review overseas facility description of decommissioning plan and suggests Kori-1 decommissioning target facilities. We are more considering the following issues for the FDP. In case of common facilities, only part of a facility is estimated to be decommissioned, that decommissioning plan is described in detail in relation to the facility remaining in operation, and the impact of decommissioning activities considering the adjacent plant should be discussed.

REFERENCES

[1] Nuclear Safety and Security Commission, Regulations of Nuclear Facilities Decommissioning Plan, such as Notice 2015-8.

[2] IAEA, Safety Reports Series No.45 “Standard Format and Content for Safety Related Decommissioning Documents”, 2005.

[3] Yankee Atomic Electric Company, Yankee nuclear power station decommissioning plan, Revision 0.0.

[4] BNFL, Report to ENRESA Zorita PWR Decommissioning Study. Issue 1. 2003.

Study on Installation of Plasma Melter Refractory

Seokju Hwang, Hyun-jae Cho, and Cheon-Woo Kim
KHNP-CRI, 70, 1312-gil, Yuseong-daero, Yuseong-gu, Daejeon, Republic of Korea
hsjhhhhh@khnp.co.kr

1. Introduction

Efforts are being made home and abroad to develop a processing method to satisfy the requirements for stable processing and disposal to treatment various radioactive wastes. KHNP-CRI have developed on Plasma Torch Melter(PTM) as a method for treating radioactive wastes with high temperature melting.

The plasma melter is composed of refractories. So, it is important to ensure the integrity of the refractory. KHNP-CRI studied building and curing of refractories to ensure integrity when installing plasma melter.

2. Conceptual Design of Melter Refractory

2.1 Plasma Melter

For PTM facility, which uses plasma torch, it is crucial to develop the technology for maintaining the integrity of plasma melter, a container for treating radioactive wastes in high-temperature plasma environments. Thus, the process of build and curing the refractory is important when installing the plasma melter.

2.2 Refractory

In the plasma melter, various refractories reflecting the thermal-flow characteristic of the melt inside are used [1]. Table 1 shows the properties of the refractories used in the plasma melter. The refractory materials used in upper inside, upper outside, lower inside and lower outside were CASTABLE, MgO-C, Al_2O_3-Cr_2O_3 and High Alumina, respectively as shown in Fig. 1.

Table 1. Properties of Refractory Materials

	Density (kg/㎥)	Cp (J/kg·K)	Thermal Conductivity (W/m·K)
CASTABLE	0.24	3.19	1.14
MgO-C	3000	0.24	3.19
Al_2O_3-Cr_2O_3	3300	0.24	3.2
High Alumina	3000	0.24	2.5

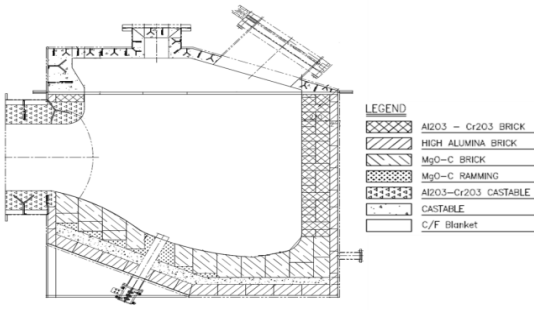

Fig. 1. Distribution of Plasma Melter Refractories.

3. Building of the Melter Refractory

3.1 Refractory Building Process

The plasma melter consists of lid, body and side discharge chamber. Among them, the lid and side

discharge chamber were built of a monolithic refractories and the body was built of a shaped refractories and a monolithic refractories.

The monolithic refractories of the lid and side discharge chamber were built using a model frame as shown in Fig. 2 and 3.

Fig. 2. Building Process of The Lid Refractories.

Fig. 3. Building Process of The Side Chamber Refractories.

The refractories of the body were built in order from the inside to the outside according to the layout as shown in Fig. 4.

Fig. 4. Building Process of The Body Refractories.

3.2 Refractory Curing and Drying

Curing and drying process are essential to ensure the physical integrity of monolithic refractories and safety in high temperature plasma environments.

The drying process was done through the process shown in Fig. 5.

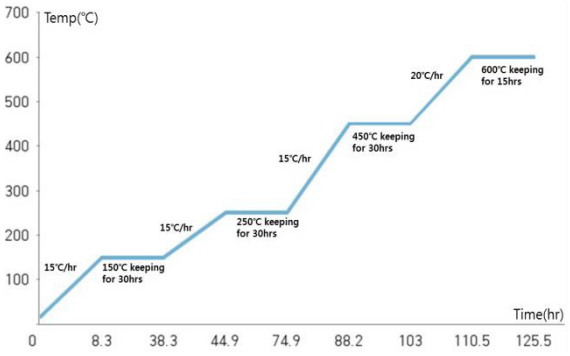

Fig. 5. Temperature Profile of Refractory Drying.

4. Conclusion

The installation process of the plasma melter refractory is very important for the stable treatment of radioactive waste in high temperature environment. Therefore, the quality of the refractories must be secured during buliding and curing process in order to ensure integrity of the plasma melter. Through this study, quality was secured during the building and curing process for the plasma melter integrity. Based on this study, KHNP-CRI plans to complete the installation of the PTM system in the near future.

REFERENCES

[1] S.J. Hwang and Y.H. Hwang, “Study on Thermal-Flow Analysis of the Plasma Melter”, Global 2017, Korea (2017).

Development of RV Decommissioning Mockup

Seokju Hwang, Young Hwan Hwang, and Cheon-Woo Kim
KHNP-CRI, 70, 1312-gil, Yuseong-daero, Yuseong-gu, Daejeon, Republic of Korea
hsjhhhhh@khnp.co.kr

1. Introduction

Since Kori unit 1 was permanently shut down, the importance of decommissioning technology has been emphasized. One of the most important technology in decommissioning activity is the segmentation and dismantling of activated large component. The reactor vessel (RV) is relatively highly activated among various systems [1]. The development of efficient RV segmentation is essential.

The development of RV decommissioning mockup for the Kori unit1 RV will be discussed in this paper. Mockup training is essential to verify segmentation process and minimize worker exposure in the radiation environment and segment the RV following the decommissioning schedule.

2. Design of RPV Mockup

2.1 Kori Unit 1 RV

The Kori unit 1 RV is a carbon steel structure with a outer diameter of about 3.8 m, a height of about 9.7 m and a weight of about 187 tons. The interior of carbon steel structure is cladded with stainless steel. As shown in Fig. 1, the RV is a cylindrical structure that contains and supports RVI. The main feature of RV is that the thickest part is the upper flange and there are four nozzles for connecting to the primary circuit.

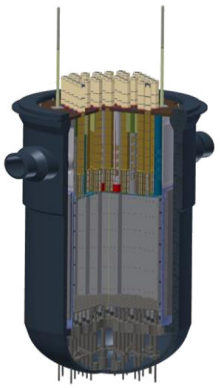

Fig. 1. Image of RV and RVI of Kori unit 1.

2.2 Conceptual Design of RV Mockup

The RV mockup should be the same size of actual RV in the form of a circular cylinder. However, since the structure is circular and symmetrical, it is not necessary to manufacture all of them. As shown in Fig. 2, the actual mockup is partially manufactured.

Fig. 2. Concept Image of the RV Mockup.

The main feature of Mockup is that the flange and nozzle, which are main parts of the RV, are designed as a module type so that they can be replaced after

segmentation process checking and segmentation scenarios validation.

3. Development of RV Mockup

3.1 Manufacture of Mockup

After completion of the design, KHNP-CRI manufactured RV mockup for segmentation process and segmentation scenarios. The nozzle specimens and flange specimens were manufactured as changeable module type after cutting. And auxiliary structure was manufactured for industrial safety.

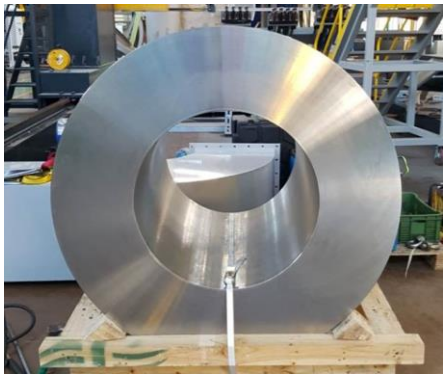

Fig. 3. Specimen of RV Nozzle.

Fig. 4. Specimen of RV Flange.

3.2 Installation of Mockup

For the RV segmentation process and segmentation scenarios, a mockup was made and installed in a field. And auxiliary structure was installed for industrial safety.

Fig. 5. RV Mockup Installation.

4. Conclusion

Development of a mockup is essential for the RV segmentation, which is high activated structure. The mockup developed in this study will be used to verify the segmentation process and to utilize it for worker training in the future decommissioning

Acknowledgments

This work was supported by the Korea Institute of Energy Technology Evaluation and Planning(KETEP) and the Ministry of Trade, Industry & Energy(MOTIE) of the Republic of Korea(20161510300430)

REFERENCES

[1] Y.H. Hwang, “Conceptual Design for Kori Unit 1 Reactor Vessel and Internal Segmentation Process”, Proc. Of the KRS 2017 Fall Conference, 26(8), Oct 18-20, 2017 Changwon.

Study on Segmentation Plan for Kori Unit 1 Reactor Vessel Internal

Young Hwan Hwang, Seok-Ju Hwang, Ju-Young Yoon, and Cheon-Woo Kim
KHNP-CRI, 70, 1312-gil, Yuseong-daero, Yuseong-gu, Daejeon, Republic of Korea
younghwan7@khnp.co.kr

1. Introduction

After the permanent shut down of Kori unit 1, the first commercial nuclear power plant (NPP) in Korea, various decommissioning activities are awaiting. The segmentation of large components are one of the primary activity. Since the reactor vessel (RV) and reactor vessel internal (RVI) are relatively highly activated, they should be carefully treated to achieve the safe and economical decommissioning. The RV and RVI had been activated by neutron from the fuel during operation. They are classified as ILW, LLW, and VLLW [1]. Since the lower part of RVI are directly irradiated by neutron from the fuel, some part of them are classified as ILW. Rest of RV and RVI are classified as LLW and VLLW. In this study, the segmentation plan for Kori unit 1 RVI and estimation of radioactive waste generation are studied.

2. RVI Segmentation Plan Development

Since the core part of RVI are directly irradiated by neutron from the fuel, the lower part of RVI is the most highly activated region in whole NPP component. The segmentation of RVI is implemented under the water to achieve ALARA principle.

2.1 Segmentation Process

The RVI is disassembled, segmented, and packaged under the water with remotely controllable equipment. The dimension of cavity and arrangement are shown in Fig. 1 [2].

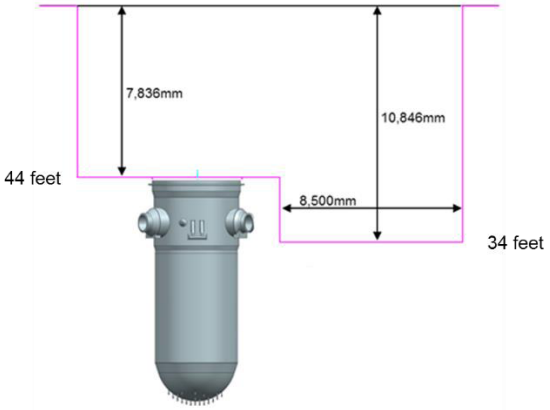

Fig. 1. Dimension and Arrangement of RV/RVI and cavity [2].

First, the cavity is filled with water and upper/lower part of RVI are moved to the stands in lower cavity, 34 feet, as shown in Fig. 2.

After the removal of RVI to the stands, the RV flange region, located near 44 feet, is sealed. The workstation, where primary segmentation process is implemented, are prepared at the upper cavity, 44 feet, with band saw, circular saw, etc. In the lower cavity region, water filtration system, fastening tool guide system, various cutting tool, etc. are equipped.

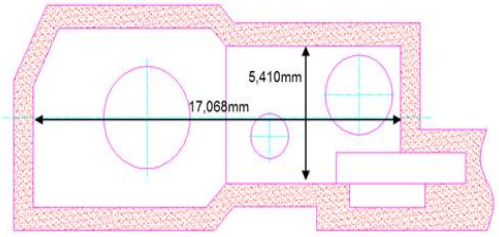

Fig. 2. Top View of Cavity.

2.2 Segmentation Plan

The RVI consists of various physical shapes: tube, thick and plates, rigid cylinder, asymmetry complex structures, etc. Various segmentation methods are required to achieve the minimization of secondary waste and process period [2]. Fine plasma cutting, contact arc metal cutting (CAMC), and mechanical cutting tools are essential for the segmentation. In addition, some part the RVI are assembled with lots of bolts, nuts, and pins. The fastening process are important to reduce the cutting time and utilize the equipment efficiently.

The preparation of equipment, including inspection, assembling, and measurement, is implemented at the operation floor, 70 feet. The additional bridge, which withstands massive segments and tools, is also equipped at the operation floor.

According to the previous experiences, the floating particle, micro bubble, and foreign substance hinder the micro observation during under water process and delay the segmentation process. The preparation of effective filtration system is prerequisite for the efficient segmentation process. The expected segmentation plan and radioactive waste generation are summarized in table1.

Table 1. Segmentation plan

Item	Results
Total cutting length	~354 m
Package generation (200L drum)	~232 drums
# of Segments	764 ea.

3. Conclusion

The segmentation of Kori unit 1 RVI is studied to achieve safe and economical decommissioning. It is suggested that the RVI is segmented under water with remotely controllable tools. The estimated cutting length, package, and number of segments are ~354 m, ~232 drums, and 764 ea., respectively. The optimized segmentation plan with new packages will be suggested in future works.

ACKNOWLEDGEMENTS

This work was supported by the Korea Institute of Energy Technology Evaluation and Planning (KETEP) and the Ministry of Trade, Industry & Energy (MOTIE) of the Republic of Korea (20161510300430).

REFERENCES

[1] H.-K. Kim et. al., “Characterization of Source Term in Nuclear Power Plant Decommissioning”, Final report (2016).

[2] C.-W. Kim et. al., “Technology Development for Pilot Test of Activated RV and RVI Decommissioning”, Intermediate report (2017).

Process Development for Kori Unit 1 Reactor Vessel Segmentation

Young Hwan Hwang, Seok-Ju Hwang, Ju-Young Yoon, and Cheon-Woo Kim
KHNP-CRI, 70, 1312-gil, Yuseong-daero, Yuseong-gu, Daejeon, Republic of Korea
younghwan7@khnp.co.kr

1. Introduction

The segmentation of reactor vessel (RV) is classified as one of the primary process among various decommissioning activities. The RV is a massive component. The inner diameter, height, and weight of RV is ~3.3 m, ~9.7 m, and ~187 ton, respectively. The stainless steel cladding covers the inner surface area of RV. The role of reactor vessel are safe containment of fuel and reactor vessel internal (RVI) during operation and allows the energy, from fuel to water, and fluid transfer. Since the Kori unit 1 RV is irradiated to large number of neutrons during operation, the RV is classified as LLW according to the previous calculation [1]. In this study, the in-situ thermal segmentation of RV is studied to achieve low radiation exposure and reduce process duration.

2. RV Segmentation Plan Development

Since the core part of RV is exposed to large number of neutrons from the fuel, the middle of RV is one of the most highly activated region in whole NPP components. The segmentation of RV is implemented with remote controllable tools to achieve ALARA principle. In addition, rapid thermal cutting tools is favorable to reduce radiation exposure and process duration.

2.1 Preparation of Segmentation

The RV segmentation consists of preparation and segmentation steps. The Fig. 1. shows the dimension and arrangement of RV and cavity, where most of the process takes place. The flange region is located at 44 feet. There are four hot and cold legs, which support massive component and path for coolant water. Installation of tent, which cover top of RV to prevent secondary contamination during segmentation, adequate ventilation system, and rigging tool to raise RV are prerequisites.

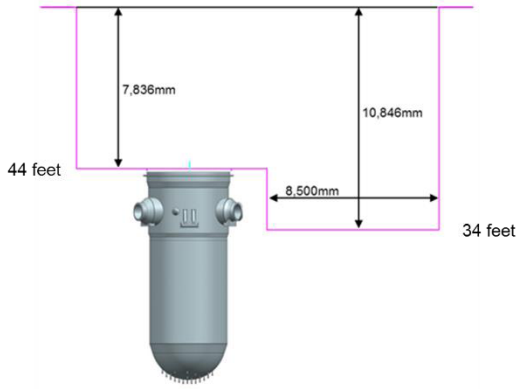

Fig. 1. Dimension and Arrangement of RV and Cavity [2].

The extension of bio-shield concrete around flange region is required to secure and install the oxy-propane torch. The insulation, which covers RV outer surface, is segmented and removed for further segmentation process.

2.2 Segmentation of RV

After preparation and installation, the RV is segmented with oxy-propane torch from top to

bottom. The example of RV cutting plan is shown in Fig. 2. Since thermal energy, which is generated from torch, melts carbon steel from outer surface and blows it into inner region, the generated slag is gathered in the RV bottom head and rigging tool.

Fig. 2. RV cutting Plan (Example) [2].

During segmentation using oxy-propane torch, it is generally accepted that the unfavorable aerosol is generated. Since the aerosol easily diffuses and increases the possibility of secondary waste generation, the additional ventilation system is strongly required for the adequate treatment of air contaminants, floating particle, and aerosol.

The shape of RV is relatively simple, cylindrical shape with rounded bottom head. Since the level of RV shell is similar in shell region, it is expected that the teaching and movement for remote segmentation of RV shell can be achieved in a short time. The detailed cutting plan is shown in Table 1.

Table 1. Segmentation plan [2]

Item	Results
Total cutting length	~530 m
Package generation (200L drum)	~484 drums
# of Segments	~510 ea.

3. Conclusion

The segmentation of Kori unit 1 RV is studied. The in-situ segmentation at the ambient surrounding with remotely controllable oxy-propane torch is suggested. The estimated cutting length, package, and number of segments are ~530 m, ~484 drums, and 510 ea., respectively. The optimized segmentation plan with new packages will be suggested in future works.

ACKNOWLEDGEMENTS

This work was supported by the Korea Institute of Energy Technology Evaluation and Planning (KETEP) and the Ministry of Trade, Industry & Energy (MOTIE) of the Republic of Korea (20161510300430).

REFERENCES

[1] H.-K. Kim et. al., “Characterization of Source Term in Nuclear Power Plant Decommissioning”, Final report (2016).

[2] C.-W. Kim et. al., “Technology Development for Pilot Test of Activated RV and RVI Decommissioning”, Intermediate report (2017).

Review of Decommissioning Radioactive Waste Management and Treatment Technology for Waste Type

Mi-Hyun Lee* and Cheon-Woo Kim
KHNP CRI, 70, 1312-gil, Yuseong-daero, Yuseong-gu, Daejeon, Republic of Korea
*mihyun.lee@khnp.co.kr

1. Introduction

Recently, the decommissioning of nuclear power plants in Korea was decided due to the permanent suspension of Kori Unit 1.

In Korea, a large amount of disposal of exempt waste and extremely low level wastes will be generated in the process of operation and decommissioning of nuclear power plants. If the decommissioning of large capacity nuclear plants is started in the future, much larger amount of disposal of low level waste and very low level waste will be generated in a short period of time.

Therefore, the disposal strategy for the decommissioning radioactive waste should be prepared first, and appropriate measures for disposal of these wastes should be followed accordingly.

In this paper, the current status of domestic and overseas radioactive waste classification standard and disposal technology for radioactive waste generated by the decommissioning was summarized and reviewed.[1],[2],[3],[4]

2. Disposal Waste Characteristics

The decommissioning radioactive waste is defined as the waste of a nuclear facility that has been discarded. These waste can be generated by various activities (e.g. decontamination and demolishment) to make the radioactivity level of nuclear site to acceptable level.

The characteristics of the decommissioning radioactive waste are as follows.

- Larger amount than operational wastes in a shorter period
- Have various forms
- Have low or very low radioactivity

In addition, they consist of metal and concrete because most of them are construction wastes.[5]

3. Classification Standard for Domestic and Overseas Radioactive Waste

Spent nuclear fuel waste should be disposed of in-depth, intermediate level waste shall be disposed of rock cavern & deep geological site, low-level and very low-level wastes shall be disposed of surface disposal site. Exempt wastes are allowed to be reclaimed or recycled in accordance with other laws and regulations.[1],[2]

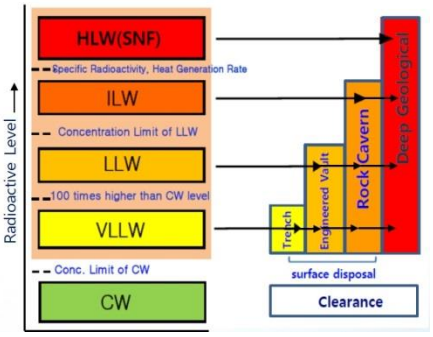

Fig. 1. Classification and Disposal of Waste in Korea.

The International Atomic Energy Agency(IAEA) has classified radioactive wastes into six categories, depending on the half-life and radioactivity content: High Level Waste(HLW), Intermediate Level Waste(ILW), Low Level Waste(LLW), Very Low Level Waste(VLLW), Very Short-Lived Waste(VSLW) and Exempt Waste(EW) as described

in Fig. 2. [3],[4]

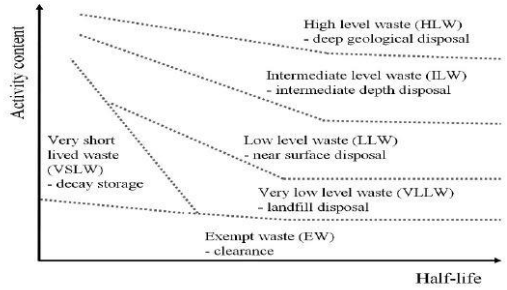

Fig. 2. Conceptual illustration of waste classification scheme.

4. Treatment Technology for Waste Disposal

In the decommissioning process of nuclear power plants decommissioning radioactive waste is mostly metal waste and concrete waste used as building construction materials.[5]

4.1 Metal Waste

Wastes when the decommissioning nuclear power plants are generated in various form such as metal pieces, concrete, and in large amounts. Some countries have acquired the techniques to minimize radioactive metal waste through long-term R&D and experiences based on recycling scenarios of waste, behavior of radionuclides, and so on. Actually, commercial treatment facility is in operation, and many R&D projects for more safe and economical recycling in the nuclear industry are continuing.

4.2 Concrete Waste

Contaminated radioactive concrete waste is the waste which is generated by the decommissioning nuclear power plants. In European Commission report, it is expected that there will be 5 million tons of concrete waste from the decommissioning nuclear power plants in Europe by 2060. Some countries such as USA, Germany had recognized the importance of recycling concrete waste and had used it as a solid form for shielding block in some cases.

5. Conclusions

The decommissioning and maintenance of nuclear power plants generate a large amount of waste, and the waste disposal site is not enough to accommodate the waste, and the disposal cost is continuously increasing. Therefore, the reduction and recycling of dismantled waste is essential in terms of environmental and economic aspects. Considering the fact that the disposal cost of radioactive waste is not easily secured and the disposal cost of radioactive waste is continuously increasing, it is one of the waste management measures to reduce the volume of bulk dismantled waste generated during dismantling of nuclear power plants or dispose of exempt waste. It is considered. The recycling of dismantled wastes that will occur when dismantling nuclear power plants in the future is an important issue for us in terms of environmental aspects and economics.

Therefore, it is necessary to study waste disposal technologies that will be developed in the future.

REFERENCES

[1] International Atomic Energy Agency, Classification of Radioactive Waste, IAEA, Safety Standards Series No. GSG-1 (2009).

[2] International Atomic Energy Agency, Application of the Concepts of Exclusion, Exemption and Clearance, IAEA Safety Standards Series No. RSG-1.7 (2004).

[3] International Atomic Energy Agency, Managing Low Radioactivity Material from the Decommissioning of Nuclear Facilities, Technical Reports Series No. 462 (2008).

[4] International Atomic Energy Agency, Disposal Aspects of Low and Intermediate Level Decommissioning Waste, IAEA-TECDOC-1572 (2007).

[5] ANDRA, National Inventory of Radioactive Materials and Waste-Synthesis Report (2009).

Discussion on Bioshield Dismantling Process of Kori Unit 1

Ju-Young Yoon※ and Cheon-Woo Kim

KHNP CRI, 70, 1312-gil, Yuseong-daero, Yuseong-gu, Daejeon, Republic of Korea

※august63@khnp.co.kr

1. Introduction

Kori unit 1 has been permanently suspended in June 2017, and preparations for decommissioning are in progress.

Activated wastes in radioactive waste include reactor vessel, reactor vessel intetnals, and bioshield.

Among them, bioshield has a large, and there is a difference in degree of pollution in each district, so a strategic dismantling plan should be established.

This paper describes the overseas case and discusses the process of disassembling the bioshield of Kori unit 1 in consideration of Korea's policies and environment.

2. Bioshield

The bioshield is surrounded by nuclear reactor vessel and has the function of reactor vessel protection and shielding from the heat as shown in Fig. 1.

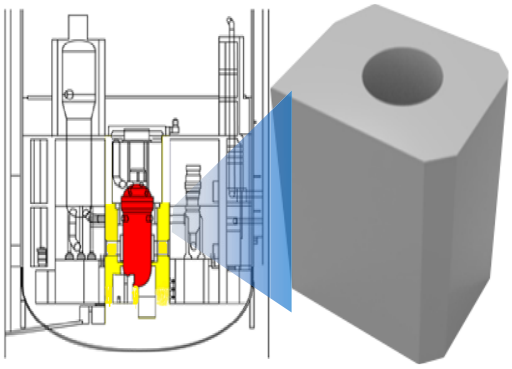

Fig. 1. Bioshield structure in Kori unit 1.

Kori unit 1 bioshield structural features are as follows.

Kori unit 1 bioshield mainly consists of concrete containing reinforcing bars, epothy, liner plate, etc.

In the lower part, there is a penetration part of the in-core measurement instrument.

In the middle, there is a structure in which the ex-core measuring instrument is inserted.

It is closest to the nuclear fuel, so it is also called the belt line, and the activity is expected to be the highest.

In the upper part, structures such as in-leg and out-leg piping are formed.

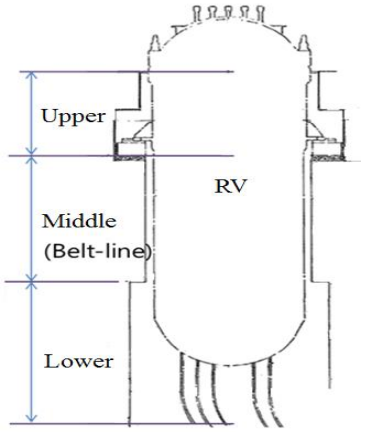

Fig. 2. Bioshield structure.

3. Dismantling Process

3.1 Activation evaluation

In order to dismantle, the bioshield characteristics must be evaluated before dismantling process is decided. The bioshield structure and material properties are assessed to perform the activation evaluation.

According to the result of proper activation evaluation, it is possible to manage the dose and to

classify the radioactive waste systematically in the dismantling process. This is more important because it directly relates to the cost of treating radioactive waste.

In the case of overseas cases, evaluation of bioshield activation includes the method of radioactivity evaluation using MCNP code and the method of directly sampling or collecting by coring or drilling as shown in Table 1.

Table 1. Oversaes status of the activation evaluation

NPP	Activation Analysis	Sampling	Activation Depth
Jose Cabrera	MCNP/ ORIGEN-S	Drilling	120cm
SONGS-1	-	Drilling	First 30cm highly activated in RV beltline region
Maine Yankee	-	Coring	Activation to 60cm, First 40cm above site release limits
Yankee Rowe	MCNP/ ORIGEN-S	Coring	First 27cm above site release limits

3.2 Establish cutting process

Once the ex-core device structure is removed, a small perforation is created in the middle and upper part of the bioshield. The cutting operation can be performed by using the penetrating portion.

This is similar to Jose Cabrera's method of cutting a bioshield into a saw recently.

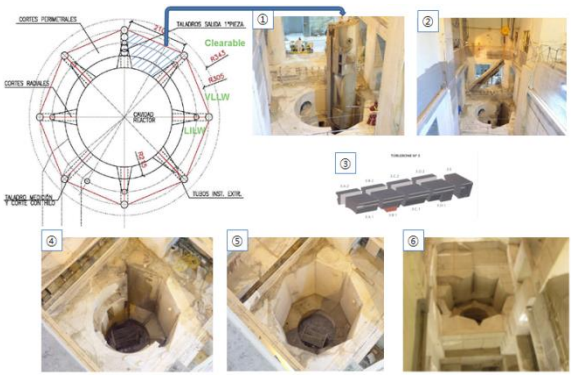

Fig. 3. Cutting process of Jose Cabrera.

According to the results of the activation evaluation, the radiation level & cutting line have been determined.

In addition, there should be a way to more effectively capture the dust generated during the cutting of concrete and a method to prevent the spread of radioactive contamination to concrete with a relatively low contamination level.

There are ways to install tents and dust collectors, which have the advantages of low contamination spread, effective dose management and dust collection, but also have the disadvantage of installation costs and secondary radioactive waste generation.

It should be decided taking into consideration various measures.

4. Conclusion

Bioshield concrete contains radioactive concrete, and its capacity is large, requiring a strategic dismantling process. It is necessary to accurately evaluate the bioshield structure and physical properties of Kori unit 1 to perform activation evaluation.

Further, by analyzing the radioactivity through the sampling, comparative analysis with the results of the activation evaluation can be performed to obtain a more accurate characteristic evaluation result.

It is necessary to design and cut the cutting line by making good use of the characteristics of the structure, and to establish the cutting process considering contamination spread, worker dose management, and secondary radioactive waste.

REFERENCES

[1] EPRI 1015502 “Concrete Characterization and Dose Modeling During Plant Decommissioning”.

[2] 15th EPRI International Nuclear Power Plant Decommissioning Workshop “Jose Cabrera NPP Characterization and Decontamination of Biological Shielding”.

Study on the Characteristics of Electro-Decontamination by Pilot Scale Equipment

Ki-Chul Kim*, Dong-Yeon Kim, and Jung-hyun Lee
KEPCO KPS, 96-1 Gilchon-Gil, Jangan-Eup, Gijang-Gun, Busan, Republic of Korea
*KICHKIM@kps.co.kr

1. Introduction

Electro-decontamination technology can be used for decontamination of the primary system of the nuclear power plant by directly applying current to the metal and simultaneously removing the base material and the oxide film.

In this study, data on the weight loss and thickness reduction of STS304 specimens, which are caused by temperature and voltage, were selected for commercial electro- decontamination process equipment, and a pilot scale electro-decontamination process was conducted to evaluate decontamination efficiency .

2. Process equipment

The electro-decontamination pilot equipment used in this study was designed based on the mock-up of the shape reduced to 75%, while the cold leg reactor coolant system pipes connecting the steam generator and the reactor coolant pump in the power plant system was cut to 1 m. The volume of electro-decontamination tank is 900 (L) x 900 (W) x 1,000 (H), 810L.

3. Experiments

3.1 Experimental method

The specimens used were STS304 (35*13*3㎜), and three pieces were vertically mounted on the PIPE type mock-up. The electrode is indirectly connected for process automation and is shown in Fig. 1. The electrolyte was used with 4 M H_3PO_4. The temperature of the electrolyte was increased to RT (10 °C), 40 °C and 60 °C, and the voltage was applied at 4, 6, 8 and 10 V for each temperature. The process time was 1 hour and the current was measured every 10 minutes. After the test, thickness reduction was calculated using the weight measurement and weight loss method of the specimen.

Fig. 1. PIPE type mock-up and jig(L).
Fig. 2. Electro-decontamination tank(R).

3.2 Thickness reduction calculation

The mole of metal for weight loss before and after the electro-decontamination process of STS304 specimen is expressed as $\alpha\, mol_{M^{n+}}$, and the formula for thickness reduction can be summarized as follows.

$$d_{M^{n+}} = \alpha\, mol_{M^{n+}} \times \frac{F.W(g/mol_{M^{n+}})}{density(cm^3/g)} \qquad (1)$$

After the electro-decontamination process, the weight loss for each of the three specimens in each experiment was added up and averaged, and the weight of the measured metal was substituted into the above formula to calculate the thickness reduction of the specimen.

3.3 Experimental result

As a result of experiments at three temperature conditions through electro-decontamination process, the current density also increased with increasing voltage. In addition, weight loss and thickness reduction were also found to increase, and data for each experiment are shown in Tables 1, 2, and 3. At the same voltage, the thickness reduction was found to be high as the temperature increased, and was shown in Fig. 3.

Table 1. Measurement results of current density by voltage and temperature

Voltage [V]	Current density [mA/cm^2]		
	RT	40 ° C	60° C
4	2.01`	5.08	5.16
6	8.29	17.87	21.13
8	19.61	32.08	34.68
10	31.23	46.66	50.99

Table 2. Measurement results of weight loss by temperature and voltage

Voltage [V]	Weight loss [mg]		
	RT	40 ° C	60° C
4	`6.6	13.5	17.8
6	24.8	52.1	69.8
8	39.9	91.9	119.5
10	42.4	154.6	181.2

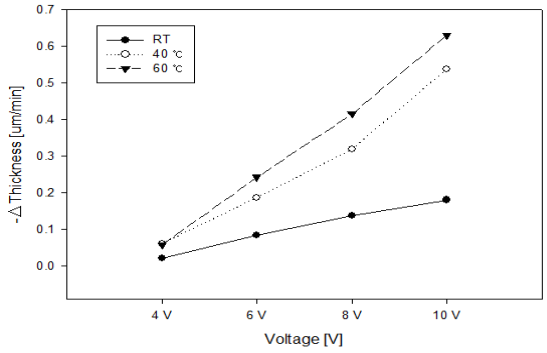

Fig. 3. Experimental results in relation to voltage and temperature.

4. Conclusion

From the results of this experiment, it was confirmed that the results are similar to the experimental results at the laboratory scale in relation to the voltage increase [1]. The measurement revealed that the average thickness removal rate was 24 μm per 1 hour on the surface area of 1.5 m^2. Therefore, it is expected that it will exhibit excellent decontamination efficiency even in the process of commercial scale.

Future research will be carried out to enhance decontamination efficiency about complex shaped segmentation by using arrangement of electrodes.

ACKNOWLEDGEMENTS

This work was supported by the Korea Institute of Energy Technology Evaluation and Planning (KETEP) and the Ministry of Trade, Industry & Energy (MOTIE) of the Republic of Korea (No. 20141510300310)

REFERENCES

[1] D.Y. Kim, "Electrolysis Characteristics of SUS304/316L for Electro-decontamination of Radioactive Contaminated Metal in Nuclear Power Plant", Kyungpook National University, August, 2017.

[2] D.Y. K, H.K. L, W.Z. O, S.J. C, “Effect of the addition of oxalic acid to the phosphoric acid electrolyte on the electro-decontamination behavior of the SUS metal surface”, Proc. of the KRS 2017 Spring Conference, 15(1), May 24-26, 2017, Busan.

A Study of Traceability and Change Management Based on Decommissioning Information for a Nuclear Facility

Yunjeong Hong*, Heeseoung Park, Jongjin Kim, and Jeong-guk Kim
Korea Atomic Energy Research Institute, Daedeok-daero989ben-gil 111,Yuseong-gu, Daejeon, Republic of Korea
*hong814@kaeri.re.kr

1. Introduction

Decommissioning information is generated from various fields related to decommissioning from permanent shutdown to site restoration when nuclear facility is decommissioned. Since this information is used for important factors such as waste management and cost estimation, it is necessary to manage information systematically and accurately. Various management systems have been developed, however, there are limits in aspect of information management because each unit system is operated independently. In order to overcome this, we have secured the connection between existing unit programs.

In this study, we will describe the traceability function that can clearly identify the affected items as the requirements for decommissioning nuclear facilities, and management function that can adjust the changes related to decommissioning activities and regulatory requirements.

2. Design of Traceability and Change Management Function

Traceability and change management based on nuclear facility decommissioning information aims at ensuring data integrity and consistency between the decommissioning information.

2.1 Main Function

Traceability and change were used with the CMD Build platform based on an open source that facilitates the management and tracking of nuclear facility decommissioning data.

2.1.1 Traceability. Data in this system is managed by defining relations between classes, and administrators and users can easily add and modify them.

- Adding of Traceability: Users can easily add / edit data through the system's 'Relations' tab list if there is a change in the relationship between the data.

- Confirmation of relationship (confirmation of traceability): It is easy to trace configuration information through 'Relation graph' function. As shown in Fig. 1, all configuration information related to each diagram can be visually confirmed, and attribute information of each configuration can be confirmed through UI 'Card' tab.

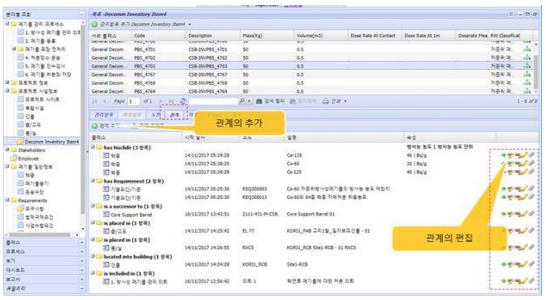

Fig. 1. Adding and editing relationships (traceability).

2.1.2 Change Management.

- When technical standards related to decommissioning regulatory requirements and activities is changed, the changes shall be carried out

in accordance with predefined change management procedures and the relevant records shall be recorded. It also supports the function to clearly identify the items affected by the change.

- History management: life-cycle history of configuration information is managed as lists.

3. Results

An example of a radioactive waste process was selected as a sample case for verifying traceability and change management function

3.1 Traceability of Decommissioning Regulatory Requirement

The radioactive waste processes to being managed as classes on the system, general information on radioactive waste, and laws information are connected to each other through relation. The user can confirm and modify the relation between the class and the other class.

Fig. 2. Traceability of radioactive waste - Relationship graph.

3.2 Change Management of Decommissioning Regulatory Requirements

The user can confirm the change process of the management item through the history tab of the management area and inputting the management item of the system. As shown in Fig. 3, the history function provides basic functions of change management such as modification start time, registration date, end time, and changer information.

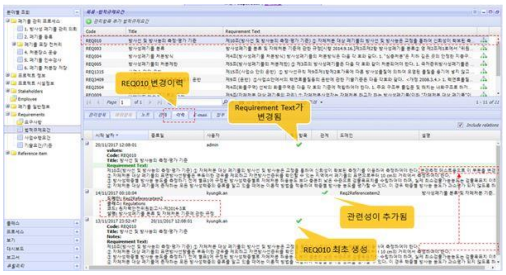

Fig. 3. Change management of radioactive waste regulatory requirements.

4. Conclusion

In this study, we described the traceability function that can clearly identify the affected items as the decommissioning regulatory requirements for nuclear facility are changed, and the management function to reflect the regulatory requirements and the changes related to the decommissioning activities based on the traceability function. The case of radioactive waste process was applied for traceability and change management as an example. Through this study, we have secured a basis for systematically tracking regulatory requirement information, decommissioning facility information, and decommissioning activity information related to decommissioning of nuclear facilities.

3D Scanner Calibration Methodology for Advanced Remote Dismantling System

Sang Min Lee[a], Jonghwan Lee[b]*, Dongjun Hyun[b], Ikjune Kim[b], and Shin Young Kang[b]
[a] Korea Univ. of Tech. and Edu., 1600, Chungjeol-ro, Byeongcheon-myeon, Cheonan, Republic of Korea
[b] Korea Atomic Energy Research Institute, 111, Daedeok-daero 989beon-gil, Yuseong-gu, Daejeon, Republic of Korea
*jhl@kaeri.re.kr

1. Introduction

Dismantling of nuclear power plants requires the remote system because human access is limited to the work place having a high radiation [1]. For this reason, teleoperation robot will be accessible with dismantling mission. But, before dismantling, actual nuclear power plant environment need to be acknowledged. So, the 3D scanner can be used for recognizing dismantling environment.

This research proposes a methodology to calibrate the transformation matrix of the 3D scanner. Position obtained by the transformation matrix of the 3D scanner may have an error of the order of a few millimeters because most 3D scanners are designed to acquire object's shape, not position. In this research, a calibration methodology based on ICP algorithm is used to find transformation matrix aligning scanned point cloud data with a true cad model. Experimental results show that localization using the calibrated matrix achieves an acceptable level of error.

2. 3D Scanner Calibration Methodology

ICP algorithm [2] is used for acquiring distance and angular differences between true data which is accurate CAD position data and scanned data. Transformation matrix is used for transforming coordinate from scanner's camera to mount origin.

2.1 3D registration with ICP algorithm

Iterative Closest Point algorithm is designed to minimize error between two-point cloud data.

$$E(R,t) = \frac{1}{N_p}\sum_{i=1}^{N_p}\|x_i - Rp_i - t\|^2 \qquad (1)$$

Where translation t and rotation R minimize the sum of the squared error. $x_i$and $p_i$are corresponding points.

2.2 Calibration Sequence

Calibration process is followed with this steps.

Step 1. Getting point cloud data from scanner

Step 2. Transform point cloud to origin of scanner mount by transformation matrix.

Step 3. Acquire calibration matrix with ICP algorithm between true data and scanned data.

2.3 Acquiring Calibrated Matrix

Raw data from scanner is just distance from camera, not actual distance from mount origin.

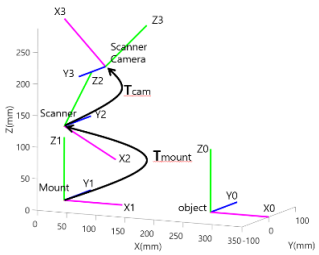

Fig. 1. Coordination System of Experiment.

Thus, data need to be transformed to mount origin with transformation calculation.

$$\mathbf{D}_{\text{modified}} = \mathbf{T}_{\text{mount}}\mathbf{T}_{\text{cam}}\mathbf{D}_{\text{raw}} \qquad (2)$$

As shown in Fig. 1, $\mathbf{T}_{\text{mount}}$ is transformation from mount origin to scanner origin, $\mathbf{T}_{\text{cam}}$ is transformation from scanner origin to main camera, $\mathbf{D}_{\text{raw}}$ is raw point cloud data. ICP algorithm is used for comparing true data and modified data. Result of ICP algorithm $\mathbf{T}_{\text{ICP}}$ is the matrix with distance and angular transformation.

$$\begin{aligned}\mathbf{D}_{\text{true}} &= \mathbf{T}_{\text{ICP}}\mathbf{T}_{\text{mount}}\mathbf{T}_{\text{cam}}\mathbf{D}_{\text{raw}} \\ &= \mathbf{T}_{\text{mount}}\mathbf{T}_{\text{cam}'}\mathbf{D}_{\text{raw}}\end{aligned} \qquad (3)$$

$\mathbf{T}_{\text{mount}}$ is different when mount changed to other environment like robot arm. Thus, $\mathbf{T}_{\text{cam}'}$ matrix which is unchanged need to be calculated.

$$\mathbf{T}_{\mathrm{cam}'} = (\mathbf{T}_{\mathrm{mount}})^{-1}\mathbf{T}_{\mathrm{ICP}}\mathbf{T}_{\mathrm{mount}}\mathbf{T}_{\mathrm{cam}} \qquad (4)$$

Invariant scanner calibration matrix $\mathbf{T}_{\mathrm{cam}'}$ is acquired by calculation (4).

3. Experiment

Experiment repeated 6 times to get average of result for reliability.

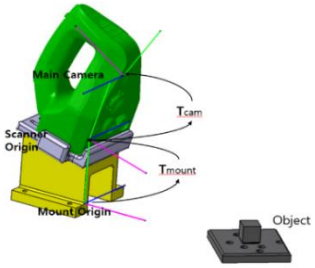

Fig. 2. Experiment Setup.

Mount and object are printed by 3D printer. Materials are fixed to test table with bolt.

4. Result

4.1 Calibrated Camera Transformation Matrix

$$\begin{bmatrix} -0.9998 & -0.0100 & 0.0148 & -0.1219 \\ -0.0053 & 0.9572 & 0.2894 & 122.4096 \\ -0.0171 & 0.2893 & -0.9571 & 16.9045 \\ 0 & 0 & 0 & 1 \end{bmatrix} \qquad (5)$$

$$\begin{bmatrix} -1 & 0 & 0 & 0 \\ 0 & 0.9547 & 0.2975 & 120.97 \\ 0 & 0.2975 & -0.9547 & 16.053 \\ 0 & 0 & 0 & 1 \end{bmatrix} \qquad (6)$$

Matrix (5) is final calibrated $T_{cam'}$ matrix which is averaged with all iteration result. Matrix (6) is given by manufacturer. Camera transformation matrix calibrate +1.44mm in direction of Y-axis, +0.85mm in direction of Z-axis, -0.12mm and -0.49 degrees on the X-axis.

4.2 Error Analysis

Fig. 3 shows verification of calibration matrix.

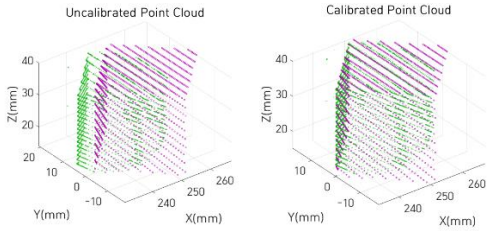

Fig. 3. Differences between True and Calibrated Data.

Result proves that method derives satisfactory calibration data. As shown in Fig. 4, RMS error of point cloud data are 0.06mm~0.07mm. Thus, Calibration method can reach accuracy with in 0.1mm expressed in scanner specification [3].

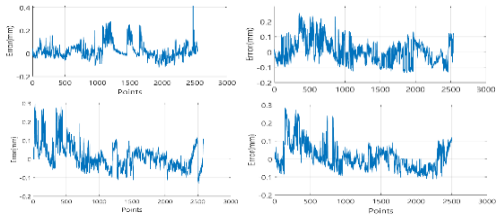

Fig. 4. Plotting 4 cases Error between True and Calibrated Point Cloud Data.

5. Conclusion

The calibration methodology proposed in this paper can get precision calibrated result that derives low error between true and scanned data. Method show that calibration using ICP algorithm is appropriate for calibrating scanner.

ACKNOWLEDGEMENT

This work was supported by the nuclear research and development program through the National Research Foundation of Korea, funded by Ministry of Science and ICT, Republic of Korea (Grant Code: 2017M2A8A5015146)

REFERENCES

[1] Hyun, D., Lee S., Seo Y., Kim G., Lee J., Jeong K., Choi B., Moon J., “Seamless remote dismantling system for heavy and highly radioactive components of Korean nuclear power plants”, Annals of Nuclear Energy, 73, 39-45 (2014).

[2] Chen, Y. and G. Medioni, “Object Modelling by Registration of Multiple Range Images.”, Vol. 10, Issue 3, April 1992, pp.145-155.

Development of Decommissioning Project Management System Platform

Kook-Nam Park [a*], In-Hye Hahm [a], Dae-Seo Koo [a], Sang-Bum Hong [a], Jung-Sup Oh [b], and Moon-Joo Gil [b]

[a] Korea Atomic Energy Research Institute, 989-111 Daedeok-daero, Yuseong-gu, Daejeon, Republic of Korea

[b] NSE Technology, 5F Convergence Technology Research Commercialization Center, Electronics and Telecommunications Research Institute, 218 Gajeong-ro, Yuseong-gu, Daejeon, Republic of Korea

knpark@kaeri.re.kr

1. Introduction

A project management system is established for carrying out a decommissioning project of nuclear facilities. First, the system will be complemented with a system that can systematically manage the history of dismantled waste, which has already been constructed and minimize the waste amount and cost. Second, we propose a decommissioning integrated management system that systemically manages dismantling information such as the scope, time, and configuration, as shown in Fig. 1 [1]. The platform of the decommissioning project management system consists of a dismantling waste platform and a configuration management platform.

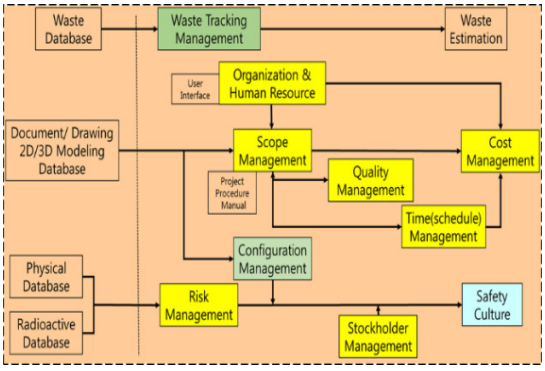

Fig. 1. Decommissioning Integration System.

2. Project Management Platform

2.1 Dismantling Waste Platform

As shown in Fig. 2, the dismantling waste platform structure manages three areas: the standard requirements, the waste characteristics information and the waste process.

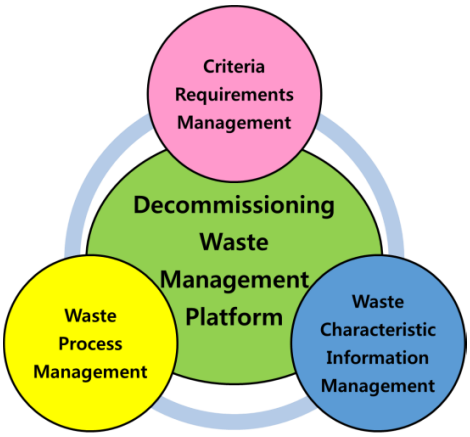

Fig. 2. Dismantling waste platform structure.

The standard requirement management has the function of linking standard requirement, design, construction, operation document and waste in the design bases of nuclear power plant operation. Waste characteristics information management consists of a facility master value for each component, the generation of waste packages, the linkage of components and unit waste, and the management of waste characteristic information. Waste process management was designed for the waste treatment process, inquiring the process status, estimating the waste throughput of each process, optimizing the process, and estimating and managing the exposure of workers.

2.2 Configuration Management Platform

The configuration management platform consists of requirement management, facility configuration information, physical configuration information, and workflow platform as shown in Fig. 3 [2].

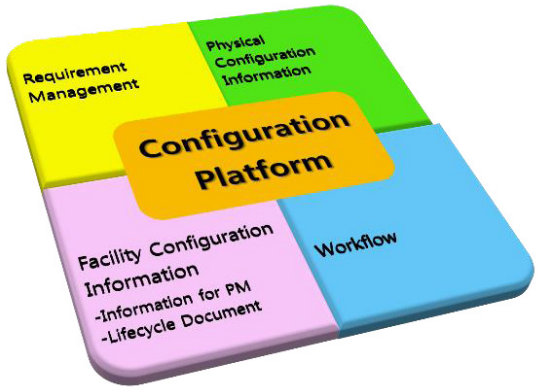

Fig. 3. Configuration management platform.

The requirement management platform supports the use of design documents and drawings that are systematically managed in the existing document management system. The facility configuration information platform maintains the number classification system based on the physical breakdown structure (PBS), the organizational breakdown structure (OBS), and the functional breakdown structure (FBS) for the design, construction and operation [3]. The physical shape information platform identifies and acts on the state and distance of the system through the panorama viewer and the 3D model viewer for the site of the nuclear facility. The workflow platform has functions such as the process design, process assignment, process execution, and process monitoring.

3. Conclusion

The decommissioning project management system platform was divided into two parts, namely, a dismantling waste platform and a configuration management platform. In particular, to allow the decommissioning project to be carried out smoothly, the configuration management platform is divided into a facility master based on the project manager information, and a document management system based on the life-cycle document information.

REFERENCES

[1] Kook-Nam Park, In-Hye Hahm, Dae-Seo Koo, and Sang-Bum Hong, etc., “Conceptual Design for Development of Decommissioning Project Management System”, Korean Nuclear Society Autumn Meeting, October 26-27, 2017, Gyeongju.

[2] Jung-Sup Oh, Moon-Joo Gil, “Development of Configuration Management Platform of Operational Nuclear Power Plant”, Korean Nuclear Society Spring Meeting, May 18-19, 2017, Jeju.

[3] Ki-Ae Jeong, etc., “A Study on the Classification System of National Construction Project based on WBS”, Information Management Research, 41(1), pp 13-15, KISTI, 2010.

Generation Characterization of Metal Wastes During the Decommissioning of PWR NPPs

Ji-Hoon Lee and Kang-Ok Cho

KHNP Central Research Institute, 70, 1312-gil Daedeok-daero, Yuseong-gu, Daejeon, Republic of Korea

*choko1004@khnp.co.kr

1. Introduction

Kori Unit 1, which was decided to be permanently shut down, will be decommissioned after approval of the final decommissioning report. During the decommissioning of nuclear power plants, various kinds of radioactive waste such as metal, concrete, and soil will be generated in a short period of time. A lot of research has been done in Korea, such as metal decontamination, which is an essential technology of nuclear power plant decommissioning. However, there is not so many researches on the utilization of metal waste that is expected to occur in large quantities during decommissioning. It is necessary to investigate the generation characterization of radioactive wastes during the decommissioning of PWR NPPs. Therefore, the status of metal wastes generated during the decommissioning of nuclear power plants will be discussed and the strategy of volume reduction of radioactive wastes during decommissioning of Kori Unit 1.

2. Status of radioactive metal wastes generated by the decommissioning

2.1 Radioactive wastes generated during the decommissioning (Foreign status)

The IAEA has predicted the amount of metal waste during decommissioning of PWR nuclear power plant (900 ~ 1,300 MWe) [1]. The amount of radioactive metal waste was generated about 58.87% of the total radioactive waste during decommissioning of NPPs.

Table 1. Estimated waste generated by decommissioning

Kinds	Generation (ton)	Share(%)
Activated metal	650	10.48
Activated concrete	300	4.84
Radioactive metal	3650	58.87
Radioactive concrete	600	9.68
Dry Active Waste	1000	16.13
Total	**6200**	**100**

In most countries, radioactive metal wastes are subject to do clearance, restricted release or disposal in accordance with national regulatory standards. The amount of radioactive metal waste generated in the US, PWR reference nuclear power plants were estimated to be 32,731 ton/ GWe for the carbon steel and 2,080 ton/GWe for the stainless steel.

The amount of radioactive waste generated by decommissioning one PWR nuclear power plant in Japan is about 2,690 to 5960 tons from 500MWe to 1100MWe. Converting these amounts into a drum, it is estimated that 12,400 ~ 31,000 drums will be generated when the weight of waste per 200 drums are assumed to be about 200 ~ 500kg. The EdF, an electric power company in France, estimates that the amount of decommissioned radioactive waste was generated about 17,100 m^3 at the time of decommissioning of one nuclear power plant [2].

2.2 Estimation of radioactive metal waste generation during decommissioning of Kori Unit 1

The amount of radioactive metal waste generated in the decommissioning of Kori Unit 1 was estimated [3]. Generation of radioactive metal waste was 11,253 m^3. It is assumed to be 56,265 drums (200L)

when the wastes generated are cut in suitable scale. After the melting of radioactive metal waste by induction method, the amount of radioactive waste generated can be reduced to 571 m^3 which is estimated as 2855 drums (200L) as volume reduction ratio is applied to 5%.as shown in Table 2. After radiological Assessment, if some metal will be applied to unrestricted release or reuse in controlled area, the disposal amount of metal waste will be more reduced (Fig. 1).

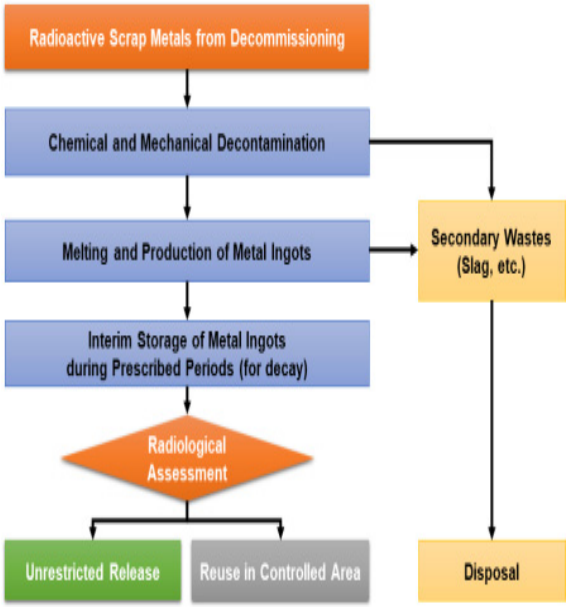

Fig. 1. VLLW and LLW radioactive metal waste treatment strategies.

Table 2. Estimation of radioactive metal waste quantity during induction heating melting and metal recycling

Level	Kinds	Waste Volume(m^3) **(200 L drum EA)**	
		Initial (1)	After melting(2)
ILW)	Small metals[1)]	8	8
LLW	Large device	832	42
	RVI	199	10
	Small metals	3,416	171
	SF storage rack	490	25
	Total	4,937	248
VLLW	Small metals	6,308	315
	Total	6,308	315
Total radioactive Waste		11,253 **(56,265)**	571 **(2855)**

1) Data from Reference [3]

2) 5% reduction of initial volume after induction melting

3. Conclusion

In the case of Kori Unit 1, the amount of metal radioactive waste was estimated to be 11,253 m^3. It is expected that metal radioactive waste will be significantly reduced through decontamination and melting process. In order to achieve this, it is necessary to further investigate the melting characteristics of target metal and the distribution of the radionuclide.

REFERENCES

[1] IAEA, Managing Low Radioactivity Material from the Decommissioning of Nuclear Facilities, Technical Report Series No. 462 (2008).

[2] Project PENLY 3, Mieux Comprendre Les Enjeux du Nucleaire (2010).

[3] Evaluation of Decommissioning Source Terms and Wastes for the Presurized Water Nuclear Power Plant and Heavy Nuclear Power Plant, KEPCO E&C Report (2016).

An Equilibrium Calculation on Removal of Sulfate and Metal Ions in a Wastewater Generated From the SP-HyBRID Decontamination Process

H.C. Eun[a,*], J.Y. Jung[a,b], S.Y. Park[a], J.S. Park[a,b], H.J. Won[a], S.B. Kim[a], and B.K. Seo[a]
[a]Korea Atomic Energy Research Institute, 989-111 Daedeok-daero, Yuseong-gu, Daejeon, Republic of Korea
[b]Department of Applied Chemistry and Biological Engineering, Chungnam National University, 99 Daehak-ro Yuseong-gu, Daejeon, Republic of Korea
[*]ehc2004@kaeri.re.kr

1. Introduction

In KAERI, the SP-HyBRID process has been developed to decontaminate the primary coolant system of a nuclear power plant[1]. The SP-HyBRID process consists of a pre-oxidative step and a reductive step, HyBRID. The pre-oxidative step is progressed using H_2SO_4 and $KMnO_4$, and the reductive step is conducted using N_2H_4 (hydrazine), H_2SO_4, and Cu^+. A wastewater is generated from the SP-HyBRID decontamination process of the coolant system. The wastewater contains not only the contamination agents but also the metal ions dissolved during the decontamination process, which typically includes radioactive metal ions such as Co-58, Co-60, Mn-54, and Cr-51, etc.

It is very effective to remove the contaminants from the wastewater for minimizing waste generation. The contaminants can be effectively removed by a precipitation method using $Ba(OH)_2$[2]. In general, when pH in a solution is increased by $Ba(OH)_2$ injection, metal ions in the solution are converted into a hydroxide form, and precipitated to the bottom of the solution[3]. $Ba(OH)_2$ is injected at an equivalent to sulfate ions, and $BaSO_4$ is removed as precipitates as shown in Eq. (1). In this precipitation reaction, the generated OH^- can be consumed to form metal hydroxide for residual metals in the solution, and the amounts of metal ions in a wastewater can be changed with operation conditions of the decontamination process. Therefore, it is necessary to evaluate effects on the removal of metal ions in a wastewater with amounts of them.

$$SO_4^{2-} + Ba(OH)_2 = BaSO_4 + 2OH^- \quad (1)$$

In this study, theoretical equilibrium calculations on removal of sulfate and metal ions in a wastewater surrogate by $Ba(OH)_2$ injection were conducted by using equilibrium calculation software (HSC-Chemistry 9.5). The removal characteristics of metal ions in the surrogate were estimated with changes in the amounts of metal ions.

2. Equilibrium Calculation

Table 1 shows the composition of the wastewater surrogate used in the equilibrium calculation. Except N_2H_4, sulfate forms as input materials were determined for the sulfate and metal ions because sulfate ions in a wastewater from the decontamination process are a main component for dissolving metals. The concentrations of the decontamination reagetns used in the SP-HyBRID process were fixed, and the amounts of dissolved metal ions were changed from 50 to 400 ppm. The concentrations were reduced into mole unit for the equilibrium calculation. The amount of $Ba(OH)_2$ was determined considering the amounts of sulfate ions in the wastewater surrogate. The equilibrium calculation was conducted using HSC-Chemistry 9.5 which is progressed on the base of Gibbs free energies of reactions between input materials[4].

Table 1. Composition of the wastewater surrogate used in the equilibrium calculation

Compounds	Concentration (ppm)
N_2H_4	1604
H_2SO_4	3632
$MnSO_4$	962
K_2SO_4	554
$CuSO_4$	81
Metal (Fe, Cr, Ni, Cu, Zn, Co) ion	50 ~ 400 (respectively)

3. Results

The equilibrium calculation results (metal ion conc.: 50 ppm, respectively) are shown in Fig. 1. According to Fig. 1, sulfate ions in H_2SO_4 is preferentially reacted with $Ba(OH)_2$, and removed into $BaSO_4$. Except for Mn, the metal (M) ions are mostly converted into $M(OH)_2$. Some of them are formed into MO. Mn ions are also mainly converted into $Mn(OH)_2$. However, a considerable amount of Mn ions are formed into liquid phase of $Mn(OH)_2$. Because of that, it is considered that removal of Mn ions in a wastewater from the SP-HyBRID decontamination process will be limited. In this equilibrium calculation, it is predicted that some of K ions are converted into KOH very soluble in water. Thus, removal of K ions by $Ba(OH)_2$ injection will be very few. When the concentrations of metal ions are 400 ppm, respectively, oxide formations of the metal ions are significantly increased. Especially, Ni ions are mainly converted NiO, and a significant amount of Zn ions are also formed an oxide form, ZnO.

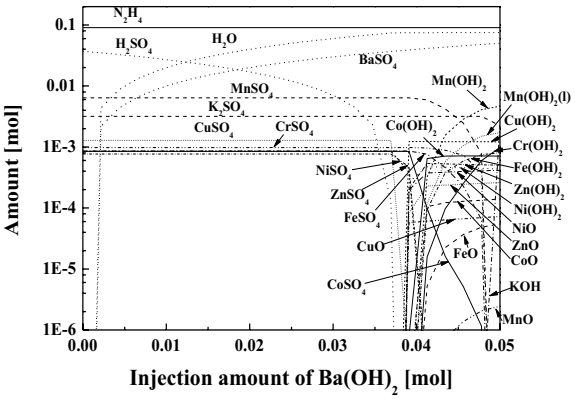

Fig. 1. Equilibrium calculation results (metal ion conc.: 50 ppm, respectively).

4. Conclusion

Through the equilibrium calculation results, it is predicted that the metal ions can be effectively removed into a hydroxide form or an oxide form, except for Mn and K. In case of Mn, it is required to evaluate a residual amount in a wastewater surrogate closely after a wastewater surrogate treatment test. For the removal of K ions, it is necessary to develop a method to separate K ions selectively as an insoluble form in water.

ACKNOWLEDGE

The authors would like to express their appreciation to the National Research Foundation of Korea (NRF) for the award of a grant funded by the Ministry of Science and ICT (MSIT) of the Republic of Korea, in support of the authors' work through the Nuclear Research and Development Program (NRF-2017M2A8A5015144).

REFERENCES

[1] S.B. Kim. H.J. Won, J.K. Moon, W.K. Choi, "Magnetite dissolution using hydrazine-acid solution for chemical decontamination", Transactions of the American Nuclear Society, Vol. 115, Las Vegas, USA (2016).

[2] S.Y. Park, W.K. Choi, S.B. Kim, H.J. Won, M.S. Choi, "Estimation of waste volume for KORI#1 decontamination using SP-HyBRID process, KRS Spring Meeting (2017).

[3] Baijnath, L. Lal, V. Gautam, V. L. Yadav, "A comparative study of the removal efficiency of calcium hydroxide and sodium hydroxide as precipitating agents for chromium (III)", J. Civil Eng. & Environ. Technol., Vol., No. 1 (2014).

[4] A. Ronie, Outokumpu HSC Chemistry for Windows, OutoKumpu Research, Pori, Finland (2002).

Development of Decommissioning Waste Information Tracking System for the Life-Cycle of Decommissioning Nuclear Facilities

Sang Bum Hong*, In Hye Hahm, Jae Hyun Ha*, Kwan Seong Jeong, Seung Kook Park, and Dae Seo Koo, Kook Nam Park, and Bum Kyoung Seo

Korea Atomic Energy Research Institute, 111, Daedeok-daero 989 beon-gil, Yuseong-gu, Daejeon, Republic of Korea

sbhong@kaeri.re.kr

1. Introduction

A large quantity of radioactive and nonradioactive waste is generated during the decommissioning nuclear facilities. The decommissioning waste is typically treated many times for minimization from the point of initial generation, sorting, decontamination until it is packaged and transported for final disposal.

The purpose of this study is to develop the waste treatment information tracking system using a waste inventory database structure of waste package and container with user-friendly interface for efficient management of waste treatment information for the life cycle of decommissioning nuclear facilities.

2. Project Management Platform

2.1 Data structure of decommissioning waste information system

The life cycle of radioactive waste consists of a number of steps such as pretreatment, treatment, conditioning, storage and disposal. The objective of radioactive treatment intended to improve safety or economy by changing the characteristics of waste such as volume reduction, decontamination and immobilization for safe disposal and clearance. Characterization of radioactive waste is an important aspect at every stage of waste management. The physical, chemical and radiological properties of the waste should be characterized and managed from generation to final disposal. [1] The waste information tracking system was developed to improve decommissioning safety and minimization of decommissioning waste. The design requirements of the system support the design document and record using modified WBS(Work Breakdown Structure) for decommissioning from the design, construction and operation. The database of the system of decommissioning waste is managed based on the waste packages as a basic unit in the system. Waste container may contain one or more packages that can be tracked science the waste package record generated main packages and waste containers are managed separately. Waste package data are merged in the containers to provide general information for waste management such as the ID, location, reference data, mass, volume, surface contamination level, dose rate and radioactivity. The package information contain data that are uniquely associated with an individual waste package. The contaminant information tables identify the radioactive and non-radioactive contaminants in a package, which are used to determine waste classification.

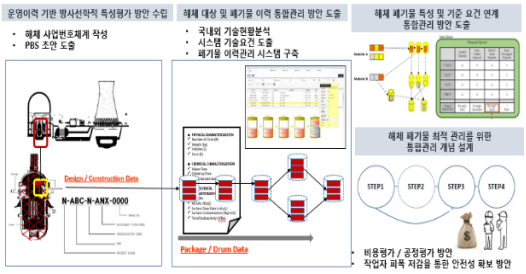

Fig. 1. Conceptual design of integrated management system for decommissioning waste.

2.2 Application of the developed system for decommissioning waste

The developed waste information tracking system was applied from the generated data of decommissioning project of KRR-1&2. Waste package and container data of decommission metal waste used for verification of the system. The waste generated data will be changed depending on the waste treatment process. The system was designed a various waste treatment such as sorting, decontamination, compaction and melting process for metal waste. Fig. 2 show the waste package and container information with waste treatment process.

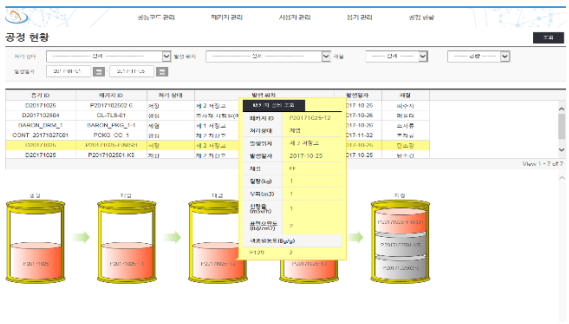

Fig. 2. Integrated information tracking system for waste treatment process.

The waste information tracing system will be expended to develop the optimized waste treatment scenarios selection using expert algorithm by comparing various factors such as a primary and secondary waste volume, treatment cost and disposal cost etc.

3. Conclusion

The waste characterization system for the life-cycle of decommissioning nuclear facilities is designed for the integrated management and evaluation of the radiological characteristics of the various types of waste generated during decommissioning process. The developed waste information tracking system for characterization of decommissioning waste from nuclear facilities will be applied and verified to prepare for the decommissioning nuclear power plant. We expected that the results can be improved the technology competitiveness and contributed to safety and optimized waste management in conducting decommissioning project.

REFERENCES

[1] IAEA, “Innovative and Adaptive Technologies in Decommissioning of Nuclear Facilities, IAEA-TECDOC-1602 (2008).

[2] IAEA, “Waste Inventory record keeping system (WIRKS) for the management and disposal of radioactive waste, IAEA-TECDOC-1222 (2001).

Review for Remediation Technology of Radiocesium-Contaminated Soil

In-Ho Yoon*, Ilgook Kim, Chan-Woo Park, Hee-Man Yang, Sung-Man Kim, and Kune-Woo Lee
Decontamination and Decommissioning Research Division, Korea Atomic Energy Research Institute (KAERI)
1045 Daedeokdaero, Yuseong-gu, Daejeon, Republic of Korea
*ihyoon@kaeri.re.kr

1. Introduction

Serious environmental contamination with radionuclides resulted from the Fukushima Daiichi nuclear accident in Japan, and a very large amount of soil (~28 million m^3) in a wide area became contaminated [1]. In addition to this critical accident, unintended leakages of radioactive substances from various nuclear facilities have also contaminated the environment, and most of the radio-contaminated soils are subject to low-level wastes [2]. Remediation of radio-contaminated soil has been attempted with various techniques, such as soil washing, phytoremediation, thermal treatment and electroremediation. Although considerable progress has been made in the development of soil remediation techniques for some radionuclides such as U and Co, the removal of radioactive cesium from soil has been relatively inefficient or has required high energy consumption owing to the strong and irreversible interaction of cesium with 2:1 clay minerals in the soil [3].

Therefore, this study was investigate the remediation technologies applicable to soils contaminated with radioactive cesium. Various soil remediation techniques were classified into soil washing, phytoremediation, thermal treatment and electroremediation. These principles and processing of various techniques were analyzed.

2. Remediation technology of radiocesium-contaminated soil

2.1 Soil washing

Soil washing is one of the most common industrial treatments for non-radioactively contaminated soils, and the soil washing process was also demonstrated for treatment of U, Ra, Th, Sr, and Cs contaminated soils. Soil washing generally uses the wet particle size separation because radionuclides have greatest affinity for particles having the highest surface area/volume ratios, such as silts and clays. During the wet separation with washing, the scrubbing action generally removes surface contaminations from the large soil particles such as sand and gravel. The fine soil particles can be separated further in a sedimentation tank, sometimes with the help of a flocculating agent. The output streams of the soil washing process include clean granular soil particles, contaminated fine soil particles, and washing solutions.

Effectiveness of soil washing process is affected by properties of contaminants and soil components. Soil washing is effective only if radionuclides can readily be desorbed from large soil fractions, and contaminated soils optimally contain less than 25% of silt and clays. To improve the removal efficiency of contaminants from soils, surfactants, acids, or solvents can be added to the washing solutions.

At a site in Texas, soil washing combined with ion exchange reduced uranium concentrations in soil from an average of 70 ppm to 20.7 ppm [4]. At the pilot plant demonstration at the Monclair/West Orange Radium Superfund site in New Jersey (USA), 323,000 cubic yards ($246,942 m^3) of soil contaminated with Ra-226, U-235, U-238, and Th-230 were treated over a period of 23 months. Contaminated soil volumes were reduced by 54% and contamination levels were reduced to 5 pCi/g. Soil washing treatment at sites in New Jersey and Tennessee reduced the mass of contaminated soils by 64 and 70% respectively. The process reduced Th-232 concentrations from 18.1 pCi/g to <5 pCi/g at the New Jersey site, and reduced Cs-137 levels from 160 pCi/g to <50 pCi/g at the Tennessee site [5].

2.2 Electrokinetic remediation

Electrokinetic (EK) remediation is an electro-chemical extraction process that can be separate and extract radionuclides from saturated or unsaturated soils. It is performed by applying a low voltage direct current across electrode pairs on each side of the contaminated soil mass. This current mobilizes ions and charged compounds to move towards the electrodes. The dissolved ionic species including radionuclides move toward the opposite-charged

electrode at a rate which depends on the local potential gradient (this transport mechanism is called electromigration). Also, the extraction of metals from soil is enhanced by an acidic condition that develops around the anode and by movement of the pore fluid in response to the electric potential difference which is called electroosmosis.

The primary advantage of the EK technique is that in-situ remediation can be accomplished without soil excavation. This in situ process inherently reduces the secondary waste generation, the transport process, and the cost associated with soil excavation, transport, and disposal. The effectiveness, however, is reduced in moisture contents less than 10 percent and where there is interference to electrical conductivity [6,7].

2.3 Thermal desorption

Heat treatment technology is a technique to increase cesium desorption by exposure contaminated soil to high temperature and inducing vaporization or interlayer expansion through pyrolysis. In addition, it has an increasing efficiency by high activity of desorbent, and expansion of interlayer between contaminated soils due to high temperature. However, the heat treatment technique is effective for purifying cesium contaminated soil, but it requires a large amount of energy compared to other treatment techniques and has a high treatment cost. Therefore, heat treatment can be used to maximize the effect of using it with other treatments than with arbitrary treatments.

2.4 Phytoremediation

Phytoremediation is a process that uses plants to remove contaminants in soil. The mechanisms of phytoremediation applicable to solid media include phytoextraction, phytodegradation, and phytostabilization. Because radionuclides including cesium cannot be biodegraded, the main mechanism applicable to remediation of radionuclides is phytoextraction.

Phytoextraction is the uptake of contaminants by plant roots and the accumulation of contaminants into plant shoots and leaves. The plants are subsequently harvested from the growing area, dried, and disposed. Phytoextraction was pilot-tested at Brookhaven National Laboratory to remove low levels of cesium and strontium from soil. Phytoextraction has also been tested in the remediation of cesium-contaminated soil at Argonne National Laboratory West in Idaho [8].

3. Conclusions

Soil contamination by cesium is a worldwide problem, therefore effective remediation approaches are necessary. A number of remediation techniques are used for effective remediation of cesium contaminated sites. In this review, we compared the principles and processing of various remediation techniques generally used to clean-up contaminated soils. However, there are some considerations for soil remediation. Considering the recent contamination of radioactive substances in wide area soil like the Fukushima accident, we must be able to process large amounts of contaminated soil quickly. Also, it must be able to perform the decontamination work in wide area. In this respect, it is necessary to apply a cleaning solution that can reduce secondary waste by the soil washing, and to develop a high performance adsorbent and to reduce the generation of secondary waste.

ACKNOWLGEMENT

This work was supported by a National Research Foundation of Korea grant funded by the Korean government (MSIP) (No. 2017M2A8A1092471).

REFERENCES

[1] Yamamoto, T. J. Nucl. Sci. Technol., 49, 1116-1133, 2012.
[2] Zhu, Y., Shaw, G. Chemosphere, 41, 121-128, 2000.
[3] Park, C.W. Kim, B.H. Yang, H.M. Seo, B.K, Lee, K.W. J. Hazar. Mater. 327, pp 127-134. 2017
[4] Technology reference guide for radioactively contaminated media, EPA, 2007
[5] Remediation of sites with dispersed radioactive contamination, IAEA, 2004
[6] Federal Remediation Technologies Roundtable. Remediation Technologies Screening Matrix and Reference Guide, Version 4.0: Electrokinetic Separation, 2002.
[7] Jung, H.B., Yang, J.S., Um, W. J Radioanal Nucl Chem, 304, 615-625, 2015.
[8] Lee, S. “Phytoremediation Application of Radionuclide Removal at Argonne National Laboratory West.” Summary of the Phytoremediation State of the Science Conference, Boston, Massachusetts, May 1-2, 2000, November 2001. EPA/625/R-0/011a.

Ferrous Oxalate Precipitation Behavior Depending on Ferrous Concentration and Temperature for Reductive Chemical Decontamination of Nuclear Power Plant

Sae-Binna Lee*, Hyun-Kyu Lee, June-Hyun Kim, Jin-Hee Kim, Yoon-Ji Park, Won-Zin Oh, and Sang-June Choi
Kyungpook National University, 80, Daehakro, Bukgu, Daegu, Republic of Korea
*dltoqlcsk@knu.ac.kr

1. Introduction

Chemical decontamination is the way to dissolve the magnetite of the radioactive corrosion oxide film inside of nuclear plant with ferrous ion using oxalic acid. The main chemical reactions are as follows.

$$Fe_3O_4 + 8H^+ \rightarrow 2Fe^{3+} + Fe^{2+} + 4H_2O \quad (1)$$

$$Fe_3O_4 + H_2C_2O_4 + 6H \rightarrow 3Fe^{2+} + 2CO_2 + 4H_2O \quad (2)$$

However, Fe ions increase above the certain concentration range, precipitation reaction is occurred by oxalic acid as follows.

$$Fe^{2+} + C_2O_4^{2-} \rightarrow FeC_2O_4 \quad (3)$$

These precipitations hinder in removing Fe ions and effective decontaminating by forming foreign substances in inner wall of treatment process. Therefore, this study was researched the behavior of precipitation reaction of ferrous ions and oxalic acid by varying ferrous ion concentrations, reaction time and temperature conditions.

2. Experimental details

Materials of this experiment were used $FeCl_2$ and oxalic acid dehydrate (DAEJUNG, Korea). All experiments were used in 500 mL volume.

To determine the effect of ferrous ion concentration on Fe-oxalate precipitate formation, experiments were performed in the 1, 2, 4 and 8 mM ferrous ions at 95 ℃.

Effect of temperature on the formation of Fe-oxalate precipitate was evaluated at 40 and 60 ℃ with initial concentration of oxalic acid of 8 mM. The times of sample extraction were the same as other experiment.

3. Results and discussion

At Fig. 1, we can see that precipitation behavior was observed at over 1 mM. And it needs almost 1 hour for precipitation reaction to occur. The slopes at 25 ℃ became gentle between 40 and 60 min. After 60 min, the precipitate amount seems to be constant.

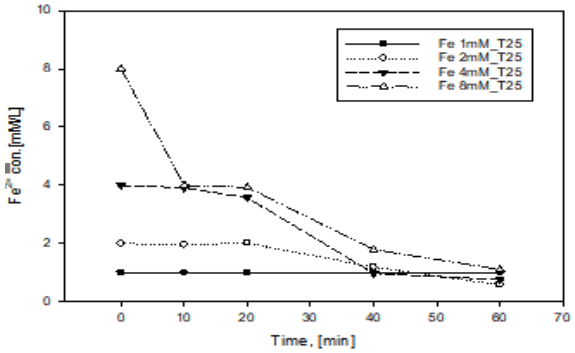

Fig. 1. Ferrous oxalate precipitation behavior depending on $FeCl_2$ concentration [mM] at 25 ℃.

At Fig. 2, precipitate behavior was not observed at 1 and 2 mM.. After 90 min, ferrous ions are constant at 4 and 8 mM. It means that precipitation reaction seems to have been completed between 40 and 60 min.

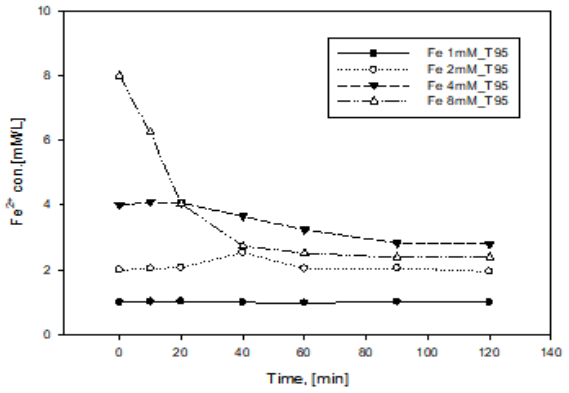

Fig. 2. Ferrous oxalate precipitation behavior depending on $FeCl_2$ concentration [mM] at 95 ℃.

In other words, precipitation reaction is dependent on temperature. Therefore, the optimal conditions of the decontamination seem to high temperature and low concentration.

4. Conclusion

The following conclusions were obtained regarding the ferrous oxalate precipitation behavior depending on the ferrous concentration and temperature which is necessary to control the excess ferrous concentration by a cation ion exchange during the reductive chemical decontamination:

1. During the reductive chemical decontamination around the temperature of 95 ℃, the ferrous ion concentration should be maintained below 2 mM to prevent from precipitation, while during decomposition of the oxalate at the room temperature, the ferrous oxalate precipitation is taken place above 1 mM.

2. The rate of ferrous oxalate precipitation is relatively slow and it takes time about 40 minutes, so that it should be taken into consideration to control the ferrous concentration during the reductive chemical decontamination.

5. Acknowledgement

This work was supported by the Korea Institute of Energy Technology Evaluation and Planning (KETEP) and the Ministry of Trade, Industry & Energy (MOTIE) of the Republic of Korea (No.20141510300310).

REFERENCES

[1] R.A. Speranzini., “Decontamination effectiveness of mixtures of citric acid, oxalic acid and EDTA”, Atomic Energy of Canada Ltd, 1990, Canada.

[2] T.Swan et al., Decontamination systems of BWRs and PWRs based on LOMI reagents, Proc.ANS-CNA Conf. on decontamination of nuclear facilities, Niagara Falls, Canada, 3-21 (1982).

Flow-Through Electrochemical Membrane System for the Selective Removal of Cobalt Ions

Joosung Park[1], Youngkun Chung[1], Keun-Young Lee[2], and Seoktae Kang[1,*]

[1]Department Civil and Environmental Engineering, Korea Advanced Institute of Science and Technology, 291, Daehak-ro, Yuseong-gu, Daejeon, Republic of Korea

[2]Decommissioning Technology Research Division, Korea Atomic Energy Research Institute, Daedeok-daero989ben-gil 111, Yuseong-gu, Daejeon, Republic of Korea

*stkang@kaist.ac.kr

1. Introduction

Recently, decommissioning of nuclear power plant becomes a hot issue for nuclear power phase-out. The main radioactive isotopes in radioactive concrete wastewater is Co-60, because of its relatively long half-life and strong γ radiation. For the selective electro-adsorption of cobalt ions in concentrated calcium ions, we synthesized multi-wall carbon nanotube based, water permeable hollow fiber membrane (MWCNT-HM), and investigated as cathodic electrode.

2. Materials and methods

2.1 Materials

For the fabrication of MWCNT-HM, multi-walled carbon nanotube (MWCNT), PVB (Polyvinyl butyral, Butvar® B-74), and NMP (N-methyl-2-pyrrolidone) were purchased from Cheap Tubes, Sigma-Aldrich, and Junsei chemical Co. Ltd., respectively.

2.2 Fabrication of hollow-fiber electrodes

Wet-spinning technique was used for the fabrication of MWCNT-HM. Spinning solution prepared by mixing MWCNT, NMP and PVB homogeneously by magnetic stirring. The wet-spinning solution extruded through hollow-fiber spinning apparatus with deionized water as bore fluid. Obtained hollow-fiber electrodes dried at room temperature and then calcined at 350 ℃ for 1 hour under Ar environment to remove PVB.

2.3 Electro-adsorption of cobalt ions

The electrochemical removal of Co^{2+} by MWCNT-HM carried out by 3-electrode electrochemical cell with potentiostat (WonA-tech ZIVE SP1) at room temperature. MWCNT-HM, graphite rod, and saturated calomel electrode (SCE) were used as working, counter, and reference electrodes with -1.0 V vs. SCE of electric potential applied to MWCNT-HM. To simulate the acidic concrete leachate, 500 mM of $CaCl_2$ at pH 1.0 were used with 0 ~ 0.5 mM $CoCl_2$ concentration.

3. Result and discussion

3.1 Microstructure of MWCNT-HM

MWCNT-HM possessed a porous, hollow-fiber structure by interconnection of MWCNTs (Fig. 1). MWCNT-HM has 77.8 m^2/g of specific surface area, and 13.9 nm of BJH pore size, which is effective for water flow through the MWCNT-HM and electrochemical Co^{2+} removal.

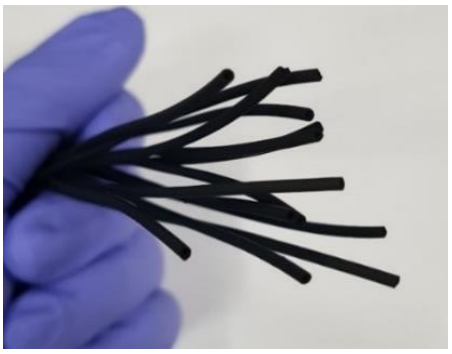

Fig. 1. Fabricated MWCNT-HM.

3.2 Selective electro-adsorption of Co^{2+}

After electrochemical reduction process, specific nanostructure appeared on the surface of MWCNT-HM. From EDS analysis, it was found that the nanostructure mainly composed with Co with minimal amount of Ca (22.7:1 mol/mol) on MWCNT-HM (Fig. 2).

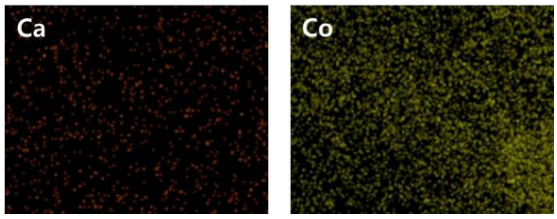

Fig. 2. EDS analysis result for appeared nanostructure on MWCNT-HM.

3.3 Co^{2+} sorption capacity of MWCNT-HM

Under electrochemical removal process of Co^{2+}, simulated acidic leachate was flown through MWCNT-HM with 80 L/m^2·h of flux. The average removal efficiency Co^{2+} was 74.5 % with 57.9 mg/g of removal capacity at pH 1. (Table 1)

Table 1. Co^{2+} removal properties of CHF

	Value
Leachate Co^{2+} concentration	12.0 mg/L
Co^{2+} concentration after reaction	3.1 mg/L
Leachate volume	55 mL
Mass of CHF	10.1 mg
Removal capacity	57.9 mg/g

4. Conclusion

In summary, MWCNT hollow-fiber membrane electrodes showed the selective removal of Co^{2+} via Ca^{2+} ion under strong acidic condition.

REFERENCES

[1] Wei, G., Chen, S., Fan, X., Quan, X., and Yu, H. "Carbon nanotube hollow fiber membranes: High-throughput fabrication, structural control and electrochemically improved selectivity", Journal of Membrane Science, 493, 97-105 (2015).

[2] K. Rekab et al., "Degradation of a cobalt(II)–EDTA complex by photocatalysis and H_2O_2/UV-C. Application to nuclear wastes containing $_{60}Co$", Journal of Radioanalytical and Nuclear Chemistry, DOI 10.1007/s10967 -014-3311-y.

Evaluation of Material Integrity by AP-OX Oxidation-Reduction Process Environments

Kyunghee Lee, Hyukchul Kwon, and Dooho Lee
Korea Hydro&Nuclear Power Co., LTD, 70, 1312-gil, Yuseong-daero, Yuseong-gu, Daejeon, Republic of Korea
*kyunghee.lee@khnp.co.kr

1. Introduction

Nuclear Utilities widely apply chemical decontamination process to remove deposited radioactivity and thereby lower exposure of plant personnel to ionizing radiation. In particular, operational decontamination is important not only to achieve the desired decontamination factor, but also to ensure the integrity of structural materials for future operation[1].

This experiment was conducted to evaluate the material integrity by AP-OX(Alkaline permanganate-Oxalic acid) oxidation-reduction process for the purpose of applying operational decontamination.

2. Experimental Methods

2.1 Experimental Apparatus

In this experiment, 'Steam Generator Chemical Cleaning Demonstration Equipment (Fig. 1)' created by KHNP-CRI was used.

Fig. 1. Experimental Apparatus.

2.2 Test Specimens

The main piping material of primary system is stainless steel cladding over carbon steel. The actual piping surface of the system will be covered with metal oxides. However, in this experiment, specimens were tested with bare metal for evaluation in the most aggressive environment.

The test specimens were as follows:

- Stainless steel : SS 304
- Carbon steel : SA 508, SA 516

Table 1. Chemical composition of specimens (from Material Certificate)

Materials	C	Mn	Ni	Cr	Mo	Si
SS 304	0.05	1.74	8.03	18.4	0.37	-
SA 508	0.19	1.35	0.83	0.13	0.49	0.2
SA 516	0.21	1.04	0.07	0.06	0.02	0.19

2.3 Experimental Conditions

In this experiment, the AP-OX process was applied for 1 cycle as shown below.

2.3.1 Oxidation step (AP process).

- Conc. : 1,000 ppm $KMnO_4$ + 100 ppm NaOH
- Temp. : 95±2℃
- Holding Time : 6 hours

2.3.2 Reduction step (OX process).

- Conc. : 2,000 ppm Oxalic acid
- Temp. : 95±2℃
- Holding Time : 4 hours

2.4 Evaluation Methods

2.4.1 Surface Analysis. Before and after the

experiment, the surfaces of the specimens were observed using Videoscope and SEM.

2.4.2 Calculation of Corrosion Rate. The weights of the specimens were measured before and after the experiment. Then, each corrosion rate was calculated according to the following equation.

$$C.R = \frac{1{,}550 \times W}{D \times A \times T} \quad (1)$$

C.R : corrosion rate(μm/hr), W: mass loss(g),
D : specimen density(g/cm^3), A : surface area(in^2),
T : exposure time(hr)

3. Results and Discussion

3.1 Surface Analysis

In the case of the stainless steel(SS 304) specimens, no corrosion pattern was found. The carbon steel(SA 508, SA 516) specimens were uniformly eroded.

Table 2. Surfaces of specimens before and after experiment

SS 304		SA 508		SA 516	
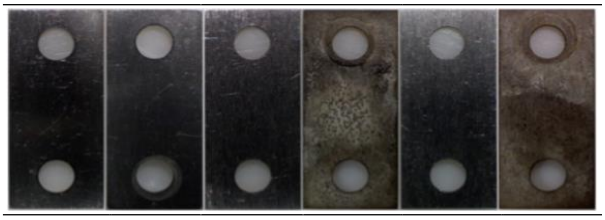					
before	after	before	after	before	after

3.2 Corrosion Rate

The corrosion rates calculated according to the above equation was as follows.

Table 3. Corrosion rate

Materials	SS 304	SA 508	SA 516
C.R (μm/hr)	< 0.01	0.27	0.27

3.3 Others

During the experiment, dark brown precipitate was formed in large quantities immediately after the injection of oxalic acid. The precipitate was excessively injected and the residual permanganate reacted with oxalic acid to form manganese dioxide($MnO_{2(s)}$). It was deposited on the bottom of the reactor and adhered to the specimen surface(Fig. 2, left). Further observation using SEM, it is considered that the precipitate did not cause local corrosion(Fig. 2, right).

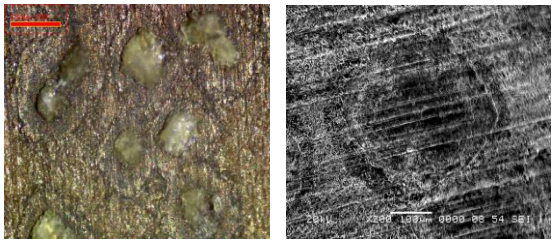

Fig. 2. Carbon Steel Surface.
(Videoscope, x300(left) / SEM, x200(right)).

4. Conclusion

As a result of the corrosion test of AP-OX chemical decontamination process, stainless steel(SS 304) specimens showed almost no corrosion and carbon steel(SA 508, SA 516) specimens showed uniform general corrosion.

The piping material in contact with primary system water is stainless steel. Therefore, if this decontamination process is applied, the impact on the material corrosion will be very low.

And when the process is actually applied, it is necessary to review the injection concentration of the oxidizing and reducing agents to minimize the generation of $MnO_{2(s)}$ precipitates.

REFERENCES

[1] EPRI, “Decontamination Handbook”, TR-112352 (1999).

Review on North Korea's Critical Nuclear Facilities Decommissioning From the Planning Point of View

Yong-soo Kim
Nuclear Engineering Department, Hanyang university, 222, Wangsimni-ro, Seongdong-gu, Seoul, Republic of Korea
yongskim@hanyang.ac.kr

1. Introduction

There have been some reports on the decommissioning of DPRK's nuclear facilities but, in most of cases, principally disabling part has been focused on. In this paper, decommissioning works following the disabling are reviewed from their characteristics to decommissioning cost. Even with limited access to the real information, practical factors are variably taken into consideration in the assessing the decommissioning works in addition to the available information.

2. DPRK's Critical Nuclear Facilities

Fig. 1. Yongbyon Nuclear Scientific Research Center [1].

In fact, although it has been reported that there are more than ten nuclear facilities all over the DPRK including small uranium enrichment facilities, most significant Plutonium-relevant facilities are located in Yongbyon area. Particularly two facilities, 5 MWe nuclear reactor and radiochemical laboratory, are the key facilities for the global CVID (Complete, Verifiable, and Irreversible Dismantlement) issue.

2.1 Characteristics of 5 MWe Nuclear Reactor

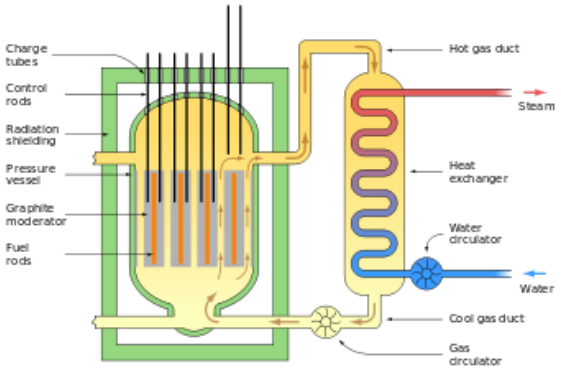

This reactor is a gas-cooled, graphite-moderated reactor (GCR) that uses MAGNOX fuel, which consists of natural-uranium alloyed with aluminum, clad in magnesium-aluminum alloy. In actuality, it is a smaller version of Britain's Calder Hall reactor so its characteristics are compared with those of Calder Hall reactor [2]. This shows that irradiation-power history is shorter and lower than that of Calder Hall reactor.

	Yongbyon	Calder Hall
MWth	25	225
avg Bu	635 MTU/T	2700 MTU/T
fast n flux	?	7.1×10^{12}
moderator	300 t	650 t
reflector	300 t	490 t
vessel(cm)	880ϕx1648x4	1125ϕx2182x5
bio-shield (side/top)	300 cm thick	243 cm thick
	450 cm thick	213 cm thick
th-shield inner dia.	7 cm thick	15.3 cm thick
	1100ϕ cm	1825ϕ cm

2.2 Characteristics of Radiochemical Laboratory

The radiochemical laboratory is the main reprocessing facility at Yongbyun complex. Main process building is 192 m long, 27 m wide and 6 stories high, consisting of six process cells (on 1st floor), three sampling cells (on 2nd floor), 30 mixer-settlers, and five glove boxes. It was reported that the construction of second process line was completed around in 1994 [3,4].

3. Influential Factors to Determine the Decommissioning Strategies

3.1 Review of Operational History

Even with experiencing some abnormalities, 5 MWe reactor started operation in 1986 and continued to operate for eight years until when the freeze began in 1994. Later DPRK restarted it in February 2003 and shutdown in February 2007 when Six Party Talks were agreed. Again they restarted it in 2013 and it is now claimed to operate at full power. Therefore, maximum operation period is 17 years, however, effective full power years must be less than the period, which is one of the critical factors affecting the radioactivity inventory in the constituting system materials [4,5].

DPRK is believed to operate the Radiochemical Laboratory for two main series of campaigns—the first from 1989 to 1991 and the second during the first six months of 2003. It is suspected that they may be operating the Lab to reprocess the discharged fuels from the 5 MWe reactor. They claim that the capacity of the Laboratory is 110 metric tons of uranium per line per year [4].

3.2 Radiological Characteristics

Based on the international experiences, most radio-activities in the 5 MWe reactor are expected to arise from the reactor vessel made of steel (95 ~ 98%) and principal radioisotope is Co^{60}. Total activity expected to be 1.82×10^{16} Bq so specific radioactivity is 2.68×10^{6} Bq/g [2]. In actuality, this value is one order magnitude lower than that of the typically decommissioned LWR pressure vessel. Next is the graphite moderator block whose radioactivity inventory consists of 2 ~ 5% of the total. It is expected to be 2.5×10^{14} Bq, equivalent to 2.2×10^{4} Bq/g at most. Major constituent radio-nuclides are H^{13} and C^{14}.

Decommissioning of reprocessing plant will result in generation of a large amount of steel and concrete waste. Most of them will be surface contaminated by mainly alpha radioactivity.

3.3 Decommissioning Strategies

Deferred dismantlement of the reactor may be favored because of cooling requirement of activated graphite moderator block, however, security concerns based on the CVID would make immediate decommissioning as quickly as possible after the disabling of the reactor more suitable. Site restoration needs to be greenfield. The disabling strategy can refer to the 'cocooning' of US Hanford reactor.

Unlike the 5 MWe reactor, suitable strategy for the decommissioning of Radiochemistry lab. would be an immediate dismantlement because there are no difficult technical barriers for the option.

3.4 Decommissioning Cost

Detailed engineering studies must be surely carried out to best-estimate the cost. Though not strongly correlated, however, a simple relationship between the costs and MWe may predict that the total decommissioning cost of the 5 MWe reactor may range 4 – 70 MUSD. Practically we understand that there are a few factors to significantly reduce the costs, including very low labor cost in North Korea [6].

Decommissioning cost of a reprocessing facility is determined by several factors such as the number of main process cells, complexity of the facility, etc. Compared to the cost of the Eurochemical facility with 40 main process cells, the cost could be estimated to be around or less than 50 MUSD.

In any case, if soil and underwater in their sites are seriously contaminated, time and cost for decommissioning would be significantly influenced by the restoration activities.

4. Conclusions

For the proper decommissioning planning of the Yongbyon facilities, we absolutely need thorough investigations. In this study, only brief review of the task is provided as a guidance for the following studies. This review shows that decommissioning works of the DPRK's nuclear facilities will be challenging but manageable, if prepared well since power-irradiation history is shorter and lower than other international GCRs which retired after lifetime-long operation.

REFERENCES

[1] 38 NORTH, March 5, 2018.
[2] KAERI/RR-3286/2011
[3] KAERI/RR-3091/2009
[4] SAND 2005-1981P (2005).
[5]http://cisac.fsi.stanford.edu/sites/default/files/khucisacfinalreport_compressed.pdf
[6] H. Zhang, Decomm. NK Nucl. Facilities: Approaches and Costs, Kennedy School, Harvard Univ.

6분과

방사선환경 및 안전 (Oral)

Fukushima Mapping Project After the Fukushima Dai-ichi Nuclear Power Station Accident

Satoshi Mikami*

Japan Atomic Energy Agency, 11601-13 Nishi-Jusanbugyou, Hitachinaka-shi Ibaraki, 311-1206, Japan

*mikami.satoshi@jaea.go.jp

1. Introduction

An enormous amount of radionuclides were released from the Fukushima Dai-ichi Nuclear Power Station (FDNPS) accident, and part of them were deposited on ground in Japan. In order to obtain basic data to evaluate the impact of the accidental release, a national project for comprehensive environmental monitoring was launched in June 2011 [1], and is still continuing. In the so-called Fukushima mapping project, a series of large-scale environmental monitoring with diverse methods have been conducted, aiming to obtain information on contamination conditions in different aspects.

Several radionuclides released from the accident were observed in soil over wide areas soon after the accident. However, it turned out from rough estimation that radiocesium was far more important than other observed radionuclides from a viewpoint of long-term exposure doses [2]. Then, the environmental monitoring in the mapping project was mainly focused on radiocesium. Actually, gamma-radiation emitting radionuclides other than radiocesium have not been detected since 2013.

This article presents the measurement methodologies for distribution mapping of air dose rates and radionuclides deposition density adopted in our mapping project, and also discuss the temporal change in air dose rate and radiocesium deposition density through repeatedly conducted measurements.

2. Monitoring Methods

2.1 Monitoring in undisturbed field

To obtain fundamental data on contamination conditions in standardized places, measurements on air dose rate and deposition density have been carried out in undisturbed flat fields where the basic topographical features were similar and disturbance by human activities or flooding was unlikely to happen.

Air dose rates were measured using standard surveymeters basically at approximately 6500 locations in 80-km zone from the FDNPS [3]. While, for determining deposition densities, soil samples were collected and analyzed at laboratories in 2011[2], In-situ measurement using portable germanium detectors have been adopted basically at approximately 380 locations within the 80 km zone since 2012 [4].

2.2 Monitoring along roads

Important technology for measuring the air dose rate was the second generation of the car-borne survey system, KURAMA-II developed at Kyoto University [5]. KURAMA-II is compact and easy to operate; anyone can run the system by connecting a plug to a power supply of a car. This feature enabled us to construct a detailed air dose rate distribution map in a short time in collaboration with staff of municipalities. Consequently, the total mileage of the roadway measured per a campaign was approximately 85,000 km at maximum. Further, by carrying a KURAMA-II on walker's back, the air dose rate in living environment along roads including small paths where vehicles are difficult to access can be measured.

3. Result and discussion

Fig. 1 shows distribution maps of the air dose rates at 1 m above the ground as of six different occasions over five years (2011 – 2016) that were created from the obtained dose rate data and positional data. The air dose rates drastically decreased in five years after the accident. Excessive dose-rate reduction than physical decay in undisturbed flat fields is observed. The air dose rates above roads have decreased much faster than those at undisturbed flat fields. Human activities such as decontamination, car driving, cultivation, cleaning, weeding, etc. were considered to accelerate dose rate reduction. In contrast, the average deposition density of radiocesium in non-decontaminated filed was observed to have decreased almost according to physical decay both for ^{134}Cs and ^{137}Cs [4].

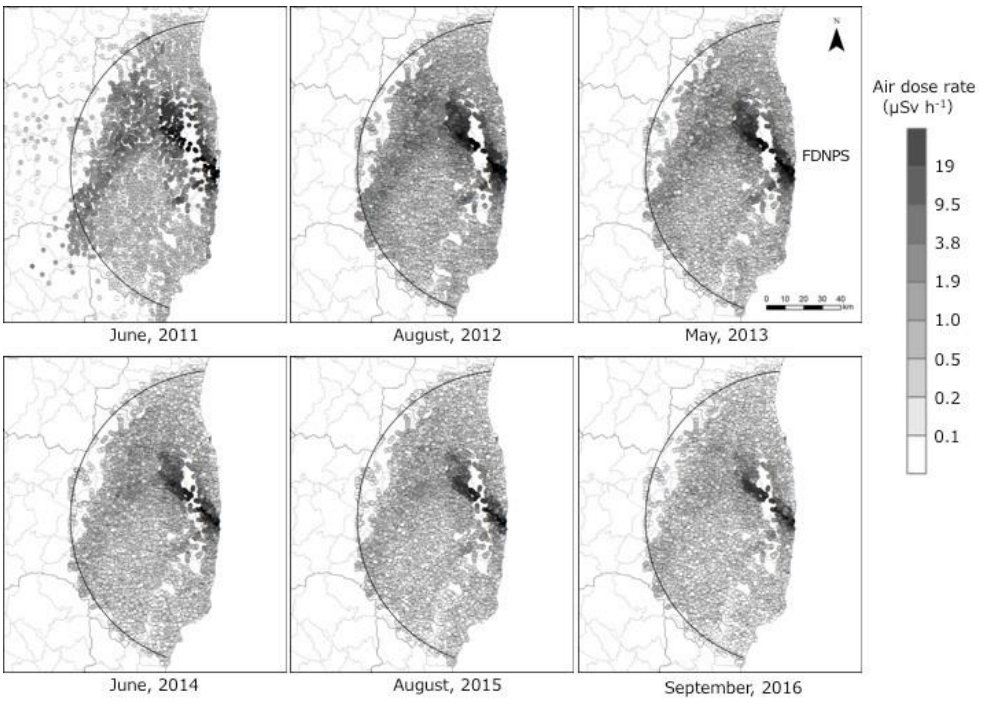

Fig. 1. Distribution maps of air dose rate around the Fukushima Dai-ichi Nuclear Power Station by handheld surveymeters.

4. Conclusion

The distribution maps on air dose rate and radiocesium deposition density were constructed on the measured data at different occasions. Then, the time-dependent deceasing tendency of air dose rate, and that of deposition density were shown on the basis of the monitoring results.

Acknowledgement

This report summarized the knowledge obtained in a series of commissioned studies called distribution- mapping project from the Nuclear Regulation Authority.

REFERENCES

[1] Saito, K., Onda, Y., Outline of the national mapping projects implemented after the Fukushima accident. J. Environ. Radioact. 139, 240-249. 2015.

[2] Saito, K., Tanihata, I., Fujiwara, M., Saito, T., Shimoura, S., Otsuka, T., Onda, Y., Hoshi, M., Ikeuchi, Y., Takahashi, F., Kinouchi, N., Saegusa, J., Seki, A., Takemiya, H., Shibata, T., 2015. Detailed deposition density maps constructed by large-scale soil sampling for gamma-ray emitting radioactive nuclides from the Fukushima Daiichi Nuclear Power Plant accident. J. Environ. Radioact. 139, 308-319.

[3] Mikami,S., Maeyama, T., Hoshide, Y., Sakamoto, R., Sato, S., Okuda, N., Sato, T., Takemiya, H., Saito, K., The air dose rate around the Fukushima Dai-ichi Nuclear Power Plant: its spatial characteristics and temporal changes until December 2012. J. Environ. Radioact. 139, 250-259. 2015.

[4] Mikami, S., Maeyama, T., Hoshide, Y., Sakamoto, R., Sato, S., Okuda, N., Demongeot, S., Gurriaran, R., Uwamino, Y., Kato, H., Fujiwara, M., Sato, T., Takemiya, H., Saito, K., Spatial distributions of radionuclides deposited onto ground soil around the Fukushima Dai-ichi Nuclear Power Plant and their temporal change until December 2012. J. Environ. Radioact. 139, 320-343. 2015.

[5] Tsuda, S., Yoshida, T., Tsutsumi, M., Saito, K., Characteristics and verification of a car-borne survey system for dose rates in air: KURAMA-II. J. Environ. Radioact. 139, 260-265. 2015.

Review on the Optimized Public Protective Action on NPP Having 30km UPZ Risk Based on the New Protective Action Guidance

Goanyup Lee*, Bongseok Kim, Hyunki Kim, Haecho Lee, Jongsoo Kim, Kanghyeon Lee, and Seungyeon Baek
Korea Atomic Energy Research Institute, 111, Daedeok-daero 989beon-gil, Yuseong-gu, Daejeon, Republic of Korea
*gylee@kaeri.re.kr

1. Introduction

The emergency planning zone (EPZ) is separated to precautionary action zone (PAZ) and urgent protective action planning zone (UPZ) in nuclear emergency preparedness act on 2014. The PAZ for nuclear power plant (NPP) is defined as 3 to 5 km radius, and the UPZ as 20 to 30km radius in the act. EPZ is normally considered as the zone for the evacuation of the residents in its area. PAZ is the precautionary evacuation zone before exposure by an accident and UPZ is the urgent evacuation zone according to the measurement at a field. But some people think all residents in EPZ should be evacuated. In this research, the optimized protective action was reviewed based on ICRP-103 recommendation and IAEA recent requirement.

2. Meaning of 30km UPZ

2.1 Meaning in IAEA Safety guide

PAZ and UPZ in the nuclear preparedness act is from IAEA safety guide for emergency preparedness [1]. The IAEA safety guide suggested PAZ as 3-5km and UPZ as 5-30km for the reactors greater than 1000MW(th). PAZ radius is the approximate distance for which the acute (2day) dose to bone marrow is 1Gy and the acute dose to lung is 6Gy, for preventing a deterministic health effects. UPZ radius is the approximate distances for which the total effective dose for inhalation, cloud shine and ground shine for 48hours will not exceed 1-10 times of the 50mSv for evacuation. This result is from the calculation in the condition of average meteorological condition, no rain, ground release. The maximum does during emergency (2days) of 30km UPZ reactor considered by IAEA can be simply described as under description.

1Gy(1Sv=1000mSv) at 5km of PAZ
500mSv(10 times of 50mSv) at 5km of UPZ
50mSv(1 times of 50mSv) at 30km of UPZ

2.2 Assumption of dose by distance

U.S. NRC considered under simple equation during 10mile EPZ determination for U.S. nuclear power plants [2].

$$D = D_0 \times (\frac{r}{r_0})^{-1.5} \quad (1)$$

Where, D_0 is the dose at the distance r_0, D is the dose at the distance r. From the above equation, if the plume centerline dose at 30km away from a nuclear power plant is 50mSv, and then the dose by distance can be calculated like under Fig. 1.

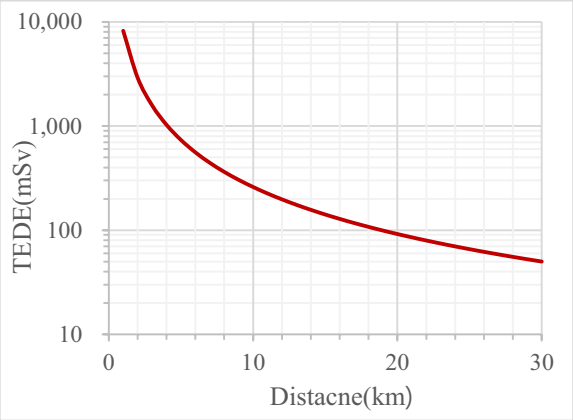

Fig. 1. Dose by distance of 30km UPZ NPP.

3. Protective Action Strategy

3.1 New protective action guidance

ICRP 103 recommends 20-100mSv residual dose as reference level during emergency exposure situation. IAEA general safety requirements part 3 selected 100mSv projected dose in the first7days for the protective action.

3.2 Review on the optimized protective action

U.S. EPA published protective action guides (PAG) for nuclear emergency. The PAG describes the exposure reduction factor from nuclear fallout like under Fig. 2.

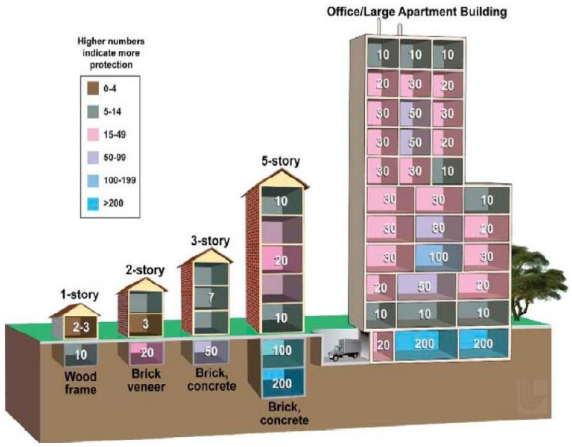

Fig. 2. Reduction factor from nuclear fallout.

If people stay in their home for 12hrs in a day and outside for 12hrs in a day and the reduction factor is 10, then the reduction ratio is 55%. It means normal life after accident, then the dose can be reduced like under table 1 from Fig. 1.

Table 1. Dose in normal life after accident

Distance(km)	TEDE(mSv)
2.734	1000
12.7	**100**
20.1	50
30	28

If no protection action implemented, then the public to 12.7km from nuclear power plant will receive more than 100mSv residual dose.

4. Results and Consideration

The public in 2.734km should be evacuated ungently to avoid deterministic health effects, the public in 12.7km should be evacuated in several hours to get the residual dose less than 100mSv. The protective action for the public outside the 12.7km can be considered with time and field measurement results.

REFERENCES

[1] IAEA, “Arrangements for Preparedness for a Nuclear or Radiological Emergency”, Safety Guide No. GS-G-2.1 (2007).

[2] U.S. NRC, “Planning Basis for the Development of State and Local Government Radiological Emergency Response Plans in support of Light Water Nuclear Power Plants”, NUREG-0396 (1978).

Radiological Risk Assessment of ^{232}Th and ^{238}U in Water Leach Purification (WLP) Residue Using Modified SPLP Method

Nur Shahidah Abdul Rashid[a,*], Zetty Izzaty Saleh[b], Nurul Syiffa Mahzan[b], Khoo Kok Siong[b], Wooyong Um[a], and Syazwani Mohd Fadzil[b]
[a]Division of Advanced Nuclear Engineering (DANE), Pohang University of Science and Technology (POSTECH), Republic of Korea.
[b]School of Applied Physics, Faculty of Science and Technology, Universiti Kebangsaan Malaysia (UKM), 43600 Bangi, Selangor, Malaysia.
*nurshahidah@postech.ac.kr

1. Introduction

Lynas Advanced Material Plant (LAMP) which is the largest rare earth processing plant in the world is located at Gebeng Industrial State (GIE) in Kuantan, Pahang, Malaysia. Lanthanide concentrate (LC) was processed by LAMP in order to extract rare earth elements. Using leaching and purification process, water leach purification (WLP) residue was yielded from the calcined and cracked concentrate of water soluble lanthanide components. The WLP residue contain radioactive elements such as thorium (^{232}Th) and uranium (^{238}U). The aim of this case study is to estimate potential level of ^{232}Th and ^{238}U in WLP residue to enter the human body using modified Synthetic Precipitation Procedure (SPLP) (Method 1312)[1]. In order to determine potential radiation doses hence taking measures to evade radiation exposure to consumers, it is vital to evaluate the radionuclides content of WLP residue. Additionally, knowledge of ^{232}Th and ^{238}U daily intake are crucial for evaluating metabolic parameters of radionuclides uptake and retention in human body.

2. Methods and results

WLP residue samples were collected from LAMP, Kuantan, Malaysia. The initial concentrations of ^{232}Th and ^{238}U in WLP residue are 206.1 mg kg^{-1} and 6.6 mg kg^{-1}, respectively by using X-Ray Fluorescence Spectrometer (XRF, Bruker/S8 Tiger/2009).

2.1 The modified SPLP method

To deduce the concentration of ^{232}Th and ^{238}U in leachate, SPLP method was implemented by modifying pH and reaction time parameters. About 10 g of WLP residue were reacted with 200 mL leaching fluid for about 20:1 solid-to-solution ratio under various pH conditions (4, 5, 7, and 8). All samples were prepared and tested for different reaction times (1, 2, 7, 14 days) at room temperature. The target radionuclides, ^{232}Th and ^{238}U in leachate were analysed using Inductively Coupled Plasma-Mass Spectrometry (ICP-MS).

2.2 The leaching results

Based on Fig. 1, on the 14th day of reaction, the reading for ^{232}Th and ^{238}U concentrations in leachate were at maximum, which were 8.23 mg kg^{-1} and 0.36 mg kg^{-1}, respectively. These results represent the maximum amount of radionuclides that are potentially available for intestinal absorption and diffusion into bloodstream. 1 to 14 days of contact intervals were applied to simulate average period of flooding in Malaysia. This approach depicted the correlation between leachates and contact time.

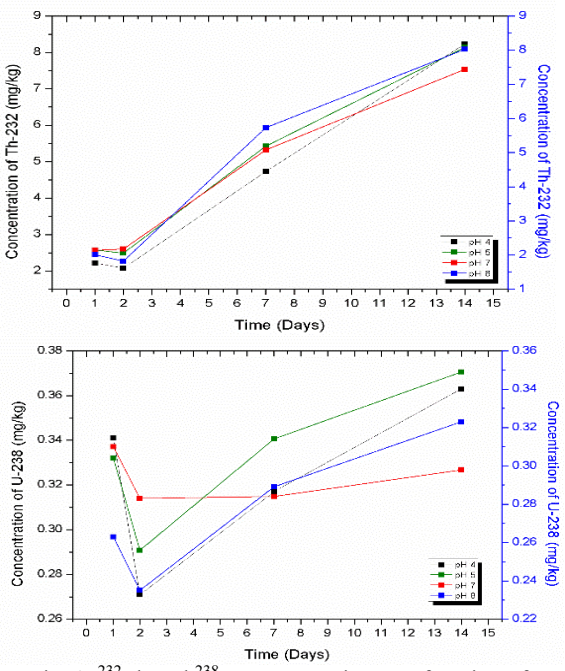

Fig. 1. ^{232}Th and ^{238}U concentration as a function of reaction time and pH by practicing SPLP method.

The leaching fluid pH was prepared for acidic rain and groundwater pHs to simulate the potential remobilization of ^{232}Th and ^{238}U after periods of heavy flooding in LAMP area. The maximum leached concentrations of ^{232}Th and ^{238}U were found at low pH (= 4), while the leached amounts of ^{238}U and ^{232}Th were at minimum which is pH 7 and 8 conditions. The effects of varying pHs prior to ^{232}Th and ^{238}U concentration were studied and the result showed that the rate of concentration value by leaching was very much influenced by pH

value used.

2.3 The committed equivalent and effective dose

To understand better the effects of modified SPLP method on human exposure, ^{232}Th and ^{238}U effective and equivalent dose coefficients were used to estimate committed effective and equivalent dose ingested by public adults and occupational workers [2]. The result for committed equivalent and effective dose of ^{232}Th and ^{238}U are presented in Table 1. The topmost committed equivalent doses of ^{232}Th and ^{238}U were found in red marrow and bone surface, respectively. ^{238}U committed effective dose for workers was higher than ^{232}Th. However, the committed effective dose of ^{232}Th and ^{238}U ingested by public were very low.

Table 1. Committed equivalent and effective dose of ^{232}Th and ^{238}U using modified SPLP method

		pH			
		4	**5**	**7**	**8**
Committed Equivalent dose (mSv)					
Bone surface	^{232}Th	2.340	2.300	2.110	2.280
	^{238}U	0.001	0.001	0.001	0.001
Kidney	^{232}Th	0.030	0.030	0.020	0.030
	^{238}U	0.001	0.001	0.001	0.001
Liver	^{232}Th	0.030	0.020	0.020	0.020
	^{238}U	0.001	0.001	0.001	0.001
Red marrow	^{232}Th	0.670	0.070	0.060	0.070
	^{238}U	0.001	0.001	0.001	0.001
Committed Effective dose (mSv)					
Public	^{232}Th	0.010	0.010	0.010	0.010
	^{238}U	0.001	0.001	0.001	0.001
Workers	^{232}Th	6.680	6.560	6.040	6.520
	^{238}U	8.960	8.620	7.660	7.980

To conduct this research, MONDAL 3 modelling was utilized to analyse the acute intake internal dose of occupational workers' whole body[3]. The data gained from MONDAL 3 are depicted in Figure 2, which shows ^{232}Th and ^{232}U internal dose via ingestion decrease with the reaction time. Indeed, the ingestion dose coefficients are the predominant factor.

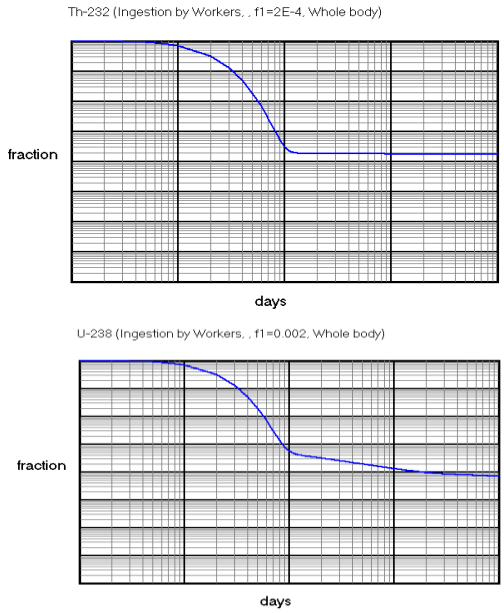

Fig. 2. Internal dose of ^{232}Th and ^{238}U of occupational workers using MONDAL 3.

3. Conclusions

^{232}Th and ^{238}U concentrations have been evaluated by using modified SPLP method. The maximum concentrations of ^{232}Th (8.23 mg kg^{-1}) and ^{238}U (0.363 mg kg^{-1}) in WLP residue were found at low pH (= 4), while the leached amounts of ^{238}U and ^{232}Th were minimum at pH 7 and 8 conditions. The committed equivalent and effective dose from WLP residue of ^{232}Th and ^{238}U by ingestion were affected by the dose coefficient of ^{232}Th and ^{238}U.

References

[1] Townsend, Timothy, Thabet Tolaymat, Helena Solo-Gabriele, Brajesh Dubey, Kristin Stook, and Lakmini Wadanambi. "Leaching of CCA-treated wood: implications for waste disposal." Journal of Hazardous Materials 114, no. 1-3: 75-91. 2004.

[2] IAEA, International Atomic Energy Agency. Methods For Assessing Occupational Radiation Doses Due to Intakes of Radionuclides. 2004.

[3] Ishigure N, Matsumoto M, Nakano T, Enomoto H. MONDAL 3: Support System for Internal Dosimetry. Chiba,Japan: National Institutes of Radiological Sciences. 2005.

Acknowledgement

The authors would like to thank The National University of Malaysia for financial support under the project code GGPM-2016-040. A portion of work was supported by the National Research Foundation of Korea (NRF) grant funded by the Korean government (MSIP: Ministry of Science, ICT and Future Planning) (No. NRF-2016R1D1A1B02013310)

Experience of Airborne Radiation Monitoring After the Fukushima Dai-ichi Nuclear Station Accident

Yukihisa Sanada*

Japan Atomic Energy Agency, 45-169, Sukakejo, Kaihama-aza, Haramachi-ku, Minami-soma, Fukushima, 975-0036, Japan

*sanada.yukihisa@jaea.go.jp

1. Introduction

In order to evaluate the influence of radionuclides emitted by the accident at the Fukushima Dai-ichi Nuclear Power Station (FDNPS) of the Tokyo Electric Power Company Holdings, Inc. caused by the Great East Japan Earthquake, various types of environmental radiation monitoring data have been obtained by many governmental institutes and universities. An airborne radiation monitoring technique is suitable to grasp the overall distribution of the ambient dose rate (referred to hereinafter as the air dose rate) and the deposition of radionuclides.

After the FDNPS accident, the radiation measurement using a manned helicopter (MRM: Manned helicopter Radiation Monitoring) national project was started [1]. Even though the MRM initially monitored only the area around the FDNPS, the surveyed areas were gradually expanded and eventually airborne radiation monitoring was used in eastern Japan, excluding Hokkaido, after October 2011 and in western Japan and Hokkaido, after May 2012 [3]. The distributions of the air dose rate at a height of 1 m above ground level (agl.) and of the contamination concentration of radioactive cesium (^{134}Cs and ^{137}Cs) on the ground surface were monitored for all areas in Japan via this MRM project. This monitoring project is ongoing with regularly repeating surveys conducted [3]. While conducting the MRM project, we developed and established an analysis method concurrently with the development of the monitoring method [3].

A radiation measurement technique that is more detailed than the method using a manned helicopter is required to form a decontamination plan and to evaluate the effect of decontamination. Radiation measurement using an unmanned helicopter (URM: Unmanned helicopter Radiation Monitoring) is one solution because an unmanned helicopter can make detailed air dose rate maps by flying below 150 m, in accordance with Japanese aviation law. The URM was developed for monitoring high air dose-rate areas [4]. This article presents the methods and results of the MRM and URM missions performed around the FDNPS.

2. Method and Results

2.1 Monitoring system

The dedicated MRM radiation detection system (RSX-3, Radiation solution Inc., Mississauga, Canada), which was installed on a manned helicopter. This system consists of six large NaI detectors (dimensions: 2” × 4” × 16”, total NaI crystal volume: 12.6 L), a data processing unit (RS501 and RS701), and a Global Positioning System (GPS) receiver.

Unmanned helicopters, R-MAX G1 (manufactured by YAMAHA Co., Ltd., Iwata, Japan), originally developed for spraying pesticides, were used for radiation measurements. An unmanned helicopter can conduct a programmed flight with the help of detailed self-localization using a Real-time Kinematic Global Positioning System (RTK-GPS), and we can set its flight waypoints and altitude. Three LaBr3:Ce scintillation detectors (dimensions, 1.5”φ × 1.5”H; total LaBr3:Ce crystal volume, 0.13 L) are used in the URM radiation monitoring system.

2.2 Analytical methods

This section describes the method used to analyze the measurement data. The detailed analysis methods of MRM and URM are described in our previous articles [4, 5]. In order to convert MRM and URM data at the flight altitude to the air dose rate at a height of 1 m agl., a straight topographically flat road with a relatively flat distribution of the air dose rate was set as the test line. A conversion factor (CD:μSv h−1

cps-1) is used to convert the count rate at the flight altitude in the air to the air dose rate at a height of 1 m agl. Furthermore, flights at various altitudes from 150 m to 1,000 m (URM: from 10 m to 150 m) were performed over the test line and the effective attenuation factor in the air (AF) was obtained from the relationship between the count rate and the flight altitude.

Mapping was performed by supplementing unmeasured areas via an interpolation of the measured results. The inverse distance weighted (IDW) method was applied to the MRM. The URM data were interpolated using Kriging because this dataset is smaller than that of MRM.

3. Result and discussion

Fig. 1 shows maps of the air dose rate at 1 m agl. that were constructed from the MRM measured data. Area of high air dose rate exceeding 10 μSv h-1 was oriented toward the northwest from the FDNPS to an area approximately 30 km of the FDNPS. The area of high air dose rate (more than 1 μSv h−1) is gradually decreasing. In a recent result (2016), the air dose rates of more than half the areas within a range from 3 km to 80 km from the FDNPS were less than 0.5 μSv h−1. Conversely, the air dose rate northwest of the FDNPS remains relatively high.

Fig. 1 shows maps of the air dose rate at 1 m agl. that were constructed from the URM measured data. Four deposition patterns in which the air dose rate is particularly high extend from the FDNPS. This indicates that there were four separate releases of adioactive material to the ground side during the FDNPS accident. As in the result of the MRM, the area of high air dose rate is gradually decreasing.

4. Conclusion

In order to investigate the influence of radioactive cesium, the distributions of the air dose rate were measured via MRM and URM. In Japan, no technical experience or example measurements were available for evaluating the air dose rate distribution via wide-spread MRM and URM prior to the FDNPS accident. Therefore, we developed and established an analysis method concurrently while carrying out actual monitoring.

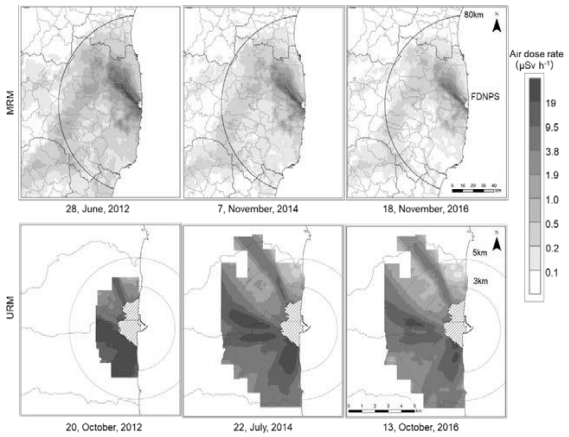

Fig. 1. Counter maps of dose rate around Fukushima Dai-ichi Nuclear Power Plant by airborne radiation monitoring.

This report summarized results that JAEA carried out as commissioned business by "the projects of the radiation monitoring using manned helicopter around the Fukushima Daiichi Nuclear Power Station" of the Nuclear Regulation Authority.

REFERENCES

[1] Lyons, C., Colton D., Aerial measuring system in Japan. Health Phys. 102, 509-515, (2012).

[2] Sanada, Y., Sugita, T., Nishizawa, Y., Kondo, A., Torii, T., The airborne radiation monitoring in Japan after the Fukushima Daiichi nuclear power plant accident. Prog. Nucl. Sci. Tech., 4, 76-80, (2014).

[3] Sanada, Y., Ishizaki, A., Nishizawa, Y., Urabe, Y., 2017, Airborne radiation monitoring using a manned helicopter. Bunseki Kagaku, 66, 149-162, (2017). in Japanese.

[4] Sanada, Y., Torii, T., Aerial radiation monitoring around the Fukushima Dai-ichi Nuclear Power Plant using an unmanned helicopter. J. Environ. Radioact, 139, 294-299, (2015).

Large-Area Compton Camera for Three-Dimensional Imaging of Radioactive Contamination in Concrete

Young-su Kim, Jae Hyeon Kim, Junyoung Lee, and Chan Hyeong Kim*

Department of Nuclear Engineering, Hanyang University, 222 Wangsimni-ro, Seongdong-gu, Seoul, Republic of Korea

chkim@hanyang.ac.kr

1. Introduction

A Compton camera provides distribution of gamma-ray sources by confining the location of the sources to conical surfaces based on Compton scattering kinematics. The camera is theoretically able to provide three-dimensional images using parallax information among the obtained conical surfaces. However, when the source-to-detector distance is farther than the extent of the component detector of the camera, the parallax among the conical surfaces becomes too small to obtain three-dimensional images. Thus, to utilize the parallax information, the extent of the component detectors should be sufficiently large.

In this point of view, a Large-Area Compton Camera (LACC) prototype has been developed in Hanyang University using large monolithic scintillation detectors [1]. In the present study, the developed LACC prototype was tested to demonstrate the three-dimensional imaging capability of radioactive contaminations inside concrete bricks or a wall.

2. Prototype setup

The developed LACC prototype had each plane with a 27×27 cm^2 monolithic NaI(Tl) scintillator (Scintitech, MA, USA) and a 6×6 array of 5×5 cm^2 square PMTs (XP3290; Photonis, France). The thicknesses of the scintillators for the first and second planes were 2 cm and 3 cm, respectively. The first and the second planes were separated by 25 cm. The raw pulses from each detector were collected by the dedicated signal processing circuits and data acquisition system developed in the previous study for a single detector [2].

3. Experimental results

Two measurements were performed with the LACC, to demonstrate the three-dimensional imaging capability. Fig. 1 shows the experimental setup of the two experiments.

Fig. 1. Experimental setup for the experiment using a stack of bricks (left) and a building wall (right).

In the first experiment, a 7.6 μCi ^{137}Cs point source was placed inside a stack of bricks (density: 1.9 g/cm^3). The ^{137}Cs source was located on the axis of the LACC at a distance of 0.3 m. The resulting Compton images were reconstructed by back-projection and maximum-likelihood expectation-maximization algorithm (MLEM). With a 300-second measurement, resulting Compton images were reconstructed as shown in Fig. 2. In the reconstructed images, the location of the sources was accurately localized within the error of voxel size (=0.01 m) of the image space.

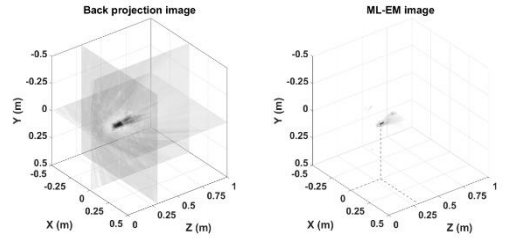

Fig. 2. Reconstructed Compton image by back-projection (left) and MLEM (right) for the ^{137}Cs at (0.0 m, 0.0 m, 0.3 m) inside the stack of bricks.

The second experiment was conducted with a concrete building wall which thickness is about 25 cm. The source-to-detector distance was set to be 30 cm. To demonstrate a multitracing capability of the LACC, a 7.6 μCi ^{137}Cs point source and a 3.0 μCi ^{60}Co point source were placed behind the wall simultaneously. The coordinates of the ^{137}Cs and ^{60}Co sources were (−0.1 m, 0.0 m, 0.3 m) and (0.1 m, 0.0 m, 0.3 m), respectively. The measurement time was 300 seconds. Fig. 3 presents the back-projection Compton images for each radioactive source. The resulting images show that the locations of the both sources were clearly localized at the true source positions. The images also show that there is no significant interference between the two sources.

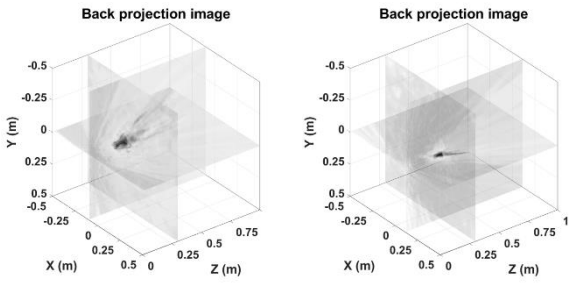

Fig. 3. Reconstructed Compton images for the ^{137}Cs (left) and ^{60}Co (right) behind the building wall.

4. Conclusion

In the present study, the three-dimensional imaging capability of the LACC prototype system was evaluated with various experiments. The results of this study served to demonstrate the great potential of the LACC for the application of the radioactive contamination monitoring, especially hot-spot in a radioactive waste drum or a concrete wall. In the near future, we will conduct various experiments for more realistic cases.

REFERENCES

[1] Y. Kim, et al., “Development and performance evaluation of large-area Compton camera,” Transactions of the Korean Nuclear Society Spring meeting, May 17-19, 2017, Jeju.

[2] Y. Kim, et al., “Position-Sensitive NaI(Tl) Detector Module for Large-Area Compton Camera,” Journal of the Korean Physical Society, 72(1), 26-32 (2018).

Experimental Setup for Accuracy Analysis of Multi-Detector Boron Meter

[a,*]Si Hyeong Sung, [b]Jin Bok Cho, and [a]Hee Reyoung Kim

[a] Department of Nuclear Engineering, Ulsan National Institute of Science and Technology, 50, UNIST-gil, Eonyang-eup, Ulju-gun, Ulsan, Republic of Korea

[b] Users Incorporated Company

[*]shlove912@unist.ac.kr

1. Introduction

PWR operated in Korea controls the combustion reaction by changing the concentration of boric acid water used as a coolant. Accurate measurement of boric acid concentration is necessary to prepare for boron dilution accidents. The boron meter, which is one of the methods for measuring the concentration of boric acid, has the advantage of being able to perform on-line measurement at all times, but shows a high error (2%) [1]. To improve the accuracy of the boron meter, a study was made on the boron meter using the selective detector. It prevents pulse pile-up and perturbation, and also enables stable counting rate measurement even at high boric acid concentration. MCNP simulation was performed to evaluate the accuracy of the multi-detector boron meter and showed a low error (0.4%) [2]. Based on the simulation conditions, the experiments were carried out in a limited environment and showed up to 65% higher accuracy than single detector boron meter detectors [3].

The accuracy of the multi - detector boron meter was confirmed through previous studies and the system was constructed for the experiment in the actual cooling water circulation environment.

2. Experimental Setup for Accuracy Analysis

2.1 Boron Meter

Fig. 1 shows the design of a multi-detector boron meter. The fast neutrons emitted from the neutron source inserted in the central column are decelerated to thermal neutrons due to the boric acid water circulating inside the boron meter and then counted by the detectors. The internal detector uses four LND 20292 BF_3 detectors (11.3 cps/nv) and two LND 2528 ^{3}He detectors (28 cps/nv).

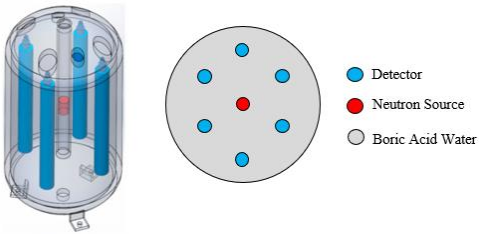

Fig. 1. Design of Boron Meter.

The neutron source inserted inside is Eckert & Ziegler N20 capsule, and the nuclide is Am-Be. To compare the accuracy with the single detector boron meter, the experiment is performed using the same activity (1 Ci). Fig. 2 shows the source information.

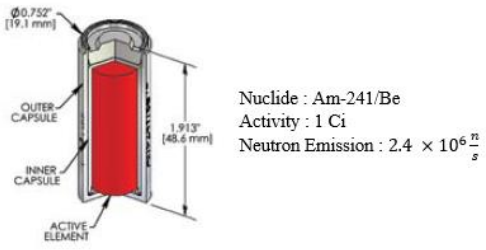

Fig. 2. Am-Be Neutron Source.

2.2 Boric Acid Water Circulation System

Fig. 3 shows the boron water circulation system including the boron meter.

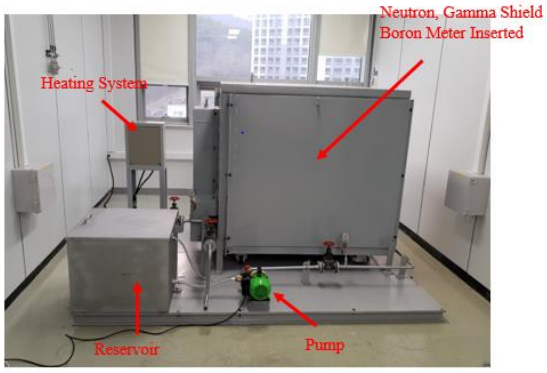

Fig. 3. Boric Acid Water Circulation System.

A shield was constructed to prevent gamma ray and neutron damage caused by the neutron source inserted into the boron meter. The whole circulation system is made of stainless steel and can be run in an environment of 200 psig (13.79 bar), which is the actual reactor coolant pipe environment. A heating system for the calibration of the boron meter accuracy according to coolant temperature was constructed. Experiment of change of count rate in environment of maximum 60 ℃ is carried out.

3. Conclusion

Accurate analysis of the multi-detector boron meter can be performed by installing a system designed based on the actual reactor coolant circulation. The development of a more accurate boron meter will enable real-time coolant concentration measurement, which will improve the stability of nuclear power plants.

ACKNOWLEDGMENTS

This work was supported by the Nuclear Power Core Technology Development Program of the Korea Institute of Energy Technology Evaluation and Planning (KETEP) granted financial resource from the Ministry of Trade, Industry & Energy (No. 20151520100930).

REFERENCES

[1] M. Zubair, R. Anmed, G. Heo, “Quantitative and qualitative analysis of safety parameters in nuclear power plants”, Int J Energy Res, 38, pp. 755-764 (2014).

[2] C. Kong, H. Lee, S.H. Kim, S. Lyou, D. Lee, “Accuracy Improvement of Boron Meter Adopting New Fitting Function and Multi-Detector, Nuclear Engineering and Technology, Volume 48, pp 1360-1367 (2016).

[3] S.H. Sung, H.R. Kim, “Experimental characterization of the accuracy of multidetector boron meter for operational safety of reactors, Int J Energy Res. 2018;1-9 (2018).

Proposed Regulatory Standards for the Industrial NORM Waste Management

Yeoungsuk Go*, Eun Lee, Jaeman Kim, and Suk K. Sim
Environment & Energy Technology, Inc., 213 R&D Building 2, 99, Gajeong-ro, Yuseong-gu, Deajeon, Republic of Korea
*ysgo@en2t.com

1. Introduction

NORM (Naturally Occurring Radioactive Material) can be artificially increased resulting in a higher radioactivity level during industrial manufacturing processes. Some domestic industries use Bauxite, Phosphate rock and TiO_2 as raw materials which include ^{238}U and ^{232}Th radioactive nuclide as well as their radioactive decay series, and they can be enhanced during manufacturing processes generating NORM wastes. Although radioactivity concentrations and radiation exposure levels for the workers or public are regulated by the "NORM Safety Management Law", currently there are no domestic regulations or guides for the safe management of the industrial NORM wastes.

Radiation characteristics are investigated for the industries using Bauxite, Phosphate rock and steel scraps to identify the industrial NORM wastes and their safety management practices to establish regulatory standards for the industrial NORM safety management.

2. Radiation Characteristics and Safety Management Practices of the Industrial NORM Wastes

In order to investigate the radioactivity and safety management of the NORM wastes, field detections were performed for the phosphate fertilizer, aluminum hydroxide manufacturing and the steel scrap industries. Tables 1 and 2 show the results of the field detections for the industrial NORM wastes.

Table 1. Radioactivity Concentration of the NORM Wastes

NORM Wastes	Nuclide	Concn. (Bq/g)	Remark
Pipe Scale A	^{238}U	0.857	Landfill
	^{232}Th	0.215	
Red Mud	^{238}U	0.182	open storage
	^{232}Th	0.318	
Phosphoric Gypsum	^{238}U	1.003	open storage
	^{232}Th	0.005	
Pipe scale B	^{238}U	0.269	separate storage
	^{232}Th	0.038	

Tables 1 and 2 also show that NORM wastes were found in the pipe scales of the manufacturing industries and large volumes of the NORM residues are generated such as red mud and phosphate gypsum.

Table 2. Radiation dose rate of the NORM wastes for the steel scrap industry

NORM Wastes	Nuclide	Dose (μSv/hr)	Remark
Pipe scale C	^{232}Th	4.0	separate storage
Pipe scale D	^{232}Th	5.4	separate storage
Pipe scale E	^{232}Th	13.7	separate storage
Pipe scale F	^{232}Th	5.5	separate storage

3. Proposed Regulatory Standards for the Industrial NORM Waste Management

IAEA and the EU have recognized the need for regulatory guides for the safety management of the NORM wastes and some EU countries regulate the NORM wastes in accordance with the EU

recommendations. In Korea, industrial NORM wastes are regulated by the "NORM Safety Management Law". Table 3 shows the NORM safety standards recommended by the IAEA and EU as well as the registration criteria of the NORM wastes in Korea. However, there are no specific regulatory guides regarding disposal and recycling of the industrial NORM wastes.

This study proposes regulatory standards for the NORM wastes to dilute below 1 Bq/g and 1 mSv/yr of the exclusion level, and may spread on the earth surface, landfill, or recycle. National NORM waste storage or landfill sites for the higher industrial NORM wastes should be considered.

Table 3. NORM safety standards

	Concentration (Bq/g)			Remark
	^{232}Th	^{238}U	^{40}K	
Korea	1	1	10	Exclusion level
IAEA	1	1	10	Exclusion level
EU	0.5	0.5	5	Clearance level
UK for landfill	5*		-	Exemption level

* Sum of ^{238}U and ^{232}Th concentrations

4. Conclusion

Regulatory standards have been proposed for the safe management, disposal and recycling of the industrial NORM wastes. Detailed safe management procedures should be further developed to implement proposed regulatory standards for the NORM wastes.

REFERENCES

[1] "Safety Standards Series No. RS-G-1.7, IAEA" (2004).

[2] "Industrial NORM Characterization", N-STAR-15NS11-01, Environment & Energy Technology, Inc. (2016).

[3] Y. Go et al., "Radioactivity Characteristics and Safety Management of Steel Scrap", ISSN 1738-1142 (2017).

6분과

방사선환경 및 안전 (Poster)

Domestic Data on the Radionuclide Transfer From Soils to Rice Plants

Yong-Ho Choi, Kwang-Muk Lim, In Jun, Dong-Kwon Keum, and Hyo-Joon Jeong
Korea Atomic Energy Research Institute, 111, Daedeok-daero 989beon-gil, Yuseong-gu, Daejeon, Republic of Korea
yhchoi1@kaeri.re.kr

1. Introduction

Radionuclides in the radioactive waste disposed into an underground repository can enter a biosphere through the movement of underground water if natural and artificial barriers are damaged by certain causes. Rice fields in Korea are usually located in low places and submerged for about half a year. Considerable amount of underground water is used for irrigating them. The above-mentioned conditions make the paddy soils comparatively vulnerable to an invasion of the radioactivity originated from such radioactive wastes. Accordingly, it is very important to have a reliable tool for evaluating the radionuclide transfer from paddy soils to rice plants. Soil-to-plant transfer of radionuclides is generally estimated using the transfer factor (TF), which is a model parameter defined as the concentration ratio between soil and plant. This study was conducted for the purpose of collating TF values for rice which have been measured over last more than 30 years by KAERI.

2. Materials and methods

Most of the TF data was produced by means of pot experiments in greenhouses. Soils were thoroughly mixed with radioactive solutions for the top about 15-20 cm layers sometime before transplanting. Field studies were also conducted for fallout ^{137}Cs in mid 1990s. Tables 1 and 2 show physicochemical properties of the soils

Table 1. Soil properties in greenhouse (GH) experiments

Soil code	Physicochemical properties						
	pH	OM (%)	CEC [a]	K [a] exch.	Ca [a] exch.	Clay (%)	Sand (%)
A	5.8	1.5	7.1	0.13	6.83	14.0	39.3
B	8.8	0.6	8.4	0.99	3.55	10.6	24.8
C	7.7	2.1	12.2	0.29	17.2	12.6	48.8
D	5.5	1.8	10.9	0.21	5.3	29.8	6.0
E	6.0	2.1	9.0	0.41	4.3	7.8	60.5
F	6.4	0.42	7.5	0.36	4.5	4.7	78.9
G	4.4	0.94	6.7	0.16	1.8	8.0	71.4
H	6.1	0.68	4.7	0.18	3.3	2.8	81.9
I	5.6	0.93	5.4	0.16	3.9	7.2	71.9
J	4.6	2.43	7.2	0.11	3.2	6.0	67.3
K	5.5	4.4	8.2	0.41	6.1	10.2	46.2
L	5.4	3.3	16.3	0.79	14.9	19.9	10.6
M	5.6	2.4	12.8	0.63	6.2	28.2	21.5
N	5.5	3.7	14.4	0.29	4.5	11.0	-
O	5.1	4.2	27.7	0.48	10.9	15.4	-
P	5.6	3.0	17.0	0.49	6.1	26.9	-
Q	5.1	4.9	43.5	0.94	20.5	25.2	-

OM: organic matter, CEC: cation exchange capacity
[a] unit: cmol kg^{-1}.

Table 2. Soil properties in field studies

Soil code	Physicochemical properties					
	pH	OM (%)	CEC [a]	Clay (%)	Silt (%)	Sand (%)
S1	5.5	3.74	11.4	14.0	27.4	58.6
S2	5.8	3.24	10.2	14.0	21.0	65.0
S3	5.5	1.69	12.8	17.0	30.1	52.9
S4	5.6	2.24	7.5	20.0	40.7	39.3
S5	5.7	6.55	14.6	14.0	38.1	47.9
S6	5.5	1.94	9.5	20.1	29.6	50.3
S7	4.9	3.12	7.3	17.5	22.3	60.2
S8	5.8	2.14	8.6	20.4	19.9	59.7
S9	4.3	2.07	14.7	25.9	51.1	23.0
S10	5.0	1.95	6.5	17.3	17.1	65.6
S11	5.6	2.52	9.1	16.4	40.1	43.5
S12	6.4	1.83	9.3	21.3	36.7	42.0

OM: organic matter, CEC: cation exchange capacity
[a] unit: cmol kg^{-1}.

Radioactivity analysis was made by means of gamma spectrometry or total-beta counting. TF values (dimensionless) were calculated as follows;

$$TF = \frac{C_{plant}}{C_{soil}} \quad (1)$$

where C_{plant} (Bq kg^{-1}-dry) is the radionuclide concentration in the plant part of interest and C_{soil} (Bq kg^{-1}-dry) is that in the soil.

3. Results and discussions

3.1 Radiocesium (^{137}Cs)

The results on the radiocesium transfer are summarized in Tables 3 and 4.

Table 3. Summary for the Cs TF data from GH experiments

Plant part	Statistics on TF values				
	N (soils) [a]	AM	GM	Min.	Max.
BR	13 (A~M)	4.9E-02	2.9E-02	8.1E-03	1.6E-01
BR	3 (K~M)	6.0E-02	3.0E-02	8.1E-03	1.5E-01
Chaff	3 (K~M)	1.8E-01	8.1E-02	2.1E-02	4.5E-01
Straw	3 (K~M)	9.9E-02	5.0E-02	1.6E-02	2.5E-01

BR:brown rice, AM:arithmetic mean, GM:geometric mean
[a] number of soils tested (See table 1.).

Table 4. Summary for the Cs TF data from field studies

Plant part	Statistics on TF values				
	N [a]	AM	GM	Min.	Max.
BR	12	5.7E-03	4.5E-03	1.2E-03	1.1E-02

3.2 Radiostrontium (^{85}Sr, ^{90}Sr)

Table 5 summarizes the TF data of radiostrontium from greenhouse experiments. Straw had the highest TF value, followed by chaff, then brown rice.

Table 5. Summary for the Sr TF data from GH experiments

Plant part	Statistics on TF values				
	N (soils) [a]	AM	GM	Min.	Max.
BR	4(F,K~M)	4.4E-02	3.0E-02	1.6E-02	1.2E-01
BR	3 (K~M)	1.9E-02	1.9E-02	1.6E-02	2.5E-02
Chaff	3 (K~M)	1.7E-01	1.5E-01	9.7E-02	2.8E-01
Straw	3 (K~M)	7.1E-01	6.6E-01	4.2E-01	1.1E+00

3.3 Technetium (^{99}Tc)

TF data for ^{99}Tc is summarized in Table 6, showing its very low mobility to seeds.

Table 6. Summary for the Tc TF data from GH experiments

Plant part	Statistics on TF values				
	N (soils) [a]	AM	GM	Min.	Max.
BR	4 (N~Q)	1.3E-03	1.1E-03	5.4E-04	2.5E-03
Straw	4 (N~Q)	8.8E-01	8.3E-01	5.3E-01	1.3E+00

3.4 Radioiodine (^{125}I)

TF data for ^{125}I is summarized in Table 7.

Table 7. Summary for the I TF data from GH experiments

Plant part	Statistics on TF values				
	N (soils) [a]	AM	GM	Min.	Max.
BR	3 (K~M)	3.6E-03	2.9E-03	1.1E-03	6.4E-03

3.5 Others (^{54}Mn, ^{60}Co, ^{65}Zn)

The other TF data is summarized in Table 8.

Table 8. Summary for the BR TFs of other radionuclides

Nuc-lide	Statistics on TF values				
	N (soils) [a]	AM	GM	Min.	Max.
^{54}Mn	5 (F~J)	2.9E-01	2.6E-01	1.2E-01	5.2E-01
^{60}Co	4 (F,G,I,J)	4.7E-03	4.3E-03	2.2E-03	6.0E-03
^{65}Zn	4 (G~J)	1.9E+00	1.7E+00	5.8E-01	2.7E+00

4. Conclusions

For a reliable estimation of the ingestion dose, it is important to use site-specific transfer data. Much additional rice TF data needs to be domestically produced for a sufficiently reliable estimation of the dose due to a repository.

5. Acknowledgements

This work was supported by the MSIT, Korea.

REFERENCES

[1] Y.H. Choi, et al., KAERI/TR-1993/2001.

[2] Y.H. Choi, et al., KAERI/TR-6132/2015.

Establishment of Alarm Management System for Radiation Emergency Response

[1,*]Hae Cho Lee, [1]G.Y. Lee, [1]J.S. Kim, [1]H.K. Kim, [1]B.S. Kim, [1]J.S. Kim, [1]G.H. Lee, [1]S.Y. Baek, [2]W.S. Heo, and [2]K.Y. Sohn

[1]Korea Atomic Energy Research Institute, Daedeok-daero989beon-gil 111,Yuseong-gu, Daejeon, Republic of Korea

[2]MIRAEEN Co., Ltd. 72, Techno Jungang-ro, Yuseong-gu, Daejeon, Republic of Korea

[*]hclee@kaeri.re.kr

1. Introduction

In the event of a radiation emergency, information sharing and rapid propagation of the radiation emergency should be done promptly in order to effectively perform emergency response in the early stage

From this point of view, this study describes an AMP (Alarm Manager Program) to disseminate the emergency situation early and call the designated emergency responders when the radiation level of the facility or environment rises to the emergency level

2. System Configuration

2.1 Hardware and Software Configuration

The hardware system consists of a computer server for collecting radiation data of facilities and environment, respectively, and a DBMS (Data Base Manager System) for managing data stored in real time as shown in Fig. 1. The facility and environmental data are stored in DBMS in real time. The AMP developed in this study compares real-time radiation data with radiation emergency settings as shown in Fig. 2. If the radiation data is exceeding than the set value, it is designed to automatically propagate the situation via SMS (Short Message Service) and call emergency personnel.

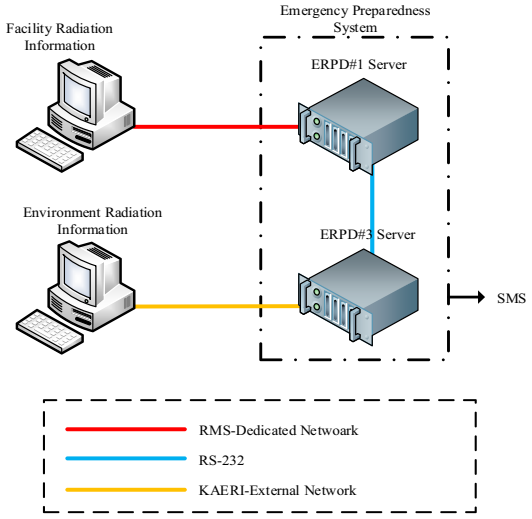

Fig. 1. Hardware Configuration.

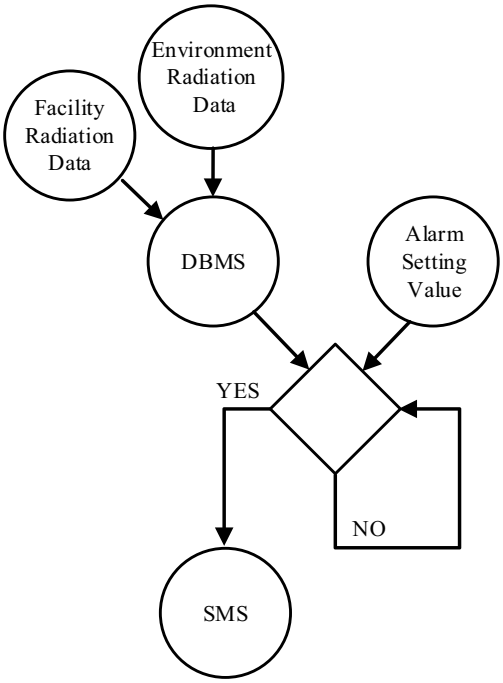

Fig. 2. Software Configuration.

2.2 Alarm Manager Program

AMP runs on MS Windows 7, and Visual Studio 2010 and MSSQL2014 software are used for development. Since the radiation data from facility has the IEEE 754 floating point structure of 1 signal bit, 8 exponent bits and 23 mantissa bits, it must be converted to a real number by applying a real number conversion function. The formula 1 shows a real-valued conversion equation. Where, s is signal bit, e and M are exponent bit and mantissa bit, respectively.

$$\text{Real Number} = (-1)^S \times (1.M) \times 2^{e-127} \quad (1)$$

The AMP can check the facility name, tag, set value and person in charge as shown in Fig 3. In addition, it has a function to periodically check the communication status of facility and environmental radiation data for the health scientist of the system and notify the maintenance person in case of trouble.

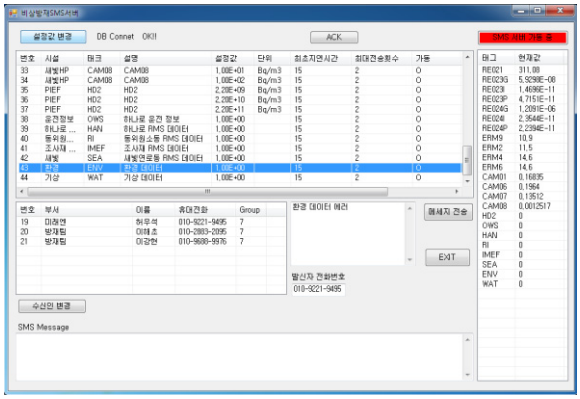

Fig. 3. Alarm Manager Program.

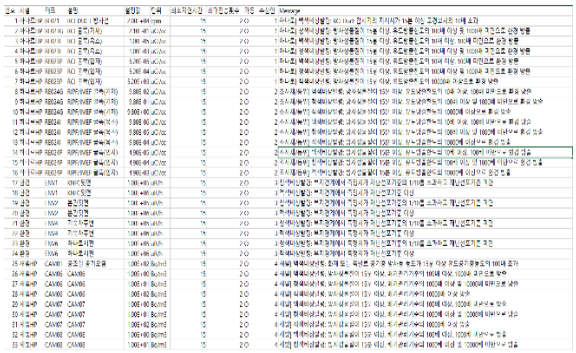

Fig. 4. Alarm Setting Value.

3. Conclusion

Radiation emergency response should be established to ensure that the protection of lives is swiftly handled. The construction of a system to realize such a purpose must be established to enable rapid emergency response. For this purpose, the AMS of this study is expected to be used effectively in the emergency personnel call-up by spreading the situation quickly in case of radiation emergency.

REFERENCES

[1] Criteria for essential digital assets such as nuclear facilities (KINAC,RS019)

[2] IEEE Standard for floating-point arithmetic-1997

[3] Visual Studio 2010 MSDN (Microsoft Developer Network)

Development of Air Suction Control System for Continuous Air Contamination Monitor

Jongsoo Kim, Sung-Ho Lee, O-Young Kwon, and Hae-Cho Lee
Korea Atomic Energy Research Institute, Daedeok-daero989ben-gil 111,Yuseong-gu, Daejeon, Republic of Korea
jskim4@kaeri.re.kr

1. Introduction

Nuclear facilities generally operate continuous air monitoring systems to monitor contamination by radioactive materials. The air intake position of the air monitoring system is determined in consideration of the working space of the work room, the air flow, and the radiation concentration. In this paper, an air suction control system for covering a relatively wide area is considered.

2. Air Suction Control System

2.1 Hardware Configuration

The ASCS (Air Suction Control System) consists of air suction valves and a controller and is connected to the air monitoring system as shown in Fig 1. The suction valve is opened or closed by the controller. The room air passes through the pipe while the valve is open. The number of valves can be set in consideration of the space or structure of the work room, but four intake valves are considered in this study. This means that air from four zones can be monitored according to a defined schedule. The instantaneous response time of each valve at opening and closing is almost 2.5 seconds. The controller consists of PLC (program control logic), clock timer, valve selection switches, and indicate lamps.

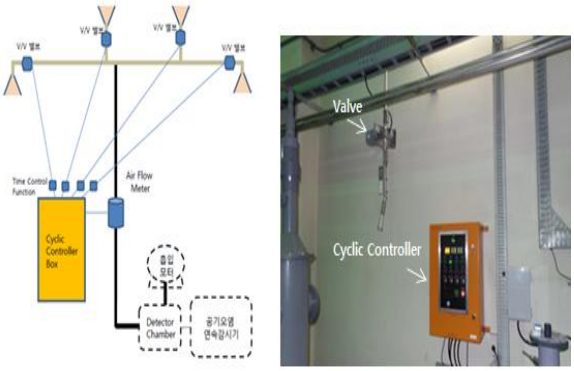

Fig. 1. Configuration of the ASCS.

2.2 Operation mode

The operating mode of the ASCS is normal, interim, and fixed operations, as shown in Fig. 2.

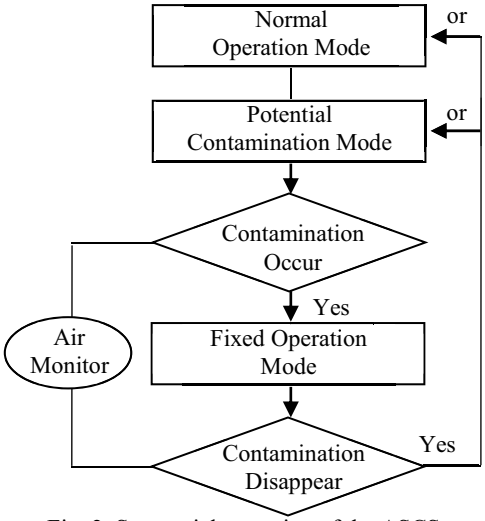

Fig. 2. Sequential operation of the ASCS.

If air contamination is not expected, the normal operating mode can be selected by an operator. In this mode, the air intake through the valve operates sequentially at regular time intervals. However, if air

contamination is anticipated, the valve can be switched to a suspicious position and the air intake will continue to operate until air contamination disappears at its position.

2.3 Error code analysis

If an error occurs while the ASCS is inhaling air, the buzzer and the lamp are designed to occur at the same time. In order to find out the error easily and to recover the error quickly, the error codes were analyzed that may cause the error, which is shown in Table 1. The error could be classified into five groups, each of which could be subdivided into sub-error codes.

Table 1. Analyzed possible error of the ASCS

Error code	Error contents
Telecommunication module error related to hardware	
E00-01	Hardware self- diagnostic error
E00-02	PLC and interface error of the module
E00-03	Power and hardware error of FOU group
E00-04	Initial error of input/output and module in slave group
Telecommunication error of the module	
E01-01	F-net telecommunication error in master and slave group
E01-02	F-net telecommunication error in FOU
PLC and interface error of telecommunication module	
E02-01	PLC and interface error in master and telecommunication module group
E02-02	F-net Input/output module with interface error in slave group
Operation error of high speed link function	
E03-01	High speed link parameter in error status communication tool
E03-02	Fault of high speed link
E03-03	HSxRLNK, HSxTRx electric contact error during high speed link
E03-04	HSxLTRBL electric contact error during high speed link
Operation error of telecommunication command service	
E04-01	Command error of ERR “ON’, STATUS “0” in F-net service mode
Operation error of GMWIM	
E05-01	No response message occurrence in remote contact
E05-02	Others error in remote contact

3. Conclusion

Most of air contamination monitoring is used air suction pathway of single channel. In the other side, the ASCS can be applied several air suction channels for the radioactive substance treatment laboratory of a large area. It will more effect than single channel method.

Equipment to be used a nuclear facility should be analyzed for error to recover quickly. In this point of view, the ASCS analyzed the possible errors and proved them through experiments.

REFERENCES

[1] LG Inc., “Fine Field I/F Module programmable Control Logic Controller”, GLOFA-GM MASTER-K

[2] HSE, “Electric Actuated Ball Valve” Series, 3 PIECE SCRD D-Type

Evaluation of Trapping Characteristics for Volatile Kr/Xe Off-Gas

Seok-Min Hong, Jae Hwan Yang, and Yung-Zun Cho

Korea Atomic Energy Research Institute, Daedeok-daero989ben-gil 111,Yuseong-gu, Daejeon, Republic of Korea

seokminhong@kaeri.re.kr

1. Introduction

An accumulation of spent fuel has brought a considerable interest due to its energy and environmental issue [1]. Pyroprocessing has been investigated in Korea Atomic Energy Research Institute (KAERI) which reduces the accumulated spent fuel and increases the efficiency of fuel cycle. In head-end process of pyroprocessing, UO_2 pellets are produced from a fuel bundle and various radioactive gases from a spent fuel are released during thermal treatment. Within these gases, Kr is a volatile gas which has a long half-life of 11 years and high radioactivity, and therefore it is imperative to capture Kr [2]. Several methods such as cryogenic distillation, absorption using solvents, and adsorption on solids have been widely applied to Kr capture. Of these approaches, adsorption has many advantages such as its low energy-consumption processes and easy regeneration. In addition, Xe also can be released from the spent fuel and it inhibits Kr trapping performance due to its relatively high adsorption affinity. Therefore, Xe should be trapped even it has lower half-life and radioactivity compared to Kr. In this study, Kr/Xe adsorption process was designed and tested using a packed bed column filled with adsorbents. The Kr/Xe adsorption performances were determined from breakthrough curves obtained from a gas chromatography, and the effects of adsorption conditions on capacities were investigated.

2. Experimental Section

2.1 Preparation of Adsorption Test

The adsorbents were pretreated at 130 °C in a vacuum oven for overnight to remove moisture and impurities. The dried adsorbents were packed in a column of a diameter of 30 mm with flowing inert gas to prevent adsorbing water from atmosphere. The flow was 126 cm^3 min^{-1} and the pressure was 1 atm.

2.2 Gas Analysis

The gas chromatography (GC, DS Science, Republic of Korea) equipped with a pulsed discharge detector (PDD) was used to measure a gas concentration which passed through the adsorption column. A 30 m of GC column (ValcoPLOT Molesieve 5A) was installed. He gas was used as a carrier gas in GC, and Kr and Xe was calibrated using standard gases. The temperature of GC was maintained at 60 °C.

2.3 Breakthrough Curve

An adsorption capacity was calculated using a breakthrough time as follows:

$$q_b = \frac{F}{M}\int_0^{t_b}(Co - C)\mathrm{d}t \quad (1)$$

where q represents adsorption capacity (mmol kg^{-1}), F is a flow rate (cm^3 min^{-1}), M is a mass of adsorbent (g), t is an adsorption time (min). Co and C are initial and measured concentration, respectively.

Breakthrough capacity (q_b) was calculated using a breakthrough time (t_b) and the breakthrough time is measured when Kr/Xe is detected at first time in GC.

3. Adsorption Test

3.1 Adsorption Conditions

The commercial adsorbents, activated carbon and zeolite, and a novel adsorbent, polymer-based porous carbon, were selected as adsorbents.

In addition, Kr/Xe adsorption was tested with controlling parameters such as Kr/Xe concentration and adsorption temperatures. From the results, it was found that the adsorption capacities were highly influenced by the Kr/Xe concentration and adsorption temperature. The both breakthrough and equilibrium capacity increase as increasing Kr/Xe concentrations (Fig. 1 and 2), however, they decrease

with increasing adsorption temperature.

Dynamic results were obtained through composition of gas using GC, and the adsorption performances such as working capacities, equilibrium capacity, and kinetic. Furthermore, the effects of adsorption condition on the adsorption capacities were investigated. These parameter effects will be further applied in optimizing adsorption process.

3.2 Adsorption performances

On the other hand, the feed gas in Pyroprocessing contains hydrogen or oxygen for reduction and oxidation, respectively, and therefore Kr/Xe adsorption test was carried out in 3.2% H_2-balanced with Ar or 21% O_2-balanced with Ar. It was confirmed that similar results were obtained in the presence of hydrogen or oxygen which indicate a feasible adsorption process in Pyroprocessing (Fig. 2).

4. Conclusion

Adsorption process was designed for Kr/Xe capture using packed bed column with adsorbents. Kr/Xe adsorption performance was investigated by varying adsorbents and process parameters. It was found that Kr/Xe adsorption was highly influenced by Kr/Xe concentration and adsorption temperature.

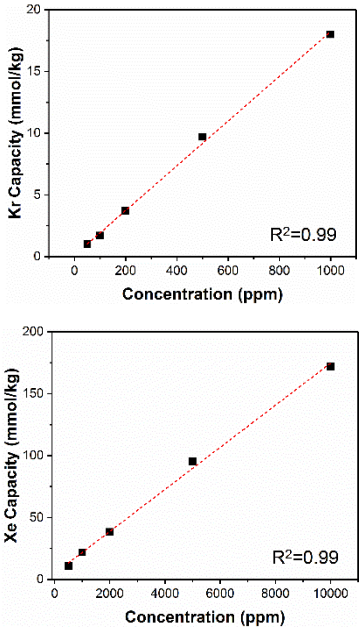

Fig. 1. Adsorption capacities at various Kr and Xe concentrations.

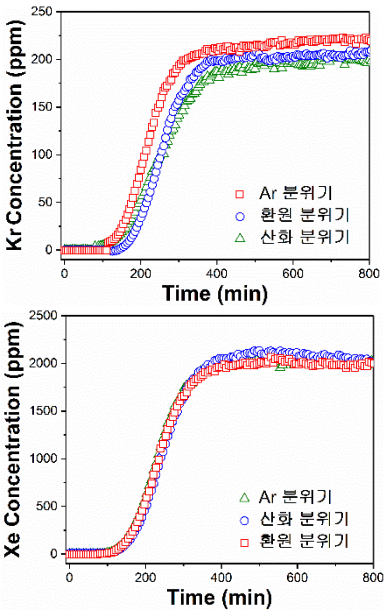

Fig. 2. Breakthrough curves measured at argon, reducing, and oxidizing condition.

REFERENCES

[1] L. Deliere, B. Coasne, S. Topin, C. Greau, C. Moulin, D. Farrusseng, “Beakthrough in Xenon capture and purification using adsorbent-supported silver nanoparticles”, Chemistry: A European Journal, 2, 9660–9666 (2016).

[2] M. Greenhalgh, T. G. Garn, J. D. Law, “Development of a hydrogen mordenite sorbent for the capture of krypton from used nuclear fuel reprocessing off-gas streams”, Journal of Nuclear Science and Technology, 51, 476481 (2014).

Analysis of the Natural Radionuclides Concentrations of Atmospheric PM_{10} Aerosols of Jeju Gosan Site in 2015

Chung-Hun Han[1*], Duk-Woo Kim[1], Hang-ku Lee[1], and Jae-Woo Park[2]
[1*]Institute for Nuclear Science and Technology, Jeju National University, Jeju-si, Jeju-do, Republic of Korea
[2]Department of Nuclear & Energy Engineering, Jeju National University, Jeju-si, Jeju-do, Republic of Korea
[*]tang007@jejunu.ac.kr

1. Introduction

In this study, we have measured radioactivity concentrations of the natural radionuclides (^{40}K, ^{232}Th and ^{238}U) contained in the atmospheric PM_{10} aerosols which were collected at the Jeju Gosan site in 2015.

2. Materials and methods

2.1 Air sampling locations

Air sampling for aerosols was conducted at the Jeju Gosan site. The site serves as a natural background site for characterizing the air pollution in Korean peninsula since the atmosphere in the area is relatively very little affected by artificial airborne matters. Chemical composition analyses have usually been conducted for the atmospheric aerosols collected at the site [1]. The samples were collected for 24 hours using a PM_{10} sampler at approximately 3-day intervals throughout the year 2015. On collecting samples, the air flow rate was kept to about 16.7 L/min, and total air flow was calculated from the flow rate and running time. A total of 127 samples have been analyzed, of which 7 samples are those collected during Asian Dust days, 62 samples collected during normal weather days (no-event days), and the remaining samples collected during the days of haze (10 samples) and fog-mist (48 samples).

2.2 Sample Analysis

For the analysis of PM_{10} elemental species, the aerosol samples were decomposed with acids using a microwave digestion system 10 mL acid solution (5.55% HNO_3/16.75% HCl). The vessel was heated at 180℃ for 15 minutes with 1000 W microwave radiation to digest the PM_{10} aerosols. The number of elements determined by ICP-DRC-MS ((Perkin Elmer, model ELAN DRC-Ⅱ, USA) instruments was 3 species such as ^{39}K, ^{232}Th and ^{238}U. For the elemental analysis, the instrumental detection limits (IDL) of ^{39}K, ^{232}Th and ^{238}U were 27.12 μg/L, 2.98 ng/L and 3.23 ng/L, respectively.

The radioactivity concentrations of the isotopes ^{40}K, ^{232}Th and ^{238}U in the collected fine dust were calculated using the following Eq. (1) (Ref. 2):

$$A_i = \frac{\ln 2}{T_{1/2}} \times \frac{\rho_i \times m_e}{M_i} \times N \quad (1)$$

3. Results and discussion

We have measured, using the ICP-DRC-MS, radioactivity concentrations of ^{40}K, ^{232}Th and ^{238}U contained in Jeju Gosan atmospheric PM_{10} aerosols in 2015.

Table 1. The associated ^{40}K, ^{232}Th and ^{238}U concentrations of airborne PM_{10} by atmospheric phenomenon at Jeju Gosan site, 2015

Atmospheric phenomenon(n)	PM_{10} (μg/m^3)	^{40}K (pg/m^3)	^{232}Th (pg/m^3)	^{238}U (pg/m^3)
Asian Dust (7)	133.11	105.66	395.17	106.73
Haze (10)	80.75	69.42	100.48	62.62
Fog-Mist (48)	32.70	17.56	26.85	31.50
Non-Event (62)	31.72	19.22	40.85	34.80
All (127)	42.48	28.16	62.42	40.34

The mean mass concentration of PM_{10} was 42.48 μg/m^3 (Table 1). During the study period, the mean concentrations of ^{40}K, ^{232}Th and ^{238}U were 28.16, 62.42 and 40.34 pg/m^3, respectively. During Asian Dust periods (7 samples), the mean mass concentration of PM_{10} was 133.11 μg/m^3, and the mean concentrations of ^{40}K, ^{232}Th and ^{238}U were 105.66, 395.17 and 106.73 pg/m^3, respectively.

The radioactive concentrations of ^{40}K, ^{232}Th and ^{238}U were 7.47, 0.25 and 0.50 μBq/m^3, respectively (Table 2). During Asian Dust periods, the radioactive concentrations of ^{40}K, ^{232}Th and ^{238}U were 27.98, 1.60 and 1.31 μBq/m^3, respectively. Furthermore, they are lower than the world averages for the mean

atmospheric activity concentrations of ^{232}Th and ^{238}U, which are 0.5 and 1.0, respectively [3]. However, the Asian Dust period values were higher than the world average. The ^{232}Th/^{238}U activity ratio of totality was 0.500. The ^{232}Th/^{238}U activity ratio of Asian Dust period value was 1.221, which was higher than other atmospheric phenomenon period ratios.

Table 2. The radioactive concentrations in PM_{10} aerosols of Jeju Gosan site, 2015

Atmospheric phenomenon	^{40}K (μBq/m^3)	^{232}Th (μBq/m^3)	^{238}U (μBq/m^3)
Asian Dust	27.98	1.60	1.31
Haze	18.39	0.41	0.77
Fog-Mist	4.65	0.11	0.39
Non-Event	5.09	0.17	0.46
All	7.47	0.25	0.50

We are analyzing five-day backward trajectories of the air inflow into the Gosan site using the HYSPLIT4 model of NOAA.

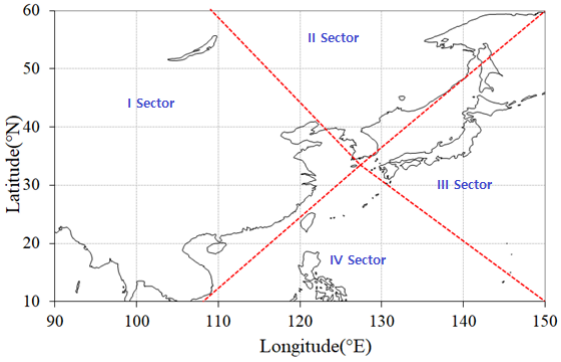

Fig. 1. Sectional classification of Northeast Asia for backward trajectory analysis based on the Jeju Gosan site.

The air movement route was classified into Sector I (China continent), II (Korean peninsula), III (Japan) and IV (North Pacific Ocean) (Fig. 1).

Table 3. Inflow pathway sectional activity concentrations of ^{40}K, ^{232}Th and ^{238}U in airborne PM_{10} at Jeju Gosan site, 2015

Sector (n)	^{40}K (μBq/m^3)	^{232}Th (μBq/m^3)	^{238}U (μBq/m^3)
I (43)	11.23	0.43	0.65
II (49)	6.28	0.19	0.40
III (19)	4.13	0.08	0.46
IV (16)	3.08	0.05	0.38
All (127)	7.47	0.25	0.50

Sector specific values are shown in Table 3. The values of sector I were higher than those of other sectors. However, they are lower than the world averages for the mean atmospheric activity concentrations of ^{232}Th and ^{238}U. The ^{232}Th/^{238}U activity ratio of sector I was 0.662, which was higher than other sector ratios.

4. Conclusions

We have measured radioactivity concentrations of the natural radionuclides contained in the atmospheric PM_{10} aerosols at the Jeju Gosan site in 2015. The radioactive concentrations of ^{40}K, ^{232}Th and ^{238}U were 7.47, 0.25 and 0.50 μBq/m^3, respectively. They are lower than the world averages for the mean atmospheric activity concentrations of ^{232}Th and ^{238}U. However, the Asian Dust period values were higher than the world average. The ^{232}Th/^{238}U activity ratio of Asian Dust period value was 1.221. The values of sector I (China continent) were higher than those of other sectors. As a result, it was confirmed that the ratio of each nuclide was slightly different according to the inflow route. It is expected that this will be a preliminary data for analyzing the sources and various weather phenomena of fine dust on the peninsula. It is judged that the results become a preliminary data on the impact of fine dust from China, which has been recently intensified, on the Korean Peninsula.

Acknowledgements

This research was supported by Basic Science Research Program through the National Research Foundation of Korea (NRF) funded by the Ministry of Education (No. NRF-2010-0020077).

REFERENCES

[1] Kim K.J., Lee S.H., Hyeon D.R., Ko H.J., Kim W.H. and Kang C.H., Composition comparison of PM_{10} and $PM_{2.5}$ fine particulate matter for Asian dust and haze events of 2010-2011 at Gosan site in Jeju Island, Analytical Science & Technology, 27(1), 1-10, (2014).

[2] J. Magill and J. Galy, "Radioactivity, Radionuclides, Radiation." Springer, Berlin (2005).

[3] United Nations Scientific Committee on Effects of Atomic Radiation, Sources and Effects of Ionizing Radiation. UNSCEAR 2000 Report Vol. I. United Nations, New York (2000).

A Preliminary Study for Residual Radioactivity Assessment After Neutron Irradiation of Silicon Carbide

Ki-Man Lee, Byung-Gun Park, and Gwang-Min Sun

Korea Atomic Energy Research Institute, 989-11 Daedeok-daero, Yuseong-gu, Daejeon, Republic of Korea

lkm@kaeri.re.kr

1. Introduction

Silicon carbide (SiC) single crystal has been an excellent substrate material for high power and high frequency electronic devices because of its excellent thermal and electrical properties compared with silicon. Neutron transmutation doping (NTD) of semiconductors is an important method for applications that require high dopant homogeneity, for example in electric power devices [1]. For neutron transmutation doping, SiC is irradiated by neutron and the components of SiC become radioactive nuclides. These radioactive nuclides can be a problem for safety and quality control. In this study, assessment of residual radioactivity after neutron irradiation of SiC is conducted using Monte Carlo simulation and most influential component is discussed.

2. Materials and methods

2.1 PHITS simulation

Assessment for the residual radioactivity after neutron irradiation of SiC is conducted using a general purpose Monte Carlo particle transport simulation code PHITS (Particle and Heavy Ion Transport code System) version 3.02. For simulating the radioactivity of components after neutron irradiation, the t-dchain tally of PHITS and DCAHIN-SP program are used. PHITS automatically generate an input file of DCHAIN-SP by using t-dchain tally and DCHAIN-SP can calculated the time variation of induced activity and ambient dose equivalent H*(10) rate at 1m away from the point source during irradiation and cooling time. Thermal energy neutron and source power of 4×10^{14} n/cm^2·sec are adopted as a source input.

2.2 Modeling of silicon carbide sample

A SiC sample for the simulation of neutron irradiation is modeled after a typical cylindrical single crystal with a diameter of 50 mm and a length of 50 mm. Aluminum, boron, iron and titanium that are major impurities in the SiC wafer are considered as components of the sample [2]. The concentration of each impurity is conservatively assumed as 10 ppm.

3. Results and discussion

Relative radioactivity, dose rate and ambient dose equivalent H*(10) of five dominant radionuclides after neutron irradiation for five minutes are listed in table 1. Most of residual radioactivity is come from silicon and radioactivity of each elemental impurity is different from each other. Aluminum-28 has dominant radioactivity (4.30 %) because of large neutron capture cross section of aluminum. Also the ambient dose equivalent from Al-28 is 98.07 percent of total dose equivalent.

Table 1. Relative radioactivity, dose rate and ambient dose equivalent of elements after neutron irradiation

Nuclide	Relative radioactivity [%]	Relative dose rate [%]	Ambient dose equivalent [μSv/h·m^2]
Be-8	0.03	0	0
B-12	0.11	0.06	4.103
Al-28	4.30	98.07	6.689×10^3
Si-31	95.46	1.19	8.131×10^1
Ti-51	0.11	0.67	4.6×10^1

Time variation of ambient dose equivalent H*(10) rate during and after neutron irradiation is showed in Fig.1. The dose rate is sharply decreased for 20 minutes because the half-life of Al-28 is 134.5 seconds.

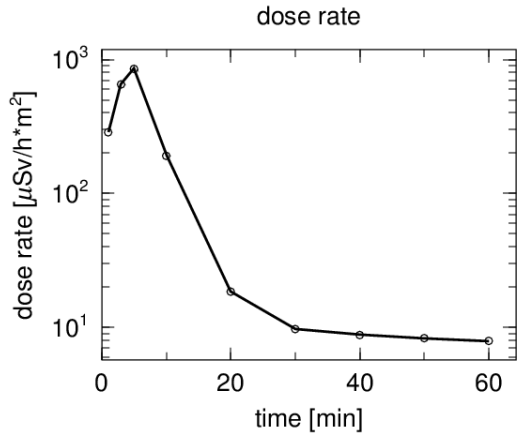

Fig. 1. Time variation of ambient dose equivalent H*(10) rate at 1m away from the SiC during and after neutron irradiation (plotted by ANGEL 4.50).

4. Conclusion

Assessment for residual radioactivity after neutron irradiation of SiC is conducted using PHITS simulation. As a result, aluminum that is an impurity in SiC has dominant residual radioactivity and ambient dose equivalent after neutron irradiation. Thus the concentration of aluminum in SiC should be controlled for safety and quality assurance.

ACKNOWLEDGMENTS

This work was supported by the National Research Foundation of Korea (NRF) Grant funded by the Korea government (MSIP) (NRF-2012M2A2A6004263 & 2014M2A8A1048615).

REFERENCES

[1] IAEA, “Neutron Transmutation Doping of Silicon at Research Reactors”, Report IAEA-TECDOC series, 1681 (2012).

[2] D. G. Shin, H. R. Son, S. Heo, B. S. Kim, J. E. Han, K. S. Min and D. H. Lee, “Impurity Behavior of High Purity SiC Powder during SiC Crystal growth”, Materials Science Forum, 778, 22-25 (2014).

Analysis of Minimum Detectable Activity for Noble Gas Monitor Using System Modeling

Sung-Ho Lee, Jong-Soo Kim, and Tae-Woo Go
Korea Atomic Energy Research Institute, Daedeok-daero989ben-gil 111,Yuseong-gu, Daejeon, Republic of Korea
leesungho@kaeri.re.kr

1. Introduction

Krypton is one of the noble gas isotopes. It has mostly generated from reprocessing of the spent fuel and fault of nuclear fuel cladding. Krypton monitoring is an important factor in determining in spent fuel's reprocessing or nuclear fuel's fault.

Radiation measurement is based on random processing; this results in inherent statistical fluctuation. By causing unwanted errors like false alarm, it may adversely affect facility operation and management.

In this paper, an analysis of minimum detectable activity (MDA) for a noble gas monitor using system modeling is presented. A determination of the suitable MDA contributes to reduction of the error by the fluctuation and the correct use of the monitor.

2. Analysis of MDA for noble gas monitor using system modeling

2.1 International Standard, ANSI N42.17B

The MDA concept which one of the most has been widely used was introduced by Currie [1]; it is a kind of guidelines for a decision whether a certain sample has activity or not.

Some regulatory agencies have their standards related to MDA such as *NUREG 1576*, *ISO 11929*, *DIN 25482*, *ANSI N42.17B*. They require

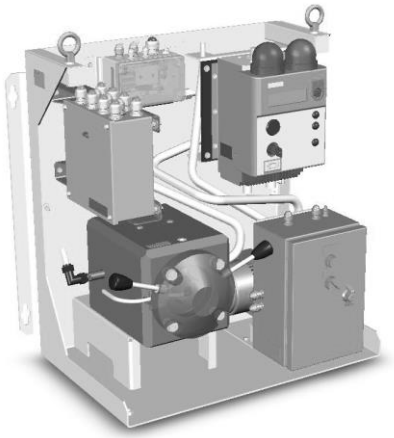

Fig. 1. Noble gas monitor, NGM204 (MGPI).

that a certain minimum detectable amount of activity be measurable while monitoring for the possible presence of radioactive contaminants.

ANSI N42.17B standard is based on the deriving MDA without signal; it means only the blank signal uncertainties are considered. The MDA in *ANSI 42.17B* is defined as

$$MDA_{ANSI\,42.17} = 4.65 \cdot u(0) \qquad (1)$$

where $u(0)$ is the uncertainty of target system with the blank signal [2].

2.2 MDA Calculation using mathematical of a noble gas Monitor

Fig. 1 shows a monitor NGM204 which has developed by MGPI; it monitors the fluid noble gas activity inside its sample chamber. With dual silicon detector, it provides dynamic gamma compensation.

Considering its hardware configuration and

calculation algorithm, noble gas volumetric activity *VA* is derived as

$$VA = \frac{C_p - kC_c - C}{Eff} \quad (2)$$

where C_p and C_c are count rate [c/s] in primary and compensation channels. They are yielded by first and second detectors, respectively. *C* is background noise [c/s]. As *k* and *Eff* are The system parameters, k is a weighting coefficient of the compensation channel, and *Eff* is detection efficiency [c/s/Bq/m^3].

For the model in (2), each term can be specified as:

$$\mu_{cp} = Eff \cdot s + \varepsilon_{\gamma p} \cdot s_\gamma + b_p \text{ and } \sigma^2_{Cp} = \frac{\mu_{cp}}{t} \quad (3)$$

$$\mu_{cc} = \varepsilon_{\gamma c} \cdot s_\gamma + b_c \text{ and } \sigma^2_{Cc} = \frac{\mu_{cc}}{t} \quad (4)$$

where

μ_{cp} : Mean of the random variable of C_p

μ_{cc} : Mean of the random variable of C_c

s : Volumetric activity [Bq/m^3]

s_r : External gamma dose rate [Sv/h]

ε_{rp} : Efficiency of gamma in the primary channel [c/s/Sv/h]

ε_{rp} : Efficiency of gamma in the compensation channel [c/s/Sv/h]

b_p : Noise in the primary channel [c/s]

b_c : Noise in the compensation channel [c/s]

t : Measurement time [s].

The variable μ_{cp} can be rearranged with Eq. (4) as

$$\mu_{cp} = Eff \cdot s + k\mu_{cc} + \mu_c$$
$$\text{where } k = \frac{\varepsilon_{\gamma p}}{\varepsilon_{\gamma c}} \text{ and } \mu_c = b_p - kb_c. \quad (5)$$

From (2)-(5), the measurement uncertainty for the noble gas volumetric activity in NGM204 is derived as

$$u^2(s) \cong \frac{Eff \cdot s + k\mu_{cp} + k^2\mu_{cp} + \mu_c}{Eff^2 t}. \quad (6)$$

Because *ANSI N42.17* considers only blank signal uncertainties, the MDA in (7) is obtained as

$$MDA = 4.65u(0) = \frac{4.56}{Eff}\sqrt{\frac{k(1+k)C_c + C}{t}}. \quad (7)$$

Table 1 shows MDA of NGM204 according to the measurement time. In this case, ambient gamma is set 10μSv/h.

Table 1. MDA of NGM204

Measurement time (min)	MDA(kBq/m^3)
2	57.9
10	25.9
60	10.6
600	3.34

3. Conclusion

In this paper, analysis of MDA for the noble gas monitor is introduced. Besides measurement time and background noise, the understanding for the characteristics of the target monitor such as processing algorithm and hardware configuration gives more accurate MDA.

REFERENCES

[1] L. A. Currie, “Limits for qualitative detection and quantitative determination”, *Anal. Chem.*, 40 (3), 586-593 (1968).

[2] “ANSI N42.17B-1989”, Occupational airborne radioactivity monitoring instrument-ation.

Review of Decommissioning Risks

Gi-Lim Kim, Taesik Yun, and Jihwan Yu*
Decommissioning Technology Team, Central Research Institute, KHNP
70, Yuseong-daero 1312beon-gil, Yuseong-gu, Daejeon, Republic of Korea
* liu20893283@khnp.co.kr

1. Introduction

Risk management is a series of process to minimize the impact of unfortunate events or to maximize the realization of economic values such as identification, evaluation, prioritization and coordination. Thus it is necessary to consider the integrated approach to maximize risk reduction (ISO 31000). In this article, we extract universal risks which can be bring about in the course of decommissioning process and suggest how to resolve those risks.

2. Decommissioning Process

Generally decommissioning consists of four periods: Preparation for decommissioning activities, Safe Storage, Decontamination and Dismantlement (D&D), and Site Restoration before final operation termination. There are so many risks in each period.

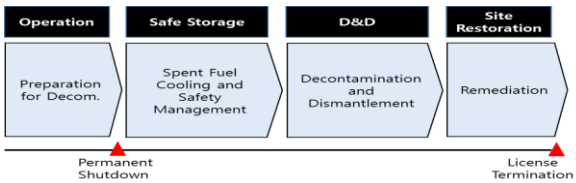

Fig. 1. Example of Major Activities of process.

3. Universal Decommissioning Risks

3.1 Irreversible risks

- A country needs capacities to be replaced for the plant decommissioned which could cause economic hardships
- Big gaps between the estimated costs and the financing allocated by EU and each country are demonstrated.
- Long-term radioactive waste facilities are the major challenges e.g. Lithuania with interim storage for spent fuel assemblies, Bulgaria with national disposal facility for low/intermediate-level waste, Slovakia with decontamination of the primary circuit
- Work on potential final disposal solutions for high-level waste and spent nuclear fuel still is at conceptual stages.

3.2 Radiological risk

Each plant has its specific physical and radiological characteristics which results in different types of contamination in the SSCs and the site it has been operated. Hence, before commencing the decommissioning in earnest, the owner of the plant to be decommissioned has to scrutinize SSCs and site. From the radiological perspective, workers could be exposed directly to the decay of radioactive materials that produces radiation in the decommissioning stage. Minimize the personnel dose as low as possible is a major issue during the decommissioning stage.

3.3 Financial risk

Decommissioning cost has been levied with the electricity selling price and accumulated until the

commencement of decommissioning. However, in reality, it is not easy to estimate the appropriate costs for decommissioning in the early stage of the project. The decommissioning costs spent in the future are influenced by the change of interest rate, material and equipment costs, staffing costs, schedule overruns, unexpected events and the like. In addition, it is important how to manage money accumulated since commencement

3.4 Regulatory risks

Each country differs in involvement of the state and its regulatory body to supervision and management of the decommissioning. The regulation with regard to decommissioning is, so called, plant or country specific; there are largely two guidelines; some countries follow US NRC rules, the others refer the IAEA guidance. Furthermore, the decommissioning projects across the world are still in the early stage, each country has to prepare its own regulation with regard to its specific political and environmental situation. On top of that, it should be responsive to change of the regulatory guidelines which have been revised to consider the current decommissioning situation and technology readiness. In addition to the risks delineated above, there are human resource risks and other risks brought up by many events happening in the process of decommissioning.

3.5 Electricity rate risks

Decommissioning a nuclear power plant provides other generating resources such as LNG, Coal, and renewable energy to produce the capacities. Accordingly electricity rate is likely to be higher than that using nuclear power plants since electricity prices had become entirely dictated by natural gas and other costly electricity sources, causing rates to go up substantially. Without viable low-cost options like coal and hydroelectric power, and with rising operating costs of plants and demand for energy, electric rates would continue to rise.

4. Conclusion

We demonstrate the risks normally arouse in the decommissioning site in this article. It is, however, made up with the economic assessment to show how much impact those risks or uncertainties can impact on the decommissioning itself as well as the whole life cycle of nuclear power plant.

REFERENCES

[1] IAEA, “Risk management: A tool for improving nuclear power plant performance, IAEA-TECDOC-1209, April 2001

A Case Study on the Effect of Filter Micron Rating Change of Filtration System in Lancing Process

Kyung-Wook Shin, Yun-Sang Jung, Sam-Hyun Kim, Yong-Seok Choi, Byeong-Mok Park, Gyung-Sun Chae, and Hee-Kon Jang

SAE-AN ENGINEERING CO., 184, Gasan digital 2-ro, Geumcheon-gu, Seoul, Republic of Korea

and9211@sae-an.co.kr

1. Introduction

Lancing is the process of remove the corrosion products deposited on the top of the of the tube side of the secondary side of the steam generator and the surface of the tube during the nuclear power plant overhaul. The purpose of lancing is remove sludge deposit on the top of the steam generator tube sheet and on the surface of the tubing to prevent stress corrosion cracking, deterioration of heat exchange performance, and unstable water level of steam generator. Thus, the solid corrosion products generated from the secondary side of the steam generator are removed from the filtration system of lacing process and the filtration system uses a bag filter at the front and a cartridge filter at the rear end.

In this case study, we confirmed the influence of the micron rating of the filter used in the filtration system on the lancing process of Unit 1 of NPP.

2. Lancing process

2.1 Overview

The mail working place of the lancing process can be divided into the secondary side of the steam generator in the containment building, the process system container outside the containment building, and the control container. On the secondary side of the steam generator, a large amount of high-pressure water is injected into the barrel spray nozzle to remove the deposited sludge in the secondary side of the steam generator. The water and sludge generated are transferred to the surge tank installed in the process system container, the water in the surge tank is collected in the filter while the sludge is collected in the filter and the water is collected in the storage tank. The water in storage tank is reused to remove the sludge by spraying with a robot using different pumps according to the type and position of the sludge. The removal of sludge is carried out in the order of soft sludge, hard sludge and deviated hard sludge on top of the tube sheet. The lancing process is shown in Fig. 1.

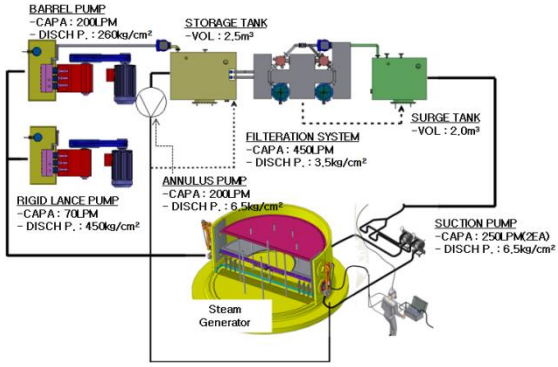

Fig. 1. Lancing process flow diagram.

2.2 Filtration system

The filtration system of the lancing process uses a bag filter to remove large particle sludge and a cartridge filter to remove small particle sludge. The filtration system consist of two filtration systems. One filtration system consist of one bag filter and nine cartridge filter, as shown in Fig. 2.

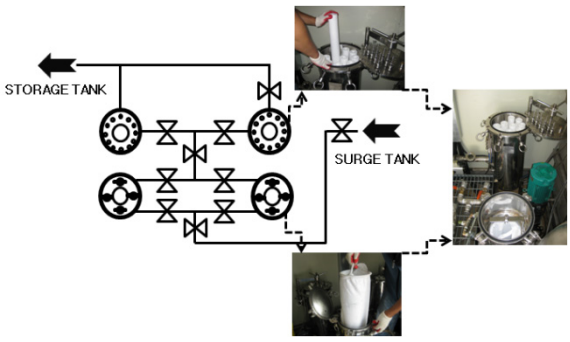

Fig. 2. Filtration system.

3. Effect of micron rating of filter

3.1 Filter usage

Table 1 shows the amount of filter used when the bag filter of 10 μm and 7.5 μm was used in the filtration system through the lacing process of S/G A, B, C. These results show that the use of the cartridge filter is significantly reduced when using a 7.5 μm bag filter, compared to using a 10 μm bag filter.

Table 1. Cartridge filter usage

Filter	S/G A		S/G B		S/G C	
	10μm	7.5μm	10μm	7.5μm	10μm	7.5μm
Bag	53	0	30	45	12	49
Cartridge	414	0	189	54	117	54

The amount of sludge removal was not significantly different between the two types of bag filters, although it may vary depending on the timing of use.

Table 2. Weight of sludge by micron rating of bag filter

Micron Rating	Quantity	Total Weight
10 μm	95EA	169.06 kg
7.5 μm	94EA	185.5 kg

3.2 Filtration system maintenance

Replacement of the filter is an important part of maintenance because the process may be stopped if the filter replacement of the filtration system is not performed in a timely manner during the lancing process. When replacing, be careful not to spill contamination on the floor. The replacement of the filter is performed when the differential pressure is 4.0 bar, and when the amount of sludge is large at the beginning of the lancing process, the differential pressure of the filter increase rapidly, and the replacement time of the filter becomes very fast.

The results of S/G B and C in Table 1 indicate that when 7.5 μm was used, the amount of cartridge filter used decreased but the amount of bag filter used increased. Therefore, when 7.5 μm is used, the bag filter replacement is increased and the replacement of the cartridge filter is decreased, so that the maintenance time is further increased.

Table 3. Number of replacements of the filter

Filter Type	10μm	7.5μm
Bag	42	94
Cartridge	33	12
Total	75	106

3.3 Waste

The spent filters generated in the process system container are to be stored temporarily with a waste label and carried out according to the procedure when moving to the radiation management area.

In the filter structure, the bag filter composed of a bag-shaped synthetic fiber and an upper ring, and the cartridge filter has a structure in which a cylindrical synthetic fiber surrounds a cylindrical plastic, so that the bag filter can be easily separated. When calculating the volume of only the synthetic fibers of the bag filter and the cartridge filter as the standard of the filter currently used, the volume of the cartridge filter is about 1.2 times larger than that of the bag filter. In addition, since cartridge filters also product plastic waste, it is advantageous to reduce the usage of cartridge filters in order to reduce waste.

3.4 Cost

The use of the filter is closely related to the cost of not only the purchase of the filter but also the processing of future filter wastes. Since the cartridge filter is many times more expensive than the bag filter and the waste disposal cost in high, it is advantageous in terms of cost to rationalize the use of the filter.

4. Conclusion

The use of filters in the filtration system during the lancing process greatly affects not only safety but also maintenance, waste treatment and purchasing costs. We plan to comprehensively estimate not only the number of years of operation of the NPP but also the amount of sludge generated in the previous cycle, and to find an efficient operation method of the filtration system corresponding to this, it is very important in the lancing process.

References

[1] SEA-AN Co. Maintenance Procedure “Removal of deposits on the secondary side of the steam generator”

[2] The Final Report “The 21th KORI NUCLEAR POWER PLANT, UNIT 3(STEAM GENERATO SECONDARY Lancing & FOSAR)”

Analysis of Exposure Dose by RESRAD Sensitivity Analysis

Sang June Park[1*], Ji Hyang Byon[1], Suhee Lee[2], and Seokyoung-Ahn[1]

[1] Pusan National University, 2, Busandaehak-ro 63beon-gil, Geumjeong-gu, Busan, Republic of Korea

[2] Korea Hydro & Nuclear Power Central Research Institute, 70, Yuseong-daero 1312beon-gil, Yuseong-gu, Daejeon, Republic of Korea

*xelidake2@pusan.ac.kr

1. Introduction

When decommissioning an old nuclear power plant, evaluation of exposure dose is essential. Dose can vary depending on the radionuclide concentration, scenario, exposure pathway and parameters. RESRAD-ONSITE code was used to evaluate exposure dose.

The RESRAD code was developed by Argonne National Laboratory (ANL) with support of the U.S. Department of Energy (DOE), and the U.S. Nuclear Regulatory Commission (NRC). This code was used for remediation standards, evaluation of doses and risks for contaminated sites.

The code used in this study is the RESRAD-ONSITE code, which can be used to assess radiation exposures of a human receptor located on top of soils contaminated with radioactive materials. [1]

The purpose of this study is to analyze the dose by changing characteristics of cover, which is one of RESRAD parameters.

RESRAD Sensitivity Analysis was performed for characterization of dose.

2. Methodology

The radionuclides used in this study are ^{240}Pu, ^{137}Cs, ^{90}Sr, and the radionuclides concentration was 1 Bq/g. In RESRAD, the main parameters related to the cover are the cover depth, the density of cover material, and the cover erosion rate.

RESRAD default values were used for the above three parameters. Sensitivity analysis was carried out after setting the density to 1.5 g/cm^3, the erosion rate to 0.001 m/yr, and the thickness to 20 cm.

We quantitatively confirmed the characteristics of the derived dose through sensitivity analysis of each parameters.

3. Results and Discussion

3.1 Cover depth

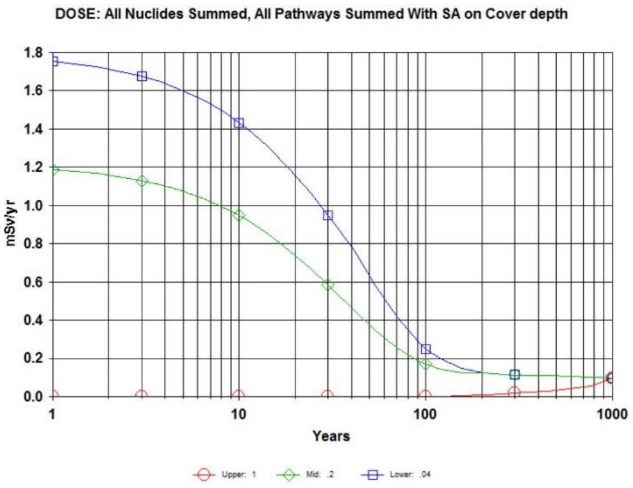

Fig. 1. Graph of dose for the cover depth.

If the thickness of the cover is 1 m, the initial dose is 0 and the maximum dose is 0.1 mSv/yr after 1000 years. In the case of 20 cm and 4 cm, the maximum dose occurs at the beginning and is 1.2 mSv/yr and 1.75 mSv/yr.

3.2 Density of cover material

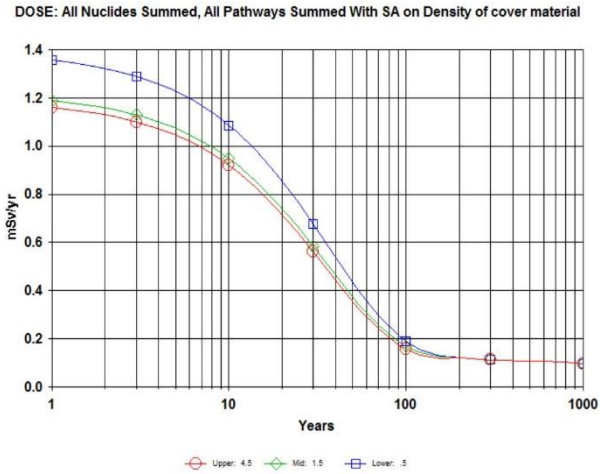

Fig. 2. Graph of dose for the density of cover materil.

The maximum dose occurred at t = 0, and dose values were 1.35 mSv/yr (0.5 g/cm^3), 1.2 mSv/yr (1.5 g/cm^3) and 1.15 mSv/yr (4.5 g/cm^3).

3.3 Cover erosion rate

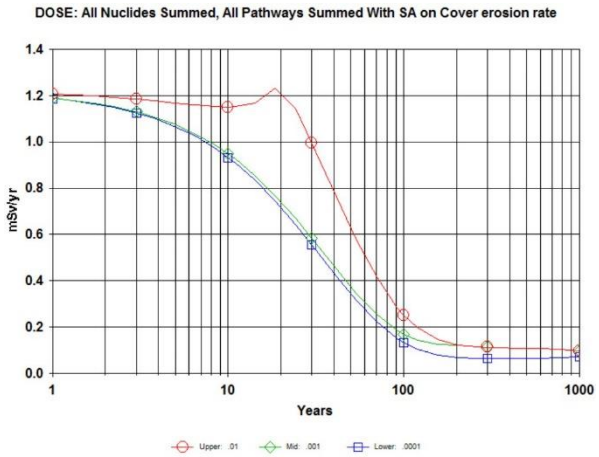

Fig. 3. Graph of dose for the cover erosion rate.

The maximum dose occurred at t = 0 except when the erosion rate was 0.1 m/yr, and the maximum dose occurred after 20 years for 0.1 m/yr erosion rate. The dose values are about 1.2 mSv/yr in all three cases.

4. Conclusion

In this study, dose were derived through sensitivity analysis of cover thickness, density, and erosion rate.

The most sensitive parameter is cover thickness. The change in dose was most prominent with the change in thickness. In the case of erosion rate, special attention should be paid to the exposure dose even after the elapse of time since it was confirmed that the maximum dose occurred at 20 years after the initial dose.

The exposure dose was quantitatively confirmed by the graph that the dose decrease with the cover thickness increased, the density increased, and the erosion rate decreased. Also, if a thick cover is used with a dense material, the exposure dose will be reduced immediately.

In Korea, because of the lack of experience in decommissioning commercial nuclear power plants, it is considered effective to reduce the exposure dose by using the cover in the case of unexpected exposure situation.

REFERENCES

[1] ANL, “User’s Manual for RESRAD version 6”.

Radiological Effect of Aerosols From Decommissioning and Decontamination

Min-Ho Lee, Nakkue Chae, and Sungyeol Choi*

Department of Nuclear and Quantum Engineering, Korea Advanced Institute of Science and Technology, 291 Daehak-ro, Yuseong-gu, Daejeon, Republic of Korea

* sungyeolchoi@kaist.ac.kr

1. Introduction

According to the US Department of Energy`s (DOE) announcement, decommissioning and decontamination (D&D) of nuclear power plants (NPPs) activities can cause additional problems for inhalation of radioactive aerosols. During D&D, various cutting technics are used to cut metals. These activities generate airborne species called aerosols that cause a negative effect on health [1].

Inhalation is the major route of internal exposure of workers to radioactive aerosols. The particle size distribution will determine whether any part of the inhaled particles to be deposited in the compartment of the respiratory tract. Therefore, the internal doses from radioactive aerosols are strongly dependent on the particle size distribution [2]. This study presents the importance of measuring the aerodynamic diameter distribution for the risk assessment of worker`s internal dose in the nuclear facility.

2. The generation of radioactive aerosol during the D&D process

During D&D, radioactive aerosols are produced by cutting the metal in large-scale components and melting the metal during recycling to achieve a reduction in volume. The cutting metal process produces radioactive aerosols by the mechanical comminution of metals and the vaporization of metals. The radioactive aerosols have very different characteristics depending on the cutting process specifications such as a cutting tool, the thickness of material, and atmosphere condition (Table 1).

The distribution of aerosols is essential parameters needed for assessment of inhalation exposures. Therefore, it is essential to analyze the aerodynamic diameter distribution of aerosols for the D&D process.

Table 1. Characterization of aerosols produced during metal cutting processes [1]

Cutting tool	Material	MMAD (μm)	Concentration (mg/m^3)
Oxy-Acetylene Torch	Stainless steel pipe	0.1~0.3	15±11
Plasma Torch		0.2~0.3	60±80
Cut Rod		0.4~0.8	53±30

(MMAD = Mass Median Aerodynamic Diameter)

In laboratory experiments, a plasma torch is used to cut metal plates of different thicknesses and measure various parameters. Mostly, the size distribution of aerosol measurements is performed using impactor. For an impactor, all particles collected at a given stage have an aerodynamic diameter greater than the cut-off diameter of that stage.

3. Inhalation of aerosol into the human respiratory model for internal dosimetry

3.1 Human Respiratory Tract Model(HRTM)

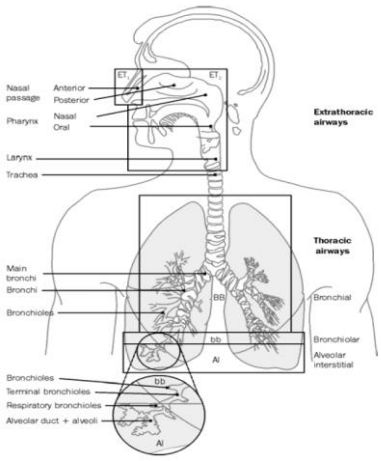

Fig. 1. The human respiratory tract is showing the various regions used within the HRTM [3].

The International Commission on Radiological Protection (ICRP) developed a human respiratory tract model (HRTM) for the assessment of internal dose by aerosol inhalation (Fig 1). ICRP provides information and guidance to the worldwide nuclear community to inform radiological protection practices.

The activity median aerodynamic diameter (AMAD) is an aerodynamic diameter for which 50% of the radioactivity in the cumulative size distribution. AMAD is a key parameter to predict internal dose from inhaling radioactive aerosols. It is used as a means to simplify the actual distribution of aerosol for internal dosimetry. The task group on lung dynamics of ICRP concluded that respiratory tract deposition was mainly related to the median of the distribution: AMAD and the breathing characteristics of the person.

Inhalation dose increased with decreasing particulate size. Committed effective doses due to inhalation of 0.01 μm sized particulates were higher than doses due to 100 μm sized particulates [4]. The aerosol particles of about 0.1 to 1 μm in size receive both aerodynamic and thermodynamic effects in the respiratory tract. Therefore, these particles in the respiratory region have a lower deposition fraction.

3.2 Internal exposure of workers depends on the aerosol diameter

Measurements of airborne particulate in a wide range of nuclear workplaces have shown that activity is distributed on airborne particulate such that the AMAD is in the region of 5 μm [5]. However, the AMAD can affect the effective dose more than tens or hundreds of times (Fig 2). Thus, when the radiation dose is evaluated without consideration of aerosol characteristics precisely, it will be significantly distorted.

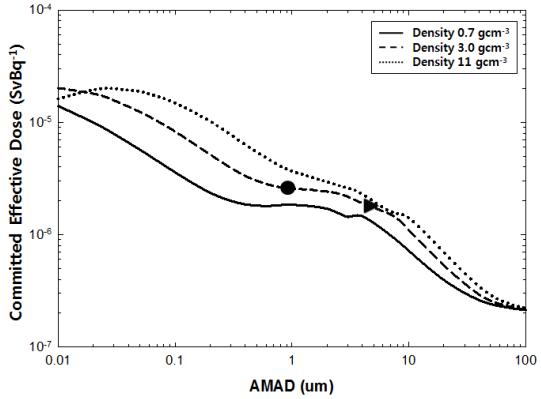

Fig. 2. Committed effective dose due to inhalation of airborne particulates by particulate mass density [4].

Internal radiation dose through radioactive aerosol inhalation depends on the particulate properties, such as size, shape, density, and absorption type. In order to the accurate assessment of worker exposure, for this reason, it is taken into consideration that both site-specific materials and the site-specific particulate properties.

4. Conclusion

It is significant to understand the distribution of radioactive aerosols according to their aerodynamic diameters, radioactive isotopes, chemical forms for the evaluating the worker's internal exposure.

ACKNOWLEDGMENTS

This work was financially supported by the National Research Foundation of Korea (NRF) by a grant funded by the Ministry of Science and ICT, Republic of Korea (Grant No. NRF-2017M2A8A4018596).

REFERENCES

[1] M. Ebadian, S. Dua, and H. Guha, “Size Distribution and Rate of Production of Airborne Particulate Matter Generated During Metal Cutting,” (2001).

[2] M.D. Dorrian, and M. Bailey, “Particle Size Distributions of Radioactive Aerosols Measured in Workplaces,” Radiation protection dosimetry, 60(2), 119-133 (1995).

[3] RWM Reports, “Review of Respirable Particle Size Range,” (2013).

[4] S.Y. Kim, C.K.Choi, Il Park, Y. G. Kim, W. C. Choi, and K. P. Kim, “Assessment of Inhalation Dose Sensitivity by Physicochemical Properties of Airborne Particulates Containing Naturally Occurring Radioactive Materials,” Journal of radiation protection and research, 40(4), 216-222 (2015).

[5] ICRP, “Human Respiratory Tract Model for Radiological Protection, Publication 66,” ICRP 24(1-3), (1994).

Effectiveness Verification of the Representative Sampling Location Scale Down to Reflect the Latest Standards

Ju-Young Yoon※ and Dong-guk Lee

KHNP CRI, 70, 1312-gil, Yuseong-daero, Yuseong-gu, Daejeon, Republic of Korea

※august63@khnp.co.kr

1. Introduction

The technical standards for gas leakage radiological monitoring of nuclear power plants are designed and constructed in accordance with ANSI N13.1.

It was revised in 1999 after it was published in 1969. Domestic nuclear power plants were designed and constructed in accordance with the revised version(1999) from Shin-Kori unit 1. The previously constructed nuclear power plant was built by the standards issued in 1969.

In order to reflect the latest standards of the power plants reflected in the existing standards, we need to perform the proof test or scale down test of the representative sampling locations. In order to perform the scale down test, we tried to verify effectiveness of the scale down.

2. Test Method

The representative sampling locations of the representative nuclear gas radiation monitors are to comply with the ANSI N13.1 code requirements, as follows: 40 CFR 60, APP. A Method 1 shall be satisfied.

Table 1. 40 CFR 60, APP. A Method 1

Item	Acceptance criteria
Flow angle	< 20°
Velocity	COV < 20%
Tracer gas	COV < 20%
	COV_{Max} < 20%
Paticle	COV < 20%

* COV : Coefficient Of Variation

2.1 Reset the sampling location

Considering the field operation and environment, we decided to carry out the scale down test in the laboratory. The CFD(Computational Fluid Dynamics) analysis was reset the representative sampling location before the proof test.

The velocity distribution COV, flow angle and trace gas concentration distribution COV at the sampling location are evaluated to meet the design requirements of ANSI/HPS N13.1-1999

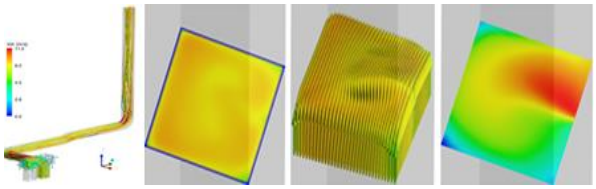

Fig. 1. CFD Analysis Results.

2.2 Effectiveness Verification tests

In order to verify the validity of the proof test model, we installed ducts of the actual and scale models for the RE-053 system and verified that they meet the requirements of ANSI N13.1 (1999).

○ Scale model validation criteria

- Obtain geometric similarity between scale model and actual duct in sampling position
- Reynolds number of scale model: 10,000 or more
- Conditions of hydraulic diameter and average flow velocity of scale model and actual duct

$$\frac{V_{actual}\, D_{h,actual}}{6} \leq V_{scale}\, D_{h,scale}$$

- Velocity homogeneity: COV 5% or less

○ Duct installation

Fig. 2. Photographs for actual model.

Fig. 3. Photographs for scale model(2.032:1).

○ Scale model scale and velocity design

Table 2. Design specification

RE-053	Actual	Scale down (V_{actual}=V_{scale})	Scale down (Re_{actual}=Re_{scale})
Streamline (CFM)	19,800	4,795	9,744
Velocity (m/sec)	8.62	8.62	17.52
Reynolds number	580,397	285,629	580,397
Hydraulic Diam.(m)	1.04	0.51	0.51
Velocity X Diam.	8.97	4.42	8.97
Scale Ratio	2.032	2.032	1

3. Test Result

Since the actual model and the scale-down model of RE-053 satisfy all 5 conditions of sampling position approval condition (flow velocity, flow angle, particle distribution, trace gas distribution, tracer gas maximum value) of ANSI N13.1 (1999) it was suitable as a sampling location.

Geometric similarity was maintained, and the COVs of the actual model, flow velocity equal-scale model, and Reynolds number equal-scale model of 2.032: 1 were 4.6%, 5.3%, and 4.1% The validity of the scale model for the verification test was verified.

Comparing the experimental results for five sampling conditions, it was found that the scale model with the same Reynolds number had the similarity with the actual model.

Table 3. Test result

RE-053	Acceptance criteria	Actual	Scale down (V_{actual}=V_{scale})	Scale down (Re_{actual}=Re_{scale})
Flow angle(°)	< 20	3.6	9.7	9.3
Velocity COV(%)	< 20	4.6	5.3	4.1
Tracer gas COV(%)	< 20	2.3	2.3	3.2
Tracer gas COV_{Max}(%)	< 30	4.8	2.6	4.9
Particle COV(%)	< 20	11.9	16	12

4. Conclusion

To validate the latest standards, the radiation monitoring system of nuclear power plants was used to verify the validity of sampling location of one representative radiological survey.

We set up sampling locations according to the design requirements of ANSI-HPS N13.1 (1999) through CFD. The validity of the scale model was verified by preparing the actual model and the scale model for the reset sampling location.

The scale model proof test was carried out under the same conditions with the actual model at the same flow rate and the same Reynolds number. All three models were satisfied with the ANSI N13.1 (1999) code sampling location requirements.

REFERENCES

[1] ANSI/HPS N13.1-1999, “Sampling and Monitoring Releases of Airborne Radioactive Substances from the Stacks and Ducts of Nuclear Facilities”, American National Standards Institute and the Health Physics Society.

[2] 40 CFR 60, Appendix A, Method 1. “Method 1— Sample and Velocity Traverses for Stationary Sources.” Code of Federal Regulations, U.S. Environmental Protection Agency.

Impact of Operating Nuclear Power Plants to Decommissioning Workers

EunHee Lee and ChangLak Kim
KEPCO International Nuclear Graduate School, 658-91 Haemaji-ro, Seosaeng-myeon, Ulju-gun, Ulsan, Republic of Korea
eunilee@kings.ac.kr

1. Introduction

During the licensing phase of construction or operation, Domestic nuclear power plant operator should prove that if the radiation dose meet the dose criteria according to requirements of Article 16 (Prevention of Environmental Hazards) of Notification (Radiation 001. Standard for Radiation Protection) to protect the residents and the environment.

Likewise, it would be also important to evaluate the exposure dose to the dismantling workers in terms of protection of workers because the dismantling worker may be affected by the radiation effluents emitted from the nuclear power plant operated nearby.

In case of Kori Unit 1, Kori Unit 2 to 4 and Shin-Kori Unit 1&2 are adjacent in the same Kori site. Close to Kori site, there is Sae-wul site which include Shin Kori Unit 3&4 and Shin Kori 5&6 which is under construction now. Thus it is essentially required to evaluate the exposure dose to the decommissioning workers by operating multiple NPP units nearby.

2. Exposure dose calculation model

ENDOS program is used to calculate the exposure dose which was developed by KAERI based on NRC Regulatory Guide 1.109. Two of sub-programs of ENDOS are used in this assessment, ENDOS-ATM which performs atmospheric transport and diffusion assessments and ENDOS-G performs exposure dose assessment by gaseous radioactive emissions.

2.1 Exposure Pathways from gaseous effluents

The most of exposure pathway for the decommissioning workers is due to the gaseous emissions. There are three main considerations for exposure pathways for workers exposed to gaseous emissions: First, external exposures due to plume; second, external exposures due to the contaminated ground; and the last, internal exposures due to the inhalation of contaminated air. In case of workers, the consideration of contaminated food intake was neglected.

2.2 Assumptions

The decommissioning work will start after the 5 years after the permanent stop of Kori Unit 1 and the decommissioning worker assumed 8 hours of work per a day. Since the maximum individual dose in the ENDOS program is based on the residents who always present 24 hours therefore, one third of the evaluation value is used to evaluate the exposure dose to the decommissioning workers.

As the input data of the ENDOS-ATM program, the atmospheric meteorological data, which was used for the radiation environmental impact assessment for the construction permit of Shin-Kori 5&6, was applied. As the input date of the ENDOS-G program, the emissions of gaseous effluents from adjacent operating NPP was used for evaluation. This emission data, in case of the Kori Unit 2~4, it is based on the operating results from 2000 to 2009 and in case of Shin-Kori Unit 1~6, it is the estimated emission by PWR-GALE code.

3. Results

Atmospheric dispersion factors and deposition factors are obtained by using ENDOS-ATM depending on distance and direction between the Kori Unit 1 and each of the adjacent NPP units as summarized in Table1.

Table 1. Atmospheric dispersion factors and deposition factors

(Kori 1)	Direction	Distance (m)	x/Q (sec/m^3)	(x/Q)D (sec/m^3)	(x/Q)DD (sec/m^3)	D/Q (sec/m^3)
Kori2	WSW	100	1.31E-04	1.30E-04	1.28E-04	1.71E-07
Kori3	W	410	6.51E-06	6.49E-06	6.15E-06	1.51E-08
Kori4	W	660	2.75E-06	2.73E-06	2.53E-06	7.22E-09
Shin-12	SW	1225	1.65E-06	1.63E-06	1.46E-06	6.42E-09
Shin-34	SW	2720	4.49E-07	4.38E-07	3.75E-07	1.64E-09
Shin-56	SW	3035	3.79E-07	3.69E-07	3.13E-07	1.36E-09

To evaluate the maximum individual dose for decommissioning workers affecting by operating nearby NPP units, ENDOS-G program was used base on dispersion and deposition factors and the emissions gaseous effluents from each of the adjacent NPP units. In this paper, exposures only causing by plume, ground, and inhalation are considered. Table 2 summarizes this results. 8 hours of work per a day is assumed in this analysis.

Table 2. Maximum individual dose (mSv/yr)

exposure pathway	plume	ground	inhalation	Sum	Evaluation value
Kori2	3.66E-03	1.80E-04	5.16E-02	**5.54E-02**	**1.85E-02**
Kori3	1.38E-04	1.11E-07	4.67E-04	**6.05E-04**	**2.02E-04**
Kori4	5.07E-04	4.17E-06	3.01E-04	**8.12E-04**	**2.71E-04**
Shin-12	3.28E-03	8.07E-05	1.10E-03	**4.46E-03**	**1.49E-03**
Shin34	2.00E-04	1.39E-05	3.61E-04	**5.75E-04**	**1.92E-04**
Shin-56	1.64E-04	1.15E-05	3.04E-04	**4.80E-04**	**1.60E-04**

4. Conclusion

In 2023, decommissioning of Kori unit 1 will be started. In consideration of Kori 2 shutdown expected in 2023, we could consider only the impacts of Kori 3,4 and Shin-Kori 1~6. As a result, the annual maximum individual dose of the decommissioning workers is estimated to be 2.31E-03mSv/yr and it is insignificant compared to the effective dose limit of 1mSv/yr.

ACKNOWLEDGEMENT

This research was supported by the Nuclear Safety Research Program through the Korea Foundation of Nuclear Safety (KOFONS), granted financial resource from the Nuclear Safety and Security Commission (NSSC), Republic of Korea (No.1605008).

REFERENCES

[1] KHNP, “Environmental Impact Assessment Report for Construction of Shin-Kori Unit 5,6” (2016).

[2] KAERI, “Environmental Impact Assessment around Nuclear Facilities”, KAERI/RR-3327 (2001).

Tritium Release Under Unlikely and Extremely Unlikely Loading Condition of the HCCR TBS at PD-1 Phase

Hyung Gon Jin [a*], Dong Won Lee [a], Jae Sung Yoon [a], Suk Kwon Kim [a], Eo Hwak Lee [a],

Seong Dae Park[a], Chang Wook Shin[a], and Seungyon Cho[b]

[a]Korea Atomic Energy Research Institute, Daedeok-daero989ben-gil 111,Yuseong-gu, Daejeon, Republic of Korea

[b]National Fusion Research Institute, 169-148, Gwahak-ro, Yuseong-gu, Daejeon, Republic of Korea

jhg@kaeri.re.kr

1. Introduction

Korea has developed a Helium Cooled Ceramic Reflector (HCCR) TBS which will be installed to the ITER [1]. It consists of two major loops, which are HCS (Helium Cooling System) and TES (Tritium Extraction System) (Fig. 1). And these systems should demonstrate safety in various operating situations. Tritium is one of the most highly permeable molecule on earth, therefore, tritium permeation takes place from HCCR TBS. This paper presents a tritium release input data set of unlikely and extremely unlikely loading condition for the HCCR TBS, assumption of the estimation and boundary conditions.

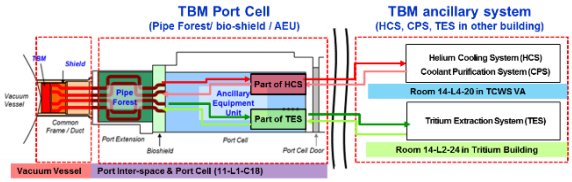

Fig. 1. Schematic Diagram of HCCR TBS.

2. Assumptions

To estimate the tritium release under unlikely and extremely unlikely loading condition followings were assumed.

-Tritium production is given by neutronics calculation. (No extra tritium flux from plasma)

-Continuous back to back plasma pulse with duty factor 0.25.

-Steady state condition (instantaneous tritium diffusion to the purge gas isotropically)

-Averaged tritium generation rate (constant over the time and uniform in the TBM volume)

-Transport mechanism through structural materials is bulk diffusion.

-Tritium concentration in space is constantly zero to estimate conservative release rate.

-Averaged temperature and pressure for each region

3. ITER Loading Conditions

ITER loading conditions are categorized into the following four classes based on the expected frequency of occurrence.

Table 1. ITER Loading Conditions

Category	Description
I	Operational Loading Conditions
II	Likely Loading Conditions
III	Unlikely Loading Conditions
IV	Extremely Unlikely Loading Conditions

4. Boundary Conditions

Boundary condition of this estimation is given in the Table 2.

Table 2. Summary of boundary condition

Tritium Production Rate	25.9 mg/day (continuous back to back with duty 0.25)
PI/PC Volume	280.264 m^3
TCWS VA Volume	500 m^3 (considering occupied by HCCR HCS/CPS)
TES Pipe Thickness	3.68 mm
HCS Pipe Thickness	8.56 mm (Vertical shaft pipe thickness 8.56 mm)
BZ Pipe Thickness	4.0 mm
N-DS at PI/PC	40 m^3/h
HVAC at TCWS	1 Vol/hr, i.e. 500 m^3/h

5. Results

Fig. 2 is pipe length and operational temperature information of each room which HCCR-TBS is allocated. Design of HCCR-TBS is evolving and this data reflects recent update of PD-1 phase.

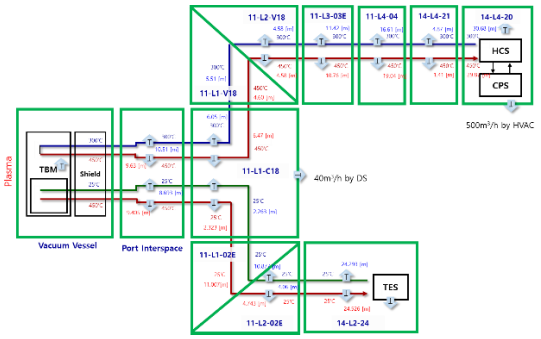

Fig. 2. Pipe length and temperature of HCCR-TBS.

6. Results

This result is outcome of input data set for the ITER Connection Pipe System Design Document, which contains total activity(Bq) of each location and amount of tritium(mg) for unlikely and extremely unlikely loading conditions of the HCCR TBS. At the PD-1 stage, it is conservatively assumed that tritium in pipes completely releases during unlikely and extremely unlikely loading. Amount of tritium highly depends on operating temperature of pipes in each room.

Table 3. Summary of tritium total activity

TBS sub-system	Function	Rooms	Total Activity (Bq) / Amount of tritium (mg) for unlikely and extremely unlikely loading conditions
HCS	Inlet	11-L1-C18	2.71E+09/7.53E-03
		11-L1-V18	2.46E+09/6.86E-03
		11-L2-V18	2.05E+09/5.71E-03
		11-L3-03E	5.11E+09/1.42E-02
		11-L4-04	7.43E+09/2.07E-02
		14-L4-21	2.18E+09/6.07E-03
		14-L4-20	1.37E+10/3.82E-02
	Outlet	11-L1-C18	2.29E+09/6.39E-03
		11-L1-V18	1.63E+09/4.54E-03
		11-L2-V18	1.62E+09/4.52E-03
		11-L3-03E	3.81E+09/1.06E-02
		11-L4-04	6.75E+09/1.88E-02
		14-L4-21	5.00E+08/1.39E-03
		14-L4-20	1.06E+10/2.95E-02
TES	Inlet	11-L1-C18	2.04E+10/5.68E-02
		11-L1-02E	9.80E+10/2.73E-01
		11-L2-02E	3.66E+10/1.02E-01
		14-L2-24	2.19E+11/6.10E-01
	Outlet	11-L1-C18	2.09E+10/5.83E-02
		11-L1-02E	9.92E+10/2.76E-01
		11-L2-02E	4.27E+10/1.19E-01
		14-L2-24	2.21E+11/6.15E-01

7. Conclusion

Total activity and tritium amount have been estimated. Design of the HCCR TBS is evolving, therefore, this input data set will be revisited at PDR and FDR phase.

8. Acknowledgement

This work was supported by the R&D Program through the National Fusion Research Institute (NFRI) funded by the Ministry of Science and ICT of the Republic of Korea (NFRI-IN1803).

REFERENCE

[1] D.W. Lee, et. al., “Current Status and R&D Plan on ITER TBMs of Korea,” Journal of Korean Physical Society, 49 S340-S344 (2006).

Vacuum Suction Force Analysis of Concrete Wall Climbing Device for Dry Cask Storage System

Kyoung Won Yoon, Jin Yoo, Misuk Jang, and Seoung Rae Kim

Nuclear Engineering Service & Solution Co., Ltd., 96, Gajeongbuk-ro, Yuseong-gu, Daejeon, Republic of Korea

kwyoon@ness.re.kr

1. Introduction

Sensor transport system(SeTS) is the wall climbing instrument developing to inspect the defects of dry cask storage system(DCSS) wall. Fig. 1 shows the conceptual frame design of SeTS. It is composed of main frame, driving axle connected with electric motor, impeller connected with adsorptive motor, impeller generating negative pressure, lower chamber connected with impeller, seal generating flexibility to contact with the ground, and etc.

Important factors to decide adsorption force of SeTS in these block diagram are the shape and discharge of impeller, a lower chamber shape of impeller, and etc. Therefore, an impeller and a lower chamber of impeller were selected as the calculation area in this analysis. The analysis conditions were selected in consideration of the suction motor specification and the lower chamber of impeller was simulated in the flow range with the highest efficiency of the impeller.

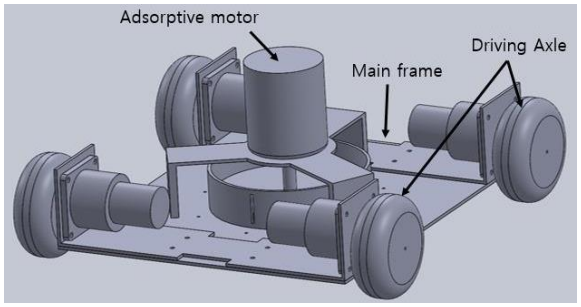

Fig. 1. Shape of SeTS.

2. Governing Equation and Calculation Method

We use ANASYS CFX 17.0, which is commercial CFD program based on FVM(Finite Volume Method) in order to get the solution of RANS governing equation.

Continuity equation and momentum equation about 3-dimensional incompressible and normal turbulence flow are as below.

- Continuity equation

$$\frac{\partial U_i}{\partial x_i} = 0 \tag{1}$$

- Momentum equation

$$U_j \frac{\partial U_i}{\partial x_j} + \frac{\partial (\overline{u_i' u_j'})}{\partial x_j} + \frac{\partial p}{\partial x_i} - \frac{1}{Re} \nabla^2 U_i = 0 \tag{2}$$

In this analysis, we used $k-\epsilon$ model among generally 2-equation turbulence models and set the the convergence condition of the solution to the residual 10^{-4}.

3. Analysis Condition and Boundary Condition

The analysis conditions were selected in consideration of the fiducial discharge for centrifugal impeller with highest lift compared to discharge. The shape of lower chamber of impeller was assumed that a fluid enters through the lower intake of 5mm and exits through outlet of impeller. In the future, we plan to derive the optimized shape through experiments. The fluid passing through centrifuge impeller was assumed to be a standard air.

Details of analysis and boundary conditions are given in Table 1 and Table 2.

Table 1. Analysis conditions

Input Item	Value
Mass flow rate [kg/s]	0.0198
Rotational speed [RPM]	7600
Outlet diameter of Impeller [mm]	130
Inlet diameter of Impeller [mm]	20
Number of blade [EA]	10
Gap between the floor and chamber [mm]	5

Table 2. Boundary conditions

Working fluid	Air
Inle	Total pressure
Outlet	Mass flow rate
Turbulent closure	$k-\epsilon$model
Interface area	Frozen-rotor
Wall	No-slip

4. Result of Analysis

Fig. 2 shows the inflow velocity vector of an impeller. As shown in the figure, pressure drop occurs at the inlet of impeller and the impeller rotation speed increases. And the flow field inside the impeller generates a complex recirculation flow and vortex due to the rapid rotation of the impeller.

Fig. 3 shows the pressure distribution in the axial center section to confirm the flow characteristics of the impeller. As shown in the figure, the lower and upper chamber are constant at atmospheric pressure, while the pressure is gradually lowered toward the impeller exit portion.

The force applied to the lower part of the impeller by using the pressure and area derived from this analysis result is about 7.8kgf. Therefore, SeTS can deliver mounting up to 3.8kg of sensors and accessories excluding device to inspect the inner surface of dry storage cask wall.

5. Conclusion

In this paper, we have examined the capacity of SeTS equipped with some sensors and accessories and climbing the walls using CFD code.

As a result, the impeller with 10 blades, 7,600 rpm speed and 0.0198kg/s flow rate was evaluated to be able to mount up to 3.8kg excluding device when the gap between the wall surface and chamber is 5mm. If sensors and accessories are determined in the future, the final design will be carried out through additional analysis that reflects these conditions. And the final SeTS will also be designed to operate under high temperature and high radiation conditions.

ACKNOWLEDGEMENTS

This work was supported by the Korea Institute of Energy Technology Evaluation and Planning(KETEP) and the Ministry of Trade, Industry & Energy(MOTIE) of the Republic of Korea(No.201715201017800).

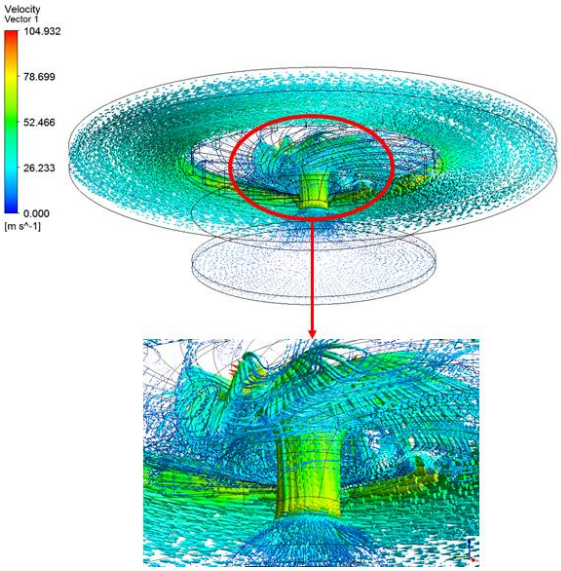

Fig. 2. Distribution of Pressure in Chamber of SeTS.

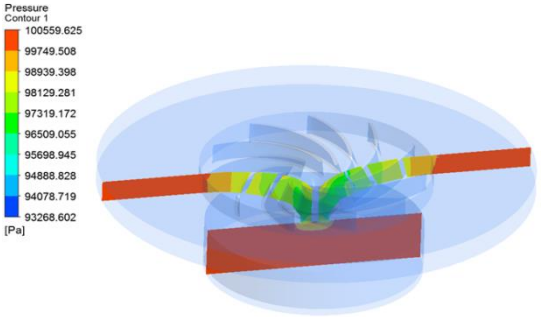

Fig. 3. Distribution of Pressure in the Chamber of SeTS.

6. References

[1] Dong chul Choi, A study on the tip clearance effect of the suction fan for a NDT robot, Master degree thesis, May 2014, Hanyang University.

[2] Choon-Man Jang, Performance Analysis for Turbo Blower According to Inlet-Vane Angles, December 2010.

[3] Jeong, Seon Yong, Optimum design and performance of marine sea water pump with impeller using CFRP. Journal of the Korea Academia-Industrial cooperation Society, November 30, 2015.

[4] Myung Seok, Kim, A Study on the Design and performance Analysis of Horizontal Single Suction Centrifugal Pump by CFD, Master degree thesis, February 2006, Korea Maritime and Ocean University.

Estimated Activity of CPP Wastewater and Radioactivity of Evaporative Concentrates

Ki Bang Sung
KHNP Central Research Institute, 70, 1312-gil, Yuseong-daero, Yuseong-gu, Daejeon, Republic of Korea
kind.sung@khnp.co.kr

1. Introduction

When the CPP regenerated waste solution is evaporated under reduced pressure, the gaseous radionuclides and tritium are not concentrated, but the other ionic and particulate gaseous species are condensed together with the non-fugitive renewable wastewater component during the decompression of the CPP regeneration wastewater.

To examine the concentration effect of CPP regeneration wastewater, the expected radioactivity concentration of the CPP wastewater was calculated from the secondary system radioactivity concentration based on the FSAR data of A nuclear plant, and the actual concentration of CPP wastewater was concentrate to analyze the radioactivity and compared to each other.

2. Experimental Methods

2.1 Experimental Apparatus

The apparatus used in this experiment is shown in Fig. 1.

Fig. 1. Experimental Apparatus.

2.2 Purification System of Condensate

Recycled wastes are collected in the condensate purification plant drainage and then transferred to the integrated wastewater treatment plant. If the radioactivity level of the CPP drainage wastes exceeds the high alarm set point(0.365 Bq/cm^3), the waste is transferred to the liquid radioactive waste system. That is, the radioactive liquid wastewater is treated in the radioactive waste treatment system and ~~does~~ not leaked out.

2.3 Expected radioactivity of CPP regeneration wastewater

In the operating NPP, the blowdown ~~estimated~~ radioactivity is estimated assuming the design leakage rate of the SG tubing during normal operation, and the equilibrium radionuclide concentration of the liquid phase and main steam of the secondary side cooling water in the steam generator is calculated considering the radioactivity concentration of the primary system water and the permissible leakage rate .

In the case of the a nuclear power plant, the design leakage rate from the primary side to the secondary side through the steam generator tube is assumed to be 34 kg / day

2.4 Expected radioactivity of CPP regeneration wastewater

The radioactivity of the CPP regeneration

wastewater is calculated from using about 32 m^3 of 6% sulfuric acid solution and then a dilution water of 120 m^3 or more is used.

During the regeneration, all the radioactive materials contained in 8 m^3 of the cation resin are transferred to the regeneration waste water of 32 m^3. Thus, the radioactive material is diluted from 8 to 32 to about 4 times

If the radioactive material is again concentrated by evaporation under reduced pressure, 32 m^3 will be concentrated to 20 times and the radioactive material will be present in the solid matter of about 1.6 m^3.

Therefore, the radioactive material after the decompression evaporation is finally converted from 8 m^3 to 1.6 m^3, which is about 5 times higher than the concentration in CPP wastewater.

That is, the Cs-137 nuclide in the reduced-pressure evaporation dried product, assuming no leakage of the coolant but assuming leakage, is about 0.7 Bq/cc.

Table 1. Estimated activity by equipment and flow path in the secondary chemical control system

nuclide	SG Blowdown (Bq/g)	Condensate (Bq/cc)	CPP Cation IX (Bq/cc)	Dried Waste (Bq/cc)
Cs-134	6.1E-03	1.4E-05	1.0E-01	5.0E-01
Cs-137	8.1E-03	1.9E-05	1.4E-01	7.0E-01
Co-58	3.4E-03	3.1E-06	2.3E-02	1,4E-02
Co-60	3.9E-04	3.5E-07	2.7E-03	8.5E-03
SUM	5.7E-02	1.2E-04	3.1E-01	1.5E+00

3. Results and Discussion

3.1. Result of radioactivity measurement of Residual CPP waste

The radioactivity of the sample was measured for the same 10,000 seconds. The reason for the measurement for 10,000 seconds is that the power plant usually measures about 3000 seconds to check the radioactive contamination at the time of discharge, so it is about 3 times more to reduce the uncertainty of the measurement and to make a clear

First, the background radioactivity was measured, and then the decompressed volatile solids of a nuclear power plant were measured.

As a result of the measurement, the background radioactivity measurement spectrum showed a little 1461 keV peak emitted from the K-40 natural radioactivity in the spectrum.

Table 2. Activity of A plants CPP waste concentrates

Detector Name: DET01
Sample Title: 신고리2호기 CPP 농축액
Peak Analysis Performed on: 2016-11-09 8:49:39 AM
Peak Analysis From Channel: 50
Peak Analysis To Channel: 8192

Peak No.	ROI start	ROI end	Peak centroid	Energy (keV)	FWHM (keV)	Net Peak Area	Net Area Uncert.	Continuum Counts
1	366-	376	370.71	92.63	1.26	1.20E+002	20.56	1.25E+002
2	740-	753	744.30	185.87	0.86	6.64E+001	21.45	1.41E+002
3	951-	960	955.71	238.64	0.74	4.59E+001	13.65	7.01E+001
4	2036-	2056	2047.21	511.06	0.34	1.96E+002	18.85	5.77E+001
5	2434-	2447	2441.30	609.42	0.53	3.99E+001	10.07	2.81E+001
6	5844-	5862	5853.51	1461.05	1.81	1.34E+002	13.14	1.71E+001

4. Conclusion

In the radioactive measurement spectrum of decompressed evaporated water samples, only K-40 natural radioactivity was detected. That is, the spectrum of the dried sample was almost identical, no specific peak indicating the presence of the nuclide was observed, and no detectable gamma ray emitting nuclide was detected at the time of operation.

The Determination of Depth Distributions of Radioactive Cesium in the Ground Using In Situ Gamma-Ray Spectrometry

Young-Yong Ji[*,1], Taehyung Lim[2], Kun Ho Chung[1], Mun Ja Kang[1], and Wanno Lee[1]

[1] Korea Atomic Energy Research Institute, Daedeok-daero989ben-gil 111,Yuseong-gu, Daejeon, Republic of Korea

[2] SI Detection Co. Ltd., 21, Yuseong-daero 1628beon-gil, Yuseong-gu, Daejeon, Republic of Korea

yyji@kaeri.re.kr

1. Introduction

In general, the depth distribution of deposited nuclides should be first determined to evaluate their radioactivities in the ground. After sampling by the depth in the ground, its analysis can make the depth profile of deposited nuclides. However, this sampling method has some drawbacks about time and cost. To overcome it, in situ measurements with specific algorithms and hardware, which means multiple photopeaks, peak-to-valley, and collimation method, have been using to estimate the depth distribution of nuclides in the ground. However, these approaches have also certain limitations, such as multiple gamma-rays from a nuclide and multiple measurements with and without collimators and lead plates.

In this study, a simple method to estimate the depth distributions of nuclides was developed by calculating the individual dose rate of detected gamma nuclides at 1 m above the ground. The dose rate spectroscopy [1-3] was then used to previously determine the individual dose rate of ^{137}Cs from the measured energy spectrum using a portable HPGe detector. In addition, theoretical individual dose rates of ^{137}Cs at 1 m above the ground were calculated by assuming several depth distributions of ^{137}Cs in the ground. The real depth distribution of ^{137}Cs was determined from the comparison between them. Finally, its radioactivity in the ground was then calculated by applying the dose conversion factor in the unit of nGy/h/Bq/m^2 in the condition of the determined depth distribution.

2. Method and Results

2.1 Depth distribution

As a parameter to determine the exponential depth profile of deposited nuclides in the ground, the parameter β, which means relaxation mass per unit area (g/cm^2), is used as shown in Fig. 1. The relaxation length, λ, means the depth with a relative source intensity of 37 % from the maximum intensity of deposited nuclide. Therefore, a parameter β is the multiplication of the relaxation length and soil density, as assuming the density of soil is constant in the ground. In general, natural radionuclides are assumed to be uniform intensity by the depth, so that they have an infinite value of β. On the other hand, the recent fallout has a zero value of β, because of its distribution only in the surface of the ground. As time passes, the value of a parameter β increases to reflect the exponential depth profile of deposited nuclides.

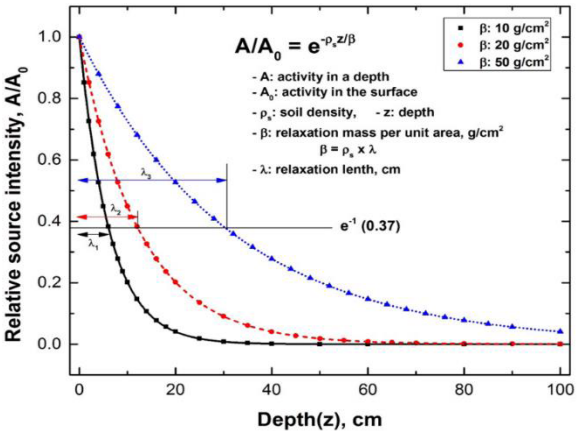

Fig. 1. The exponential depth profile of deposited nuclides.

2.2 Radioactivity and dose rate of deposited nuclides

In general, the radioactivity of deposited nuclides in the ground can be calculated from the measured count rate using in situ gamma-ray spectrometry at general 1 m height from the ground and the in situ calibration factor, as shown in Eq. (1). The dose rate due to the deposited nuclide at 1 m above the ground is then calculated from the dose conversion factor by the nuclide, as shown in Eq. (2). The in situ

calibration factor and dose conversion factor greatly depends on the parameter β, although they can be calculated from the Monte Carlo simulation. Fig. 2 shows an example of in situ calibration factor and dose conversion factor according to the parameter β.

$$A_i = \frac{(n')_E}{\left(\frac{n'}{A_\gamma}\right)_E \times \gamma_E} \quad (1)$$

$$\dot{X}_i = A_i \times d_i \quad (2)$$

where, A_i and $\dot{X}_i$ are the radioactivity in the ground and dose rate at 1 m above the ground of a nuclide, $(n')_E$ and γ_E are the measured count rate of photons with an energy E and its emission probability, $(n'/A_\gamma)_E$ is the in situ calibration factor to convert the net count rate into radioactivity, and d_i is the dose conversion factor from radioactivity in the ground to dose rate at 1 m height.

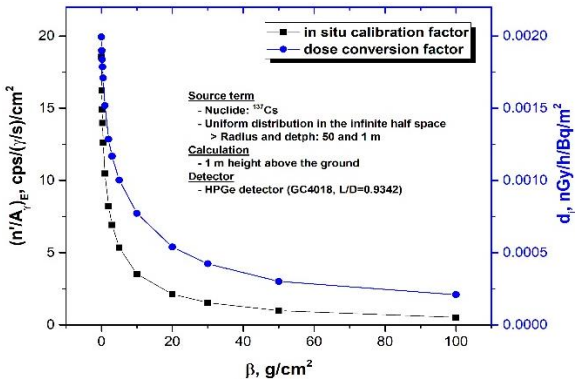

Fig. 2. The calculated in situ calibration factor and dose conversion factor of ^{137}Cs.

2.3 Determination of a parameter β

In this study, the net count rate of ^{137}Cs in the ground was first calculated, which was measured using a portable HPGe detector at 1 m above the ground in Jeju Island. From Eqs. (1) and (2), its radioactivities and dose rates according to the parameter β, as shown in Fig. 3, were calculated by applying values of in situ calibration and dose conversion factors in Fig. 2. Second, the dose rate of ^{137}Cs was then calculated using dose rate spectroscopy, by converting the measured energy spectrum for count rate into one of dose rate. The result was 1.31 nGy/h and compared with ones from Eq. (2). As a result, the parameter β of deposited ^{137}Cs in the ground was determined to be about 6.16 g/cm^2. This means the same value of dose rate of ^{137}Cs was shown at both methods in the case of selecting parameter β of 6.16 g/cm^2. Finally, the radioactivity of ^{137}Cs was analyzed to be about 1382 Bq/m^2 by using the in situ calibration factor in the condition of the determined parameter β.

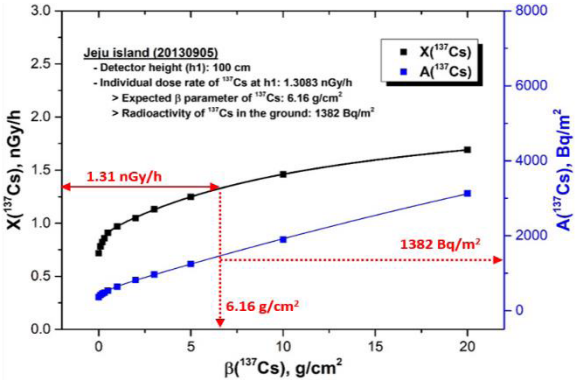

Fig. 3. The calculation of a parameter β and radioactivity of deposited ^{137}Cs.

3. Conclusion

To determine the depth profile of a deposited nuclide in the ground using in situ gamma-ray spectrometry, a simple method was developed by introducing the dose rate spectroscopy. The method was successfully applied to the measured energy spectrum using a portable HPGe detector in Jeju Island.

ACKNOWLEDGMENTS

This work was performed under the auspices of the Ministry of Science and ICT of Korea, NRF contract No. NRF-2017M2A8A4015256.

REFERENCES

[1] Ji YY, Chung KH, Lee W, Park DW, Kang MJ, "Feasibility on the spectrometric determination of the individual dose rate for detected gamma nuclides using the dose rate spectroscopy", Radiat. Phys. Chem. 97, 172-177, (2014).

[2] Ji YY, Chung KH, Kim CJ, Kang MJ, Park ST, "Application of the dose rate spectroscopy to the dose-to-curie conversion method using a NaI(Tl) detector", Radiat. Phys. Chem. 106, 320-326, (2015).

[3] Ji YY, Kim CJ, Chung KH, Choi HY, Lee W, Kang MJ, Park ST, " In situ gamma-ray spectrometry in the environment using dose rate spectroscopy", Radiat. Phys. Chem. 119, 90-102, (2016).

7분과

방사화학 (Oral)

What are Required for Ensuring the Safe Disposal of Radioactive Wastes?

Sol-Chan Han, Yongheum Jo, and Jong-Il Yun

Department of Nuclear and Quantum Engineering, KAIST, 291 Daehak-ro, Yuseong-gu, Daejeon, Republic of Korea

jiyun@kaist.ac.kr

Placing a repository of spent fuel and/or high-level radioactive waste at depth in a long-term stable geological environment has been regarded as one of the most appropriate disposal methods. Usually, a deep geological repository is equipped with the multi-barrier system, namely canister, buffer, and geological overrock to prevent the radioactivity release into the biosphere and to protect human and environment.

Over the past decades, much efforts have been devoted to improve the disposal safety of radioactive waste repositories. Up to now, a number of researches have been conducted by not only fundamental and practical experiments to understand the migration behavior of radionuclides, but also the development of THMC (Thermo-Hydro-Mechanical-Chemical) coupled models to assess the safety of radioactive waste disposal.

Even though numerous studies have shed light on the field, a number of concerns remain still unclear. For instance, a sophisticated understanding on chemical behaviors related to the retention and migration of radionuclides including transuranics in natural aquatic environments, such as complexation with various inorganic/organic ligands, redox process, sorption, colloid formation, etc. is still challenging. Furthermore, detailed geochemical processes of radionuclides are to be implemented in a numerical simulation approach for safety assessment [1]. Besides, the in-depth knowledge about the radionuclide retention mechanism of highly mobile anionic species, such as I^-, HCO_3^-/CO_3^{2-}, TcO_4^-, and Cl^- should be gained and improved for enhancing the disposal safety.

The presentation will review the state of knowledge and requirements for the safe disposal of radioactive wastes. The following three topics are mainly covered in the talk: i) the brief review of the chemical thermodynamics of transuranic elements [2], ii) the safety assessment methods reinforcing the reliability of numerical models conjugated with complementary indicators [3], and iii) highly mobile anions such as $C(IV), Tc(-I/VII), I(-I/VII), Se(-I/IV)$ and the engineered strategy for mitigating their mobility in subsurface environments.

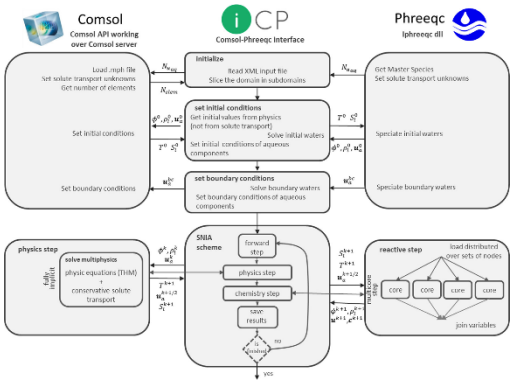

Fig. 1. Numerical model interfaces between COMSOL and PHREEQC [1].

REFERENCES

[1] A. Nardi, A. Idiar, P. Trinchero, L. M. de Vries, and J. Molinero, “Interface COMSOL-PHREEQC (iCP), an efficient numerical framework for the solution of coupled multiphyscis and geochemistry”, Computers & Geosciences, 69, 10-21 (2014).

[2] H. Geckeis and T. Rabung, “Actinide geochemistry: From the molecular level to the real system”, Journal of Contaminant Hydrology, 102, 187-195 (2008).

[3] D.-A. Becker, J.-L. Cormenzana, A. Delos, L. Duro, J. Grupa, J. Hart, J. Landa, J. Marivoet, L. Orzechowski, T.J. Schröder, A. Vokal, J. Weber, E. Weetjens, and J. Wolf, “Safety and Performance Indicators”, Deliverable 3.4.2 of the European Commission, PAMINA Project (2009).

DFT Study on the U(IV)-PNPP Complex in Water

Keunhong Jeong[a], Wansik Cha[b] , and Kyungwon Kwak[c,d*]

[a]Department of Chemistry, Korea Military Academy, Seoul, South Korea

[b]Nuclear Chemistry Research Division, Korea Atomic Energy Research Institute, Daejeon, Republic of Korea

[c]Center for Molecular Spectroscopy and Dynamics, Institute for Basic Science (IBS), Seoul, Republic of Korea

[d]Department of Chemistry, Korea University, Seoul, Republic of Korea

kkwak@korea.ac.kr

1. Introduction

Since the toxicity of U(IV) has been considered as a potentially hazardous element in the environment, understanding U(IV) chemistry is important for the treatment of the nuclear waste.

Research has been focused on the fate of U(IV) in environmental chemistry in order to manage and remediate U-contaminated sites[1].

Therefore, the molecular level study on the structures and processes in the overall behavior of U(IV) has been investigated. Both experimental and theoretical studies have discussed complexation with various ligands[2]. However, para-Nitrophenylphosphate (PNPP) was not dealt with U(IV) in complexation study even though PNPP is one of the important substrates for phosphate binding chemistry at mineral-water interfaces and spectrophotometric biochemical assays[3].

Computational chemistry is a great complement to experimental studies of U(IV) chemistry because this methodology provides valuable information that is not available through the experiment, especially for transient materials and those with short kinetic times[4]. Herein, we performed the quantum calculation study on the complexation between U(IV) and PNPP to investigate several important chemical properties of the U(IV)-PNPP complex in water.

2. Quantum calculation on U(IV)-PNPP

2.1 Computation details

The B3LYP functional was utilized for geometry optimization at gas phase with tight energy and geometry convergence criteria without symmetry constraint. The ECP60MWB relativistic effective core potential and its associated basis set, which was developed by the Stuttgart-Cologne group, was chosen for describing Uranium and 6-31G(d) is used for P, N, O, C, and H. After the optimization, frequency calculation was performed and local minimum structure was confirmed by checking all positive frequencies. Those theoretical calculations were performed using Gaussian 09 packet.

2.2 Optimized Structures

Optimized structure of U(IV) ion in water was described with 8 and 9 water molecules (Fig. 1) [5]. Two water molecules of stable structures, $U(H_2O)_8^{4+}$(IV) and $U(H_2O)_9^{4+}$(IV), were exchanged by $PNPP^-$, respectively. Each complex was optimized in order to obtain the structure of U(IV)-PNPP complex in water. And then, the most stable spin state of the complex was found after calculating the energies of possible spin states (Fig. 2).

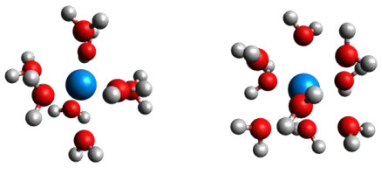

Fig. 1. Optimized structures of U(IV) ion in water.

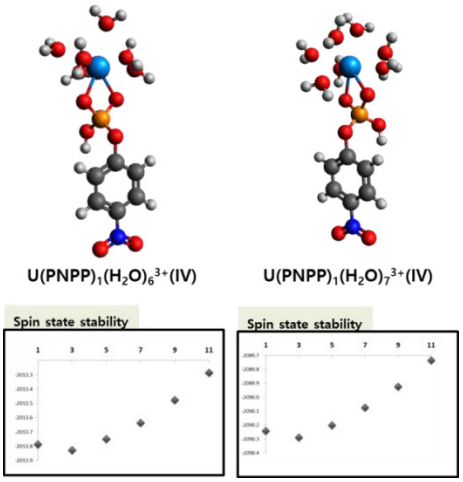

Fig. 2. Optimized structures of U(IV)-PNPP complex in water and energies of possible spin states in each complex.

2.3 Predicting Infrared Spectra

In each structure of U(IV)-PNPP complexes, Infrared spectrum was calculated by frequency calculation. And each complex shows the discernible signals (Fig. 3).

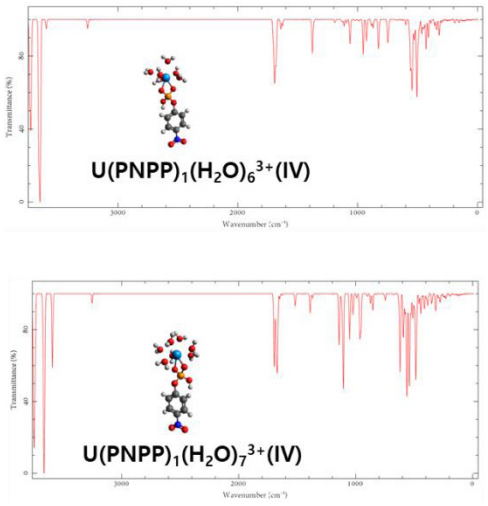

Fig. 3. Predicted infrared spectra for U(IV)-PNPP complexes in water.

3. Conclusion

Herein, we performed theoretical studies to obtain several important chemical properties of U(IV)-PNPP complex in water including their stable structures, spin state, and infrared spectra. This computational study may be a firm basis for the future applications on environmental researches of U(IV) and actinide chemistry in water.

4. Acknowledgment

This research was supported by the Nuclear Research and Development Program of the National Research Foundation of Korea [Grant No. NRF-2017M2A8A5014719].

REFERENCES

[1] S. E. Bonea, J. J. Dynes, J. Cliffc, and J. R. Bargar , “Uranium(IV) adsorption by natural organic matter in anoxic sediments”, Proceedings of the National Academy of Sciences of the United States of America, 114(4),711-716 (2017).

[2] D. E. Latta, B. Mishra, R. E. Cook, K. M. Kemner, and M. I. Boyanov, “Stable U(IV) Complexes Form at High-Affinity Mineral Surface Sites”, Environmental Science & Technology, 48(3), 1683-1691 (2014).

[3] S. J. Smith, A. Casellato, K. S. Hadler, N. Mitić, M. J. Riley, A. J. Bortoluzzi, B. Szpoganicz, G. Schenk, A. Neves, L. R. Gahan, “The reaction mechanism of the Ga(III)Zn(II) derivative of uteroferrin and corresponding biomimetics”, Journal of Biological Inorganic Chemistry, 12(8), 1207-1220 (2007).

[4] J. D. Kubicki, G. P. Halada, P. Jha and B. L. Phillips, “Quantum mechanical calculation of aqueuous uranium complexes: carbonate, phosphate, organic and biomolecular species”, Chemistry Central Journal, 3:10 (2009).

[5] S. Tsushima, T. Yang, “Relativistic density functional theory study on the structure and bonding of U(IV) and Np(IV) hydrates”, Chemical Physics Letters 401, 68–71 (2005).

First Principles Computational Studies of Spontaneous Reduction Reaction of Eu(III) in Eutectic LiCl-KCl Molten Salt

Choah Kwon[1], Seung Hyo Noh[1], Hoje Chun[1], Il Soon Hwang[2], and Byungchan Han[1*]

[1]Department of Chemical and Biomolecular Engineering, Yonsei University, Seoul 03722, Republic of Korea

[2]Department of Energy Systems Engineering, Seoul National University, Seoul 08826, Republic of Korea

kwonchoah@gmail.com, bchan@yonsei.ac.kr*

1. Introduction

Using first principles calculations, we study fundamental mechanism of spontaneous reduction reaction of Eu^{3+} to Eu^{2+} in eutectic LiCl-KCl molten salt. We decouple the reaction Gibbs free energy into enthalpy and entropy contributions using rigorous thermodynamic formalism. Key structural features of the solvation shell are characterized by the radial distribution function (RDF) and the coordination number. Compared to Eu^{2+} the Eu^{3+} ion has a more rigid framework of the solvation shells, corroborating its stronger electrostatic interaction with neighboring ligands of Cl^- ions and a more favorable state on the aspect of enthalpy. Computations on vibrational frequency, however, pose significant contribution of vibrational entropy to the reaction Gibbs free energy for the reduction. Vibration frequency of Eu^{2+} is smaller than that of Eu^{3+}, driving a more positive change of the entropy in the reduction reaction. Furthermore, an Eu^{2+} diffuses more quickly than an Eu^{3+} in the LiCl-KCl molten salt with switching mechanism of ligand Cl^- ions in the solvation shell. Our results propose that the spontaneity of the reduction reaction is driven by the entropic contribution by overcoming the penalty of the reaction enthalpy.

2. Computation Methods

All the simulations were calculated using Vienna Ab-initio Simulation Package (VASP) based on the plane wave basis sets with 500 eV cut-off energy. The generalized gradient approximation (GGA) with the Perdew-Burke-Ernzerhof (PBE)[1] was used as exchange correlation functional and the projected augmented wave (PAW) potential[2] was utilized to substitute core electrons of Li, K, Cl and Eu. Ab-initio molecular dynamics (AIMD) simulations were performed in the canonical ensemble with a Nosè-Hoover thermostat[3] conditions fixing total number of atoms (N), volume (V) and temperature (T). To distinguish the Eu^{2+} and Eu^{3+}, GGA+U parameters were obtained, which are -12 and 2 eV. The model systems were constructed as shown Fig. 1.

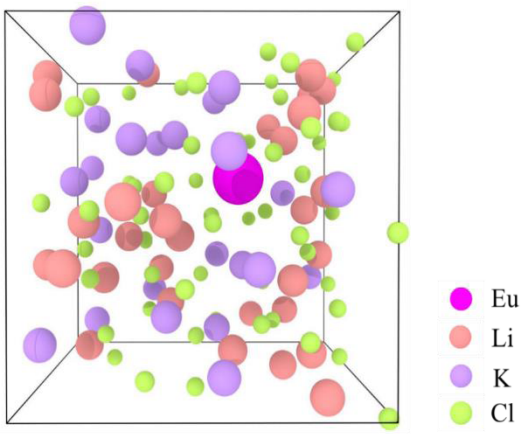

Fig. 1. Model system.

LiCl-KCl molten salt were packed in a 15^3 Å^3 cubic cell based on eutectic composition and density. To describe the Eu^{2+} (Eu^{3+}), $EuCl_2$ ($EuCl_3$) were added in the cubic cell, respectively.

3. Results and Discussion

$$Eu^{3+}(LiCl-KCl)+Cl^-(LiCl-KCl)\rightarrow Eu^{2+}(LiCl-KCl)+\frac{1}{2}Cl_2(g) \quad (1)$$

Gibbs free energy of reaction (1) was decoupled

into enthalpic and entropy contributions. Entropic contributions were confirmed by the results of AIMD simulations.

3.1 Structure of solvation shell

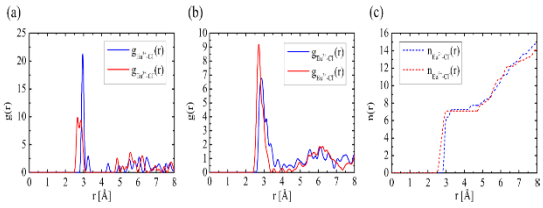

Fig. 2. The figure (a) indicates RDFs at 5 ps and the figure (b) does average RDFs that 10 samples were selected from 4 ps to 5 ps with interval of 0.1 ps. The coordination numbers of $Eu^{2+/3+}$ at 5 ps are shown in (c). Blue and red lines denote those of Eu^{2+} and Eu^{3+}, respectively.

Solvation shells of Eu^{2+} and Eu^{3+} in a LiCl-KCl molten salt were calculated. The solvation shell of Eu^{3+} was more rigid than that of Eu^{2+} becasue of stronger electrostatic interaction betweeen Eu^{3+} and Cl^-.

3.2 Vibrational frequency

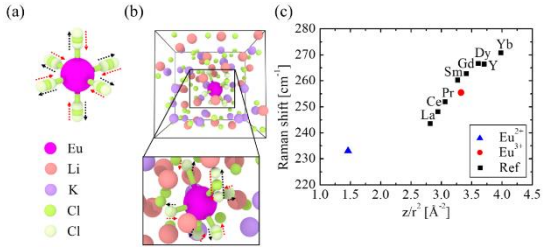

Fig. 3. Vibration mode of MCl_6 (M=Eu^{2+} and Eu^{3+}) complex in (a) vacuum and (b) molten salt. (c) Vibration frequencies of various rare-earth elements in a molten salt.

Vibration frequencies of α_{1g} mode for Eu^{2+} and Eu^{3+} were calculated. As the vibration frequency get increase, which means stronger electrostatic interactions with Cl^- ions, the entropy becomes smaller. Based on the results, the entropy of the reaction (1) is positive because Eu^{3+} has stronger electrostatic interaction with molten salt.

3.3 Diffusion coefficients of Eu^{2+} and Eu^{3+}

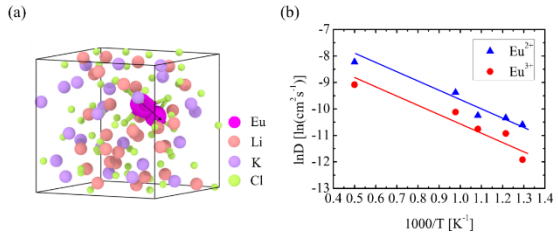

Fig. 4. (a) Diffusion mechanism of Eu ions in LiCl-KCl molten salt. (b) Diffusion coefficients of Eu^{2+} and Eu^{3+} in LiCl-KCl molten salt at various temperatures.

Diffusion coefficients of Eu^{3+} are smaller than that of Eu^{2+} because Eu^{3+} has rigid solvation shell structure comparing to Eu^{2+}.

4. Conclusion

We utilized first principles DFT calculations and AIMD simulations to understand fundamental mechanism of spontaneous reduction of Eu^{3+} to Eu^{2+} in LiCl-KCl eutectic molten salt. We decoupled reaction Gibbs free energy into enthalpic and entropic contributions. The rigidity of the solvation shells was estimated by RDF, oxidation and coordination numbers, which largely described the enthalpic change.

REFERENCES

[1] Perdew, J. P.; Burke, K., Comparison shopping for a gradient-corrected density functional. International journal of quantum chemistry 1996; 57:309-319.

[2] Blöchl, P. E., Projector augmented-wave method. Physical Review B 1994; 50:17953-17979.

[3] Hoover, W. G., Canonical dynamics: equilibrium phase-space distributions. Physical review A 1985; 31:1695.

[4] Choah Kwon, Seung Hyo Noh, Hoje Chun, Il Soon Hwang, Byungchan Han, International Journal of Energy Research, 2018, 1-9.

On-Line Monitoring of Metal Ions in LiCl-KCl Melt

Sang-Eun Bae,[1,2,*] Suhee Choi,[1] Tae-Hong Park,[1,2] Jong-Yun Kim[1], and Ji-Hye Kim[1]

[1]Nuclear Chemistry Research Division, Korea Atomic Energy Research Institute, 989-111 Daedeok-daero, Yuseong-gu, Daejeon, Republic of Korea

[2]Department of Radiochemistry, University of Science and Technology, 217 Gajeong-ro Yuseong-gu, Daejeon, Republic of Korea

sebae@kaeri.re.kr

1. Introduction

Recently, the pyrochemical process has attracted much attention in that the electrochemical process recovers the unreacted uranium and reduces the volume of high-level wastes in spent nuclear fuel. Since the uranium and transuranium (TRU) elements are recovered during the pyrochemical process [1,2], it is critical to accurately determine the material flow of actinides and fission products in an electrolyte of molten salt during the process operation. Conventionally, destructive analysis techniques are performed for quantitative and qualitative analyses of uranium and transuranium elements, but they often require tedious chemical separation procedures and radiometric or spectrometric measurements [3]. In contrast, the direct determination of elements in the molten salt may present the real-time monitoring of nuclear materials and the meaningful information on the safeguards if the electrochemical process operates as declared [1]. In this work, we developed an electrochemical technique and optimized the technique for on-line monitoring during the pyrochemical process.

2. Experimental

All the experiments were carried out in a glove box under Ar where O_2 and H_2O level were maintained to be less than 1 ppm. Lithium chloride (LiCl)/potassium chloride (KCl) eutectic salts (anhydrous beads), and silver chloride (AgCl) were obtained from Sigma Aldrich. Cerium chloride ($CeCl_3$), lanthanum chloride ($LaCl_3$), and magnesium chloride ($MgCl_2$) were purchased from Alfa Aesar (purity ≥ 99.99%). UCl_3 was made from chemical dissolution of U metal by $CdCl_2$ in LiCl-KCl.

Electrochemical measurements were performed in a quartz tube (20 mm in outer diameter and 2 mm in wall thickness). W wire (Alfa Aesar, dia. 0.2 mm) and glassy carbon (Alfa Aesar, dia. 2 mm) electrodes were used as the working and counter electrodes, respectively. The W wire electrode was mechanically polished with sand paper prior to use. The reference electrode was Ag wire immersed in 1 mol% AgCl-LiCl-KCl melt.

The Electrochemical measurements were performed using a Gamry Reference 3000. The concentrations of uranium and magnesium ions were examined using inductively coupled plasma-atomic emission spectrometer (ICP-AES) (Ultima 2C, Horiba Jobin Yvon).

3. Results and Discussion

Fig. 1 shows cyclic voltammograms (CV) obtained from s W electrode immersed in LiCl-KCl containing uranium and some lanthanides. Around -1.5 V and -2.0 V, the redox currents of $U^{0/3+}$ and $Ce^{0/3+}$ are observed. These results are well consistent in literatures[4]. Fig. 1(b) also shows CV according to

the addition of the some other lanthanides such as La, Nd. The current for U redox reaction was changed little but the currents for the lanthanide redox reactions increased as the lanthanide ions were added. These results mean that there is not the formation reaction of alloy among U and lanthanide ions.

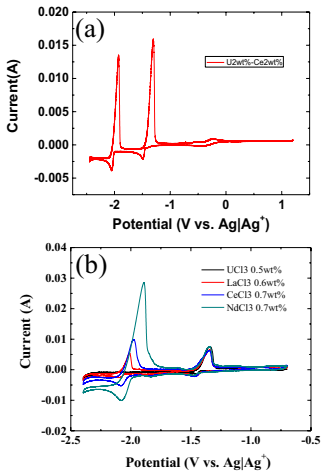

Fig. 1. CA results obtained from W wire in LiCl-KCl melt containing.

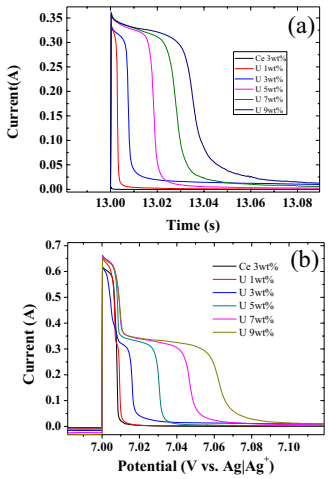

Fig. 2. CA results obtained from W wire in LiCl-KCl melt containing.

Fig. 2 shows chronoamperometry (CA) results obtained from s W electrode immersed in LiCl-KCl containing uranium and cerium cations. The dissolution reactions in Fig. 2(a) were performed for the electrodeposition of U. As the concentration of the U cation increased, the dissolution current response proportionally last more.

Fig. 2(b) shows CA results obtained after the simultaneous electrodeposition of U and Ce. In this case, new sharp peak firstly and then the second current, similar shape of U dissolution, in turn appeared. The first sharp peaks were nearly changed but the second dissolution currents last further with the concentration increment of U cation. The results denote that the passed charge, which can be calculated by the integration of the CA in Fig. 2, can be useful to extract the information for the concentration of the metal ions in LiCl-KCl melt.

4. Conclusion

To develop an on-line monitoring system for use in the pyrochemical process, electrochemical techniques, CV and CA, were employed The passed charges obtained from the integration of CA results show a good relation with the concentration of the metal ions in LiCl-KCl melt. This means that the CA technique may be one of the promising candidates for an on-line monitoring system during the pyrochemical process.

REFERENCES

[1] D.-H. Kim, S.-E. Bae, T.-H. Park, J.-Y. Kim, C.-W. Lee, and K. Song, Microchemical Journal, 114, 261-265 (2014).

[2] T. Inoue, L. Koch, Development of Pyroprocessing and its future direction, Nucl. Eng. & Technol., 40, 183-190 (2008).

[3] Y.J. Park, S.-E. Bae, Y.H. Cho, J.Y. Kim, K. Song, UV–vis absorption spectroscopic study for on-line monitoring of uranium concentration in LiCl–KCl eutectic salt, Microchem. Journal, 99, 170-173 (2011).

[4] S.-E. Bae, Y.-H. Cho, Y.J. Park, H.J. Ahn, K. Song, Oxidation State Shift of Uranium during U^{3+} Synthesis with Cd^{2+} and Bi^{3+} in LiCl-KCl melt, Electrochem. Solid State Lett., 13, F25-F27 (2010).

The Effect of Target Material and the Neutron Spectrum on Nuclear Transmutation of ^{99}Tc and ^{129}I in Nuclear Reactors

Seung Gu Kang and Hyun Chul Lee*
Pusan National University, 2, Busandaehak-ro 63beon-gil, Geumjeong-gu, Busan 46241, Korea
*hyunchul.lee@pusan.ac.kr

1. Introduction

Of the long-lived fission products in spent nuclear fuel, ^{99}Tc and ^{129}I are highly mobile in underground environment during disposal at a deep geological disposal repository. And they cause the exposure doses to the ecosystem mainly due to the release of beta rays of several hundred keV [1]. Therefore, if the two nuclides are separated from spent nuclear fuel and converted into short-lived nuclides or stable nuclides through nuclear transmutation in nuclear reactors, it can have a positive effect on safety for disposal. For this purpose, it is necessary to investigate the efficiency of transmutation of these two nuclides in the reactor. In this study, for variable nuclear reactor, the depletion calculation was performed using McCARD code [2], a neutronics analysis code of the nuclear reactor and fuel systems, and the results were compared and discussed in terms of nuclear transformations of ^{99}Tc and ^{129}I.

2. Target Material

Because ^{99}Tc has a high melting point and metal density, it is assumed to be a technetium metal target material for nuclear transmutation. On the other hand, due to be converted to gaseous xenon through beta decay, ^{129}I has a physical problem. The problem is that the melting point and boiling point of ^{129}I are lower than the core temperature and pressure. To solve this problem, CuI, CaI_2 and MgI_2 were assumed to be the chemical forms of the target material in consideration of the thermal and chemical properties of iodide [3].

In this study, the target materials were simulated using technetium metal, CuI, CaI_2 and MgI_2. Additionally, the isotope ratios of technetium and iodine were obtained from a typical PWR 16x16 nuclear fuel assembly burned up to the average discharge burnup (55000 MWD / MTU) [4].

3. Model

To simplify the calculation, only fuel assemblies and fuel bundle with the target material rod were modeled and calculated in 2 dimensions. PWR and CANDU are typically pressurized light water reactor type and heavy water reactor type. And PGSFR and MET-1000 are sodium cooled fast reactors. The difference between the two reactors is that PGSFR uses highly enriched uranium fuel and MET-1000 uses TRU as fuel [4~9]. In case of CANDU, PGSFR and MET-1000, the center rod of each assembly and bundle is replaced with the target material rod. Otherwise, the target material rod is loaded in the instrumentation tube in case of PWR.

After calculating the burnup to the average discharge burnup of each reactor [4~9], ^{99}Tc and ^{129}I of the target material rod in each case were examined.

4. Comparison of simulation results

4.1 Comparison of ^{129}I nuclear transmutation ratio by target materials

Fig. 1 shows the nuclear transmutation ratio of ^{129}I when the iodide target materials are loaded in each reactor and that the results of each target material are similar.

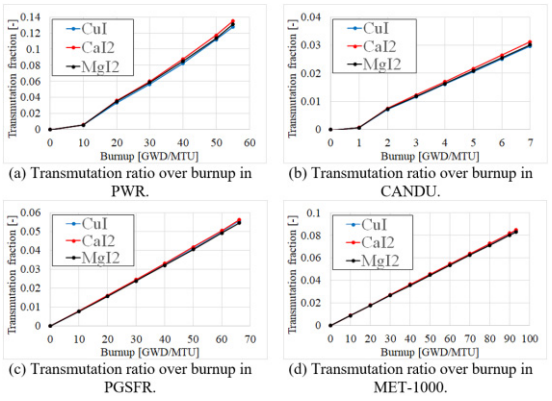

(a) Transmutation ratio over burnup in PWR. (b) Transmutation ratio over burnup in CANDU.

(c) Transmutation ratio over burnup in PGSFR. (d) Transmutation ratio over burnup in MET-1000.

Fig. 1. Transmutation ratio over burnup in each reactor.

On the other hand, as shown in Fig. 2, the transmutation amount of ^{129}I of MgI_2 is higher than the others considering the densities of iodine.

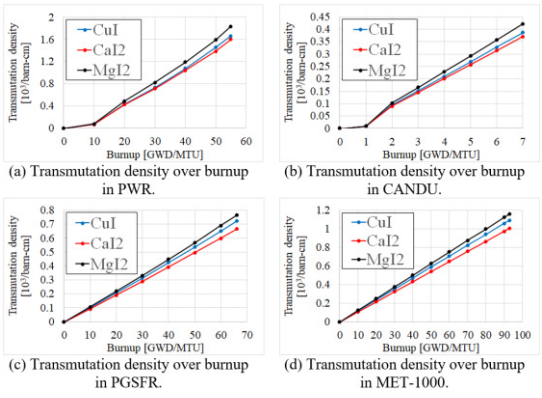

(a) Transmutation density over burnup in PWR. (b) Transmutation density over burnup in CANDU.

(c) Transmutation density over burnup in PGSFR. (d) Transmutation density over burnup in MET-1000.

Fig. 2. Transmutation density over burnup in each reactor.

4.2 Comparison of nuclear transmutation ratio by each reactor

As shown in Fig. 3, total transmutation ratios of ^{99}Tc and ^{129}I in case of PWR are more than in the other cases due to relatively larger the transmutation rate and the average discharge burnup. On the other hand, in case of CANDU, transmutation rate is larger than the others, but due to the shortest average discharge burnup, total transmutation ratio is the shortest.

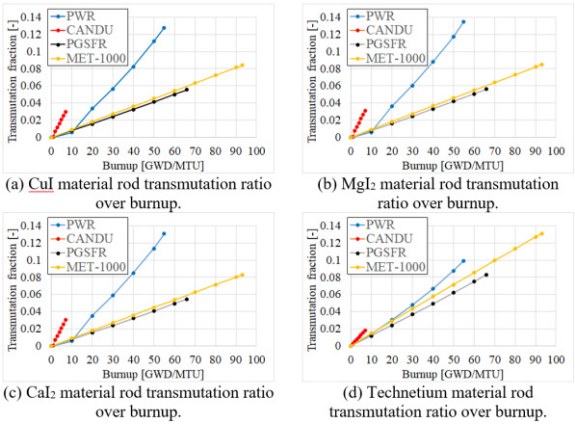

(a) CuI material rod transmutation ratio over burnup.

(b) MgI_2 material rod transmutation ratio over burnup.

(c) CaI_2 material rod transmutation ratio over burnup.

(d) Technetium material rod transmutation ratio over burnup.

Fig. 3. Transmutation rate of each target material over burnup.

5. Conclusion

The fuel assemblies of PWR, PGSFR and MET-1000 and the fuel bundle of CANDU are modeled with target materials and performed depletion calculation using the McCARD code.

As a result of transmutation ratio comparison, the nuclear transmutation ratios of the three target materials (CuI, CaI_2 and MgI_2) are almost the same, but MgI_2 is the most amount of transmutation during the same burnup.

CANDU has the most transmutation rate, but has the shortest transmutation ratio due to the shortest average discharge burnup. On the other hand, PWR has less transmutation rate than CANDU, but has the most transmutation ratio consideration in the average discharge burnup and transmutation rate.

REFERENCES

[1] L. Kun, et al., "A code development for LLFP transmutation analysis based on the whole pin-wise calculation in PWRs", Journal of Nuclear Engineering and Design, 256, 56-66 (2013).

[2] S. Hyung Jin, et al., "McCARD: monte carlo code for advanced reactor design and analysis", Journal of Nuclear Engineering and Technology, 44(2), 161–176 (2012).

[3] L. Kun, et al., "Studies on LLFP transmutation in a pressurized water reactor", Journal of Nuclear Science and Technology, 50, 581-598 (2013).

[4] KHNP Co., LTD. April 11 2011. “Status Report 103 – Advanced Power Reactor (APR1000)” Advanced Reactor Information System Database (International Atomic Energy Agency). Accessed Dec. 30 2017. Available from: https://aris.iaea.org/PDF/APR1000.pdf.

[5] KHNP Co., LTD. Design Manual, “CANDU 6 Generating Station Physics Design Manual”, Wolsong NPP 1, 59RF-03310-DM-000 Revision 0 (2009).

[6] Candu Energy Inc., “Enhanced CANDU 6 Technical Summary”, Candu Energy Inc. Press, Mississauga (2012).

[7] W. Bernnat, et al., “Benchmark for Neutronic Analysis of Sodium-cooled Fast Reactor Cores with Various Fuel Types and Core Sizes”, Nuclear Energy Agency Technical Report, NEA/NSC/R (2015)9 (2016).

[8] K. Taek K., et al., "Core Design Studies for a 1000 MWth Advanced Burner Reactor", Annals of Nuclear Energy, 36(3), 331-336 (2009).

[9] Y. Kyung Ho, et al., "Mechanical Design Evaluation of Fuel Assembly for PGSFR", Proc. of Int. Conf. on Fast Reactors and Related Fuel Cycles: Next Generation Nuclear Systems for Sustainable Development(FR17), IAEA-CN 245-017, June 26-29, 2017, Yekaterinburg, Russian Federation.

Rotating Disk Electrode Measurements of the Electrochemical Reduction Reaction of Sm^{3+} and Eu^{3+} in LiCl-KCl Melt

Suhee Choi*, Sang-Eun Bae, and Tae-Hong Park

Korea Atomic Energy Research Institute, Daedeok-daero989ben-gil 111, Yuseong-gu, Daejeon, Republic of Korea

*shchoi926@kaeri.re.kr

1. Introduction

Electrochemical behaviors of actinide and lanthanide ions have been widely studied to explain the fundamental electrochemical reactions in the pyrochemical processing [1]. In particular, electrochemical parameters, such as diffusion coefficient, exchange current density, were measured using cyclic voltammetry, chronoamperometry, etc. However, there is some disagreement between the values obtained by different groups.

The rotating disk electrode (RDE) is well-known, one of the effective electrochemical techniques, for determining various electrochemical parameters.

In the present work, we investigated various electrochemical parameters of Sm^{3+} and Eu^{3+} in LiCl-KCl melts by using the RDE technique.

2. Experimental

All the experiments were carried out in a glove box under Ar. The O_2 and H_2O level were maintained to be less than 1 ppm. LiCl-KCl eutectic salts and AgCl were obtained from Sigma Aldrich. $SmCl_3$ and $EuCl_3$ were purchased from Alfa Aesar (purity $\geq$ 99.998%).

Tungsten (Alfa Aesar, dia. 6.3mm) and glassy carbon (Alfa Aesar, dia. 2 mm) electrodes were used as the working and counter electrodes, respectively. The reference electrode was Ag wire that was immersed in 1 mol% AgCl in the LiCl-KCl eutectic melt.

The electrochemical experiments were performed using a Gamry Reference 3000. RDE data were obtained using a Pine Model MSRX rotator.

3. Results and Discussion

Fig. 1 shows the cyclic voltammograms (CVs) of Sm^{3+} and Eu^{3+} in the LiCl-KCl melt at 723 K and 783 K. Sm^{3+} and Eu^{3+} reduction peaks appear at -0.96 V and 0.25 V at 723 K, respectively. The temperature increase led to the anodic shift of the peak potential and the increaseof the peak current. We calculated the diffusion coefficients of Sm^{3+} and Eu^{3+} using the Randles-Sevick equation:

$$\frac{I_p}{\sqrt{v}} = 0.446 \frac{(nF)^{3/2}}{\sqrt{RT}} CS\sqrt{D} \quad (1)$$

where I_p is the reduction peak current, v is the scan rate, n is the number of electrons, F is the faraday constant, R is the gas constant, T is temperature, C is the concentration of bulk, S is area of electrode, and D is diffusion coefficient. The diffusion coefficients of Sm^{3+} and Eu^{3+} were estimated to be 5.6 x 10^{-6} and 5.4 x 10^{-6} cm^2/s at 723 K, respectively.

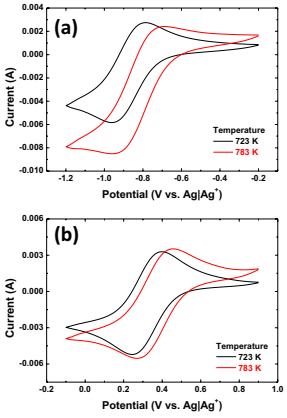

Fig. 1. CVs obtained in LiCl-KCl melt at 723 K and 783 K containing 1.5 wt.% (a) $SmCl_3$ and b) $EuCl_3$. Scan rate = 200 mV/s.

Fig. 2 shows linear sweep voltammograms (LSVs) of Sm^{3+} and Eu^{3+} at 723 K and 783 K in the LiCl-KCl melt using a W RDE. The Sm^{3+} and Eu^{3+} reduction currents show up at -0.6 V and 0.5 V at 723 K, respectively. The peak potentials shifted positively and the peak currents increased with increased temperature. We determined diffusion coefficient using the Levich equation:

$$i_L = 0.62nFAD_0^{2/3}\omega^{1/2}\nu^{-1/6}C \quad (2)$$

where i_L is the limiting current, A is the electrode area, is the rotation speed, ν is the kinematic viscosity, and C is the bulk concentration of the ion. The diffusion coefficients of Sm^{3+} and Eu^{3+} were estimated to be 5.4 x 10^{-6} and 6.1 x 10^{-6} cm^2/s at 723 K, respectively. These calculated values were close to the reported ones [2], [3].

We also built Tafel graphs for the reduction reactions and estimated Tafel slope, exchange current density, transfer coefficient, etc.

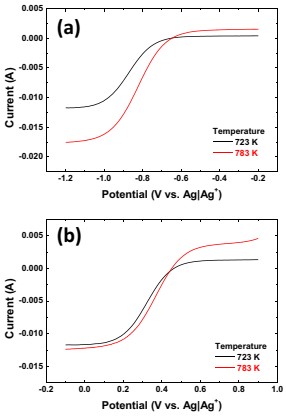

Fig. 2. LSVs obtained using W RDE in LiCl-KCl melt at 723 K and 783 K containing 1.5 wt.% (a) $SmCl_3$ and (b) $EuCl_3$. A rotation rate and scan rate are 1200 rpm and 5 mV/s, respectively.

4. Conclusion

Here, we studied the reduction of Sm^{3+} and Eu^{3+} at the various temperatures in the LiCl-KCl melt. The exchange current densities and transfer coefficients were determined for Sm^{3+} and Eu^{3+}.

REFERENCES

[1] S. Choi, S.–E. Bae, T.–H. Park, "Electrochemical and spectroscopic monitoring of interactions of oxide ion with U (III) and Ln (III)(Ln=Nd, Ce, and La) in LiCl-KCl metls" J. Electrochem. Soc., 164, H5068-H5073 (2017).

[2] G. Cordoba, C. Caravaca, "An electrochemical study of samarium ions in the molten eutectic LiCl+KCl", 572, 145-151 (2004).

[3] S. A. Kuznetsov, M. Gaune-Escard, "Kinetics of electrode processes and thermodynamic properties of europium chlorides dissolved in alkali chloride melts", Journal of Electroanalytical Chemistry, 595, 11-22 (2006).

Luminescence Studies of U(VI)-Laponite System in Aqueous Phase

Wansik Cha*, Hee-Kyung Kim, Sue Young Hong, and Euo Chang Jung

Korea Atomic Energy Research Institute, Daedeok-daero989ben-gil 111,Yuseong-gu, Daejeon, Republic of Korea

*wscha@kaeri.re.kr

1. Introduction

Mineral surface adsorption of radionuclides is one of fundamental geochemical processes to be elucidated for long-term safety analysis of deep geological disposal techniques of spent fuels. Uranium(VI) adsorption onto clay minerals has been studied to understand the sorption mechanism particularly at the surface of the characteristic platelet structures. For decades time-resolved laser-induced fluorescence spectroscopy (TRLFS) has been a valuable tool for the chemical speciation of U(VI) adsorbed on various mineral phases. Although the surface-adsorbed U(VI) species exhibit strong luminescence enhancement in general, however, the TRLFS-based U(VI) speciation data of colloidal mineral phases are still limited and inconsistent within literature available [1].

In this study, we attempt to understand the basic U(VI) luminescence characteristics arising from the interaction with a synthetic nano-clay mineral, i.e., Laponite RD®. Although laponite shares a 2:1 silicate structure with the smectite natural clays such as montmorillonite, its primary particles are fairly monodispersed with a disk-like shape having a diameter in the range 25−30 nm and thickness of 0.92 nm. So, it offers a large area of surface binding sites, particularly from the edge of the platelet structures. At low concentration it can form a homogeneous and transparent aqueous solution depending on pH and electrolyte concentrations (ionic strength). Thus, U(VI)-laponite system can be a good model system for investigating U(VI)-clay interactions and speciation using TRLFS.

2. Results and Discussion

2.1 Properties of laponite aqueous solutions

Laponite RD® (Southern Clay Products Inc. USA) was used as received. It forms highly thixotropic, clear gels when dispersed in water at a 2 wt% concentration. In this study the final concentration of laponite in aqueous samples was maintained at 0.1-0.2 wt%, where completely dissolved forms of laponite can be obtained. Due to the non-spherical shape of laponite platelets, the particle size distribution appears multi-modal when analyzed using dynamic light scattering (DLS) (Zetasizer NanoZS, Malvern), as shown in Fig. 1. It is evident that at such low concentration levels cluster or aggregate formation of laponite particles is effectively suppressed for more than a week.

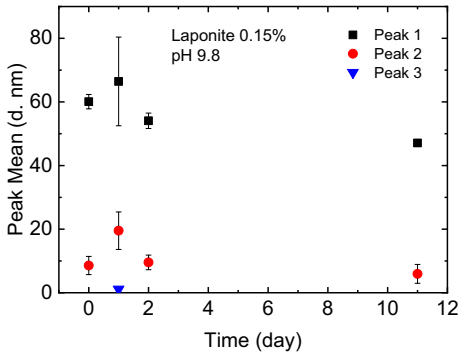

Fig. 1. Monitoring the particle size distribution of an aqueous sample containing 0.15% Laponite (pH 9.9). DLS analysis results show 2-3 main peaks at different sizes.

2.2 U(VI) sorption equilibria

Strong sorption behaviors of U(VI) are observed in a wide pH range, i.e., 4-9. When monitored using an ultracentrifuge technique, only trace amount of U(VI) is detected in a supernatant solution in this pH range after the removal of laponite-gel precipitates. (data not shown). Thus, we conclude that the majority of U(VI) exists in forms of surface complexes on the laponite nano-colloids in the pH region explored in this study. The zetapotential values of the aqueous U(VI)-laponite colloidal system are measured in the range of -30 ~ -40 mV, which indicates the negative charges of the basal plane of clay particles play dominant role in the colloidal behaviors of laponite. In recent studies, however, the U(VI) sorption equilibrium on smectite clay occurs primarily via the reactive edge sites, i.e., silanol (≡SiOH) and aluminol (≡AlOH) surface groups [2,3].

2.3 TRLFS study of U(VI)-laponite system

For TRLFS study a pulse laser (355 nm, 2~3 mJ) was used with a repetition rate of 10 Hz. An intensified CCD (iStar, Andor Technol.) was employed for the gated detection of luminescence. Deconvolution of TRLFS data using PARAFAC analysis was carried out by implementing N-way331 in Matlab [4]. Ten data sets of 10 μM U(VI) in a pH range of 7 to 10 were analyzed (0.1 wt% of laponite). Deconvolution with three components converged with a core-consistency value (75%). Details of TRLFS techniques and spectral deconvolution methods will be discussed in the presentation. The summarized results of the PARAFAC analysis with three components are shown in Figs. 2-3.

In this study our investigation aims to analyze the long lifetime luminescent species, of which typical luminescence lifetimes are > 50 μs. Fig. 2 displays the deconvoluted luminescence spectra of three major U(VI) species identified from the PARAFAC analysis. Interestingly, the species of the longest lifetime appears as a dominant adsorbed species at < pH 7.5 (A in Fig. 2).

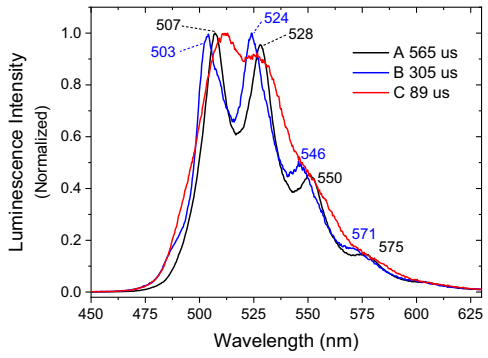

Fig. 2. Normalized deconvoluted luminescence spectra of the three U(VI) species adsorbed on laponite at pH 7-10. The luminescence lifetime of each species is shown in the legend.

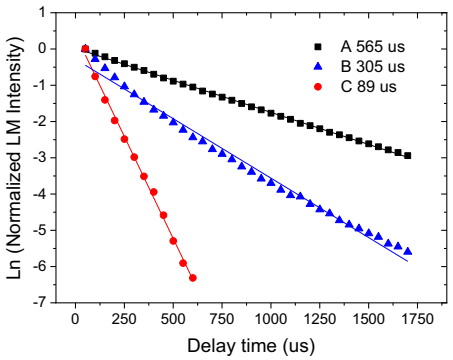

Fig. 3. Luminescence decays of the three species of Fig. 2 as a function of delay time.

On the other hand the species B and C are observed at higher pH regions, i.e., 7.5-8.5 and > 8.5, respectively. Species C is found to contribute to the featureless luminescence spectra with absence of the multiple peak pattern at higher pH region. Combined with the batch sorption results we conclude that all three U(VI) species represent adsorbed species on laponite, specifically inner-sphere complexes at edge sites of the plate structures. More details will be discussed in the conference presentation.

3. Conclusion

By using a synthetic nano-clay mineral material (laponite) and TRLFS techniques the fundamental sorption behaviors of U(VI) were investigated. Luminescence kinetic data were deconvoluted using PARAFAC analysis and examined with the results from on the batch sorption equilibrium analysis. Three major luminescent U(VI) species are identified, each of which appears as an adsorbed species on laponite in a pH-dependent manner.

REFERENCES

[1] G. Geipel, “Some aspects of actinide speciation by laser-induced spectroscopy”, Coordination Chemistry Reviews, 250 844–854 (2006).

[2] A. Kremleva, S. Krüger and N. Rösch, “Uranyl adsorption at solvated edge surfaces of 2 : 1 smectites. A density functional study”, Phys. Chem. Chem. Phys., 17, 13757 (2015).

[3] E. R. Sylwester, E. A. Hudson and P. G. Allen, “The structure of uranium (VI) sorption complexes on silica, alumina, and montmorillonite”, Geochim. Cosmochim. Acta, 2000, 64, 2431−2438 (2000).

[4] R. Bro, “PARAFAC. Tutorial and applications”, Chemometrics and Intelligent Laboratory Systems, 38, 149-171 (1997).

7분과

방사화학 (Poster)

Electrochemical Behavior of Er Ion and Bi Ion in LiCl-KCl Molten Salt

Beom Kyu Kim, Hwa Jeong Han, Ji Hye Park, Won Ki Kim, and Byung Gi Park
Department of Energy & Environmental Engineering, Soonchunhyang University, Soonchunghyangro 22, Asan, Chungnam, Republic of Korea
qu@sch.ac.kr

1. Introduction

The pyro separation process using molten salts is one of the most promising options for extracting lanthanides (Lns) and actinides from the fission products. The pyro separation process using chlorides or fluorides as solvent, having some advantageous properties, such as high level radiation resistances of the process, are considered as a promising technique for the resolution of the problem of actinide and fission product partitioning. The most developed pyroprocess techniques include electrorefining, electroextraction with reactive cathodes, liquid–liquid metal reductive extraction. The electrochemical extraction of lanthanides was investigated in molten chlorides using reactive working electrode, Bismuth electrode.[1-3]

Since there are many advantages (No change of the electrode surface, easier aggregation and moving) using liquid metal as working electrode, the electrochemical extracting Lns on liquid bismuth electrode from molten salts have a strong point for pyrochemical reprocessing of spent nuclear fuels. For liquid Bi as cathodic material, the electrochemical behavior of Ln(III) La, Ce and Pr was studied in the LiCl-KCl system. However, the concentration changes of Erbium ions in the melts of electrochemical extraction process was not explored on liquid Bi electrode.

This study is to establish therefore, we focused on the electrochemical behavior of Bismuth ions and Erbium ions. The technique is applied to investigate electrode reactions of erbium ion and Bismuth ion in the molten salt LiCl-KCl. Finally, we analyze the effect of Bi ion concentration on the electrochemical reduction of Er.

2. Experimental

Electrochemical tests were conducted in a glove box and the electrochemical cell was set up inside a steel furnace connected under the glove box. The cell was fabricated to accommodate both working electrode(tungsten wire), counter electrode(tungsten wire), reference electrode(silver wire) and thermocouple. All the electrodes and chlorides were contained in a quartz cell. The electrochemical measuring instrument was Versa State from Princeton Applied Research Inc. and the software used was Versa studio. The electrochemical methods involved were cyclic voltammetry, square wave voltammetry, and open circuit chrono-potentiometry.

3. Results and Discussion

As a first result, the behavior of Er was confirmed by electrochemical measurement of Cyclic Voltammetry. At a temperature of 773K, the standard potential of Er is about -2.05V. The results confirm the current and potential through various scan rates.The Value of the potential and Current are shown in Table 1.

The cyclic voltammogram of LiCl-KCl+$ErCl_3$(1wt%) at 773 K showed a single redox peak corresponding to the Er^{3+}/Er couple under potential window between -2.3V and -1.5V (vs. Ag/AgCl reference electrode). Analysis of voltammogram exhibited that a formal standard potential of Er^{3+}/Er redox couple was obtained to -1.8V/-2.03V (vs. reference electrode). As a result of adding $BiCl_3$(1wt%), various intermetallic compounds redox peaks were observed in Fig. 2.

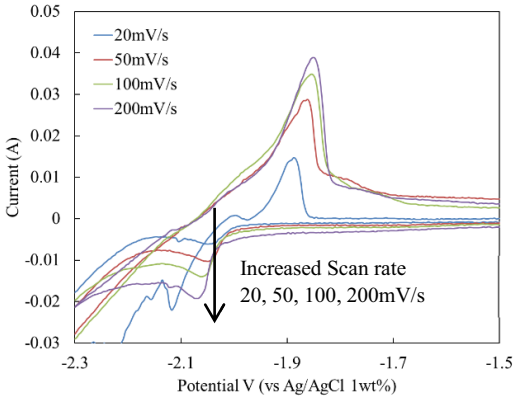

Fig. 1. Cyclic voltammogram obtained for Er^{3+} in LiCl-KCl melt using the tungsten electrode (A=0.332 cm^2) at 773K, 1wt%, scan rate: 20, 50, 100, 200mV/s.

Table 1. The Value of the Potential and Current at 773K

Scan Rate	Reaction	Potential(V)	Current(A)
20mV/s	$Er \rightarrow Er^{3+} + 3e^-$	-1.88	0.014
	$Er^{3+} + 3e^- \rightarrow Er$	-2.03	-0.007
50mV/s	$Er \rightarrow Er^{3+} + 3e^-$	-1.86	0.028
	$Er^{3+} + 3e^- \rightarrow Er$	-2.04	-0.01
100mV/s	$Er \rightarrow Er^{3+} + 3e^-$	-1.84	0.033
	$Er^{3+} + 3e^- \rightarrow Er$	-2.06	-0.014
200mV/s	$Er \rightarrow Er^{3+} + 3e^-$	-1.84	0.038
	$Er^{3+} + 3e^- \rightarrow Er$	-2.07	-0.019

The -1.8/-2.0V are the redox peak of Er and 0.3/0.5V is the peak of Bi metal. Except the B peak in the CV shown, the R1/O1, R2/O2 and R3/O3 are an intermetallic compounds and it can be seen that was also confirmed at the peak of oxidation-reduction behavior. According to the Phase Diagram, five intermetallic compounds Bi2Er and BiEr are observed in the Er-Bi system at 773K. [4]

But we various Lu-Bi intermetallic compounds were formed in LiCl-KCl and the corresponding potentials were observed using CV. We applied Semi-Reduction Cyclic Voltammogram (concentration of Bi/Er ratio 0.7) to software Fityk 0.9.8 and searched for reduction peaks. The reduction peak of R_3/O_3 was not observed at Bi/Er molar ratio 0.7, but it was confirmed at Bi/Er molar ratio 1.14.

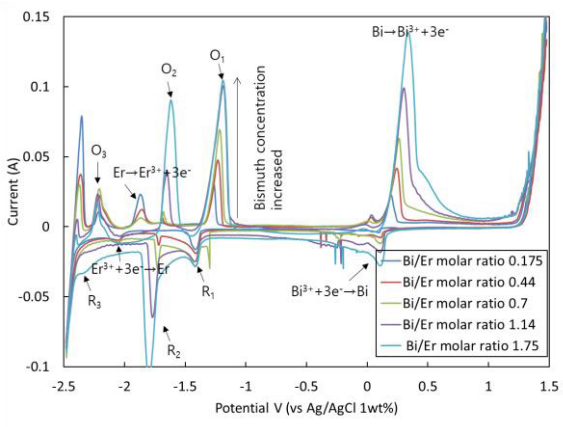

Fig. 2. Cyclic voltammogram obtained for $ErCl_3$(1wt%) add $BiCl_3$(0~2wt%)in LiCl-KCl melt using the tungsten electrode (A=0.332 cm^2) at 773K, Scan Rate 0.1V/s.

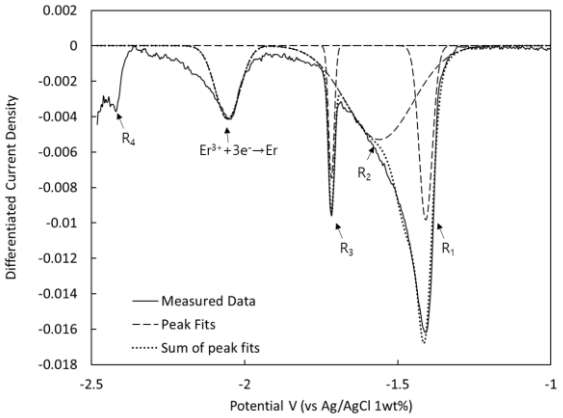

Fig. 3. Fitting of semi-differentiated cyclic voltammograms curve for reduction potential of concentration Bi/Er molar ratio 0.44.

4. Conclusion

The electrochemical behavior of bismuth ion and erbium ion was carried out by CV, and various intermetallic compound were confirmed. The -2.4V(O_3/R_3) redox potential is expected to be an unidentified IMC and will be closely monitored.

REFERENCES

[1] Y. Castrillejo, et al., "The electrochemical behaviour of the Pr(III)/Pr redox system at Bi and Cd liquid electrodes in molten eutectic LiCl–KCl", *J. Electroanal. Chem.*, 579, 343 (2005).

[2] M. Li, et al., Electrochemical behavior of La(III) on liquid Bi electrode in LiCl–KCl melts. Determination of thermodynamic properties of La–Bi and Li–Bi intermetallic compounds, *RSC,* 5, *pp.*82471 *(2015).*

[3] Y. Castrillejo, et al., Electrode reaction of cerium into liquid bismuth in the eutectic LiCl-KCl, *Electrochemistry,* 73, 636 *(*2005).

[4] H. Okamoto, "Supplemental Literature Review of Binary Phase Diagrams: Bi-Ce, Bi-Er, C-Ce, C-La, C-Pr, Cd-I, Cr-Cu, Cu-Er, Er-Sb, F-Sm, F-Yb, and Fe-Gd", Journal of Phase Equilibria and Diffusion, 34(4) 350–362 (2013).

Preliminary Test of ^{55}Fe and ^{63}Ni Analysis Method in Concrete Sample

Kahee Jeong[1)], Jong-Ki Choi[1),] Kyu-Min Song[1)], and Jong-Myoung Lim[2)]

[1)] KHNP Central Research Institute, 70-1312 gil, Yuseong-daero, Yuseong-gu, Daejeon, 34101

[2)]Korea Atomic Energy Research Institute, 111, Deadeok-daero 989 beon-gil, Yuseong-gu, Daejeon, 34057

kaheejeong@khnp.co.kr

1. Introduction

The radiochemical analysis is an essential necessity for the management and disposal of radioactive wastes. Both ^{55}Fe and ^{63}Ni are neutron activation products. ^{55}Fe ($t_{1/2}$=2.7y) decays via electron capture to stable ^{55}Mn with the emission of Auger electrons and low energy X-rays (5.89 keV, 16.9%). ^{63}Ni is a pure beta emitting radionuclide with maximum beta energy of 66.95 keV and half life of 100.1 y. Due to low beta energy emitted from ^{55}Fe and ^{63}Ni, both have to be separated completely from other radionuclides before the counting. In this study, a sample procedure based on anion exchange is investigated for the simultaneous determination of ^{55}Fe and ^{63}Ni. The recovery rate of stable isotope Fe and Ni were also confirmed for the standard solution and concrete samples.

2. Experimental

2.1 Equipment and chemicals

Inductively coupled plasma optical emission spectrometry (ICP-OES, Teledyne leeman laboratory Inc, Prodigy) is used for the determination of stable Fe and Ni. The automatic fusion system (K2 prime, Katanax) is used to melt the concrete samples. Fe and Ni standard solution was purchased from the AccuSandard, Inc., (Accutrace reference standard, MES-16-1). This standard solution contains stable isotopes such as Ca, Co, Cu, Pb, etc. In order to primarily separate Fe and Ni, Bio-Rad anion exchange resin was purchased from Bio-Rad laboratory(USA).

2.2 Preparation of samples

The stable isotope Fe and Ni carrier are 25 mg and 2 mg, respectively, and 1mL of cobalt standard (1,000ug/mL) is added to the sample. The prepared sample is adjusted to pH 8~9 using 8M NaOH. The precipitate is separated by centrifugation, and then dissolved with concentrated nitric acid, transferred to a teflon beaker and evaporated to dryness. This sample is dissolved with 10 mL of 9M HCl solution to prepare a sample for separation.

2.3 Separation of Fe and Ni from interfering radionuclides by anion exchange chromatography

The solution is then loaded to a Bio-Rad AG 1x4 anion exchange column, which has been conditioned with 20mL of 9M HCl solution. 9M HCl is added to elute Ni^{2+} and wash the column, 6M HCl is added to elute Co^{2+} and Cu^{2+}, finally DIW(or 0.05M HCl) is added to elute Fe^{3+}. The effluent, washes and eluate are collected in polyethylene vials of 2mL each. These vials are then measured by ICP-OES.

2.4 Applied to concrete samples

Concrete samples are completely melted by automatic fusion system and then separated according to 2.3.

2.5 Determination of Fe and Ni by ICP-OES

2mL of each eluate in accordance with 2.3 was diluted and the concentration was measured with ICP-OES. Then the recovery rate was calculated.

3. Results and discussion

In a concentrated HCl solution, many metals form anion complexes with Cl^-, and will therefore be absorbed on an anion exchange resin. Depending on the stabilities of the metal chloride anion complexes in different concentration of HCl, Fe, Ni and other metals can be separated by anion exchange chromatography. Fig. 1 shows the eluting curves of Fe, Ni and other metals on an anion exchange column. Ni^{2+} does not absorb on the column even in 9M HCl, so Ni can be separated from Co^{2+} and Fe^{3+} very well. Fe^{3+} retained on the column can be isolated by elution of Cu^{2+}, Co^{2+}, etc., with 6M HCl, and then eluting Fe with DIW.

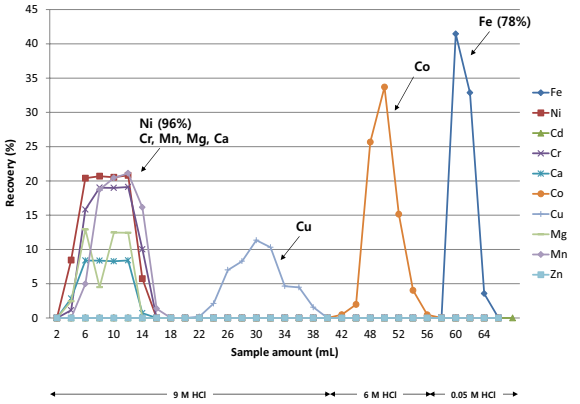

Fig. 1. Eluting curves on anion exchange column.

4. Conclusion

The Fe and Ni were separated each other by an anion exchange chromatography and the recovery rate of Fe and Ni are higher than 90%, 80%, respectively.

REFERENCES

[1] Xiaolin Hou, Lars Frøsig Østergaard, Sven P. Nielsen, "Determination of ^{63}Ni and ^{55}Fe in nuclear waste samples using radiochemical separation and liquid scintillation counting", Analytica chimica acta, 535, 297-307 (2005).

[2] Jukka Lehto and Xiaolin Hou., "Chemistry and analysis of radionuclides", Wiley-vch(2011).

[3] Michael F.L' Annunziate, "Handbook of radioactivity analysis", Academic press (2012).

Determination of Cerium Isotopes and Total Burnup in Irradiated Pellet Based on Isotope Dilution Mass Spectrometric Measurement

Jung Suk Kim*, Yang-Soon Park, Byungman Kang, Kyungwon Suh, Kwang Soon Choi, and Yeong Keong Ha
Korea Atomic Energy Research Institute, 111, Daedeok-daero 989beon-gil, Yuseong-gu, Daejeon, Republic of Korea
*njskim1@kaeri.re.kr

1. Introduction

The burnup of important fissile isotopes and the composition of an irradiated fuel depend on the nature of the fuel and on the conditions of an irradiation. A detailed knowledge of these quantities is useful for a reactor work as well as for the effective utilization of a nuclear fuel. Burnup determination by destructive method, which is based on the determination of specific nuclides, e.g. U, Pu and ^{148}Nd by a chemical analysis after an appropriate separation of the heavy elements and a monitoring of the fission product, is widely used as a reference method to measure the burnup of an irradiated fuel [1]. The ^{140}Ce and ^{142}Ce were recommended as useful nuclear fuel burnup monitors of total fission because they satisfy most of the necessary requirements for a good burnup monitor of PWR fuel, and can be determined easily using isotope dilution mass spectrometric techniques (IDMS) [2].

The aim of the present work is to determine the isotopic compositions and its contents of Ce for the samples from sintered solid and annular pellets of PWR type irradiated in the Hanaro reactor at KAERI, and to determine the total burnup using the measured results, so as to determine the respective validity of the methods

2. Experiments

2.1 Chemicals

The Certified ^{140}Ce (99.84 atom%) spike was obtained from Oak Ridge National Laboratory (ORNL). This spike solution was prepared by dissolving its oxide in hot c-HNO_3 added H_2O_2. The concentration of the spike solution was determined by calibrating that with a Ce standard solution and inductively coupled plasma–atomic emission spectrometer (ICP-AES).

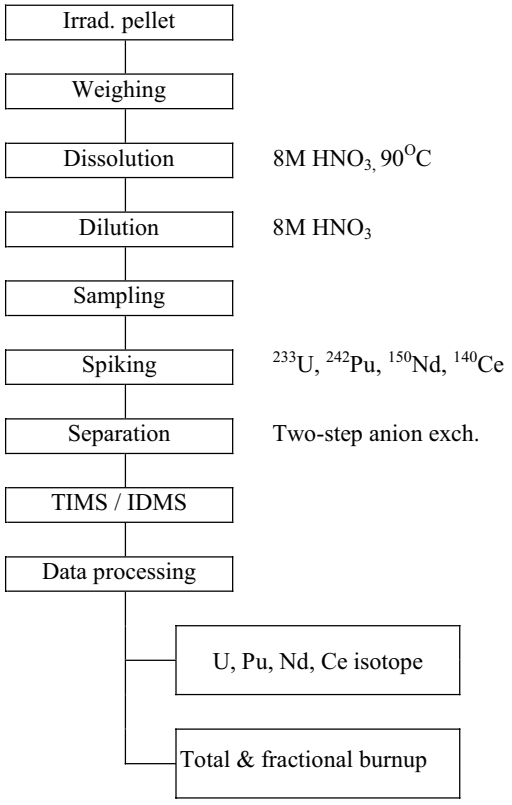

Fig. 1. Analytical processes for the determination of U, Pu, Nd and Ce isotopes, and burnup in an irradiated pellet.

2.2 Chemical Separation and Isotopic Determination

The basic processes in the analytical laboratory for the determination of U, Pu, Nd, Ce, and burnup are shown in Fig. 1. Chemical separation was carried out for both the unspiked and the spiked sample solutions in the same experimental conditions in a glove box without any heavy shieldings. Nd is eluted from other fission products on the second anion exchange resin column (AG 1X4, 200-400 mesh) with 0.04M HNO_3-99.8% MeOH (1:9) eluent, followed by Ce elution with 0.007M HNO_3-99.8% MeOH (1.5:8.5) eluent. The isotopic compositions of U, Pu, Nd and Ce in the unspiked and spiked pellet samples were determined using a thermal ionization mass spectrometer (TIMS, Finnigan TRITON).

2.3 Determination of the Ce and total burnup

The concentrations of Ce in the sample solutions were determined by the IDMS according to Eq. (1):

$$C_n = C_a \cdot G_a/G_n \cdot M_n/M_a \cdot (R_a-R_m)/(R_m-R_n) \cdot (\sum nRi)/(\sum aRi) \quad \text{------ (1)}$$

Where,

C_n : concentration of Ce in sample soln. (μg-Ce/ mL)
C_a : concentration of Ce in spike soln. (μg-Ce/mL)
G_n : volume of sample soln. taken (mL)
G_a : volume of spike soln. taken (mL)
M_n : mean atomic weight of Ce in sample
M_a : mean atomic weight of Ce in spike
R_a : ratio of two basic isotopes in spike ($^{142}Ce/^{140}Ce$)
R_m: ratio of two basic isotopes in mixture($^{142}Ce/^{140}Ce$)
R_n : ratio of two basic isotopes in sample ($^{142}Ce/^{140}Ce$)
$\sum nRi$: sum of ratios of total isotopes for basis isotope in sample
$\sum aRi$: sum of ratios of total isotopes for basis isotope in spike

The total burnup in atom% fission for the pellet sample was determined by using Nd and Ce isotope monitors according to Eq. (2) [3]:

$$\text{Atom\% fission} = (N/Y)\ x100 / [(N/Y) +(N/U) +(N/Pu)] \quad \text{------ (2)}$$

Where,

N : number of atoms of the monitor Nd or Ce isotope in the sample solution,
Y : effective fission yield of the monitor Nd or Ce isotope from the fissile elements,
N(U), *N*(Pu) : number of U and Pu atoms in the sample solution , respectively.

3. Results & Discussion

3.1 Isotopic Compositions of Ce in Irradiated Fuel

The Ce isotopes in irradiated pellets include two major ^{140}Ce and ^{142}Ce, and trace ^{144}Ce (γ-emitter). Table 1 shows the isotopic compositions of Ce in the irradiated pellet samples (B3 and BO3), and their spiked samples measured by the TIMS .

3.2 Determination of the effective fission yield

The effective fission yields of the Ce isotope monitors were calculated from the fission yields for each of the fissioning isotopes weighted according to their contribution to the fission (Table 2). The concentration of fissionable isotopes used those determined by the IDMS.

Table 1. Isotopic compositions of the Ce separated from the irradiated pellet samples

	Atom%		
Sample	^{140}Ce	^{142}Ce	^{144}Ce
B3 (S)	53.225	46.308	0.467
BO3 (S)	53.123	46.380	0.497
B3 (S+SP)	73.900	25.841	0.259
BO3 (S+SP)	76.170	23.605	0.225

S : sample, S+SP : spiked sample

Table 2. Estimated effective fission yields of Ce isotopes for the irradiated pellet samples

Isotope	Effective fission yield (%)	
	B3	BO3
^{140}Ce	5.9219	5.8898
^{142}Ce	5.4830	5.4400

4. Conclusion

The contents of U, Pu, Nd, Ce and their isotopes in irradiated pellet samples and the total burnup by using Nd and Ce isotope monitors can be determined simultaneously by the isotope dilution mass spectrometric techniques. The Nd and Ce isotope patterns provide information on the real irradiation characteristics which are necessary for evaluating a fuel's performance in a reactor. A comparison between independently determined burnup values provides a check on the validity of the results

REFERENCES

[1] ASTM, "Standard Test Method for Atom Percent Fssion in Uranium and Plutonium Fuel (Neodymium-148 Method)", Annual Book of ASTM Standards 12.02, E321-96 (reapproved 2012), (2012).

[2] F. L. Lisman, W. J. Maeck, and J. E. Rein, "Determination of Nuclear Fuel Burnup from Fission Product **Analysis**", Nucl. Sci. & Eng., 42, 215-219 (1970).

[3] J. S. Kim, Y. S. Jeon, S. D. Park, S. H. Han, and J. G. Kim, "Burnup Determination of High Burnup and Dry Processed Fuels Based on Isotope Dilution Mass Spectrometric Measurements", J. Nucl. Sci. & Technol., 44(7), 1015-1033 (2007).

2018 춘계학술논문요약집

발행인 김창락

발행처 한국방사성폐기물학회

주 소 대전광역시 유성구 대덕대로 989번길 111
한국원자력연구원 원자력성과확산관(E7) 202호

연락처 **Tel** +82-42-861-5851, +82-42-866-4205
Fax +82-42-861-5852 **E-mail** krs@krs.or.kr

인쇄처 신진기획인쇄사 **Tel** +82-42-638-7887

Abstracts of Proceedings of the
Korean Radioactive Waste Society Spring 2017

www.krs.or.kr

KOREAN RADIOACTIVE WASTE SOCIETY

사단 한국방사성폐기물학회
법인 Korean Radioactive Waste Society